Polymer Physics

Applications to Molecular Association and Thermoreversible Gelation

FUMIHIKO TANAKA

This page intentionally left blank

Polymer Physics

The field of polymer science has advanced and expanded considerably in recent years, encompassing broader ranges of materials and applications. In this book, the author unifies the subject matter, pulling together research to provide an updated and systematic presentation of polymer association and thermoreversible gelation, one of the most rapidly developing areas in polymer science. Starting with a clear presentation of the fundamental laws of polymer physics, subsequent chapters discuss a new theoretical model that combines thermodynamic and rheological theory. Recent developments in polymer physics are explored, along with important case studies on topics such as self-assembly, supramolecules, thermoreversible gels, and water-soluble polymers. Throughout the book, a balance is maintained between theoretical descriptions and practical applications, helping the reader to understand complex physical phenomena and their relevance in industry. This book has wide interdisciplinary appeal and is aimed at students and researchers in physics, chemistry, and materials science.

Fumihiko Tanaka is Professor in the Department of Polymer Chemistry at the Graduate School of Engineering, Kyoto University. Professor Tanaka has published extensively and his current research interests are in theoretical aspects of phase transitions in polymeric systems, polymer association, and thermoreversible gelation.

Polymer Physics

Applications to Molecular Association and Thermoreversible Gelation

FUMIHIKO TANAKA

Kyoto University, Japan

CAMBRIDGE
UNIVERSITY PRESS

Dedicated to the memory of
Professor Walter H. Stockmayer
and to
Sir Sam Edwards

Miracle of polymer science

Contents

Preface

Polymer science has expanded over the past few decades and shifted its centre of interest to encompass a whole new range of materials and phenomena. Fundamental investigations on the molecular structure of polymeric liquids, gels, various phase transitions, alloys and blends, molecular motion, flow properties, and many other interesting topics, now constitute a significant proportion of the activity of physical and chemical laboratories around the world.

But beneath the luxuriance of macromolecular materials and observable phenomena, there can be found a common basis of concepts, hypotheses, models, and mathematical deductions that are supposed to belong to only few theories.

One of the major problems in polymer physics which remain unsolved is that of calculating the materials properties of self-assembled supramolecules, gels, molecular complexes, etc., in solutions of associating polymers from first principles, utilizing only such fundamental properties as molecular dimensions, their functionality, and intermolecular associative forces (hydrogen bonding, hydrophobic force, electrostatic interaction, etc.).

Theoretical studies of polymer association had not been entirely neglected, but their achievements were fragmentary, phenomenological, and lacked mathematical depth and rigor. What I have tried to do, therefore, is to show how certain physically relevant phenomena derive from the defining characteristics of various simple theoretical model systems.

The goal of this book is thus to present polymer physics as generally as possible, striving to maintain the appropriate balance between theoretical descriptions and their practical applications.

During the decade that has just ended the application of the method of lattice theory (by Flory and Huggins), the scaling theory (by de Gennes) of polymer solutions, and the theory of gelation reaction (by Flory and Stockmayer) has resulted in the development of what has become known as the "theory of associating polymer solutions." This has brought the aforementioned unsolved problem markedly nearer to the resolution.

In this book special reference is made to polymer associations of various types – binding of small molecules by polymers, polymer hydration, block-copolymerization, thermoreversible gelation, and their flow properties. These topics do not, by any means, exhaust the possibilities of the method. They serve, however, to illustrate its power. The author hopes that others will be stimulated by what has already been done to attempt further applications of the theory of associating polymer solutions.

Most of the subject matter treated in the present book has been hitherto available only in the form of original papers in various scientific journals. These have been very diverse and fragmented. Consequently, they may have appeared difficult to those who start the research and practice on the subjects. The opportunity has therefore been taken to develop the theoretical bases from the unified view and to give the practical applications in somewhat greater detail.

The first four chapters, making up the fundamental part, contain reviews of the latest knowledge on polymer chain statistics, their reactions, their solution properties, and the elasticity of cross-linked networks. Each chapter starts from the elementary concepts and properties with a description of the theoretical methods required to study them. Then, they move to an organized description of the more advanced studies, such as coil–helix transition, hydration, the lattice theory of semiflexible polymers, entropy catastrophe, gelation with multiple reaction, cascade theory, the volume phase transition of gels, etc. Most of them are difficult to find in the presently available textbooks on polymer physics.

Next, Chapter 5 presents the equilibrium theory of associating polymer solutions, one of the major theoretical frameworks for the study of polymer association and thermoreversible gelation.

This is followed by three chapters on the application of the theory to nongelling and gelling solutions. Chapter 6 on nongelling associating solutions includes block polymerization by hydrogen bonding, hydration of water-soluble polymers, hydrogen-bonding liquid crystallization, and micellization by hydophobic aggregation. Chapter 7 treats more interesting but difficult gelling solutions, with stress on phase separation and thermoreversible gelation with junctions of variable multiplicity. Chapter 8 presents two major methods for the study of gels near the sol–gel transition point. One is the topological method on the basis of graph theory, and the other is scaling theory on the basis of the percolation picture.

Chapter 9 presents the transient network theory of associating polymer solutions, which is the other one of the two major theories treated in this book. It studies the dynamic and rheological flow properties of structured solutions from a molecular point of view. Thus, linear complex modulus, nonlinear stationary viscosity, start-up flows, and stress relaxation in reversible polymer networks are studied in detail.

Chapter 10 presents an application of the two theoretical frameworks to more complex, but important systems, such as a mixture of polymers and surfactants, and network formation accompanied by polymer conformational transitions.

This work is a result of the research the author has done over the past two decades with many collaborators. I would like to thank Dr. A. Matsuyama and Dr. M. Ishida (Shoji) for their outstanding contribution to the hydration and thermoreversible gelation of water-soluble polymers while they were graduate students at Tokyo University of Agriculture and Technology. I would also like to thank Dr. Y. Okada who, while studying for his Ph.D under my supervision at Kyoto University, took the initiative of studying the cooperative hydration of temperature-sensitive polymers, giving me no option but to get up to date on this topic. The contribution by Dr. T. Koga to the rheological study of transient networks must also be acknowledged.

It is also a great pleasure to thank Professor Françoise M. Winnik for her research collaboration over the past decade: she has never stopped stimulating and encouraging me with her enthusiasm in the research of water-soluble polymers.

Finally, it is my great pleasure and honor to thank Professor Ryogo Kubo and Sir Sam Edwards, who in my early career introduced me to the fascinating world of statistical mechanics.

Fumihiko Tanaka
Kyoto July 2010

1 Statistical properties of polymer chains

This chapter reviews the elementary statistical properties of a single polymer chain in solvents of different nature. Starting with the ideal random coil conformation and its tension–elongation relation, the excluded-volume effect is introduced to study the swelling and collapse of a random coil. We then focus on the conformational transition of a polymer chain by hydrogen bonding. Coil–helix transition by the intramolecular hydrogen bonding between neighboring monomers, hydration of a polymer chain in aqueous media, and competition in hydrogen bonding in the mixed solvents are detailed.

1.1 Conformation of polymers

1.1.1 Internal coordinates of a polymer chain and its hindered rotation

The complete set of space coordinates which specifies the conformation of a polymer in three-dimensional space is called its **internal coordinates**. To study the positions of the carbon atoms along the linear chain of a polymer, let us consider three contiguous atoms -C-C-C- along the chain (gray circles in Figure 1.1). Because they are connected by covalent bonds, the length l of a bond is fixed at $l = 0.154$ nm, and the angle θ between the successive bonds is fixed at $\theta = 70.53°$ (tetrahedral angle with $\cos\theta = 1/3$). The bond to the fourth carbon atom, however, can rotate around the axis of the second bond although its length and angle are fixed. Such freedom of rotational motion is called the **internal rotation** of the polymer chain [1–5].

The rotation angle ϕ is conventionally measured in a clockwise direction relative to the reference position called the **trans position**. The trans position (t) is on the plane formed by the first three carbon atoms. Due to the molecular interaction, the potential energy of the fourth atom is a function of the rotation angle ϕ. For a simple symmetric polymer like polyethylene, the potential energy becomes minimum at the trans position, and there are two local minima at the angle $\phi = 120°, 240°$ (or equivalently $\pm 120°$). They are called the **gauche position**, and are indicated by the symbols g′, g″ (or g$^+$, g$^-$). Transition between these minima is hindered by the potential barriers separating them. The conformations with different rotation angles which a polymer chain can take are called the **rotational isomeric states**. When all carbon atoms on the chain take the trans conformation, the chain is extended on a plane in zigzag form. This is called **planar zigzag conformation**.

(a)   (b)
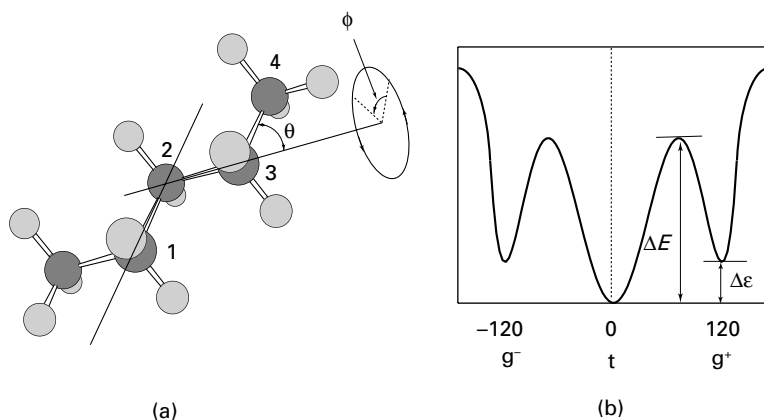
Fig. 1.1   Internal rotation of the carbon atom 4 in a contiguous sequence on a polymer chain. (a) The bond angle θ is fixed at $\cos\theta = 1/3$, while its rotational motion is described by the angle ϕ around the bond axis 2–3. (b) The potential energy is shown as a function of the rotation angle. For polyethylene, there are three minima at $\phi = 0$ (t) and $\phi = \pm 120°$ ($g^{\pm}$).

The energy difference $\Delta\epsilon$ between the t position and the g′, g″ positions decides the average population of the carbon atoms in thermal equilibrium state. It is related to the flexibility of the chain. For instance, the average length λ of the continuous trans sequence ttttt... is given by

$$\lambda = l \exp(\Delta\epsilon/k_{\mathrm{B}}T), \tag{1.1}$$

where T is the absolute temperature, and k_{B} is the Boltzmann constant. This average length is called the **persistence length** of the polymer. It is, for example, approximately $\lambda = 5.1$ nm at room temperature if the energy difference is $\Delta\epsilon = 2.1$ kcal mol^{-1}.

On the other hand, the frequencies of the transition between different isomeric states are determined by the potential barrier ΔE between t and g′, g″ positions (Figure 1.1). The average time τ for the transition from t to g′, g″ is given by

$$\tau = \tau_0 \exp(\Delta E/k_{\mathrm{B}}T), \tag{1.2}$$

where τ_0 is the microscopic time scale of the torsional vibration of a C-C bond ($\tau_0 \approx 10^{-11}$ s). When the temperature is lowered, there is a point where τ becomes sufficiently longer than the duration of observation so that the internal motion looks frozen. Such a transition from a random coil with thermal motion to a frozen rigid coil is called the **glass transition** of a single chain.

Polymers with simple chemical structure take values of order $\Delta\epsilon \simeq 1$ kcal mol^{-1}, $\Delta E \simeq 4$–5 kcal mol^{-1}, but the barrier height ΔE can be higher if the side groups are replaced with larger ones, and also if there is strong interaction, such as dipole interaction, hydrogen bonds, etc., between them.

1.1.2 Coarse-grained models of polymer chains

The **rotational isomeric state** model (RIS) is a model chain in which chain conformation is represented by the set of three states, t, g$^\pm$.

The RIS incorporates the potential of internal rotation, and is one of the most precise descriptions of a chain that preserves its chemical structure. To describe the assemblies of polymers such as polymer solutions, blends, melts, crystals, and glasses, however, RIS is still too complex and difficult to treat. To simplify the treatment of the many chain statistics, coarse-grained model chains are often used. Typical examples are described in Figure 1.2.

Random flight model

A model chain consisting of rigid rods linearly connected by freely rotating joints is called the **random flight model** (RF) (Figure 1.2(a)). Let a be the length of each rod and n the total number of the rods. Since the joint does not necessarily correspond to a single monomer but represents a group of monomers, a may be larger than the length of the C-C chemical bond. Also n may be smaller than the degree of polymerization of the chain. Let us call each unit (a set of joint and rod) a **statistical repeat unit**.

The probability $\rho(\mathbf{x}_i; \mathbf{x}_{i-1})$ to find the i-th joint at the position $\mathbf{x}_i$ when the $(i-1)$-th joint is fixed at the position $\mathbf{x}_{i-1}$ is given by

$$\rho(\mathbf{x}_i; \mathbf{x}_{i-1}) = \frac{1}{4\pi a^2} \delta(l_i - a), \tag{1.3}$$

where $\mathbf{l}_i \equiv \mathbf{x}_i - \mathbf{x}_{i-1}$ is the **bond vector**, $l_i \equiv |\mathbf{l}_i|$ is its absolute value, and $\delta(x)$ is Dirac delta function. The probability ρ characterizes a linear sequence of the statistical repeat units, and is often referred to as the **connectivity function**. The vector **R** which connects both ends of a chain is the **end-to-end vector**. Figure 1.3 shows an RF chain with $n = 200$ which is generated in three dimensions projected onto a plane.

Bead–spring model

A model chain with $n + 1$ beads linearly connected by n springs is called the **bead–spring model** (BS) (Figure 1.2(b)). Each spring is assumed to have a spring constant

(a) (b) (c)
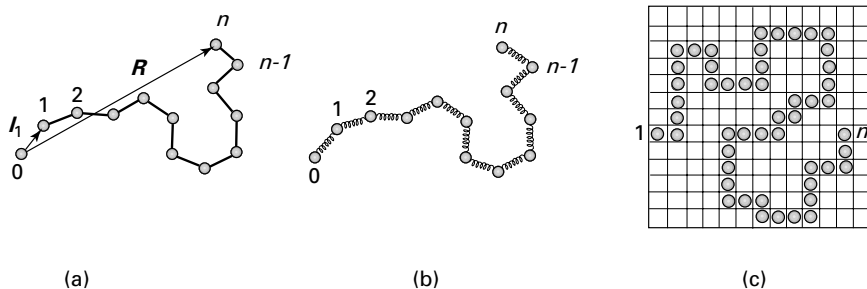
Fig. 1.2 Typical coarse-grained models of a polymer chain: (a) random flight model, (b) bead–spring model, (c) lattice model.
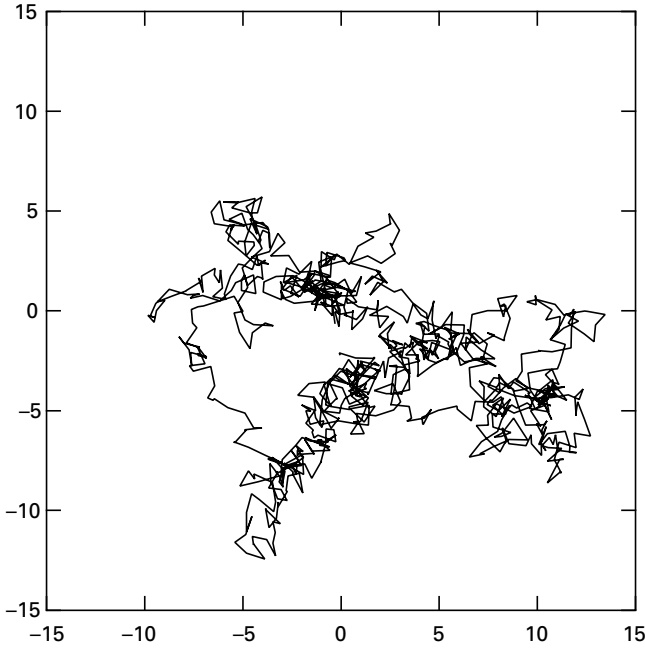
Fig. 1.3   Random coil formed with the random flight model with 200 bonds produced in three dimensions and projected onto a plane.

$k = 3k_B T/a^2$ with 0 equilibrium length. Because the energy of a spring stretched to length l is $kl^2/2$, its statistical weight is given by the Boltzmann factor

$$\rho(\mathbf{x}_i; \mathbf{x}_{i-1}) = \frac{1}{(2\pi a^2/3)^{3/2}} \exp(-3l_i^2/2a^2). \tag{1.4}$$

This is a Gaussian distribution with a mean square separation $\langle l_i^2 \rangle = a^2$ between adjacent beads. The bead in a BS chain also indicates a group of monomers as in RF.

The Gaussian bond (1.4) can easily be stretched to high extension, and allows unphysical mutual passing of bonds. To prevent this unrealistic mechanical property, the model potential, called the **finitely extensible nonlinear elastic potential** (FENE), and described by

$$\rho(\mathbf{x}_i; \mathbf{x}_{i-1}) = C \exp\left[\frac{k}{2}(l_{max} - a)^2 \ln\left\{ 1 - \left(\frac{l_i - a}{l_{max} - a} \right)^2 \right\} \right], \tag{1.5}$$

is often used in the molecular simulation [6], where k is the spring constant and C is the normalization constant. The bond is nonlinear; its elongation is strictly limited in the finite region around the mean bond length a so that bonds can never cross each other.

Lattice model

A chain model described by the trajectory of a random walk on a lattice is called the **lattice model** (Figure 1.2(c)). The lattice constant a plays the role of the bond length. The simplest lattice model assumes that each step falls on the nearest neighboring lattice cell with equal probability [1], so that the connectivity function is given by

$$\rho(\mathbf{x}_i; \mathbf{x}_{i-1}) = \frac{1}{z} \sum_{\mathbf{e}} \delta(\mathbf{l}_i - a\mathbf{e}), \tag{1.6}$$

where z is the lattice coordination number, and the sum should be taken over all lattice vectors $\mathbf{e}$. For instance, $\mathbf{e}$ takes $\pm \mathbf{e}_x, \pm \mathbf{e}_y, \pm \mathbf{e}_z$ for the simple cubic lattice. In a more sophisticated lattice model, one of the nearest neighboring cells is selected as trans position and the rest are regarded as gauche position by introducing the energy difference $\Delta \epsilon$ described in Figure 1.1 [7, 8].

Because the statistical unit of a chain has finite volume, the condition implies that, in the random walk, a lattice cell should never be passed again once it is passed. A random walk with such a constraint is called a **self-avoiding random walk**.

1.2 The ideal chain

1.2.1 Single-chain partition function

A polymer chain changes its conformation by thermal motion. The probability of finding a particular conformation of the chain in the heat reservoir of the absolute temperature T is given by the canonical distribution function. If one end $\mathbf{x}_0$ of a chain is fixed at the origin of the coordinates (Figure 1.4), and the other end $\mathbf{x}_n$ is fixed at the position vector $\mathbf{R}$, the end-to-end vector $\mathbf{R}$ is given by the sum of all bond vectors

$$\mathbf{R} = \sum_{i=1}^{n} \mathbf{l}_i. \tag{1.7}$$

The canonical partition function for the statistical distribution of the specified end-to-end vector is defined by

$$Z(\mathbf{R}, T) = \int \cdots \int d\mathbf{x}_1 d\mathbf{x}_2 ... d\mathbf{x}_{n-1} \exp[-\beta(U+V)] \prod_{j=1}^{n} \rho(\mathbf{x}_j; \mathbf{x}_{j-1}), \tag{1.8}$$

where $\beta \equiv 1/k_B T$ is the reciprocal temperature, and ρ is the connectivity function described in Section 1.1.2.

The interaction energy between the repeat units is separated into two fundamentally different types U and V. The part U is the potential energy of the internal rotation of
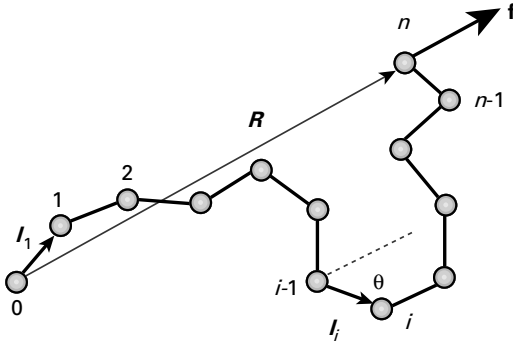
Fig. 1.4   The bond vectors $\mathbf{l}_i$, the first bond vector $\mathbf{l}_1$, and the end-to-end vector $\mathbf{R}$. Tension is applied at one end bead ($i = n$) with the other end bead ($i = 0$) fixed.

each repeat unit, and described in the sum

$$U = \sum_i u_1(\phi_i) + \sum_i u_2(\phi_{i-1}, \phi_i) + \cdots \tag{1.9}$$

by using the rotational angle ϕ of the bonds. The first term depends only upon the angle of the repeat unit under study (one-body term), the second term depends on the nearest neighboring pairs (two-body term), etc. Because the potential energies of the internal rotation involve only local neighbors along the chain, their interaction is called **local**, or **short-range interaction**. When interactions other than the one-body interaction are negligible, the rotation is called **independent internal rotation**. When all U is small enough to be neglected, the rotation is called **free rotation** [1, 2].

However, the potential energy V describes the interaction between the repeat units when they come close to each other in the space, even if the distance along the chain is far apart. It is usually given by the sum

$$V = \sum_{i<j} u(r_{ij}) \tag{1.10}$$

over all pairwise interactions, where $r_{ij} \equiv |\mathbf{x}_i - \mathbf{x}_j|$ is the distance between the i-th and j-th units. Such interaction between distant statistical units along the chain is called **long-range interaction**. For instance, van der Waals force, Coulomb force, etc., belong to this category [1].

A chain for which the interaction energy is negligibly small is called an **ideal chain**. For an ideal chain, we may treat $U = V = 0$, so that we have only to study the connectivity function ρ.

The Helmholtz free energy of a chain can be found by the logarithm of the partition function

$$F(\mathbf{R}, T) = -k_{\mathrm{B}} T \ln Z(\mathbf{R}, T). \tag{1.11}$$

From the Helmholtz free energy, we can find the entropy S and the average tension $\mathbf{f}$ of the chain using the law of thermodynamics:

$$dF = -SdT + \mathbf{f} \cdot d\mathbf{R}. \tag{1.12}$$

To find the free energy of the ideal chain, we consider the integral

$$Z_0(\mathbf{R}, T) = \int \cdots \int \prod_{i=1}^{n} \rho(\mathbf{l}_i) d\mathbf{l}_1 d\mathbf{l}_2 \cdots d\mathbf{l}_n, \tag{1.13}$$

for the partition function. We have changed the integration variables from the position vectors of the joints (beads) to the bond vectors. The subscript 0 indicates that the chain is ideal. Because of the constraint (1.7), we cannot complete the integration in this form.

To remove this constraint, we consider its Laplace transform

$$Q(\mathbf{f}, T) \equiv \int Z(\mathbf{R}, T) e^{\beta \mathbf{f} \cdot \mathbf{R}} d\mathbf{R}, \tag{1.14}$$

where $\beta \equiv 1/k_B T$. The integration of the bond vectors is independent of each other in Q. We find

$$Q(t, T) = \tilde{g}(t)^n, \tag{1.15}$$

after integration, where the new function $\tilde{g}(t)$ is defined by the Laplace transform of the connectivity function

$$\tilde{g}(t) \equiv \int d\mathbf{l} \rho(\mathbf{l}) e^{\beta \mathbf{f} \cdot \mathbf{l}}. \tag{1.16}$$

It is a function of the dimensionless tension t defined by the work fa to elongate the chain by the fundamental length unit a divided by the thermal energy $k_B T$:

$$t \equiv fa/k_B T. \tag{1.17}$$

Let us define the new function $G(\mathbf{f}, T)$ by the log of the Laplace transformed partition function $Q(\mathbf{f}, T)$:

$$G(\mathbf{f}, T) \equiv -k_B T \ln Q(\mathbf{f}, T). \tag{1.18}$$

Because the independent variable is changed from $\mathbf{R}$ to $\mathbf{f}$, the small change of G is given by

$$dG = -SdT - \mathbf{R} \cdot d\mathbf{f}. \tag{1.19}$$

Hence we find that G is identical to the Gibbs free energy. For the ideal chain, it takes the form

$$G_0(\mathbf{f}, T) = -nk_B T \ln \tilde{g}(t), \tag{1.20}$$

from (1.15).

The function ρ of the RF chain (1.3) leads to

$$\tilde{g}(t) = \frac{\sinh t}{t}, \tag{1.21}$$

and hence the Gibbs free energy is

$$G_0(\mathbf{f}, T) = -nk_B T \ln[(\sinh t)/t]. \tag{1.22}$$

The BS chain (1.4) gives the form

$$\tilde{g}(t) = \exp(t^2/6), \tag{1.23}$$

and hence

$$G_0(f, T) = -\frac{n}{6} k_B T t^2. \tag{1.24}$$

For small elongations of the chain, these two models give the same result.

1.2.2   Tension–elongation curve

Using the thermodynamic relation (1.19), we can find the average end vector $\mathbf{R}$ under a given tension $\mathbf{f}$ by the differentiation

$$\mathbf{R} = -\left(\frac{\partial G}{\partial \mathbf{f}}\right)_T. \tag{1.25}$$

Because the vector $\mathbf{R}$ lies in parallel to the tension, we can write the result for the RF model in terms of its absolute value as

$$\frac{R}{na} = L\left(\frac{fa}{k_B T}\right), \tag{1.26}$$

where the function $L(t)$ is defined by

$$L(t) \equiv \frac{d}{dt}\left[\ln\left(\frac{\sinh t}{t}\right)\right] = \coth t - \frac{1}{t}, \tag{1.27}$$

and called the **Langevin function** [4]. The tension–elongation relation is shown in Figure 1.5.

In the linear region where the elongation is small, the graph is a straight line with slope 3, but there is an upturn in the high-extension region due to the nonlinear stretching of the chain. Such a nonlinear amplification in the tension in the high-elongation region is referred to as the **hardening effect**.
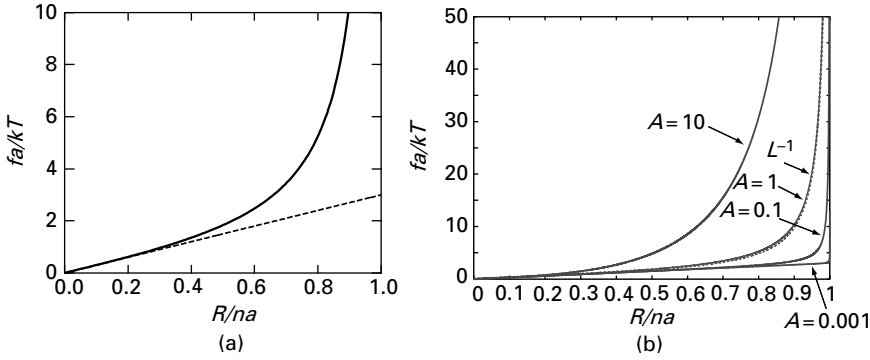
Fig. 1.5 (a) Tension–elongation curve of the Langevin chain (solid line) and its Gaussian approximation (broken line). (b) Simplified model (1.30) of a nonlinear chain for different nonlinear amplitude A. The curve with $A = 1$ (dotted line) is close to that of the Langevin chain.

The Langevin function $\tilde{r} = L(t)$, described by the dimensionless elongation $\tilde{r} \equiv R/na$, is measured relative to the total chain length na, and its inverse function can be expanded in the power series

$$\tilde{r} = L(t) = \frac{1}{3}t - \frac{1}{45}t^3 + \frac{2}{945}t^5 - \frac{1}{4725}t^7 + \cdots, \tag{1.28a}$$

$$t = L^{-1}(\tilde{r}) = 3\tilde{r} + \frac{9}{5}\tilde{r}^3 + \frac{297}{175}\tilde{r}^5 + \frac{1539}{875}\tilde{r}^7 + \cdots. \tag{1.28b}$$

Hence, in the linear region, the tension is proportional to the elongation as

$$f = \frac{3k_B T}{na^2} R, \tag{1.29}$$

so that it obeys **Hooke's law**. A chain that obeys Hooke's law is called a **Gaussian chain**. The proportionality constant depends on the temperature. The BS model with a linear spring obeys a similar law. Because the origin of the tension is not the intermolecular force but the entropy of the chain conformation, the spring constant of the chain increases in proportion to the temperature. This is the opposite tendency to the elastic constant of solids made up of low molecular weight molecules such as metals.

Because the Langevin function and its inverse function are mathematically difficult to treat, we introduce here a simple nonlinear model chain whose tension is described by

$$t = 3\tilde{r}\left[1 + \frac{2}{3}A\frac{\tilde{r}^2}{1 - \tilde{r}^2}\right], \tag{1.30}$$

where A is a parameter to specify the degree of nonlinearity of the chain (Figure 1.5(b)), and referred to as the nonlinear amplitude [9, 10]. When $A = 0$, the chain is Gaussian. It deviates from Gaussian with an increase in A, and the nonlinear effect caused by chain

stretching becomes stronger. For $A = 1$, the chain is close to a Langevin chain with very high accuracy (95%). This simplified model of the tension is used extensively for the study of shear thickening and strain hardening in transient networks in Chapter 9.

We can describe the **temperature coefficient of chain tension** $(\partial f / \partial T)_R$ in terms of the coefficient of the **thermal expansion** $\alpha \equiv (\partial R / \partial T)_f / R$ at constant tension and the extensivity $\kappa_T \equiv (\partial R / \partial f)_T / R$ as

$$\left(\frac{\partial f}{\partial T} \right)_R = \frac{\alpha}{\kappa_T}. \tag{1.31}$$

We thus recognize the similarity to the thermodynamic law

$$(\partial p / \partial T)_V = \alpha / \kappa_T, \tag{1.32}$$

for gases, and hence infer that the origin of the chain elasticity is the entropy as for the temperature coefficient of gases.

1.2.3   Distribution of the end-to-end vector

From the thermodynamic law (1.12), the Helmholtz free energy at a constant temperature is given by the work $\int_0^{\mathbf{r}} \mathbf{f} \cdot d\mathbf{R}$ done for stretching the end vector from $\mathbf{0}$ to $\mathbf{R}$. By the relation (1.11), the partition function is given by

$$Z(\mathbf{R}, T) = \exp \left\{ -n \int_0^{R/na} L^{-1}(y) dy \right\}$$

$$= \exp \left\{ -\frac{3R^2}{2na^2} \left[1 + C_1 \left(\frac{R}{na} \right)^2 + C_2 \left(\frac{R}{na} \right)^4 + \cdots \right] \right\}, \tag{1.33}$$

where C_1 and C_2 are numerical constants. They are found to be $C_1 = 3/10, C_2 = 33/125$ from the expansion (1.28b) for a Langevin chain.

The partition function, when regarded as a function of the end vector, is proportional to the probability of finding the end vector at a position $\mathbf{R}$. It gives the **canonical distribution function** of the end vector after normalization. If the chain is sufficiently long, or the degree of elongation is small, terms higher than C_1 can be neglected, so that the probability is found to be

$$\Phi_0(\mathbf{R}) = \left(\frac{3}{2\pi na^2} \right)^{3/2} \exp \left(-\frac{3R^2}{2na^2} \right). \tag{1.34}$$

Since this is a Gaussian distribution, a chain with this probability distribution function is called a **Gaussian chain**. The mean square end-to-end distance of a Gaussian chain is given by

$$\langle R^2 \rangle_0 = na^2. \tag{1.35}$$

It is proportional to the number n of repeat units, and hence the molecular weight of the polymer. The tension–elongation relation (1.29) of the Gaussian chain gives the free energy

$$F_0(R) = \frac{3k_B T}{2na^2} R^2 \qquad (1.36)$$

by integration. It is proportional to the temperature and the square of the end-to-end distance.

By expanding the Laplace transformed partition function (1.14) in powers of the dimensionless tension, we find

$$\frac{Q(t,T)}{Q(0,T)} = 1 + \frac{\langle R^2 \rangle_0}{6a^2} t^2 + \cdots, \qquad (1.37)$$

and hence we can find the mean end-to-end distance of a free chain from the coefficient of t^2.

Because the energy of orientation measured from the reference direction parallel to the end vector is $f \mathbf{l}_i \cdot \mathbf{R}/R = fa \cos \theta_i$, the orientational distribution function of the bond vector is proportional to $\exp[fa \cos \theta_i / k_B T]$. Because the tension is related to the end-to-end distance by (1.28b), the orientational distribution under a fixed $\mathbf{R}$ is given by the probability

$$f(\theta) = C \exp[L^{-1}(R/na) \cos \theta]. \qquad (1.38)$$

The **orientational order parameter** of the chain is then defined by

$$\eta \equiv \langle P_2(\cos \theta) \rangle, \qquad (1.39)$$

by using the Legendre polynomial of the second-order $P_2(x) \equiv (3x^2 - 1)/2$, where $\langle \cdots \rangle$ is the average over the **orientational distribution function** $f(\theta)$. By taking the average over (1.38), we find

$$\eta(\tilde{r}) = 1 - 3\tilde{r}/L^{-1}(\tilde{r}), \qquad (1.40)$$

for a RF model.

1.3   Fundamental properties of a Gaussian chain

We have seen that a chain has a Gaussian property irrespective of the details of the model employed when the number n of the repeat units is large. This is a typical example of the **central limit theorem** in probability theory.

A Gaussian chain has the following fundamental properties:

(1) The probability distribution function of finding an arbitrary pair i and j of the repeat units at the relative position vector $\mathbf{r}_{ij} \equiv \mathbf{x}_i - \mathbf{x}_j$ is given by

$$\Phi_0(\mathbf{r}_{ij}) = \left(\frac{3}{2\pi a^2 |i-j|} \right)^{3/2} \exp \left(-\frac{3\mathbf{r}_{ij}^2}{2a^2 |i-j|} \right), \tag{1.41}$$

and hence we have $\langle \mathbf{r}_{ij}^2 \rangle_0 = a^2 |i-j|$.

(2) Let $\mathbf{s}_i \equiv \mathbf{x}_i - \mathbf{X}_G$ be the relative position vector of the i-th repeat unit as seen from the center of mass of the chain

$$\mathbf{X}_G \equiv \sum_{i=0}^{n} \mathbf{x}_i / n. \tag{1.42}$$

The square average

$$\langle s^2 \rangle \equiv \frac{1}{n} \sum_{i=0}^{n} \langle s_i^2 \rangle \tag{1.43}$$

of $\mathbf{s}_i$ is the **mean radius of gyration**. The mean radius of gyration of a Gaussian chain is

$$\langle s^2 \rangle_0 = \frac{1}{6} n a^2. \tag{1.44}$$

(3) The probability of finding the relative position vector $\mathbf{r}_{ij}$ connecting the two repeat units to be found at $\mathbf{r}$ is

$$G(\mathbf{r}) = \frac{1}{n} \sum_{i,j} \langle \delta(\mathbf{r} - \mathbf{r}_{ij}) \rangle. \tag{1.45}$$

This function is called the **pair correlation function**. The Fourier transformation

$$\tilde{S}(\mathbf{q}) \equiv \int G(\mathbf{r}) e^{-i\mathbf{q}\cdot\mathbf{r}} d\mathbf{r} = \frac{1}{n} \sum_{i,j} \langle e^{-i\mathbf{q}\cdot\mathbf{r}_{ij}} \rangle \tag{1.46}$$

of the pair correlation function is directly measurable by scattering experiments of light, X-rays, neutrons, etc., and is called the **scattering function** of the chain. Since the Gaussian average is

$$\langle e^{-i\mathbf{q}\cdot\mathbf{r}_{ij}} \rangle_0 = \exp \left\{ -\frac{1}{2} q^2 a^2 |i-j| \right\}, \tag{1.47}$$

we find (1.46), by replacing the sum over i, j in (1.46) by the integral, as

$$\tilde{S}(\mathbf{q}) = n D(\langle s^2 \rangle_0 q^2), \tag{1.48}$$

for a Gaussian chain, where the function $D(x)$ is defined by

$$D(x) \equiv \frac{2}{x^2} \left(e^{-x} - 1 + x \right), \tag{1.49}$$

and called the **Debye function** [11].

The scattering function (1.48) can be expanded as

$$\tilde{S}(q)/n = 1 - \frac{1}{3} \langle s^2 \rangle_0 q^2 + \cdots, \tag{1.50}$$

by using the power expansion $D(x) \simeq 1 - x^2/3 + \cdots$ of the Debye function for small x. By plotting the intensity of scattered light in the limit of long wavelength $q \ll \sqrt{\langle s^2 \rangle_0}$ as a function of the scattering angle, we can find the mean radius of gyration from its slope.

Conversely, in the short wavelength limit of $q \gg \sqrt{\langle s^2 \rangle_0}$, the scattering function is approximately

$$\tilde{S}(q)/n = \frac{2}{x} \simeq \frac{2 \langle s^2 \rangle_0^{1/2}}{q} \sim q^{-1}. \tag{1.51}$$

This shows that the random coil locally looks like a rod-shaped molecule, because the scattering function of a rod is proportional to the inverse power q^{-1}.

1.4 Effect of internal rotation and stiff chains

1.4.1 Characteristic ratio

In this section, we study the effects of local interaction on chain properties. A real chain has a fixed bond length ($l = 0.154$ nm) and a fixed bond angle ($\theta = 109.47°$) between subsequent carbon atoms. The internal rotation experiences a potential energy which depends upon the rotational angle ϕ_i. It is generally described by (1.9).

Because the one-body potential $u_1(\phi)$ has minima at the trans and two gauche angles (Figure 1.1(b)), a simple model in which only the three states t, g^-, g^+ are allowed may be proposed (the **rotational isomeric state model**, or RIS).

The internal hindered rotation affects the chain statistics in many ways, but the fundamental nature of a Gaussian chain, such that its mean square end-to-end distance and radius of gyration are proportional to the molecular weight of the chain, remains unaltered, although the rotional potential energy modifies the proportionality constants. Therefore, to study the proportionality constant, we introduce the **characteristic ratio**

$$C_n \equiv \langle R^2 \rangle / na^2, \tag{1.52}$$

as a function of the potential of rotation. A polymer chain with a large characteristic ratio is difficult to bend. It takes an extended conformation along its axis.

Table 1.1 Characteristic ratios of common polymers

Polymer	Temperature [°C]	C_∞
polyethylene	138	6.7
polystyrene	34	10.2
polypropylene	74	7.0
polyisobutylene	24	6.6
poly(vinyl acetate)	29	9.2

Let us first consider the free rotation model. The free rotation model has a mean square end-to-end distance

$$\langle R^2 \rangle = \sum_{i,j=1}^{n} \langle \mathbf{l}_i \cdot \mathbf{l}_j \rangle = \sum_{i=1}^{n} \langle l_i{}^2 \rangle + 2 \sum_{i<j}^{n} \langle \mathbf{l}_i \cdot \mathbf{l}_j \rangle$$

$$= a^2[n + 2(n-1)(\cos\theta) + 2(n-2)(\cos\theta)^2 + \cdots + 2(\cos\theta)^{n-1}]$$

$$= na^2 \left[\frac{1+\cos\theta}{1-\cos\theta} - \frac{2\cos\theta}{n} \frac{1-(\cos\theta)^n}{(1-\cos\theta)^2} \right], \tag{1.53}$$

due to the independent nature of the rotational motion, where θ is the bond angle.

For a large n, the second term can be neglected. The characteristic ratio is then given by the **Eyring formula** [12]:

$$C_\infty = \frac{1+\cos\theta}{1-\cos\theta}. \tag{1.54}$$

When the potential is not uniform, the characteristic ratio takes the more general form

$$C_\infty = \frac{1+\cos\theta}{1-\cos\theta} \frac{1+\langle\cos\phi\rangle}{1-\langle\cos\phi\rangle}, \tag{1.55}$$

where $\langle \cos\phi \rangle$ is the thermal average over the rotational angle using the Boltzmann factor

$$\exp(-u_1(\phi)/kT). \tag{1.56}$$

This is called the **Oka formula** [13]. For the RIS model, the average is $\langle \cos\phi \rangle = (1-\sigma)/(1+2\sigma)$, where $\sigma \equiv \exp(-\beta\Delta\epsilon)$ ($\Delta\epsilon$ is the energy difference between trans state and gauche state (Figure 1.1)(b)), the Oka formula takes the form

$$C_\infty = \frac{1+\cos\theta}{1-\cos\theta} \frac{2+\sigma}{3\sigma}. \tag{1.57}$$

The textbook by Flory [2] includes the major results on the potentials of rotation and the characteristic ratios calculated on the basis of the chemical structure of polymers.

The experimental values C_∞ of some typical polymers are shown in Table 1.1. Polyethyrene has $\Delta\epsilon = 0.5$ kcal mol^{-1}, $\cos\theta = 1/3$, and hence $\sigma = 0.54$ at $T = 413$ K.

The RIS model (1.57) gives $C_\infty = 3.1$, but the experimental value is $C_\infty = 6.7$, almost twice as large. This discrepancy is attributed to the effect of two-body and higher body interactions.

1.4.2 Persistence length and the stiff chain

The length of the end vector $\mathbf{R}$ projected onto the first bond vector $\mathbf{l}_1$

$$l_p \equiv \langle \mathbf{R} \cdot \mathbf{l}_1 \rangle / a, \tag{1.58}$$

is called **persistence length**. The memory of the initial bond direction is lost in the contour distance l_p along the chain. For the free rotation model, we find

$$\frac{\langle \mathbf{R} \cdot \mathbf{l}_1 \rangle}{a} = \frac{1}{a} \left\langle \sum_{i=1}^{n} \mathbf{l}_i \cdot \mathbf{l}_1 \right\rangle = a \sum_{i=1}^{n} (\cos\theta)^{i-1} = a \frac{1 - (\cos\theta)^n}{1 - \cos\theta}. \tag{1.59}$$

Hence, in the limit of the long chain $n \to \infty$, the persistence length reduces to

$$l_p \equiv \lim_{n \to \infty} \frac{\langle \mathbf{R} \cdot \mathbf{l}_1 \rangle}{a} = \frac{a}{1 - \cos\theta}. \tag{1.60}$$

When there is a potential of internal rotation, the formula is refined to

$$l_p = a \frac{1 + \cos\theta \langle \cos\phi \rangle}{(1 - \cos\theta)(1 - \langle \cos\phi \rangle)}. \tag{1.61}$$

If we take the special limit of $n \to \infty, a \to 0, \theta \to 0$ under a fixed value of the total length $L = na$ in the free rotation model, we find from (1.60)

$$(\cos\theta)^n = (1 - a/l_p)^n \to \exp(-L/l_p), \tag{1.62}$$

and hence we have

$$\langle R^2 \rangle = 2l_p^2 (e^{-L/l_p} - 1 + L/l_p) = L^2 D(x) \tag{1.63}$$

for the mean square end-to-end distance (1.53), where $x \equiv L/l_p$. The function $D(x)$ is Debye function defined by (1.49). The ratio $x \equiv L/l_p$ (the number of the persistence length in the chain) is called the **Kuhn step number**. A chain defined this way in the limit of small bond angles in the free rotation model is called a **Kratky–Porod chain** (KP chain) or **wormlike chain** [14].

A KP chain has a nature similar to the Gaussian chain when the total length is longer than the persistence length ($L \gg l_p$); its mean end-to-end distance becomes $\langle R^2 \rangle \simeq 2l_p L$, which is proportional to L. In the opposite case where the total length is shorter than the persistence length ($L \ll l_p$), it has a similar nature to the rigid rod because $\langle R^2 \rangle \simeq L^2$.
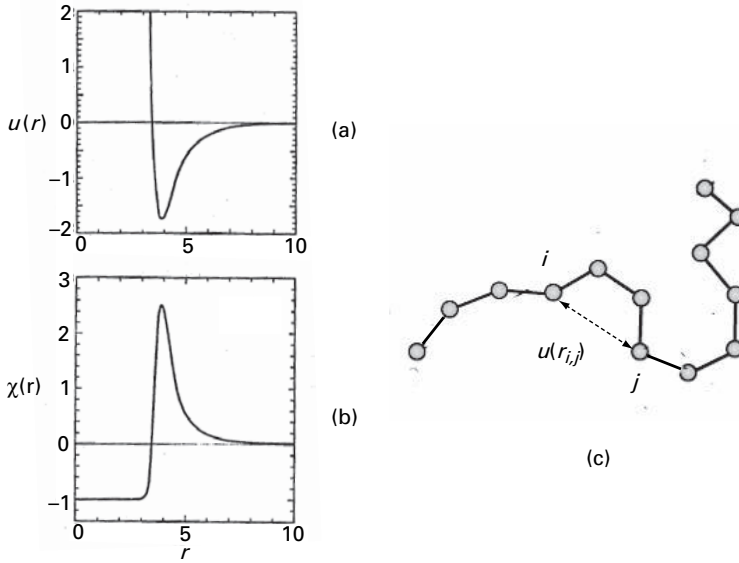
Fig. 1.6   (a) Potential energy $u(r)$ of Lenard–Jones type as a function of the distance between a pair of repeat units on a chain shown in (c). (b) Mayer function constructed from the potential energy (a).

1.5   Excluded-volume effect

This section studies the effect of long-range interaction. Molecular interaction through van der Waals forces, hydrogen bonding, electrostatic forces, and hydrophobic forces, all fall into this category.

We first consider the van der Waals force. The total interaction energy is given by the sum of the pairwise potential

$$V = \sum_{i<j} u(r_{i,j}), \tag{1.64}$$

where $u(r)$ is the effective interaction potential between the monomer i and j in the solvent. It is assumed to have a hard core repulsive part and a long-range attractive part (Figure 1.6(a)).

The partition function (1.8) for a given end-to-end vector $\mathbf{R}$ is

$$Z(\mathbf{R}, T) = \int \cdots \int d\mathbf{x}_1 d\mathbf{x}_2 \cdots d\mathbf{x}_{n-1} \exp\left[-\beta \sum_{i<j} u(r_{i,j})\right] \prod_{j=1}^{n} \rho(\mathbf{x}_j; \mathbf{x}_{j-1}). \tag{1.65}$$

Following Mayer's perturbation theory in the classical statistical mechanics of interacting particles, let us try to expand it in powers of the strength of the interaction [15].

The interaction potential $u(r)$ goes to infinity when the two monomers come into contact, and hence a simple expansion in powers of it leads to the divergence of each

term in the series. To avoid this problem, we introduce the **Mayer function**, defined by

$$\chi(r) \equiv e^{-\beta u(r)} - 1,$$ (1.66)

and expand the interaction part in the partition function in powers of this function as

$$\prod_{i<j}\left[1+\chi(r_{i,j})\right] = 1 + \sum_{i<j}\chi(r_{i,j}) + \sum_{i<j}\sum_{k<l}\chi(r_{i,j})\chi(r_{k,l}) + \cdots.$$ (1.67)

We then carry out the integration term by term. This is the method referred to as **cluster expansion**, which was developed in the theory of condensation of interacting gases [15]. For a polymer chain, the condition of linear connectivity is added.

To calculate term by term in the power expansion, let us introduce a further approximation. The Mayer function takes the form shown in Figure 1.6(b). It can be roughly replaced by

$$\chi(r) \simeq v(T)\delta(r)$$ (1.68)

in order to study the chain properties in scales larger than the size of monomers, where the **excluded volume** of a monomer $v(T)$ is defined by the integral

$$v(T) \equiv -\int \chi(r)d\mathbf{r}.$$ (1.69)

Carrying out this integration separately from the repulsive force inside the diameter σ of the hard core and from the repulsive force outside of it, we find

$$v(T) = \frac{4\pi}{3}\sigma^3 + \beta\int_{\sigma}^{\infty} u(r)4\pi r^2 dr,$$ (1.70)

where the attractive part is expanded in powers of $u(r)$ because it is finite. The first term $v_0 \equiv 4\pi\sigma^3/3$ gives the volume of the space region to which the monomers cannot enter due to the existence of other monomers. This is the origin of the term "excluded volume." The second term takes a negative value due to the attractive nature of $u(r)$. When summed, they are combined as

$$v(T) = v_0(1 - \theta/T).$$ (1.71)

The parameter θ is defined by

$$\theta \equiv -\frac{3}{k_B\sigma^3}\int_{\sigma}^{\infty} u(r)r^2 dr,$$ (1.72)

which is a positive number with the dimension as temperature. This gives the reference temperature for the study of the polymer chain, and called the **theta temperature**.[1] In

---

[1] The theta temperature of polymer solutions is conventionally defined by the temperature at which the second virial coefficient of the osmotic pressure vanishes. In this book, we write Θ for this theta

Table 1.2 Coefficients in the expansion factors

Expansion factor	Mean end-to-end distance	Radius of gyration
C_1	$4/3 = 1.333$	$134/105 = 1.276$
C_2	2.075	2.082
C_3	6.297	–

the following, we measure the temperature in terms of the dimensionless temperature deviation

$$\tau \equiv 1 - \theta/T, \tag{1.73}$$

from the reference theta temperature.

In the high-temperature region $\tau > 0$, the repulsive force is dominant. The monomers mutually repel each other, and as a result the chain swells from the ideal state. The solvent serves as a **good solvent**. On the contrary, in the low-temperature region $\tau < 0$, the chain contracts due to the attractive interaction among the monomers. The solvent serving such an environment is a **poor solvent**. At the theta temperature lying in between them, these two effects exactly cancel each other, so that the chain remains ideal.

If the integrals are carried out term by term in the power series of the cluster expansion for the BS model chain (1.4), the series turns out to be in powers of the parameter

$$z \equiv \left(\frac{3}{2\pi a^2}\right)^{3/2} v(T)\sqrt{n} \simeq \tau\sqrt{n}. \tag{1.74}$$

This parameter is called the **excluded-volume parameter**.

On the basis of this perturbational method, we can calculate the statistical averages of various physical quantities [17, 16]. For instance, the mean square end-to-end distance is expressed in the asymptotic series

$$\alpha_R^2 \equiv \langle R^2 \rangle / \langle R^2 \rangle_0 = 1 + C_1 z - C_2 z^2 + C_3 z^3 - \cdots \tag{1.75}$$

which has alternating coefficients. The series does not converge, but the absolute value gradually approaches the exact value as higher terms are included. The ratio α_R^2 defined by the left of this equation is called the **expansion factor** of the mean end-to-end distance. The expansion factor α_S of the radius of gyration is similarly defined. The results obtained so far are summarized in Table 1.2. We can see clearly that the chain expands or shrinks, depending on the temperature.

The perturbational analysis is theoretically clear in principle, but has weak points such as (1) calculation of the higher-order terms is seriously difficult, (2) it is not a convergent

temperature of the solutions to distinguish from the single-chain θ at which the attractive and repulsive interactions balance and the total excluded volume vanishes. The relation between the two is studied in the following chapters.

series, and (3) the series has physical meaning only in the vicinity of the theta temperature because the excluded-volume parameter is proportional to $\sqrt{n}$. Therefore, we need a more efficient method to understand the statistical properties of the polymer chain over a range temperature wide.

In fact, experiments report that the average end-to-end distance obeys the power law

$$\langle R^2 \rangle^{1/2} \simeq an^{\nu}, \quad \nu = 3/5. \tag{1.76}$$

The exponent of n changes from 1/2 to this **Flory's 3/5 law** at high temperatures [18]. The exponent 3/5 of the polymer dimensions is called the **Flory exponent**. We cannot reach this result by continuing the calculation of higher-order terms in the cluster expansion.

1.6 Scaling laws and the temperature blob model

The critical exponent ν of the polymer dimension is found to be $\nu = 0.60$ in the high-temperature region by light scattering measurements, $\nu = 0.55-0.57$ by measurements of the diffusion coefficient, and $\nu = 0.55-0.57$ by viscometry. In this section, we propose a physical picture by which we can view the statistical properties of the polymer chain over the entire temperature region.

First, we know that polymer chains show the properties of a Gaussian chain in the narrow region near the theta temperature where the excluded volume parameter z is sufficiently small. We have

$$R_{\theta} \simeq an^{\nu_{\theta}}, \quad \nu_{\theta} = 1/2. \tag{1.77}$$

In this section, we focus on the dependence on the temperature and DP, so that we may neglect the unimportant numerical prefactor of order unity. Therefore, R_{θ} on the right-hand side can also be interpreted as the mean radius of gyration, R_G.

In the high-temperature region, the chain expands not uniformly but forms **temperature blobs**, groups of correlated monomers consisting of an average number g of monomers [16] (see Figure 1.7). Each of the blobs has the nature of a Gaussian chain with the scaling law, but they repel each other due to the excluded-volume effect. The average radius of gyration of a blob is given by

$$\xi = ag^{\nu_{\theta}}. \tag{1.78}$$

The polymer takes a conformation which looks like a pearl-necklace made up of blobs.

The number g of monomers inside the blob can be found using the condition such that in the length scale larger than ξ the excluded-volume effect is significant. The boundary is given by

$$v(T)\frac{g}{\xi^3} \simeq 1, \tag{1.79}$$
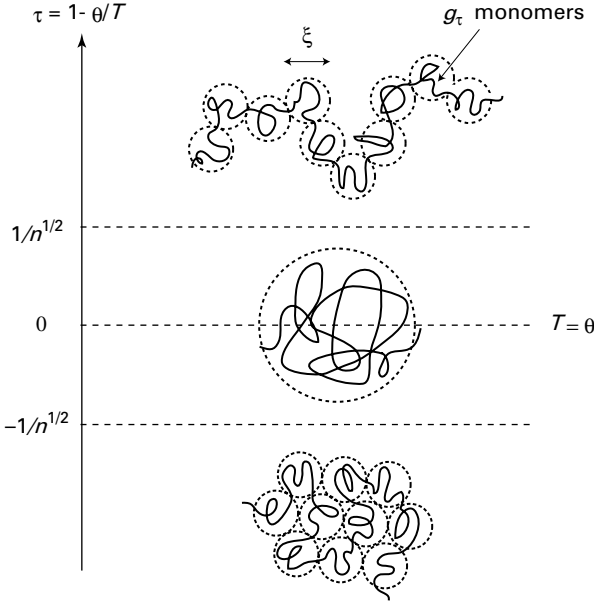
Fig. 1.7   Thermal blob model describing the conformational change of a polymer chain with the temperature. The vertical axis is the dimensionless reduced temperature τ with the theta temperature as the reference temperature.

where v is the excluded volume (1.71). Substituting ξ and v into this equation, we find

$$g_\tau \simeq 1/\tau^2. \tag{1.80}$$

This number depends on the temperature, and hence we write it as g_τ.

Now, the total number of blobs is n/g_τ. As they obey Flory's law (1.76), the radius of gyration of the chain becomes

$$R_F \simeq (a g_\tau{}^{v_\theta}) \cdot \left(\frac{n}{g_\tau}\right)^{v_F} = \tau^{1/5} n^{3/5}, \tag{1.81}$$

where $v_F = 3/5$ is the Flory exponent. This is Flory's 3/5 law shown with the temperature factor.

The **crossover temperature** where the theta region changes into the high-temperature swollen region is decided by the condition $\xi \simeq R_\theta$. This gives $\tau \simeq 1/n^{1/2}$ for the boundary between them.

At low temperatures, the chain forms blobs as in the high-temperature region, but the blobs attract each other and are packed into a compact form by the negative excluded-volume interaction (see Figure 1.7). If we assume **close packing** of the blobs, the radius of gyration of the chain becomes

$$R_G \simeq (a g_\tau{}^{v_\theta}) \cdot \left(\frac{n}{g_\tau}\right)^{v_c} = a\tau^{-1/3} n^{1/3}, \tag{1.82}$$

where $\nu_c = 1/3$ is the critical exponent for close packing.[2] The close packed blobs form what is called a **polymer globule**.

The change from Gaussian chain to globule by cooling is generally a gradual crossover, but discontinuous change (**collapse transition**) is also reported in the literature [19–22] Under what conditions the collapse transition takes place remains an open question. Such a discontinuous collapse is considered to be thermally reversible, and is called **coil–globule transition** (referred to as CG transition).

1.7 Coil–globule transition of a polymer chain in a poor solvent

Monomers on a polymer chain in a solvent interact with each other through the effective long-range force. The temperature blob model predicts a **crossover** from a random coil to a compact globule. On the basis of the mean-field free energy, this section studies the possibility of a sharp CG transition [16, 20].

Let $\alpha \equiv R/R_0$ be the expansion factor of the average radius R of the chain measured relative to the reference value $R_0 = a\sqrt{n}$ in the Gaussian state. The volume $V = 4\pi R^3/3$ occupied by the chain has an average of n/V monomer density. The free energy can be described by

$$\beta F(R) = A(\alpha) + \beta F_{\text{int}}(R), \tag{1.83}$$

where $A(\alpha)$ is the elastic free energy due to the change in the polymer conformational entropy. It is

$$A(\alpha) = \frac{3}{2}(\alpha^2 - 1) - 3\ln\alpha, \tag{1.84}$$

from (1.36) when the reference value at $\alpha = 1$ is subtracted.[3]

The second term F_{int} is the energy due to the monomer interaction. Following the standard procedure for the study of interacting gases, it can be expanded as

$$\beta F_{\text{int}}(\phi) = n\left[v(T)\left(\frac{n}{V}\right)^2 + w\left(\frac{n}{V}\right)^3 + \cdots\right] \tag{1.85}$$

in the density virial series, where $v(T)$ is the two-body interaction parameter (1.71), w is the three-body cluster integral, etc. Taking up to the third-order term, and minimizing the total free energy (1.83) with respect to α, we find the equation

$$f(\alpha) \equiv \alpha^5 - \alpha^3 - \frac{y}{\alpha^3} - C\tau\sqrt{n} = 0, \tag{1.86}$$

for α. We have employed the form $v(T) = v_0\tau$ for the excluded volume, and introduced two constants $y \equiv w/2\omega^2$ and $C \equiv v_0/\omega$ ($\omega \equiv 4\pi a^3/3$ is the volume of a monomer). They both have numerical values of order unity.

---

[2] If we pack n rigid spheres of radius a as closely as possible into a spherical form, the radius of the body formed is proportional to $n^{1/3}$.

[3] The final term $-3\ln\alpha$ is necessary when the volume change is associated with the deformation.

Solving (1.86) with respect to α, we find the following results:

(1) Under the assumption that y is independent of the temperature, α is a function of the combined variable $z \equiv \tau \sqrt{n}$.
(2) In the high-temperature region, where $\tau \sqrt{n} \gg 1$, $\alpha \simeq (\tau \sqrt{n})^{1/5}$, and hence $R \simeq \tau^{1/5} n^{3/5}$. The chain is swollen compared to the ideal state. Thus, Flory's 3/5 law is confirmed.
(3) In the low-temperature region, where $-\tau \sqrt{n} \gg 1$, $\alpha \sim |\tau \sqrt{n}|^{-1/3}$, and hence $R \simeq (-\tau)^{-1/3} n^{1/3}$. The 1/3 law indicates that the chain takes a close-packed globular conformation.
(4) In the transition region, where $|\tau \sqrt{n}| \lesssim 1$, the expansion factor is close to unity $\alpha \simeq 1$. The nature of the transition depends on the value of y. If y takes a value larger than the critical value $y_c = 0.0228$, the transition from swollen coil to globule is a gradual crossover. If it is smaller than the critical value, the equation (1.86) has three solutions, so that the transition becomes discontinuous similarly to the first-order phase transition (Figure 1.8(a)). The transition temperature τ_c lies $1/\sqrt{n}$ below the temperature θ. It approaches the temperature θ in the limit of infinite molecular weight.
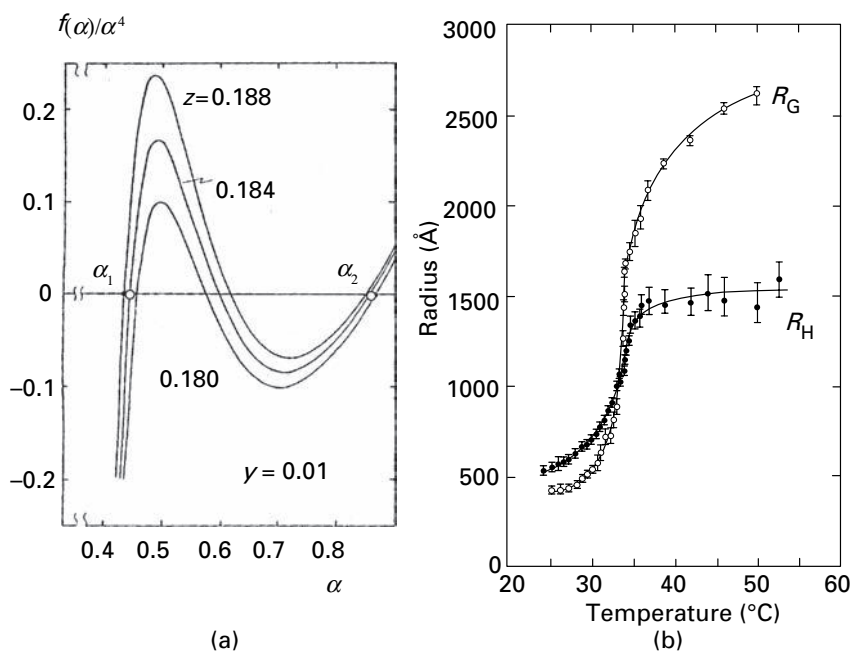
Fig. 1.8 (a) Function $f(\alpha)$ (divided by α^4 to show Maxwell's rule of equal areas) plotted against α. There is a discontinuous coil–globule transition for $y < 0.0228$. (b) Radius of gyration R_G and hydrodynamic radius R_H of a polystyrene (PS) chain in cyclohexane measured by static and dynamic light scattering plotted against the temperature. The molecular weight of PS is $M_w = 2.6 \times 10^7$. (Reprinted with permission from Ref. [22].)

In the region occupied by the polymer chain, solvent molecules are mixed. Let $\Delta\mu_0$ be the chemical potential of the solvent molecule measured from the value in the pure solvent. From the thermodynamic condition $\Delta\mu_0 = (\partial\Delta F/\partial N_0)_n = -(\phi/n)(\partial\Delta F/\partial\phi) = 0$ that the chemical potential of a solvent molecule inside the region occupied by the polymer should be equal to that in the outside region, we can derive **Maxwell's rule of equal area** for the osmotic pressure in the form

$$\beta\Delta F \equiv \beta(F_2 - F_1) = \int_{\alpha_1}^{\alpha_2} 3f(\alpha)\frac{d\alpha}{\alpha^4} = 0, \qquad (1.87)$$

for the free energy, where α_1 is the swollen state and α_2 is the collapsed state (Figure 1.8(a)).

The nature of the CG transition has been investigated by many researchers. A typical example is polystyrene (PS) in the solvent cyclohexane ($\theta = 34.5°C$). Neutron scattering, light scattering, osmotic pressure measurements, and viscosity measurements have all confirmed the points (1)–(3) above, but no consensus has yet been reached about the nature of the transition (4). Light scattering experiments on PS of ultrahigh molecular weight ($M_w = 2.6 \times 10^7$) indicate that the transition is very close to the discontinuous one with $y \simeq y_c$ (Figure 1.8(b)) [21].

1.8 Coil–helix transition

Some polymers, such as isotactic polypropyrene (iPP), polyisobutadiene (PIB), and poly(ethylene oxide) (PEO), form **helices** in the crystalline state. A **helical structure** is represented by p_m with p number of monomers and m the number of turns in one period of the helix. The length d of one period is called **pitch of the helix**. The length along the helical axis *per monomer* is then given by

$$b \equiv d/p. \qquad (1.88)$$

For example, iPP forms a 3_1 helix with $d = 0.65$ nm, and hence $b = 0.22$ nm; PIB forms an 8_5 helix with $d = 1.863$ nm, $b = 0.233$ nm; and PEO forms a 7_2 helix with $d = 1.93$ nm, $b = 0.28$ nm (see Figure 1.9). Short-range interactions (local interactions), in particular hydrogen bonds, are important for stabilization of a helical conformation.

Several synthetic polypeptides, such as the poly(L-amino acid)s, the poly(γ-L-glutamate) (PBLG), poly(β-benzyl-L-asparate) (PβBA), and poly(L-glutamic acid)
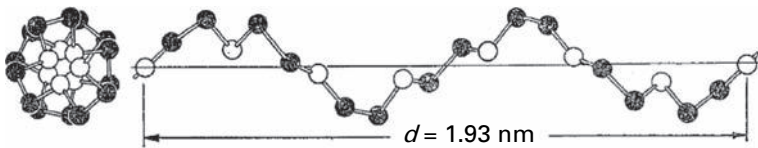
Fig. 1.9 Helix structure 7_2 of poly(ethylene oxide). The period is $d = 1.93$ nm. One period includes seven ethylene oxide monomers and forms two turns.
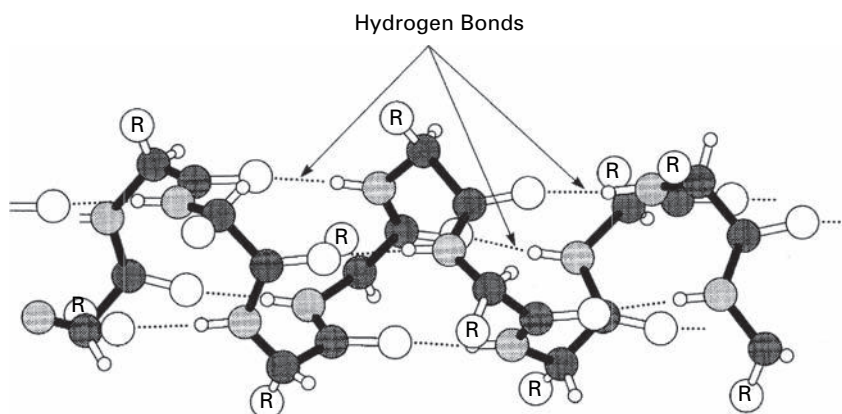
Fig. 1.10   Alpha helix of polypeptide. Type 18_5 has a period of 2.7 nm. Hence, 3.6 residues (0.54 nm) form a turn. The pitch per monomer is $b = 0.15$ nm.

(PLGA), also form **α-helices** in the solid state (see Figure 1.10). When they are dispersed in strongly interacting solvents, polymer chains are not merely separated from each other but also change their conformation from helical to random coil. For instance, PBLG forms an α-helix with $b = 0.15$ nm in chloroform (CF), but melts into a statistical random coil in dichloroacetic acid (DCA). Hence, the chain changes its conformation in mixed solvents of CF and DCA depending on the solvent composition. Such a conformation change is an example of **coil–helix transition** (referred to as CH transition). In the transition state, a chain generally takes a conformation with rod-like rigid helices of polydisperse length that are sequentially connected by random coil segments. CH transition may also be induced by changing other environmental parameters, such as temperature or pH.

Theoretical studies of CH transitions focus attention on the behavior of the poly(amino acid) in the transition region. The most basic information is the change in the fraction of the residues in helical states as functions of the molecular weight of the chain and of the environmental parameters (solvent composition x, temperature T, and pH).

From the late 1950s, many papers in the literature studied this problem [23]. Most of them employed either the matrix method or the generating function method to calculate the chain partition function. However, in order to apply the theoretical method directly to many chain problems in solutions and gels, we here reformulate the single chain problem using the combinatorial counting method.

Consider a polymer chain carrying a total number n of statistical units (Figure 1.11). Let the symbol 0 indicate a monomer (an amino acid) in the random coil part, and let 1 indicate the same in the helical part. Let u be the statistical weight of the adjacent pair $(0,0)$ of monomers, v be that of a pair $(1,1)$, and w be that of the pairs $(0,1)$ and $(1,0)$. These can be derived by integrating over the rotational angle of a monomer under the potential of internal rotation (1.9). Because a hydrogen bond is formed between
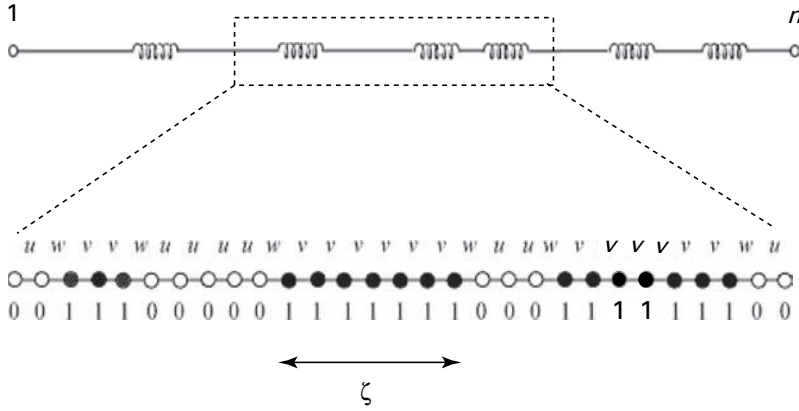
Fig. 1.11   Statistical weight of the conformation of a chain with mixed helical parts (1) and random coil parts (0). After integration over the internal rotation angle, we find the statistical weights u, v, and w for the adjacent pair (0,0), (1,1) and (0,1), (1,0). The number of repeat units (an amino acid) in the helix is designated ζ.

neighboring pairs in the helical part, the statistical weight v is different from u for the pair in a coil part.

The partition function of the chain is then given by the form

$$Z_m(T) = \sum (u) w(vv) w(uuuu) w(vvvvvv) \cdots, \tag{1.89}$$

where the summation should be taken over all possible distributions of the helical parts along the chain under the given number m of the helical monomers.

Let us study this partition function from a different viewpoint. In order for the helices to be generated on this chain, helical sequences must be selected from the finite length n. Let j_ζ be the number of helices with length $\zeta = 1, 2, 3, \ldots, n$ (counted in the number of statistical repeat units).

We first consider that helices are temporarily contracted into single units. The total length is therefore reduced to $n' = n - \sum \zeta j_\zeta$. (In order to distinguish the neigboring helices, we assume that there should be at least one nonhelical monomer between them.)

The number of ways to choose $\sum j_\zeta$ units from n' is given by $n'!/(\sum j_\zeta!)(n' - \sum j_\zeta)!$, but since we cannot distinguish the states that are obtained by exchanging helices of the same length, we instead have to multiply by the factor $(\sum j_\zeta)!/(\prod j_\zeta!)$.

We thus find that the number of different ways to select $\mathbf{j} \equiv \{j_1, j_2, j_3, \ldots\}$ sequences is given by

$$\omega(\mathbf{j}) = \frac{(n - \sum \zeta j_\zeta)!}{(\prod j_\zeta!)(n - \sum \zeta j_\zeta - \sum j_\zeta)!}. \tag{1.90}$$

We next divide the partition function by its value u^n in the reference state of the perfect random coil, and introduce the relative statistical units $s(T) \equiv v/u$. The ratio w/u is then

expressed as $\sigma s(T)$, where $\sigma \equiv w/v$ is associated with each boundary between the neighboring coil part and the helical part.

In general, for a run of ζ helical monomers, the statistical weight

$$\eta_\zeta = \sigma s(T)^\zeta \tag{1.91}$$

is assigned [24]. The parameter σ associated with the helix boundary is called the **helix initiation (nucleation) parameter**, or the **cooperativity parameter**. If it is small, the probability to create the first hydrogen bond to generate the helix (nucleation of the helix) is low due to the large penalty for adjusting the local conformation to form the hydrogen bond. But once one bond is formed, adjacent bonds are formed more easily, so that there is a strong tendency to form continuous chains of bonds.

The partition function of a chain measured relative to the random-coil conformation is then given by

$$Z_m(T) = \sum_{\mathbf{j}} \omega(\mathbf{j}) \prod_\zeta (\eta_\zeta)^{j_\zeta}. \tag{1.92}$$

Because the total number $m \equiv \sum \zeta j_\zeta$ of helical monomers is not a fixed number but thermally controlled, we introduce the activity λ of the helical monomers, and move to the grand canonical partition function

$$\Xi(\lambda, T) \equiv \sum_{m \geq 0} Z_m(T) \lambda^m. \tag{1.93}$$

This function is the helical counterpart of the **binding polynomial** in the literature [25] on biomacromolecules, which is frequently used to study the adsorption of ions, legands, protons, etc. onto proteins.

In order to find the most probable distribution (m.p.d.) of helices, we maximize the partition function (1.93) with $\lambda = 1$, or minimize the free energy $G(T)$ of a chain, by changing $\mathbf{j}$. The condition is

$$\frac{\partial}{\partial j_\zeta} \left[\ln \omega(\mathbf{j}) + \sum_\zeta j_\zeta \ln \eta_\zeta \right] = 0. \tag{1.94}$$

By using the Stirling formula for $\ln \omega(\mathbf{j})$, we find that the m.p.d. is given by

$$j_\zeta/n = (1 - \theta - v)\eta_\zeta z^\zeta, \tag{1.95}$$

where

$$\theta \equiv \sum_{\zeta=1}^n \zeta j_\zeta/n \tag{1.96}$$

is the average helical content (number of statistical units in the helical parts divided by the total number of units), and

$$\nu \equiv \sum_{\zeta=1}^{n} j_{\zeta}/n \tag{1.97}$$

is the average number of helices on the chain. The parameter z in (1.95) is defined by

$$z \equiv (1-\theta-\nu)/(1-\theta). \tag{1.98}$$

Substituting the distribution (1.95) into these definitions, we find θ and ν as

$$\theta = zV_1(z)/[1+zV_1(z)], \tag{1.99}$$

and

$$\nu = zV_0(z)/[1+zV_1(z)], \tag{1.100}$$

where the functions $V(x)$ are defined by

$$V_0(z) \equiv \sum_{\zeta=1}^{n} \eta_{\zeta} z^{\zeta}, \qquad V_1(z) \equiv \sum_{\zeta=1}^{n} \zeta \eta_{\zeta} z^{\zeta}. \tag{1.101}$$

Similarly, substituting (1.95) back into the original partition function (1.92), we find

$$\Xi(T) = z^{-n}, \tag{1.102}$$

where $\Xi(T) \equiv \Xi(1,T)$, or equivalently,

$$G(T) = k_B T \ln z. \tag{1.103}$$

By definition (1.98), the parameter z must satisfy the equation

$$\frac{z}{1-z} V_0(z) = 1. \tag{1.104}$$

If n is allowed to go to infinity in $V_0(z)$, this is the same equation as that found by Zimm and Bragg [24] (referred to as ZB):

$$\frac{z}{1-z} \frac{\sigma sz}{1-sz} = 1. \tag{1.105}$$

The solution z corresponds to the reciprocal λ_0^{-1} of the larger eigenvalue λ_0 of the original ZB secular equation. However, because the upper limit of the sum in V_k is limited to the total number n of repeat units, the effect of the molecular weight on the transition is easy to study in the present theoretical framework.
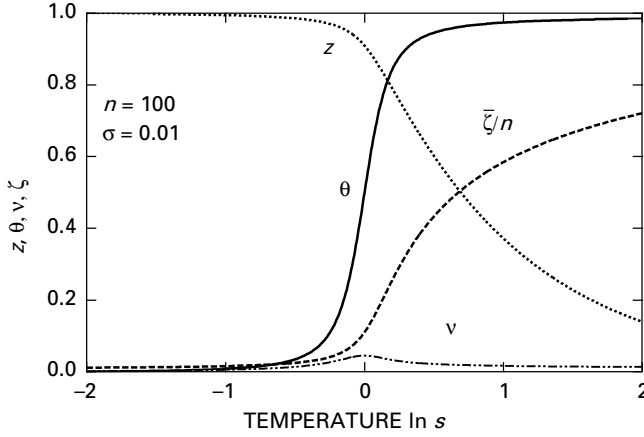
Fig. 1.12   Helix content θ (solid line), number of helices ν (broken dotted line), mean helix length $\bar{\zeta}$ (broken line), and probability z (thin broken line) for a randomly chosen monomer to belong to the random coil part shown as functions of the temperature. The temperature is measured in terms of $\ln s = \text{const} + |\epsilon_H|/k_B T$ by using the probability s of hydrogen-bond formation.

Substituting the form (1.91), we find

$$V_0(z) = \sigma s z w_0(sz), \qquad V_1(z) = \sigma s z w_1(sz), \tag{1.106}$$

where the functions w_0 and w_1 are defined by

$$w_0(x) \equiv \sum_{\zeta=1}^{n} x^{\zeta-1}, \qquad w_1(x) \equiv \sum_{\zeta=1}^{n} \zeta x^{\zeta-1}. \tag{1.107}$$

Lifson and Roig [26] used a slightly different weight for η_ζ:

$$\eta_\zeta = v \ (\text{for } \zeta = 1), \qquad v^2 w^{\zeta-2} \ (\text{for } \zeta \geq 2). \tag{1.108}$$

The result does not differ significantly, so that, in the following study, we employ the simpler ZB weight.

Figure 1.12 plots z, θ, ν, and the mean helix length $\bar{\zeta} \equiv \theta/\nu$ as functions of the temperature. Temperature is measured in terms of $\ln s(T)$. The CH transition takes place at around $\ln s = 0$. The transition becomes sharper for a smaller nucleation parameter σ (stronger cooperativity). The transition also becomes sharper with molecular weight, and becomes a real phase transition with discontinuous θ in the limit of infinite chain length.

Consider next the CH transition of a polymer chain under tension applied at the chain end (Figure 1.13) [27]. For simplicity, let us also assume that the helices are rigid rods and have a pitch d with p monomers in one period. The length along the rod axis per monomer is then given by b (1.88). The length of a helix with monomer sequence ζ is given by $b\zeta$.
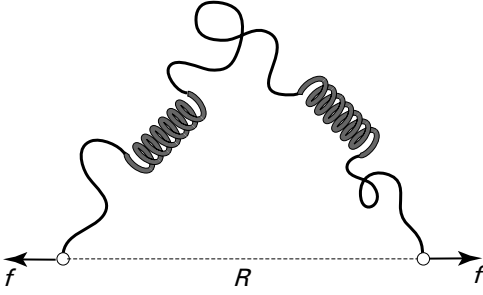
Fig. 1.13   Polymer chain forming helices under an applied tension $\mathbf{f}$. Coil parts and helical parts appear alternately along the chain.

Let $\mathbf{e}_i$ be the unit vector specifying the direction of the i-th helix along the chain, and let $\mathbf{r}_k$ be the end-to-end vector of the k-th random coil part along the chain. We then have the relation

$$\mathbf{R} = \sum_k \mathbf{r}_k + b \sum_i \zeta_i \mathbf{e}_i \tag{1.109}$$

for the end-to-end vector of a chain.

Let m be the total number of repeat units in the helical parts. The canonical partition function of a chain with specified m and $\mathbf{R}$ is written as

$$Z_m(T,\mathbf{R}) = \sum_{\{j\}} \omega(\mathbf{j}) \prod_\zeta (\eta_\zeta)^{j_\zeta} \int \cdots \int \prod_k \rho(\mathbf{l}_k) d\mathbf{l}_k \prod_i \rho_\zeta(\mathbf{l}_i) d\mathbf{l}_i, \tag{1.110}$$

under the condition (1.109), where $\rho_\zeta(\mathbf{l})$ is the connectivity function (1.3) for the helix of length ζ.

We next move to the ensemble where the external tension $\mathbf{f}$ is the independent variable, and integrate over end-to-end vectors $\mathbf{R}$ and orientation $\mathbf{e}_i$ of helical rods. We then find

$$Q_m(T,\mathbf{f}) \equiv \int d\mathbf{R}\, Z_m(T,\mathbf{R}) e^{\beta \mathbf{f} \cdot \mathbf{R}} = \tilde{g}(t)^{n-m} \sum_{\mathbf{j}} \omega(\mathbf{j}) \prod_\zeta (\eta_\zeta)^{j_\zeta} \prod_{i=1}^n \tilde{g}(\kappa t \zeta)^{j_\zeta}, \tag{1.111}$$

where the function $\tilde{g}(t)$ is the Laplace transform (1.16) of the connectivity function $\rho(\mathbf{l})$, $t \equiv fa/k_B T$ is the dimensionless tension, and

$$\kappa \equiv b/a \tag{1.112}$$

is the helical pitch per monomer in the unit of the fundamental step length of a repeat unit.

We next introduce the activity λ for a helical monomer, and move to the grand partition function

$$\Xi(T,\lambda,\mathbf{f}) \equiv \sum_{m=0}^{n} \lambda^m Q_m(T,\mathbf{f})$$

$$= \tilde{g}(t)^n \sum_{\mathbf{j}} \omega(\mathbf{j}) \prod_{\zeta} (\eta_\zeta \phi_\zeta(t)\lambda^\zeta)^{j_\zeta}, \qquad (1.113)$$

where the new function ϕ_ζ is defined by

$$\phi_\zeta(t) \equiv \tilde{g}(\kappa t \zeta)/\tilde{g}(t)^\zeta. \qquad (1.114)$$

At this stage, we can see clearly the effect of tension on the CH transition. The statistical weight η_ζ of a helix with length ζ is changed to

$$\eta_\zeta \longrightarrow \eta_\zeta \phi_\zeta(t), \qquad (1.115)$$

where the factor ϕ_ζ includes the effect of the orientation $\tilde{g}(\kappa \tau \zeta)$ of a rod-like helix, and the entropic force $\tilde{g}(\tau)^{-\zeta}$ from the corresponding random coil segments. In fact, by taking the logarithm of the total statistical weight of a helix, we find that the free energy of a helical sequence of length ζ is given by

$$\Delta f_\zeta(\tau)/k_B T = -\ln \eta_\zeta - \ln[\sinh(\kappa \tau \zeta)/\kappa \tau \zeta] + \zeta \ln[\sinh \tau/\tau] - \zeta \ln \lambda. \qquad (1.116)$$

By minimizing this free energy with respect to ζ for a given statistical weight η_ζ, we can see in a simple way that the average helix length is increased by stretching to the limit where they are finally destroyed. The physical reason why helices are enhanced by tension is that the linear growth of rod-like helices gains a larger end-to-end distance than that of the random coils, and hence it is advantageous for a chain under tension.

The m.p.d. of helices is found by maximizing the grand partition function (1.113) by changing j_ζ. As before, we find

$$j_\zeta/n = (1-\theta-\nu)\eta_\zeta \phi_\zeta(t)(\lambda z)^\zeta \qquad (1.117)$$

by variational calculation. The parameter z is defined by

$$z \equiv (1-\theta-\nu)/(1-\theta). \qquad (1.118)$$

To see the physical meaning of this parameter, we substitute the equilibrium distribution (1.117) into the grand partition function, and fix at $\lambda = 1$. We find that it is given by

$$\Xi(T,t) = [\tilde{g}(t)/z]^n. \qquad (1.119)$$

Since the probability $p(m=0)$ for finding a completely random coil is given by $\tilde{g}(t)^n/\Xi(T,t)$, we find

$$p(m=0)=z^n, \tag{1.120}$$

and hence the physical interpretation of the parameter z is the probability such that an arbitrarily chosen monomer belongs to the random coil part.

Repeating the same procedure given above under no tension, we find

$$\theta = zV_1(t,z)/[1+zV_1(t,z)], \tag{1.121}$$

and

$$\nu = zV_0(t,z)/[1+zV_1(t,z)], \tag{1.122}$$

where the functions $V(t,z)$ are defined by

$$V_0(t,x)\equiv\sum_{\zeta=1}^{n}\eta_\zeta\tilde{\phi}_\zeta(t)z^\zeta, \qquad V_1(t,x)\equiv\sum_{\zeta=1}^{n}\zeta\eta_\zeta\tilde{\phi}_\zeta(t)z^\zeta. \tag{1.123}$$

The condition to find z is

$$\frac{z}{1-z}V_0(t,z)=1. \tag{1.124}$$

This is basically the ZB equation, but here it is properly extended to include the effect of tension. The solution of this equation gives the probability $z(t)$ as a function of the temperature and the external force.

Let us next find the tension–elongation curve. The average end-to-end distance R can be found by the fundamental relation

$$R=\frac{\partial}{\partial f}[k_\mathrm{B}T\ln\Xi(T;\lambda,t)], \tag{1.125}$$

so that we have

$$\begin{aligned}R/na&=L(t)-(\partial z/\partial t)/z\\&=(1-\theta(t))[L(t)+\kappa zW_1(t,\lambda z)],\end{aligned} \tag{1.126}$$

where $L(t)$ is the Langevin function (1.27), and W_k is defined by

$$W_k(t,x)\equiv\sum_{\zeta=1}^{n}\zeta^k\eta_\zeta\phi_\zeta(t)L(\kappa t\zeta)x^\zeta, \tag{1.127}$$

for $k=0,1,2,\ldots$.

To find the average square end-to-end distance $\langle R^2 \rangle_0$ *in the absence of the external force* we expand the partition function $\Xi(T,t)$ in powers of the dimensionless force t. Formal expansion gives

$$\Xi(T,t)/\Xi(T,0) = 1 + (\langle R^2 \rangle_0 / 6a^2)t^2 + \cdots, \tag{1.128}$$

so that we can find $\langle R^2 \rangle_0$ from the expansion

$$z = z_0 + z_1 t^2 + \cdots \tag{1.129}$$

of the parameter z and the expansion of the relation (1.119) in the form

$$\langle R^2 \rangle_0 / na^2 = 1 - 6z_1/z_0. \tag{1.130}$$

Here, z_0 is the solution of (1.124) under no force $t = 0$.

Explicit calculation of z_1 leads to

$$\langle R^2 \rangle_0 / na^2 = [1 - \theta(0)] + \kappa^2 \bar{\zeta}_w \theta(0), \tag{1.131}$$

where $\theta(0)$ is the helix contents at $t = 0$, which was studied in the preceding section, and

$$\bar{\zeta}_w \equiv V_2(0, z_0)/V_1(0, z_0) \tag{1.132}$$

is the **weight-average helix length** of the chain under no tension (see Figure 1.14).

The end-to-end distance as a function of the tension is calculated in a similar way as before. We find

$$R(t) = R^{(c)}(t)[1 - \theta(t)] + \kappa R^{(h)}(t)\theta(t), \tag{1.133}$$
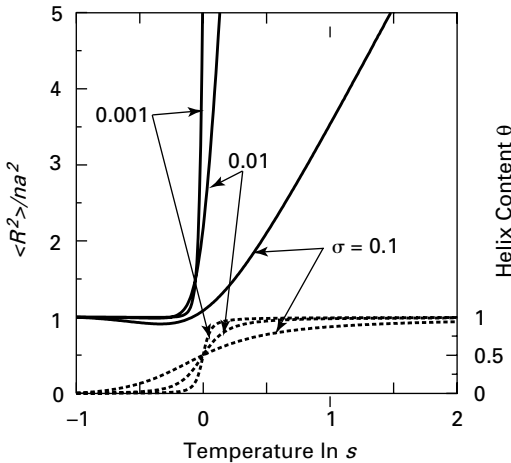
Fig. 1.14   Mean square end-to-end distance (solid lines) and helix content (dotted lines) plotted against the temperature. A minimum appears in $\langle R^2 \rangle$ at the coil–helix transition temperature.

where $R^{(c)}$ and $R^{(h)}$ are the end-to-end functions defined for the coil part and helical part in a similar way as above [28, 29].

1.9 Hydration of polymer chains

Water-soluble polymers often collapse upon heating. Such inverted CG transitions cannot be explained by a simple excluded-volume interaction of the type (1.71), because $v(T)$ increases with temperature and hence monomers on the chain repel each other, resulting in the chain swelling at high temperature. For a chain to collapse at high temperature, we should consider additional molecular interaction such as hydrogen bonding and hydrophobic association.

Hydration of a neutral polymer can roughly be classified into two categories: direct hydrogen bonds (referred to as H-bonds) between a polymer chain and water molecules (p-w), and the hydrophobic hydration of water molecules surrounding a hydrophobic group on a chain in a cage structure by water–water (w-w) H-bonds. In this section, we extend the combinatorial method for the partition function presented in the previous section to suit for the problem of solvent adsorption, and study polymer conformation change in aqueous solutions due to the direct p-w H-bonds.

1.9.1 Statistical models of hydrated polymer chains

At low temperature, a polymer chain is hydrated and dissolves in water. On heating, bound water molecules dissociate (dehydrate). The hydrophobic segments aggregate into globules to repel water. To study such a high-temperature collapse, we assume that a polymer chain takes a pearl-necklace conformation (Figure 1.15) [27–30]. are the compact spherical globules formed by close-packed hydrophobic aggregates of the dehydrated chain segments. They are connected in series by the hydrated swollen random coils. Such a polymer chain with an alternating secondary structure can be studied using a general theoretical framework similar to the one employed for CH transition.

Let i_ζ be the number of pearls that consist of a number ζ of contiguous repeat units, and let j_ζ be the number of swollen hydrated coils of the length ζ connecting them. Chain conformation is specified by the indices $\mathbf{i} \equiv \{i_1, i_2, \ldots\}$ and $\mathbf{j} \equiv \{j_1, j_2, \ldots\}$ as shown in Figure 1.15. The partition function (1.8) of a chain with no specification of its end-to-end vector takes the form

$$\Xi(T) = \sum_{\mathbf{i},\mathbf{j}} \exp[-\beta A(\mathbf{i}, \mathbf{j})], \qquad (1.134)$$

where the statistical weight is given by

$$\exp[-\beta A(\mathbf{i}, \mathbf{j})] \equiv \omega(\mathbf{i}, \mathbf{j}) \prod_\zeta (\lambda_\zeta)^{i_\zeta} (\eta_\zeta)^{j_\zeta}. \qquad (1.135)$$
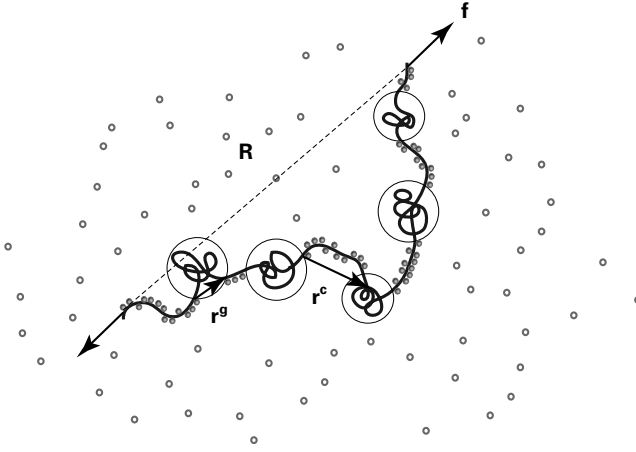
Fig. 1.15   Sequential hydration along the polymer chain, with the end-to-end vector **R** under tension **f**, due to the cooperative interaction between the nearest-neghboring bound water molecules. The vector $\mathbf{r}^g$ connects the incoming and outgoing point of a globule, while the vector $\mathbf{r}^c$ is the end-to-end vector of a hydrated coil. (Reprinted with permission from Ref. [30].)

The combinatorial factor ω is the number of different ways to place the sequences specified by $(\mathbf{i}, \mathbf{j})$, and is given by

$$\omega(\mathbf{i}, \mathbf{j}) = \frac{(\sum i_\zeta)!(\sum j_\zeta)!}{\prod i_\zeta! \prod j_\zeta!}. \tag{1.136}$$

This method is generally applicable to any chain along which two different structures are alternately formed [30].

The statistical weight λ_ζ for a globule of size ζ can be modeled by considering its condensation free energy Δf_ζ. The cohesive energy of the globule due to hydrophobic aggregation is given by $-\epsilon\zeta$, where $\epsilon(>0)$ is the binding energy per repeat unit. The globule has a surface tension γ at the surface in contact with water, so that the total free energy is given by $\Delta f_\zeta = -\epsilon\zeta + \gamma\zeta^{2/3}$. Thus the statistical weight takes the form

$$\lambda_\zeta(T) = e^{-\gamma\zeta^{2/3}} \lambda(T)^\zeta, \tag{1.137}$$

where $\lambda(T) \equiv \exp(\beta\epsilon)$ is the association constant. (Dimensionless $\beta\gamma$ of the surface free energy is simply written as γ.)

For the statistical weight η_ζ a swollen random coil, we can incorporate the cooperativity of H-bonds by assuming the Zimm–Bragg form (1.91)

$$\eta_\zeta = \sigma s(T)^\zeta, \tag{1.138}$$

where $s(T)$ is the association constant for the H-bonding of a water molecule onto a repeat unit of the polymer chain. It can be written as $s(T) \equiv \exp[\beta(\epsilon_H + \Delta\epsilon)]$ in terms of the H-bonding energy ϵ_H. The parameter $\sigma \equiv \exp(-\beta\Delta\epsilon)$ is a measure of the **cooperativity**

of hydration due to the interaction free energy $-\Delta\epsilon$ between the nearest-neghboring bound water molecules. Smaller σ gives stronger cooperativity as in CH transition.

For instance, a sequence

$$\cdots \text{GGGGG}\underline{\text{CCCCC}}\text{GGGGGGG}\cdots \qquad (1.139)$$

of five contiguous hydrated repeat units on the coil part has a statistical weight of $s(T)^5$ with an additional factor $(\sqrt{\sigma})^2$ from the two boundaries in contact with the globular parts.

Instead of summing over all possible distributions $(\mathbf{i},\mathbf{j})$, we find the m.p.d. that minimizes the free energy $A(\mathbf{i},\mathbf{j})$ under the condition

$$\sum_{\zeta=1}^{n} i_\zeta = \sum_{\zeta=1}^{n} j_\zeta, \qquad (1.140)$$

because a pearl and string appear alternately, and also under the condition that the total number of repeat units is fixed at

$$\sum_{\zeta=1}^{n} \zeta(i_\zeta + j_\zeta) = n. \qquad (1.141)$$

Let us introduce two Lagrange indeterminate coefficients α and μ for these constraints, and minimize

$$\beta A(\mathbf{i},\mathbf{j}) = -\ln\omega(\mathbf{i},\mathbf{j}) - \sum_\zeta (i_\zeta \ln\lambda_\zeta + j_\zeta \ln\eta_\zeta)$$

$$-\alpha \sum_\zeta (i_\zeta - j_\zeta) - \mu \left[\sum_\zeta \zeta(i_\zeta + j_\zeta) - n \right], \qquad (1.142)$$

by changing $\mathbf{i}$ and $\mathbf{j}$. From the conditions $\partial A(\mathbf{i},\mathbf{j})/\partial i_\zeta = \partial A(\mathbf{i},\mathbf{j})/\partial j_\zeta = 0$, we find

$$i_\zeta / \sum i_\zeta = e^\alpha \lambda_\zeta z^\zeta, \quad j_\zeta / \sum j_\zeta = e^{-\alpha} \lambda_\zeta z^\zeta, \qquad (1.143)$$

where the new parameter z is introduced by the definition $z \equiv e^\mu$.

By taking the sum over $\zeta = 1,\ldots,n$, we find that the Langrange constants must satisfy the coupled equations

$$e^\alpha U_0(z) = 1, \quad e^{-\alpha} V_0(z) = 1, \qquad (1.144)$$

where

$$U_k(z) \equiv \sum_{\zeta=1}^{n} \zeta^k \lambda_\zeta z^\zeta, \quad V_k(z) \equiv \sum_{\zeta=1}^{n} \zeta^k \eta_\zeta z^\zeta \quad (k=0,1,2,\ldots) \qquad (1.145)$$

are the k-th moments of the distributions i_ζ and j_ζ, respectively. By eliminating α, the Lagrange constant z can be found by the equation

$$U_0(z)V_0(z) = 1. \tag{1.146}$$

This is equivalent to the **Zimm–Bragg equation** (1.104) if λ_ζ is replaced by 1 and the weight (1.138) for η_ζ is employed. In what follows, therefore, we will call this the ZB equation.

Substituting the m.p.d. into the condition (1.141), we find that the average number ν of pearls (also of coils) is given by

$$\nu \equiv \sum_\zeta i_\zeta/n = \sum_\zeta j_\zeta/n = [U_1(z)/U_0(z) + V_1(z)/V_0(z)]^{-1}. \tag{1.147}$$

By the ZB equation, it can be written as

$$\nu = [U_1(z)V_0(z) + U_0(z)V_1(z)]^{-1}. \tag{1.148}$$

The fraction of the hydrated part, or the number of bound water molecules, is given by

$$\theta \equiv \sum_\zeta \zeta\, j_\zeta/n = U_0(z)V_1(z)/[U_1(z)V_0(z) + U_0(z)V_1(z)]. \tag{1.149}$$

The fraction of the globules is given by $1 - \theta$. This equation can be written in a more compact form as

$$\theta = h(z)V_1(z)/[1 + h(z)V_1(z)], \tag{1.150}$$

where the function $h(z)$ is defined by

$$h(z) \equiv U_0(z)^2/U_1(z). \tag{1.151}$$

In the original ZB (1.146) for CH transition with $\lambda_\zeta = 1$, the factor $h(z)$ is reduced to z. (The upper limit of the sum is allowed to go to infinity.)

The number-average size of the globules is given by

$$\bar{\zeta}_n^{(g)} \equiv \sum_\zeta \zeta\, j_\zeta / \sum_\zeta j_\zeta = U_1(z)/U_0(z) = U_1(z)V_0(z). \tag{1.152}$$

Similarly, the number-average sequence length of the hydrated random coils is given by

$$\bar{\zeta}_n^{(c)} \equiv \sum_\zeta \zeta\, j_\zeta / \sum_\zeta j_\zeta = V_1(z)/V_0(z) = U_0(z)V_1(z). \tag{1.153}$$

The superscript (c) indicates the random coils swollen by bound water.

Finally, by substituting the m.p.d. into the original partition function (1.134), we find $Z(T) = 1/z^n$, as in (1.102).

In order to find the average end-to-end distance as a function of the tension $\mathbf{f}$ applied at the chain end, we change the independent variable from $\mathbf{R}$ to $\mathbf{f}$ by carrying out the Laplace transformation as in (1.14). Introducing the Laplace transformation

$$\tilde{g}_\zeta(t) \equiv \int \rho_\zeta^g(\mathbf{r}) e^{\beta \mathbf{f} \cdot \mathbf{r}} d\mathbf{r}, \quad \mathfrak{p}_\zeta(t) \equiv \int \rho_\zeta^c(\mathbf{r}) e^{\beta \mathbf{f} \cdot \mathbf{r}} d\mathbf{r}, \tag{1.154}$$

we can easily see that the partition function $Q(\mathbf{f}, T)$ takes a form similar to Z as

$$Q(\mathbf{f}, T) = \sum_{\mathbf{i}, \mathbf{j}} \omega(\mathbf{i}, \mathbf{j}) \prod_\zeta [\lambda_\zeta \tilde{g}_\zeta(t)]^{i_\zeta} [\eta_\zeta \mathfrak{p}_\zeta(t)]^{j_\zeta}, \tag{1.155}$$

where $t \equiv fa/k_{\mathrm{B}}T$, as defined in (1.17), is the dimensionless tension in the unit of the thermal energy. The statistical weight is now renormalized by the effect of tension as

$$\lambda_\zeta \to \tilde{\lambda}_\zeta(t) \equiv \lambda_\zeta \tilde{g}_\zeta(t), \qquad \eta_\zeta \to \tilde{\eta}_\zeta(t) \equiv \eta_z \mathfrak{p}_\zeta(t). \tag{1.156}$$

By differentiating the free energy with respect to the tension, we find

$$R(t) = R^{(g)}(t)[1 - \theta(t)] + R^{(c)}(t)\theta(t), \tag{1.157}$$

where

$$R^{(g)}(t) \equiv na \frac{\partial U_0(t, z)/\partial t}{U_1(t, z)}, \quad R^{(c)}(t) \equiv na \frac{\partial V_0(t, z)/\partial t}{V_1(t, z)}. \tag{1.158}$$

The solution $z(t)$ of the ZB equation,

$$U_0(t, z) V_0(t, z) = 1, \tag{1.159}$$

must be used for z. Thus the total length is decomposed into a globular part and a swollen coil part.

The mean square end-to-end distance is written in compact form as

$$\langle R^2 \rangle_0 = \langle R^2 \rangle_0^{(g)}(1 - \theta_0) + \langle R^2 \rangle_0^{(c)} \theta_0, \tag{1.160}$$

where $\theta_0 \equiv \theta(0)$ is the degree of hydration at $t = 0$, and

$$\langle R^2 \rangle_0^{(g)} \equiv 6na^2 \frac{U^{(1)}(z_0)}{U_1(0, z_0)}, \quad \langle R^2 \rangle_0^{(c)} \equiv 6na^2 \frac{V^{(1)}(z_0)}{V_1(0, z_0)} \tag{1.161}$$

are the average square end-to-end distance of each component, where $U^{(1)}(z_0)$, $V^{(1)}(z_0)$ are the coefficients of the $O(t^2)$ terms in U_0, V_0.

1.9.2   Models of the globules and hydrated coils

Let us introduce a simple model of the globules. A globule of size ζ is assumed to take a spherical shape into which repeat units are close packed. The radius R is given by the condition $4\pi R^3/3 \simeq \zeta a^3$.

We then have the diameter $2R \simeq \kappa a \zeta^{1/3}$, where $\kappa = 2(3/4\pi)^{1/3}$ is a numerical constant. We also assume that the incoming random coil goes out from a point exactly opposite to the sphere, so that the connecting vector $\mathbf{r}^g$ has the absolute value $2R$ of the diameter. Hence we have

$$2Rf/k_B T = \kappa \zeta^{\nu_G} t, \qquad \nu_G = 1/3. \tag{1.162}$$

The Laplace transform of the end-vector distribution for a globule then takes the form

$$\tilde{g}_\zeta(t) = \sinh(\kappa \zeta^{\nu_G} t)/\kappa \zeta^{\nu_G} t \equiv \tilde{g}(\kappa \zeta^{\nu_G} t), \tag{1.163}$$

where $\tilde{g}(t)$ is the Laplace transform (1.21) for the orientational distribution of one bond vector of the chain segment.

We next introduce a simple model for the swollen hydrated coils. The mean end-to-end distance of the chain segment with length ζ is given by

$$R = \kappa_w a \zeta^{\nu_F}, \qquad \nu_F = 3/5, \tag{1.164}$$

according to Flory's law (1.76) for a swollen chain with the excluded-volume effect, where $\nu_F = 3/5$ is Flory's exponent and κ_w is a numerical constant of order unity. The Laplace transform of the end-vector distribution for a hydrated coil then takes the form

$$\text{þ}_\zeta(t) = \tilde{g}(\kappa_w \zeta^{\nu_F} t). \tag{1.165}$$

We first solve the ZB equation (1.149), and obtain θ_0 by (1.149). The end-to-end distance can be calculated from the explicit formula

$$\langle R^2 \rangle_0 / na^2 = \kappa^2 \overline{\zeta^{2\nu_G - 1}}(1 - \theta_0) + \kappa_w^2 \overline{\zeta_w^{2\nu_F - 1}} \theta_0, \tag{1.166}$$

where

$$\overline{\zeta^{2\nu_G - 1}} \equiv \sum_{\zeta=1}^{n} \zeta^{2\nu_G} \lambda_\zeta z_0^\zeta / \sum_{\zeta=1}^{n} \zeta \lambda_\zeta z_0^\zeta, \tag{1.167a}$$

$$\overline{\zeta_w^{2\nu_F - 1}} \equiv \sum_{\zeta=1}^{n} \zeta^{2\nu_F} \eta_\zeta z_0^\zeta / \sum_{\zeta=1}^{n} \zeta \eta_\zeta z_0^\zeta. \tag{1.167b}$$

For the numerical calculation, we assume the form $s(T)/\lambda(T) = \lambda_0 \exp[\gamma(1 - \tau)]$ for the association constant of the H-bond, where $\tau \equiv 1 - \Theta/T$ is the reduced temperature deviation (1.73) from the theta temperature of the polymer solution without H-bonds,

and $\gamma \equiv (\epsilon_H + \Delta\epsilon - \epsilon)/k_B\Theta$. (The fraction θ and the expansion factor α_R depend only upon the ratio $s(T)/\lambda(T)$.)

Figure 1.16(a) shows the test calculation to see how the coil–globule transition becomes sharper with cooperativity. The DP is fixed at $n = 100$ and the cooperativity parameter is varied from curve to curve. We can see clearly that the transition becomes sharper with σ. The broken lines show the fraction of the hydrated parts.

Figure 1.16(b) shows the tension–elongation curves at three different temperatures. At $\tau = -0.5$ in the transition region, there appears a wide plateau in R, and we notice the existence of the critical tension $t_c \simeq 3.0$ for $\tau = -0.5$ at which chain segments start to be **reeled out** from the globules. For the balance between a globule of the size ζ and a hydrated coil of the same size, we find a scaling law

$$t_c^2 \simeq \Delta\tau. \tag{1.168}$$

The critical tension becomes smaller as the transition temperature is approached. Hence, we can expect that chain segments are easily reeled out from the globules by a small tension near the transition temperature. If the chain is stretched by tension above a critical value (the critical tension t_c), segments are reeled out from the globules, and exposed to water. Hydration proceeds while the random coils grow, so that the collapse temperature is shifted to a higher value. The tension stays constant during the reel-out process, and hence a plateau appears in the tension–elongation curve [30].

1.9.3 Competitive hydrogen bonds in mixed solvents

Some water-soluble polymers, such as PEO and PNIPAM, exhibit a peculiar conformational change in water upon mixing of a second water-miscible good solvent such as
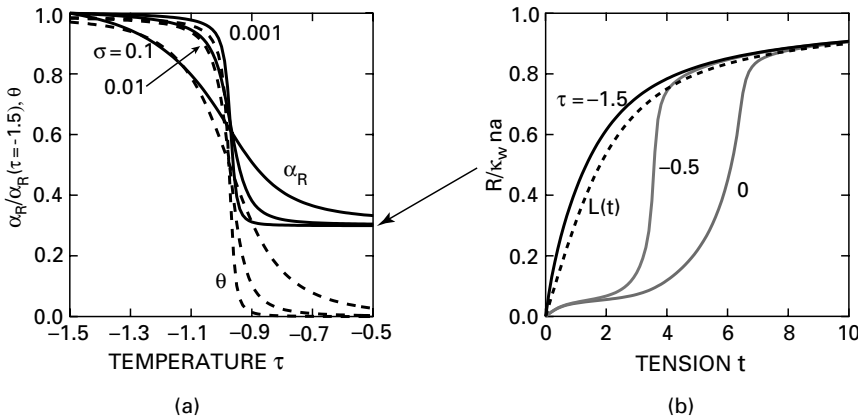
Fig. 1.16 (a) Theoretical calculation of the expansion factor α_R (solid lines) and the degree of hydration θ (broken lines) plotted against temperature for three different cooperativity parameters $\sigma = 10^{-3}, 10^{-4}$, and 10^{-5} ($n = 100, \kappa_w/\kappa = 0.31$). (b) Tension–elongation curves at three different temperatures. (Reprinted with permission from Ref. [30].)
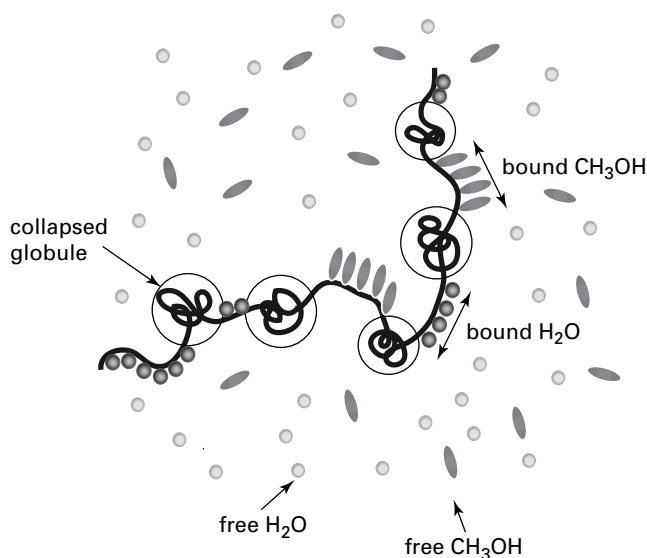
Fig. 1.17   Competitive H-bonding between PNIPAM–water (p-w) and PNIPAM–methanol (p-m). When there is strong cooperativity, continuous sequences of each species are formed along the chain. As a result, the chain takes a pearl-necklace conformation. (Reprinted with permission from Ref. [10].)

methanol, tetrahydrofuran, or dioxane. For PNIPAM, although the second solvent is a good solvent for the polymer, the chain sharply collapses at the molar fraction $x_m \simeq 0.2$ of methanol, stays collapsed up to $x_m \simeq 0.4$, and finally recovers the swollen state at $x_m \simeq 0.6$ in a majority of methanol [31]. Such a transition from coil to globule, followed by an expansion from globule to coil, is called **reentrant coil–globule–coil transition**.

Considering that methanol molecules are also H-bonded onto the chain, we expect that there is a competition in forming the p-w and p-m H-bonds. The statistical weight of a sequence for each is given by

$$\eta_\zeta{}^{(\alpha)} = \sigma_\alpha s_\alpha(T)^\zeta, \qquad \alpha = \text{w}, \text{m}. \tag{1.169}$$

To take into consideration the difference in molecular volume of the solvents, let p be the volume of methanol molecule relative to that of water. It has a numerical value of between 2 and 3. We assume that the chain segments covered by bound water and bound methanol are swollen because both solvents are good, and the remaining free segments are collapsed by hydrophobic aggregation (see Figure 1.17).

Now, the number of different ways to choose such sequences from the finite total number n is given by

$$\omega(\mathbf{i}, \mathbf{j}) = \frac{(\sum i_\zeta)!(\sum j_\zeta^{(\text{w})})!(\sum j_\zeta^{(\text{m})})!}{\prod_\zeta [i_\zeta! j_\zeta^{(\text{w})}! j_\zeta^{(\text{m})}!]}. \tag{1.170}$$

The canonical partition function of a chain for given numbers $n^{(w)}, n^{(m)}$ of bound water and bound methanol under tension $\mathbf{f}$ is given by

$$Q(n^{(w)}, n^{(m)}, t) = \sum_{\mathbf{j}} \omega(\mathbf{i}, \mathbf{j}) \prod_{\zeta} [\tilde{\lambda}_{\zeta}(t)]^{i_{\zeta}} [\tilde{\eta}_{\zeta}^{(w)}(t)]^{j_{\zeta}^{(w)}} [\tilde{\eta}_{\zeta}^{(m)}(t)]^{j_{\zeta}^{(m)}}, \qquad (1.171)$$

where $\tilde{\eta}_{\zeta}^{(\alpha)}(t)$ is the statistical weight of length ζ for a solvent α under tension, and $n^{(\alpha)} \equiv \sum_{\zeta \geq 1} \zeta j_{\zeta}^{(\alpha)}$ is the total number of adsorbed molecules of the solvent α.

Since the mixed solvent is a particle reservoir of both components, we introduce the activity a_{α} of each type of solvent as independent variables (functions of the solvent composition), and move to the grand partition function:

$$\Xi(\{a\}, t) \equiv \sum_{n^{(w)}, n^{(m)}=0}^{n} a_{w}^{n^{(w)}} a_{m}^{n^{(m)}} Q(n^{(w)}, n^{(m)}, t). \qquad (1.172)$$

The m.p.d. of sequences that maximizes this grand partition function under the conditions

$$\sum_{\zeta} i_{\zeta} = \sum_{\zeta} (j_{\zeta}^{(w)} + j_{\zeta}^{(m)}), \qquad (1.173)$$

and

$$\sum_{\zeta} \zeta(i_{\zeta} + j_{\zeta}^{(w)} + p j_{\zeta}^{(m)}) = n, \qquad (1.174)$$

are given by

$$j_{\zeta}^{(w)}/n = (1-\theta)\eta_{\zeta}^{(w)} z(a_{w}z)^{\zeta}, \qquad (1.175a)$$

$$j_{\zeta}^{(m)}/n = (1-\theta)\eta_{\zeta}^{(m)} z(a_{m}z^{p})^{\zeta}, \qquad (1.175b)$$

as in the preceeding section. Here,

$$\theta = \theta^{(w)} + p\theta^{(m)} \qquad (1.176)$$

is the total coverage with $\theta^{(\alpha)} \equiv \sum_{\zeta \geq 1} \zeta j_{\zeta}^{(\alpha)}/n$ being the mean coverage by each solvent. Similarly,

$$\nu = \nu^{(w)} + \nu^{(m)} \qquad (1.177)$$

is the total number of sequences with $\nu^{(\alpha)} \equiv \sum_{\zeta \geq 1} j_{\zeta}^{(\alpha)}/n$ being the number of sequences of each solvent. The parameter z is defined by $z \equiv 1 - \nu/(1-\theta)$, and is the probability that an arbitrarily chosen monomer belongs to the free part. The grand partition function is given by $\Xi(\{a\}, t) = z(t)^{-n}$.

Following the same procedure as before, we find the equation

$$U_0(t,z)\left\{V_0^{(w)}(t,a_w z)+V_0^{(m)}(t,a_m z^p)\right\}=1, \tag{1.178}$$

for z for the mixed solvents. This is basically the same as the ZB equation in the preceding section, but here it is properly extended to describe competiton in p-w and p-m H-bonding. The functions V_k are defined by

$$V_k^{(\alpha)}(t,x)\equiv\sum_{\zeta=1}^{n^*}\zeta^k\tilde{\eta}_\zeta^{(\alpha)}(t)x^\zeta. \tag{1.179}$$

The upper limit of the sum is $n^*=n$ for water, and $n^*=[n/p]$ for methanol, where $[k]$ means the maximum integer smaller than, or equal to k.

By using the solution z of the ZB equation, we find that the total coverage θ is given by

$$\theta=\frac{h(t,z)\left[V_1^{(w)}(t,a_w z)+pV_1^{(m)}(t,a_m z^p)\right]}{1+h(t,z)\left[V_1^{(w)}(t,a_w z)+pV_1^{(m)}(t,a_m z^p)\right]}, \tag{1.180}$$

where

$$h(t,z)\equiv U_0(t,z)^2/U_1(t,z). \tag{1.181}$$

The end-to-end distance as a function of the tension is given in a similar way as before by

$$R(t)=\kappa R^{(g)}(t)[1-\theta^{(w)}(t)-\theta^{(m)}(t)]+\kappa_w R^{(w)}(t)\theta^{(w)}(t)+\kappa_m R^{(m)}(t)\theta^{(m)}(t), \tag{1.182}$$

where $R^{(g)}(t)$ and $R^{(\alpha)}(t)$ are defined by a similar equation as in a pure water.

The mean square average end-to-end distance of a free chain can be calculated by the equation [10, 29, 30]

$$\langle R^2\rangle_0/na^2=\kappa^2\overline{\zeta^{2\nu_G-1}}(1-\theta_0^{(w)}-\theta_0^{(m)})+\kappa_w^2\overline{\zeta_w^{2\nu_F-1}}\theta_0^{(w)}+\kappa_m^2\overline{\zeta_m^{2\nu_F-1}}\theta_0^{(m)}. \tag{1.183}$$

If we employ the ZB form for the statistical weight η_ζ, the arguments of the V functions become the combined variable $a_w s_w t$ for water, and $a_m s_m t^p$ for methanol. We assume that the solvent–solvent interaction is weak, compared to the solvent–polymer interaction, and neglect it. The mixed solvent is regarded as an ideal mixture.[4] Then the activity is proportional to the mole fraction of each component. We can write $a_w s_w=a_w^\circ(T)(1-x_m)$ and $a_m s_m=a_m^\circ(T)x_m$, where a°s are functions of the temperature only.

---

[4] The activity of w/m mixture can be treated more rigorously by using the theory of associated solutions.
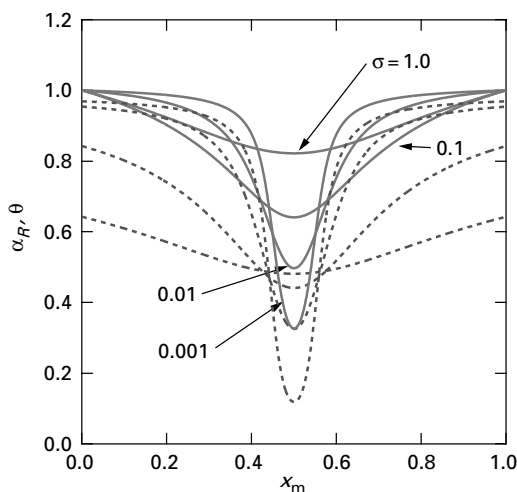
Fig. 1.18 Normalized end-to-end distance (solid lines), the total of the bound water and of bound methanol (dotted lines), plotted against the mole fraction of methanol. The DP of the polymer chain is fixed at $n = 100$ for a test calculation. For a test calculation, perfect symmetry is assumed. The volume ratio of the solvents is fixed at $p = 1$. The cooperativity parameter $\sigma_w = \sigma_m$ is varied from curve to curve. The association constants are fixed at $a_w^\circ = a_m^\circ = 1.8$. The monomer expansion factors are fixed at $\kappa_w/\kappa = \kappa_m/\kappa = 2.0$ (Reprinted with permission from Ref. [10].)

Figure 1.18 shows the expansion factor for the end-to-end distance $\alpha_R^2 \equiv \langle R^2 \rangle_0(x_m)/\langle R^2 \rangle_0(0)$ (solid lines) and the total coverage θ_0 (broken lines) plotted against the molar fraction x_m of methanol. Here, $\langle R^2 \rangle_0(0)$ is the value in pure water.

The calculation was done as a test case by assuming that all parameters are symmetric and with $p = 1$. The cooperativity parameter σ varies from curve to curve. We can clearly see that the coverage takes a minimum value at $x_m = 0.5$ (stoichiometric concentration) as a result of the competition, so that the end-to-end distance also takes a minimum value at $x_m = 0.5$. As cooperativity becomes stronger, the depression of the end-to-end distance becomes narrower and deeper. In a real mixture, the association constant and cooperativity parameter are different for water and methanol, so that we expect asymmetric behavior with respect to the molar fraction.

Figure 1.19 shows a comparison between the experimental mean radii of gyration (circles) obtained from laser light scattering measurements [31] and the mean end-to-end distances obtained from theoretical calculations (solid line). Both are normalized by the reference value in pure water. The total coverage $\theta = \theta^{(w)} + p\theta^{(m)}$, including bound water and bound methanol, is also plotted (broken line). The molecular weight of the polymer used in the experiment is as high as $M_w = 2.63 \times 10^7 \, \text{g} \, \text{mol}^{-1}$, and hence we fixed $n = 10^5$. The volume ratio is set to be $p = 2$ from the molecular structure of methanol.

For larger p, it turns out that the recovery of the expansion factor at high methanol composition is not sufficient. In order to have a sharp collapse at around $x_m \simeq 0.17$ the cooperativity must be as high as $\sigma_w = 10^{-4}$. Similarly, to produce a sharp recovery at around $x_m \simeq 0.4$, we used $\sigma_m = 10^{-3}$.
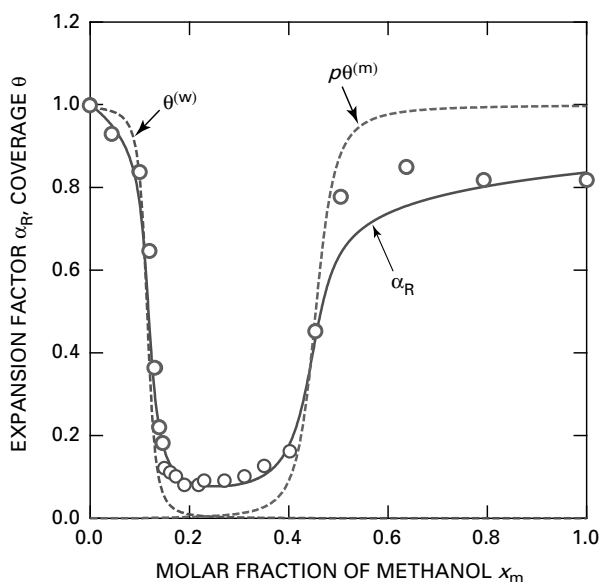
Fig. 1.19   Comparison between the theoretical calculation (solid line) of the expansion factor for the mean square end-to-end distance for $n = 10^5$ and $p = 2$ and the experimental data of the radius of gyration (circles). The degree of hydration (p-w H-bonding) $\theta^{(w)}$ and of p-m H-bonding $\theta^{(m)}$ are also plotted (broken line). The fitting parameters are $a_w^\circ = 1.13$, $a_m^\circ = 2.20, \kappa_w/\kappa = 1.15, \kappa_m/\kappa = 1.06$. (Reprinted with permission from Ref. [10].)

References

[1] Flory, P. J., *Principles of Polymer Chemistry*, Chap. X. Cornell University Press: Ithaca, NY, 1953.

[2] Flory, P. J., *Statistical Mechanics of Chain Molecules*. Wiley: New York, 1968.

[3] Tobolsky, A. V.; Mark, H. F., *Polymer Sience and Materials*. Wiley: New York, 1971.

[4] Rubinstein, M.; Colby, R. H., *Polymer Physics*. Oxford University Press: Oxford, 2003.

[5] Graessley, W. W., *Polymeric Liquids & Networks: Structure and Properties*. Garland Science: London, 2004.

[6] Kremer, K.; Grest, G. S., *J. Chem. Phys.* **92**, 5057 (1990).

[7] Gibbs, J. H.; Dimarzio, E. A., *J. Chem. Phys.* **28**, 373 (1958).

[8] Dimarzio, E. A.; Gibbs, J. H., *J. Chem. Phys.* **28**, 807 (1958).

[9] Indei, T.; Tanaka, F., *Macromol. Rapid Commun.* **26**, 701 (2005).

[10] Tanaka, F.; Koga, T., *Macromolecules* **39**, 5913 (2006).

[11] Debye, P., *J. Phys. Chem.* **51**, 18 (1947).

[12] Eyring, H., *Phys. Rev.* **39**, 746 (1932).

[13] Oka, S., *Proc. Math. Phys. Soc. Japan* **24**, 657 (1942).

[14] Kratky, O.; Porod, G., *Rec. Trav. Chim.* **68**, 1106 (1949).

[15] Mayer, J. E.; Mayer, M. G., *Statistical Mechanics*. Wiley: New York, 1940.

[16] de Gennes, P. G., *Scaling Concepts in Polymer Physics*. Cornell University Press: Ithaca, 1979.

[17] Yamakawa, H., *Modern Theory of Polymer Solutions*. Harper & Row: New York, Pub. 1971.

[18] Flory, P. J., *J. Chem. Phys.* **17**, 303 (1949).

[19] Ptitsyn, O. B.; Kron, A. K.; Eizner, Y. Y., *J. Polym. Sci. Part C* **16**, 3509 (1968).

[20] de Gennes, P. G., *J. Physique Lett.* **36** L-55; **39** L-299 (1975).

[21] Nishio, I.; Sun, S.-T.; Swislow, G.; Tanaka, T., *Nature* **281**, 208 (1979); Sun, S.-T.; Nishio, I.; Swislow, G.; Tanaka, T., *J. Chem. Phys.* **73**, 5971 (1980).

[22] Park, I. H.; Wang, Q.-W.; Chu, B., *Macromolecules* **20**, 1965 (1987).

[23] Poland, D.; Scheraga, H. A., *Theory of Helix-Coil Transitions in Biopolymers*. Academic Press: New York and London, 1970.

[24] Zimm, B. H.; Bragg, J. K., *J. Chem. Phys.* **31**, 526 (1959).

[25] Wyman, J.; Gill, S. J., *Binding and Linkage*. University Science Books: Mill Valley, 1990.

[26] Lifson, S.; Roig, A., *J. Chem. Phys.* **34**, 1963 (1961).

[27] Toda, M.; Tanaka, F. *Macromolecules* **38**, 561 (2004).

[28] Okada, Y.; Tanaka, F. *Macromolecules* **38**, 4465 (2005).

[29] Tanaka, F.; Koga, T.; Winnik, F. M., *Phys. Rev. Lett.* **101**, 028302 (2008).

[30] Tanaka, F.; Koga, T.; Kojima, H.; Winnik, F. M., *Macromolecules* **42**, 1231 (2009).

[31] Zhang, G.; Wu, C., *J. Am. Chem. Soc.* **123**, 1376 (2001).

2 Polymer solutions

Gibbs' principle of multiple phase equilibria is applied to model polymer solutions to explore the possible types of heterophase coexistence and phase transitions. The fundamental properties of dilute polymer solutions and liquid–liquid phase separation driven by van der Waals-type interaction is reviewed within the framework of Flory–Huggins theory. No specific molecular interactions are assumed. Refinement of the polymer–solvent contact energy beyond Flory–Huggins' description is attempted to study the glass transition of polymer solutions at low temperatures. The scaling description of semiconcentrated polymer solutions is summarized.

2.1 Thermodynamics of phase equilibria

2.1.1 Gibbs' phase rule and phase diagrams

In this section, we present the necessary and sufficient conditions for a multicomponent mixture consisting of A_i $(i = 1, 2, \ldots c)$ molecules of c species to separate into n different phases in thermal equilibrium under the temperature T and pressure p (Figure 2.1).

We use superscript $\alpha = 1, 2, \ldots, n$ to distinguish phases. In each phase α, there are $c - 1$ independent variables of intensive nature to specify its composition. The chemical potential $\mu_i^{(\alpha)}(p, T, \{x^\alpha\})$ of any species i is a function of $c + 2 - 1 = c + 1$ intensive variables, where $\{x\} \equiv \{x_1, x_, \ldots, x_{c-1}\}$ are the mole fraction of the species.

For such n phases to remain stable in equilibrium, the temperature and pressure must be uniform. In addition, the chemical potential of each species must be uniform throughout the system, so that we have the Gibbs conditions

$$\mu_1^{(1)} = \mu_1^{(2)} = \cdots = \mu_1^{(n)},$$

$$\vdots$$

$$\mu_c^{(1)} = \mu_c^{(2)} = \cdots = \mu_c^{(n)}. \tag{2.1}$$

If such balance breaks, the free energy can be reduced by the appropriate transfer of materials between the phases.

The total number of these conditions is $c(n-1)$. The total number of intensive variables necessary to describe the system is $n(c-1) + 2$ (the number $n(c-1)$ added by 2 for T and p). Hence the total number f of the independent variables is given by

$$f = n(c-1) + 2 - c(n-1) = c - n + 2. \tag{2.2}$$
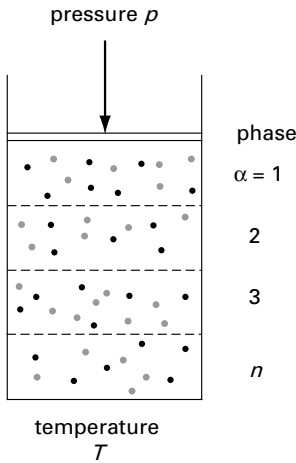
Fig. 2.1 Phase equilibrium of a multicomponent mixture under the given pressure p and temperature T. The mixture is separated into $\alpha = 1, 2, \ldots, n$ phases.

This result is called **Gibbs' phase rule**. The **variance**, or **thermodynamic degree of freedom**, f, is the number of intensive variables that can be independently changed without breaching the thermal equilibrium of the system.

A system with $f = 0$ is **invariant**; all intensive variables are fixed, and hence the state can be represented by a point in the phase space.

A system with $f = 1$ is **monovariant**, with $f = 2$ it is **bivariant**, with $f = 3$ it is **trivariant**, etc. In the phase space, the boundary between two distinct phases is described by a line for a monovariant system, a plane for bivariant system, and a cube for a trivariant system.

When some reactions take place in the phases, the variance is reduced. Consider the reversible reaction

$$\nu_1 A_1 + \nu_2 A_2 + \cdots \rightleftharpoons \nu_1' A_1' + \nu_2' A_2' + \cdots . \tag{2.3}$$
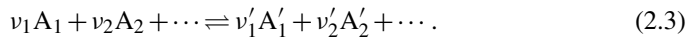
Equation (2.3) is in equilibrium in phase α. The condition for the chemical equilibrium is

$$\sum \nu_i \mu_i^{(\alpha)} = \sum \nu_i' \mu_i'^{(\alpha)}, \tag{2.4}$$

which is added to the original Gibbs conditions (2.1), and hence one degree of freedom is reduced. If there are r reactions in the entire system, the number of independent variables is reduced from c to $c - r$, and hence the variance is given by

$$f = (c - r) - n + 2 \tag{2.5}$$

in a generalized form.

For a one component system with $c = 1$, we have $f = 3 - n$. Hence, for a uniform state with $n = 1$, the variance is $f = 2$. For a two-phase equilibrium with $n = 2$, it is $f = 1$.
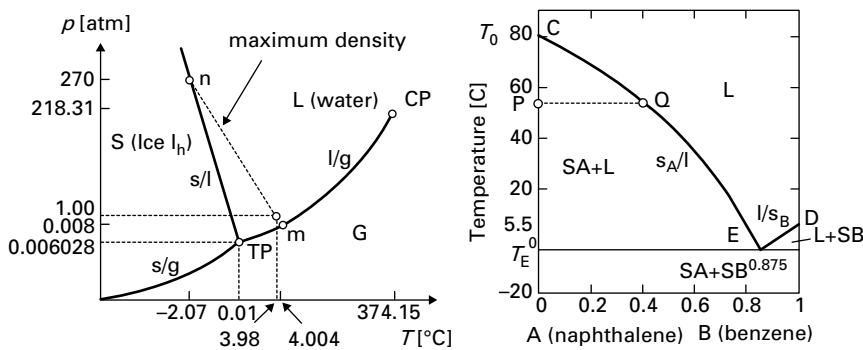
Fig. 2.2   Examples of phase diagrams: (a) one-component system (water), (b) two-component system (naphtalene/benzene).

For the three-phase equilibrium $n = 3$, it is $f = 0$, etc. Because the maximum variance is 2, we can describe any state by using two intensive variables. The temperature and the pressure are usually chosen, and the **phase diagram** can be represented on the $T - p$ plane. On this phase plane, $f = 2$ indicates an area, $f = 1$ indicates a line, and $f = 0$ indicates a point. Therefore, three-phase equilibrium, for instance, is possible only at a point on the plane.

Figure 2.2(a) shows the phase diagram of water. Liquid–gas (l/g), solid–liquid (s/l), solid–gas (s/g) equilibrium are all in two-phase equilibrium and shown by the corresponding three lines (each $f = 1$). The crossing point of the three lines ($f = 0$) indicates the triple point (TP) of water. The liquid-gas line ends at the critical point (CP), but the solid-liquid line has no end.

A two-component system has a uniform phase ($n = 1, f = 3$), a two-phase equilibrium ($n = 2, f = 2$), a three-phase equilibrium ($n = 3, f = 1$), and a four-phase equilibrium ($n = 4, f = 0$). Because the maximum variance is 3, we can specify the phases in the three-dimensional space of T, p, x, where x is the mol fraction of one component. The projection of this phase space onto the $T - p$, $T - x$, and $p - x$ planes is often used for the phase diagram.

Figure 2.2(b) shows an example of the projection onto the $T - x$ plane of the phase diagram of a two-component mixture of naphthalene and benzene. The line CQE(s_A/l) is the boundary between the liquid mixture and the solid SA phase, while the line DE is the boundary between the liquid mixture and the solid SB phase. At temperature near 60°C, for instance, a crystalline solid SA of pure naphthalene (point P) is in equilibrium with the liquid mixture of the composition at point Q. The special point E at temperature T_E where s_A/l and l/s_B cross is called the **eutectic point**. Below T_E, the solid is separated into two pure crystals SA and SB.

2.1.2   Stability of a phase

This section describes the necessary conditions for an arbitrary system to remain stable in a specified uniform phase under the given environmental conditions. In order for a
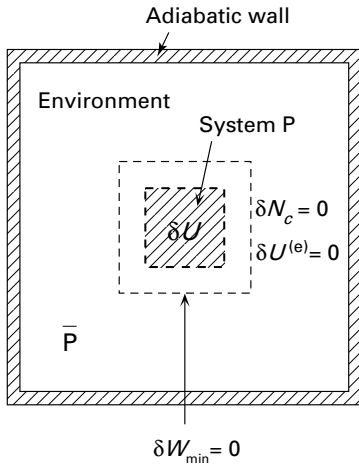
Fig. 2.3 Minimum work required to change the state of a part P in the closed system.

state to be stable, the system does not change spontaneously, i.e., it can change only if a positive work is applied to it from the environment [1–5].

Consider a part P of the system surrounded by an adiabatic wall where a small change is caused by work applied from the environment (Figure 2.3). The minimum work $\delta W_{\min}$ to cause this change is that of a **quasi-static process**. It is given by

$$\delta W_{\min} = \delta U + \delta U^{(e)}, \tag{2.6}$$

where δU is the change of the internal energy of P, and $\delta U^{(e)}$ is the change of the internal energy of the remaining part $\bar{P}$ of the system outside of P (regarded as an environment to P). If we take a part of the system containing a fixed amount of the special component (usually the solvent $i = c$), we have $\delta N_c = 0$ during this change. The infinitesimal change of the environment $\bar{P}$ is

$$\delta U^{(e)} = T^{(e)}\delta S^{(e)} - p^{(e)}\delta V^{(e)} + \sum_{i=1}^{c-1}\mu_i^{(e)}\delta N_i^{(e)}. \tag{2.7}$$

Because the entire system is isolated, we also have the conditions

$$\delta V^{(e)} = -\delta V, \quad \delta N_i^{(e)} = -\delta N_i. \tag{2.8}$$

Because the entropy of an isolated system must increase (or stay constant) due to the second law of thermodynamics, the inequality

$$\delta S + \delta S^{(e)} \geq 0 \tag{2.9}$$

holds. For a quasi-static process, the equality holds, and hence the minimum work is

$$\delta W_{\min} = \delta U - T^{(e)}\delta S + p^{(e)}\delta V - \sum_{i=1}^{c-1} \mu_i^{(e)}\delta N_i. \tag{2.10}$$

Let us expand δU in powers of the small deviation. Up to second-order terms, we have

$$\delta W_{\min} = \left(T - T^{(e)}\right)\delta S - \left(p - p^{(e)}\right)\delta V + \sum_{i=1}^{c-1}\left(\mu_i - \mu_i^{(e)}\right)\delta N_i$$

$$+ \frac{1}{2}\left\{\left(\frac{\partial^2 U}{\partial S^2}\right)(\delta S)^2 + \left(\frac{\partial^2 U}{\partial V^2}\right)(\delta V)^2 + 2\left(\frac{\partial^2 U}{\partial S \partial V}\right)(\delta S)(\delta V)\right.$$

$$\left. + \sum_{i,j}\left(\frac{\partial^2 U}{\partial N_i \partial N_j}\right)(\delta N_i)(\delta N_j) + \cdots\right\}. \tag{2.11}$$

This work must be positive, $\delta W_{\min} \geq 0$, to ensure the stability of the system, and hence the right-hand side of (2.11) must be positive-definite.

First, the coefficients of the linear terms must vanish because the sign of the terms can change if they are nonzero. Hence the conditions

$$T = T^{(e)}, \quad p = p^{(e)}, \quad \mu_i = \mu_i^{(e)} \tag{2.12}$$

must hold. The temperature, pressure, and chemical potentials must be the same as the remaining part.

The second-order terms are a quadratic form of the independent variables δS, δV, δN_i $(i = 1, 2, \ldots, c-1)$, and hence the matrix made up of these coefficients must be a positive-definite matrix. We can express this matrix by using the thermodynamic relations $\partial U/\partial S = T$ and $\partial U/\partial V = -p$ in the form

$$\begin{bmatrix} \left(\frac{\partial T}{\partial S}\right)_V & -\left(\frac{\partial p}{\partial S}\right)_V & & & \\ & & & & * & \\ \left(\frac{\partial T}{\partial V}\right)_S & -\left(\frac{\partial p}{\partial V}\right)_S & & & & \\ \hdashline & & & \frac{\partial \mu_1}{\partial N_1} & \cdots & \frac{\partial \mu_{c-1}}{\partial N_1} \\ & * & & \vdots & & \vdots \\ & & & \frac{\partial \mu_{c-1}}{\partial N_1} & \cdots & \frac{\partial \mu_{c-1}}{\partial N_{c-1}} \end{bmatrix}. \tag{2.13}$$

This is called the **Gibbs matrix**.

Since $C_V = T(\partial S/\partial T)_V$, the $(1,1)$ element of this Gibbs matrix is inversely proportional to the specific heat C_V at constant volume. The $(2,2)$ element is inversely

proportional to the adiabatic compressibility $\kappa_S = -(\partial V/\partial p)_S/V$. The off-diagonal elements indicated by the symbol $*$ are not necessary for finding the stability condition.

It is well known in linear algebra that the necessary and sufficient condition for a matrix to be positive-definite is that all principal minors of the determinant are positive. We then immediately find that C_V and κ_S must be positive:

$$C_V > 0, \quad \kappa_S > 0. \tag{2.14}$$

By the thermodynamic relations

$$C_p - C_V = \frac{\alpha^2}{\kappa_T} TV, \tag{2.15}$$

the specific heat C_p at constant pressure must also be positive. The general relation

$$\kappa_S = \frac{C_V}{C_p}\kappa_T \tag{2.16}$$

indicates that the isothermal compressibility κ_T must also be positive.

Let us specifically consider a change under the constant temperature and pressure $(dT = dp = 0)$. The partial matrix $(\partial \mu_i/\partial N_j)_{p,T} = (\partial^2 G/\partial N_i \partial N_j)_{p,T}$ must be positive-definite, but this condition is equivalent to the condition for the matrix

$$\left[\frac{\partial^2 \bar{G}}{\partial x_i \partial x_j}\right]_{p,T} \equiv \begin{bmatrix} \frac{\partial^2 \bar{G}}{\partial x_1^2} & \cdots & \frac{\partial^2 \bar{G}}{\partial x_1 \partial x_{c-1}} \\ \vdots & & \\ \frac{\partial^2 \bar{G}}{\partial x_{c-1} \partial x_1} & \cdots & \frac{\partial^2 \bar{G}}{\partial x_{c-1}^2} \end{bmatrix} \tag{2.17}$$

to be positive-definite, where $\bar{G}$ is the molar Gibbs free energy of the system. The state where the determinant D of this matrix vanishes is the state where the system changes from stable to unstable. For a such **stability limit**, an extra condition is added to the Gibbs conditions, and hence the variance is reduced to $f = c - n + 1$.

For instance, for a two-component system $(c = 2)$ the stability limit of the uniform state $(n = 1)$, called **spinodal**, is a surface with $f = 2$.

The point where two coexisting phases $(n = 2)$ merge into one uniform phase $(n = 1)$ is called the **critical point**, and the merged phase is called the **critical phase**. At the critical point, two conditions,

$$D = 0, \quad D' = 0, \tag{2.18}$$

are added, where determinant D' is the new determinant obtained by replacing the last row of D by

$$\frac{\partial D}{\partial x_1}, \frac{\partial D}{\partial x_2}, \ldots, \frac{\partial D}{\partial x_{c-1}}. \tag{2.19}$$

The variance of the critical phases is given by $f = c - n$.

Because two phases merge into one, we have $n=1$, and hence $f=0$ (critical point) for $c=1$, $f=1$ (critical line) for $c=2$, and $f=2$ (critical surface) for $c=3$.

Let us specifically consider a two-component system. Because the Gibbs determinant is simply $D=(\partial^2\bar{G}/\partial x_1^2)_{p,T}$, the critical condition is

$$\frac{\partial^2\bar{G}}{\partial x_1^2} = \frac{\partial^3\bar{G}}{\partial x_1^3} = 0. \tag{2.20}$$

By using the Gibbs–Dühem relation

$$x_1 d\mu_1 + x_2 d\mu_2 = 0, \tag{2.21}$$

the differential of

$$\frac{\partial\bar{G}}{\partial x_1} = \mu_1 - \mu_2 \tag{2.22}$$

is transformed into

$$\frac{\partial^2\bar{G}}{\partial x_1^2} = \frac{\partial\mu_1}{\partial x_1} - \frac{\partial\mu_2}{\partial x_1} = \left(1 + \frac{x_1}{x_2}\right)\frac{\partial\mu_1}{\partial x_1} = \frac{1}{1-x_1}\left(\frac{\partial\mu_1}{\partial x_1}\right). \tag{2.23}$$

One more differentiation leads to

$$\frac{\partial^3\bar{G}}{\partial x_1^3} = \frac{1}{(1-x_1)^2}\left(\frac{\partial\mu_1}{\partial x_1}\right) + \frac{1}{1-x_1}\left(\frac{\partial^2\mu_1}{\partial x_1^2}\right). \tag{2.24}$$

By using these relations, we can express the spinodal condition as

$$\left(\frac{\partial\mu_1}{\partial x_1}\right)_{T,p} = 0, \tag{2.25}$$

and the critical condition as

$$\left(\frac{\partial\mu_1}{\partial x_1}\right)_{T,p} = \left(\frac{\partial^2\mu_1}{\partial x_1^2}\right)_{T,p} = 0, \tag{2.26}$$

in terms of the chemical potential of one components of the two.

2.1.3   Liquid–liquid separation by a semipermeable membrane

A membrane through which solvent molecules can pass freely but solute molecules cannot is called a **semipermeable membrane**. For a solution L and a pure solvent S separated by a semipermeable membrane M, the pressure of L is higher than the pressure of S (Figure 2.4), and hence the surface of L is higher by h than that of S. The pressure difference $\pi = \rho g h$ is called the **osmotic pressure**. The osmotic pressure is caused by the thermal motion of the solute molecules.
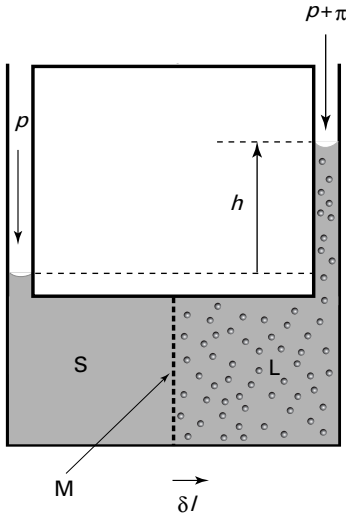
Fig. 2.4   Schematic representation of the osmotic pressure. The liquid part is separated into the solution and the pure solvent by a semipermeable membrane M. The gas phase is in equilibrium with the two liquid phases. The solute is assumed to be involatile.

Since the solvent molecules can pass freely through M, the chemical potential of the solvent ($i = 0$) must be the same,

$$\mu_0{}^\circ(T,p) = \mu_0(T, p+\pi, \{x\}), \tag{2.27}$$

in the equilibrium state of L and S, where p is the external pressure. Developing the right-hand side of this equation in powers of π, and taking the first-order term only, we find

$$\pi = -\frac{\Delta\mu_0}{\bar{V}_0}, \tag{2.28}$$

where $\bar{V}_0$ is the molar volume of the solvent. We have used the relation $(\partial\mu_0/\partial p)_T = \bar{V}_0$. It stays approximately the same as that of the pure solvent. The difference $\Delta\mu_0 \equiv \mu_0(T, p, \{x\}) - \mu_0^\circ(T, p)$ is the chemical potential of the solvent measured relative to the pure solvent.

Let p_0 be the pressure of the vapor G (assumed to be an ideal gas) in equilibrium with the solution. The osmotic pressure is connected to the activity $a_0 = e^{\Delta\mu_0/RT}$ and the ratio of the vapor pressure p_0/p_0° of the solvent through the relation

$$\pi = -\frac{RT}{\bar{V}_0} \ln\left(\frac{p_0}{p_0^\circ}\right). \tag{2.29}$$

If we assume the semipermeable membrane is mobile in Figure 2.4, and give it an imaginary displacement of an infinitesimal distance δl toward one side of the solution,

the total work necessary is

$$\delta F = \pi \, S \delta l - \mu_0 \delta N_0 + \mu_0^\circ \delta N_0, \tag{2.30}$$

where S is the area of the membrane. In a state of equilibrium, this work must be zero, i.e., $\delta F = 0$. Because $S \delta l$ is the volume change, the ratio $S \delta x / \delta N_0 = \bar{V}_0^\circ$ is the molar volume of the pure solvent. Hence, we confirm the relation (2.28).

For an ideal solution, the chemical potential of the solvent is given by

$$\Delta \mu_0 = RT \ln x_0 = RT \ln \left(1 - \sum_{i \neq 0} x_i \right), \tag{2.31}$$

where the solvent is excluded in the sum over the component. The vapor pressure is

$$p_0 / p_0^\circ = 1 - \sum_{i \neq 0} x_i, \tag{2.32}$$

so that it is reduced in proportion to the solute concentration (**Raoult's law**).

Expanding the logarithm, and taking the linear term only for dilute solutions, the solvent chemical potential is approximately

$$\Delta \mu_0 \simeq -RT \sum_{i \neq 0} x_i, \tag{2.33}$$

so that the osmotic pressure is given by

$$\pi = \frac{RT}{\bar{V}_0} \sum_{i \neq 0} x_i. \tag{2.34}$$

Because weight concentration is more often used than the mole fraction, let us convert the unit of concentration. For a dilute solution, we have

$$\sum_{i \neq 0} x_i = \frac{\sum_{i \neq 0} n_i}{n_0 + \sum_{i \neq 0} n_i} \simeq \frac{\sum_{i \neq 0} n_i}{n_0}, \tag{2.35}$$

but since the volume of the solution is approximately given by $V = n_0 \bar{V}_0 + \sum n_i \bar{V}_i \simeq n_0 \bar{V}_0$, the osmotic pressure can be written as

$$\pi = \frac{RT}{V} \sum_{i \neq 0} n_i = \frac{RT c}{\bar{M}_\mathrm{n}}, \tag{2.36}$$

where

$$c = \sum_{i \neq 0} M_i n_i / V \tag{2.37}$$

is the weight concentration [kg dm^{-3}] of the solution (M_i is the molecular weight of the component i). The average

$$\bar{M}_n \equiv \frac{\sum_{i \neq 0} M_i n_i}{\sum_{i \neq 0} n_i} \tag{2.38}$$

is the **number average molecular weight** of the solute molecules, i.e., the molecular weight averaged by the number distribution function. Equation (2.36) is **van't Hoff's law**.

Because the osmotic pressure of a polydisperse polymer solution in which polymers of the same chemical species but different molecular weight are dissolved is related to the average molecular weight of the polymers, we can infer the molecular weight of the polymers by measuring the osmotic pressure of their solutions.

For nonideal dilute solutions we can study the osmotic pressure using **virial expansion**. For simplicity, let us specifically assume that the solute is one component. The virial expansion of the osmotic pressure,

$$\pi(c, T) = RT \left[\frac{c}{M} + A_2(T)c^2 + A_3(T)c^3 + \cdots \right], \tag{2.39}$$

in powers of the concentration is just the same as the virial expansion of interacting gases in powers of the density. The first term shows van't Hoff's law because $c/M = n/V$ is the mole concentration. The rest are corrections to this ideal law. The coefficient $A_m(T)$ of the m-th power term is the m-th **virial coefficient**.

In dilute solutions, the second virial coefficient, which appears as a result of the intermolecular interaction, is important. Plotting the ratio π/c as a function of the concentration, we can find RT/M from the intercept by extrapolating the data into the infinite dilution $c \to 0$, and hence we can estimate the molecular weight M of the solute polymers. The initial slope of this curve in dilute region is A_2. We will see this in Section 2.2 in more detail.

2.1.4 Spontaneous liquid–liquid phase separation

Equilibria of two phases in two-component systems have a variance $f = c - n + 2 = 2$ (bivariant), and hence they are represented by two-dimensional surfaces in the phase space.

Let us specifically consider an equilibrium between two different liquid phases α and β. We take the mole fraction of the second component (solute) as the independent variable, and assume that they are given by x_B^α in α phase and x_B^β in β phase. The Gibbs conditions are

$$\mu_A(p, T, \{x^\alpha\}) = \mu_A(p, T, \{x^\beta\}), \tag{2.40a}$$

$$\mu_B(p, T, \{x^\alpha\}) = \mu_B(p, T, \{x^\beta\}). \tag{2.40b}$$

The slope of the tangent line drawn at a given value of x_B on the molar Gibbs free energy,

$$\bar{G} \equiv x_A \mu_A + x_B \mu_B, \tag{2.41}$$

is given by $\mu_B - \mu_A$. If a common tangent of $\bar{G}$ can be drawn, the two phases with the compositions corresponding to the two contact points are in equilibrium. The condition for the common tangent is

$$\mu_B^\alpha - \mu_A^\alpha = \mu_B^\beta - \mu_A^\beta = \frac{\bar{G}^\beta - \bar{G}^\alpha}{x_B^\beta - x_B^\alpha}. \tag{2.42}$$

From the condition (2.22), it is evident that this condition is equivalent to the condition for the phase equilibrium (2.40).

The stability limit of a phase is found by the condition

$$\left(\frac{\partial \mu_B}{\partial x_B}\right)_{p,T} = 0, \tag{2.43}$$

or, equivalently,

$$\left(\frac{\partial^2 \bar{G}}{\partial x_B^2}\right)_{p,T} = 0. \tag{2.44}$$

The inner region inside the boundary determined by this condition is an unstable region with $\partial^2 \bar{G}/\partial x_B^2 < 0$.

For the critical point, the additional condition

$$\left(\frac{\partial^2 \mu_B}{\partial x_B^2}\right)_{T,p} = 0, \tag{2.45}$$

or

$$\left(\frac{\partial^3 \bar{G}}{\partial x_B^3}\right)_{p,T} = 0, \tag{2.46}$$

is necessary. All of these results are summarized in Figure 2.5.

In an unstable region, the total free energy of the separated phases is lower than in a uniform state. The free energy difference between the unstable uniform phase and the separated two phases at a given composition x_B is

$$\Delta \bar{G} \equiv \bar{G}(x_A, x_B) - \left(\mu_A^{(\alpha)} x_A + \mu_B^{(\alpha)} x_B\right). \tag{2.47}$$

Substituting (2.41), we find the free energy difference, given by

$$\Delta \bar{G} = \left(\mu_A - \mu_A^{(\alpha)}\right) x_A + \left(\mu_B - \mu_B^{(\alpha)}\right) x_B, \tag{2.48}$$

on quenching the temperature from a stable uniform state with the composition x_B to the temperature inside the unstable region as shown in Figure 2.5. The solution eventually
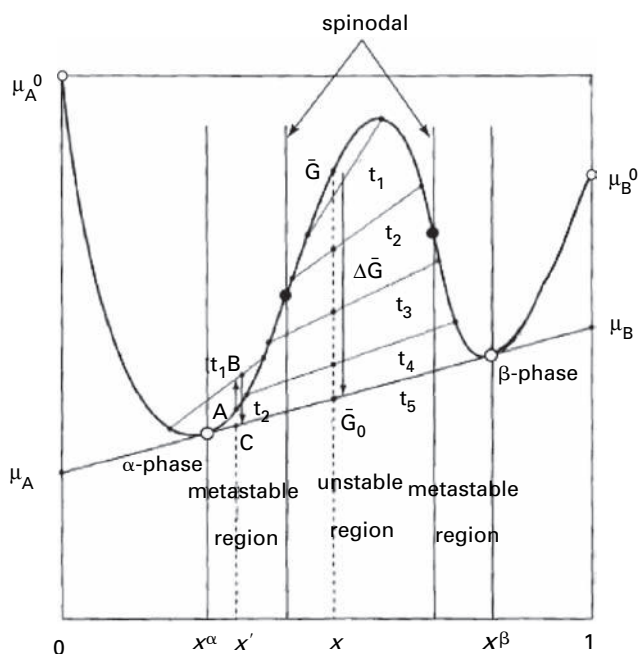
Fig. 2.5   The composition (x^{α}, x^{β}) in a two-phase equilibrium (white circles) and the spinodal point of the stability limit (black circles). The free energy difference between the uniform state at the composition x and the phase separated state is indicated by the line $\overline{G_0 G}$.

decomposes into two phases which are indicated by the endpoints of the lines $t_1, t_2, \ldots$ in Figure 2.5, and approaches the final state with α and β. Such decomposition of a solution into two phases by **temperature quenching** is called **spinodal decomposition**.

If similar quenching is carried out at the composition $x_B = x'$ lying inside the **metastable region** between the binodal and spinodal lines, the free energy of the solution once goes up to the line t_1 (A→B), and then after passing the change B→C, the solution decomposes into α and β phases. Because the free energy will not increase spontaneously, thermal excitation or external work is necessary to realize such an activation process.

2.2   Characteristic properties of polymer solutions

Polymers in solution phases have a high degree of freedom for translational and internal motion. They change their conformations randomly by Brownian movements. The purpose of this section is to see how these molecular characteristics of polymers lead to the macroscopic properties of the polymer solutions.

Measurements to find the characteristics of each polymer chain are carried out by separating them from each other in solution. Knowing the fundamental properties of polymer solutions, in particular **dilute solutions**, is very important for the molecular

characterization of polymers. Studies on dilute polymer solutions have historically played an important role in polymer science [6]. In addition, concentrated polymer solutions have practical applications to polymer processing. This section provides an overview of the nature of polymer solutions with a comparison to solutions of low-molecular weight solutes.

The following conventional units of concentration will be used:

- Mole fraction $x_i = n_i / \sum_i n_i$
  The number of i-component molecules/total number of molecules in the mixture (dimensionless).
- Volume fraction $\phi_i = V_i / V$
  The volume occupied by i-component molecules/total volume of the mixture (dimensionless).
- Weight % $w_i = n_i M_i / \sum_i n_i M_i$
  The weight of the i-component/total weight of the mixture (dimensionless [wt %]).
- Molarity $m_i = n_i / n_0 M_0$
  The number of i-component molecules in a unit weight of the solvent ([mol kg^{-1}]).
- Mole concentration $v_i = n_i / V$
  The number of moles of the i-component in a unit volume of the mixture ([mol dm^{-3}]).
- Weight concentration $c_i = n_i M_i / V$
  The mass of the i-component in a unit volume of the mixture ([kg dm^{-3}]).

For simplicity, let us assume that the volume a^3 of a statistical repeat unit of a polymer is the same as that of a solute molecule. If there are N_0 solvent molecules and N_1 polymer chains of the length n in terms of the number of repeat units in a volume $V = (N_0 + n N_1) a^3$ of the solution, the concentration is

$$v = \frac{N_1}{V}, \quad c = \frac{m n N_1}{V}, \quad x = \frac{N_1}{N_0 + N_1}, \quad \phi = \frac{n N_1}{N_0 + n N_1},$$

in terms of the unit given above, where m is the mass of a repeat unit.

The characteristic feature of polymer solutions is that they largely deviate from the ideal solution. We will look at this step-by-step in the following subsections.

2.2.1   Vapor pressure and osmotic pressure

The vapor pressure of a polymer solution deviates downwards largely from the **Raoult's law**. Figure 2.6 plots the pressure of the solvent vapor in equilibrium with a solution of uncrosslinked rubber in benzene. The depression becomes larger with the molecular weight of the polymer. Thus, polymers of high molecular weights significantly suppress the solvent activity.

As for the osmotic pressure of a polymer solution, the first term c/M in the virial expansion (2.39) is small due to the factor M^{-1} when compared with the same concentration c of a low-molecular weight counterpart. The second virial coefficient A_2, which
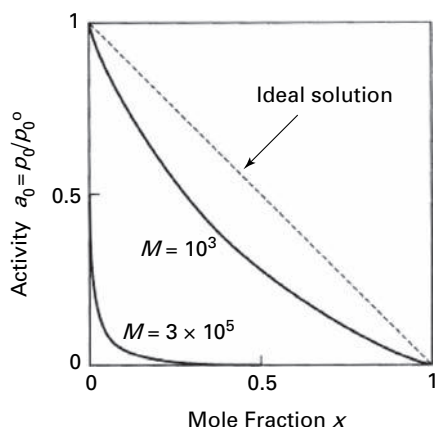
Vapor pressure depression of polymer solutions. The solvent activity (vapor pressure normalized by the reference value of the pure solvent) is plotted against the molar fraction of the polymers.
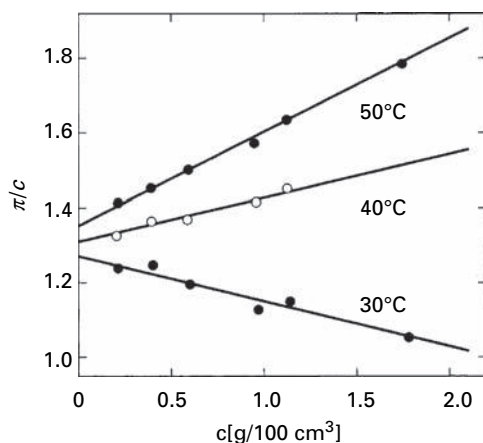
Osmotic pressure of polystyrene/cyclohexane solutions. The molecular weight of polystyrene is 203 000. The figures beside the curves show their temperatures (Reprinted with permission from Krigbaum, W. R., *J. Am. Chem. Soc.* **76**, 3758 (1954).)

originates in the interchain interaction, is very important. Figure 2.7 plots π/c of the solutions of polystyrene in cyclohexane against the weight concentration c. In the limit of dilution $c \to 0$, we can find RT/M, and hence we can find the molecular weight M of the polymer. The initial slopes of these lines give A_2. Its sign changes between the temperatures 30°C and 40°C from negative to positive. The temperature at which the condition

$$A_2(T) = 0 \qquad (2.49)$$

Table 2.1 Theta temperature of common polymer solutions

Polymer	Solvent	Theta temperature [°C]
polyethylene	diphenylether	161.4
polystyrene	decalin	31
	cyclohexane	34.5
polypropylene	cyclohexanone	92
	isoamyl acetate	34
poly(vinyl chloride)	benzyl alcohol	155.4
Poly(methyl methacrylate)	2-heptanone	11
	acetonytril	30
	2-octanone	52
poly(dimethyl siloxane)	methylethylketon	20
	chlorobenzene	68

is fulfilled is called the **theta temperature**[1] of a solution, and denoted $T = \Theta$. The theta temperature is fixed by the combination of polymer and solvent. It takes a different value for the same polymer if the solvent is different. The theta temperature of polystyrene/cyclohexane is $\Theta = 34.5°C$. Table 2.1 summarizes the theta temperatures of common polymer solutions.

We can roughly estimate the second virial coefficient of the osmotic pressure by regarding a polymer as a rigid sphere with the same radius R as the radius of gyration of the random coil (**thermodynamic equivalent sphere**). As shown in Figure 2.8, A_2 of the hard sphere system is the volume of the region where the sphere cannot enter due to the presence of other spheres. It is equal to the volume of the spherical region with the radius $2R$, the diameter of the rigid sphere, and hence we have

$$A_2 = \frac{4\pi}{3}(2R)^3 \frac{1}{M^2},\tag{2.50}$$

where M^2 in the denominator is required to change the number of the sphere to the mass density c used in the definition. Because the radius of gyration of a random coil in a good solvent is $R \sim M^\nu$, we have

$$A_2 \sim M^{3\nu-2},\tag{2.51}$$

and hence the power law $A_2 \sim M^{-0.2}$ holds for the swollen chain with the Flory exponent $\nu = 3/5$. Experiments report that the exponent lies in the range 0.1–0.5, with a typical value of 0.2. Detailed calculation of the second virial coefficient on the basis of the perturbation expansion is presented in the classic textbook by Yamakawa [7].

---

[1] In this book, we discriminate it from the molecular theta temperature θ defined in Chapter 1 based on the intramolecular interaction. Θ depends on both intra- and intermolecular interaction. If the interaction between the statistical repeat units can be described by a single excluded volume parameter v in (1.71), these two are identical. In the perturbational calculation of the third virial coefficient, simple substitution of (1.71) cannot explain the observation of positive $A_3 > 0$ at the Θ temperature. In such a case, the third cluster integral must be introduced in addition to the binary cluster integral v.

2R
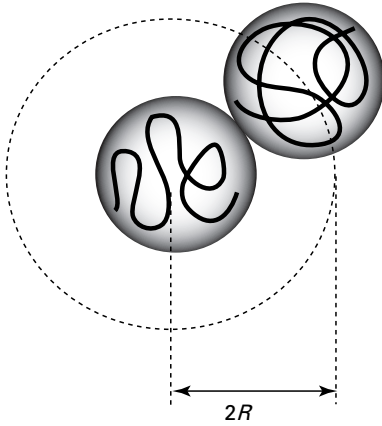
Fig. 2.8 Excluded volume (broken line) between the equivalent spheres representing polymer chains. The second virial coefficient of the osmotic pressure is proportional to the excluded volume.

2.2.2 Viscosity

The viscosity of a liquid is defined as follows. Keep a liquid between the two parallel plates, and apply a force σ_{xy} per unit area to the upper plate in the x-direction perpendicular to the y-axis. The force σ_{xy} is called the **shear stress**. The first index indicates the force direction, and the second indicates the direction of the normal vector perpendicular to the surface. The liquid flows in the x-direction, and the stationary velocity field $v_x(y)$ with a constant velocity gradient (**shear rate**)

$$\dot{\gamma} \equiv \frac{\partial v_x}{\partial y}, \tag{2.52}$$

is established after a sufficiently long time (Figure 2.9).

The stationary viscosity η is defined by the ratio of the shear stress to the velocity gradient

$$\eta(\dot{\gamma}) = \frac{\sigma_{xy}}{\dot{\gamma}}. \tag{2.53}$$

The viscosity η of the polymer solution depends in general on the shear rate $\dot{\gamma}$. The term "viscosity" usually indicates $\eta(\dot{\gamma})$ in the limit of the small shear rate $\dot{\gamma} \to 0$,

$$\eta_0 \equiv \lim_{\dot{\gamma} \to 0} \eta(\dot{\gamma}). \tag{2.54}$$

Whenever its dependence on the shear rate is studied, $\eta(\dot{\gamma})$ is referred to as the **nonlinear stationary viscosity**. The CGS unit of the viscosity $[\mathrm{g\,cm\,s^{-1}}]$ is called poise. Its MKS unit is $[\mathrm{kg\,m\,s^{-1}}] \equiv [\mathrm{Pa\,s}]$.

The viscosity is related to the energy dissipation in the liquid. Let d be the separation between the two plates, and let us consider the lower part with area S. The upper area moves by a distance $\dot{\gamma} d$ in the x-direction per unit time, and hence the stress does the work $(\dot{\gamma} d)(\sigma_{xy} S)$ on the liquid. This work is dissipated as heat generated by the friction
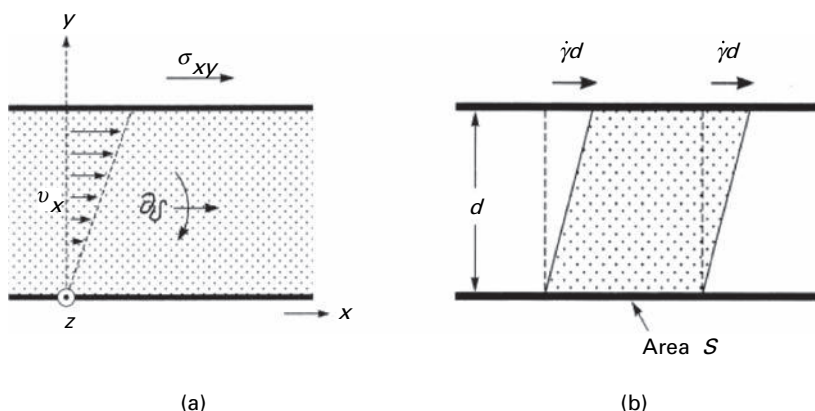
Fig. 2.9   (a) Shear flow and viscosity of the solution. Polymers flow toward downstream while they rotate. (b) The work done by the shear stress in a unit time for the solution to flow.

between the molecules in the liquid. By definition, the stress is $\sigma_{xy} = \eta\dot{\gamma}$, and the work done by the stress is $(\dot{\gamma}d)(\sigma_{xy}S) = (\eta\dot{\gamma}^2)(Sd)$, so that the heat quantity generated in a unit time in a unit volume is proportional to the viscosity as $\eta\dot{\gamma}^2$.

The small shear rate region where the nonlinear viscosity is independent of the shear rate is called **Newtonian region**. With an increase in the shear rate, the viscosity of ordinary polymer solutions decreases. This phenomenon is known as **shear thinning**. In polymer solutions in which polymers associate with each other by strongly attractive forces, such as hydrogen bonding, hydrophobic association, etc., the viscosity increases with the shear rate, reaches a maximum, and then decreases. The increase of the viscosity by shear is called **shear thickening**. Typical examples of **thickening solutions** are solutions of associating polymers. Shear thickening caused by nonlinear stretching of the polymer chains will be studied in Chapter 9.

The viscosity η of a solution is a function of the concentration. Its increment due to the solvent relative to the reference value η_0 of the pure solvent is the **specific viscosity**

$$\eta_{sp} \equiv \frac{\eta - \eta_0}{\eta_0}. \tag{2.55}$$

The specific viscosity is proportional to the concentration in the dilute region; the **reduced viscosity** defined by $\eta_{red} \equiv \eta_{sp}/c$ is often used. It can be developed in a power series of the concentration:

$$\frac{\eta_{sp}}{c} = [\eta] + k_2c + k_3c^2 + \cdots. \tag{2.56}$$

The first term $[\eta]$ is the **intrinsic viscosity** (or **limiting viscosity number**). It has the dimension of the reciprocal of concentration, and has a value of order unity when measured by the unit of $g\,dm^{-3}$. More precisely,

$$[\eta]c^* \simeq 1, \tag{2.57}$$

where c^* is the overlap concentration, the concentration at which polymer random coils start to overlap with each other. The overlap concentration will be described in detail in Section 2.4.1.
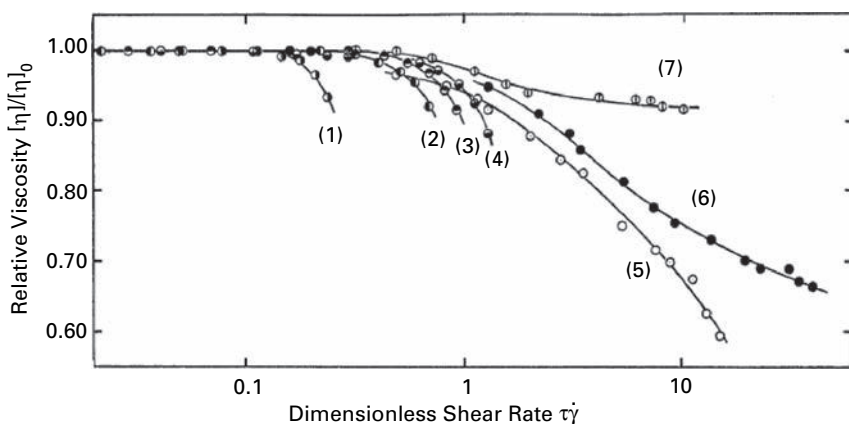
Figure 2.10 shows an example of the viscosity of a polymer solution measured as a function of the shear rate. The relative intrinsic viscosity $[\eta](\dot{\gamma})/[\eta](\dot{\gamma}=0)$ is plotted against the reduced shear rate $\tau\dot{\gamma}$, where τ is the characteristic relaxation time. Crossover from the Newtonian region to the thinning region can be seen.

The coefficient of the second term k_2 gives the effect of **hydrodynamic interaction** between two polymer chains. The interaction is mediated by the flow of the solvent around them. The strength of the hydrodynamic interaction is usually described by the dimensionless number called the **Huggins coefficient**:

$$k_{\mathrm{H}} \equiv k_2/[\eta]^2. \tag{2.58}$$

In commonly occurring polymer solutions, the Huggins coefficient takes the value in the range 0.3–0.7 (see Figure 2.11).

The intrinsic viscosity contains the information on the conformation and molecular motion of each individual polymer chain. It depends on the molecular weight in the power law (the **Mark–Houwink–Sakurada relation**)

$$[\eta] = K M^a, \tag{2.59}$$

where the **Sakurada constant** K is a constant depending on the combination of the polymer and solvent. The power index a takes a value in the range 0.5–0.8. Table 2.2 lists several examples.
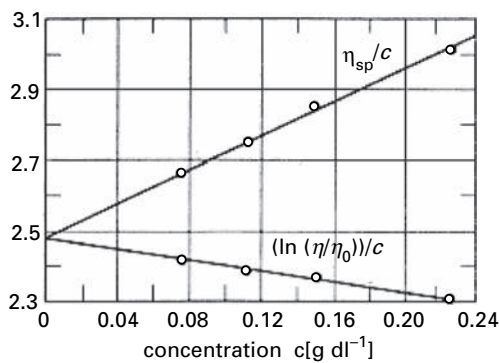
Fig. 2.11   Specific viscosity of polystyrene in benzene plotted against the polymer concentration [g dm^{-3}]. The molecular weight of the polymer is $M_w = 360\,000$.

Table 2.2 Intrinsic viscosity and the molecular weight

Polymer	Solvent	Temp. [°C]	$K\ 10^3$ [dm^3 g^{-1}]	a
polystyrene	cyclohexane	34.5	84.6	0.50
	butanone	25	39	0.58
(cis-)polybutadiene	benzene	30	33.7	0.72
poly(ethyl acrylate)	acetone	25	51	0.59
poly(methyl methacrylate)	acetone	20	55	0.73
poly(vinyl acetate)	benzene	30	22	0.65
poly(tetrahydrofuran)	toluene	28	25.1	0.78

Let us derive the relation (2.59) by comparing the random coil of a polymer with a hard sphere. It is known for a suspension of rigid hard spheres of mass m and volume v that the specific viscosity is given by

$$\eta_{sp} = \frac{5}{2}\phi + \kappa_2\phi^2 + \cdots, \tag{2.60}$$

where $\phi \equiv Nv/V$ is the volume fraction of the spheres in the suspension. The coefficient 5/2 was found by Einstein in 1906. The exact value of the second coefficient κ_2 is difficult to find, but is estimated to be 7.6 from the approximate solution of the hydrodynamic equation. Because $\phi = vc/m$, we find that $[\eta] = 5v/2m$ by comparing this equation with (2.56). The intrinsic viscosity depends on the mass density m/v of the sphere and is independent of the total mass (molecular weight). Hence we have $a = 0$.

Let us assume the random coil in the solution as a hard sphere of the radius R_H as in the thermodynamic sphere (Figure 2.8). This hypothetical sphere is not the representative of the segment distribution, but shows the region inside the coil where the solvent flow cannot pervade. It is called the **hydrodynamically equivalent sphere** (Figure 2.12). Its volume is $v_H = 4\pi R_H^3/3$. The radius R_H is not the same as the radius of gyration, but is
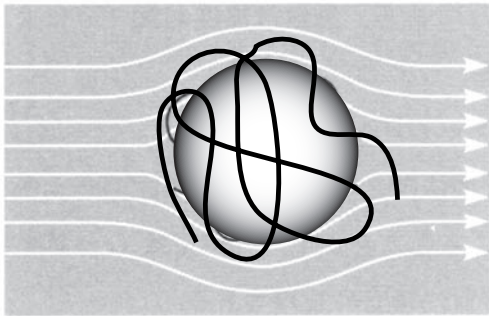
Hydrodynamically equivalent sphere defined by the region into which the solvent flow does not pervade.

expected to be proportional to it. Therefore, let us introduce the proportionality constant by the relation $R_H = \lambda \langle s^2 \rangle^{1/2}$. The constant λ shows the degree of solvent pervasion. A uniform rigid sphere has $\lambda = (5/2)^{1/2} = 1.58$, while a random Gaussian coil has a value of the order of $\lambda \simeq 0.69$. From the Einstein coefficient for the rigid sphere, we find

$$[\eta] = 2.5 \frac{v_H}{m} = \Phi \frac{\langle s^2 \rangle^{3/2}}{M}. \tag{2.61}$$

Because the relations $m = M/N_A, v_H = 4\pi R_H^3/3$ hold, we find $\Phi = 2.5 \times 4\pi \lambda^3 N_A$. This constant is known to take the value $\Phi = (2.1 \pm 0.2) \times 10^{23}\ \mathrm{g}^{-1}\ \mathrm{mol}^{-1}$ by measurement, and is regarded as a universal constant independent of the materials studied.

Because (2.61) can be transformed to

$$[\eta] = \left[\Phi (\frac{\langle s^2 \rangle_0}{M})^{3/2} \right] M^{3\nu - 1}, \tag{2.62}$$

the Sakurada constant is given by

$$K = \Phi (\langle s^2 \rangle_0 / M)^{3/2}, \tag{2.63}$$

and the index a is $a = 3\nu - 1$. (The subscript 0 indicates a Gaussian coil. The radius of gyration $\langle s^2 \rangle_0$ of a Gaussian chain is proportional to the molecular weight M.) K is a constant independent of M. At the theta temperature, polymer chains can be regarded as Gaussian with $\nu = 0.5$, and hence $a = 0.5$. At high temperatures where chains are swollen by the excluded volume effect with the Flory index, $\nu = 3/5$, and hence $a = 0.8$. The experimental results summarized in Table 2.2 can thus be explained.

2.2.3 Diffusion of a polymer chain

If the concentration is not uniform in the solution, but depends on the position, the solute molecules diffuse from regions of high concentration to regions of low concentration. This is due to random Brownian motion of the solute molecules.
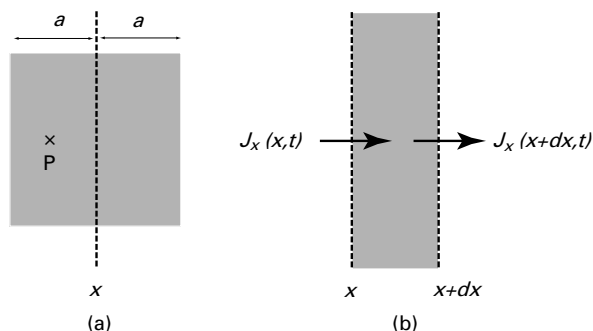
Fig. 2.13   Molecular diffusion. (a) Counting the number of molecules moving across a hypothetical unit area in the solution. (b) Counting the number of molecules entering and exiting the region between parallel planes separated by an infinitesimal distance dx.

The mass of the solute molecules moving across an infinitesimal area dS in the solution in a unit time is given by $\mathbf{J} \cdot \mathbf{n} dS$, where $\mathbf{n}$ is the unit normal vector perpendicular to this area, and $\mathbf{J}$ is the **flux vector**. For instance, the mass flux of solute molecules moving across the unit area perpendicular to the x-axis is J_x.

The flux is proportional to the gradient of the concentration,

$$\mathbf{J} = -D\nabla c, \tag{2.64}$$

because of the diffusion. This is **Fick's law**. The negative sign shows that the diffusion takes place from a region of high concentration to a region of low concentration. The proportionality constant D is the **diffusion constant**. It is a material constant of the solute molecules in a given solvent.

To derive Fick's law, consider a fictitious plane perpendicular to the x-axis at the position x, and count the number of molecules that cross the small area dS on this plane (Figure 2.13(a)). To describe the random Brownian motion of the solute molecules due to thermal agitation, let us assume for simplicity that each molecule moves by one step of width a in a fixed short time τ in random directions with equal probability. Because there are three axes in the space, and each axis has $\pm$ direction, on average 1/6 of the total molecules move to the $+$ direction of the x-axis. The number of molecules that pass the area during the time interval τ is therefore 1/6 of the molecules in the cylindorical volume adS in the left-hand side of the plane. If the number density in the volume is represented by $n(x - a/2, t)$ at the central position P($x - a/2$) of the volume, then a total of

$$\frac{1}{6}n(x - a/2, t)adS$$

molecules cross the area to the positive direction. A similar formula holds for the molecules moving in the negative direction. Taking the difference and dividing by the area, we find

$$j_x = \frac{1}{6}\left\{(n(x - a/2, t) - n(x + a/2, t))\right\}a \times \frac{1}{\tau} \simeq -\left(\frac{a^2}{6\tau}\right)\frac{\partial n}{\partial x} \tag{2.65}$$

for the number flux to the positive direction. The multiplication of the mass of a molecule to this equation leads to Fick's law for the mass flux $J_x \equiv m j_x$. Hence the diffusion constant is given by

$$D = \frac{a^2}{6\tau}.$$ (2.66)

(The squared step length a^2 divided by the fundamental time scale τ necessary for one step of movement.) The number 6 comes from the space dimensions d multiplied by 2 for the $\pm$ directions. The diffusion of a marked particle obtained in such a way is the **self-diffusion constant** or **marker diffusion constant**.

Let us next count the number of molecules that are entering and exiting the region between the parallel planes at the position x and $x + dx$ separated by an infinitesimal distance dx in the system (Figure 2.13(b)). Because mass $J_x(x,t)$ enters from the left-hand plane per unit area per unit time, and mass $J_x(x + dx, t)$ exits from the right-hand plane, the mass inside the region changes by

$$\frac{\partial}{\partial t}(c\,dx) = J_x(x,t) - J_x(x+dx,t) \simeq -\frac{\partial J_x}{\partial x}dx.$$

Substituting Fick's law (2.64) into this equation, we find that the concentration obeys the **diffusion equation**

$$\frac{\partial c}{\partial t} = D\frac{\partial^2 c}{\partial x^2}.$$ (2.67)

If we observe the displacement of a Brownian particle over a long time interval t, it looks like the conformation of a random flight polymer chain with a fundamental step length a and number of repeat units $n = t/\tau$ (Figure 1.4). The displacement **R** of the particle corresponds to the end-to-end distance, and its square average should be equal to

$$\langle R^2 \rangle = na^2 = \frac{ta^2}{\tau} = 6Dt.$$ (2.68)

(For the x-component, the relation is $\langle x^2 \rangle = 2Dt$.)

The diffusion constant is related to the friction of the particle with the media. Let ζ be the friction constant of the diffusing particle. Einstein found that the relation

$$D = \frac{k_B T}{\zeta}$$ (2.69)

holds, where k_B is the Boltzmann constant (**Einstein relation**).

When a rigid sphere of radius a moves in a solvent of viscosity η_0, the friction coefficient is given by **Stokes' law**

$$\zeta = 6\pi a \eta_0.$$ (2.70)

In the case of polymers diffusing in a solvent, we can replace the random coil by the hydrodynamically equivalent sphere of radius R_H. We find

$$\zeta = 6\pi \eta_0 R_H,$$ (2.71)

Table 2.3 Some examples of diffusion constants

Solute	Molecular weight	Solvent	$D\ [10^{-7}\mathrm{cm}^2\,\mathrm{s}^{-1}]$
sodium chloride	58	water	80.0
polystyrene	10 600	benzene	11.7
polystyrene	67 000	benzene	4.1
polystyrene	606 000	benzene	1.5

and hence the friction coefficient should obey the power law $\zeta \propto M^{\nu}$. The molecular weight of the polymer can therefore be estimated by measuring the diffusion constant. The absolute values of the diffusion constant for different materials are in the range 10^{-7}–$10^{-6}\mathrm{cm}^2\,\mathrm{s}^{-1}$. Table 2.3 shows some examples.

The diffusion constant obtained by tracing the selected particle among many is the **marker diffusion constant**. The marker diffusion constant is indicated by the labeling symbol *, as D^*. In contrast, the diffusion constant in Fick's law is defined for the many particles involved in the local concentration, and is called the **concentration diffusion coefficient**. In dilute solutions where particles move independently of each other, these two diffusion constants are the same. In concentrated solutions, the assumption of independent motion of the particles breaks down by molecular interaction, so that the two diffusion coefficients are not identical.

To study the concentration diffusion coefficient, let us focus on a solute particle in solution. Its average velocity $\mathbf{u}$ is decided by the balance condition between the thermal driving force $-\nabla\mu$ and the viscous resistance force $\zeta\bar{\mathbf{u}}$,

$$\zeta\bar{\mathbf{u}} = -\nabla\mu, \tag{2.72}$$

where $\mu(\mathbf{r},t)$ is the chemical potential of the particle at the position $\mathbf{r}$, and ζ is the friction constant. The mass flux $\mathbf{J} = c\bar{\mathbf{u}}$ then takes the form

$$\mathbf{J} = -(c/\zeta)\nabla\mu = -(c/\zeta)(\partial\mu/\partial c)_T\nabla c, \tag{2.73}$$

and hence the concentration diffusion coefficient is given by

$$D = \left(\frac{c}{\zeta}\right)\left(\frac{\partial\mu}{\partial c}\right)_T. \tag{2.74}$$

Although the marker diffusion coefficient is always positive, the concentration diffusion coefficient may become negative when the thermodynamic instability condition $(\partial\mu/\partial c)_T < 0$ is fulfilled (Section 2.3). Particles spontaneously move from the regions of low concentration to the regions of high concentration. When a solution is quenched from a high-temperature uniform state to a low-temperature unstable state in the spinodal region, it separates into two phases through such negative diffusion. The method used to observe the time development of the phase separation process by such a temperature quenching is called the **spinodal decomposition** method.

The chemical potential of the solute particles in a solution can be written as

$$\mu(c,T) = \mu_0(T) + k_B T \ln(\gamma c), \tag{2.75}$$

(where $\mu_0(T)$ is the reference value) by using the activity coefficient γ. The concentration diffusion coefficient is

$$D(c) = \frac{k_B T}{\zeta(c)} \left\{ 1 + \left(\frac{\partial \ln \gamma}{\partial \ln c} \right)_T \right\}, \tag{2.76}$$

where the friction coefficient may also depend on the concentration as

$$\zeta(c) = \zeta_0 (1 + k_f c + \cdots). \tag{2.77}$$

When there is no interaction, the activity is given by $\gamma = 1$ and $\zeta = \zeta_0$, so that the diffusion coefficient reduces to the marker diffusion coefficient

$$D = k_B T / \zeta_0 = D^*. \tag{2.78}$$

The factor in the parenthesis of (2.76) appears due to the molecular interaction, and is called the **thermodynamic factor** of the diffusion coefficient. The diffusion coefficient can be expanded in powers of the concentration in the dilute region as

$$D(c) = D^* (1 + k_D c + \cdots), \tag{2.79}$$

where k_D is the **mutual diffusion concentration coefficient**. It is related to the second virial coefficient A_2 and the friction coefficient k_f as

$$k_D = 2 A_2 M - k_f. \tag{2.80}$$

due to the relation (2.76).

2.3   Lattice theory of polymer solutions

We modify the conventional regular solution model [5] of low-molecular weight molecules to apply it to solutions of long chain molecules in which the molecular weight of the solute molecules is much larger than that of the solvent molecules. The entropy of mixing decreases with the molecular weight of polymers due to the reduction of the freedom in the translational motion of the molecules.

2.3.1   The free energy of mixing

To find the entropy of mixing [6,8–11],we first introduce a hypothetical lattice cells for the solution of the total volume V. We choose the unit volume to be that of the unit cell and make the customary simplifying assumption that the solvent molecules and the statistical repeat units of the polymer chains occupy the same volume a^3. We count the
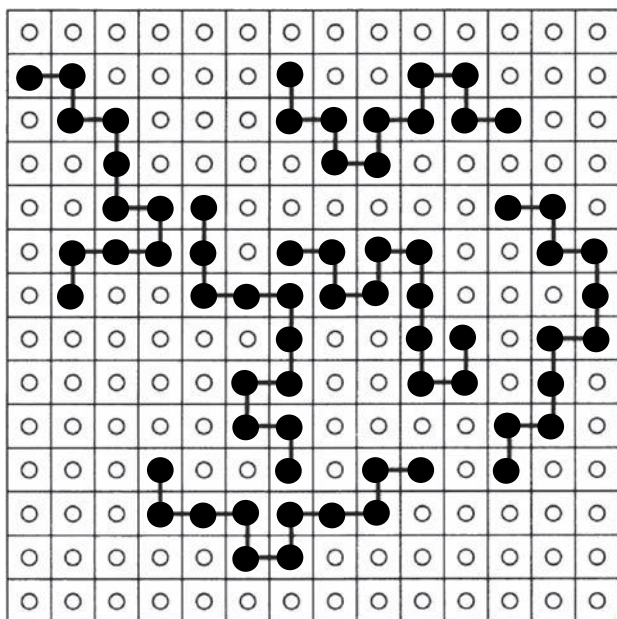
Fig. 2.14   Hypothetical lattice introduced to find the mixing entropy of polymers and solvent.

number $W(N_0, N_1)$ of different ways to place N_1 chains and N_0 solvent molecules on this hypothetical lattice, whose total number of cells is $N \equiv V/a^3$ (Figure 2.14). We assume that the solution is incompressible, and hence $N = N_0 + nN_1$ holds. The configurational entropy is given by the Boltzmann's principle

$$S(N_0, N_1) = k_B \ln W(N_0, N_1). \tag{2.81}$$

The entropy of mixing, as measured from the standard reference state in which polymers and solvent are separated in the hypothetical crystalline states, is then given by the difference

$$\Delta_{\mathrm{mix}} S = S(N_0, N_1) - S(0, N_1) - S(N_0, 0). \tag{2.82}$$

To find $W(N_0, N_1)$, we tentatively assign the number $1, 2, 3, \ldots, N_1$ to the polymers. Let ν_{j+1} be the number of possible ways to place the $(j+1)$-th chain on the lattice without double occupancy, one repeat unit by one starting from one end unit, under the condition that all polymers to the j-th are already placed on the lattice.

The number W is then given by

$$W(N_0, N_1) = \frac{1}{N_1! \sigma^{N_1}} \prod_{j=0}^{N_1-1} \nu_{j+1}, \tag{2.83}$$

where the prefactor $1/N_1!$ is the correction for the overcounting by assigning the sequence number to the identical polymers. The factor σ is the symmetry number, which takes the

value 2 for a symmetric polymer, and 1 for an asymmetric polymer. (For a symmetric polymer, there is no difference in placing the polymer at one end unit or the other.)

The first repeat unit of the $j+1$-th chain can be placed on any vacant cell, and the number of its placement is $N - jn$. The second unit can be placed on one of the vacant cells in the nearest neighboring z cells of the first unit. There are $zR_{j,1}$ ways to do this, where $R_{j,k}$ is the probability for one of the nearest neighboring cells to be vacant when j chains and the first k units of the $j+1$-th chain are already placed.

Similarly, the third unit has $(z-1)R_{j,2}$ different ways to place. We assume that all repeat units after the third one ($k \geq 4$) have similar $(z-1)R_{j,k}$ ways of placing, although some of them may hit a cell that is already occupied by the former repeat units by forming loops.

We then have

$$\nu_{j+1} = \delta_{\max} \cdot (N - jn) \prod_{k=1}^{n-1} R_{j,k}, \tag{2.84}$$

where $\delta_{\max} \equiv z(z-1)^{n-2}$ is the **maximum flexibility** of a chain, i.e., the maximum possible number of internal conformations the chain can take.

The probability $R_{j,k}$ of the nearest neighboring cell of the (j,k)-th repeat unit being unoccupied may be given by the condition that the position of the repeat unit under investigation is the surface of the vacant cell. Because the total number of surface cells, including those of polymer chains already arranged on the lattice and those of the vacant sites, is $z(N - jn - k) + [(z-2)(n-2) + 2(z-1)]j + (z-2)k + 2$, the probability is given by the ratio

$$R_{j,k} = \frac{z(N - jn - k)}{z(N - jn - k) + [(z-2)n + 2]j + (z-2)k + 2}. \tag{2.85}$$

For completely random mixing, it is approximately equal to the volume fraction

$$R_{j,k} \simeq 1 - jn/N \tag{2.86}$$

of the vacancy, when j and k are assumed to be small compared to N and n. The approximation of replacing the nonoccupancy probability by this volume fraction is called the **molecular field approximation**. In this section, we look at the solution within such molecular-field treatment.

We thus find

$$\nu_{j+1} \simeq \left(\frac{\delta_{\max}}{\sigma}\right) N \left(1 - \frac{jn}{N}\right)^n. \tag{2.87}$$

Detailed study using a more rigorous formula (2.85) will be presented in Section 2.3.4.

Substituting (2.87) into (2.83), and using **Starling's formula**, $\ln N! \simeq N \ln N - N$ for a large number N, we find

$$S(N_0, N_1)/k_B = -N_1 \ln \phi_1 - N_0 \ln \phi_0 + N_1 \ln \left(\frac{n\delta_{\max}}{\sigma e^{n-1}}\right) \tag{2.88}$$

for the conformational entropy, where $\phi_0 \equiv N_0/N$, $\phi_1 \equiv nN_1/N$ are the volume fraction of the polymer and solvent. Unlike the solutions of low-mass solutes, the volume fractions have appeared in place of the molar fractions.

The conformational entropy of pure polymers can be found by fixing $N_0 = 0$ as

$$S(0, N_1) = N_1 k_B \ln \left(\frac{n\delta_{max}}{\sigma e^{n-1}} \right). \tag{2.89}$$

Each chain thus gains the **entropy of disorientation**

$$S_{dis}(n) = k_B \ln \left(\frac{n\delta_{max}}{\sigma e^{n-1}} \right), \tag{2.90}$$

when it is transformed from the hypothetical straight rods to amorphous states of random conformation.

For the pure solvent, there is only the unique arrangement, so that $S(N_0, 0) = 0$ holds. The entropy of mixing is then

$$\Delta_{mix} S(N_0, N_1) = -k_B (N_0 \ln \phi_0 + N_1 \ln \phi_1). \tag{2.91}$$

Figure 2.15 summarizes the method to find the entropy of mixing.

If all bonds of the chains were cut and the repeat units were separated from each other, the entropy of mixing would be

$$\Delta_{mix} S' = -k_B (N_0 \ln \phi_0 + nN_1 \ln \phi_1). \tag{2.92}$$
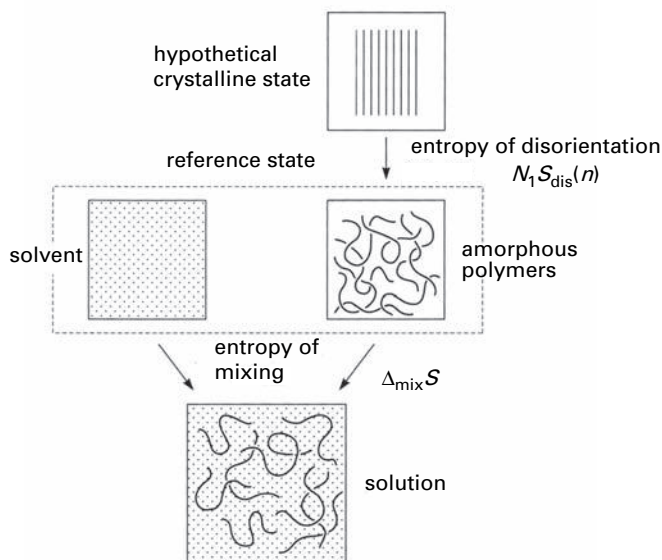
Fig. 2.15   Method to find the entropy of disorientation and the entropy of mixing in polymer solutions.

Hence, the mixing entropy has reduced by $k_B(n-1)|\ln\phi_1|$ per chain through chemical bonds. Every time a repeat unit is connected to the chain, the center of mass degree of freedom is reduced by 1. The entropy of mixing in polymer solutions is thus smaller than that of the solutions of low-molecular weight molecules.

Let us next find the enthalpy (internal energy) of the solution with the assumption of random mixing. Let $\epsilon_{0,0}$ be the interaction energy between a neighboring pair of the solvent molecules, $\epsilon_{1,1}$ be that between repeat units, and $\epsilon_{0,1}=\epsilon_{1,0}$ be that between a solvent molecule and a repeat unit. We then have

$$U = \epsilon_{0,0}N_{0,0} + \epsilon_{1,1}N_{1,1} + \epsilon_{0,1}N_{0,1}. \tag{2.93}$$

If the average probability for one of the $z-2$ available nearest neighboring sites of a repeat unit (except the chain ends) to be occupied by a solvent is ϕ_0, the number of solvent–monomer pairs is $N_{0,1}=N_{1,0}=nN_1(z-2)\phi_0$. Similarly, $N_{0,0}=N_0 z\phi_0/2$, $N_{1,1}=nN_1(z-2)\phi_1/2$. If we replace $z-2$ with z for simplicity in these relations, we find

$$U = \left(\frac{1}{2}zN_0\right)\phi_0\epsilon_{0,0} + \left(\frac{1}{2}znN_1\right)\phi_1\epsilon_{1,1} + (znN_1)\phi_0\epsilon_{0,1}. \tag{2.94}$$

The first two terms are the internal energy of each component. By subtraction, the mixing energy is given by

$$\Delta_{\text{mix}}U = \left[znN_1\phi_0\epsilon_{0,1} + \frac{1}{2}zN_0\phi_0\epsilon_{0,0} + \frac{1}{2}znN_1\phi_1\epsilon_{1,1}\right]$$
$$- \left[\frac{1}{2}znN_1\epsilon_{1,1} + \frac{1}{2}zN_0\epsilon_{0,0}\right] = zN\phi_0\phi_1\Delta\epsilon, \tag{2.95}$$

where $\Delta\epsilon$ is the energy difference caused by molecular contact

$$\Delta\epsilon \equiv \epsilon_{0,1} - \frac{1}{2}(\epsilon_{0,0}+\epsilon_{1,1}). \tag{2.96}$$

The dimensionless interaction energy

$$\chi(T) \equiv z\Delta\epsilon/k_B T \tag{2.97}$$

is conventionally called **Flory's χ-parameter** in polymer solution theory. The mixing enthalpy takes the **van Laar form**,

$$\Delta_{\text{mix}}U = Nk_B T\chi(T)\phi_0\phi_1, \tag{2.98}$$

by using this χ-parameter. The mole fraction is replaced by the volume fraction.

If $\chi > 0$, the solution tends to separate into two phases with different concentrations because the energy increases when molecules of different species are brought into contact. If $\chi < 0$, on the other hand, molecules of different species tend to mix. If $\chi = 0$, there is no mixing heat, and the solution is called an **athermal solution**.

Putting the entropy and enthalpy together, the free energy of mixing is found to be

$$\Delta_{\text{mix}} F / k_B T = N_0 \ln \phi_0 + N_1 \ln \phi_1 + N \chi(T) \phi_0 \phi_1. \tag{2.99}$$

Alternatively, it is written in dimensionless form as

$$
\begin{aligned}
\mathscr{F}(\phi, T) &\equiv \Delta_{\text{mix}} F / N k_B T \\
&= \frac{\phi}{n} \ln \phi + (1 - \phi) \ln(1 - \phi) + \chi(T) \phi (1 - \phi)
\end{aligned}
\tag{2.100}
$$

per a lattice cell using the unit of thermal energy. The mean field approximation on the basis of random mixing is called the **Flory–Huggins theory** [8–11].

The approximation becomes poor for the systems in which concentration fluctuations are large. For instance, in dilute polymer solutions, monomers distribute unevenly inside and outside the region occupied by the polymer chains. The spatial variation of the concentration is so high that the mean field assumption cannot be expected to hold. Also, in the region near the critical point of phase separation, where the concentration fluctuation is large, the mean field picture breaks down.

2.3.2   Properties of polymer solutions predicted by Flory–Huggins lattice theory

In the following sections, we take the volume fraction of the polymer as an independent variable and write it as $\phi_1 \equiv \phi$.

Osmotic pressure
The mole chemical potential of the solvent is

$$\Delta \mu_0 = RT \left[\ln(1 - \phi) + \left(1 - \frac{1}{n} \right) \phi + \chi \phi^2 \right], \tag{2.101}$$

by the definition $\Delta \mu_0 = (\partial \Delta_{\text{mix}} F / \partial N_0)_{N_1, T}$. The osmotic pressure $\pi = -\Delta \mu_0 / a^3$ takes the form

$$\pi = \frac{RT}{a^3} \left[\frac{1}{n} \phi + \left(\frac{1}{2} - \chi \right) \phi^2 + \frac{1}{3} \phi^3 + \cdots \right] \tag{2.102}$$

by expanding (2.101) in powers of the polymer volume fraction. Comparing with (2.39), and after changing the volume fraction to the weight concentration, the second virial coefficient is found to be

$$A_2(T) = \frac{a^3}{m^2} \left[\frac{1}{2} - \chi(T) \right], \tag{2.103}$$

where m is the molecular weight of a repeat unit.

The coefficient A_2 depends on the temperature through the χ-parameter, but is independent of the polymer molecular weight. It vanishes at the temperature where $\chi = 1/2$ is fulfilled, and hence the theta temperature is found by the condition

$$\chi(\Theta) = 1/2. \tag{2.104}$$

We can expand $\chi(T)$ in terms of the dimensionless temperature difference $\tau \equiv 1 - \Theta/T$ in the form

$$\chi(T) = \frac{1}{2} - \psi\left(1 - \frac{\Theta}{T}\right), \tag{2.105}$$

where ψ is a constant of order unity. It is a material constant fixed by the combination of the polymer and solvent.

This equation has the form

$$\chi(T) = A + B/T, \tag{2.106}$$

and is different from the form obtained by the mixing energy (2.97). However, if we add the entropy Δs to the energy $\Delta\epsilon$ of molecular contact, and replace it with the free energy $\Delta f \equiv \Delta\epsilon - T\Delta s$ of interaction, these two are identified. In fact, when molecules of different species come into contact, not only the interaction energy but also the entropy of orientation, rotation, etc., may change. From the experimental data, separating χ into an energy part and an entropy part, we can often see that the entropy change is larger than the energy change. The form (2.105) is called the **Shultz–Flory formula**.

Solubility parameter

The interaction energy $\Delta\epsilon$ between neighboring molecules is related to the **cohesive energy** of each species. The cohesive energy of a pure A component in a crystalline state is $E_{AA} = (zN_A/2)\epsilon_{AA}$. Per unit volume, it is $E_{AA}/V_A = (z/2a^3)\epsilon_{AA}$. Since ϵ_{AA} is negative, let us introduce the **solubility parameter** δ_{AA} by

$$E_{AA}/V_A \equiv -\delta_{AA}{}^2 \tag{2.107}$$

For species B, δ_{BB} is similarly defined.

If we assume the relation $\epsilon_{AB} = -(\epsilon_{AA}\epsilon_{BB})^{1/2}$ for the interaction energy between the different species, the energy part of the χ-parameter can be written in terms of the solubility parameters as

$$\chi_H(T) = \frac{a^3}{k_B T}(\delta_{AA} - \delta_{BB})^2. \tag{2.108}$$

The constant B in (2.106) turns out to be $B = a^3(\delta_{AA} - \delta_{BB})^2/k_B$, and takes a positive value.

The solubility parameter is known to obey an additivity rule; it is given by the sum of all the solubility parameters of the fundamental chemical groups contained in the molecule. We can therefore estimate the solubility parameter of a polymer chain by using the standard values of the fundamental groups listed in the table. The **group contribution method** to find the mixing enthalpy of polymers proposes the following formula for the solubility parameter δ of a polymer:

$$\delta = \frac{\rho}{m}\sum_i G_i, \tag{2.109}$$

where ρ is the density of the monomer, m is its molecular weight and G_i is the **molar attraction constant**, which is a numerical value assigned to the each fundamental group.

Group		G
$-CH_3$		214
$-CH_2-$	single-bonded	133
$-CH<$		28
$>C<$		–93
$CH_2=$		190
$-CH=$	double-bonded	111
$>C=$		19
$-CH=C<$		285
$-C=C-$		222
Phenyl		735
Phenylene	(o,m,p)	658
Naphthyl		1146

(a)

$G = 133$ $G = 28$

H_2C CH

$G = 735$
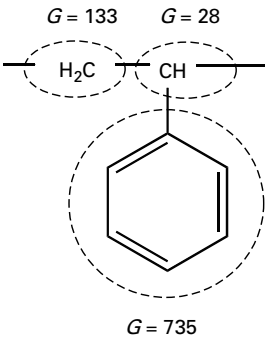
(b)

Fig. 2.16 (a) Molar attraction constants G at 25°C assigned to the fundamental groups. (b) Example of calculation of the solubility parameter. Each monomer of polystyrene is decomposed into three fundamental groups. The solubility parameter of polystyrene is estimated from the sum of their molar attraction constants.

For instance, polystyrene has $\rho = 1.05 \, \text{g cm}^{-3}$, $m = 104 \, \text{g mol}^{-1}$. The molar attraction constant can be found from the table in Figure 2.16(a). The solubility parameter is estimated to be (Figure 2.16(b))

$$\delta = 1.05 \times (133 + 28 + 735)/104 = 9.05 \quad (\text{cal cm}^{-3})^{1/2}. \tag{2.110}$$

The tables of solubility parameters edited by Hansen [12] accommodate all the presently available values in the form of a database.

The solubility parameter of many materials can be decomposed into three parts as

$$\delta^2 = \delta_D^2 + \delta_P^2 + \delta_H^2, \tag{2.111}$$

where δ_D is the part contributed by the dispersion force, δ_P by the polar force (permanent dipole–dipole interaction), and δ_H by hydrogen bonds.

Osmotic compressibility
Osmotic compressibility is defined by

$$K_T \equiv \frac{1}{\phi} \left(\frac{\partial \phi}{\partial \pi} \right)_T, \tag{2.112}$$

analogously to the compressibility of gases, and serves as the measure of the relative change of the concentration due to small change of the osmotic pressure.[2] Taking the

---

[2] The compressibility of the solution need not be considered because the solution is assumed to be incompressible.

derivative by the volume fraction, we find

$$K_T = \frac{a^3/k_B T}{\phi^2 \mathscr{F}''(\phi, T)} \tag{2.113}$$

for the osmotic compressibility, where

$$\mathscr{F}''(\phi) = \frac{1}{n\phi} + \frac{1}{1-\phi} - 2\chi(T) \tag{2.114}$$

is the second derivative of the free energy (2.100). As shown in Section 2.1, K_T must be positive for stable systems. If it is negative, the osmotic pressure becomes lower in the region where the concentration is higher, and hence polymers spontaneously move to the region of high concentration. Such a **negative diffusion** indicates that the system is unstable against phase separation.

The boundary between the stable and unstable states can be found by the **spinodal condition**

$$\mathscr{F}''(\phi) = 0, \tag{2.115}$$

where K_T is divergent.

Phase equilibria

The chemical potential of the polymer is similarly found to be

$$\Delta\mu_1 = RT\{\ln\phi - (n-1)(1-\phi) + \chi n(1-\phi)^2\}. \tag{2.116}$$

The Gibbs condition for the phase equilibria can be written in the form of the coupled equations

$$\Delta\mu_0(\phi^\alpha, T) = \Delta\mu_0(\phi^\beta, T), \tag{2.117a}$$

$$\Delta\mu_1(\phi^\alpha, T) = \Delta\mu_1(\phi^\beta, T), \tag{2.117b}$$

whose solutions give the **coexistence curve**, or **binodal curve**, for liquid–liquid phase separation into a dilute phase with a volume fraction ϕ^α and a concentrated phase with ϕ^β. This Gibbs condition is equivalent to drawing a common tangent to the total free energy (2.100) of mixing.

Comparison between the theoretical calculation of the coexistence curve and the experimental cloud-point curve is made in Figure 2.17(a). The experimental data (dotted lines) are wider than the theoretical binodals, but the shape of the curves, including the molecular weight dependence, is well reproduced.

The critical point is the point where both binodal and spinodal conditions

$$\frac{\partial \Delta\mu_0}{\partial \phi} = \frac{\partial^2 \Delta\mu_0}{\partial \phi^2} = 0 \tag{2.118}$$
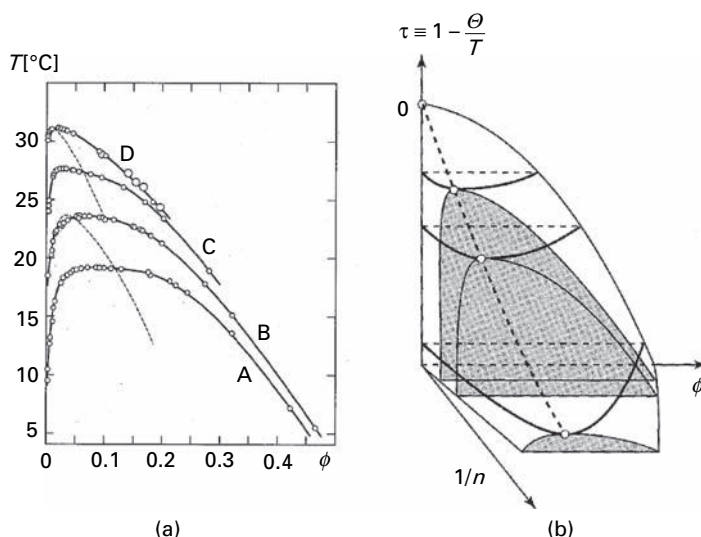
Fig. 2.17   (a) Comparison of the experimental cloud-point curves (symbols) and theoretical coexistence curves (dotted lines) of the solutions of polystyrene in cyclohexane. Data for the different molecular weight polymers: A (43 600), B (89 000), C (250 000), D (1 270 000). (Reprinted with permission from Ref. [13].) (b) Coexistence surface in three-dimensional phase space with an extra axis for the reciprocal molecular weight.

are fulfilled. Solving these coupled equations with respect to ϕ and T, we find

$$\phi_c = \frac{1}{1+\sqrt{n}}, \tag{2.119}$$

$$\chi_c = \frac{(1+\sqrt{n})^2}{2n}. \tag{2.120}$$

For the high-molecular weight polymers with a large number of repeat units, the critical concentration is approximately given by $\phi_c \simeq 1/\sqrt{n} \ll 1$. It is extremely small for high-molecular weight polymers. The critical temperature is approximately $\chi(T_c) \simeq 1/2 + 1/\sqrt{n}$, hence T_c is lower by $1/\sqrt{n}$ than the theta temperature. (The temperature coefficient of χ is assumed to be positive $B > 0$.) The theta temperature is the critical temperature of the solutions of infinitely large molecular weight polymers.

Figure 2.18 shows the molecular weight dependence of the critical temperature. From (2.105) and (2.120), T_c is given by

$$\frac{1}{T_c} = \frac{1}{\Theta} + \frac{1}{\psi\Theta}\left(\frac{1}{\sqrt{n}} + \frac{1}{2n}\right). \tag{2.121}$$

The extrapolation point to the vertical axis in the limit of $n \to \infty$ gives the theta temperature, while the slope of the curve gives the Shultz–Flory constant ψ. Such an analysis is called a **Shultz–Flory plot**.
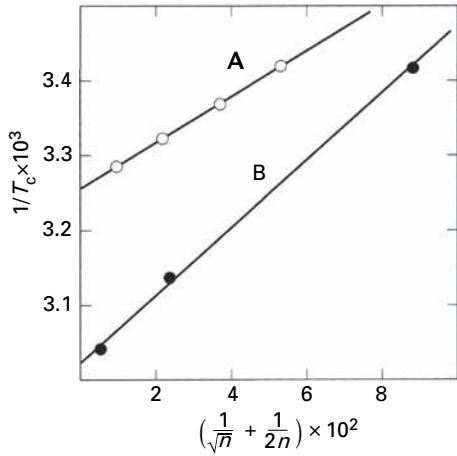
Fig. 2.18 Relation between the critical temperature of polymer solutions and the molecular weight of the polymer. A (polystyrene/cyclohexane), B (polystyrene/diisobuthylketon). (Reprinted with permission from Ref. [13].)

2.3.3 Extension to many-component polymer solutions and blends

Similar consideration of the configurational entropy to arrange two species of polymers with n_1 and n_2 repeat units leads to the free energy of mixing per lattice site,

$$\mathscr{F}(\phi) = \frac{\phi_1}{n_1}\ln\phi_1 + \frac{\phi_2}{n_2}\ln\phi_2 + \chi(T)\phi_1\phi_2, \tag{2.122}$$

where ϕ_i is the volume fraction of each species. The relation $\phi_1 + \phi_2 = 1$ holds. By differentiation, the chemical potentials are found to be

$$\frac{\beta\Delta\mu_1}{n_1} = \frac{1}{n_1}(1+\ln\phi_1) - \nu + \chi(T)\phi_2^2, \tag{2.123a}$$

$$\frac{\beta\Delta\mu_2}{n_2} = \frac{1}{n_2}(1+\ln\phi_2) - \nu + \chi(T)\phi_1^2, \tag{2.123b}$$

where

$$\nu \equiv \phi_1/n_1 + \phi_2/n_2 \tag{2.124}$$

is the total degree of freedom for translational motion (the number of mass centers in the system). If $\phi_2 = \phi$ is taken as an independent variable for the concentration, the critical point of the binary blend is given by

$$\phi_c = \sqrt{n_1}/(\sqrt{n_1} + \sqrt{n_2}), \quad \chi_c = (\sqrt{n_1} + \sqrt{n_2})^2/2n_1n_2. \tag{2.125}$$

In particular, for a symmetric blends for which $n_1 = n_2$ is satisfied, they are reduced to $\phi_c = 1/2$, $\chi_c = 2/n$.

We can extend the theory still further to the many-component polymer blends whose components are indicated by $i \ (= 1, 2, \ldots, c)$, each carrying n_i repeat units. The free energy per lattice site is

$$\mathscr{F}(\{\phi\}) = \sum_i \frac{\phi_i}{n_i} \ln \phi_i + \sum_{i<j} \chi_{i,j} \phi_i \phi_j. \tag{2.126}$$

By using the relation $\Delta\mu_i = (\partial \Delta F/\partial N_i)_{N_j, T}$, we can find the chemical potential $\Delta\mu_i$ of the i-th component as

$$\frac{\beta \Delta\mu_i}{n_i} = \frac{1}{n_i}(1 + \ln \phi_i) - \nu + \sum_k \chi_{i,k} \phi_k - \sum_{j<k} \chi_{j,k} \phi_j \phi_k, \tag{2.127}$$

where the number N_i of chains of the i-th component is related to the total number $N = \sum_i n_i N_i$ of lattice cells. As in the two-component blends and solutions, the total number of mass centers in the system is given by

$$\nu \equiv \sum_{i=1}^{c} \phi_i / n_i. \tag{2.128}$$

In particular, for the three-component blends P1/P2/P3, the Gibbs determinant is

$$D = \begin{vmatrix} \partial \Delta\mu_1/\partial \phi_1, & \partial \Delta\mu_1/\partial \phi_2 \\ \partial \Delta\mu_2/\partial \phi_1, & \partial \Delta\mu_2/\partial \phi_2 \end{vmatrix}, \tag{2.129}$$

because the chemical potentials fulfill the Gibbs–Dühem relation, and hence two of the three components are independent.

The condition $D = 0$ should be calculated to find the stability limit. We find that the spinodal condition is given by

$$\sum_{i=1,2,3} n_i \phi_i - 2 \sum_{i<j} \chi_{i,j} n_i n_j \phi_i \phi_j - \tilde{\chi} n_1 n_2 n_3 \phi_1 \phi_2 \phi_3 = 0, \tag{2.130}$$

where $\tilde{\chi} \equiv \chi_{1,2}^2 + \chi_{2,3}^2 + \chi_{3,1}^2 - 2\chi_{1,2}\chi_{2,3} - 2\chi_{2,3}\chi_{3,1} - 2\chi_{3,1}\chi_{1,2}$.

If we assume the interaction parameter takes the form (2.106), the temperature coefficient B is positive; the polymers are more easily dissolved into the solvents at higher temperature. Hence the solutions phase separate at low temperatures with an **upper critical solution temperature** (UCST). Many polymers dissolved in organic solvents show a phase separation of the UCST type. Aqueous solutions of polymers, however, often exhibit the opposite tendency. They dissolve more easily at low temperatures. Hence the solutions separate into two phases with a **lower critical solution temperature** (LCST) on heating.

Some water-soluble polymers, such as poly(ethylene oxide), have the phase separation region of loop shape on the temperature–concentration plane. The cohesive energy due to van der Waals interaction is not sufficient to explain their phase behavior. Hydrogen

bonds and hydrophobic interaction, combined with van der Waals-type interaction, must be considered to have a negative temperature coefficient ($B < 0$).

Phenomenological analyses are often attempted by using the free energy in the form

$$\mathscr{F}(\phi) = \frac{\phi_1}{n_1} \ln \phi_1 + \frac{\phi_2}{n_2} \ln \phi_2 + g(\phi, T)\phi_1\phi_2 \qquad (2.131)$$

with the interaction parameter $g(\phi, T)$, which is allowed to vary with the concentration. In particular, the form

$$g(\phi, T) = h/T + g_1(\phi_2) \qquad (2.132)$$

is often used, where h is a constant, or depends only upon the pressure [11]. Such analyses were first applied to the mixtures of interacting gases by Van Laar, and later developed for liquid mixtures by Heitler [14], Hildebrand [5], and Scatchard [15]. Because the molecular foundation of the phenomenological description was done by Bragg and Williams for metallic alloys, the theoretical framework is called **VLBW theory** in [11], after their initials.

2.3.4 Refinement beyond the simple mean field approximation

Many refinements of the Flory–Huggins theory (FH theory) of polymer solutions have been attempted ever since it was proposed in the 1940s. The first one is the detailed study of the mixing entropy and its improvement. The second is to take the semiflexibility of the polymer chains into the theoretical framework. The third is to consolidate its interaction term to accommodate specific interactions such as hydrogen bonds, dipole interaction, hydrophobic force, etc.

Refinement of the mixing entropy

The mixing entropy (2.91) of FH theory is known to be widely applicable under the condition that the **free volume** of each component in the mixture is proportional to its molecular volume, as was pointed out by Huggins [9] and Hildebrand [5, 16]. We try to derive its refined form by employing the detailed probability (2.85) of the monomer–solvent contact in the counting problem of the number of possible arrangements of polymers on the lattice.

Let us start from the number of possible arrangements $W(N_0, N_1)$ (2.83), and use the detailed form (2.85) of the monomer-solvent contact probability (**surface contact**) for ν_{j+1}.

Because the product of $R_{j,k}$ can be transformed to

$$\prod_{k=1}^{n-1} R_{j,k} = \left(\frac{z}{2}\right)^{n-1} \frac{(N - jn - 1)![zN/2 - (n-1)(j+1)]!}{[N - n(j+1)]![zN/2 - (n-1)j]!}, \qquad (2.133)$$

we find

$$W(N_0, N_1) = \frac{N!}{N_1!N_0!} \left(\frac{\delta_{\max}}{\sigma}\right)^{N_1} \left(\frac{z}{2}\right)^{(n-1)N_1}$$

$$\times \frac{[\{[(z-2)n+2]N_1+zN_0\}/2]!}{(zN/2)!}. \quad (2.134)$$

By applying Starling's formula,

$$(\alpha N)! \simeq (\alpha N/e)^{\alpha N} \simeq (N!)^{\alpha} \alpha^{\alpha n}, \quad (2.135)$$

this is approximately equal to

$$W(N_0, N_1) \simeq \left(\frac{\delta_{\max}}{\sigma}\right)^{N_1} \frac{N!}{N_1!N_0!} \left\{\frac{(N_0+qN_1)!}{(N_0+nN_1)!}\right\}^{z/2}, \quad (2.136)$$

where parameter q is the numerical constant defined by the relation

$$\frac{z}{2}(n-q) = n-1. \quad (2.137)$$

For the entropy, we have

$$-\Delta_{\mathrm{mix}}S(N_0, N_1)/k_B = N_0 \ln \frac{N_0}{N_0+nN_1} + N_1 \ln \frac{nN}{N_0+nN_1}$$

$$+ \frac{1}{2}z(N_0+qN) \ln \frac{N_0+nN_1}{N_0+qN_1} - \frac{1}{2}zqN_1 \ln \frac{n}{q}. \quad (2.138)$$

The last two terms are corrections to the FH mixing entropy.

Guggenheim generalized this result to the mixtures of two components with arbitrary molecular volumes, and found that the mixing entropy is given by [17]

$$- \Delta_{\mathrm{mix}}S(N_A, N_B)/k_B$$

$$= N_A \ln \frac{n_A N_A}{n_A N_A + n_B N_B} + N_B \ln \frac{n_B N_B}{n_A N_A + n_B N_B}$$

$$+ \frac{1}{2}zq_A N_A \ln \frac{q_A(n_A N_A + n_B N_B)}{n_A(q_A N_A + q_B N_B)} + \frac{1}{2}zq_B N_B \ln \frac{q_B(n_A N_A + n_B N_B)}{n_B(q_A N_A + q_B N_B)}, \quad (2.139)$$

where q_A, q_B are the numerical constants defined by the relations

$$\frac{z}{2}(n_i - q_i) = n_i - 1 \qquad (i = A, B). \quad (2.140)$$

These results are an improvement of the simple molecular-field approximation, and are referred to as the **quasi-chemical approximation**. It is known to be equivalent to the **Bethe approximation** in the theory of ferromagnets.

Lattice theory of semiflexible polymers

So far, polymer chains have been assumed to be perfectly flexible; there is no energy difference in trans and gauche. Each subsequent statistical unit can be placed in any one of the nearest neighboring (n.n) cells at equal probability. For semiflexible chains, the energy for bending the chain should be considered.

Consider the second bond from one end of a polymer chain and all the rest of the bonds. Each of these bonds can be connected to one of the $z - 1$ n.n. cells, among which the one in the straight direction produces a trans position, and the other $z - 2$ produces gauche positions. Let the trans conformation be the reference position for which the energy is $\epsilon = 0$ (trans), and let $\epsilon_i = \epsilon$ (gauche) be the energy for a gauche position.

Let f be the probability for an arbitrarily chosen bond to be in the gauche position. In lattice theory, the hypothetical crystalline state in which polymers are all trans position and regularly arranged is chosen as the reference state (see Figure 2.15). For semiflexible chains, the disorientation is not complete. The chain entropy remains at

$$\Delta_{\mathrm{conf}} S(n, f)/k_{\mathrm{B}} = \ln \left[\frac{nz(z-2)^{(n-2)f}}{\sigma e^{n-1}} \right]$$
$$- (n-2)[f \ln f + (1-f) \ln (1-f)], \qquad (2.141)$$

in the state defined above. The factor $(z-2)^{(n-2)f}$ appears because there are $(n-2)f$ gauche bonds.[3] The second term is the entropy to choose the trans bonds among the total $n - 2$ bonds.

The enthalpy change accompanying such conformation change is

$$\Delta_{\mathrm{conf}} H = f\epsilon(n-2). \qquad (2.142)$$

The entropy of mixing solvent to the polymers in such disoriented chains is the same as that of FH theory, so that the total free energy is

$$\beta \Delta F(N_0, N_1; f) = N_0 \ln \phi_0 + N_1 \ln \phi_1 + N \chi(T)\phi_0 \phi_1 + N_1 \beta \Delta_{\mathrm{conf}} F(n, f), \quad (2.143)$$

where

$$\beta \Delta_{\mathrm{conf}} F(n, f) \equiv -\ln \left[\frac{nz(z-2)^{(n-2)f}}{\sigma e^{n-1}} \right]$$
$$+ (n-2)[f \ln f + (1-f)\ln(1-f) + \beta\epsilon f] \qquad (2.144)$$

is the conformational free energy per chain.

Let us minimize the total free energy by changing f, and find the most probable (equilibrium) value f^*. By differentiation, we find

$$f^* = (z-2)e^{-\beta\epsilon}/[1 + (z-2)e^{-\beta\epsilon}]. \qquad (2.145)$$

---

[3] In the original paper [8], the second bond is not included in the trans-gauche category because of its strict definition presented in Figure 1.1 in Section 1.1. Hence the number of gauche bonds is $(n-3)f$.

On substitution back into the total entropy, we find it is given by

$$\Delta S(N_0, N_1; f^*)/k_B$$
$$= -N_0 \ln \phi_0 - N_1 \ln \phi_1$$
$$+ (n-2)N_1 \left\{ \left[\frac{(z-2)e^{-\beta\epsilon}}{1+(z-2)e^{-\beta\epsilon}} \right] \beta\epsilon + \ln[1+(z-2)e^{-\beta\epsilon}] - \frac{n-1}{n-2} \right\}. \tag{2.146}$$

For instance, $f^* = (z-2)/(z-1)$ for completely flexible chains for which $\epsilon = 0$, and hence

$$\Delta_{conf} S(n, f^*)/k_B = \ln \left[\frac{nz(z-1)^{(n-2)}}{\sigma e^{n-1}} \right]. \tag{2.147}$$

The entropy reduces to the FH form $\delta_{max} = z(z-1)^{n-2}$.

For a perfectly rigid rod, the bending energy takes the limiting value $\epsilon \to \infty$, so that we have $f^* \to 0$, and

$$\Delta_{conf} S(n, 0)/k_B = \ln \left[\frac{nz}{\sigma e^{n-1}} \right]. \tag{2.148}$$

This is the entropy of rigid rods in the disordered phase.

Entropy catastrophe and the glass transition

To study the volume change (compressibility) of the melts of semiflexible polymers, we consider a special case where the solvent component is the vacancy. Because the volume occupied by the **vacancy** (the **free volume**) is $N_0 a^3 = (N - nN_1)a^3$, the mixing free energy is given by $\Delta_{mix} F(N - nN_1, N_1)$ in (2.143). The pressure is therefore derived by the differentiation

$$pa^3 = -\left(\frac{\partial \Delta_{mix} F}{\partial N} \right), \tag{2.149}$$

from fundamental law of thermodynamics. The pressure turns out to be the chemical potential of the vacancy $pa^3 = -\Delta\mu_0$.

For flexible polymers, this relation leads to the equation of state

$$\ln(1-\rho) + (1-1/n)\rho + \chi\rho^2 + \tilde{p} = 0, \tag{2.150}$$

where $\rho \equiv \phi$ is the density of the polymer, $\tilde{p} \equiv pa^3/k_B T$ is the dimensionless pressure, and χ is the polymer–vacancy surface interaction parameter.

For semiflexible polymers, however, one realizes that there is a temperature T_2 at which the total entropy (2.146) satisfies the condition

$$\Delta S(N_0, N_1; f^*) = 0, \tag{2.151}$$

under a given volume fraction $\phi_0 = 1 - \rho$ of the free volume. At temperatures below T_2, polymer chain rigidity is so high that chain packing at a given free volume ϕ_0 becomes impossible ($\Delta S = 0$). The system is frozen in the state at temperature T_2. Gibbs and

Dimarzio [18] identified this state of vanishing entropy as the **entropy catastrophe** introduced by Kauzmann [19], and regarded T_2 as the **glass transition temperature T_g** of the polymer. Because the temperature derivative of the entropy is discontinuous if the entropy is kept constant at $\Delta S = 0$ below T_2, the glass transition on the basis of this picture is classified into a second-order transition by **Ehrenfest's definition**.

As an example, for polystyrene of $n = 200$, the trans-gauche energy difference is $\epsilon = 1.44\,\mathrm{kcal\,mol^{-1}}$, or $\epsilon/k_B T_g = 1.27$. For the observed free volume $\phi_0 = 0.025$ at the glass transition temperature, the flexibility is estimated to be $f^* = 0.359$. Therefore, 36% of the bonds are in the gauche position.

Let us next consider the total free energy (2.143) for a polymer melt with no vacancy ($\phi_0 = 0, N_1 \equiv N$). If $\Delta F(0, N; f) < 0$, the disordered amorphous state is thermally more stable than the crystalline state chosen as the reference state. In order for this condition to be fulfilled, the flexibility must satisfy [20]

$$f > 1 - \left[\frac{nz(z-1)}{\sigma e^{n-1}} \right]^{1/(n-2)} \tag{2.152}$$

In the limit $n \to \infty$ of high-molecular weight polymers, this condition reduces to

$$f_c = 1 - 1/e = 0.63 \tag{2.153}$$

The flexibility must be larger than 0.63 for the existence of a stable disordered phase. Compared with the maximum flexibility $f^* = 0.80$ for $z = 6, \epsilon = 0$, this critical value is very high. If this condition breaks down, or if there exists a temperature T_m at which the condition

$$\Delta F(0, N; f) = 0 \tag{2.154}$$

is fulfilled, **crystallization** of the liquid state takes place. Crystallization is a first-order phase transition and associated with the latent heat $(1 - 1/e)[-T^2(\partial(\epsilon/T)/\partial T)_p]$

Counting problem of the Hamiltonian paths

Let us consider the conformation of a single chain in the special case of a disordered state with no vacancy. Fixing $N_0 = 0, N_1 = 1$ in the theory developed above, the number $W_H(n)$ of paths that visit all lattice points (cells) without overlap, referred to as **Hamiltonian path**, is found [21]. Within the theoretical framework (2.146) described in the preceding sections, the entropy of Hamiltonian paths is estimated by

$$\Delta S = (n-2) \left\{ \left[\frac{(z-2)e^{-\beta\epsilon}}{1 + (z-2)e^{-\beta\epsilon}} \right] \beta\epsilon + \ln[1 + (z-2)e^{-\beta\epsilon}] - 1 \right\}. \tag{2.155}$$

The single-chain glass transition temperature is found by the condition

$$\frac{(z-2)e^{-\beta\epsilon}}{1 + (z-2)e^{-\beta\epsilon}} \beta\epsilon + \ln[1 + (z-2)e^{-\beta\epsilon}] - 1 = 0. \tag{2.156}$$

By fixing $\epsilon = 0$ in ΔS, in the limit of long chain the number takes the form

$$\lim_{n \to \infty} \frac{1}{n} \ln W_H(n) \equiv \ln \omega_H, \qquad (2.157)$$

where ω_H is the number of Hamiltonian paths per monomer.

For example, the entropy of polymers within FH theory described above gives

$$\omega_H = (z-1)/e. \qquad (2.158)$$

Quasi-chemical approximation gives

$$\omega_H = (z-1) / \left[\frac{z}{z-2} \right]^{(z-2)/2} \qquad (2.159)$$

The following are known regarding the number of Hamiltonian paths:

(1) The exact solution on the honeycomb lattice ($z=3$) in two dimensions [21] is given by

$$W_H(n) = (\sqrt{6n} - 3)2^{\sqrt{n/6}} \qquad (2.160)$$

where $\sqrt{n/6}$ is the number of layers counted from the central cell. The entropy per monomer vanishes in the long chain limit, so that the residual entropy (2.157) is 0, and $\omega_H = 1$. Hence the degeneracy does not reach $O((\text{const})^n)$

(2) For a two-dimensional square lattice ($z=4$), FH theory gives $\omega_H = 1.104$. The upper bound can be estimated by using **ice model** [22] to be $\omega_H = (4/3)^{3/2} = 1.5396$. Numerical simulation evaluates $\omega_H = 1.38$. The estimate of the lower bound is possible by using the model of the Manhattan walk [23]. The **Manhattan walk** is a Hamilton walk on the **directed lattice**. Walks have to follow the arrows on the edges, which are alternately up/down and left/right, as the traffic regulation in Manhattan downtown.

Exact solution of Manhattan walks on the square lattice is known. The number of walks is given by

$$W_H(n) = e^{Cn/\pi} = (1.338\,515\,152\ldots)^n = e^{0.292n}, \qquad (2.161)$$

where the constant C (Catalan's constant) is defined by the series

$$C \equiv 1 - \left(\frac{1}{3} \right)^2 + \left(\frac{1}{5} \right)^2 - \cdots = 0.915\,965\,594 \cdots . \qquad (2.162)$$

(3) Miscellaneous [21]–for a three-dimensional diamond lattice ($z=4$), the lower bound is known to be $\omega_H = 1.398$. For the simple cubic lattice, the lower bound is $\omega_H = 1.810$, while FH theory gives $\omega_H = 1.84$.

2.4 Scaling laws of polymer solutions

In Section 1.6, we referred to the scaling laws for the conformation of a single chain in dilute solutions. Starting with them, we develop in this section scaling laws for the structural and thermodynamic properties of polymer solutions in concentrations that range from dilute to concentrated, and also cover a wide temperature range [24].

2.4.1 Overlap concentration

Random coils of polymers are separated from each other in a dilute solution. With an increase in the concentration of the solution, the mean distance between them is reduced, and they start to overlap. With a further increase in concentration, the polymers interpenetrate each other so deeply that the properties of each individual chain become difficult to observe (Figure 2.19). The concentration at which polymers start to overlap is called the **overlap concentration**. The overlap concentration can be found by the condition such that the volume fraction na^3/R^3 of monomers within the region occupied by the random coil of each polymer becomes the same order as that of the concentration ϕ of the solution

$$na^3/R^3 \simeq \phi, \tag{2.163}$$

where R is the mean radius of gyration of the random coil. (We shall neglect the numerical factor of order unity in all equations in this section as in Section 1.6.)

Let us first find the overlap concentration for various temperature regions. In the high-temperature region where Flory's law $R = R_F = a\tau^{1/5}n^{3/5}$ holds, we find from (2.163) that

$$\phi^* = \tau^{-3/5}n^{-4/5}. \tag{2.164}$$

The overlap is indicated by the symbol $*$. The superscript indicates that the property is in the high-temperature region. For high-molecular weight polymers, the number n of the repeat units is so large that the overlap concentration is small. For example, it is approximately $\phi^* = 0.1\%$ for $n = 10^4$.

dilute region   overlap concentration   semiconcentrated region
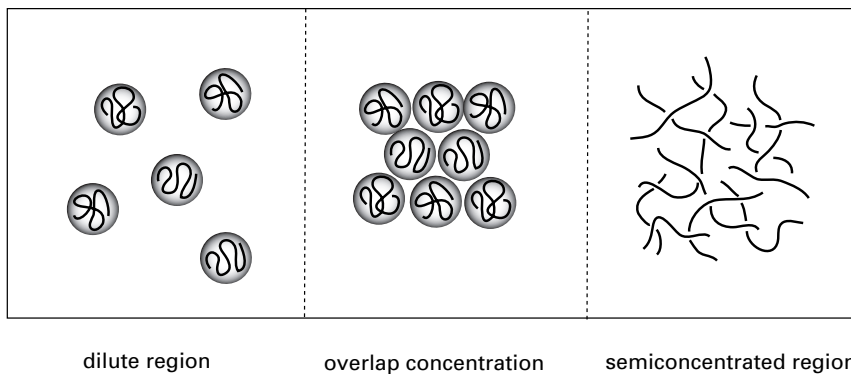
Fig. 2.19   Change in the structure of a polymer solution with varied concentration.

Alternatively, the overlap concentration can be defined as the concentration at which the number of chains contained in the volume occupied by one random coil chain is just one. If R is considered to be the hydrodynamic radius R_H, this number is $(4\pi R_H^3/3)(c/M) \simeq c[\eta]$. Therefore we have

$$c^*[\eta] \simeq 1 \tag{2.165}$$

at the overlap concentration.

Similarly, in the theta region where $R = R_\theta = an^{1/2}$ holds, we find

$$\phi* = n^{-1/2}. \tag{2.166}$$

It is independent of the temperature. The symbol $*$ at the side of a letter indicates that the property is in the theta region.

Finally, in the low-temperature region where $R = R_G = a\tau^{-1/3}n^{1/3}$ holds, we find

$$\phi_* = |\tau|. \tag{2.167}$$

The subscript $*$ indicates that the property is in the low-temperature region. The results are summarized by the boundary lines (thick lines) on the temperature–concentration phase plane in Figure 2.20. The liquid–liquid phase separation line (coexistence curve) in the low-temperature region is shown by the solid line in the figure.
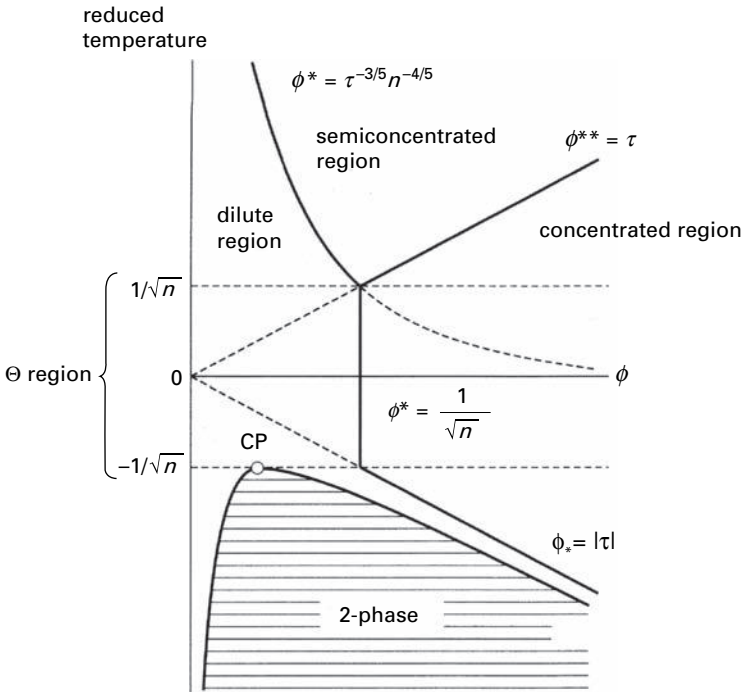
Fig. 2.20   Scaling laws of polymer solutions shown on the temperature–concentration phase plane.

2.4.2 Correlation length

At concentrations higher than the overlap concentration, polymers interpenetrate each other and form a structure like entangled network. The average size ξ of the mesh in such a network, the region where there is no polymer segment, is the **correlation length** (Figure 2.21). It is more precisely defined by the mean distance where the effect of fluctuation in the concentration at one space point is propagated (the correlation length of the concentration fluctuations). Above the overlap concentration, the correlation length is smaller than the mean radius of gyration.

To find ξ as a function of the concentration and temperature, let us assume that it obeys the power law

$$\xi = R \left(\frac{\phi}{\phi^*} \right)^m \tag{2.168}$$

of the ratio ϕ/ϕ^*, the polymer concentration divided by the reference value of the overlap concentration. Such an assumption that a physical quantity does not depend on the temperature and concentration independently, but depends on the combined variable ϕ/ϕ^*, is called the **scaling assumption**.

For concentrations well above the overlap concentration, the radius of gyration of a random coil is larger than the correlation length ($R \gg \xi$), so that the molecular weight will not affect the correlation length. In the high-temperature region, by using Flory's exponent for $R = R_F$, and assuming that (2.168) is independent of n in the region $\phi \gg \phi^*$, we find the power exponent m to be $m = -3/4$. Hence, the correlation length depends on the concentration and the temperature as

$$\xi = a(\phi \tau^{1/3})^{-3/4}. \tag{2.169}$$

A similar argument for the theta region leads to $\xi = a\phi^{-1}$; the correlation length is independent of the temperature.

For the low-temperature region, it is impossible to find the solution for which ξ is independent of n. This indicates that it is impossible for the compact globules to
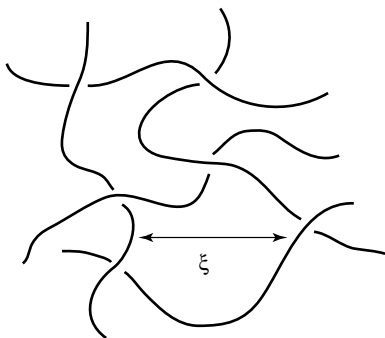
Fig. 2.21 Correlation length in a semiconcentrated polymer solution.

interpenetrate each other no matter how high the concentration becomes. Hence, the concept of correlation length does not work in this region.

2.4.3   Radius of gyration

When polymer chains overlap, they take conformations that are different from those of isolated individual chains because monomers interact in a different way. Figure 2.22 schematically shows the conformation of a polymer chain in a concentration well above the overlap concentration. It has a structure like a pearl-necklace; a train of blobs (called a **concentration blob**) made up of groups of monomers connected in sequence. The size of each concentration blob is called the correlation length ξ. The monomers in the blob are directly in contact with the solvent so that they swell by the excluded-volume effect, in the same way as an isolated random coil does.

Let g_ϕ be the number of monomers in a concentration blob. Since the number density g_ϕ/ξ^3 inside the blob must be equal to the concentration ϕ/a^3 of the solution, we find

$$g_\phi/\xi^3 = \phi/a^3. \tag{2.170}$$

Substituting (2.169) into this, we find

$$g_\phi = (\phi\tau^{3/5})^{-5/4}. \tag{2.171}$$

This is much larger than the number of monomers $g_\tau = 1/\tau^2$ in the temperature blob studied in Section 1.6.

Similarly, in the theta region, we fix $\xi = a/\phi$ and find

$$g_\phi = \phi^{-2}. \tag{2.172}$$
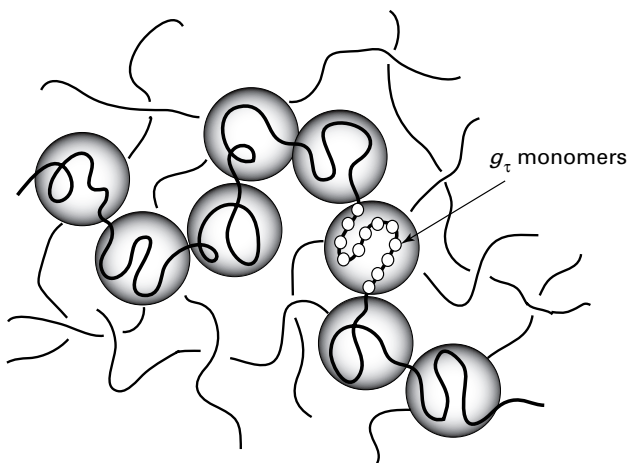
Fig. 2.22   Concentration blob describing the conformation of a polymer in a semiconcentrated solution. Blobs of the diameter ξ are sequentially connected.

When the chain is seen as a whole with blobs as the structural repeat unit, the excluded-volume effect by monomer interaction is screened by the presence of the blobs of other chains, and hence considered to behave as an ideal chain. If we assume such a **screening effect**, the radius of gyration is given by

$$R^2 = \left(\frac{n}{g_\phi}\right)\xi^2,\tag{2.173}$$

since there are n/g_ϕ blobs per chain. In the high-temperature region, this relation gives

$$R^2 = (na^2)\left(\frac{\tau}{\phi}\right)^{1/4}.\tag{2.174}$$

This result is called the **Daoud radius of gyration**, since it was found by Daoud [24].

This equation suggests that, if the concentration is increased still further at a fixed temperature τ, the radius of gyration becomes the same order as the Gaussian chain $R^2 = na^2$ at the concentration satisfying the condition

$$\phi \simeq \phi^{**} \equiv \tau.\tag{2.175}$$

In other words, the screening is so perfect that a blob reaches the size of a monomer. Although many chains are entangled and interpenetrated with each other in complex ways in the concentrated solution, each chain takes a very simple Gaussian conformation as a result of the cancelation of the excluded-volume interaction. Because Flory first noticed this fact [10], it is sometimes referred to as the **Flory theorem**. The assertion that the chain conformation becomes simple in the limit of high concentration was initially difficult for researchers to accept, but it was proved in the 1970s when neutron scattering experiments using labeled polymers succeeded in directly observing polymer conformation.

The high-temperature concentrated region can therefore be divided into two parts: the lower one covering the range $\phi^* < \phi < \phi^{**}$ is called the **semiconcentrated region**, while the higher one with $\phi^{**} < \phi$ is called the **concentrated region** (Figure 2.20).

In the theta temperature region, the solution changes directly into the concentrated region on crossing the overlap concentration. All of these results are summarized in the phase diagram shown in Figure 2.20.

2.4.4 Osmotic pressure

Let us apply the scaling concept to the osmotic pressure of polymer solutions in a good solvent (in the high-temperature region). The osmotic pressure π, when multiplied by the volume of a repeat unit a^3, gives the negative chemical potential of a solvent molecule (2.28), or equivalently the free energy necessary to remove a solvent molecule from the solution. If we compare this with the thermal energy $k_B T$, the ratio should give the number density ϕ/n of the polymer chains by van't Hoff's law (2.36) in the dilute region.

In the semiconcentrated region, let us assume the scaling form

$$\frac{\pi a^3}{k_B T} = \frac{\phi}{n} \left(\frac{\phi}{\phi^*} \right)^m,$$

(2.176)

as usual with the fractional power m of the reduced concentration. The power index is fixed to be $m = 5/4$ by the condition that the osmotic pressure should not depend on the molecular weight of the polymer. Hence we have

$$\frac{\pi a^3}{k_B T} = (\tau \phi^3)^{3/4}.$$

(2.177)

As this depends on the fractional power $9/4$ of the concentration, it is impossible to reach this result no matter how higher-order terms in the perturbational calculation are obtained. It has an exponent higher by $1/4$ than the exponent of the second virial term. Around the overlap concentration where the volume fraction is numerically $\phi \sim 10^{-3}$, this discrepancy cannot be neglected.

The result can be summarized in compact form as

$$\frac{\pi \xi^d}{k_B T} = C,$$

(2.178)

where $d = 3$ is the space dimension, C is a numerical constant of order unity. The left-hand side of this equation gives the dimensionless free energy contained in a space region of size ξ in the solution. Comparing with van't Hoff's law $\pi V = N k_B T$ for an ideal solution (V is the total volume, N the number of polymer chains), the volume V/N per chain is replaced by the correlation volume ξ^3 in the semiconcentrated solutions. The result (2.178) for the osmotic pressure is called **des Cloizeaux's scaling law**.

2.4.5   Phase equilibria (reduced equation of states)

We saw in Section 2.3 that polymers have generally low solubility; they easily separate into different phases, or precipitate in the solutions. The molecular weight plays a very important role in the solubility of polymers. Because the phase boundaries shift with the molecular weight, phase diagrams are usually constructed for samples with different molecular weights. The result may be presented by using three-dimensional phase space with an extra axis of molecular weight added to the temperature and concentration (Figure 2.17(b)).

The phase diagrams of polymer solutions reveal asymmetric characteristics due to the volume difference between solute and solvent molecules. The critical concentration is very low, and shifts toward a lower concentration with the molecular weight (Figure 2.17(a)). The critical point approaches the theta point in the limit of high molecular weight.

In Figure 2.17(b), temperature is measured by the dimensionless temperature deviation $\tau \equiv 1 - \Theta/T$ from the theta temperature. The molecular weight is represented by
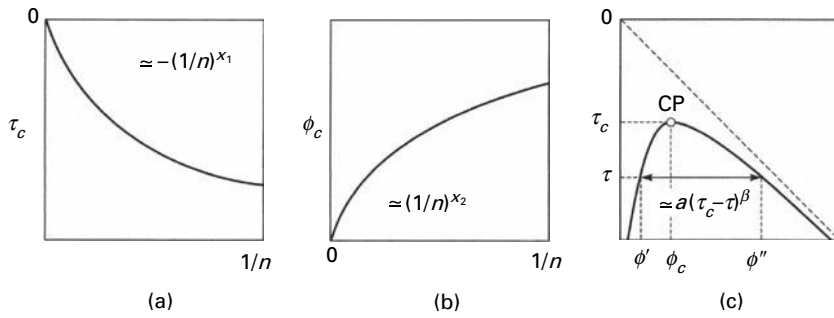
Fig. 2.23 Scaling laws near the critical point of the polymer solutions. (a) Critical line on the temperature–molecular weight plane, (b) critical line on the concentration–molecular weight plane, (c) coexistence line on the temperature–concentration plane

the reciprocal of the number of the repeat units. The coexistence curves for different molecular weight form a **coexistence surface**. The line connecting the critical points is the **critical line**.

The critical line when projected onto the $(\tau, 1/n)$ plane rises from the origin in the form

$$|\tau_c(n)| \sim g_1 \left(\frac{1}{n}\right)^{x_1}, \tag{2.179}$$

where g_1 is a numerical constant and x_1 is the **crossover index** (Figure 2.23(a)). The crossover index takes a value of around 0.5.

Similarly, when projected onto the $(\phi, 1/n)$ plane, the critical line rises as

$$\phi_c(n) \sim g_2 \left(\frac{1}{n}\right)^{x_2}, \tag{2.180}$$

where the other crossover index is given by $x_2 = \nu_\theta d - 1$ ($\nu_\theta = 1/2$ is the scaling index of the radius of gyration (1.77) in the theta region, and d is the space dimension) (Figure 2.23(b)). It takes a value around 0.5.

The coexistence curve on the (τ, ϕ) plane for a fixed molecular weight can be scaled in the form

$$\frac{\tau}{\tau_c} = F\left(\frac{\phi}{\phi_c(n)}\right), \tag{2.181}$$

by using the critical values. This is the **reduced equation of state** for the polymer solutions. The width of the coexistence curve obeys the scaling law

$$\phi'' - \phi' = a(n)(\tau_c(n) - \tau)^\beta, \tag{2.182}$$

near the critical point (Figure 2.23(c)), where ϕ'' is the concentration of the higher concentration phase, and ϕ' is that of the lower concentration phase. The **critical exponent** β takes a value around $\beta = 0.31$.

The osmotic compressibility is divergent near the critical temperature in the form

$$K_T \propto |\tau - \tau_c(n)|^{-\gamma}, \tag{2.183}$$

where the exponent γ is around 1.25. The divergence originates in the concentration fluctuations with large spatial scales. The power laws that characterize the type of singularity are called the **scaling laws of critical phenomena**. The critical exponents are known to be universal; they do not depend on the details of the materials studied, but only on the spatial dimensions, the internal symmetry of the system, and the range of interaction (short- or long-range interaction). The critical exponents of polymer solutions are known to be the same as those of the Ising model for ferromagnets [24].

2.4.6   Molecular motion

Let us next consider how the blob chains move in the semiconcentrated solution. The chain cannot move freely because it is entangled with other chains in the neighborhood. Such a constraint is called a **topological constraint**, since the force originates in the entanglements and has a more topological nature than a geometrical one.

When there is a fluctuation in the concentration, the polymer under study tries to move to fill the vacancy in the low-concentration region, but it is impossible for the whole chain to move simultaneously due to the topological constraints. Instead, a blob plays a role of the moving unit. It can diffuse into the neighborhood to restore the concentration back to the average value. This movement can be seen as a diffusion of a rigid sphere of radius ξ in the solvent, so that the diffusion constant D_c is estimated to be

$$D_c = \frac{k_B T}{6\pi \eta_0 \xi} = D_0 \tau^{1/4} \phi^{3/4}, \qquad (2.184)$$

by the Einstein relation, where $D_0 \equiv k_B T / 6\pi \eta_0 a$ is the self-diffusion constant of a repeat unit, and η_0 is the viscosity of the solvent. Such a diffusive motion of the chain segments to adjust the concentration without violating topological constraint is called **cooperative diffusion**, or **gel mode**. The diffusion constant D_c is the **cooperative diffusion coefficient**.

Cooperative diffusion can be seen in a different way using the scaling idea. Let us assume that it takes a scaling form

$$D_c = D \left(\frac{\phi}{\phi^*} \right)^m, \qquad (2.185)$$

by using the marker diffusion constant $D = k_B T / 6\pi \eta_0 R_H$ (2.69). We apply the condition that D_c is independent of the molecular weight in the region $\phi > \phi^*$, and find $m = 3/4$.

The other possible motion under the topological constraints is that the blob moves along the confining tube surrounding it without large perpendicular motion. The movement is similar to that of snakes or earthworms, and is hence called **reptation** [25] (Figure 2.24).

Since there are n/g_ϕ blobs in a chain, the total length of the tube is $L_t = n\xi/g_\phi$. The friction coefficient of the viscous resistance working on a blob is $\zeta_b = 6\pi \eta_0 \xi$, the total friction is given by $\zeta_b n/g_\phi$. Hence, the diffusion coefficient D_t of the reptation is

$$D_t = k_B T / (n\zeta_b/g_\phi). \qquad (2.186)$$
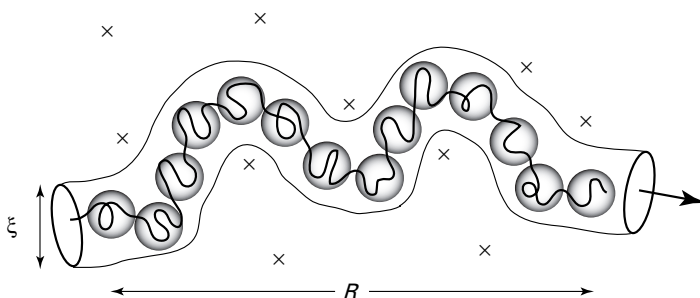
Fig. 2.24   The blob model of a polymer chain which reptates along the tube formed by the surrounding chains.

The time required for the original tube to disappear by the motion of the blob is the time for the chain to reptate the distance L_t, and hence it is given by $\tau_t = L_t^2/D_t$. Sustituting the relation $\xi = a(\phi\tau^{1/3})^{-3/4}$ and $g_\phi = (\tau^{1/3}\phi)^{-5/4}$ into this equation, we find

$$\tau_t = \tau_0 n^3 \phi^{3/2} \tau^{3/2}. \tag{2.187}$$

However, the displacement of the center of mass of the chain in the space is only its radius of gyration R. Therefore, by the fundamental relation (2.66) for the diffusion, the diffusion constant D_{rep} of the chain by reptation is

$$D_{rep} = R^2/\tau_t, \tag{2.188}$$

and from (2.187)

$$D_{rep} = D_0 n^{-2} \phi^{-7/4} \tau^{-5/4}, \tag{2.189}$$

where D_0 is the diffusion constant of a repeat unit, and $\tau_0 \equiv a^2/D_0$ is the microscopic time for a repeat unit to move a distance a.

The time τ_t is the relaxation time by reptation; it becomes longer in proportion to the third power of the molecular weight $\tau_t \simeq M^3$. The diffusion constant D_{rep} becomes smaller in proportion to $1/M^2$.

References

[1] Lewis, G. N.; Randel, M., *Thermodynamics*, 2nd ed. McGraw Hill: New York, 1961.
[2] Guggenheim, E. A., *Thermodynamics*. North-Holland: Amsterdam, 1967.
[3] Prigogine, I.; Defay, R., *Chemical Thermodynamics*. Longman: London, 1954.
[4] Prigogine, I., *The Molecular Theory of Solutions*. North-Holland: Amsterdam, 1957.
[5] Hildebrand, J. H.; Prausnitz, J. M.; Scott, R. L., *Regular and Related Solutions*. Van Nostrand Reinhold: New York, 1970.
[6] Graessley, W. W., *Polymeric Liquids & Networks: Structure and Properties*. Garland Science: London, 2004.
[7] Yamakawa, H., *Modern Theory of Polymer Solutions*. Harper & Row: 1971.

[8] Flory, P. J., *J. Chem. Phys.* **12**, 425 (1944).

[9] Huggins, M. L., *J. Chem. Phys.* **46**, 151 (1942).

[10] Flory, P. J., *Principles of Polymer Chemistry*, Chap. XII. Cornell University Press: Ithaca, 1953.

[11] Koningsveld, R.; Stockmayer, W. H.; Nies, E., *Polymer Phase Diagrams*, Oxford University Press: Oxford, 2001.

[12] Hansen, C. M., *Hansen Solubility Parameters – A User's Handbook*, 2nd edn. CRC Press: Boca Raton, 2007.

[13] Shultz, A. R.; Flory, P. J., *J. Am. Chem. Soc.* **74**, 4760 (1952).

[14] Heitler, W., *Ann. Physik* **80**, 630 (1926).

[15] Scatchard, G., *Chem. Rev*. **8**, 321 (1931).

[16] Hildebrand, J. H., *J. Chem. Phys.* **15**, 225 (1947).

[17] Guggenheim, E. A., *Mixtures*. Clarendon Press: Oxford, 1952.

[18] Gibbs, J. H.; Dimarzio, E. A., *J. Chem. Phys.* **28**, 373 (1958).

[19] Kauzmann, W., *Chem. Rev.* **43**, 219 (1948).

[20] Flory, P. J., *Proc. Roy. Soc., London* **A234**, 60 (1956).

[21] Gordon, M.; Kapadia, P.; Malakis, A., *J. Phys. A: Math. Gen.* **9**, 751 (1976).

[22] Lieb, E. H., *Phys. Rev. Lett.* **18**, 692 (1967).

[23] Kasteleyn, P. W., *Physica* **29**, 1329 (1963).

[24] de Gennes, P. G., *Scaling Concepts in Polymer Physics*. Cornell University Press: Ithaca, NY, 1979.

[25] Doi, M.; Edwards, S. F., *The Theory of Polymer Dynamics*. Oxford University Press: Oxford, 1986.

3 Classical theory of gelation

This chapter presents the definition of gels and gives some typical examples, followed by a description of their structures and fundamental properties. A statistical mechanical treatment of the chemical gels in the polycondensation reaction is developed to find the molecular weight distribution, average molecular weight, gel point, and the gel fraction.

3.1 What is a gel?

3.1.1 Definition of a gel

Gels are three-dimensional networks made up of molecules, polymers, particles, colloids, etc., that are connected with each other by the specific parts on them such as **functional groups** and **associative groups**. The connected parts are called **cross-links**. Gels usually contain many solvent molecules inside their networks, and hence they are close to liquid in composition, but show solid-like mechanical properties due to the existence of the cross-links [1–4].

Although this statement can be adopted as a formal definition of gels, there are many exceptional ones that do not fall neatly into this categorization. For instance, colloidal suspensions exhibit gel-like rheological behavior at high densities. Entanglements of long rigid fibrillar molecules or an assembly of molecules mutually hinder their motion, and lead to gel-like rheology due to jamming of the rigid segments. In such materials, there are no direct cross-links, but geometrical or topological constraints play similar roles to the cross-links, although they are delocalized. Therefore, to define gels by connectivity only is not sufficient to include these materials.

3.1.2 Classification of gels

Gels can be classified by their constituents. Gels made up of aggregated particles or colloids are **particulate gels**. Networks made up with covalent bonds, H-bonds, etc., of low molecular weight molecules are **low-mass gels**. Networks formed by cross-linking of the primary polymers are **polymeric gels**. If the primary molecules are biopolymers, gels are specifically called **biopolymer gels** [2].

Gels are also classified into chemical and physical ones by the persistence time (lifetime) of their cross-links. **Chemical gels** (or **strong gels**) have covalent bonds as the cross-links, so that the connection cannot be broken by thermal motion of the constituent

molecules. The topological structure of a chemical gel is therefore preserved as it is pre-pared [5]. Random variables with fixed statistical property but different assigned values depending on the sample are called **frozen variables**. A system with random variables as structural parameters is called a **random system**. Chemical gels are examples of ran-dom systems. A general theoretical scheme to treat random systems was developed by Edwards and his collaborators [6,7].

On the other hand, **physical gels** (or **weak gels**) are networks cross-linked by physical bonds. The binding energy is of the order of thermal energy, and hence cross-links can be reversibly formed and destroyed by a change in temperature. If the cross-links are sufficiently weak to be created and destroyed by the thermal motion of the constituents, the gels are often called **transient gels**.

In physical gels, the equilibrium between connected and disconnected states is reached if the average lifetime τ of the cross-links is shorter compared with the time of obser-vation. In the opposite case, the topological structure of the network is observed to be frozen [5]. Because gels are reversibly formed and melted by changing temperature and concentration, physical gels are also called **thermoreversible gels** [3,4]. However, not all gels are clearly classified into chemical and physical ones, but are distributed in-between the two extremities according to their lifetime.

According to this classification, gels with mobile cross-links, such as **sliding ring gels** [8], are chemical gels because the number of junctions is preserved. **Jamming gels** with delocalized cross-links should be regarded as viscoelastic fluids with long relaxation times. There are many gels in which both chemical and physical cross-links coexist.

3.1.3   Structure of gels and their characterization

Global structure of a network

A gel has the general network structure shown in Figure 3.1. The part of the chain connecting the neighboring cross-links is a **subchain**. The **branching number** of a cross-link is the number of subchains connected in it. It is shown by the number beside each cross-link. A chain with one end connected to a cross-link and the other end free to move is called a **free end chain** or **dangling chain**. A path circulating around part of the network along the subchains is a **cycle**. The total number of independent cycles is the **cycle rank** of the network. An entangled subchain whose topological relation is preserved is a **trapped entanglement**. The skeletal structure that remains after all free end chains have been removed is the **skeleton** of the network.

To characterize the structure of gels, parameters such as the number of cross-links μ, the number of **subchains** ν, and their average molecular weight M, the branching index of the cross-links ϕ, the number of free ends ν_{end}, and the cycle rank ξ should be specified [1].

For networks with cross-links of a fixed branch number ϕ, the following two geometrical relations hold:

$$\nu = (\mu\phi + \nu_{\text{end}})/2, \tag{3.1a}$$

$$\xi = \nu - (\mu + \nu_{\text{end}}) + 1. \tag{3.1b}$$
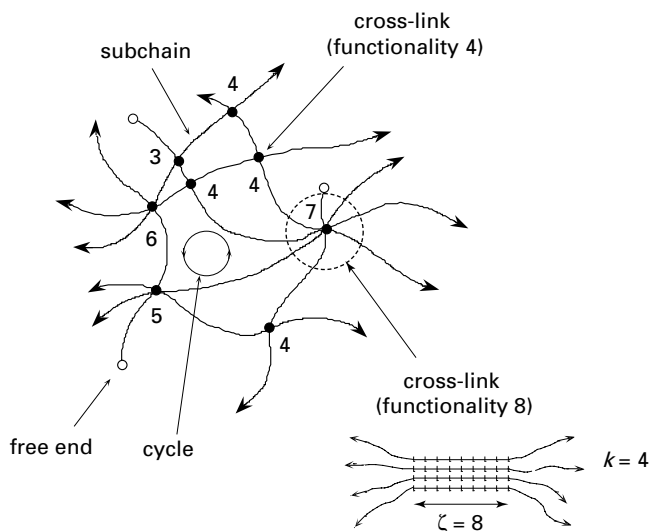
Fig. 3.1 Global structure (network topology) and local structure (cross-links) of a network. There are several fundamental parameters that characterize these structures.
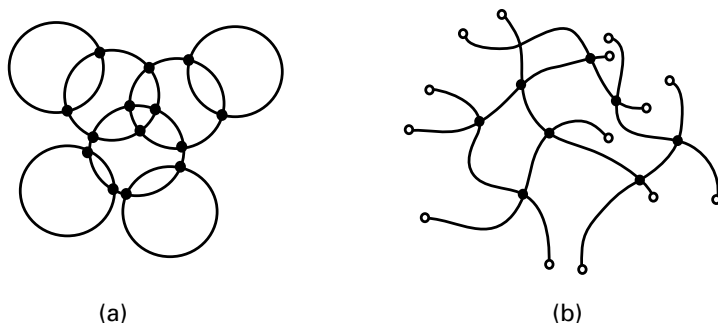
Fig. 3.2 Model networks: (a) perfect network, (b) network made by random cross-linking of primary polymers.

A network with no free ends is called a **perfect network** (Figure 3.2(a)). A network formed by pairwise cross-linking of the primary polymers is a **polymer network** whose number of free ends is twice as large as the number of primary chains (Figure 3.2(b)).

Local structure of the cross-links

Cross-link junctions are important for the elastic properties of gels. The number of chains k combined in a junction is its **multiplicity**, and the length ζ (in terms of the number of repeat units) is the **cross-link length** (Figure 3.1). Figure 3.3 shows a network formed by multiple cross-linking of trifunctional molecules. The number beside each junction shows its multiplicity. The multiplicity of the cross-links formed in polycondensation reaction, by cross-linking agencies, etc., is usually $k = 2$.
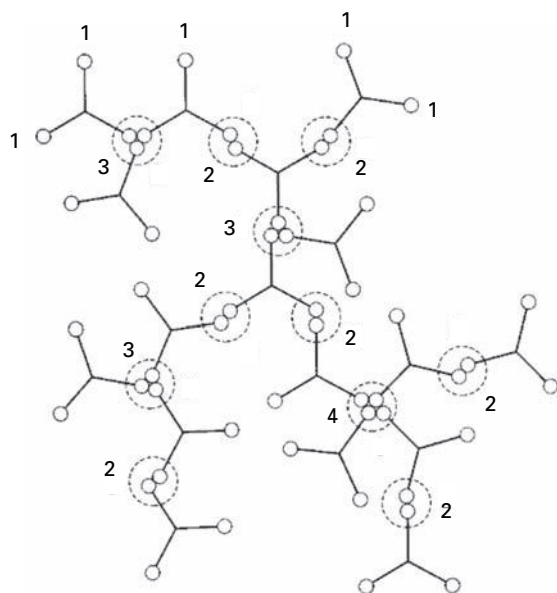
Fig. 3.3   Multiplicity of the cross-link junctions in the polycondensation of trifunctional molecules. Numbers beside the junction show their multiplicities. Unreacted groups can be regarded as cross-links with multiplicity 1.

3.1.4   Examples of gels

Chemical gels

Branched polymers are produced by the polycondensation of multifunctional molecules whose **functionality** is greater than or equal to 3. If the reaction proceeds to the stage where the products grow as large as the space dimensions of the entire system, a three-dimensional network whose parts are connected by covalent bonds is formed. This is the **gel point**. The reaction continues after this gel point is passed. The polycondensation reaction is irreversible under ordinary conditions, so that the gelation of chemical gels is irreversible.

Let us use the symbol R$\{A_f\}$ for a monomer unit carrying the number f of A functional groups, R$\{AB_{f-1}\}$ for a monomer carrying one A functional group and $f-1$ of B functional groups, etc.

As an example, let us consider esterification of tricalvaryl acid and ethyrene glicohol (Figure 3.4). Let us use the symbol A for a –COOH group, and –B for an –OH group. Tricalvaryl acid is the trifunctional monomer R$\{A_3\}$ and ethyrene glicohol is the bifunctional monomer R$\{B_2\}$. Since the esterification reaction is,

$$\underset{\underset{O}{\|}}{-\,C}\text{–O–H} + \text{HO–CH}_2\text{—} \longrightarrow \underset{\underset{O}{\|}}{-\,C}\text{–O–CH}_2\text{—} + \text{H}_2\text{O}$$
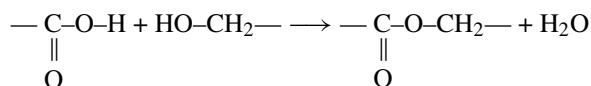
three-dimensional branched polymers are produced (Figure 3.4).
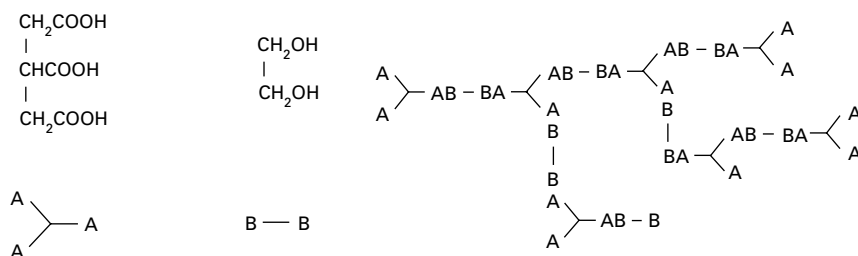
Fig. 3.4 Gelation by the polycondensation of trifunctional and bifunctional molecules.
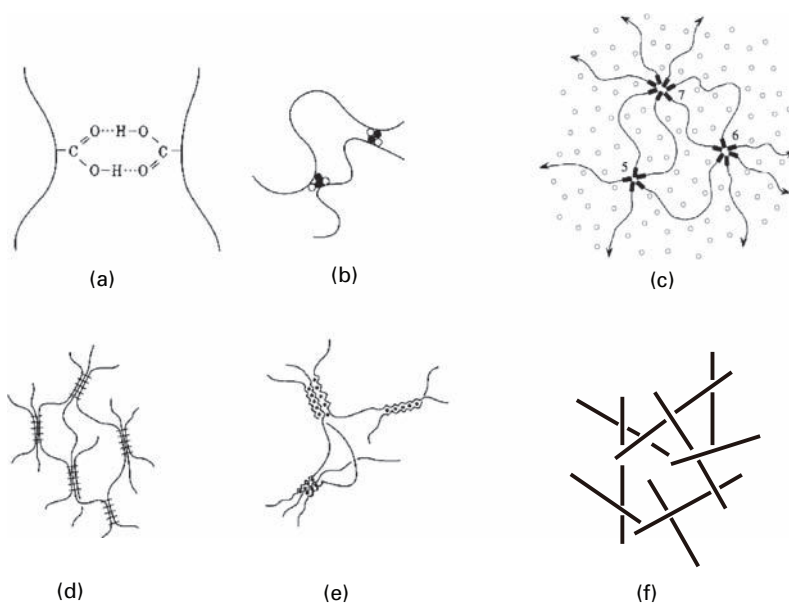
Fig. 3.5 Various types of physical cross-links: (a) hydrogen bonds, (b) dipole association, (c) micellar formation of hydrophobic groups, (d) microcrystalline junction, (e) ion association and complex formation, (f) entanglements of long rigid polymers.

Physical gels

Physical cross-linking often makes complex junctions. The cross-links are not strictly localized but extend in the form of junction zones.

(1) Hydrogen bonding

H-bonds between polymer chains form pairwise cross-links and bridge them (Figure 3.5(a)). The binding energy of an H-bond in a solution is of the order of the thermal energy, so that the bonds may easily break and recombine. If there is strong correlation between adjacent H-bonds, as in the complex formation between poly(ethyrene oxide)

and poly(acrylic acid), there is a tendency to form zipper-like contiguous sequences of H-bonds. These are called **cooperative H-bonds**. Cooperative H-bonds are often observed in the hydration of biopolymers and water-soluble polymers (Section 1.9). They can be the origin of the sharp conformational transitions of these polymers.

(2) Dipole interaction

If polymers carry dipole moments that are sparsely dispersed along the chains, they are cross-linked by aggregation of the dipole moments (Figure 3.5(b)). The aggregates (multiplets) are surrounded by the chain segments, so that there is an upper limit to the multiplicity. Ionomers, such as metal-sulfonated polystyrene, in a nonpolar solvent, are typical examples.

(3) Hydrophobic association

Water-soluble polymers carrying hydrophobic groups, such as short alkyl chains, fluorocarbon chains, etc., form gels by micellization of the hydrophobic groups in water (Figure 3.5(c)). Micelles serve as the cross-links that can dissociate and associate by temperature, external force, added agents, etc. Water-soluble polymers partially modified by hydrophobic associative groups are called **associating polymers**. Poly(ethylene oxide) and poly(N-isopropylacryl amide), which carry short alkyl chains ($-C_nH_{2n+1}$, $n = 12$–25) at their chain ends, are typical examples. They are called **telechelic polymers** as both chain ends are active in forming micelles. Because the molecular weight of the main chain and the length of the associative groups can be tuned, telechelic associating polymers serve as model systems for transient networks in which the junctions can break and recombine. One of the main purposes of this book is to present the recent developments in the research on associating polymers. These will be detailed at the end of Chapters 7 and 9.

(4) Gels with microcrystalline junctions

When crystallizable polymers are quenched below their melting point, they often form gels with microcrystals involving many chains at their junctions (Figure 3.5(d)). Junctions may have a fringed micellar structure, folded-chain microcrystals, etc. In order for a microcrystal to stay stable, its size should be above the critical nucleus size, and hence there is a lower limit in the multiplicity and sequence length of the junctions. The crystal structure inside the junction may be different from that of the bulk crystals. Gels with small junctions melt at low temperatures. The way that gels form by avoiding crystalization depends on the cooling speed, concentration, and other experimental conditions. Fast cooling, while keeping the system away from the thermal equilibrium state, may often lead to gels – as in the formation of glass. For example, isotactic polystyrene, poly(vinyl alcohol), etc., form gels when supercooled.

(5) Complex formation

Gels with zipper-like cross-links of sequential H-bonds, with double or triple helices, with eggbox-shaped complexes involving ions, as shown in Figure 3.5(e), may be classified as gels with extended junction zones of complexes. Conformation change of prepolymers

is necessary to form such complex junction zones, so that coil–helix transition often takes place before gelation. The gelation of polysaccharides, such as carrageenan and alginate, falls into this category.

(6) Gels with sliding junctions

Recently, new gels have been synthesized by cross-linking ring-shaped cyclodextrins after threading them into poly(ethylene oxide) chains [8]. The gels have junctions that are mobile along the chains to release the stresses caused by deformation. Gels with such mobile junctions fall into the category of chemical gels in the sense that the number of cross-links is preserved. However, since they can relax the external force by sliding their junctions, their rheological properties are more like physical gels.

(7) Entanglement

Entanglements of long rigid polymers in concentrated solutions and melts often lead to gel-like rheological properties (Figure 3.5(f)) [9]. The entanglements are regarded as delocalized cross-links whose spatial range is difficult to specify. They are created and destroyed by the thermal motion of the polymers or by external force. The number of cross-links is not conserved. The name pseudo-networks is therefore more appropriate for such viscoelastic liquids.

3.2   Classical theory of gelation

The critical point for the appearance of an infinitely large product (a gel) can be found by the condition that the weight average molecular weight of the products is divergent. Mathematically, this is written as

$$\langle M \rangle_{\mathrm{w}} = \infty. \tag{3.2}$$

This gel point uses the definition of a gel based on the connectivity of the system [10, 11, 12, 1]. The gel point is the point at which the reacting system is geometrically percolated by the connected objects. The appearance of a macroscopic object in the products is called **gelation**, or **sol–gel transition**. In chemical gels, the transition is irreversible, while in physical gels it is generally thermoreversible.

For the polycondensation of polyfunctional molecules, we can theoretically find the molecular weight distribution of the products, and hence the average molecular weight, as a function of the reactivity of the system under the assumption of equal reactivity.

The **principle of equal reactivity** states that all functional groups of the same species are equivalent, that is, the reactivity of all functional groups on the polymers is the same irrespective of their molecular weight and structure [1]. In other words, there is an intrinsic reactivity of the polycondensation. We shall derive the molecular weight distribution function of nonlinear polymers under the assumption of equal reactivity.

3.2.1   Random branching

Consider the polycondensation of functional monomers of the type $R\{AB_{f-1}\}$. The reaction is assumed to take place between the A group and B group only [1]. Nonlinear polymers with a tree structure are formed by reaction. They may have intramolecular cycles, but to find the exact solution we consider only branched tree-type polymers which have no cycles (Figure 3.6). These are sometimes called **Cayley trees**, named after the mathematician who studied tree-type graphs. The approximation under this assumption of no intramolecular cycles is called the **tree approximation**.

Let N_m be the number of m-mers (nonlinear polymers consisting of m monomers), and let p be the reactivity of the A groups and q that of the B groups. Then, we have the stoichiometric relation $p = (f - 1)q$. In what follows, we use q as the independent variable, and write it as $q = \alpha$. It varies in the range $0 \le \alpha \le 1/(f - 1)$.

An m-mer has a total number m of A groups and $(f - 1)m$ of B groups, among which $m - 1$ of A groups and $m - 1$ of B groups are pairwisely reacted. A total of $(f - 1)m - (m - 1) = fm - 2m + 1$ B groups remain unreacted. Because each m-mer carries only one unreacted A group (A* in Figure 3.6), the probability for an arbitrarily chosen unreacted A group to belong to an m-mer, i.e., the fraction of unreacted A groups in the m-mer among the total of unreacted A groups in the system, is given by the number distribution of the m-mers

$$f_m \equiv N_m / \sum_j N_j, \tag{3.3}$$

where N_m is the number of m-mers produced by reaction. This is given by

$$f_m = \omega'_m \alpha^{m-1} (1 - \alpha)^{fm - 2m + 1}, \tag{3.4}$$
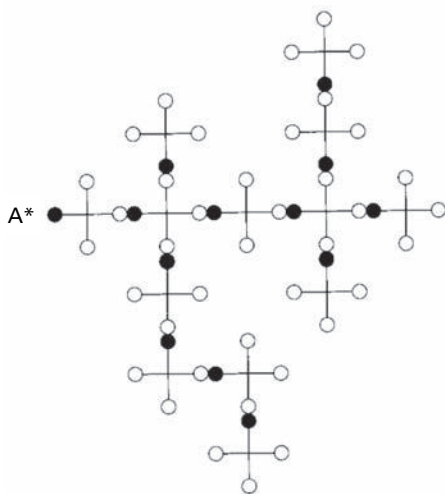
Fig. 3.6   Tree structure formed by polyfunctional molecules of type AB_3 carrying one reactive A group (black circles) and three reactive B group (white circles).

where ω'_m is the number of different ways to form an m-mer from its constituent m monomers. The number ω'_m can be found in the following way.

First, we give a sequence of numbers from 1 to m to the total of m monomers. Overcounting by labeling a sequence for the identical molecules will be corrected later. We then choose $m-1$ of B groups from the total $fm - m$. The number of different ways of choosing them is $_{fm-m}C_{m-1} = (fm-m)!/(m-1)!(fm-2m+1)!$. We connect them to the A groups without forming cycles. There are $(m-1)!$ ways to do this. Finally, we correct the overcounting by dividing the result by $m!$. Thus we find

$$\omega'_m = \frac{(fm-m)!}{m!(fm-2m+1)!}.\tag{3.5}$$

The number distribution function of the m-mers (clusters) is then

$$f_m = \frac{1-\alpha}{\alpha}\omega'_m\beta^m,\tag{3.6}$$

where β is defined by

$$\beta = \alpha(1-\alpha)^{f-2}.\tag{3.7}$$

The physical meaning of β will be detailed later. The first three moments of the distribution (3.6) are calculated in Appendix 3.A.

Because the number of monomer units is reduced by 1 every time a new bond is formed, the total number of clusters is

$$M \equiv \sum_{m\geq 1} N_m = N - (f-1)\alpha N = N[1-(f-1)\alpha].\tag{3.8}$$

This is equal to the number of A groups that remain unreacted in the system. From the first few moments shown in Appendix 3.A, we can find

$$\langle m \rangle_{\mathrm{n}} = \frac{1}{1-(f-1)\alpha}\tag{3.9}$$

for the number average degree of polymerization, and

$$\langle m \rangle_{\mathrm{w}} = \frac{1-(f-1)\alpha^2}{[1-(f-1)\alpha]^2}\tag{3.10}$$

for the weight average degree of polymerization.

Because both averages are divergent at $\alpha = \alpha^* \equiv 1/(f-1)$, this is identified as the gel point. Since the gel point thus found is the point where the reactivity of A groups is 1 (complete reaction), networks are formed in the limiting state where all A groups are reacted. In other words, there is no postgel regime in this system.

3.2.2 Polycondensation

We next consider the condensation reaction of polyfunctional molecules of the type $R\{A_f\}$. The molecular weight distribution for the special case $f = 3$ was first studied by Flory [10]. The result was later extended to the general case of f by Stockmayer [11] under the assumption of no intramolecular cycle formation. Their theories are called the **classical theory of gelation reaction**.

Pregel regime

Let p be the reactivity of A groups, and write it as α (the reason for this will be detailed below). Let N be the total number of monomers in the reacting system. An m-mer contains $2(m-1)$ reacted groups, and $fm - 2(m-1) = fm - 2m + 2$ unreacted groups (Figure 3.7). The probability for an unreacted A group, which is arbitrarily chosen from $fN(1-\alpha)$ unreacted A groups in the system, to belong to an m-mer is

$$P_m = \frac{[(f-2)m+2]N_m}{fN(1-\alpha)}. \tag{3.11}$$

The number of different ways of connecting the remaining $m-1$ monomers is the same as ω'_m derived in the preceding section, and hence we find

$$P_m = \omega'_m \alpha^{m-1}(1-\alpha)^{fm-2m+1}. \tag{3.12}$$

Comparing with (3.11), we find

$$N_m = fN\frac{(1-\alpha)^2}{\alpha}\omega_m\beta^m, \tag{3.13}$$

where the parameter β is the same as (3.7). The new number of configurations,

$$\omega_m \equiv \frac{(fm-m)!}{m!(fm-2m+2)!}, \tag{3.14}$$

has appeared instead of ω'_m.
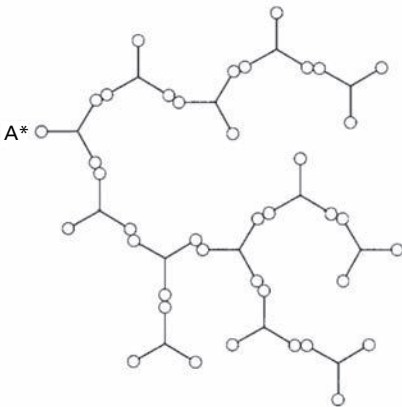
Fig. 3.7   Tree structure formed by polyfunctional monomers of the type $R\{A_3\}$.

Because one monomer is connected every time a new bond is formed in the tree structure, the number of molecules reduces by one. The number of reacted A groups, or equivalently the number of bonds, is $(fN)\alpha/2$, and the total number of clusters $M \equiv \sum_{m \geq 1} N_m$ is given by

$$M = N - (fN)\alpha/2 = N(1 - f\alpha/2), \tag{3.15}$$

from which the number distribution function $f_m \equiv N_m/M$ of the products takes the form

$$f_m = \frac{f(1-\alpha)^2}{\alpha(1-f\alpha/2)} \omega_m \beta^m. \tag{3.16}$$

By using the first few moments calculated in Appendix 3.A, we find that the number average degree of polymerization is

$$\langle m \rangle_n = \frac{1}{1 - f\alpha/2}. \tag{3.17}$$

Similarly, the weight distribution function

$$w_m \equiv m N_m / \sum_{m \geq 1} m N_m, \tag{3.18}$$

is found to be

$$w_m = \frac{f(1-\alpha)^2}{\alpha} m \omega_m \beta^m. \tag{3.19}$$

Hence the weight average molecular weight is

$$\langle m \rangle_w = \frac{1+\alpha}{1 - (f-1)\alpha}. \tag{3.20}$$

Gel point

Since the weight average molecular weight diverges when the reactivity α reaches

$$\alpha = 1/(f-1) \equiv \alpha^*, \tag{3.21}$$

we find that this is the gel point in the tree approximation. The number average remains at a finite value $\langle m \rangle_n = 2(f-1)/(f-2)$ at the gel point. The solid lines in Figure 3.8 below α^* show these two averages together with the z-average defined by

$$\langle m \rangle_z \equiv \sum m^2 w_m / \sum m w_m. \tag{3.22}$$

The explicit form of the z-average is given in Appendix 3.B.
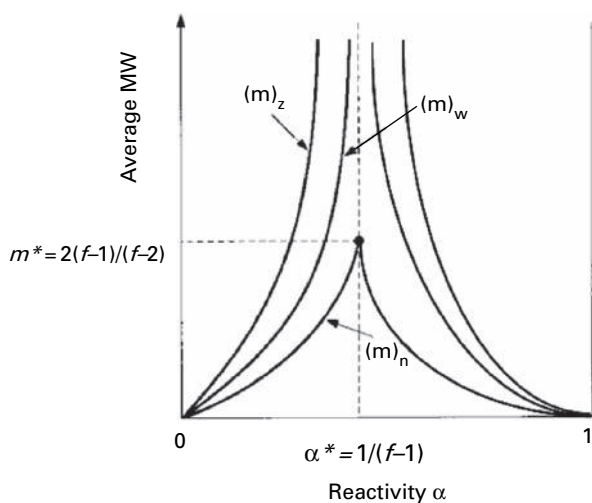
Fig. 3.8 Number-, weight-, and z-average molecular weights as functions of the reactivity in the gelation reaction of polyfunctional molecules $R\{A_f\}$.

Postgel regime

After the gel point is passed, the gel part coexists with the sol part in the reacting system. The reactivity α in each part may in principle be different. Let α^S be the reactivity of the sol part, and let α^G be that of the gel part. The average reactivity α of the entire system should then be given by

$$\alpha = \alpha^S (1-w) + \alpha^G w, \tag{3.23}$$

where w is the fraction of the A groups that are connected to the gel part, and called the **gel fraction**. It agrees with the weight fraction of the gel for the monodisperse system consisting of polyfunctional molecules whose functionality (the number of reactive groups) and molecular weight are uniquely fixed. The sol fraction is $1-w$.

If we take the limit of infinite molecular weight in the tree approximation, it is natural to assume that the gel network remains in the tree structure. Because the gel can be regarded as the $m \to \infty$ of an m-mer, its reactivity is

$$\alpha^G = \lim_{m \to \infty} 2(m-1)/fm = 2/f \equiv \alpha_0. \tag{3.24}$$

Therefore, in the postgel regime where the average reactivity is larger than the critical gel value α^*, we see that clusters of finite sizes are connected to the gel in the way such that the reactivity of the sol part stays at a constant value $\alpha^S = \alpha^*$. The relation (3.23) then gives

$$w = \frac{(f-1)\alpha - 1}{1 - \alpha_0} \tag{3.25}$$

for the gel fraction. It rises linearly from $\alpha^* = 1/(f-1)$, and reaches unity at $\alpha_0 = 2/f$. All monomers are connected to the gel before the reaction is completed. The sol part stays at the critical condition $\alpha = \alpha^*$. Such a theoretical treatment is first proposed by
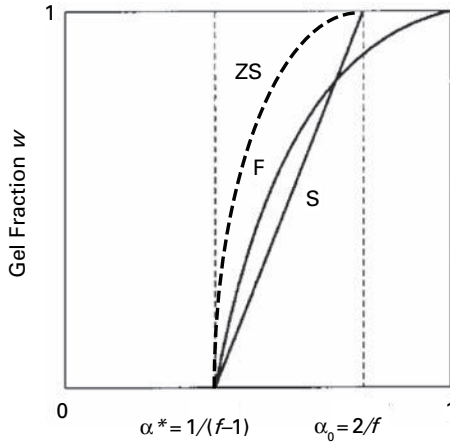
Fig. 3.9 Weight fraction of the gel part plotted against the reactivity. (Stockmayer's treatment (S), Flory's treatment (F), and Ziff–Stell's treatment (ZS).)

Stockmayer, and is called **Stockmayer's treatment** of the postgel regime (the solid line S in Figure 3.9).

This theoretical treatment is, however, not a unique way of describing the reaction in the postgel regime. Flory postulated that the reactivity of the sol part α^S should be found by the condition

$$\beta = \alpha(1-\alpha)^{f-2} = \alpha'(1-\alpha')^{f-2}. \tag{3.26}$$

In other words, for the average reactivity α larger than the critical value α^*, the equation

$$\beta \equiv \alpha(1-\alpha)^{f-2} \tag{3.27}$$

has two roots, and α^S should be the other root α' (the shadow root) which lies below the critical value. Hence, $\alpha^S = \alpha'$ is assumed.

The molecular weight distribution function of the sol part is therefore given by replacing α by α' in (3.19). The weight fraction of the sol in the postgel regime is then calculated to be

$$\sum_{m \geq 1} w_m = 1 - w = \frac{(1-\alpha)^2 \alpha'}{(1-\alpha')^2 \alpha}, \tag{3.28}$$

and hence the gel fraction is

$$w = 1 - \frac{(1-\alpha)^2 \alpha'}{(1-\alpha')^2 \alpha}. \tag{3.29}$$

Substituting into (3.23) and solving for the reactivity α^G of the gel part, we find

$$\alpha^G = \frac{\alpha + \alpha' - 2\alpha\alpha'}{1 - \alpha\alpha'}. \tag{3.30}$$

This α^G takes a value larger than $\alpha_0 = 2/f$. Therefore, in **Flory's treatment**, cycle formation is allowed in the gel network. The number of independent cycles, or the cycle
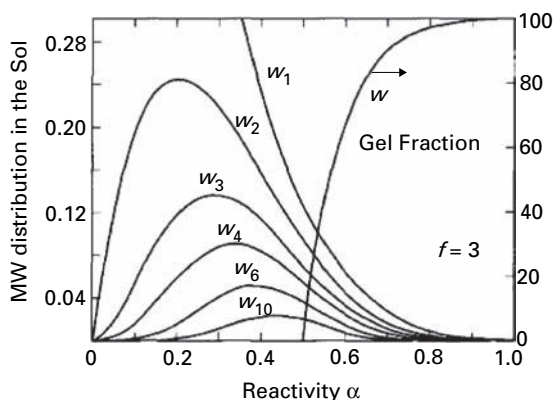
Fig. 3.10   The molecular weight distribution function w_m and the gel fraction w for polycondensation reaction of trifunctional monomers R{A$_3$} plotted against the reactivity.

rank, of the network is given by

$$\xi = \frac{f}{2}\alpha^G - 1. \tag{3.31}$$

All monomers belong to the gel part only in the limit of complete reaction $\alpha = 1$ (the solid line F in Figure 3.9).

Figure 3.10 shows the molecular weight distribution function and the gel fraction for the polycondensation of trifunctional monomers by Flory's treatment plotted against the average reactivity. The gel fraction w rises linearly from the gel point $\alpha = 0.5$ and approaches unity in the limit of $\alpha \to 1$. This result leads to the three curves for the number-, weight-, and z-average in the postgel regime in Figure 3.8.

The difference in the two approaches was later clarified from a kinetic point of view by Ziff and Stell [13]. It was shown that Stockmayer's treatment allows reaction neither between sol and gel, nor between gel and gel. The increase of the gel fraction is only by the cascade growth of the sol clusters to infinity, while in Flory's treatment sol and gel interact, and reaction within the gel is also allowed. Ziff and Stell proposed a new treatment in which intramolecular reaction of the gel is not allowed but reaction between sol and gel is allowed. Their result on the gel fraction is shown in Figure 3.9 by the broken line (ZS).

In the classical tree statistics, the number of the functional groups on the surface of a tree-like cluster is of the same order of that of the groups inside the cluster, so that a simple thermodynamic limit without surface term is impossible to take. The equilibrium statistical mechanics for the polycondensation was refined by Yan [14] to treat surface correction in such finite systems. He found the same result as Ziff and Stell. Thus the treatment of the postgel regime is not unique. The rigorous treatment of the problem requires at least one additional parameter defining relative probability of occurrence of intra- and intermolecular reactions in the gel.
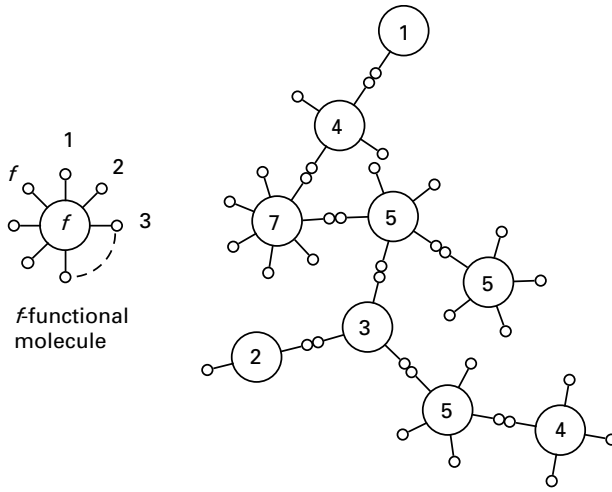
Fig. 3.11 Nonlinear polymer of the type $\mathbf{m} = (1, 1, 1, 2, 3, 0, 1)$ produced in condensation reaction of polydisperse functional monomers.

3.2.3 Polydisperse functional monomers

This section studies the gelation reaction of polydisperse functional monomers carrying different numbers of functional groups [11]. Let us consider the condensation system in which the number N_f of f-functional monomers is given by R{A_f}($f = 1, 2, \ldots$) (Figure 3.11). The total number of monomers is $\sum N_f \equiv N$, and the total number of functional group is $\sum f N_f \equiv \Psi$. Let us define the distribution function of the functional groups by[1]

$$\rho_f \equiv f N_f / \sum f N_f. \tag{3.32}$$

This is defined not by the number of monomers but by the functional groups. The number average functionality of the monomers is

$$f_n \equiv \sum f N_f / \sum N_f = \left(\sum \rho_f / f \right)^{-1}, \tag{3.33}$$

and the weight average is

$$f_w \equiv \sum f^2 N_f / \sum f N_f = \sum f \rho_f. \tag{3.34}$$

To specify the type of products during reaction, we use the index $\mathbf{m} = (m_1, m_2, \ldots)$. It indicates that the cluster consists of m_f f-functional monomers (Figure 3.11). For example, the label of the cluster in Figure 3.11 is $\mathbf{m} = (1, 1, 1, 2, 3, 0, 1)$.

---

[1] We use the symbol ρ_f for the distribution function of the reactants to avoid confusion with the molecular weight distribution w_m of the reacted products.

By repeating the similar counting method as in the previous section, we find that the number $N(\mathbf{m})$ of clusters specified by the type $\mathbf{m}$ is given by

$$N(\mathbf{m}) = \left(\sum f N_f\right) \frac{\left(\sum f m_f - \sum m_f\right)!}{\left(\sum f m_f - 2\sum m_f + 2\right)!}$$

$$\times \alpha^{\sum m_f - 1}(1-\alpha)^{\sum f m_f - 2\sum m_f + 2} \prod_{f\geq 1} \frac{(\rho_f)^{m_f}}{m_f!} \qquad (3.35)$$

at the reactivity α. This result can be easily found by replacing the factors as $fN \to \sum f N_f, m \to \sum m_f, fm \to \sum f m_f, 1/m! \to \prod (\rho_f)^{m_f}/m_f!$ in the monodisperse system (3.13).

Because the weight average molecular weight is

$$\left\langle \sum f m_f \right\rangle_{\mathrm{w}} = \frac{f_{\mathrm{w}}(1+\alpha)}{1-(f_{\mathrm{w}}-1)\alpha}, \qquad (3.36)$$

the gel point condition is given by

$$(f_{\mathrm{w}} - 1)\alpha = 1. \qquad (3.37)$$

Let us consider the special case of the binary mixture of $f = 2$ (unbranching monomers) and $f(\geq 3)$ (multifunctional branching monomers). Types of clusters can be specified by the label (m_2, m_f). To simplify the notation, write $m_2 = l$ and $m_f = m$. The number of clusters is then

$$N_{l,m} = \left(\sum f N_f\right) \frac{(l+fm-m)!}{(fm-2m+2)!} \alpha^{l+m-1}(1-\alpha)^{fm-2m+2} \frac{\rho_2^l \rho_f^m}{l!\,m!}. \qquad (3.38)$$

Let $\rho_f \equiv \rho$ be the fraction of the functional groups which belong to the branching monomers. We then have the relation $\rho_2 = 1 - \rho$, and

$$N_{l,m} = \left(\sum f N_f\right) \frac{(1-\alpha)^2}{\rho\alpha} \omega_{l,m} \eta^l \zeta^m, \qquad (3.39)$$

where $\omega_{l,m} \equiv (l+fm-m)!/l!m!(fm-2m+2)!$, and the parameters η and ζ are defined by

$$\eta \equiv (1-\rho)\alpha, \qquad (3.40)$$

$$\zeta \equiv \rho\alpha(1-\alpha)^{f-2}. \qquad (3.41)$$

The special case $\rho = 0$ reduces to the linear polymerization, and $\rho = 1$ reduces to the condensation of f-functional monomers. The molecular distribution (3.39) connects these extreme cases.

The total number of clusters $M \equiv \sum N_{l,m}$ decreases by one every time a bond is formed, and hence

$$M = \underbrace{N_2 + N_f}_{\text{monomers}} - \underbrace{\alpha(2N_2 + fN_f)/2}_{\text{cross-links}} \qquad (3.42)$$

holds. Because the weight average functionality of the monomers is $f_w = f\rho + 2(1-\rho) = (f-2)\rho + 2$, the gel condition (3.37) turns out to be

$$[(f-2)\rho + 1]\alpha = 1. \tag{3.43}$$

3.2.4 Cross-linking of prepolymers

Let us next consider that the primary molecules are polymers. Mixing cross-linkers, exposure to γ-ray radiation, etc., results in the random cross-linking of monomers on the prepolymers [12, 1]. We assume that the prepolymers are monodisperse with n repeat units, and the cross-linking process is independent and random. Each monomer on the chain can be regarded as a functional molecule, so that we can fix $f = n$ in the previous studies. The DP of the polymer is assumed to be sufficiently large that we may take the limit of $n \to \infty$ under the condition that the number of reacted monomers on a chain

$$\alpha n \equiv \gamma \tag{3.44}$$

is kept constant. We may take the limit of $\alpha \to 0$ with a constant **cross-link index** γ.

By using the approximations

$$\beta \equiv \alpha(1-\alpha)^{n-2} \simeq \frac{\gamma e^{-\gamma}}{n} \ll 1, \tag{3.45}$$

$$\omega_m = \frac{(nm-m)!}{m!(nm-2m+2)!} \simeq \frac{(nm)^{m-2}}{m!} \tag{3.46}$$

in the molecular weight distribution (3.19) for large n, we find that the molecular weight distribution function takes the limiting form

$$w_m \simeq \frac{m^{m-1}}{\gamma m!}(\gamma e^{-\gamma})^m \simeq \frac{1}{m\gamma}(\gamma e^{1-\gamma})^m. \tag{3.47}$$

Hence, the gel point is found to be

$$\gamma^* = 1, \tag{3.48}$$

by the condition that $\gamma e^{-\gamma}$ reaches the maximum value as a function of γ. It turns out that one cross-link on average per chain is sufficient for gelation.

In the postgel regime, we take the similar limit in the relation

$$\sum_{m \geq 1} w_m = \frac{f(1-\alpha)^2}{\alpha} S_1(\alpha') \tag{3.49}$$

in Flory's treatment, and find

$$1 - w = \gamma'/\gamma, \qquad w = 1 - \gamma'/\gamma \tag{3.50}$$

for the sol and gel fractions, where α' (or γ') is the shadow root of the equation

$$\beta = \alpha'(1-\alpha')^{f-2} \simeq \frac{\gamma'}{n} e^{-\gamma'},$$

for a given β. For this shadow root γ', which is smaller than unity, the relation

$$S_1(\alpha') = \frac{\alpha'}{f(1-\alpha')^2} \simeq \frac{\gamma'}{n^2}$$

holds.

3.3   Gelation in binary mixtures

3.3.1   Finding the gel point using the branching coefficient

In this section, we study gelation by **heteromolecular condensation reaction** in binary mixtures. Typical model systems are condensation of f-functional monomers of the type R$\{A_f\}$ and g-functional monomers of the type R$\{B_g\}$. They form binary mixed networks. The mixtures are indicated by R$\{A_f\}$/R$\{B_g\}$. For simplicity, the reaction is limited to only between the A and B functional groups (Figure 3.12).

Before detailed study of the molecular weight distribution function, we consider a simple method to find the gel point by using the branching coefficient [1]. The **branching coefficient** α is defined by the probability that any one of the functional groups on an arbitrarily chosen branching monomer (functional monomer with functionality more than or equal to 3) reaches the next branching monomer of the *same species* by a connected path (Figure 3.13).

Consider that a reacted path reaches a branching monomer R$\{A_f\}$. In order for the path to extend to infinity without breakage, at least one of the number $(f-1)$ possible directions of the extension must reach the next branching monomer with probability 1 (Figure 3.14). Hence the gel condition is given by

$$(f-1)\alpha = 1. \tag{3.51}$$
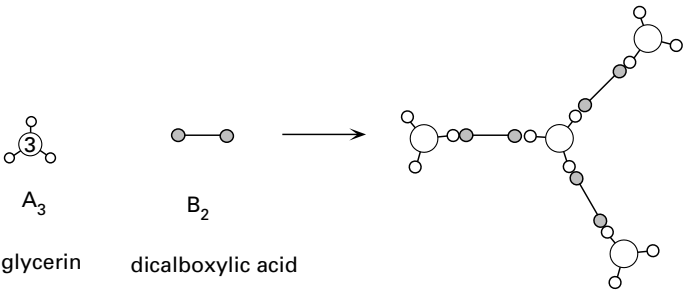
Fig. 3.12   Esterification of trifunctional monomers R$\{A_3\}$ and bifunctional monomers R$\{B_2\}$.
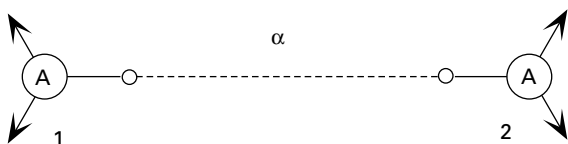
Fig. 3.13 Branching coefficient α of a branching monomer $R\{A_f\}$. The monomer 1 is connected by the next monomer 2 of the same species by a reacted path.
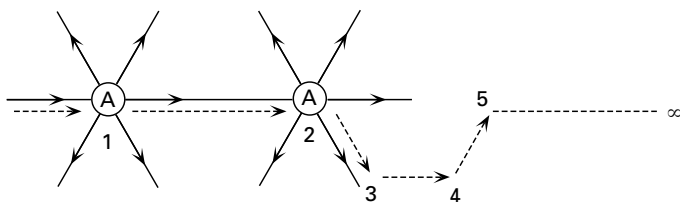
Fig. 3.14 Gel point condition as seen from the existence of a path that continues to infinity.
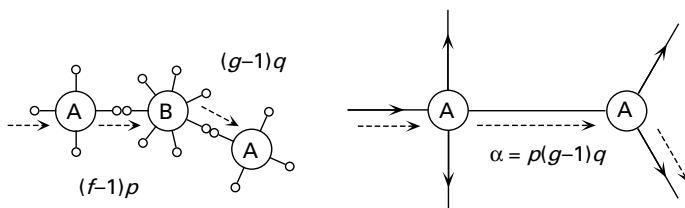
Fig. 3.15 Branching coefficient of the mixture A_f/B_g.

The method for finding the gel point by the branching coefficient is very convenient because it does not require information of the molecular weight distribution.

For the binary mixture $R\{A_f\}/R\{B_g\}$, the condition (3.51) gives

$$(f-1)p(g-1)q = 1, \tag{3.52}$$

since the probability for a pair of $R\{A_f\}$ monomers to be connected by a reaction path is $\alpha = p(g-1)q$ (Figure 3.15), where p and q are the reactivity of the A and B groups, respecitvely.

Let us study the slightly more complex mixtures of $R\{A_f\}/R\{A_2\}/R\{B_2\}$. $R\{A_2\}$ and $R\{B_2\}$ are nonbranching monomers. The structure of the branched polymers is shown in Figure 3.16. Let $\rho \equiv fN_f/(2N_2 + fN_f)$ be the fraction of functional A groups on the branching monomers among all A groups in the system. Summing up all the possible reaction paths from one branching monomer $R\{A_f\}$ to the next one (the bottom part of
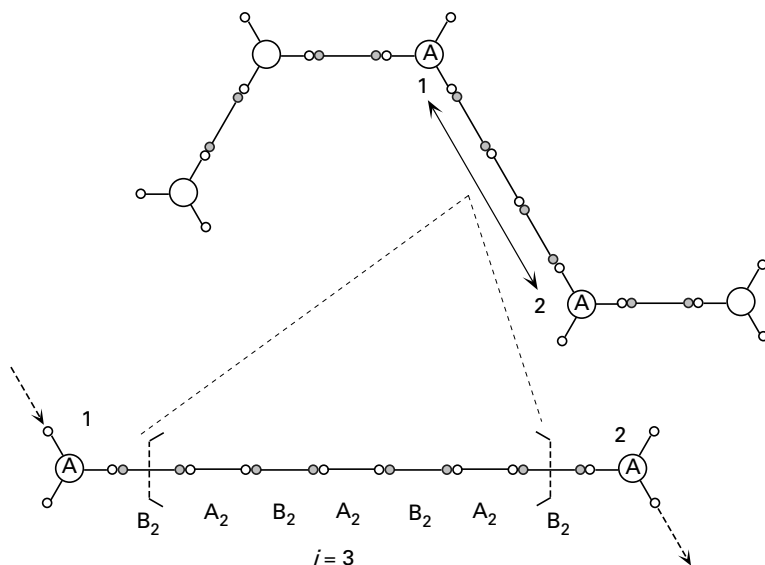
Fig. 3.16   Branching coefficient of the mixture $A_f/A_2/B_2$.

Figure (3.16), we find the branching coefficient to be

$$\alpha = \sum_{i=0}^{\infty} p\{q(1-\rho)p\}^i q\rho = \frac{pq\rho}{1-pq(1-\rho)}. \tag{3.53}$$

The gel point is found by the condition

$$[(f-2)\rho+1]pq=1, \tag{3.54}$$

from (3.51). Because the average functionality of R{A} monomers is $f_w = 2(1-\rho) + f\rho = (f-2)\rho+2$, the gel point condition is equivalent to

$$(f_w-1)pq=1. \tag{3.55}$$

In particular, for stoichiometric mixtures with the same number of A and B groups, the reactivities are equal, $p=q$, so that $\alpha = p^2\rho/[1-p^2(1-\rho)]$.

If there are no R{A$_2$} monomers, $\rho=1$ and $\alpha = pq$ hold, so that the gel point is $(f-1)pq=1$. If there is no R{A$_f$}, we have random copolymerization of R{A$_2$} and R{B$_2$}, for which $\alpha = p^2$. The polymerization point is the point with $\alpha_c = 1$ where all groups are reacted.

3.3.2   Molecular weight distribution function of the binary mixtures R{A$_f$}/R{B$_g$}

Consider the binary mixture R{A$_f$}/R{B$_g$}. Let N_A be the number of R{A$_f$} molecules, and N_B be the number of R{B$_g$} molecules. The number of functional groups in the

system is $\Psi_A = f N_A$ and $\Psi_B = g N_B$ for each species. The reaction is assumed to take place only between A and B.

Under the assumption of tree statistics (no intramolecular reaction allowed), Stockmayer [15] found that the number of clusters consisting of l A monomers and m B monomers is given by

$$\lambda N_{l,m} = \frac{(fl-l)!(gm-m)!}{l!m!(fl-l-m+1)!(gm-l-m+1)!} x^l y^m, \tag{3.56}$$

where λ is the equilibrium constant of the reaction of bond formation

$$A + B \rightleftharpoons A \cdot B \tag{3.57}$$

By putting $(l,m) = (1,0)$, or $(0,1)$, parameters x and y turn out to be

$$x = \lambda f N_{10}, \ y = \lambda g N_{01}. \tag{3.58}$$

These are the numbers of A and B monomers that remain unreacted in the system, multiplied by the equilibrium constant λ.

Because $f N_{10}$ is the number of A monomers on the unreacted monomers, it must be equal to $\Psi_A(1-p)^f$ by the definition of the reactivity p. Therefore, x can be written as $x = \lambda \Psi_A(1-p)^f$. Similarly, $y = \lambda \Psi_B(1-q)^g$ holds.

Let us express x and y in terms of the reactivity p and q. Because the number of reacted A groups $\Psi_A p$ is the same as the number of reacted B groups $\Psi_B q$, let us write it as γ. This is also equal to the number of bonds formed by reaction. The equilibrium constant λ can be found by the equilibrium condition in the reaction (3.57) as

$$\lambda = \frac{\Psi_A p}{\Psi_A(1-p)\Psi_B(1-q)} = \frac{\Psi_B q}{\Psi_A(1-p)\Psi_B(1-q)}. \tag{3.59}$$

We then have the relation $\lambda \Psi_A = q/(1-p)(1-q)$, and hence

$$x = \frac{q}{(1-p)(1-q)} \cdot (1-p)^f = \frac{q(1-p)^{f-1}}{1-q}. \tag{3.60}$$

Similarly, we have

$$y = \frac{p}{(1-p)(1-q)} \cdot (1-q)^g = \frac{p(1-q)^{g-1}}{1-p}. \tag{3.61}$$

Next, let us express the number of bonds γ in terms of Ψ_A, Ψ_B, and λ:

$$\gamma = \lambda \Psi_A \Psi_B (1-p)(1-q). \tag{3.62}$$

Substituting the relations $p = \gamma/\Psi_A$, $q = \gamma/\Psi_B$, we find

$$\gamma = \lambda \Psi_A \Psi_B (1 - \gamma/\Psi_A)(1 - \gamma/\Psi_B), \tag{3.63}$$

which is regarded as the equation to find γ. Solving for γ, we find

$$\lambda\gamma = \frac{1}{2}\left\{1+\lambda(\Psi_A+\Psi_B)-\left[1-2\lambda(\Psi_A+\Psi_B)+\lambda^2(\Psi_A-\Psi_B)^2\right]^{1/2}\right\}.$$

(The sign is chosen so that the equation holds in the limit of $\lambda \to 0$.) The equilibrium number γ of bonds can thus be found for the given concentration in the preparation stage.

The number of molecules is reduced by one every time a new bond is formed. Hence the total number of molecules (clusters) in the system is

$$\sum_{lm} N_{l,m} = \frac{\Psi_A}{f}+\frac{\Psi_B}{g}-\gamma. \tag{3.64}$$

From the information of $N_{l,m}$, we can find the weight average molecular weight by

$$\langle M\rangle_w \equiv \sum_{lm}(M_A l+M_B m)^2 N_{l,m}/\sum_{l,m}(M_A l+M_B m)N_{l,m} \tag{3.65}$$

where M_A and M_B are the molecular weights of the monomers. By using the distribution (3.56), the sum turns out to be

$$\langle M\rangle_w = \frac{\frac{[(f-1)pM_B^2+(g-1)qM_A^2+2M_A M_B]pq}{1-(f-1)(g-1)pq}+\frac{q}{f}M_A^2+\frac{p}{g}M_B^2}{\frac{q}{f}M_A+\frac{p}{g}M_B}. \tag{3.66}$$

The gel point is

$$(f-1)(g-1)pq=1, \tag{3.67}$$

from the divergence condition of $\langle M\rangle_w$, as is expected from the branching coefficient (3.52).

3.3.3   Polydisperse binary mixture R{A_f}/R{B_g}

Let us generalize the above results to the polydisperse binary mixture R{A_f}/R{B_g} in which functional monomers carry various numbers of functional groups. Let N_f^A ($f=1,2,\ldots$) be the number of f-functional monomers, and N_g^B ($g=1,2,\ldots$) be the number of g-functional monomers. The total number of A and B groups are then given by $\Psi_A=\sum f N_f^A$, $\Psi_B=\sum g N_g^B$. Let us introduce the distribution function of the functional groups as $\rho_f^A \equiv f N_f^A/\Psi_A$ and $\rho_g^B \equiv g N_g^B/\Psi_B$. These are the fractions of the functional groups on the monomers of specified functionalities.

Under the assumption of the tree statistics, Stockmayer [15] generalized the monodisperse mixtures to polydisperse ones, and found that the number of clusters consisting of

$\mathbf{l} \equiv (l_1, l_2, \ldots)$ A monomers and $\mathbf{m} \equiv (m_1, m_2, \ldots)$ B monomers is given by

$$\lambda N(\mathbf{l}, \mathbf{m}) = \frac{\left(\sum f l_f - \sum l_f\right)! \left(\sum g m_g - \sum m_g\right)!}{\left(\sum f l_f - \sum l_f - \sum m_g + 1\right)! \left(\sum g m_g - \sum l_f - \sum m_g + 1\right)!}$$
$$\times \prod_f \left(\frac{x_f^{l_f}}{l_f!}\right) \prod_g \left(\frac{y_g^{m_g}}{m_g!}\right), \tag{3.68}$$

where x_f and y_g are generalizations of (3.60) and (3.61), defined by

$$x_f \equiv \rho_f^A \frac{q(1-p)^{f-1}}{1-q}, \quad y_g \equiv \rho_g^B \frac{p(1-q)^{g-1}}{1-p}. \tag{3.69}$$

The reaction constant λ is given by

$$\lambda \equiv \frac{p \, \Psi_A}{\Psi_A (1-p) \Psi_B (1-q)} = \frac{q \, \Psi_B}{\Psi_A (1-p) \Psi_B (1-q)} \tag{3.70}$$

By using the average functionalities of the functional monomers

$$f_w \equiv \sum f \rho_f^A, \quad g_w \equiv \sum g \rho_g^B, \tag{3.71}$$

and the weight average molecular weights

$$\langle M \rangle_A \equiv \sum M_f \rho_f^A, \quad \langle M \rangle_B \equiv \sum M_g \rho_g^B, \tag{3.72}$$

the weight average molecular weight of the products can be found by replacing M_A/f, M_B/g by $\langle M \rangle_A/f$, $\langle M \rangle_B/g$ in (3.66). The gel point condition is

$$(f_w - 1)(g_w - 1) p \, q = 1. \tag{3.73}$$

3.3.4 Gels with multiple junctions

Let us consider the limit of the complete reaction of functional B groups in the preceding section (Figure 3.17). In such a limit, a reactive B group can be regarded as a cross-linker producing a junction of multiplicity g. The **multiplicity** of the junction is the number of functional groups combined into it (see Figure 3.3). The B molecules act as glues to paste the A groups.

Let us indicate the multiplicity by k as in the convention. We then replace the notations as $m_g \rightarrow j_k$ and $\rho_f^A \rightarrow \rho_f$, $\rho_g^B \rightarrow p_k$ in the molecular distribution (3.68) while the notation l_f is kept as it is. Here, p_k gives the probability for a chosen A group to belong to the junction of multiplicity k. The average functionality of B monomers becomes $g_w = \sum k p_k$, and we write this as $\bar{\mu}_w$, where $\bar{\mu}_w$ shows the average multiplicity of the cross-links.
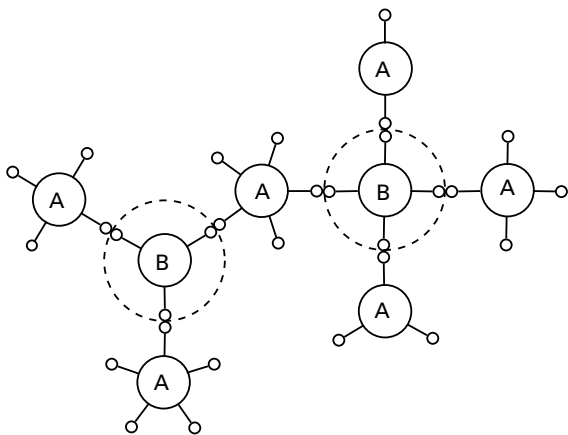
Fig. 3.17   Multiple junction as seen from cross-linking by glue molecules B.

There are two fundamental geometrical relations which hold for clusters of tree type with multiple junctions. For the total number of monomers in the cluster, the relation

$$\sum l_f = \sum (k-1) j_k + 1 \qquad (3.74)$$

holds. For the total number of functional groups, the relation

$$\sum f l_f = \sum k j_k \qquad (3.75)$$

holds.

The combinatorial factor in the molecular weight distribution function (3.68) simplifies as the factor $p(1-p)q(1-q)$ disappears, and the limit $q \to 1$ of complete reaction can be taken. As a result, the molecular weight distribution is transformed to

$$N(\mathbf{j},\mathbf{l}) = \left(\sum f N_f \right) \left(\sum j_k - 1 \right)! \left(\sum l_f - 1 \right)! \prod_f \frac{(\rho_f)^{l_f}}{l_f!} \prod_k \frac{(p_k)^{j_k}}{j_k!}, \qquad (3.76)$$

which agrees with the tree statistics with multiple junctions derived by Fukui and Yamabe [16] directly by using the statistical-mechanical method.

The gel point turns out to be given by

$$(f_w - 1)(\bar{\mu}_w - 1) = 1, \qquad (3.77)$$

after the replacement of the symbols as above. We will derive these results more efficiently in Appendix 3.B by using the **probability generating function** (p.g.f.) of the cascade theory.

The branching coefficient of this system when regarded as an A/B mixture is found to be $\alpha = (g_w - 1) pq$ by generalizing (3.52) to polydisperse systems. Fixing $q = 1$ in
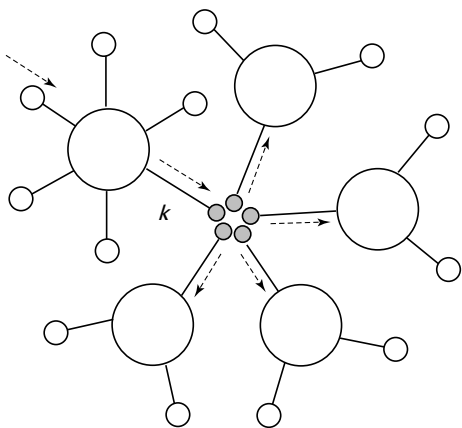
Fig. 3.18   Branching coefficient of multiple cross-linking systems.

the gel point condition (3.73), and replacing $(g_\mathrm{w} - 1)p$ by $\sum(k-1)p_k$, we find that the branching coefficient for the multiple cross-linking is

$$\alpha = \bar{\mu}_\mathrm{w} - 1. \tag{3.78}$$

Because there are $k - 1$ paths going out of the k junction, the result can be understood in the form (Figure 3.18)

$$\alpha = \sum_{k \geq 1}(k-1)p_k = \bar{\mu}_\mathrm{w} - 1. \tag{3.79}$$

Thus, the gel point condition (3.77) is also derived from the branching coefficient method.

Most physical gels have multiple cross-links. They are formed by the association of the particular segments on the polymer chains. Therefore, gels with multiple junctions may be understood more profoundly when they are treated by thermodynamic theory rather than reaction theory. In Section 7.1, we shall present some of the equilibrium thermodynamics of physical gels with multiple junctions.

Appendices to Chapter 3

3.A   Moments of the Stockmayer distribution function

We define the k-th moments for the power series with coefficients ω'_m and ω_m as

$$S'_k \equiv \sum_{m=1}^{\infty} m^k \omega'_m \beta^m, \quad S_k \equiv \sum_m^{\infty} m^k \omega_m \beta^m.$$

For S'_k, the normalization condition $\sum_{m \geq 1} f_m = 1$ leads to

$$S'_0 = \alpha/(1-\alpha).$$

The first moment is calculated by the relation $S_1' = \beta(dS_0'(\beta)/d\beta)$. Because $dS_0'/d\beta = (dS_0'(\beta)/d\alpha)(d\alpha/d\beta)$, and $dS_0'/d\alpha = -1/(1-\alpha)^2$, $d\beta/d\alpha = (1-\alpha)^{f-3}[1-(f-1)\alpha]$, we have

$$S_1' = \frac{\alpha}{(1-\alpha)[1-(f-1)\alpha]}.$$

Similarly, from $S_2'(\beta) = \beta^2(d^2S_0'(\beta)/d\beta^2) + S_1'(\beta)$, we find

$$S_2' = \frac{\alpha[1-(f-1)\alpha^2]}{(1-\alpha)[1-(f-1)\alpha]^3}.$$

For S_k, the normalization condition leads to

$$S_0 = \alpha(1 - f\alpha/2)/f(1-\alpha)^2.$$

By differentiation, we find

$$S_1 = \frac{\alpha}{f(1-\alpha)^2}, \quad S_2 = \frac{\alpha(1+\alpha)}{f(1-\alpha)^2[1-(f-1)\alpha]}.$$

3.B Cascade theory of gelation

After the classical theory of gelation reaction was developed by Flory and Stockmayer, a very efficient mathematical machinery was invented on the basis of the cascade theory of stochastic **branching processes**. By the use of the cascade theory, we can calculate the average molecular weights, the reactivity at the gel point, the sol fraction, etc., without any detailed knowledge of the molecular weight distribution function. Furthermore, the molecular weight distribution function itself can be obtained from elementary calculus without reading to solve any complex combinatorial problems.

Cascade theory starts with the weight fraction generating function, or the **probability generating function** (p.g.f.) [17, 18]

$$W(\alpha;\theta) \equiv \sum_{m=1}^{\infty} w_m(\alpha)\theta^m, \tag{3.80}$$

where α is the reactivity (the fraction of functional groups that have reacted), $w_m(\alpha)$ is the weight distribution function (3.19), and θ is the dummy parameter used to construct the p.g.f. The **sol fraction** is given by

$$w^S \equiv S = W(\alpha, 1). \tag{3.81}$$

In the pregel regime, the weight fraction is normalized as

$$\sum_{m=1}^{\infty} w_m(\alpha) = 1,$$

so that (3.81) has a trivial solution $S = 1$, while in the postgel regime it has a nontrivial solution in the region $0 \leq S < 1$. The number average molecular weight is calculated by the relation

$$\frac{1}{\langle m \rangle_{\mathrm{n}}} \equiv \sum_{m=1}^{\infty} \frac{w_m(\alpha)}{m} = \int_0^1 W(\alpha;\theta) \frac{d\theta}{\theta}.$$

The weight average, z-average, and higher averages are calculated by

$$\langle m \rangle_{\mathrm{w}} = \left(\frac{\partial W}{\partial \theta} \right)_{\theta=1},$$

$$\langle m \rangle_{\mathrm{z}} = \frac{1}{\langle m \rangle_{\mathrm{w}}} \left[\frac{\partial}{\partial \theta} \left(\theta \frac{\partial W}{\partial \theta} \right) \right]_{\theta=1},$$

and so on.

Starting with the 0-th generation, the p.g.f. for the total number of molecules in the first, second, …, r-th generations, can be seen to be

$$W(\alpha;\theta) = \theta F_0(\theta F_1(\theta F_2(\theta \cdots F_r(\theta))\cdots)), \tag{3.83}$$

where $F_i(\theta)$ is the p.g.f. for the children of the molecules in the i-th generation (Figure 3.19). Rigorous proof of this relation is given by Good for the vectorial cascade random branching problem [19]. For an infinite tree ($r \to \infty$), all F_i for $i \geq 1$ have the same structure as F_1, so this relation can be written as

$$W(\theta) = \theta F_0(x), \tag{3.84a}$$

$$x = \theta F_1(x). \tag{3.84b}$$

$i = 0$ \qquad\qquad $i = 1$ \qquad\qquad $i = 2$
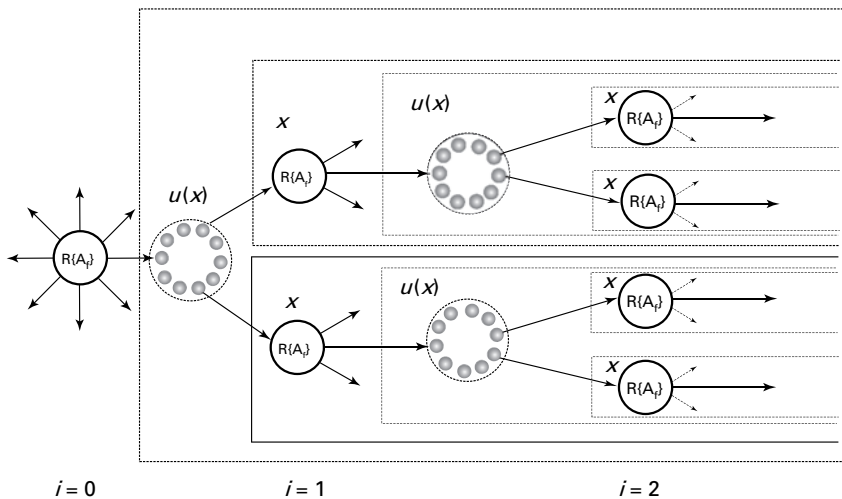
Fig. 3.19   Diagram for the p.g.f. of the cascade tree. Each junction is accompanied by a factor $u(x)$. The 0-th generation has f branches, while the generations higher than the first have $f - 1$ branches.

For the condensation of f-functional monomers, F_0 and F_1 are given by

$$F_0(x) = u(x)^f, \qquad F_1(x) = u(x)^{f-1},$$

where

$$u(x) \equiv 1 - \alpha + \alpha x, \tag{3.85}$$

for the pairwise reaction. (An arbitrarily chosen functional group may either remain unreacted with the probability $1 - \alpha$ or react with the probability α.) For multiple reactions, it is given by

$$u(x) = \sum_{k \geq 1} p_k x^{k-1}.$$

In the case of more complex mixtures of polydisperse functional primary molecules with the distribution function ρ_f, F functions are

$$F_0(x) = \sum_f \rho_f u(x)^f, \qquad F_1(x) = \sum_f \rho_f u(x)^{f-1}.$$

From (3.84a), we have $u(x) = (W(\theta)/\theta)^{1/f}$, and from (3.84b), we have $u(x) = (x/\theta)^{1/f'}$, where $f' \equiv f - 1$. These two must be the same, so that

$$x = \theta^{1/f} W(\theta)^{f'/f}$$

holds. By putting $\theta = 1$ and $W(1) = S$, we find

$$x = S^{f'/f},$$

and hence

$$u(x) = S^{1/f}.$$

In particular for pairwise reaction (3.85), this relation may be solved with respect to α as

$$\alpha = (1 - S^{1/f})/(1 - S^{f'/f}).$$

For $S = 1$, the reactivity at the gel point $\alpha = \alpha_c = 1/f'$ is obtained.

Let us find the average molecular weight by the p.g.f. By taking the derivative of (3.84b), we find

$$d\theta = \frac{1 - \theta F_1'(x)}{F_1(x)} dx.$$

Hence we have

$$\frac{1}{\langle m \rangle_n} = \int_0^x \frac{F_0(x)}{F_1(x)} \left\{ 1 - \frac{d \ln F_1(x)}{d \ln x} \right\} dx = \int_0^x u(x) \left\{ 1 - f'x \frac{u'(x)}{u(x)} \right\} dx$$

$$= f \int_0^x u(x) dx - f' x u(x) \Big|_0^x,$$

where $x = S^{f'/f}$. For the pairwise reaction,

$$\frac{1}{\langle m \rangle_{\mathrm{n}}} = S^{f'/f} \left\{ 1 - \alpha - \frac{f''}{2} \alpha S^{2f'/f} \right\}.$$

In the pregel regime, we have $S = 1$, and hence we find (3.17). For the multiple reaction

$$\frac{1}{\langle m \rangle_{\mathrm{n}}} = \sum_{k \geq 1} \left(\frac{f}{k} - f' \right) p_k S^{f'k/f},$$

which leads to

$$\langle m \rangle_{\mathrm{n}} = \frac{1}{f[1/\bar{\mu}_{\mathrm{n}} + 1/f - 1]}$$

in the pregel regime, where $\bar{\mu}_{\mathrm{n}}$ is the number average junction multiplicity.

Similarly, from the relation

$$\frac{\partial W}{\partial \theta} = F_0(x) + \frac{\theta F_1(x) F_0'(x)}{1 - \theta F_1'(x)},$$

we find

$$\langle m \rangle_{\mathrm{w}} = F_0(x) + \frac{F_0'(x)}{1 - F_1'(x)}.$$

In the pregel regime of pairwise reaction, this equation reduces to (3.20). For multiple reaction, this equation gives

$$\langle m \rangle_{\mathrm{w}} = \frac{1}{f[1/\bar{\mu}_{\mathrm{w}} + 1/f - 1]},$$

where $\bar{\mu}_{\mathrm{w}}$ is the weight average junction multiplicity, and hence the gel point condition is

$$(f - 1)(\bar{\mu}_{\mathrm{w}} - 1) = 1,$$

which is the monodisperse case of (7.96).

Higher order average may be calculated in a similar way. For instance, the z-average molecular weight of pairwise reaction is

$$\langle m \rangle_z = \frac{2\alpha[1 - (f-1)\alpha] + (1+\alpha)[1 - (f-1)\alpha^2]}{(1+\alpha)[1 - (f-1)\alpha]^2},$$

in the pregel regime. Similar calculation of the average molecular weights in binary mixtures in which different functional groups A and B react with each other in the form of multiple polycondensation is presented in the literature [20, 21].

We can also find the weight fraction distribution function $w_m(\alpha)$ from the cascade equations (3.84a) and (3.84b) by expanding the function $F_0(x)$ in powers of the dummy parameter θ. This procedure is easily feasible if we apply the following **Lagrange theorem** [22, 23]. The theorem states that if the variable x is related to θ by the equation

$$x = \theta \phi(x), \tag{3.85}$$

with an analytic function $\phi(x)$, then any analytic function $f(x)$ can be expanded as

$$f(x) = f(0) + \sum_{n \geq 1} \frac{\theta^n}{n!} \left(\frac{d}{dx}\right)^{n-1} \left[f'(x)\phi(x)^n\right]. \tag{3.86}$$

In the present case, we have $\phi(x) = \sum_f \rho_f u(x)^{f'}$ and $f(x) = \sum_f \rho_f u(x)^f$, and hence $\phi(x) = f(x)/u(x)$. Since

$$f'(x)\phi(x)^n = \frac{f(x)^n f'(x)}{u(x)^n} = \frac{1}{u(x)^n} \frac{1}{n+1} \frac{d}{dx} f(x)^{n+1},$$

we find

$$f(x) = f(0) + \sum_{n \geq 1} \frac{\theta^n}{n!(n+1)} \left(\frac{d}{dx}\right)^{n-1} \frac{1}{u(x)^n} \frac{d}{dx} f(x)^{n+1}.$$

By using the polynomial theorem, we have

$$f(x)^{n+1} = (n+1)! \sum_{\{m\}} \prod_f \left(\frac{\rho_f^{m_f}}{m_f!}\right) u(x)^{\sum f m_f},$$

where m_f are integers satisfying the condition $\sum_f m_f = n+1$.

On substitution, the function $f(x)$ has the expansion

$$f(x) = f(0) + \sum_{n \geq 1} \theta^n \left(\frac{d}{dx}\right)^{n-1} \frac{1}{u(x)^n} \frac{d}{dx} \left[\sum_{\{m\}} \prod_f \left(\frac{\rho_f^{m_f}}{m_f!}\right) u(x)^{\sum f m_f}\right]$$

$$= f(0) + \sum_{n \geq 1} \theta^n \sum_{\{m\}} \frac{\sum f m_f}{(\sum f m_f - n)} \prod_f \left(\frac{\rho_f^{m_f}}{m_f!}\right) \left(\frac{d}{dx}\right)^n u(x)^{\sum f m_f - n}.$$

By using the polynomial theorem again, we have

$$u(x)^{\sum f m_f - n} = \left(\sum p_k x^{k-1}\right)^{\sum f m_f - n}$$

$$= \left(\sum f m_f - n\right)! \sum_{\{j\}} \prod_k \left(\frac{p_k^{j_k}}{j_k!}\right) x^{\sum (k-1) j_k},$$

where $\sum_{k \geq 1} j_k = \sum_f f m_f - n$ must hold. After taking the derivatives n times and putting $x = 0$, the only term satisfying the condition $\sum_{k \geq 1}(k-1) j_k = n = \sum_f m_f - 1$ remains. Hence, we have

$$f(x) = f(0) + \sum_{n \geq 1} \theta^n \sum_{\{j,m\}} \left(\sum f m_f\right) \left(\sum j_k - 1\right)!$$

$$\times \left(\sum m_f - 1\right)! \prod_f \left(\frac{\rho_f^{m_f}}{m_f!}\right) \prod_k \left(\frac{p_k^{j_k}}{j_k!}\right)$$

The first term corresponds to the $n = 0$ term in the p.g.f. We therefore finally find

$$W(\theta) = \sum_{n \geq 1} \theta^n \sum_{\{j,m\}} (\sum f m_f)(\sum j_k - 1)!(\sum m_f - 1)! \prod_f \left(\frac{\rho_f^{m_f}}{m_f!} \right) \prod_k \left(\frac{p_k^{j_k}}{j_k!} \right),$$

which is equivalent to Fukui–Yamabe distribution (3.76).

References

[1] Flory, P.J., *Principles of Polymer Chemistry*. Cornell University Press: Ithaca, NY, 1953.

[2] Clark, A.H.; Ross-Murphy, S.B., *Adv. Polym. Sci.* **83**, 57 (1987).

[3] Guenet, J.M., *Thermoreversible Gelation of Polymers and Biopolymers*. Academic Press: London, 1992.

[4] te Nijenhuis, K., *Adv. Polym. Sci.* **130**, 1 (1997).

[5] de Gennes, P. G., *Scaling Concepts in Polymer Physics*. Cornell University Press: Ithaca, NY, 1979.

[6] Deam, R.T.; Edwards, S.F., *Phil. Trans. Roy. Soc. London* **280**, 317 (1976).

[7] Ziman, J.M., *Models of Disorder*. Cambridge University Press: Cambridge, 1979.

[8] Okumura, Y.; Ito, K., *Adv. Mater.* **2001**, *13*, 485.

[9] Weiss, R. G.; Terech, P., *Molecular Gels: Materials with Self-Assembled Fibrillar Networks*. Springer: London, 2006.

[10] Flory, P.J., *J. Am. Chem. Soc.* **63**, 3091 (1941).

[11] Stockmayer, W.H., *J. Chem. Phys.* **11**, 45 (1943).

[12] Stockmayer, W.H., *J. Chem. Phys.* **12**, 125 (1944).

[13] Ziff, R. M.; Stell, G., *J. Chem. Phys.* **73**, 3492 (1980).

[14] Yan, J.F., *J. Chem. Phys.* **78**, 6893 (1983).

[15] Stockmayer, W.H., *J. Polym. Sci.* **4**, 69 (1952).

[16] Fukui, K.; Yamabe, T., *Bull. Chem. Soc. Jpn* **40**, 2052 (1967).

[17] Gordon, M., *Proc. Roy. Soc. London A* **268**, 240 (1962).

[18] Good, I.J., *Proc. Roy. Soc. London A* **272**, 54 (1963).

[19] Good, I.J., *Proc. Camb. Phil. Soc.* **45**, 360 (1949).

[20] Tanaka, F., *J. Polym. Sci., Part B: Polym. Phys.* **41**, 2405 (2003).

[21] Tanaka, F., *J. Polym. Sci., Part B: Polym. Phys.* **41**, 2413 (2003).

[22] Good, I.J., *Proc. Camb. Phil. Soc.* **56**, 367 (1960).

[23] Whittaker, E. T.; Watson, G. N., *A Course of Modern Analysis*, 4th edn. Cambridge University Press: Cambridge, 1969, p. 133.

4 Elasticity of polymer networks

Rubbers and gels are three-dimensional networks composed of mutually cross-linked polymers. They behave like solids, but they still have high internal degrees of freedom that are free from constraints of external force; the random coils connecting the cross-links are free in thermal Brownian motion. The characteristic elasticity of polymeric materials appears from the conformational entropy of these random coils. In this chapter, we study the structures and mechanical properties of rubbers on the basis of the statistical-mechanical models of polymer networks.

4.1 Thermodynamics of rubber elasticity

Elastic properties of rubbers and gels are markedly different from those of metals, ceramics, and glasses. The properties of rubbers may be summarized as follows:

- Their elastic moduli (Young modulus and rigidity) are very small (as small as 10^{5-6} $\mathrm{N\,m^{-2}}$, about 10^{-5} times as small as those of metals).
- They have very high extensivity and restorability. They endure large deformation without rupture. They return to their initial dimensions even after being stretched to five to ten times their original size.
- Their elastic moduli increases with temperature.
- They are heated by adiabatic elongation, and cooled by adiabatic compression.

Thus, rubbers seem to be peculiar materials. We can, however, understand these unique properties very naturally if we consider that the main cause of the elasticity comes not from the interaction energy of the constituent molecules but from the conformational entropy of the chain segments, which are free to move.

4.1.1 Energetic elasticity and entropic elasticity

Consider a rectangular rubber sample to be stretched in the x-direction by an external tension f. The law of thermodynamics for the infinitesimal process of stretching the sample from the length L to $L+dL$ is

$$dU = TdS - pdV + fdL, \qquad (4.1)$$

where U is the internal energy, S the entropy, and V the volume of the sample. Because the volume stays constant during deformation of rubber, we set $dV = 0$.

Dividing this relation by dL under the condition of constant pressure and temperature, we find the tension

$$f = \left(\frac{\partial U}{\partial L}\right)_{p,T} - T\left(\frac{\partial S}{\partial L}\right)_{p,T}. \tag{4.2}$$

As for the Gibbs free energy, we have the relation

$$dG = -SdT + Vdp + fdL. \tag{4.3}$$

Comparing with the mathematical relation

$$dG = \left(\frac{\partial G}{\partial T}\right)_{p,L} dT + \left(\frac{\partial G}{\partial L}\right)_{p,T} dL, \tag{4.4}$$

at a constant pressure, we find that **Kelvin's relation** connecting the two second derivatives of the thermodynamic functions

$$-\left(\frac{\partial S}{\partial L}\right)_{p,T} = \left(\frac{\partial f}{\partial T}\right)_{p,L} \tag{4.5}$$

holds as one of the Maxwell relations.

The tension can be transformed to

$$f = \left(\frac{\partial U}{\partial L}\right)_{p,T} + T\left(\frac{\partial f}{\partial T}\right)_{p,L} \tag{4.6}$$

by the use of Kelvin's relation.

The first term $f_e \equiv (\partial U/\partial L)_{p,T}$ gives the part of the tension due to the internal energy, and the second term $f_S \equiv T(\partial f/\partial T)_{p,L}$ gives the part due to entropy. Thus, the tension is separated into two parts with different origin. These are called **energetic elasticity** and **entropic elasticity**.

Consider the plot of measured tension as a function of the temperature under a constant pressure by keeping the sample at a fixed length L (Figure 4.1). The relation (4.6) demonstrates that, if a tangent line is drawn at a temperature T, the value at its intercept with the vertical axis (point C) when extrapolated to the absolute zero temperature gives the energetic part of the tension. The entropic part is given by the rest (line AB). We can thus experimentally separate the tension into two parts at a given temperature [1, 2].

Figure 4.2 shows an example of such an analysis [3]. The total tension f (curve f), energetic f_e (curve A), and entropic f_S (curve B) parts of a vulcanized natural rubber at $T = 20°C$ are plotted against the relative deformation $\lambda - 1$, where $\lambda \equiv L/L_0$ is the elongation ratio. (L_0 is the initial value.) The horizontal axis is the degree of elongation $\lambda - 1$. It turns out that the main part of the tension comes from the entropic part for the vulcanized rubber.

The fraction of energetic elasticity in the tension is

$$\frac{f_e}{f} = 1 - \left(\frac{\partial \ln f}{\partial \ln T}\right)_{p,L} = -T\left[\frac{\partial \ln(f/T)}{\partial T}\right]_{p,L}, \tag{4.7}$$
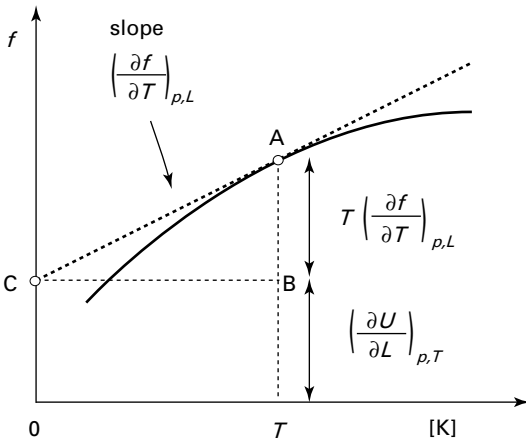
Fig. 4.1 Experimental method to separate the tension into energetic and entropic parts.
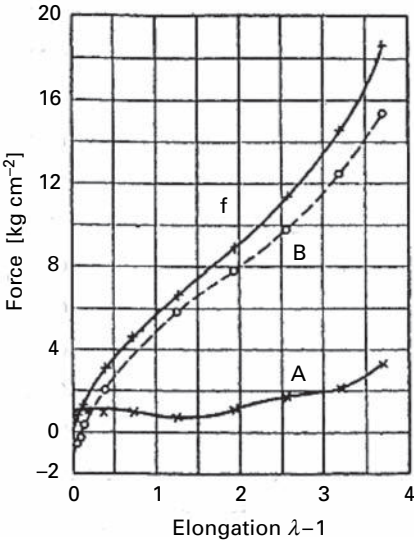
Fig. 4.2 Separation of the tension f into the energy part (curve A) and the entropy part (curve B). It turns out that the major part of the elasticity originates in the entropy for rubber. (Reprinted with permission from Ref. [3].)

from (4.6). The partial derivative $(\partial f/\partial T)_{p,L}$ on the right-hand side is the **temperature coefficient of tension**, which is analogous to (1.31). According to the molecular theory of rubber elasticity, this fraction is connected to the mean end-to-end distance $\langle r^2 \rangle_0$ of the subchains connecting two adjacent cross-links through the relation [4]

$$\frac{f_e}{f} = T \frac{d \ln \langle r^2 \rangle_0}{dT}. \tag{4.8}$$

Table 4.1 Energy part in the tension at $T = 298\,$K.

	f_e/f	$d\ln\langle r^2\rangle_0/dT \times 10^3\,(\text{K}^{-1})$
natural rubber	0.18	0.60
cis-1,4-polybutadiene	0.13	0.44
polydimethylsiloxane	0.20	0.67
polyisobutylene	-0.06	-0.20
polyethylene	-0.42	-1.41
elastine	0.26	0.87

We shall discuss this relation in the following sections presenting the molecular theory of rubber elasticity.

Because the left-hand side is a thermodynamic quantity, the macroscopic phenomenological picture is related to the microscopic picture through equation (4.8). Table 4.1 [5] shows a comparison of both sides of this relation at $T = 298$ K.

Polyethyrene (PE) has a negative value $f_e/f = -0.42$. This is because the extended trans zigzag conformation of $-CH_2-CH_2-CH_2-$ at low temperatures changes to the gauche conformation upon heating, so that end-to-end distance reduces. Poly(dimethylsiloxane) (PDMS) has a large positive value $f_e/f = 0.20$. The skeletal form of -Si-O-Si-O- takes a compact structure in the trans conformation, but with an increase in the gauche conformation upon heating, the end-to-end distance increases sharply.

4.1.2 Thermoelastic inversion

Figure 4.3 plots the tension of a rubber vulcanized with sulfur as a function of temperature under the constant length L in the small deformation region. The elongation $L/L_0 - 1$ is indicated by the figures beside the curves. The reference value L_0 is chosen to be that of the equilibrium state of the sample at $T = 20°$C. In the small elongation region below 3–6%, the temperature coefficient $(\partial f/\partial T)_{p,L}$ is negative, while it is positive at higher elongation. The sign change of the temperature coefficient at small deformation is called **thermoelastic inversion**. It is natural that the tension increases with the temperature because the origin of elasticity is entropic, but there is thermal expansion of the sample that leads to a reduction of the tension with temperature. Thermoelastic inversion indicates that thermal expansion exceeds the entropy reduction when the deformation is sufficiently small.

4.1.3 Gough–Joule effect

In 1805, Gough[1] discovered that a rubber shrinks when heated under a constant load. The rubber was restored to its initial length when cooled down, which showed that the change was thermoreversible. Contraction of a rubber by heat was confirmed in detail by

---

[1] John Gough (1757–1825) was an English natural philosopher.
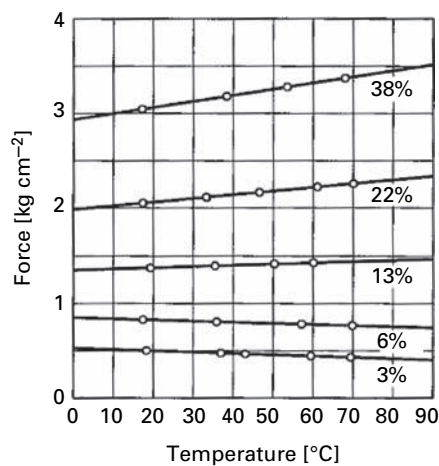
Fig. 4.3   Tension of a vulcanized rubber plotted against the temperature. The tension is measured by varying temperature under a constant length L of the sample. The elongation is shown by the ratio $\lambda = L/L_0$ by using the reference value L_0 at 20°C. The value $\lambda - 1$ is converted into %. (Reprinted with permission from Ref. [3].)
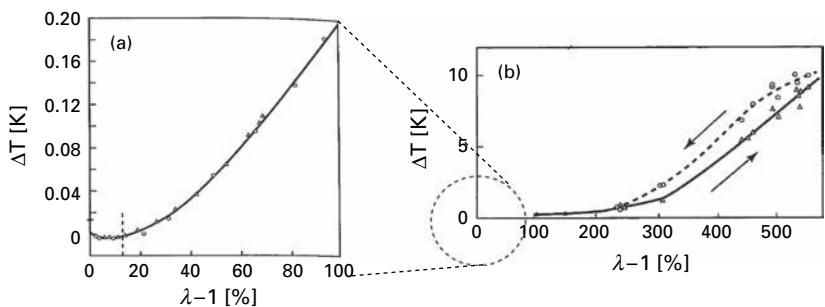
Fig. 4.4   (a) Magnification of the small deformation region. Thermoelastic inversion is seen around $\lambda = 1.13$, as indicated by the thin broken line. (b) Temperature rise (depression) by adiabatic elongation (contraction) of a rubber.

Joule in 1859, and hence it is called the **Gough–Joule effect**. The Gough–Joule effect suggests that the temperature coefficient of tension is positive.

The phenomenon of heat production when a rubber is adiabatically elongated is closely related to the Gough–Joule effect. When a rubber is quickly elongated, it produces heat and the temperature of the sample goes up. The temperature rise by such an adiabatic elongation is plotted in Figure 4.4 [6]. At high stretching ($\lambda - 1 \approx 500\%$), the temperature increase is as high as 10 K (Figure 4.4(b)), but there is a region of temperature drop as shown in Figure 4.4(a) for small elongation (below 20%). By releasing the tension, the sample restores its initial equilibrium state with the initial temperature.

The entropy change of the rubber sample under a constant pressure is given by

$$dS = \left(\frac{\partial S}{\partial T}\right)_{p,L} dT + \left(\frac{\partial S}{\partial L}\right)_{p,T} dL. \tag{4.9}$$

Rewriting the first term in terms of the specific heat $C_p \equiv T(\partial S/\partial T)_{p,L}$ under constant pressure and length, and by using Kelvin's relation (4.5) for the second term, we find

$$dS = \frac{C_p}{T} dT - \left(\frac{\partial f}{\partial T}\right)_{p,L} dL. \tag{4.10}$$

Because the entropy change is $dS = 0$ for the adiabatic process, the temperature change of the sample is proportional to the temperature coefficient of tension

$$\left(\frac{\partial T}{\partial L}\right)_S = \frac{T}{C_p} \left(\frac{\partial f}{\partial T}\right)_{p,L}, \tag{4.11}$$

so that the sign of the temperature change is the same as that of the temperature coefficient of tension. Comparison of Figure 4.3 with Figure 4.4(a) suggests that thermoelastic inversion can be studied in the region below 13% elongation (for details see Section 4.4).

Thus, the Gough–Joule effect can be understood as the manifestation of the thermoelastic inversion when seen from a different viewpoint.

4.2   Affine network theory

4.2.1   Local structure of cross-linked rubbers

Rubbers have complex structures made up of mutually entangled polymer chains. Let us focus on a cross-link point P in the sample, and study the chain paths and spatial distribution of the cross-links around it (Figure 4.5) [4, 5].

The next cross-link along the path of the selected subchain starting from the cross-link P is a **topological neighbor** of the cross-link (● in Figure 4.5). In contrast, the cross-links that lie far from P along the path of the subchains, but very close to P in spatial distance, are **spatial neighbors** (× in Figure 4.5). Let

$$\Gamma \equiv \left(\frac{4\pi}{3} \langle s^2 \rangle_0^{3/2}\right) \frac{\mu}{V} \tag{4.12}$$

be the number of spatial neighbors in the spherical region (the broken line in Figure 4.5) with the radius $\langle s^2 \rangle_0^{1/2}$, the mean radius of gyration of the subchains, where μ is the total number of cross-links in the sample and V its volume. For common rubbers, Γ is as large as $\Gamma = 25$–100. There are many cross-links in the neighborhood which are not directly connected to the particular one in focus. For random cross-linking of prepolymers, $\langle s^2 \rangle_0 \simeq \mu^{-1}$, so that Γ is proportinal to $1/\sqrt{\mu}$; it decreases with the degree of cross-linking.
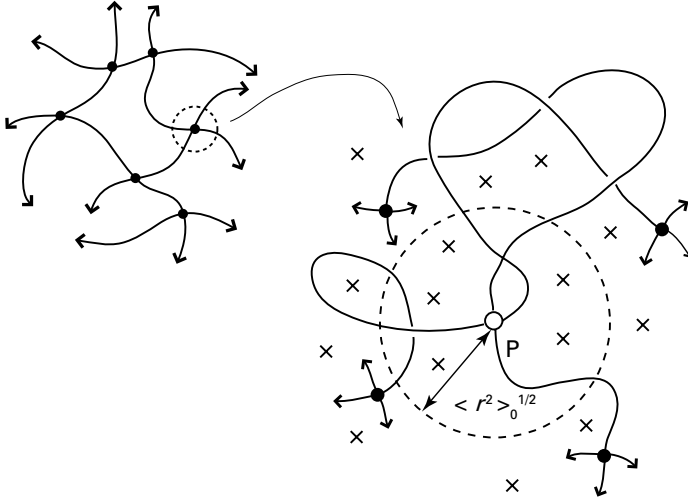
Fig. 4.5   Spatial ($\times$) and topological ($\bullet$) neighborhoods around a cross-link in a rubber sample.

Due to such densely packed molecularly interpenetrated structures, rubbers are incompressible under deformation. Each chain takes a Gaussian conformation following the Flory theorem for screened excluded-volume interaction. On the basis of these characteristics, we can derive the elastic properties of rubbers from a microscopic point of view.

4.2.2   Affine network theory

Consider a cubic rubber sample with side length L in equilibrium state to be elongated along its x-axis by a tension f to λ_x times its initial length (Figure 4.6). The sides in the y and z directions are deformed $\lambda_y = \lambda_z$ times. At the initial equilibrium state before the force is applied, each subchain in the sample has its end-to-end vector $\mathbf{r}_0$ with the probability with Gaussian distribution

$$P_0(\mathbf{r}_0) = \left(\frac{3}{2\pi \langle r^2 \rangle_0} \right)^{3/2} \exp \left(-\frac{3r_0{}^2}{2\langle r^2 \rangle_0} \right), \tag{4.13}$$

with the mean square value $\langle r^2 \rangle_0 = na^2$ (n is the number of repeat units on the subchain). This is called **Gaussian assumption**. The **chain vector** $\mathbf{r}_0$ connects the neighboring two junctions.

Kuhn [7] and Wall [8] assumed further that the chain vector $\mathbf{r}_0$ deforms in proportion to the macroscopic deformation $(\lambda_x, \lambda_y, \lambda_z)$ in spite of the molecular interaction and topological entanglements in the network. On the basis of this **affine deformation**, they found the relationship between the applied force and the deformation of the sample.

This assumption of affine deformation is written as

$$\mathbf{r}_0 \longrightarrow \mathbf{r} = \hat{\lambda} \cdot \mathbf{r}_0, \tag{4.14}$$
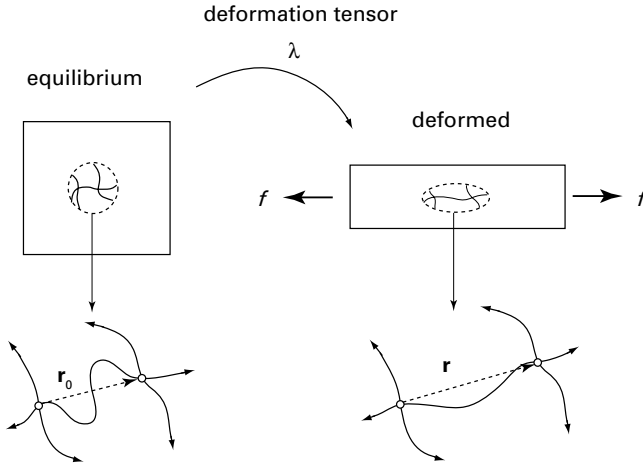
Fig. 4.6 Relation between macroscopic and microscopic deformation of a rubber sample.

where $\hat{\lambda}$ is the deformation tensor, and $\mathbf{r}_0$ and $\mathbf{r}$ are chain vectors before and after the deformation. The deformation tensor takes the form

$$\hat{\lambda} \equiv \begin{bmatrix} \lambda_x & 0 & 0 \\ 0 & \lambda_y & 0 \\ 0 & 0 & \lambda_z \end{bmatrix} \tag{4.15}$$

for a uniaxial elongation. In more general deformation, the tensor has finite off-diagonal elements.

The physical base of affine deformation lies in the intricate structure of rubber described above; polymer chains are randomly coiled, highly interpenetrated and entangled, but may follow the deformation freely by adjusting the positions of the chain segments.

Let ν be the total number of subchains in the sample. The number of subchains whose chain vector falls in the region $\mathbf{r}_0$ and $\mathbf{r}_0 + d\mathbf{r}_0$ is given by $\nu P_0(\mathbf{r}_0)d\mathbf{r}_0$. They take the vector between $\mathbf{r}$ and $\mathbf{r} + d\mathbf{r}$ after deformation, and hence the following relation holds:

$$\nu P_0(\mathbf{r}_0)d\mathbf{r}_0 = \nu P(\mathbf{r})d\mathbf{r}, \tag{4.16}$$

where $P(\mathbf{r})$ is the chain distribution after deformation. The assumption of affine deformation connects $\mathbf{r}$ to $\mathbf{r}_0$ by the relation (4.14). Because the free energy stored in a subchain whose chain vector is $\mathbf{r}$ is given by (1.36)

$$\phi(\mathbf{r}) = \frac{3k_B T}{2\langle r^2 \rangle_0} r^2, \tag{4.17}$$

in Gaussian approximation, the total free energy of the deformed sample is

$$F(\hat{\lambda}) = \int \phi(\mathbf{r})\nu P(\mathbf{r})d\mathbf{r}. \tag{4.18}$$

Substituting (4.17) into this equation, and by using the affine deformation (4.14), we find

$$F(\hat{\lambda}) = \frac{3\nu k_B T}{2\langle r^2 \rangle_0} \int (\hat{\lambda} \cdot \mathbf{r}_0)^2 P_0(\mathbf{r}_0) d\mathbf{r}_0$$

$$= \frac{\nu k_B T}{2\langle r^2 \rangle_0} (\lambda_x^2 + \lambda_y^2 + \lambda_z^2)\langle r^2 \rangle_0. \tag{4.19}$$

By subtraction of the free energy before deformation ($\lambda_x = \lambda_y = \lambda_z = 1$), we find that the free energy change $\Delta_{\text{def}} F(\hat{\lambda}) \equiv F(\hat{\lambda}) - F(1)$ by deformation is given by

$$\Delta_{\text{def}} F(\hat{\lambda}) = \frac{\nu}{2} k_B T (\lambda_x^2 + \lambda_y^2 + \lambda_z^2 - 3). \tag{4.20}$$

In the usual deformation of rubber, the volume change is negligibly small, so that we can set $\lambda_x = \lambda$, $\lambda_y = \lambda_z = 1/\sqrt{\lambda}$.

The tension can be found by differentiation $f = (\partial \Delta_{\text{def}} F / \partial(\lambda L))_T$ to be

$$f = \frac{\nu k_B T}{L} \left(\lambda - \frac{1}{\lambda^2} \right). \tag{4.21}$$

Dividing (4.21) by the initial area L^2 of the cross section gives the elongational stress σ (tension by a unit area). The stress–elongation relation turns out to be

$$\sigma = \frac{\nu k_B T}{L^3} \left(\lambda - \frac{1}{\lambda^2} \right). \tag{4.22}$$

Because the cross section under deformation is L^2/λ, the stress τ per unit area of the cross section under deformation is

$$\tau = \frac{\nu k_B T}{L^3} \left(\lambda^2 - \frac{1}{\lambda} \right). \tag{4.23}$$

The number of subchains ν/L^3 in a unit volume is given by $\nu/L^3 = \rho N_A/M$ in terms of the density ρ, and the molecular weight M of the subchain. Hence we have

$$\tau = \frac{\rho R T}{M} \left(\lambda^2 - \frac{1}{\lambda} \right). \tag{4.24}$$

The molecular theory of rubber elasticity on the basis of affine deformation assumption is the **affine network theory**, or the **classical theory of rubber elasticity**.

Young's modulus
The Young's modulus E of a rubber is found by further differentiation of the stress

$$E = \lambda \left(\frac{\partial \sigma}{\partial \lambda} \right) = \frac{\rho R T}{M} \left(\lambda + \frac{2}{\lambda^2} \right) \tag{4.25}$$

The linear Young's modulus E is defined by the Young's modulus for an infinitesimal deformation. Fixing at $\lambda = 1$ in the above equation, we find

$$E = \frac{3\rho RT}{M} \qquad (4.26)$$

For example, a sample of $M = 10^4$, $\rho = 1\,\mathrm{g\,cm^{-3}}$ at $T = 300\,\mathrm{K}$ gives $\nu/L^3 = 10^{-4}\,\mathrm{mol\,cm^{-3}}$ and $E = 7.4 \times 10^6\,\mathrm{dyne\,cm^{-2}}$. It is 10^{-5} times smaller than the Young modulus of iron $9 \times 10^{11}\,\mathrm{dyne\,cm^{-3}}$.

The Young's modulus increases in proportion to the absolute temperature because the thermal agitation grows stronger with temperature. The result is opposite to metals, which become softer with temperature. In a metal, atoms are regularly positioned to minimize interaction energy in the form of crystal. Thermal motion intensifies on heating, so that the force for restoring the original positions is weakened with temperature, which results in a decrease in the elasticity.

In rubbers, however, the modulus increases in proportion to the temperature due to the reduction of the entropy by the constraint brought by deformation. Thus, entropic elasticity and energetic elasticity have opposite tendencies as a function of the temperature.

Tension–elongation curve

The main characteristics of rubber elasticity is well described by affine network theory, but the profile of the tension–elongation curve deviates in the high-elongation region from the experimental observation. Figure 4.7 compares the experimental data (circles) of the tension f with the theoretical calculation (broken line) as functions of the elongation λ [9]. Data show the shape of the letter S. There is a sharp increase in the high-elongation region. They largely deviate from the theory because the chains are stretched beyond the linear regime, and the Gaussian assumption of the affine network theory breaks down at high elongation.

Toreloar improved this deficiency of the Gaussian assumption by introducing the Langevin chain (1.26) instead of the Gaussian chain to incorporate chain nonlinearity [9] (see Section 4.6). The effect of nonlinear stretching can thus be studied by refining the single-chain properties of the subchains.

Chain entanglements

There are also some discrepancies between theory and experiments regarding the nonlinear stretching effect. Figure 4.8 plots the ratio $\sigma/(\lambda - 1/\lambda^2)$ against the reciprocal deformation λ^{-1} for a cross-linked natural rubber (**Mooney–Rivlin plot**) [10–13].Because the ratio increases in proportion to λ^{-1}, the experiments can be fitted by the linear curve

$$\sigma = 2C_1\left(\lambda - \frac{1}{\lambda^2}\right) + 2C_2\left(1 - \frac{1}{\lambda^3}\right), \qquad (4.27)$$

with two constants C_1 and C_2. Equation (4.27) is called the **Mooney–Rivlin empirical formula**.
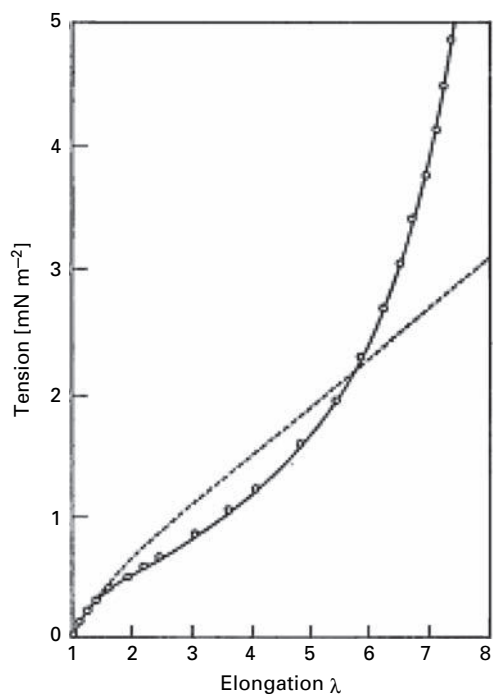
Fig. 4.7   Tension–elongation curve of a cross-linked rubber. Experimental data (circles), affine network theory by Gaussian chain (broken line), affine network theory (4.107) by Langevin chain (solid line).
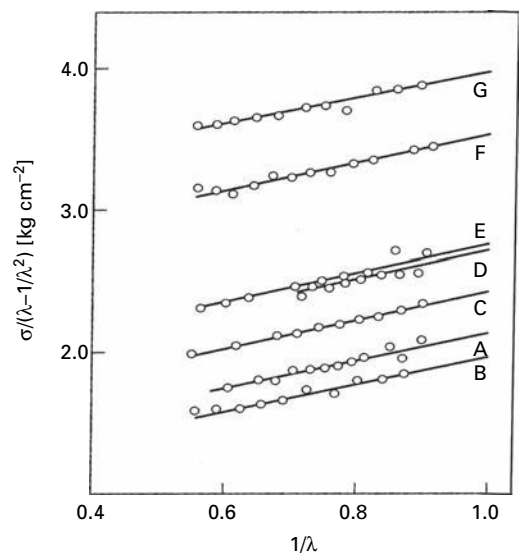
Fig. 4.8   Mooney–Rivlin plot of a cross-linked natural rubber. The curves A–G have different degrees of cross-linking with sulfur content covering from 3% to 4%. (Reprinted with permission from Gumbrell, S. M.; Mullins, L.; Rivlin, R. S., *Trans. Faraday Soc.* **49**, 1495 (1953).)

Because the constant C_2 decreases when the rubber is swollen by solvents, this extra term is deduced to be caused by the topological entanglements of the subchains. The entangled parts serve as the delocalized cross-links which increase the elasticity. Networks are disentangled on swelling, and the **Mooney constant** C_2 decreases.

4.2.3 Elastically effective chains

Apart from the problem of entanglements, there remains another difficult problem in affine network theory. It is how to count the number ν of subchains that contribute to the elasticity. Obviously, dangling chains and self-loops should not be counted. They are elastically inactive because they do not transmit the stress.

Flory clarified the activity of subchains by using the words **elastically effective chain**, or **active chain** [1]. An elastically effective chain is a chain that connects two neighboring cross-link junctions in the network.

Flory's correction
When networks are formed by cross-linking of the prepolymers, the end parts of the pre-polymers remain as dangling ends in the network. Flory made a correction by subtracting the number of such trivial free ends from the number ν of chains which appeared in the stress [14].

Let M be the molecular weight of the prepolymers, and let M_c be that of the subchains after cross-linking. The latter is the average value over the subchains whose distribution is assumed to be sufficiently narrow. The number of subchains in a unit volume is $\nu = \rho/M_c$, where ρ is the density of the rubber sample. Because the number of ends of the prepolymers is given by $2\rho/M$, the number of the effective chains should be

$$\nu_{\text{eff}} = \frac{\rho}{M_c}\left(1 - \frac{2M_c}{M}\right), \tag{4.28}$$

by subtraction (Figure 4.9). The tension is then

$$\tau = \frac{\rho RT}{M_c}\left(1 - \frac{2M_c}{M}\right)\left(\lambda^2 - \frac{1}{\lambda}\right), \tag{4.29}$$

where the factor $1 - 2M_c/M$ has appeared to exclude the free ends.

Criterion for elastic activity
There remain many inactive subchains after such an end correction is made. For instance, a group of chains, such as shown in Figure 4.10, may be dangling from one junction as a whole. They are inactive. Scanlan and Case applied the graph theory and introduced a criterion for judging the activity of a given subchain [15, 16]. It is stated as follows.

Let (i, k) be the index to characterize the topological nature of a junction; the index i (**path number**) is the number of paths emerging from it and connected to the skeletal structure of the network, and k is the multiplicity of the junction (the number of subchains connected to the junction). Let $\mu_{i,k}$ be the number of junctions whose index is (i, k).
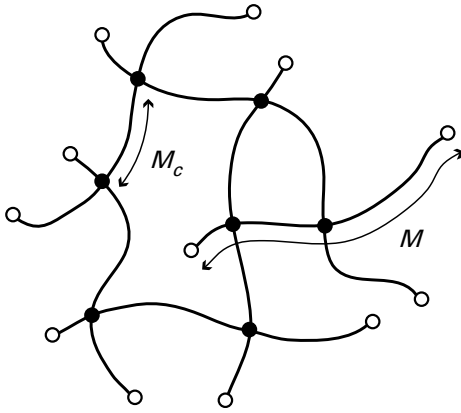
Fig. 4.9   Flory's correction for the dangling chains.
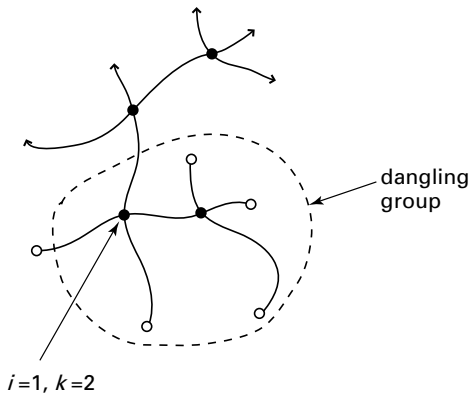
Fig. 4.10   An end group which is dangling from a junction by a single path.

Junctions whose path number is larger than or equal to 3 are called **elastically effective junctions**. Junctions with path number 1 connect dangling chains (Figure 4.10); junctions with path number 2 are not active because they merely extend the already existing paths. Both types should not be counted as effective chains.

The **Scanlan–Case (SC) criterion** states that a subchain is elastically effective if both its ends are connected to the elastically active junctions, i.e., whose path numbers i and i' are larger than or equal to 3 (Figure 4.11). The criterion leads to

$$v_{\text{eff}} = \frac{1}{2} \sum_{k=2}^{\infty} \sum_{i=3}^{2k} i \mu_{ik} \tag{4.30}$$

for the number of elastically effective chains, where the factor 1/2 is necessary to avoid counting the same subchain twice.
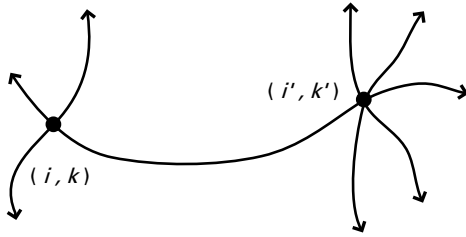
Fig. 4.11 Scanlan–Case criterion for elastically effective chains. Chains with $i \geq 3$ and $i' \geq 3$ are effective.

The number $\mu_{i,k}$ of junctions with specified type can be found as a function of the degree of reaction for polycondensation systems and the random cross-linking of pre-polymers. Also, there has been much research into the nature of the active chains and elastic moduli near the gelation point. Some results will be presented in Section 8.2.

4.2.4 Simple description of thermoelastic inversion

As a simple application of the affine network theory, let us study thermoelastic inversion by taking the effect of thermal expansion into the theory [17]. Consider a sample of rubber to be elongated by $\lambda_0 = 1 + \epsilon_0$ $(\epsilon_0 \ll 1)$ at a reference temperature T_0. The tension is $\sigma \cong 3\nu k_B T_0 \epsilon_0$. If the sample is heated to the temperature T under the constant length, the sample increases its volume, so that the length in equilibrium at T_0 is elongated, which results in a reduction in the degree of elongation by

$$\epsilon = \epsilon_0 - \frac{\beta}{3}(T - T_0), \tag{4.31}$$

where

$$\beta \equiv \frac{1}{V}\left(\frac{\partial V}{\partial T}\right)_p \tag{4.32}$$

is the **thermal expansion coefficient at a constant pressure**. The thermal expansion is caused by the motion of subchains and their molecular interaction.

The tension should be given by

$$\sigma \simeq 3\nu k_B T \left\{ \epsilon_0 - \frac{\beta}{3}(T - T_0) \right\}. \tag{4.33}$$

If the temperature coefficient is calculated under the condition that the degree of elongation ϵ_0 measured relative to the equilibrium length at the reference temperature T_0 is constant, it is

$$\left(\frac{\partial \sigma}{\partial T}\right)_{\epsilon_0} = 3\nu k_B \left\{ \epsilon_0 - \frac{\beta}{3}(2T - T_0) \right\}. \tag{4.34}$$

The critical degree of elongation at which the sign changes is found to be

$$\epsilon_0 = \frac{\beta}{3}(2T - T_0). \tag{4.35}$$

The tension reduces on heating in the small elongation region below this critical value. For instance, if we take $T_0 = 293$ K, $T = 343$ K, and $\beta = 6.6 \times 10^{-4}\,\mathrm{K}^{-1}$, the critical elongation is $\epsilon_0 = 0.086$. It turns out that, for the deformation below 8.6%, thermal expansion dominates the entropic elasticity.

4.3   Phantom network theory

The assumption of Gaussian chains in the affine network theory can be removed by using nonlinear chains, such as the RF model (Langevin chain), stiff chain model (KP chain), etc. These models show enhanced stress in the high-stretching region. The effect of nonlinear stretching will be detailed in Section 4.6.

In contrast, the assumption of affine deformation is difficult to remove. The affine network theory assumes that each subchain deforms in proportion to the macroscopic deformation tensor. However, because the external force neither directly works on the chain nor on the cross-links it bridges, the assumption lacks physical justification. In fact, the junctions change their positions by thermal motion around the average position. It is natural to assume that the nature of such thermal fluctuations remains unchanged while the average position is displaced under the effect of strain.

James and Guth developed a theory of rubber elasticity without the assumption of affine deformation [18, 19, 20]. They introduced the macroscopic deformation as the boundary conditions applied to the surface of the samples. Junctions are assumed to move freely under such fixed boundary conditions. The network chains (assumed to be Gaussian) act only to deliver forces at the junctions they attach to. They are allowed to pass through one another freely, and they are not subject to the volume exclusion requirements of real molecular systems. Therefore, the theory is called the **phantom network theory**.

The main conclusions of this theory are as follows:

JG1: The mean positions of the junctions deform affinely to the strain, while their instantaneous positions are not affine to the strain.

JG2 (**fluctuation theorem**): The fluctuations $\Delta\mathbf{r}$ around the mean positions are Gaussian with a mean square value that is independent of the strain, and is given by

$$\langle (\Delta\mathbf{r})^2 \rangle = \frac{2}{\phi}\langle r_0^2 \rangle, \tag{4.36}$$

where $\phi = 2k$ is the functionality (branch number) of the junctions. For pairwise cross-linking, the branch number is $\phi = 4$, so that the region of thermal fluctuations reaches half of the mean distance between the neighboring junctions [4].

JG3: The elastic free energy of the phantom network theory is

$$(\Delta_{\mathrm{def}} F)_{\mathrm{ph}} = \frac{\xi}{2}k_{\mathrm{B}}T(\lambda_x^2 + \lambda_y^2 + \lambda_z^2 - 3), \tag{4.37}$$

where ξ is the cycle rank of the network. For networks with a constant branch number ϕ, the cycle rank is $\xi = \nu(1 - 2/\phi)$. For instance, $\xi = \nu/2$ for $\phi = 4$.
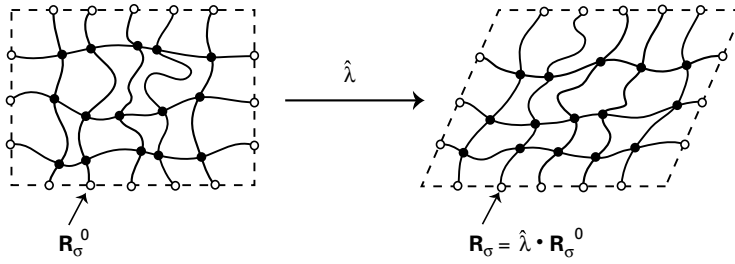
Phantom network theory. Network junctions are classified into σ-junctions at the surface and τ-junctions lying inside the rubber sample.

Therefore, the phantom network theory gives smaller elastic free energy due to the free fluctuations of the junctions.

The main idea of the phantom network theory (Figure 4.12) is summarized as follows [1, 5]. It first classifies the junctions into two categories: σ-junction and τ-junction. The σ-junctions are those fixed on the surface of the sample. They deform affinely to the strain $\hat{\lambda}$.

The τ-junctions are those inside the sample. The external force does not act directly on them. They only receive the stress transmitted through the chains. They are free from the constraints, so that they may fluctuate around their average positions.

To find the free energy of the phantom network, we count the total number of possible conformations of the subchains by integrating over all possible displacements of the τ-junctions. However, because there is no definite criterion to distinguish the surface from the inside of the sample from the microscopic viewpoint, it is difficult to identify the σ- and τ-junctions uniquely. We therefore start here from a microscopic network for which one can find the exact free energy, and grow the junctions step by step to reach the macroscopic one.

4.3.1 Micronetworks of tree form

To clarify the idea of the phantom network, let us first consider finite networks of tree form in which, starting from the central junction A, chains are generated from the junctions with a fixed branch number ϕ one after another (Figure 4.13) [21–23].

In a tree composed of l generations from the center, the number of end points on the outer surface of the network are given by

$$\mu_l = \phi(\phi-1)^{l-1}. \tag{4.38}$$

These end points are assumed to be σ-junctions that deform affinely to the strain. The internal junctions are all regarded as τ-junctions. The total number of chains in the network is

$$\nu_l = \phi[1+(\phi-1)+\cdots+(\phi-1)^{l-1}] = \phi[(\phi-1)^l-1]/(\phi-2). \tag{4.39}$$
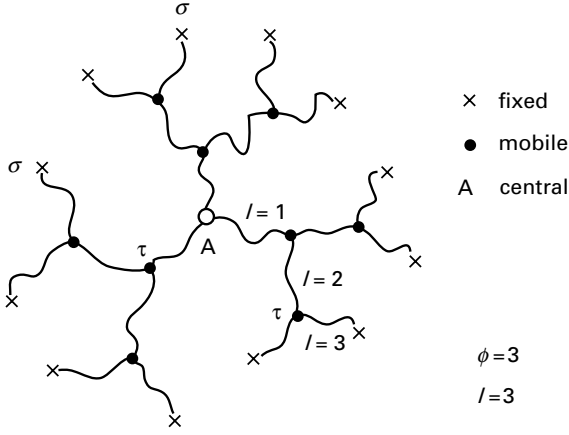
Fig. 4.13   Micronetwork of tree form with l generations.

Starting from the central τ-junction A, we can integrate over possible positions of the τ-junctions one generation after another, and find the elastic free energy

$$(\Delta_{\mathrm{def}} F)_{\mathrm{micro}} = R_l(\phi) \frac{v_l}{2} k_{\mathrm{B}} T \ (\lambda_x^2 + \lambda_y^2 + \lambda_z^2 - 3), \tag{4.40}$$

where $R_l(\phi)$ is the prefactor

$$R_l(\phi) \equiv \frac{\mu_l - 1}{v_l} \cong \frac{(\phi - 2)(\phi - 1)^{l-1}}{(\phi - 1)^l - 1}, \tag{4.41}$$

which indicates the difference from the affine network [22, 23].

For instance, if we fix $l = 2$, we have

$$R_2(\phi) = \frac{\phi - 1}{\phi}. \tag{4.42}$$

This agrees with the result of the tetrahedra model studied by Flory and Rehner [24] to investigate the effect of junction fluctuations in a micronetwork consisting of four chains which start from the corners of the tetrahedra and are connected by one central junction.

For a macroscopic network, the prefactor becomes

$$\lim_{l \to \infty} R_l(\phi) = \frac{\phi - 2}{\phi - 1}, \tag{4.43}$$

by taking $l \to \infty$ limit. It is $R_\infty(4) = 2/3$ for a tetrafunctional tree, $R_\infty(3) = 1/2$ for a trifunctional tree. Both are smaller than the affine network value.

The micronetwork of tree form, however, has a significantly large fraction of σ-junctions relative to the total number of junctions. A correction to improve this deficiency is necessary for application to real networks [22].

There are μ_l subchains with one end of type σ and other end of type τ (σ, τ), and there are $\nu_l - \mu_l$ chains of type (τ, τ). The fraction of each type to the total number of chains is $\mu_l / \nu_l = (\phi - 2)/(\phi - 1)$ and $1 - \mu_l / \nu_l = 1/(\phi - 1)$. Because the factor R_∞ is $(\phi - 1)/\phi$ for type (σ, τ), it can be decomposed into two types as

$$R_\infty = \frac{\phi - 2}{\phi - 1} = \frac{\phi - 1}{\phi} \times \underbrace{\frac{\phi - 2}{\phi - 1}}_{(\sigma, \tau)} + \frac{\phi - 2}{\phi} \times \underbrace{\frac{1}{\phi - 1}}_{(\tau, \tau)}. \tag{4.44}$$

The prefactor R is therefore identified to be $(\phi - 2)/\phi$ for type (τ, τ).

For real samples in which the τ-junctions are dominant, the free energy must be

$$(\Delta_{\mathrm{def}} F)_{\mathrm{ph}} = \frac{\nu}{2} \left(1 - \frac{2}{\phi} \right) k_{\mathrm{B}} T \, (\lambda_x^2 + \lambda_y^2 + \lambda_z^2 - 3). \tag{4.45}$$

This is the free energy (4.37) of the phantom network theory.

Because of the topological relations of the networks, $\nu(1 - 2/\phi)$ is identified to be of cycle rank ξ, and hence the free energy is given by

$$(\Delta_{\mathrm{def}} F)_{\mathrm{ph}} = \frac{\xi}{2} k_{\mathrm{B}} T \, (\lambda_x^2 + \lambda_y^2 + \lambda_z^2 - 3). \tag{4.46}$$

4.3.2 Fluctuation theorem and the elastic free energy

The elastic free energy (4.46) of the phantom network theory can be derived directly from the fluctuation theorem for the junctions [4]. According to (4.18), the free energy change by deformation is equivalent to

$$\Delta_{\mathrm{def}} F(\hat{\lambda}) = \frac{3 \nu k_{\mathrm{B}} T}{2 \langle r_0^2 \rangle} (\langle r^2 \rangle - \langle r_0^2 \rangle), \tag{4.47}$$

where $\mathbf{r}$ is the chain vector after deformation, and $\mathbf{r}_0$ is that before deformation. The symbol $\langle \cdots \rangle$ indicates the average over all possible distributions of the chain vector before deformation.

For the affine networks, the relation $\mathbf{r} = \hat{\lambda} \cdot \mathbf{r}_0$ is assumed, but the phantom networks discard this relation. Let us separate the chain vector into its average and the deviation from the average as

$$\mathbf{r} = \bar{\mathbf{r}} + \Delta \mathbf{r}, \tag{4.48}$$

where $\bar{\mathbf{r}}$ is the average chain vector that minimizes the free energy before deformation under the constraints of the fixed positions of the σ-junctions. Its mean square average is

$$\langle r^2 \rangle = \langle \bar{r}^2 \rangle + \langle (\Delta \mathbf{r})^2 \rangle, \tag{4.49}$$

due to the assumption of the independence between $\bar{\mathbf{r}}$ and $\Delta \mathbf{r}$. In particular

$$\langle r_0^2 \rangle = \langle \bar{r}_0^2 \rangle + \langle (\Delta \mathbf{r})^2 \rangle \tag{4.50}$$

for the undeformed state, so that we have

$$\langle \bar{r}_0^2 \rangle = \left(1 - \frac{2}{\phi} \right) \langle r_0^2 \rangle, \tag{4.51}$$

by the fluctuation theorem (JG2).

If we employ the assumption of the affine displacement $\langle \bar{r}^2 \rangle = \langle (\hat{\lambda} \cdot \mathbf{r}_0)^2 \rangle$ for the average chain vector, we have in (4.47)

$$\langle r^2 \rangle - \langle r_0^2 \rangle = \left\{ \frac{\lambda_x^2 + \lambda_y^2 + \lambda_z^3}{3} - 1 \right\} \langle \bar{r}_0^2 \rangle. \tag{4.52}$$

By the relations (4.47) and (4.51), the free energy turns out to be

$$(\Delta_{\text{def}} F)_{\text{ph}} = \frac{\xi}{2} k_B T (\lambda_x^2 + \lambda_y^2 + \lambda_z^2 - 3), \tag{4.53}$$

where $\xi = (1 - 2/\phi)\nu$ is the cycle rank.

4.4   Swelling experiments

The number of elastically effective chains $\xi = \nu(1 - 2/\phi)$ in phantom network theory is smaller than its affine value ν. In an affine network, all junctions are assumed to displace under the strict constraint of the strain, while in a phantom network they are assumed to move freely around the mean positions. In real networks of rubbers, the displacement of the junctions lies somewhere between these two extremes. To examine the microscopic chain deformation and displacement of the junctions, let us consider deformation of rubbers accompanied by the swelling processes in the solvent (Figure 4.14) [1, 5, 14, 25].

Let L_0 be the length of one side of a cubic sample (volume $V_0 = L_0^3$) when it is made. We choose it as the reference state before deformation. If the sample is synthesized and
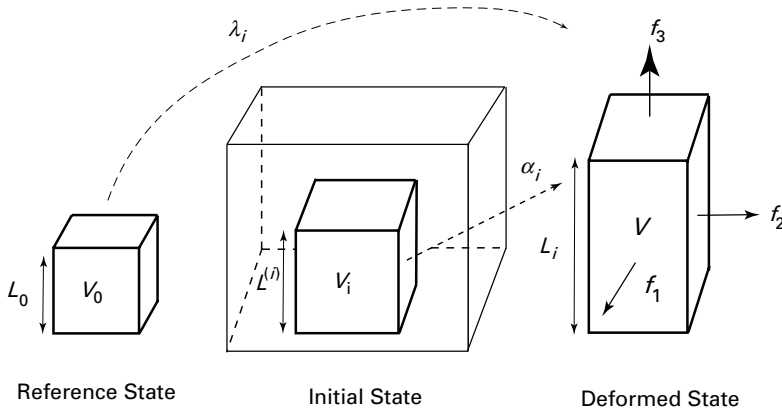
Fig. 4.14   Swelling experiments. The sample swollen by the solvent is deformed by the applied force.

cross-linked in a solvent, this cube includes solvent molecules. In such cases, let V_{dry} be the volume of the network when it is dried, and let

$$\phi_c \equiv V_{dry}/V_0 \tag{4.54}$$

be the volume fraction of the polymer in the reference state.

The sample is then immersed in a solvent for the swelling experiment. It is swollen to the length $L^{(i)}$ of one side. The volume is $V_i = (L^{(i)})^3$, so that the volume fraction becomes

$$\phi \equiv V_{dry}/V_i. \tag{4.55}$$

This is taken as the initial volume fraction of the deformation experiment.

The force $\mathbf{f}$ is given to the sample to bring it to the final equilibrium in the deformed state. The stress in this final state is then measured (Figure 4.14).

Let L_x, L_y, L_z be the length of each side of the sample in the final state. The macroscopic deformation tensor $\hat{\lambda}$ takes the form

$$\lambda_j \equiv \frac{L_j}{L_0} \qquad (j = x, y, z). \tag{4.56}$$

When the volume change by deformation can be neglected, the relation $V_i = V = L_x L_y L_z$ holds. The deformation tensor *relative to the initial state* is then given by

$$\alpha_j \equiv \frac{L_j}{L^{(i)}} = \left(\frac{V_0}{V}\right)^{1/3} \lambda_j. \tag{4.57}$$

The difference between λ and α should be noticed in the swelling experiments.

In the case of uniaxial elongation in the x direction by an applied tension f, the deformation tensor has the elements

$$\lambda_x = \alpha \left(\frac{V}{V_0}\right)^{1/3}, \tag{4.58a}$$

$$\lambda_y = \lambda_z = \frac{1}{\sqrt{\alpha}} \left(\frac{V}{V_0}\right)^{1/3}, \tag{4.58b}$$

where $\alpha \equiv \alpha_x$ is the elongation relative to the initial swollen state.

By the derivative of the free energy $f = (\partial \Delta_{def} F / \partial \lambda_x)_T / L_0$, the tension is found to be

$$f = \frac{\mathcal{F} k_B T}{L_0} \left(\lambda_x - \left(\frac{V}{V_0}\right) \frac{1}{\lambda_x^2}\right) = \left(\frac{\mathcal{F} k_B T}{L^{(i)}}\right) \left(\frac{V}{V_0}\right)^{2/3} \left(\alpha - \frac{1}{\alpha^2}\right). \tag{4.59}$$

The prefactor $\mathcal{F}$ takes the value ν for the affine networks, and ξ for the phantom networks. By dividing the area $A = (L^{(i)})^2/\alpha$ of the sample under deformation, the stress τ_x is given by

$$\tau_x = \frac{\mathcal{F} k_B T}{V} \left(\frac{V}{V_0}\right)^{2/3} \left(\alpha^2 - \frac{1}{\alpha}\right). \tag{4.60}$$

To compare with the experimental data with the theoretical prediction, we introduce **reduced stress** $[f]$ by the definition

$$[f] \equiv \frac{f\phi^{1/3}}{A_{\text{dry}}(\alpha - \alpha^{-2})}.$$

The area in the denominator is not the area in the reference state, but in the dry state. From (4.59), it is given by

$$[f] = \left(\frac{\mathcal{F}k_{\text{B}}T}{V_{\text{dry}}}\right)\phi_c^{2/3}, \tag{4.61}$$

which is independent of the degree α of elongation.

Figure 4.15 plots the reduced tension of a natural rubber against the reciprocal degree of elongation α^{-1}. As predicted by the theories, the experimental data lie in-between the upper limit of the affine network theory and the lower limit of the phantom network theory [5].

The data depend on the elongation α, however, suggesting that the fluctuation of the junctions is not completely free from the strain. The degree of constraint depends on the elongation.

The upturn of the data in the limit of high elongation indicates partial crystallization of the polymer segments that are oriented in parallel to the direction of elongation. For uniaxial compression of the sample, the stress in the swollen state is much smaller than the unswollen states. This may be attributed to the disentanglement of chains due to swelling; swelling reduces the topological constraints, and makes the motion of the junctions easier.

Figure 4.16 shows the detailed experimental data on the depression of the stress. The extrapolation to $\alpha \to \infty$ gives the **first Mooney constant** $2C_1$, which turns out to be independent of the polymer volume fraction ϕ. In contrast, the slope of the lines decreases
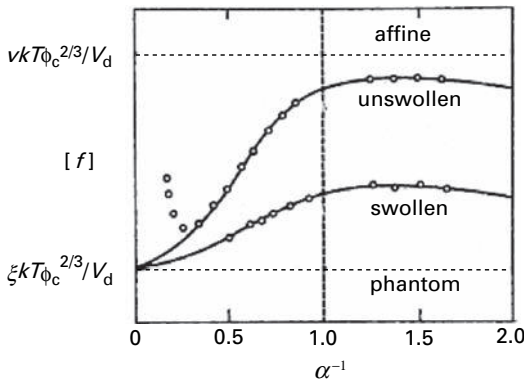
Fig. 4.15   Reduced stresses in the swollen (upper line) and unswollen (lower line) states. Experimental data lie in-between the limits predicted by the affine and phantom network theories. The tension reduces on swelling. (Reprinted with permission from Ref. [5], Chap. 8.)
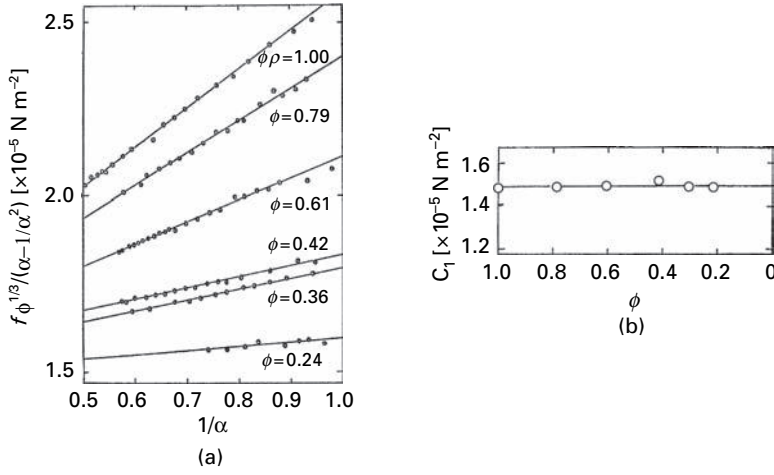
Fig. 4.16 (a) Detailed data of the reduced stress in the range $0.5 \leq \alpha^{-1} \leq 1.0$ plotted against α^{-1}. (b) The first Mooney constant C_1 is obtained by the extrapolation into $\alpha^{-1} \to 0$. (Reprinted with permission from Ref. [26].)

by dilution of the rubber. Thus the **second Mooney constant** $2C_2$ decreases by swelling, suggesting that it is related to the degree of entanglement of the chains.

We can understand the thermoelastic inversion by noticing the difference between the two distinct concepts of elongations; one defined relative to the reference state (λ), and the other defined relative to the initial state (α).

Suppose the volume expansion from V_0 to V is induced not by swelling but by thermal expansion. Then, the volume in the initial state is $V = V_0(1 + \beta \Delta T)$, where $\Delta T \equiv T - T_0$. For a small deformation $\lambda = 1 + \epsilon$ ($\epsilon \ll 1$), the stress (4.59) takes the form

$$f = \frac{\mathcal{F} k_B T}{L_0} \left\{ 1 + \epsilon - \frac{1 + \beta \Delta T}{(1+\epsilon)^2} \right\} \simeq \frac{3\mathcal{F} k_B T}{L_0} \left(\epsilon - \frac{\beta}{3} \Delta T \right). \tag{4.62}$$

The temperature coefficient of the tension f at constant ϵ is then given by

$$\left(\frac{\partial f}{\partial T} \right)_\epsilon = \frac{3\mathcal{F} k_B}{L_0} \left\{ \epsilon - \frac{\beta}{3} (2T - T_0) \right\}. \tag{4.63}$$

We thus reach the result (4.34) in a simple way.

We next briefly describe **two-dimensional deformation**. Consider a biaxial expansion in the x and y directions caused by applying the stresses τ_x and τ_y. We will find the relation between the stresses and the elongation α_x and α_y [5].
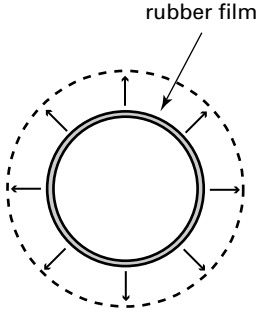
rubber film

Fig. 4.17   Extension of a rubber film. A spherical balloon made of rubber film is swollen by a gas, and the two-dimensional stress is measured.

By definition, we have $\lambda_x = \alpha_x (V/V_0)^{1/3}$, $\lambda_y = \alpha_y (V/V_0)^{1/3}$, and $\lambda_z = (1/\sqrt{\alpha_x \alpha_y})(V/V_0)^{1/3}$. The stresses are then given by

$$\tau_x = 2\left(\frac{\mathcal{F}k_{\mathrm{B}}T}{V}\right)\left(\frac{V}{V_0}\right)^{2/3}\left(\alpha_x^2 - \frac{1}{\alpha_x^2 \alpha_y^2}\right),\tag{4.64a}$$

$$\tau_y = 2\left(\frac{\mathcal{F}k_{\mathrm{B}}T}{V}\right)\left(\frac{V}{V_0}\right)^{2/3}\left(\alpha_y^2 - \frac{1}{\alpha_x^2 \alpha_y^2}\right),\tag{4.64b}$$

from (4.59). In the special case of the expansion of a spherical balloon made of rubber film (Figure 4.17), we have a symmetry $\alpha_x = \alpha_y \equiv \alpha$, so that

$$\tau = 2\left(\frac{\mathcal{F}k_{\mathrm{B}}T}{V}\right)\left(\frac{V}{V_0}\right)^{2/3}\left(\alpha^2 - \frac{1}{\alpha^4}\right).$$

In the case where a shear deformation in the x direction is given while the y direction is kept undeformed by adjusting the force f_y, we have $\alpha_x \equiv \alpha, \alpha_y = 1$, so that the stresses are

$$\tau_x = 2\left(\frac{\mathcal{F}k_{\mathrm{B}}T}{V}\right)\left(\frac{V}{V_0}\right)^{2/3}\left(\alpha^2 - \frac{1}{\alpha^2}\right),\tag{4.65a}$$

$$\tau_y = 2\left(\frac{\mathcal{F}k_{\mathrm{B}}T}{V}\right)\left(\frac{V}{V_0}\right)^{2/3}\left(1 - \frac{1}{\alpha^2}\right).\tag{4.65b}$$

The relation (4.59) has thus many applications.

4.5   Volume transition of gels

When rubbers and gels are immersed in a good solvent, they absorb solvent molecules and swell. If the tendency for the solvent to permeate into the network (osmotic pressure

reference state

$V_0 = (N^* + n_V)a^3 = L_0{}^3$

ΔF

f

$\lambda_x L_0$

V

n

$\lambda_y L_0$
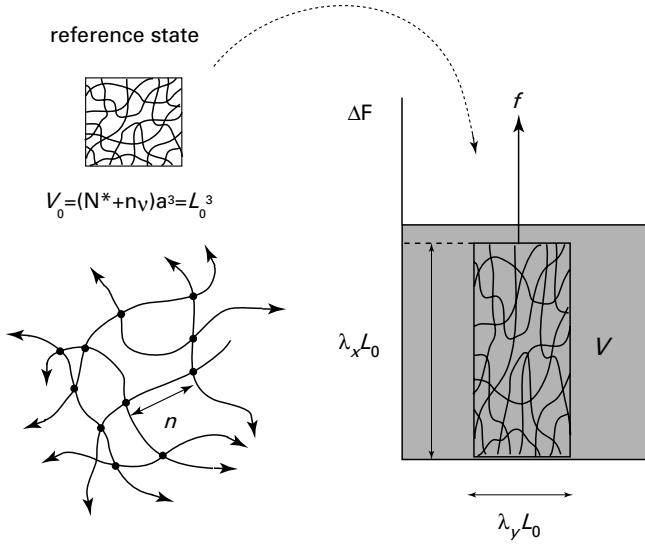
Fig. 4.18 Sample of a gel consisting of subchains of length n in the reference state (volume V_0) is immersed in a solvent and swollen to the equilibrium state (volume V) under a constant force f.

of the network) and for the network to restore its initial state (elastic force) balance, the mixed system reaches an equilibrium state. Combining the elastic free energy of the network with the free energy of mixing, we study the swelling equilibrium of the cross-linked polymer networks under specified environmental conditions [1, 28].

The volume in the reference state of the gel when it is prepared (cross-linked) is written as

$$V_0 \equiv L_0{}^3 = (N_0^* + nN)a^3, \tag{4.66}$$

where N_0^* is the number of the solvent molecules in the preparation stage, N is the total number of subchains, and n the average number of repeat units on a subchain. The length a is the size of a repeat unit, which is for simplicity assumed to be the same as the size of a solvent molecule (Figure 4.18). The volume fraction of polymers in the reference state is $\phi_c = nNa^3/V_0$. When the gel is immersed after being dried, the reference volume is $V_{\text{dry}} = nNa^3$ or $\phi_c = 1$.

The gel adsorbs solvent molecules and swells to the volume V. If the number of solvent molecules inside the gel network is N_0 in the initial state, the volume is $V = (N_0 + nN)a^3$. The volume fraction of the polymer inside the gel is $\phi \equiv V_{\text{dry}}/V$, and the **degree of swelling** is

$$Q \equiv V/V_0 = \phi_c/\phi. \tag{4.67}$$

Let $\lambda_x, \lambda_y, \lambda_z$ be the expansion factor of the side in each direction. The swelling ratio is then given by $Q = \lambda_x \lambda_y \lambda_z$.

In particular, when the gel swells under no tension, it undergoes an isotropic free expansion, so that $\lambda_x = \lambda_y = \lambda_z$. Let λ be the expansion ratio

$$\lambda_x = \lambda_y = \lambda_z \equiv \lambda = (\phi_c/\phi)^{1/3}. \tag{4.68}$$

When the gel swells under uniaxial tension in the x direction, the expansion ratios are by symmetry

$$\lambda_x = \lambda, \qquad \lambda_y = \lambda_z = \left(\frac{\phi_c}{\lambda\phi}\right)^{1/2}, \tag{4.69}$$

where λ is the elongation in the x direction.

The free energy of a swollen gel consists of two parts of different origin: the elastic free energy $\Delta_{\mathrm{def}} F$ of the network and the free energy $\Delta_{\mathrm{mix}} F$ of mixing. The total free energy is considered to be the sum $\Delta F = \Delta_{\mathrm{def}} F + \Delta_{\mathrm{mix}} F$.

The elastic free energy is

$$\Delta_{\mathrm{def}} F = \frac{\nu}{2} k_{\mathrm{B}} T \left[\lambda^2 + \frac{2}{\lambda}\left(\frac{\phi_c}{\phi}\right) + \mu \ln\left(\frac{\phi}{\phi_c}\right)\right], \tag{4.70}$$

within the theoretical scheme of the affine network (4.20). The last term $\mu \ln(\phi/\phi_0)$ is the correction term for the volume change. The coefficient μ depends on the cross-link density.

For **free swelling**, (4.68) gives

$$\Delta_{\mathrm{def}} F = \frac{\nu}{2} k_{\mathrm{B}} T \left[3\left(\frac{\phi}{\phi_c}\right)^{-2/3} + \mu \ln\left(\frac{\phi}{\phi_c}\right)\right]. \tag{4.71}$$

The free energy of mixing is given by

$$\Delta_{\mathrm{mix}} F = \frac{V}{a^3} k_{\mathrm{B}} T \left[(1-\phi)\ln(1-\phi) + \chi(T)\phi(1-\phi)\right] \tag{4.72}$$

by the Flory–Huggins lattice theory, where the mixing entropy term due to the translational motion of mass center has been neglected because the molecular weight of the polymer (gel) is infinity.

The tension can be found from the differential of the free energy with respect to L_x. It turns out to be

$$f = \left(\frac{\partial \Delta F}{\partial L_x}\right)_T = \frac{k_{\mathrm{B}} T}{L_0}\left(\frac{\partial \beta \Delta F}{\partial \lambda}\right) \equiv \frac{\nu k_{\mathrm{B}} T}{L_0} t, \tag{4.73}$$

where t is the dimensionless tension, given by

$$t \equiv \frac{f L_0}{\nu k_{\mathrm{B}} T} = \lambda - \frac{1}{\lambda^2}\left(\frac{\phi_c}{\phi}\right). \tag{4.74}$$

For free swelling under $t = 0$, this relation goes back to $\phi_c/\phi = \lambda^3$.

In the equilibrium state, solvent molecules are free to pass between the inner and outer regions of the gel. Hence the chemical potential of the solvent molecule inside the gel

$$\beta \Delta \mu_0 = \eta \frac{\phi}{n} A(\phi, \lambda) + \ln(1 - \phi) + \phi + \chi(T)\phi^2, \tag{4.75}$$

should be equal to the chemical potential in the environment $\Delta \mu_0 (= 0)$. The number ν of elastically effective chains differs in general from the total number of chains N, so that it is written as $\nu = \eta N$, where η is the fraction of effective chains. For uniaxial elongation, the elastic part of the free energy is

$$A(\phi, \lambda) = \frac{1}{\lambda} \left(\frac{\phi_c}{\phi} \right) - \frac{\mu}{2}, \tag{4.76}$$

and for free swelling it is

$$A(\phi, \lambda) = \left(\frac{\phi_c}{\phi} \right)^{2/3} - \frac{\mu}{2}. \tag{4.77}$$

The rest of the terms in (4.75) represent the effect of the osmotic pressure of the network.

The equilibrium condition takes the form

$$\eta \frac{\phi}{n} A(\phi, \lambda) + \ln(1 - \phi) + \phi + \chi(T)\phi^2 = 0. \tag{4.78}$$

The solution of the coupled equations (4.74) and (4.78) gives the degree of elongation λ and the volume fraction ϕ as functions of the temperature and the tension.

4.5.1   Free swelling

Because the swelling ratio Q lies above 10 in common gels, the volume fraction ϕ is small enough to expand the logarithm in (4.78) in powers of ϕ. Taking (4.78) up to the second order, we have

$$\frac{\eta}{n} \phi \left[\left(\frac{\phi_c}{\phi} \right)^{2/3} - \frac{\mu}{2} \right] \simeq \left(\frac{1}{2} - \chi \right) \phi^2. \tag{4.79}$$

If we further neglect $\mu/2$ in $[\cdots]$ on the left-hand side, we find the swelling ratio as

$$Q_0 \cong \left(\frac{n\psi\tau}{\eta \phi_c^{2/3}} \right)^{3/5}. \tag{4.80}$$

We have employed the interaction parameter χ of the Shultz–Flory type (2.105) with $\tau \equiv 1 - \Theta/T$ the dimensionless temperature deviation from the theta temperature.[2] As we are studying swelling by good solvents, therefore we have $\tau > 0$.

Thus, the volume of the gel increases continuously with the temperature if we employ the usual Shultz–Flory interaction parameter. However, it was observed that cross-linked

---

[2] τ should not be confused with the stress.
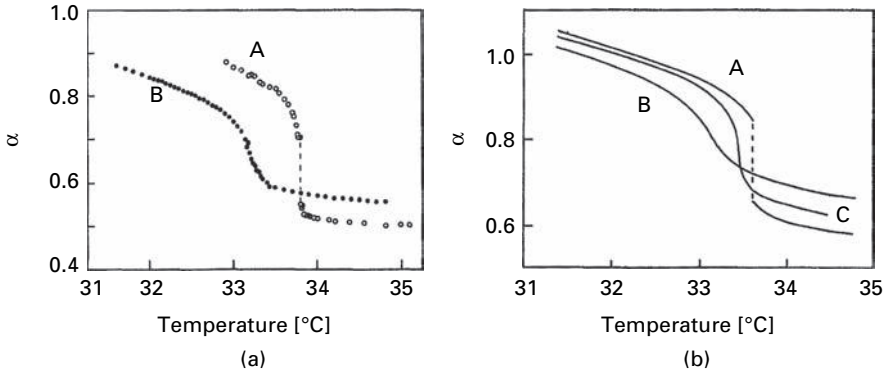
Fig. 4.19   Volume transition of gels. (a) Experimental data of cross-linked PNIPAM gels. (b) Phenomenological description by the concentration-dependent interaction parameter. Discontinuous transition can be derived by a special form of (4.81) and (4.82) with $\Delta h = -7.505\,\text{kJ}\,\text{mol}^{-1}$, $\Delta s = -2.841\,\text{J}\,\text{K}^{-1}\,\text{mol}^{-1}$, $\chi_2 = 0.518$, $\eta = 1$. Curve A: $\phi_0 = 0.075$, $N/V_0 = 0.017\,\text{mol}\,\text{dm}^{-3}$; curve B: $\phi_0 = 0.114$, $N/V_0 = 0.040\,\text{mol}\,\text{dm}^{-3}$; curve C: critical value $\phi_0 = 0.090$, $N/V_0 = 0.023\,\text{mol}\,\text{dm}^{-3}$. (Reprinted with permission from Ref. [30].)

gels of a temperature-sensitive water-soluble polymer, **poly(N-isopropylacrylamide)** (PNIPAM), reveal a discontinuous volume change if certain conditions are fulfilled in the preparation stage [28]. The volume transition of PNIPAM is a reverse transition; gels collapse on heating. Therefore, the interaction parameter must increase with the temperature.

To explain the discontinuous reverse transition of PNIPAM gels, Hirotsu introduced the concentration-dependent χ parameter in the simple form

$$\chi(\phi, T) = \chi_1(T) + \chi_2(T)\phi, \tag{4.81}$$

as in the VLBW treatment (2.131), and attempted to reproduce the discontinuous swelling curve [29, 30]. He separated the first term into enthalpy and entropy parts as

$$\chi_1(T) = (\Delta h - T\Delta s)/RT, \tag{4.82}$$

where both Δh and Δs are negative. If $\Delta h - T\Delta s < 0$, χ_1 increases with the temperature, leading to high-temperature collapse. Figure 4.19 shows some swelling curves with different values for $\Delta h, \Delta s$, and χ_2. The molecular modeling for the origin of these parameters of PNIPAM chains is possible through the detailed study of hydration.

4.5.2   Swelling under uniaxial elongation

For **uniaxial elongation**, the equilibrium condition is

$$\frac{\eta}{n}\phi\left[\frac{1}{\lambda}\left(\frac{\phi_c}{\phi}\right) - \frac{\mu}{2}\right] \simeq \left(\frac{1}{2} - \chi\right)\phi^2. \tag{4.83}$$
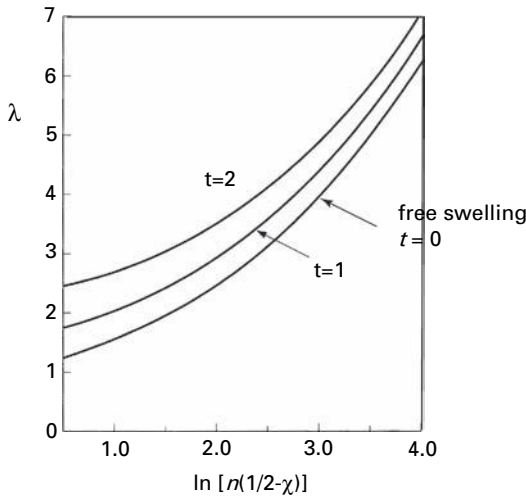
Fig. 4.20   Ratio λ for a uniaxial elongation under a constant tension plotted against the reduced temperature. The dimensionless tension is varied from curve to curve.

Eliminating ϕ by using the relation (4.74), and neglecting $\mu/2$ on the left-hand side, we find the relation between the tension and elongation as

$$\frac{\eta}{n}\lambda^3(\lambda - t)^2 \simeq \left(\frac{1}{2} - \chi\right)\phi_c. \tag{4.84}$$

Solving for the tension t, we find

$$t = \lambda - \frac{1}{\lambda^{3/2}}\left(\frac{n}{\eta}\psi\tau\phi_c\right)^{\frac{1}{2}}. \tag{4.85}$$

In Figure 4.20, the elongation ratio λ is plotted as a function of the reduced temperature $\ln(n\psi\tau/\eta)$. The swelling ratio increases with the tension t, and hence the gel absorbs more solvent molecules when stretched.

The ratio between the deformation parallel with and perpendicular to the tension,[3]

$$\sigma = -\frac{\ln\lambda_y}{\ln\lambda_x}, \tag{4.86}$$

is the **Poisson ratio**.

For homogeneous isotropic materials, it is identical to

$$\sigma = \frac{3K - 2\mu}{2(3K + \mu)}, \tag{4.87}$$

---

[3] Do not confuse this with the stress σ.

where K is the bulk modulus and μ is the shear modulus[4] [31]. Since K and μ must be positive for a stable matter, σ must take a value in the range $-1 \leq \sigma \leq 1/2$. If the material is incompressible ($K \to \infty$), then $\sigma = 1/2$. This is the upper limit of the ratio. For the soft limit $K \to 0$, the lower bound of the Poisson ratio $\sigma = -1$ is reached [31].

In reality, most materials have σ between 0 and 1/2. For a single chain swollen in a good solvent, scaling argument leads to $\sigma = 1/4$ [32]. The measurement of the ratio K/μ of the swollen polyacrylamide gels [33] showed that μ takes a value between 0.26 and 0.29 depending on the preparation condition.

For a gel swollen under tension, the Poisson ratio (4.86) is given by

$$\sigma = \frac{1}{4}\left[1 - \frac{\ln(n\psi\tau/\eta)}{\ln\lambda}\right]. \tag{4.88}$$

Hence, it may take negative values in a certain temperature range. When gels are stretched in the x direction, they absorb solvent molecules and enhance swelling, so that they expand in the y and z directions as well. Because they are open systems that solvent molecules can enter and leave, a negative Poisson ratio is possible. It does not contradict with the stability condition of the matter.

4.6   Networks made up of nonlinear chains

In both the affine and phantom network theories, the chains have so far been assumed to be Gaussian. In practical experiments, complex situations arise such as the effect of stretching beyond the Gaussian regime, conformational change, partial crystallization of the subchains, etc. This section focuses on the nonlinear effect induced by the high elongation of rubbers, paying special attention to the S-shaped stress–strain curve (the **stress upturn** in the high-elongation region). An improvement of the theory is attempted by using a Langevin chain in place of a Gaussian chain.

The single chain partition function $Q_1(f,T)$ under the action of the tension f for the random flight model chain with a bond length a takes the asymptotic form

$$Q_1(f,T) \simeq \lambda_0(t)^n, \tag{4.89}$$

in the limit of large n by (1.15), where $t \equiv fa/k_B T$ is the dimensionless tension, and

$$\lambda_0(t) = \sinh t/t. \tag{4.90}$$

is the factor that appears after integration over the rotational angle. It is regarded as the maximum eigenvalue for the partition function. The mean end-to-end distance is derived from the relation

$$R = \frac{\partial}{\partial f}(nk_B T \ln \lambda_0), \tag{4.91}$$

---

[4] Do not confuse this with the numerical coefficient μ in (4.70).

Its normalized value $l \equiv R/na$ is

$$l = \frac{\partial}{\partial t} \ln \lambda_0(t). \tag{4.92}$$

Let us solve this relation for t, and express it as $t = \psi(l)$. The free energy of the chain is then given by

$$\phi(l) = \int_0^{\mathbf{R}} \mathbf{f} \cdot d\mathbf{R} = nk_{\mathrm{B}}T \int_0^l t \, dl$$

$$= nk_{\mathrm{B}}T \int_0^t t \frac{dl}{dt} dt = nk_{\mathrm{B}}T \left[lt - \int_0^t l \, dt \right], \tag{4.93}$$

or equivalently,

$$\phi(l) = nk_{\mathrm{B}}T [l\psi(l) - \ln \lambda_0(\psi(l))]. \tag{4.94}$$

Hence, the distribution function of the end vector $\mathbf{R}$ is

$$P_0(l) = Ce^{-\beta\phi(l)} = Ce^{-ng(l)}, \tag{4.95}$$

where $g(l)$ is the dimensionless free energy, defined by

$$g(l) \equiv l\psi(l) - \ln \lambda_0(\psi(l)). \tag{4.96}$$

The normalization constant C is given by

$$C = \int_0^1 4\pi l^2 e^{-ng(l)} dl. \tag{4.97}$$

The elastic free energy of an affine network made up of such Langevin chains is written as

$$\Delta_{\mathrm{def}} F(\hat{\lambda}) = \nu \int [\phi(\hat{\lambda} \cdot \mathbf{R}_0) - \phi(\mathbf{R}_0)] P_0(\mathbf{R}_0) d\mathbf{R}_0, \tag{4.98}$$

by using the single chain free energy $\phi(\mathbf{R})$ similarly to (4.20), where $\hat{\lambda}$ is the deformation tensor, $\mathbf{R}_0$ is the chain vector before deformation, $P_0(\mathbf{R}_0)$ is its distribution function, and ν is the number of elastically effective chains. This is transformed to

$$\frac{\Delta_{\mathrm{def}} F(\hat{\lambda})}{\nu k_{\mathrm{B}}T} = n \int [g(\hat{\lambda} \cdot \mathbf{l}) - g(\mathbf{l})] P_0(\mathbf{l}) d\mathbf{l}, \tag{4.99}$$

by using the normalized chain vector $\mathbf{l} \equiv \mathbf{R}/na$.

For uniaxial elongation with $\lambda_x = \lambda$, $\lambda_y = \lambda_z = 1/\sqrt{\lambda}$, we have

$$|\hat{\lambda} \cdot \mathbf{l}| = [\lambda^2 x^2 + (y^2 + z^2)/\lambda]^{1/2} \equiv \eta(\lambda, \theta) l, \tag{4.100}$$

where the factor η is

$$\eta(\lambda, \theta) \equiv \left[\left(\lambda^2 + \frac{1}{\lambda} \right) \cos^2 \theta - \frac{1}{\lambda} \right]^{1/2}. \tag{4.101}$$

The tension f is derived by the differential $f = \partial \Delta F(\hat{\lambda})/\partial(\lambda L_0)$ with L_0 being the length before the deformation is given. It is

$$\frac{f L_0}{\nu k_\mathrm{B} T} = n \int_0^1 2\pi l^3 dl \int_0^1 \frac{\zeta(\lambda,\theta)}{\eta(\lambda,\theta)} \psi(\eta l) P_0(l) d\cos\theta, \qquad (4.102)$$

where the relation

$$\frac{\partial g(|\hat{\lambda}\cdot\mathbf{l}|)}{\partial\lambda} = \frac{\partial}{\partial\lambda} g(\eta l) = g'(\eta l)\frac{d\eta}{d\lambda} l = \psi(\eta l)\frac{\zeta}{\eta} l \qquad (4.103)$$

has been used for the differentiation of $g(|\hat{\lambda}\cdot\mathbf{l}|)$. The factor $\zeta(\lambda,\theta)$ is defined by

$$\zeta(\lambda,\theta) \equiv \left(2\lambda + \frac{1}{\lambda^2}\right)\cos^2\theta - \frac{1}{\lambda^2}. \qquad (4.104)$$

For a Gaussian chain, in particular, we have $\lambda_0 = e^{t^2/6}$, $\ln\lambda_0 = t^2/6$, $\lambda = t/3$, so that we find $t \equiv \psi(l) = 3l$. The free energy is $g(l) = 3l^2 - (3l)^2/6 = 3l^2/2$. Using the relations $\psi(\eta l)\zeta/\eta = 3l\zeta$, $\int_0^1 d\cos\theta\,\zeta(\lambda,\theta) = 2(\lambda - 1/\lambda^2)/3$, the dimensionless tension is given by $f L_0/\nu k_\mathrm{B} T = \lambda - 1/\lambda^2$. We have thus confirmed the previous results on Gaussian affine networks.

For a **Langevin chain**, we have $\lambda_0 = (\sinh t)/t$, $\ln\lambda_0 = \ln(\sinh t/t)$, $l = L(t) = \coth t - 1/t$, so that $\psi(l) = L^{-1}(l)$ is described by the inverse Langevin function. The dimensionless tension is

$$\frac{f L_0}{\nu k_\mathrm{B} T} = 2n\pi \int_0^1 dl\, l^3 P_0(l) \int_0^1 \psi(\eta l)\frac{\zeta}{\eta} d\cos\theta. \qquad (4.105)$$

Wang and Guth [34] and Treloar [2] simplified the result by introducing three independent representative chains instead of carrying out the integral of $\cos\theta$. The chain under consideration is replaced by its three projections onto the x-,y-,z-axis, and their summation is taken. These projected chains have $\theta = 0$ (x direction), $\pi/2$ (y,z direction). Because $\zeta/\eta = 2$ for $\theta = 0$ (one chain), $\zeta/\eta = -1/\lambda^{3/2}$ for $\theta = \pi/2$ (two chains), we find for such a three-chain model that

$$\frac{f L_0}{\nu k_\mathrm{B} T} = n \int_0^1 \left[\psi(\lambda l) - \frac{1}{\lambda^{3/2}}\psi\left(\frac{l}{\sqrt{\lambda}}\right)\right] P_0(l) 4\pi l^3 dl. \qquad (4.106)$$

Moreover, the integration with respect to l is approximated by the value at the mean square end-to-end distance $R_0 = \sqrt{n}\,a$ of a Gaussian chain, or equivalently $l = l_0 \equiv \sqrt{n}\,a/na = 1/\sqrt{n}$, so that the tension takes a simple form

$$\frac{f L_0}{\nu k_\mathrm{B} T} = \frac{n^{1/2}}{3}\left[L^{-1}\left(\frac{\lambda}{n^{1/2}}\right) - \frac{1}{\lambda^{3/2}} L^{-1}\left(\frac{1}{\lambda^{1/2} n^{1/2}}\right)\right]. \qquad (4.107)$$

Due to the nonlinear property of a Langevin chain, the S-shaped tension–elongation profile as shown in Figure 4.7 (solid line with data points) is well reproduced by this theory.

References

[1] Flory, P. J., *Principles of Polymer Chemistry*, Chap. XI. Cornell University Press: Ithaca, NY, 1953.

[2] Treloar, L. R. G., *The Physics of Rubber Elasticity*, Chap. 2. Oxford Univ. Press: New York, 1975.

[3] Anthony, R. L.; Caston, R. H.; Guth, E., *J. Phys. Chem.* **46**, 826 (1942). Copyright (1942) American Chemical Society.

[4] Flory, P. J., *Proc. R. Soc. London, Ser. A* **1976**, *351*, 351-380.

[5] Mark, J. E.; Erman, B., *Rubberlike Elasticity: A Molecular Primer*. Wiley.: New York, 1988.

[6] Dart, S. L.; Anthony, R. L.; Guth, E., *Ind. Eng. Chem.* **34**, 1340 (1942).

[7] Kuhn, W., *Kolloid-Zeitschrift* **68**, 2 (1934).

[8] Wall, F. T., *J. Chem. Phys.* **10**, 485 (1942).

[9] Treloar, L. R. G., *Trans. Faraday Soc.* **40**, 59 (1944).

[10] Mooney, *J. Appl. Phys.* **11**, 582 (1940).

[11] Mooney, M., *J. Appl. Phys.* **19**, 434 (1948).

[12] Rivlin, R. S., *Trans. Roy. Soc. (London)* **A240**, 459; 491; 509 (1948).

[13] Rivlin, R. S., *Trans. Roy. Soc. (London)* **1948**, *A241*, 379.

[14] Flory, P. J., *Chem. Rev.* **35**, 51 (1944).

[15] Scanlan, J., *J. Polym. Sci.* **43**, 501 (1960).

[16] Case, L. C., *J. Polym. Sci.* **45**, 397 (1960).

[17] Shen, M., *Macromolecules* **2**, 358 (1969).

[18] James, H. M.; Guth, E., *J. Chem. Phys.* **11**, 455 (1943).

[19] James, H. M., *J. Chem. Phys.* **15**, 651 (1947).

[20] James, H. M.; Guth, E., *J. Chem. Phys.* **15**, 669 (1947).

[21] Graessley, W. W., *Polymeric Liquids & Networks: Structure and Properties*. Garland Science: London, 2004.

[22] Graessley, W. W., *Macromolecules* **1975**, *8*, 186–190.

[23] Graessley, W. W., *Macromolecules* **1975**, *8*, 865–868.

[24] Flory, P. J.; Rehner, J., *J. Chem. Phys.* **11**, 512 (1943).

[25] Flory, P. J.; Rehner, J. J., *J. Chem. Phys.* **11**, 521 (1943).

[26] Flory, P. J., *Polym. J.* **17**, 1 (1985).

[27] Hill, T. L., *An Introduction to Statistical Thermodynamics*. Dover: New York, 1986.

[28] Hirokawa, Y.; Tanaka, T., *J. Chem. Phys.* **81**, 6379 (1984).

[29] Hirotsu, S., *J. Chem. Phys.* **88**, 427 (1988).

[30] Hirotsu, S. *J. Chem. Phys.* **94**, 3949 (1991).

[31] Landau, L. D.; Lifshitz, E. M., *Theory of Elasticity*, Section 5. Pergamon Press: New York, 1981.

[32] Geissler, E.; Hecht, A. M., *Macromolecules* **13**, 1276 (1980).

[33] Geissler, E.; Hecht, A. M.; Horkay, F.; Zrinyi, M., *Macromolecules* **21**, 2594 (1988).

[34] Wang, M. C.; Guth, E., *J. Chem. Phys.* **20**, 1144 (1952).

5 Associating polymer solutions and thermoreversible gelation

This chapter presents a general theoretical framework for the study of polymer solutions in which polymers are associated with each other by strongly attractive forces, such as hydrogen bonding and hydrophobic interaction. The Flory–Huggins free energy is combined with the free energy of association (reversible reaction) to study the mutual interference between phase separation and molecular association. The effective interaction parameters renormalized by the specific interactions are derived as functions of the polymer concentration.

5.1 Historical survey of the study of associating solutions

The molecular association in liquid phases has been one of the classical problems of chemical thermodynamics ever since physico-chemical studies were initiated at the beginning of the 20th century. Dolezalek [1] showed that the observed deviation from Raoult's law and the melting point depression in water/alcohol mixtures can be explained by dimer formation of alcohol molecules due to hydrogen bonding. Kempter and Mecke [2, 3] proposed that in some cases association may be developed into an infinite series (**KM series**):

$$A \rightleftharpoons A_2 \rightleftharpoons A_3 \rightleftharpoons \cdots, \tag{5.1}$$

and in others particular types of oligomers such as cyclic m-mer (A_m(ring)) are stabilized. They studied the molecular association (**chain–ring equilibrium**) within the theoretical framework of **athermal associated solutions**. Prigogine and coworkers focused on the strong orientational effects seen in hydrogen bonding, such as in acetic acid, benzoic acid, etc., and augmented the conventional theory of **regular solutions** to include dimerization, hetero-dimerization (addition complex), chain association, and three-dimensional networks. Their works are compiled in two books [4, 5]. The main problems posed by them were: (1) Is association equilibrium established in the solution? (The existence of a well-defined equilibrium constant.) (2) Do solutions separate into two phases only through molecular association? (3) Do associated molecules disperse to unimers through dilution? However, the relationship between association and phase separation was not clarified in their studies, and, ever since, these problems have been the main issues in the study of associated solutions.

On the other hand, Hirschfelder *et al.* [6] pointed out that the lower critical solution temperature appears as a result of **heteromolecular association** in solutions of water or alcohol with ammonia derivatives. The problem posed by them has been studied in relation to **reentrant phase separation** in liquid mixtures.

In contrast to the history of science of low-molecular weight associating molecules, the main stream in the study of polymer solutions had been confined until recently to chain conformation in dilute solutions and the excluded-volume effect in semiconcentrated solutions caused by van der Waals-type nonspecific interactions [7–10]. The studies of association in polymer solutions by hydrogen bonding and hydrophobic interaction are relatively new. In the following sections we reformulate the theory of regular associated solutions in an attempt to apply it to high-molecular weight polymer solutions. The KM infinite series, which drives the solution into three-dimensional networks (gelation), is studied in detail by incorporating the classical theory of gelation (Section 3.2) into the conventional Flory–Huggins theory of polymer solutions (Section 2.3).

5.2 Statistical thermodynamics of associating polymers

Consider a binary mixture of linear polymers $R\{A_f\}$ and $R\{B_g\}$ carrying associative groups A and B. The number of statistical repeat units on a chain (for simplicity referred to as the degree of polymerization, DP) is assumed to be n_A for $R\{A_f\}$ chains and n_B for $R\{B_g\}$ chains. Although we use the word "polymer" for the primary molecules before they form associated complexes, we may apply our theory to low-molecular weight molecules equally well by simply fixing n_A and n_B at small values.

These polymers are assumed to carry a fixed number f of reactive groups A and g of reactive B groups, both of which are capable of forming reversible bonds that can thermally break and recombine. Hydrogen bonds, hydrophobic interaction, electrostatic interaction, etc., are important examples of such associative forces. The type of associative interaction does not need to be specified at this stage, but it will be given in each of the following applications. We symbolically indicate this binary model system as $R\{A_f\}/R\{B_g\}$.

In the extreme limit of strong bonds, such as covalent ones, the formation of associated clusters is thermally irreversible and should be regarded as a chemical reaction. The molecular weight distribution of such irreversible reactions is studied in detail in Section 3.2.

In the experiments, various types of solvents are commonly used, so that we should consider a mixture $R\{A_f\}/R\{B_g\}/S$, where S denotes the solvent. Extension of the following theoretical consideration to such ternary systems is straightforward as long as the solvent is inactive. Therefore, for simplicity, we will mainly confine the discussion to binary systems.

Forces working among the associative groups form intermolecular clusters whose aggregation numbers cover a wide range. If either of the functionalities f or g exceeds the critical value (3 for pairwise association, but it can be 2 for multiple association, see Section 3.3), a cluster grows to the macroscopic dimensions as soon as a threshold in

the temperature, or in the composition (concentration), is reached. Above this threshold, three-dimensional networks, most generally comprising of the mixed components, are formed [11–15].

To describe such reversible network formation in associating mixtures, we start from the conventional lattice theoretical picture of polymer solutions described in Section 2.3 and references [7–11], with an attempt to include association [16–18] in the form of reaction equilibrium by taking the simplest theoretical viewpoint described in Section 3.2.

Let us first divide the total volume V of the system into small cells of size a of the monomeric unit on a chain [7]. There are a total number $\Omega \equiv V/a^3$ of microscopic cells. We first specify the part of the system containing only clusters of finite size, which will be referred to as *sol*.

Let $N_{l,m}$ be the number of connected clusters consisting of l $R\{A_f\}$ molecules (referred to as A-chains) and m $R\{B_g\}$ molecules (B-chains). We introduce the symbol (l,m) to specify such a cluster. The total volume fraction of A-chains in the sol must then be equal to

$$\phi_A^S = n_A \sum_{l,m} l\nu_{l,m},\tag{5.2}$$

where $\nu_{l,m} \equiv N_{l,m}/\Omega$ is the number of clusters per lattice cell. Similarly, the total volume fraction of B-chains in the sol is

$$\phi_B^S = n_B \sum_{l,m} m\nu_{l,m},\tag{5.3}$$

The total volume fraction of the sol in the system is $\phi^S = \phi_A^S + \phi_B^S$. This should be equal to unity for nongelling systems, or in the **pregel regime** of gelling systems, but can be smaller than unity after an infinite network (*gel*) appears (i.e., in the **postgel regime** of the gelling systems).

In the postgel regime, we have infinite clusters. Let N_i^G be the number of chains of species i in such macroscopic clusters. The total volume is

$$\Omega = \sum_{l,m}(n_A l + n_B m)N_{l,m} + n_A N_A^G + n_B N_B^G.\tag{5.4}$$

The volume fraction of the chains of species i in the gel network is given by $\phi_i^G = n_i N_i^G/\Omega$ for $i = A,B$, and

$$\phi_i^S + \phi_i^G = \phi_i\tag{5.5}$$

holds for normalization, where ϕ_i is the total volume fraction of species i that is fixed at the preparation stage of the experiments. The gel fraction w_i^G for each component is defined by the fraction

$$w_i^G \equiv \phi_i^G/\phi_i \qquad (i = A,B).\tag{5.6}$$

Reference state

$\Delta_{\mathrm{rea}}F$

(0,1)   (0,1)   (l, m)   Gel

$\Delta_{\mathrm{mix}}F$

Real mixture
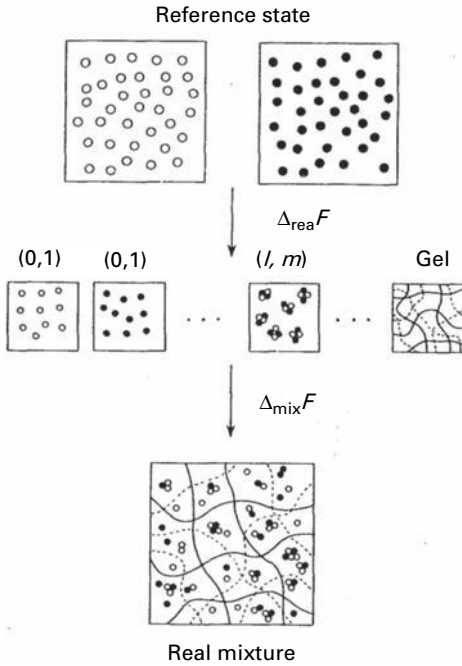
Fig. 5.1 Construction of the free energy of associating mixtures. The total free energy is the sum of the free energy of reaction and that of mixing. The standard reference state is chosen in such a way that each species of molecules is regularly placed on a hypothetical crystalline lattice with reference intramolecular conformation (a straight rod in the case of polymers).

Similarly, the number density v_i^{G} of species i in the gel is given by

$$v_i^{\mathrm{G}} \equiv \phi_i^{\mathrm{G}}/n_i = N_i^{\mathrm{G}}/\Omega \qquad (i = \mathrm{A}, \mathrm{B}). \tag{5.7}$$

Such decomposition into a sol part and a gel part automatically takes place in the mixture by thermal processes. Since we have the identity $\phi_{\mathrm{A}} + \phi_{\mathrm{B}} = 1$, we can take ϕ_{A} as an independent variable and write it as ϕ. The volume fraction of B is then $\phi_{\mathrm{B}} = 1 - \phi$.

The cluster distribution $N_{l,m}$ and the gel fractions w_i^{G} are unknown at this stage, but will soon be decided by the equilibrium condition in association.

In order to study thermodynamic properties, we start from the **standard reference state** in which unconnected A-chains and B-chains are prepared separately in a hypothetical crystalline state [7, 9] (see Figure 5.1). We first consider the free energy change $\Delta_{\mathrm{rea}}F$ to bring the system from the reference state to a fictitious intermediate state in which chains are disoriented and connected in such a way that the cluster distribution is exactly the same as the real one [18–20]. It is given by

$$\beta \Delta_{\mathrm{rea}}F/\Omega = \sum_{l,m} \Delta_{l,m} v_{l,m} + \delta_{\mathrm{A}} v_{\mathrm{A}}^{\mathrm{G}} + \delta_{\mathrm{B}} v_{\mathrm{B}}^{\mathrm{G}}, \tag{5.8}$$

where $\Delta_{l,m}$ is the free energy change when a single (l,m) cluster is formed from l A-chains and m B-chains in the reference state. We refer to this as the **free energy of reaction**.

Let $\mu_{l,m}^{\circ}$ be the internal free energy of an (l,m) cluster. The free energy difference $\Delta_{l,m}$ is given by

$$\Delta_{l,m} = \beta(\mu_{l,m}^{\circ} - l\mu_{1,0}^{\circ} - m\mu_{0,1}^{\circ}). \tag{5.9}$$

Under a constant pressure, $\mu_{l,m}^{\circ}$ is equivalent to the internal free energy necessary for combination, configurational change, and bond formation of the constitutional primary molecules. Specific forms of these contributions will be considered in each problem we study in the following chapters.

Similarly, δ_i $(i = $ A,B$)$ is the free energy change produced when an isolated chain of species i is connected to the gel network. They are given by

$$\delta_A = \beta(\mu_A^{\circ G} - \mu_{1,0}^{\circ}), \tag{5.10a}$$

$$\delta_B = \beta(\mu_B^{\circ G} - \mu_{0,1}^{\circ}), \tag{5.10b}$$

where $\mu_i^{\circ G}$ is the internal free energy of an i-chain in the gel network. The two last terms in (5.8) are necessary in the postgel regime because the number of molecules contained in the gel part becomes macroscopic; it is a finite fraction of the total number of molecules in the system.

In the second step, we mix these clusters with each other to reach the real mixture we study (see Figure 5.1). According to the conventional lattice theory of polydisperse polymer mixtures (see Section 2.3) [9, 10], the mixing free energy $\Delta_{\text{mix}} F$ in this process is given by

$$\beta \Delta_{\text{mix}} F / \Omega = \sum_{l,m} \nu_{l,m} \ln \phi_{l,m} + \chi(T)\phi(1-\phi) \tag{5.11}$$

per lattice site, where

$$\phi_{l,m} \equiv (n_A l + n_B m)\nu_{l,m} \tag{5.12}$$

is the volume fraction occupied by the (l,m)-clusters, and χ is Flory's χ-parameter (2.105), which specifies the strength of van der Waals type non-associative interaction between monomers of different species. Since clusters formed by association are generally polydisperse, and have largely different volumes, a mixing entropy of the Flory–Huggins type must be used even if the primary molecules are low-molecular weight molecules. Macroscopically connected clusters, such as gel networks, infinitely long linear aggregates, etc., do not have the mixing entropy since their centers of mass lose the translatonal degree of freedom.

The number of contacts between the two species may change upon molecular association, and hence the mixing enthalpy, the last term of (5.11), may be modified. We assume

here, however, that the same form remains valid after association except when the modification is significant due to polymer conformational change, etc. We can improve this term whenever necessary.

The total free energy from which our theory starts is given by the sum of the above two parts:

$$\Delta F = \Delta_{\mathrm{rea}} F + \Delta_{\mathrm{mix}} F. \tag{5.13}$$

We next derive the chemical potentials of the clusters in order to study the solution properties. By the thermodynamic definition of the chemical potential $\Delta\mu_{lm} \equiv (\partial \Delta F/\partial N_{lm})_{T,N_{l'm'}\cdots}$ for clusters of size (l,m), we find

$$\beta\Delta\mu_{lm} = 1 + \Delta_{lm} + \ln\phi_{lm} - (n_A l + n_B m)\nu^S + \chi\{n_A l(1-\phi) + n_B m\phi^2\}$$
$$+ \left[n_A l(1-\phi) - n_B m\phi\right]\left[\delta'_A(\phi)\nu^G_A - \delta'_B(\phi)\nu^B_G\right], \tag{5.14}$$

where

$$\nu^S \equiv \sum_{l,m} \nu_{lm} \tag{5.15}$$

is the total number of finite clusters (per lattice cell) in the mixture. This number gives the total number of molecules and clusters that possess translational degree of freedom. Within the ideal solution approximation, they equally contribute to the osmotic pressure. Obviously, the gel part is excluded from ν^S because it is macroscopic, and its center of mass is localized. The ratio defined by

$$P_n \equiv [\phi/n_A + (1-\phi)/n_B]/\nu^S \tag{5.16}$$

gives the **number-average cluster size**, or **number-average aggregation number** of clusters.

In particular, we have for molecules that remain unassociated

$$\frac{\beta\Delta\mu_{10}}{n_A} = \frac{1 + \ln\phi_{10}}{n_A} - \nu^S + \chi(1-\phi)^2 + \left[\delta'_A(\phi)\nu^G_A - \delta'_B(\phi)\nu^G_B\right](1-\phi), \tag{5.17a}$$

$$\frac{\beta\Delta\mu_{01}}{n_B} = \frac{1 + \ln\phi_{01}}{n_B} - \nu^S + \chi\phi^2 - \left[\delta'_A(\phi)\nu^G_A - \delta'_B(\phi)\nu^G_B\right]\phi. \tag{5.17b}$$

Similarly, the chemical potentials of the polymer chains included in the gel part are given by

$$\beta\Delta\mu^G_A/n_A = \delta_A/n_A - \nu^S + \chi(1-\phi)^2 + \left[\delta'_A(\phi)\nu^G_A - \delta'_B(\phi)\nu^G_B\right](1-\phi), \tag{5.18a}$$

$$\beta\Delta\mu^G_B/n_B = \delta_B/n_B - \nu^S + \chi\phi^2 - \left[\delta'_A(\phi)\nu^G_A - \delta'_B(\phi)\nu^G_B\right]\phi. \tag{5.18b}$$

To find the equilibrium distribution of clusters, we impose the **multiple equilibrium conditions**

$$\Delta\mu_{l,m} = l\Delta\mu_{1,0} + m\Delta\mu_{0,1}, \tag{5.19}$$

for all possible combinations of the integers (l, m). Upon substitution of the specific forms of the chemical potentials, we find that the volume fractions of the clusters are given by

$$\phi_{l,m} = K_{l,m}x^l y^m, \tag{5.20}$$

where for simplicity we have used x and y for the concentrations $\phi_{1,0}$ and $\phi_{0,1}$ of unassociated molecules. These unassociated molecules in the solution are sometimes called **unimers** to avoid confusion with monomers. The new constant $K_{l,m}$ (**equilibrium constant**) is defined by

$$K_{l,m} \equiv \exp(l + m - 1 - \Delta_{l,m}), \tag{5.21}$$

which depends only on the temperature through $\Delta_{l,m}$ but is independent of the concentration. Similarly, the number density of clusters is given by

$$\nu_{l,m} = \frac{K_{l,m}}{n_A l + n_B m}x^l y^m. \tag{5.22}$$

To simplify the notations and to stress analogy to the condensation phenomena of classical interacting gases, we introduce the coefficients $b_{l,m}$ by

$$b_{l,m} \equiv K_{l,m}/(n_A l + n_B m). \tag{5.23}$$

We then have

$$\nu^S(x, y) = \sum_{l,m} b_{l,m}x^l y^m \equiv G_{0,0}(x, y), \tag{5.24a}$$

$$\phi^S(x, y) = \sum_{l,m}(n_A l + n_B m)b_{l,m}x^l y^m$$

$$\equiv n_A G_{1,0}(x, y) + n_B G_{0,1}(x, y), \tag{5.24b}$$

where the G functions are the moments of the cluster distribution function of various orders, and defined by

$$G_{i,j}(x, y) \equiv \sum_{l,m} l^i m^j b_{l,m}x^l y^m. \tag{5.25}$$

5.2.1   Pregel regime

In nongelling mixtures, or a pregel regime of gelling ones, the total volume fraction should be given by

$$\phi^S(x, y) = 1 \tag{5.26}$$

since all clusters are included in the sum. The volume fraction of each species form the coupled equations

$$G_{1,0}(x, y) = \phi/n_A, \tag{5.27a}$$

$$G_{0,1}(x, y) = (1 - \phi)/n_B, \tag{5.27b}$$

for the unknown variables x and y. We solve these equations with respect to x and y, and substitute the result into the physical quantities we consider. For instance, the number-average numbers of A-chains and B-chains in the finite clusters are

$$\langle l \rangle_n = \frac{\partial \ln \nu^S(x, y)}{\partial \ln x} = \frac{G_{1,0}(x, y)}{G_{0,0}(x, y)}, \tag{5.28a}$$

$$\langle m \rangle_n = \frac{\partial \ln \nu^S(x, y)}{\partial \ln y} = \frac{G_{0,1}(x, y)}{G_{0,0}(x, y)}, \tag{5.28b}$$

where the average symbol

$$\langle Q_{l,m} \rangle_n \equiv \frac{\sum Q_{l,m} \nu_{lm}}{\sum \nu_{lm}} \tag{5.29}$$

shows the number average of the quantity $Q_{l,m}$.

Similarly, the weight-average is defined by

$$\langle Q_{l,m} \rangle_w \equiv \frac{\sum Q_{l,m} \phi_{lm}}{\sum \phi_{lm}}. \tag{5.30}$$

The weight-averages of the aggregation numbers l and m in the clusters are then given by

$$\langle l \rangle_w = \frac{\partial \ln \phi^S(x, y)}{\partial \ln x} = n_A G_{2,0} + n_B G_{1,1}, \tag{5.31a}$$

$$\langle m \rangle_w = \frac{\partial \ln \phi^S(x, y)}{\partial \ln y} = n_A G_{1,1} + n_B G_{0,2}. \tag{5.31b}$$

The weight-average DP of the clusters is obtained by the sum of these two as

$$\langle M \rangle_w \equiv \sum (n_A l + n_B m) \phi_{lm} = n_A \langle l \rangle_w + n_B \langle m \rangle_w$$

$$= n_A^2 G_{2,0}(x, y) + 2 n_A n_B G_{1,1}(x, y) + n_B^2 G_{0,2}(x, y). \tag{5.32}$$

5.2.2   Sol–gel transition and postgel regime

We have so far tacitly assumed that the infinite double summation in ϕ^{S} (and hence in ν^{S}) converges. These are double power series with positive coefficients, so that they are monotonically increasing functions. For mixtures capable of gelling, a borderline on the (x, y) plane exists, which separates the unit square into a convergent region and a divergent one. Exactly on the boundary line, the sol composition ϕ^{S} takes a finite value, but it diverges outside this line. Since the radius of convergence generally depends on the composition, let us express the boundary by a parametric form $(x^{*}(\phi), y^{*}(\phi))$ for $0 \leq \phi \leq 1$. The value $\phi^{S}(x^{*}, y^{*})$ can be smaller than unity for a certain region of the composition and the temperature because the sum *does not include* contributions from the gel part appearing in the postgel regime. Hence we can find the sol–gel transition line by mapping the condition $\phi^{S}(x^{*}, y^{*}) = 1$ back to the original temperature–concentration plane.

In the postgel regime, a chain participating in the gel must be in chemical equilibrium with an unassociated chain of the same species. This imposes the additional conditions

$$\Delta\mu_{1,0} = \Delta\mu_{A}^{G} \quad \text{and} \quad \Delta\mu_{0,1} = \Delta\mu_{B}^{G}, \tag{5.33}$$

and hence we find x and y to be functions of the concentration in the form

$$\delta_{A}(\phi) = 1 + \ln x, \qquad \delta_{B}(\phi) = 1 + \ln y \tag{5.34}$$

for the gelling component in the postgel regime. The chemical potential of each species takes a uniform value in the solution, so we can write them as $\Delta\mu_{A}$ and $\Delta\mu_{B}$ instead of $\Delta\mu_{1,0}$ and $\Delta\mu_{0,1}$.

5.3   Renormalization of the interaction parameters

We now substitute all relations obtained by equilibrium conditions back into the original free energy (5.13), or equivalently, we use the Gibbs–Dühem relation

$$\Delta F / \Omega = \Delta\mu_{A}\phi/n_{A} + \Delta\mu_{B}(1 - \phi)/n_{B}, \tag{5.35}$$

and find that the free energy takes the form

$$\beta\Delta F / \Omega = \frac{1 + \ln x}{n_{A}}\phi + \frac{1 + \ln y}{n_{B}}(1 - \phi) - \nu^{S}(x, y) + \chi(T)\phi(1 - \phi). \tag{5.36}$$

This free energy can be decomposed into two parts as

$$\mathscr{F} \equiv \beta\Delta F / \Omega = \mathscr{F}_{FH}(\phi) + \mathscr{F}_{AS}(\phi), \tag{5.37}$$

where

$$\mathscr{F}_{FH}(\phi) \equiv \frac{\phi}{n_{A}}\ln\phi + \frac{(1 - \phi)}{n_{B}}\ln(1 - \phi) + \chi(T)\phi(1 - \phi) \tag{5.38}$$

is the conventional Flory–Huggins free energy of the nonassociative counterpart, and

$$\mathscr{F}_{AS}(\phi) \equiv \frac{\phi}{n_A} \ln\left(\frac{x}{\phi}\right) + \frac{1-\phi}{n_B} \ln\left(\frac{y}{1-\phi}\right) + \frac{\phi}{n_A} + \frac{1-\phi}{n_B} - v^S(x,y) \qquad (5.39)$$

gives the effect of association.

The effect of association can be regarded as a **renormalization** of Flory's χ-parameter. It produces a shift from χ to $\chi + \Delta\chi$ in (5.13), where

$$\Delta\chi(\phi, T) \equiv \mathscr{F}_{AS}(\phi)/\phi(1-\phi) \qquad (5.40)$$

is the associative part of the interaction. The short-range associative interaction energy originally introduced in the reaction terms is now interpreted as a composition-dependent modification of the χ-parameter. We can expand the renormalization term in powers of the concentration

$$\Delta\chi = \chi_0 + \chi_1\phi + \chi_2\phi^2 + \cdots, \qquad (5.41)$$

with temperature-dependent coefficients $\chi_i = \chi_i(T)$. We thus go back to the phenomenological VLBW description (2.131), but now the molecular origin of the concentration-dependent χ-parameter is clear. Specifically, we find $\chi_0 = \mathscr{F}_1, \chi_1 = \mathscr{F}_1 + \mathscr{F}_2$, where $\mathscr{F}_1, \mathscr{F}_2$ are explicitly given in Appendix 5.A.

5.4 Phase separation, stability limit, and other solution properties

Let us now find some important physical quantities of the mixture.

Osmotic pressure
The osmotic pressure π of the A component is essentially the chemical potential of the B component with the opposite sign. It is given by

$$\beta\pi a^3/n_B = -(1 + \ln y)/n_B + v^S(x,y) - \chi\phi^2 + \left[\delta'_A(\phi)v_A^G - \delta'_B(\phi)v_B^G\right]\phi \qquad (5.42)$$

In a polymer solution in which the B component is a low-molecular weight nonassociative solvent ($n_B = 1$ and $\delta_B(\phi) = 0$), this definition reduces to the osmotic pressure in the conventional meaning.

If we expand this pressure in powers of the concentration with $n_B = 1$, we have the virial series

$$\pi a^3/k_B T = \phi/n_A + A_2\phi^2 + A_3\phi^3 + \cdots, \qquad (5.43)$$

where $A_2 = 1/2 - \chi + \Delta A_2$, with a negative temperature-dependent constant of binary association (see Appendix 5.A) given by

$$\Delta A_2 = -K_{2,0}/2n_A \qquad (5.44)$$

Hence, the second virial coefficient has a reduction from $1/2 - \chi$ due to the associative interaction. The explicit form of ΔA_2 will be shown in the following sections for some specific systems.

At a higher concentration across the gel point, the osmotic compressibility $K_T \equiv (\partial \phi / \partial \pi)_T / \phi$, or its higher derivatives, may have a discontinuity due to the appearance of the gel part.

Phase separation

The two-phase equilibrium conditions, or a **binodal** line, can be found by equating the chemical potential of each component [9, 10]:

$$\Delta \mu_A(\phi', T) = \Delta \mu_A(\phi'', T), \tag{5.45a}$$

$$\Delta \mu_B(\phi', T) = \Delta \mu_B(\phi'', T), \tag{5.45b}$$

where ϕ' and ϕ'' are the compositions of the A component in the dilute and concentrated phase respectively. If either phase, or both of them, lies inside the postgel regime, the chemical potentials must be replaced by their postgel forms.

Stability limit

The thermodynamic stability limit, or a **spinodal** line, can be found for the binary system by the single condition $(\partial \Delta \mu_A / \partial \phi)_T = 0$, or equivalently, $\partial (\Delta \mu_A / n_A - \Delta \mu_B / n_B) / \partial \phi = 0$. We have the equation

$$\frac{\kappa_A(\phi)}{n_A \phi} + \frac{\kappa_B(\phi)}{n_B(1 - \phi)} - 2\chi = 0, \tag{5.46}$$

where the new functions are defined by

$$\kappa_A(\phi) \equiv \phi \frac{d}{d\phi} \left(1 + \phi_A^G \frac{d}{d\phi} \right) \ln x, \tag{5.47a}$$

$$\kappa_B(\phi) \equiv -(1 - \phi) \frac{d}{d\phi} \left(1 - \phi_B^G \frac{d}{d\phi} \right) \ln y. \tag{5.47b}$$

In the pregel regime, these equations are related to the weight-average aggregation number of clusters. For homopolymer association where only A-chains are associated, for instance, κ_A reduces to the reciprocal of the weight-average cluster size as in conventional polydisperse polymer solutions [10, 21]. In heteropolymer association, however, κ is related to the average cluster sizes in a more complicated way.

5.5   Scattering function of associating polymer mixtures

To study microphase separation transition (MST), we next consider the correlation function of concentration fluctuations, whose Fourier components give the intensity of scattered waves. We have polydisperse clusters whose polydispersity is controlled by the temperature T and the composition ϕ.

To study the scattering intensity from such polydisperse binary blends, we tentatively give a sequential number $\alpha = 1, 2, \ldots, N = \Omega \nu^S$ to the clusters. Let the set of the numbers (α, i) show the i-th monomer in the α-th cluster. The monomer density for (α, i) at lattice site $\mathbf{r}$ is then defined by

$$\rho_i^\alpha(\mathbf{r}, t) \equiv \delta(\mathbf{r} - \mathbf{x}_i^\alpha(t)), \tag{5.48}$$

where $\mathbf{x}_i^\alpha(t)$ is an instantaneous position of the monomer at time t, and $\delta(\mathbf{r})$ is Kronecker's delta. In the following we consider equal-time correlations only, so that we ignore the time variable.

Since the thermal average of ρ_i^α gives $1/\Omega$, we can rewrite it as

$$\rho_i^\alpha(\mathbf{r}) = 1/\Omega + \delta\rho_i^\alpha(\mathbf{r}), \tag{5.49}$$

where $\delta\rho_i^\alpha$ shows the fluctuating part of the density. The **incompressibility condition** $\sum_{\alpha, i} \rho_i^\alpha(\mathbf{r}) = 1$ leads to

$$\sum_{\alpha, i} \delta\rho_i^\alpha(\mathbf{r}) = 0, \tag{5.50}$$

for any position $\mathbf{r}$.

The intensity of the scattered waves (of X-ray or neutrons) with the scattering vector $\mathbf{q}$ is most generally given by the formula

$$I(\mathbf{q}) = \sum_{\substack{\alpha, \beta \\ i, j}} b_i^\alpha b_j^\beta T_{ij}^{\alpha\beta}(\mathbf{q}) \tag{5.51}$$

in the Fourier space, where b_i^α is the scattering amplitude of the (α, i) monomer, and

$$T_{ij}^{\alpha\beta}(\mathbf{q}) \equiv \langle \delta\rho_i^\alpha(\mathbf{q}) \delta\rho_j^\beta(-\mathbf{q}) \rangle \tag{5.52}$$

is the density correlation function for the pair (α, i) and (β, j).

Let us assume that the scattering amplitude b_i^α takes the value $b_i^\alpha = A$ for A monomers and $b_i^\alpha = B$ for B monomers. We then decompose it into the form

$$b_i^\alpha = A\tau_i^\alpha + B(1 - \tau_i^\alpha) \tag{5.53}$$

for a binary mixture, where τ_i^α is an Ising variable, defined by

$$\tau_i^\alpha = \begin{cases} 1 & \text{if } (\alpha, i) \text{ is an A monomer,} \\ 0 & \text{if } (\alpha, i) \text{ is a B monomer,} \end{cases} \tag{5.54}$$

which specifies the species of the (α, i) monomer.

Substituting (5.53) into (5.51) and using the incompressibility condition (5.50), we find

$$I(\mathbf{q}) = (A - B)^2 T(\mathbf{q}), \tag{5.55}$$

where

$$T(\mathbf{q}) = \sum_{\substack{\alpha,\beta \\ i,j}} \tau_i^\alpha T_{ij}^{\alpha\beta}(\mathbf{q}) \tau_j^\beta. \tag{5.56}$$

In order to obtain the specific form of $T(\mathbf{q})$, we now apply the **random phase approximation** (RPA) [22–26] to our system. The RPA provides a classical treatment of concentration fluctuations for incompressible mixtures of very large molecular weight molecules. It assumes a self-consistent potential uniformly acting on all species of monomers to ensure the incompressibility condition. The details of the RPA method, as applied to our polydisperse block copolymer blend, are given in Appendix 5.B. The result leads to

$$T(\mathbf{q}) = \frac{1}{S(q)/W(q) - 2\chi}, \tag{5.57}$$

for the scattering strength, where

$$S(q) \equiv S_{\mathrm{AA}}^\circ(q) + S_{\mathrm{BB}}^\circ(q) + 2S_{\mathrm{AB}}^\circ(q), \tag{5.58}$$

and

$$W(q) \equiv S_{\mathrm{AA}}^\circ S_{\mathrm{BB}}^\circ(q) - [S_{\mathrm{AB}}^\circ(q)]^2, \tag{5.59}$$

are both related to the **intracluster scattering functions**. (The superscript ∘ shows the scattering intensity contributed from a single cluster.) The RPA assumes Gaussian statistics for each chain, which leads to the result

$$S_{\mathrm{AA}}^\circ(q) \equiv \frac{1}{\Omega} \sum_\alpha \sum_{i,j} J_{ij} \tau_i^\alpha \tau_j^\alpha, \tag{5.60a}$$

$$S_{\mathrm{BB}}^\circ(q) \equiv \frac{1}{\Omega} \sum_\alpha \sum_{i,j} J_{ij} (1 - \tau_i^\alpha)(1 - \tau_j^\alpha), \tag{5.60b}$$

$$S_{\mathrm{AB}}^\circ(q) \equiv \frac{1}{\Omega} \sum_\alpha \sum_{i,j} J_{ij} \tau_i^\alpha (1 - \tau_j^\alpha), \tag{5.60c}$$

for the intracluster scattering functions [27] with $J_{ij} \equiv \exp(-\kappa n_{ij})$, where n_{ij} is the distance between i-th and j-th monomers along the chain measured in terms of the number of monomers, and $\kappa \equiv (aq)^2/6$ being the dimensionless squared wavenumber. This result provides a complete set for the calculation of the scattering function for the binary blends made up of the assembly of block copolymers.

For our associating blends clusters are characterized by the set of two figures (l,m), so that the sum over α can be replaced by the sum over the type (l,m). Hence we have

$$S_{AA}^{\circ}(q) = \sum_{l,m} A_{lm}(q) v_{l,m}, \tag{5.61a}$$

$$S_{BB}^{\circ}(q) = \sum_{l,m} B_{lm}(q) v_{l,m}, \tag{5.61b}$$

$$S_{AB}^{\circ}(q) = \sum_{l,m} C_{lm}(q) v_{l,m}, \tag{5.61c}$$

where

$$A_{lm}(q) \equiv \sum_{i,j \in (l,m)} J_{ij} \tau_i \tau_j, \tag{5.62a}$$

$$B_{lm}(q) \equiv \sum_{i,j \in (l,m)} J_{ij} (1 - \tau_i)(1 - \tau_j), \tag{5.62b}$$

$$C_{lm}(q) \equiv \sum_{i,j \in (l,m)} J_{ij} \tau_i (1 - \tau_j), \tag{5.62c}$$

are the monomer correlation functions of an isolated single cluster of the type (l,m).

We now consider the divergence condition for $I(\mathbf{q})$. This is equivalent to

$$\frac{S(q)}{W(q)} - 2\chi = 0, \tag{5.63}$$

within RPA. If this condition is satisfied for a finite q, the system becomes unstable against the concentration fluctuation whose spatial dimensions are characterized by q^{-1}. If it is satisfied for $\mathbf{q} = 0$ on the other hand, it is unstable against demixing into two coexistent macroscopic phases. In fact, as we will show in Appendix 5.C explicitly, the RPA condition (5.63) for $\mathbf{q} = 0$ gives exactly the same equation as (5.46) for the spinodal curve. Owing to this fact, the study of the phase behavior on the entire temperature–concentration plane can start from a single equation (5.63).

Appendices to Chapter 5

5.A   Renormalization of the interaction parameters

From the material conservation laws (5.27a) and (5.27b), it is possible to expand x and y in powers of the volume fraction ϕ of the A component (polymer) as

$$x = \phi(x_1 + x_2\phi + x_3\phi^2 + \cdots), \tag{5.64a}$$

$$y = y_0 + y_1\phi + y_2\phi^2 + \cdots. \tag{5.64b}$$

Obviously, $x_1 = 1$, $y_0 = 1$, $y_1 = -1$, and other coefficients are 0 if there is no association. We first split the total number density of the clusters in accordance with the power of x as

$$\nu^S(x, y) = G_0(x, y) = g_0(y) + g_1(y)x + g_2(y)x^2 + \cdots,$$

where

$$g_0(y) \equiv \sum_{m=1}^{\infty} \frac{K_{0,m}}{n_B m} y^m,$$

$$g_1(y) \equiv \sum_{m=1}^{\infty} \frac{K_{1,m}}{n_A + n_B m} y^m,$$

$$g_2(y) \equiv \sum_{m=1}^{\infty} \frac{K_{2,m}}{2n_A + n_B m} y^m.$$

The function $g_0(y)$ is related to the association within the B component (solvent), $g_1(y)$ is related to the adsorption of the B molecules onto the polymers, and $g_2(y)$ is related to the pairwise cross-links of polymers by B component molecules. The fraction of the B molecules associated to the polymers is related to $g_1(y)$ by

$$\theta(y) = y g_1'(y) / g_1(y).$$

Substituting these power expansions into $\mathscr{F}_{AS}$ (5.39), and expanding it in powers of the concentration, we find

$$\mathscr{F}_{AS} = \mathscr{F}_0 + \mathscr{F}_1 \phi + \mathscr{F}_2 \phi^2 + \cdots,$$

after a lengthy calculation, where

$$\mathscr{F}_0 = \frac{1 + \ln y_0}{n_B} - g_0(y_0),$$

$$\mathscr{F}_1 = \frac{\ln x_1}{n_A} - \frac{\ln y_0}{n_B},$$

$$\mathscr{F}_2 = \frac{1}{n_A} \left(\frac{x_2}{x_1} \right) - \frac{1}{2n_B} \left(1 + \frac{y_1}{y_0} \right) - \frac{1}{2} y_0^2 g_0''(y_0) \left(\frac{y_1}{y_0} \right)^2$$
$$- x_1 y_0 g_1'(y_0) \left(\frac{y_1}{y_0} \right) - x_2 g_1(y_0) - x_1^2 g_2(y_0).$$

If we write the association free energy in the form

$$\mathscr{F}_{AS} \equiv \Delta \chi(\phi) \phi (1 - \phi),$$

in terms of the additional interaction parameter $\Delta \chi(T)$ due to the specific interactions, the original Flory–Huggins interaction parameter of the van der Waals-type nonspecific

interaction in the background is renormalized to $\chi(\phi, T) = \chi_{\mathrm{FH}}(T) + \Delta\chi(\phi, T)$. The first two coefficients in the power expansion

$$\chi(\phi, T) = \chi_0(T) + \chi_1(T)\phi + \cdots,$$

are found to be

$$\chi_0(T) = \chi_{\mathrm{FH}}(T) + \mathscr{F}_1,$$
$$\chi_1(T) = \mathscr{F}_1 + \mathscr{F}_2.$$

To find the coefficients x_i and y_j, we substitute the power expansion (5.64a) into the material conservation laws (5.27a) and (5.27b), and compare term by term. The results are summarized as follow. The 0-th term y_0 should be the solution of the equation

$$y_0 g_0'(y_0) = 1/n_{\mathrm{B}}.$$

By using y_0, x_1, x_2 and y_1 are given by

$$x_1 = \frac{1}{n_{\mathrm{A}} g_1(y_0)}, \quad \frac{y_1}{y_0} = -\frac{1 + bx_1}{1 + a_0'}, \quad \frac{x_2}{x_1} = \frac{a_1}{1 + a_0'} + \left[\frac{b}{1 + a_0'} - \frac{2g_2(y_0)}{g_1(y_0)}\right],$$

where $a_0' \equiv (d \ln g_0'/d \ln y)_0, a_1 \equiv (d \ln g_1'/d \ln y)_0$ and $b \equiv g_1'(y_0)/g_0'(y_0)$.

For instance, if association takes place only within the A component, we find $\mathscr{F}_0 = \mathscr{F}_1 = 0$ and

$$\mathscr{F}_2 = -K_{2,0}/2n_{\mathrm{A}}.$$

If B molecules are adsorbed onto the A component as in hydration, side-chain association, etc., $y_0 = 1, b = n_{\mathrm{B}}\theta(y_0)$. We find $\mathscr{F}_0 = \mathscr{F}_1 = 0$ and

$$\mathscr{F}_2 = \theta(y_0)\left[1 + \frac{n_{\mathrm{B}}}{2}\theta(y_0)\right],$$

where $\theta(y_0)$ is the fraction of adsorbed B molecules in the limit of infinite dilution. Some specific examples will be presented in the following chapters.

5.B   Scattering function in RPA

To derive the RPA scattering function in a compact form, we here introduce vector notations. Let τ be an Ω-component columnar vectorial whose (α, i)-th component is defined by τ_i^{α} given in (5.54), so that we can write $\tau = [\tau_i^{\alpha}]$. Similarly let $\mathbf{e}$ be the columnar vector whose components are all unity. We have by definition

$$^{t}\mathbf{e} \cdot \tau = \sum_{\alpha, i} \tau_i^{\alpha} = \Omega\phi,$$

where $^t\mathbf{e}$ is a transposed vector of $\mathbf{e}$. The monomer density (5.49) can be expressed as

$$\rho = \frac{1}{\Omega}\mathbf{e} + \delta\rho,$$

by the use of this notation. According to the conventional lattice theory, the monomer–monomer contact energy takes the value χ when the neighboring pair is (A,B), while it is zero for a (A,A) or (B,B) pair. We must therefore introduce a matrix $\hat{\chi}$ defined by

$$\hat{\chi} = \chi[\tau:^t(\mathbf{e}-\tau) + (\mathbf{e}-\tau):^t\tau],$$

where $\mathbf{a}:^t\mathbf{b}$ shows a dyad formed by the two vectors. Specifically we have a relation

$$^t\mathbf{e}\cdot\hat{\chi}\cdot\mathbf{e} = 2\chi\Omega^2\phi(1-\phi).$$

We now consider linear response $\langle\delta\rho_i^\alpha\rangle$ of the density to an arbitrary external field acting on each monomer with strength U_i^α. Linear response theory gives

$$\langle\delta\rho(\mathbf{q})\rangle = -\hat{\mathbf{T}}\cdot\mathbf{U}(\mathbf{q}), \tag{5.68}$$

where $\hat{\mathbf{T}}$ is a matrix whose components are given by the correlation (5.52). The RPA assumes that this average is approximately equivalent to

$$\langle\delta\rho\rangle = -\hat{\mathbf{S}}\cdot(\mathbf{U}+\delta\mathbf{U}^{\text{eff}} - \hat{\chi}\cdot\langle\delta\rho\rangle), \tag{5.69}$$

if the effective potential $\delta\mathbf{U}^{\text{eff}}$ is judiciously chosen, where $\hat{\mathbf{S}}$ is a correlation function of monomers belonging to the *same* single cluster [24]. Gaussian statistics give [28]

$$S_{ij}^{\alpha\beta}(\mathbf{q}) = \delta_{\alpha,\beta}J_{ij},$$

in terms of $J_{ij} = \exp(-\kappa n_{ij})$. The effective potential $\delta\mathbf{U}^{\text{eff}}$ is a **self-consistent potential** to ensure the incompressibility condition (5.50), or equivalently

$$^t\mathbf{e}\cdot\delta\rho = 0, \quad \text{and hence} \quad ^t\mathbf{e}\cdot\hat{\mathbf{T}} = 0.$$

It is assumed to act uniformly on all species of monomers in a bulk system

$$\delta\mathbf{U}^{\text{eff}} = \mathbf{e}\delta U, \tag{5.70}$$

where δU is a scalar. To find δU, we substitute (5.68) and (5.70) into (5.69) and multiply $^t\mathbf{e}$ from the left. Solving the result for δU, we find

$$\delta U = -\frac{^t\mathbf{e}\cdot\hat{\mathbf{S}}\cdot(\hat{\mathbf{1}}+\hat{\chi}\cdot\hat{\mathbf{T}})\cdot\mathbf{U}}{(^t\mathbf{e}\cdot\hat{\mathbf{S}}\cdot\mathbf{e})}.$$

Substituting this equation back into (5.69), and solving it with respect to $\langle \delta\rho \rangle$, we finally find

$$\hat{\mathbf{T}} = \frac{1}{\hat{\mathbf{1}} - \hat{\mathbf{Q}} \cdot \hat{\chi}} \cdot \hat{\mathbf{Q}},$$

where

$$\hat{\mathbf{Q}} \equiv \hat{\mathbf{S}} - \frac{(\hat{\mathbf{S}} \cdot \mathbf{e}) : ({}^t\mathbf{e} \cdot \hat{\mathbf{S}})}{({}^t\mathbf{e} \cdot \hat{\mathbf{S}} \cdot \mathbf{e})}.$$

The true correlation function $\hat{\mathbf{T}}$ is thus expressed in terms of the intracluster correlation function $\hat{\mathbf{S}}$; this is the fundamental idea of the RPA. Now the simple algebra gives

$$ {}^t\tau \cdot \hat{\mathbf{T}} \cdot \tau = \frac{1}{S(q)/W(q) - 2\chi}, $$

which is equivalent to (5.57).

Two extreme cases of the polymer blends of A-chains/B-chains and chemically connected block copolymers A-*block*-B have been historically important, and will be detailed in Section 6.1.

5.C   Spinodal condition in RPA

Let us prove that the RPA condition (5.63) reduces to the spinodal condition (5.46) if the wavenumber is allowed to go to zero. To simplify the notation we define $n \equiv n_A + n_B$ for the sum of the DP of both species and write $n_A \equiv na, n_B \equiv nb$ with $a + b = 1$.

For $\mathbf{q} = 0$ we have $J_{ij} = 1$, and $A_{lm}(0) = (nal)^2$, $B_{lm}(0) = (nbm)^2$, and $C_{lm} = n^2ablm$. Hence we have $S_{AA}^\circ = n^2a^2\langle l^2 \rangle v^S$, $S_{BB}^\circ = n^2b^2\langle m^2 \rangle v^S$, and $S_{AB}^\circ = n^2ab\langle lm \rangle v^S$, where a bracket $\langle \cdots \rangle$ abbreviates the number-weighted average $\langle \cdots \rangle_n$. By definition we obtain

$$\frac{S(0)}{W(0)} = \frac{\langle (al + bm)^2 \rangle}{(nab)^2(\langle l^2 \rangle \langle m^2 \rangle - \langle lm \rangle^2)v^S}.$$

To express the κ-functions in terms of the average quantities, we take the derivative of the two relations (5.27a) and (5.27b) with respect to ϕ, and find

$$na[x'v_x + x(v_{xx}x' + v_{xy}y')] = 1, \tag{5.71a}$$

$$nb[y'v_y + y(v_{yx}x' + v_{yy}y')] = -1, \tag{5.71b}$$

where a prime indicates the derivative with respect to ϕ, and v_{xy}, etc., are the partial derivatives of v^S. By the use of the identities $x^2v_{xx} = \sum l(l-1)v_{l,m} = (\langle l^2 \rangle - \langle l \rangle)v^S$, $y^2v_{yy} = (\langle m^2 \rangle - \langle m \rangle)v^S$, and $xyv_{xy} = \langle lm \rangle v^S$, we eliminate the partial derivatives

in favor of the number-averages. The relations (5.71a) are transformed into

$$\frac{\langle l^2 \rangle}{\langle l \rangle} \kappa_\mathrm{A} - \frac{a}{b} \frac{\langle lm \rangle}{\langle m \rangle} \kappa_\mathrm{B} = 1,$$

$$\frac{b}{a} \frac{\langle lm \rangle}{\langle l \rangle} \kappa_\mathrm{A} - \frac{\langle m^2 \rangle}{\langle m \rangle} \kappa_\mathrm{B} = -1,$$

which, when solved with respect to κ, give

$$\kappa_\mathrm{A}(\phi) = \frac{a \langle lm \rangle + b \langle m^2 \rangle}{b(\langle l^2 \rangle \langle m^2 \rangle - \langle lm \rangle^2)} \langle l \rangle,$$

$$\kappa_\mathrm{B}(\phi) = \frac{a \langle l^2 \rangle + b \langle lm \rangle}{a(\langle l^2 \rangle \langle m^2 \rangle - \langle lm \rangle^2)} \langle m \rangle.$$

The κ-functions have thus been expressed in terms of the average cluster sizes and their fluctuations. Substituting the result into (5.46), we confirm that it is equivalent to (5.63) with $q = 0$. The RPA scattering function has thus been most generally proved to give the lattice-theoretical spinodals in the limit of vanishing wavenumber.

References

[1]   Dolezalek, F., *Z. Phys. Chem. Stoechiom. Verwandschaftlehre* **64**, 727 (1908).

[2]   Kempter, H.; Mecke, R., *Naturwissenschaften* **27**, 583 (1939).

[3]   Kempter, H.; Mecke, R., *Z. Phys. Chim. Abt. B* **46**, 229 (1940).

[4]   Prigogine, I.; Bellemans, A.; Mathot, V., *The Molecular Theory of Solutions*. North-Holland: Amsterdam, 1957.

[5]   Prigogine, I.; Defay, R., *Chemical Thermodynaics*, 4th ed. Longman: London, 1954.

[6]   Hirschfelder, J.; Stevenson, D.; Eyring, H., *J. Chem. Phys.* **5**, 896 (1937).

[7]   Flory, P. J., *J. Chem. Phys.* **12**, 425 (1944).

[8]   Huggins, M. L., *J. Chem. Phys.* **46**, 151 (1942).

[9]   Flory, P. J., *Principles of Polymer Chemistry*. Cornell University Press: Ithaca, NY, 1953.

[10] Koningsveld, R.; Stockmayer, W. H., Nies, E., *Polymer Phase Diagrams–A Text Book*. Oxford University Press: Oxford, 2001.

[11] Clark, A. H.; Ross-Murphy, S. B., *Adv. Polym. Sci.* **83**, 57 (1987).

[12] Russo, R. S., in *Reversible Polymeric Gels and Related Systems*, Russo, R. S. (ed.). American Chemical Society: New York, 1987.

[13] Kramer, O., *Biological and Synthetic Polymer Networks*. Elsevier: London and New York, 1988.

[14] Guenet, J. M., *Thermoreversible Gelation of Polymers and Biopolymers*. Academic Press: London, 1992.

[15] te Nijenhuis, K., *Adv. Polym. Sci.* **130**, 1 (1997).

[16] Tanaka, F., *Macromolecules* **22**, 1988 (1989).

[17] Tanaka, F.; Matsuyama, A., *Phys. Rev. Lett.* **62**, 2759 (1989).

[18] Tanaka, F., *Macromolecules* **23**, 3784; 3790 (1990).

[19] Tanaka, F.; Koga, T., *Bull. Chem. Soc. Jpn* **74**, 201 (2001).

[20] Tanaka, F., *Polym. J.* **34**, 479 (2002).

[21] Solc, K., *Macromolecules* **3**, 665 (1970).

[22] de Gennes, P. G., *J. Phys. (Paris)* **31**, 235 (1970).

[23] de Gennes, P. G., *Faraday Disc. Roy. Soc. Chem.* **68**, 96 (1979).

[24] de Gennes, P. G., *Scaling Concepts in Polymer Physics*. Cornell University Press: Ithaca, NY, 1979.

[25] Leibler, L., *Macromolecules* **13**, 1602 (1980).

[26] Bates, F. S., *Science* **251**, 898 (1991).

[27] Tanaka, F.; Ishida, M.; Matsuyama, A., *Macromolecules* **24**, 5582 (1991).

[28] For example see (i) Burchard, W., In *Light Scattering from Polymers*; Springer-Verlag: Heidelberg, 1983; p.1 (ii) Picot, Cl. in *Static and Dynamic Properties of the Polymeric Solid State* Pethrick, R. A. Richards, R. W., (eds.). Reidel: New York, 1982, p. 127.

6 Nongelling associating polymers

This chapter presents some important nongelling binary associating mixtures. Throughout this chapter, we assume the pairwise association of reactive groups, the strength of which can be expressed in terms of the three *association constants* for A·A, B·B, and A·B association. We apply the general theory presented in Chapter 5 to specific systems, such as dimerization, linear association, side-chain association, hydration, etc. The main results are summarized in the form of phase diagrams.

6.1 Dimer formation as associated block-copolymers

The first system we study is a mixture of R{A$_1$} and R{B$_1$} chains, each carrying a functional group A or B at one end. Diblock copolymers are formed by the end-to-end association (**hetero-dimerization**) [1,2]. End groups A and B are assumed to be capable of forming pairwise bonds A·B by thermoreversible hetero-association. The hydrogen bond between acid and base pair is the most important example of this category.

For such mixtures, composite diblock copolymers R{A$_1$}-*block*-R{B$_1$} with a temporal junction are formed (Figure 6.1). The system is made up of a mixture of diblock copolymers (1,1), and unassociated homopolymers of each species (1,0) and (0,1). It is similar to the mixture of chemically connected diblock copolymers dissolved in their homopolymer counterparts [3, 4], but its phase behavior is much richer because the population of the block copolymers varies with both temperature and composition.

Let $n \equiv n_A + n_B$ be the total number of the statistical units on a block copolymer chain, and let $a \equiv n_A/n$ ($b \equiv n_B/n$) be the fraction of A-chain (B-chain). The relation $a + b = 1$ holds by definition.
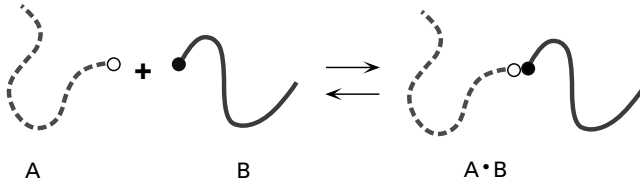
Our starting free energy is given by

$$\mathscr{F} = \nu_{11}\Delta + \nu_{10}\ln\phi_{10} + \nu_{01}\ln\phi_{01} + \nu_{11}\ln\phi_{11} + \chi(T)\phi(1-\phi), \tag{6.1}$$

where

$$\Delta \equiv \beta(\mu^{\circ}_{A\cdot B} - \mu^{\circ}_{A} - \mu^{\circ}_{B}) \tag{6.2}$$

is the free energy of dimer formation. By differentiation, we find the chemical potentials for each component as

$$\beta\Delta\mu_{10} = 1 + \ln x - n_A\nu^{S} + \chi n_A(1-\phi)^2, \tag{6.3a}$$

Fig. 6.1 Associated diblock copolymer formed by a pairwise bond between the end groups.

$$\beta \Delta \mu_{01} = 1 + \ln y - n_B v^S + \chi n_B \phi^2, \tag{6.3b}$$

$$\beta \Delta \mu_{11} = 1 + \Delta + \ln z - n v^S + \chi [n_A (1 - \phi)^2 + n_B \phi^2], \tag{6.3c}$$

where $v^S \equiv v_{10} + v_{01} + v_{11}$ is the total number of molecules that possess translational degree of freedom, and the abbreviated notations $x \equiv \phi_{1,0}, y \equiv \phi_{0,1}, z \equiv \phi_{1,1}$ have been used.

The association equilibrium condition (5.19) then leads to

$$z = K x y \tag{6.4}$$

for the volume fraction z of the block copolymers, where $K \equiv \exp(1 - \Delta)$ is the temperature-dependent equilibrium constant. Because of the nongelling nature, we have the identity

$$\phi^S = x + y + K x y \equiv 1. \tag{6.5}$$

The number density of clusters is given by

$$v^S = v = \frac{1}{n} \left(\frac{x}{a} + \frac{y}{b} + K x y \right). \tag{6.6}$$

The coupled equations (5.27a) and (5.27b) take the form

$$x(1 + a K y) = \phi, \tag{6.7a}$$

$$y(1 + b K x) = 1 - \phi. \tag{6.7b}$$

The solution is given by

$$x(\phi) = \left\{ \phi - a - K^{-1} + \sqrt{D(\phi)} \right\} / 2b, \tag{6.8a}$$

$$y(\phi) = \left\{ a - \phi - K^{-1} + \sqrt{D(\phi)} \right\} / 2a, \tag{6.8b}$$

where $D(\phi) \equiv [a(1 - \phi) + b\phi + K^{-1}]^2 - 4ab\phi(1 - \phi)$. Hence we have

$$z(\phi) = \frac{1}{2ab} \left[a(1 - \phi) + b\phi + K^{-1} - \sqrt{D(\phi)} \right]. \tag{6.9}$$

The logarithmic derivatives of x and y yield specific forms of the κ-functions for the dimerization

$$\kappa_A(\phi) = \frac{1 - az'}{1 - az/\phi}, \qquad \kappa_B = \frac{1 + bz'}{1 - bz/(1 - \phi)}, \tag{6.10}$$

where $z'(\phi)$ is the concentration derivative of $z(\phi)$. Explicitly, it is $z'(\phi) = K(y-x)/[1+K(ay-bx)]$.

Let us consider the free energy (6.2) of the dimer formation. The conformational free energy appears because the entropy of disorientation is reduced when two chains are combined. If we use the lattice-theoretical entropy of disorientation (2.90), we have

$$\Delta S_{dis} \equiv S_{dis}(n_A + n_B) - S_{dis}(n_A) - S_{dis}(n_B) = k_B \ln\left\{\frac{\sigma(\zeta-1)^2}{\zeta\,enab}\right\}, \qquad (6.11)$$

for the entropy change. The free energy is given by $\Delta f_{conf} = -T\Delta S_{dis}$. Combining the free energy of bonding $\Delta f_0 = \Delta\epsilon - T\Delta s$, we find that the equilibrium constant is given in the form

$$K = \lambda_0 e^{-\beta\Delta\epsilon}, \qquad (6.12)$$

where $\lambda_0 \equiv \sigma(\zeta-1)^2 e^{\Delta s/k_B}/\zeta\,enab$ is a temperature-independent constant.

Let us proceed to the calculation of the scattering functions. Simple algebra gives

$$A_{10} = A_{11} = \sum_{i,j=1}^{n_A} \exp(-\kappa|i-j|) = (na)^2 D(aQ), \qquad (6.13)$$

for the AA component of the intramolecular scattering function, where $Q \equiv n\kappa = n(aq)^2/6 = (R_G q)^2$ is the dimensionless squared wavenumber measured relative to the unperturbed gyration radius $R_G \equiv a\sqrt{n/6}$ of a diblock copolymer. The entire scattering function depends on Q, T, and ϕ. The function $D(x)$ is Debye function (1.49). The amplitude A_{lm} is the same for both A-unimer (1,0) and copolymer (1,1).

Similar calculation leads to

$$B_{01} = B_{11} = (nb)^2 D(bQ), \qquad (6.14)$$

for the BB components, and

$$C_{11} = \sum_{i\in A}\sum_{j\in B} \exp(-\kappa|i-j|) = \frac{n^2}{2}\{D(Q) - a^2 D(aQ) - b^2 D(bQ)\}, \qquad (6.15)$$

for the AB component of a block copolymer. Putting these results together, we find

$$S^\circ_{AA} = A_{10}\frac{x}{na} + A_{11}\frac{z}{n} = na D(aQ)\phi, \qquad (6.16a)$$

$$S^\circ_{BB} = B_{01}\frac{y}{nb} + B_{11}\frac{z}{n} = nb D(bQ)(1-\phi), \qquad (6.16b)$$

$$S^\circ_{AB} = C_{11}\frac{z}{n} = \frac{n}{2}\{D(Q) - a^2 D(aQ) - b^2 D(bQ)\}z, \qquad (6.16c)$$

and the condition for stability limit (5.63) to be solved is given by

$$F(Q) - 2n\chi = 0, \qquad (6.17)$$

where the function F, defined by $F(Q) \equiv nS(Q)/W(Q)$, takes the form

$$F(Q) = \frac{ax D(aQ) + by D(bQ) + z D(Q)}{ab\phi(1-\phi)D(aQ)D(bQ) - \frac{1}{4}z^2[D(Q) - a^2 D(aQ) - b^2 D(bQ)]^2}. \quad (6.18)$$

This function $F(Q)$ covers the two extreme limits:

(i) Nonassociating **binary blends** ($K = 0$):

$$F(Q) = \frac{1}{a\phi D(aQ)} + \frac{1}{b(1-\phi)D(bQ)} \quad (6.19)$$

This RPA scattering function of a binary blends was analyzed by de Gennes [5] in relation to the spinodal decomposition. The function $F(Q)$ shows no peak at finite Q.

(ii) Chemically connected **block copolymers** ($K = \infty$):

$$F(Q) = \frac{D(Q)}{a^2 b^2 D(aQ)D(bQ) - \frac{1}{4}[D(Q) - a^2 D(aQ) - b^2 D(bQ)]^2} \quad (6.20)$$

The microphase formation in this limit was elaborated by Leibler [6] and Bates [7].

The function F defined by (6.18) bridges these two. It can either be a steadily increasing function or exhibit a single maximum at finite Q. At sufficiently high temperatures we have $F(Q; \tau, \phi) > 2n\chi(\tau)$ for any Q, so that the homogeneously mixed state is stable. As the temperature is decreased the condition (6.17) is first satisfied for $Q = 0$ in a certain range of the concentration, where $F(Q)$ is the monotonic function

$$F(0; \tau, \phi) - 2n\chi(\tau) = 0. \quad (6.21)$$

This is the spinodal point (SP). This condition is met for the concentration ϕ, which is either small or large so that the population of the produced diblock copolymers is insufficient to form a microphase.

However, when the numbers of A- and B-chains are comparable, $F(Q)$ exhibits a maximum at finite Q^*. Sufficiently many copolymers are produced to form a microphase. In this case the instability condition is first fulfilled at this wavenumber as the temperature is lowered, which indicates that the **microphase separation transition** (MST) takes place before SP. The condition for this situation to be realized is given by

$$\frac{\partial F(Q; \tau, \phi)}{\partial Q} = 0, \quad \text{for} \quad Q = Q^* > 0, \quad (6.22)$$

together with (6.17) for $Q = Q^*$. Even in this concentration region the spinodal condition is met if one goes further down into the low-temperature region. The microphase remains stable only in the region surrounded by the MST and SP.
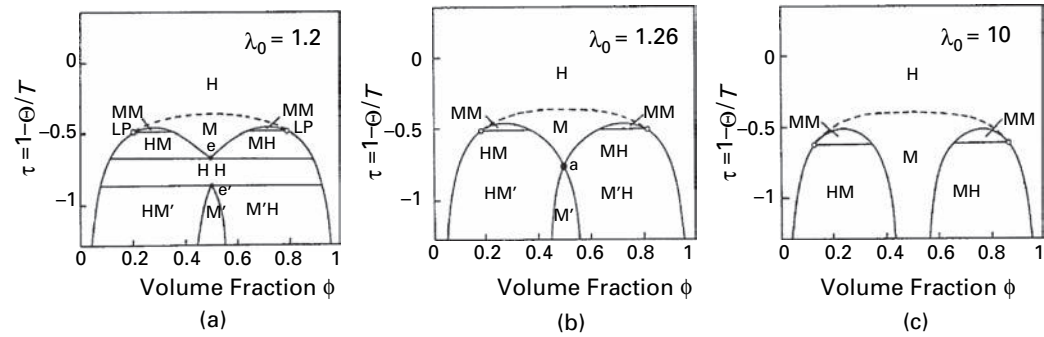
Fig. 6.2 Typical example of the phase diagrams for the associating diblock copolymer blends of relatively short chains ($n_A = n_B = 20$). MST (broken line) and SP (solid lines) are shown on the temperature–concentration plane. Points indicated by (LP) are Lifshitz points, while those shown by (e) and (e$'$) are eutectic points. Existence of a reentrant microphase (M$'$) is one of the remarkable features of the associating systems. $\gamma \equiv \Delta \in / k_B \Theta = 3$. (a) $\lambda_0 = 1.20$, (b) $\lambda_0 = 1.26$, (c) $\lambda_0 = 10.0$. (Reprinted with permission from Ref. [1].)
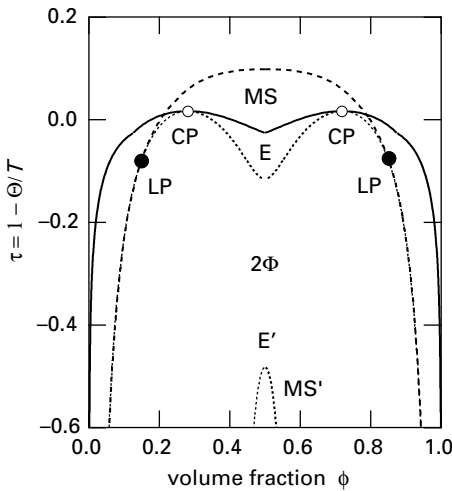
Fig. 6.3 Typical phase diagram of associating diblock copolymers in which macro- and microphase separation compete. Binodal (solid line), spinodal (dotted line), and MST (broken line) are drawn. Critical points are indicated by CP. At the crossing of the spinodal and MST lines, Lifshitz points (LP) appear. At the stoichiometric composition where the number of A groups equals that of B groups, a eutectic point (E, E$'$) appears. (Reprinted with permission from Ref. [2].)

In the following numerical calculations, the association constant is described in the form $\lambda(T) = \lambda_0 \exp(|\Delta \in| / k_B T) = \lambda_0 \exp[\gamma(1 - \tau)]$ in terms of the reduced temperature $\tau \equiv 1 - \Theta / T$ and the dimensionless association energy $\gamma \equiv |\Delta \in| / k_B \Theta$.

Figures 6.2 and 6.3 show theoretical calculation of the phase diagram for a symmetric blend where both chains have the same length [1]. The solid lines show the binodal, the broken lines MST, and dotted lines the SP. MST and SP meet at the two symmetric points (indicated by LP) at which the two conditions (6.17) and (6.21) reduce to a single one.

They are examples of a **Lifshitz point** – a point where an order parameter with finite wave number starts to appear [3, 8].

The whole plane is divided into several regions, each indicated by capital letters. The region with the letter H has a homogeneously mixed fluid phase. Those shown by M and M′ exhibit microscopically ordered phases where the microdomains are regularly ordered. The region with the letters 2Φ in the figure is a **biphasic region** (or **miscibility gap**) where two distinct phases coexist.

The point indicated by the letter E in the middle of the phase diagram is a **eutectic point**, where the single microphase melts into the two coexisting homogeneously mixed fluids when the temperature is lowered (see Figure 6.3).

At extremely low temperatures, we observe that the miscibility gap starts to split again at the point E′ in the center of the concentration axis, and a new homogeneous microphase (shown by MS′) is stabilized in between. Such a low-temperature microphase (called a **reentrant microphase**) is stabilized simply because the population of block copolymers becomes so large in this low-temperature region that they homogenize the two demixed fluid phases into a single one.

Experimentally, hydrogen bonds are expected to lead to a thermoreversible MST if they are strong enough compared to the repulsive interaction between the polymer segments, but still weak enough to break by temperature. In this respect, a single hydrogen bond is not strong enough, but through elaborate effort [9, 10] a reversible lamellar formation was confirmed to be possible for semi-crystalline block copolymers, i.e., a blend of one-end-aminated polystyrene and one-end-carboxylated polyethylene glycol. In contrast, a variety of liquid-crystalline ordered phases induced by **multiple hydrogen bonds** have been the focus of recent research interest [11–14].

The mutual interference between MST and SP is strongest around the Lifshitz point. Near the LP, the order parameter has smaller wave numbers, so that we can expand the function $F(Q)$ in powers of Q as

$$F(Q) = F_0 + F_1 Q + F_2 Q^2 + \cdots. \tag{6.23}$$

Here the coefficients F_i are functions of τ and ϕ. (F_0 is identical to $F(0; \tau, \phi)$, which appeared in the SP condition.) Then, the LP is the point at which F_1 changes its sign from positive to negative. Combination of the condition (6.21) with $F_1(\tau, \phi) = 0$ determines the position of the LP.

In the microphase region near the LP, we can write

$$F(Q; \tau, \phi) - 2n\chi = \epsilon + F_2(Q - Q^*)^2, \tag{6.24}$$

by keeping up to the second order of Q, where

$$\epsilon \equiv F_0 - \frac{F_1^2}{4F_2} - 2n\chi, \tag{6.25}$$

and

$$Q^* = -\frac{F_1}{2F_2} \quad (>0). \tag{6.26}$$

The parameter ϵ measures the temperature deviation from the LP. The squared wavenumber Q^* gives the periodicity of the unstable mode. Near the LP, where $\tau = \tau_L$ and $\phi = \phi_L$ hold, F_1 is proportional to $|\tau - \tau_L|$ or $|\phi - \phi_L|$ in accordance with the direction we approach on the phase diagram. Hence we find $q^* \sim |\tau - \tau_L|^{1/2}$ or $q^* \sim |\phi - \phi_L|^{1/2}$.

6.2   Linear association and ring formation

Consider the association of polymer chains R{A_2} carrying two functional groups at their ends (**telechelic polymers**) in a solution. We assume pairwise association in this section, so that the polymers R{A_2} form either linear chains or rings (**chain–ring equilibrium**). The problem of ring formation was studied by Jacobson and Stockmayer [15] in an attempt to incorporate **intramolecular reaction** into the classical tree statistics of gelation. Later, the similar consideration was applied to the study of **thermal polymerization** of sulfur by Tobolsky and Eisenberg [16], and by Scott [17] and Wheeler and Pfeuty [18–20]. In the solution, ring sulfurs S_8 first open the rings by thermal agitation, and form long chains by end reaction. The authors of [16–20] found interesting phase diagrams in which LCST phase separation and polymerization coexist.

More general cases of multiple association where polymer networks with multiple junctions of varied structures are formed will be treated as the gelling case in the next section.

Let N_m^C be the number of m-mer open chains, and let N_m^R be the number of m-mer rings in the system. The total number of primary polymer chains ($n_A \equiv n$) is given by

$$N = \sum_{m=1}^{\infty} m(N_m^C + N_m^R). \tag{6.27}$$

Let N_0 be the total number of solvent molecules ($n_B \equiv 1$). The number of cells is $\Omega = N_0 + nN$. Let $\phi_m^C \equiv nm N_m^C / \Omega$ and $\phi_m^R \equiv nm N_m^R / \Omega$ be the volume fraction of chains and rings. The volume fraction of polymers is then given by

$$\phi = \sum_{m=1}^{\infty} (\phi_m^C + \phi_m^R) = 1 - \phi_0, \tag{6.28}$$

where ϕ_0 is the volume fraction of the solvent. The fraction of rings among the total polymers is

$$\rho \equiv \sum_{m=1}^{\infty} \phi_m^R / \phi. \tag{6.29}$$

We follow the general strategy given in Chapter 5, and start with the free energy of the solution

$$\beta \Delta F = \sum_{m \geq 1} \left\{ \Delta_m^C N_m^C + \Delta_m^R N_m^R \right\} \tag{6.30}$$

$$+ N_0 \ln \phi_0 + \sum_{m \geq 1} \left\{ N_m^C \ln \phi_m^C + N_m^R \ln \phi_m^R \right\} + \chi \phi (1 - \phi) \Omega,$$

where Δ are the free energies of reaction, defined for chains and rings as

$$\Delta_m^C \equiv \beta(\mu_m^{C\circ} - m\mu_1^\circ),\tag{6.31a}$$

$$\Delta_m^R \equiv \beta(\mu_m^{R\circ} - m\mu_1^\circ),\tag{6.31b}$$

We first consider open chains. The number of different ways to connect m identical polymers into a linear array is given by 2^m, but since the connected chain is symmetric, we have to divide it by the symmetry number $\sigma_C = 2$, and hence we have 2^{m-1} for the combinatorial factor. The conformational term is given by the difference $\Delta S_{\mathrm{conf}}(m) = S_{\mathrm{dis}}(mn) - mS_{\mathrm{dis}}(n)$ as before. The bonding free energy is assumed to be given by Δf_0 for each bond.

Hence, for the equilibrium constant of the chains, we find

$$K_m^C = 2^{m-1} m \left[\frac{\sigma_C(\zeta-1)^2}{n\zeta} \right]^{m-1} (e^{-\beta\Delta f_0})^{m-1} \equiv m \left(\frac{2\lambda}{n} \right)^{m-1},\tag{6.32}$$

where $\lambda(T) \equiv [\sigma_C(\zeta-1)^2/\zeta]e^{-\beta\Delta f_0}$ is the association constant. We thus have

$$\frac{2\lambda}{n}\phi_m^C = mx^m,\tag{6.33}$$

for the volume fraction of chains, where $x \equiv 2\lambda\phi_1^C/n$ is the number density of associative groups on the unassociated chains.

However, the equilibrium constant for the rings includes an extra factor of the probability to form a ring. This factor is proportional to $(mn)^{-3/2}$ for a Gaussian chain of the length mn, but again we have to divide it by the symmetry factor $\sigma_R = m$ for a ring, because we can close a chain at any one of m bonds to form a ring.

We thus have

$$K_m^R = 2^{m-1} \cdot m \left[\frac{\sigma_C(\zeta-1)^2}{n\zeta} \right]^{m-1} (e^{-\beta\Delta f_0})^{m-1} \cdot \frac{B_0}{m^{5/2}}$$

$$= m \left(\frac{2\lambda}{n} \right)^{m-1} \frac{B}{m^{5/2}},\tag{6.34}$$

for rings, where

$$B \equiv B_0 e^{-\beta\Delta f_0}\tag{6.35}$$

is a temperature-dependent constant. The volume fraction of rings is given by

$$\frac{2\lambda}{n}\phi_m^R = m \cdot \frac{B}{m^{5/2}} x^m.\tag{6.36}$$

The total volume fraction of polymers is given by the sum of the two

$$\frac{2\lambda}{n}\phi = \frac{2\lambda}{n}(\phi^C + \phi^R) = \sum_{m \geq 1} mx^m + B \sum_{m \geq 1} \frac{x^m}{m^{3/2}}$$

$$= \frac{x}{(1-x)^2} + B\Phi(x; 3/2) \tag{6.37}$$

where the new function Φ is introduced by the infinite sum

$$\Phi(x; \alpha) \equiv \sum_{m \geq 1} \frac{x^m}{m^\alpha} \tag{6.38}$$

The upper limit of the summation is given by the maximum possible aggregation number and should not exceed the total number N of polymers. But here we have taken the thermodynamic limit, and allow N to go to infinity.

Similarly, the total number of clusters and molecules is given by

$$\lambda \nu^S = \lambda(1-\phi) + \sum_{m \geq 1} x^m + B \sum_{m \geq 1} \frac{x^m}{m^{5/2}}$$

$$= \lambda(1-\phi) + \frac{x}{1-x} + B\Phi(x; 5/2) \tag{6.39}$$

Solving (6.37) with respect to x, and substituting the result into (6.39), we complete our general procudure, and can find the equilibrium solution properties. The extent of reaction p is given by

$$p = x + (1-x)B\Phi(x; 3/2)/\lambda \psi \tag{6.40}$$

The functions $\Phi(x; \alpha)$ with $\alpha = 3/2, 5/2$ appear in the study of Bose–Einstein condensation of ideal quantum particles [21] that obey Bose–Einstein statistics. Their mathematical properties were studied by Truesdell [22] in detail, so that it is called the **Truesdell functions**. Their radius of convergence is given by $x = 1$. Both the functions $\Phi(x; 3/2)$ and $\Phi(x; 5/2)$ remain at a finite value at $x = 1$, but diverge as soon as x exceeds unity.

Jacobson and Stockmayer [15] showed the fraction of chains and rings on the temperature–concentration phase plane, and found very interesting phenomena that are analogous to Bose–Einstein condensation. When the parameter B exceeds a certain critical value, 100% rings are formed below a critical concentration of polymers. In fact, when $p = 1$, we have the coupled equations

$$\lambda \psi / B = \Phi(x; 3/2), \tag{6.41a}$$

$$\lambda \nu / B = \Phi(x; 5/2), \tag{6.41b}$$

($\psi \equiv 2\phi/n$), which are analogous to

$$\lambda_T^3 N/V = \Phi(x; 3/2), \tag{6.42a}$$

$$\lambda_T^3 p/k_B T = \Phi(x; 5/2), \tag{6.42b}$$

for the density and pressure of an ideal Bose–Einstein gas. Such a transition appears from the singularity in the Truesdell functions, and hence loop entropy. This is an interesting example of Bose–Einstein condensation in classical statistical mechanics.

Another singular property of this model is the divergence of the weight-average molecular weight at the point $x = 1$. The condition gives the **thermal polymerization** line when mapped onto the temperature–concentration plane, because at this point the average chain length goes to infinity. Application of our theory gives essentially the same results as those originally found by Scott [17], and later refined by Wheeler and Pfeuty [18,19,20] on the thermal polymerization of sulfur. More recently, Dudowicz *et al.* [23,24] theoretically studied living polymerization using a similar approach.

In a similar way, we can study the mixed linear association of $R\{A_2\}$ molecules and $R\{B_2\}$ ones. The sequence distribution along an associated chain can be alternative, sequential, or statistically random, depending upon the strength of association constants. All these associated chains, or rings, are block copolymers if the primary molecules are polymers, so that they undergo microphase separation transition as well as macroscopic phase separation. This problem of **competing micro- and macrophase separation** in associating polymers is one of the important unsolved problems to be studied.

In the case of the linear association of low-molecular weight rigid molecules, the problem we are studying is related to the fibrillar association of bifunctional molecules by (multiple) hydrogen bonds, such as seen in hydrogen-bonded supramolecular liquid crystals [11,12,13], low-molecular weight gelators [25,14], etc. Readers can study their equilibrium properties and phase diagrams within the theoretical framework presented here.

6.3 Side-chain association

The next system we study is a mixture of high-molecular weight polymers $R\{A_f\}$ (DP $\equiv n_A \gg 1$) bearing a number f of associative A groups, and low-molecular weight monofunctional molecules $R\{B_1\}$ (DP$\equiv n_B$) [26,14]. The latter can be solvent molecules S ($n_B = 1$) [29]. We assume that a B group, or solvent molecule, can attach onto an A group from the side of the polymer chain. The adsorption of surfactant molecules onto polymer backbones by hydrogen bonds (Figure 6.4) is an important example of the former. The hydration of water molecules in an aqueous polymer solution (Figure 6.7) is an important example of the latter.

To simplify the theoretical description, we write the DP of molecules as $n_A \equiv na$ and $n_B \equiv nb$ by using $n \equiv n_A + n_B$. The type of clusters formed is specified by $(1, m)$ with $m = 0, 1, 2, \ldots$, while the unassociated $R\{B_1\}$ molecule is indicated by $(0, 1)$.

As in the general theoretical scheme, we start with the free energy of the mixture

$$\beta \Delta F = \sum_{m=0}^{f} \Delta_m N_{1m} + N_{01} \ln \phi_{01} + \sum_{m=0}^{f} N_{1m} \ln \phi_{1m} + \Omega \chi \phi (1 - \phi). \qquad (6.43)$$
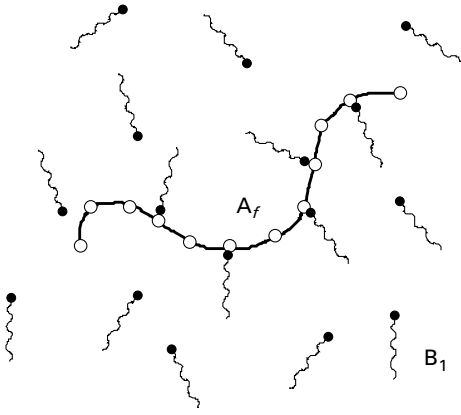
Fig. 6.4   Association of end-functional low-molecular weight molecules R{B$_1$} to the side of a long polymer chain R{A$_f$}. Comb-like block copolymers are formed.

The volume fraction of R{A$_f$} molecules is given by

$$\phi \equiv \sum_{m=0}^{f} \frac{a}{a+mb} \phi_{1m}.$$

(6.44)

The free energy change to form a $(1, m)$-mer from the primary molecules in the reference state is

$$\Delta_m \equiv \beta(\mu_{1m}^{\circ} - \mu_{10}^{\circ} - m\mu_{01}^{\circ}).$$

(6.45)

The chemical potentials for each type of molecule are

$$\beta\Delta\mu_{1,m} = 1 + \ln\phi_{1,m} - n(a+bm)v + n\chi[a(1-\phi)^2 + bm\phi^2],$$

$$\beta\Delta\mu_{0,1} = 1 + \ln\phi_{0,1} - nbv + \chi nb\phi^2.$$

(6.46a)

Imposing the chemical equilibrium conditions (5.19), we find the distribution function of the clusters in the form

$$\phi_{1m} = K_m\phi_{10}\phi_{01}{}^m,$$

(6.47)

where $K_m \equiv \exp(m - \Delta_m)$ is the equilibrium constant.

Let us write $\phi_{10} \equiv x, \phi_{01} \equiv y$, and define the coefficients b_m by $K_m \equiv (n_A + n_B m)b_m$. The variables x, y can be expressed by the controlling parameters ϕ and T by solving the coupled equations

$$n_A x G_0(y) = \phi,$$

(6.48a)

$$y + n_B x G_1(y) = 1 - \phi,$$

(6.48b)

where the functions G_k are defined by

$$G_k(y) \equiv \sum_{m=0}^{f} m^k b_m y^m. \tag{6.49}$$

By eliminating x, we find the equation for y in the form

$$y = 1 - \left[1 + \frac{b}{a} f \theta(y)\right] \phi, \tag{6.50}$$

where

$$\theta(y) \equiv G_1(y)/f G_0(y) = \langle m \rangle / f \tag{6.51}$$

is the fraction of the adsorbed sites.

The chemical potentials are

$$\beta \Delta \mu_A = 1 + \ln \phi_{1,0} - n_A \nu + n_A \chi (1 - \phi)^2 \tag{6.52a}$$

$$\beta \Delta \mu_B = 1 + \ln \phi_{0,1} - n_B \nu + \chi n_B \phi^2 \tag{6.52b}$$

The condition for a low-concentration homogeneous phase with ϕ' to coexist with a high concentration homogeneous phase with ϕ'' is given by the coupled equations

$$\Delta \mu_A(\phi', T) = \Delta \mu_A(\phi'', T), \tag{6.53a}$$

$$\Delta \mu_B(\phi', T) = \Delta \mu_B(\phi'', T). \tag{6.53b}$$

If one of the phases lies in the microphase separated region, its chemical potential must be replaced by that of the corresponding ordered state. The chemical potential of the microphase depends on the ordered structure and its precise form is unknown for the associating polymers at this moment. Therefore, in what follows we show in the phase diagrams the binodal lines calculated on the basis of (5.6), together with the MST boundary and spinodal lines, to examine under what conditions the microphases remain thermodynamically stable.

The parts of these binodal lines lying inside the microphase separated region should shift to some extent if the free energy of ordering is correctly taken into account. Their positions therefore only suggest the possibility of the phase equilibrium near them. Because

$$\kappa_A(\phi) = 1 - f \phi \theta(y) y'/y, \tag{6.54a}$$

$$\kappa_B(\phi) = -(1 - \phi) y'/y, \tag{6.54b}$$

the spinodal condition is

$$\frac{1}{n_A \phi} - \frac{[1 + (b/a) f \theta(y)] y'}{n_B y} - 2\chi = 0. \tag{6.55}$$

By differentiating (6.50), and expressing y' in terms of y, we find

$$\frac{d \ln y}{d \ln \phi} = -\frac{1-y}{y+(b/a) f \phi \theta(y) \Delta \bar{m}}, \tag{6.56}$$

by which the spinodal condition is described in terms of ϕ and T through y, where

$$\Delta \bar{m} \equiv G_2(y)/G_1(y) - G_1(y)/G_0(y) = \langle m \rangle_{\mathrm{w}} - \langle m \rangle_{\mathrm{n}}, \tag{6.57}$$

is the difference between weight- and number average of the adsorbed sites, or equivalently, the fluctuation in the number of bound molecules.

The spinodal condition can be written as

$$\frac{1}{n_{\mathrm{A}}\phi} + \frac{[1+(b/a) f \theta(y)]^2}{n_{\mathrm{B}}[y+(b/a) f \phi \theta(y) \Delta \bar{m}]} - 2\chi = 0. \tag{6.58}$$

The spinodal condition depends not only on the average degree of association $\theta(y)$ but also their fluctuations $\Delta \bar{m}$.

We can find the renormalization $\Delta \chi(\phi)$ of the interaction parameter. Expanding x and y in powers of the concentration, and substituting the results into (5.40), we find

$$\Delta \chi(\phi) = \chi_0 + \chi_1 \phi + \chi_2 \phi^2 + \cdots, \tag{6.59}$$

where $\chi_0 = 0$ and

$$\chi_1 = \theta_0 \left[1 + \frac{1}{2} n_{\mathrm{B}} \theta_0 \right], \tag{6.60}$$

with $\theta_0 \equiv \theta(y_0) = \lim_{\phi \to 0} \theta(\phi)$.

If the association takes place randomly and independently, we can find the equilibrium constant K_m. As usual, we split the free energy Δ_m into combinatorial, conformational, and bonding terms as

$$\Delta_m = -\frac{1}{k_{\mathrm{B}}}(\Delta S_{\mathrm{comb}} + \Delta S_{\mathrm{conf}}) + m \beta \Delta f_0. \tag{6.61}$$

The combinatorial entropy is given in terms of the number $_f C_m$ of different ways to attach m molecules onto f available sites on a polymer. If the attaching process occurs *independently*, it is

$$\Delta S_{\mathrm{comb}} = k_{\mathrm{B}} \ln(_f C_m). \tag{6.62}$$

When there is strong attractive interaction between the attached R{B$_1$} molecules along the chain, they are adsorbed in contiguous sequences. These sequences may induce **helical order** on the main chain due to the steric hindrance of adjacent adsorbed molecules. The combinatorial factor changes to the number of different ways to select the specified sequences from the finite total length n. Such a **correlated adsorption**, or **cooperative adsorption**, was recently studied in detail in relation to helix formation on polymers by adsorption of chiral molecules [27, 28] (Section 1.8). Cooperative hydration will be detailed in Section 6.5.

The conformational entropy is given by

$$\Delta S_{\mathrm{conf}}(m) = S_{\mathrm{dis}}(n_A + mn_B) - S_{\mathrm{dis}}(n_A) - m S_{\mathrm{dis}}(n_B)$$

$$= k_B \ln \left[\frac{a+bm}{a} \left\{ \frac{\sigma(\zeta-1)^2}{n_B \zeta e} \right\}^m \right], \tag{6.63}$$

by using the entropy of disorientation as before.

Putting the results together, we find

$$K_m = \frac{a+bm}{a} {}_f C_m \left[\frac{\lambda(T)}{n_B} \right]^m, \tag{6.64}$$

for the equilibrium constant, where $\lambda(T) \equiv [\sigma(\zeta-1)^2/e\zeta] \exp(-\beta \Delta f_0)$ is the association constant. The cluster distribution function takes the form

$$f\lambda \nu_{1m} = {}_f C_m x y^m. \tag{6.65}$$

The two unknown variables are defined by

$$x \equiv f\lambda(T)\phi_{10}/n_A, \qquad y \equiv \lambda(T)\phi_{01}/n_B. \tag{6.66}$$

These give the number density of A and B groups on the molecules that remain unassociated in the solution. They are always accompanied by the association constant λ, so that the concentration can be scaled by this factor. The association constant therefore works as a **temperature shift factor** of the concentration.

By counting the number of molecules and clusters moving together, the total number density is

$$\lambda \nu^S(x,y) = y + \frac{x}{f} G_0(y). \tag{6.67}$$

The G functions are $G_0(y) = (1+y)^f$, $G_1(y) = fy(1+y)^{f-1}$. The average number $\langle m \rangle$ of B-chains associated to an A-chain is calculated by using the distribution $\nu_{1,m}$ as

$$\theta(y) = \langle m \rangle / f = y/(1+y). \tag{6.68}$$

Hence the degree of adsorption (coverage) of A-chain defined by θ takes Langmuir form (**Langmuir adsorption**).

The coupled equations are transformed to

$$xG_0(y) = f\lambda\phi/n_A, \tag{6.69a}$$

$$y + xG_1(y)/f = \lambda(1-\phi)/n_B. \tag{6.69b}$$

Elimination of x leads to

$$y + \left(\frac{f\lambda\phi}{n_A} \right) \theta(y) = \frac{\lambda(1-\phi)}{n_B}, \tag{6.70}$$

for the equation to be solved for y.

Since the concentrations appear with the association constant as in the right-hand side of these equations, we introduce the new variables

$$c_A \equiv \lambda f\phi/n_A, \qquad c_B \equiv \lambda(1-\phi)/n_B, \tag{6.71}$$

to describe the concentrations. These variables give the total number density of A and B groups. Eliminating y, we have the equation

$$y + c_A\theta(y) = c_B. \tag{6.72}$$

Hence we find

$$y(\phi) = \left[c_B - c_A - 1 + \sqrt{D(\phi)} \right]/2, \tag{6.73}$$

where

$$D(\phi) \equiv 1 + 2(c_A + c_B) + (c_A - c_B)^2 \tag{6.74}$$

is a function of the concentration. The parameter x is given by

$$x = y/(1+y)^f. \tag{6.75}$$

Substituting these results into physical properties, in particular into $v^S(x,y)$, we find them as functions of the temperature and concentration.

The scattering functions of the mixture are calculated in the forms

$$S_{AA}^\circ = \sum_{m=0}^{f} (S_{AA}^\circ)_{1,m} v_{1,m} = n_A\phi D(n_A\kappa), \tag{6.76a}$$

$$S_{AB}^\circ = \sum_{m=0}^{f} (S_{AB}^\circ)_{1,m} v_{1,m} = \frac{n_A(1-\phi-n_B y/\lambda)E(n_B\kappa)}{fE(n_A\kappa/f)}$$
$$\times \{ fD(n_A\kappa) - D(n_A\kappa/f) + E(n_A\kappa)E(n_A\kappa/f) \}, \tag{6.76b}$$

$$S_{BB}^\circ = \sum_{l=0,1}\sum_{m=0}^{f} (S_{BB}^\circ)_{l,m} v_{l,m} = n_B(1-\phi)D(n_B\kappa)$$
$$+ \frac{n_A(1-\phi-n_B y/\lambda)^2 E(n_B\kappa)^2}{f\phi E(n_A\kappa/f)^2}$$
$$\times \{ fD(n_A\kappa) - D(n_A\kappa/f) \}e^{-n_A\kappa/f}, \tag{6.76c}$$

where $D(x)$ is the Debye function (1.49), and $E(x) \equiv (1-e^{-x})/x$. From the RPA formula (5.63), we can find phase boundaries of the MST.
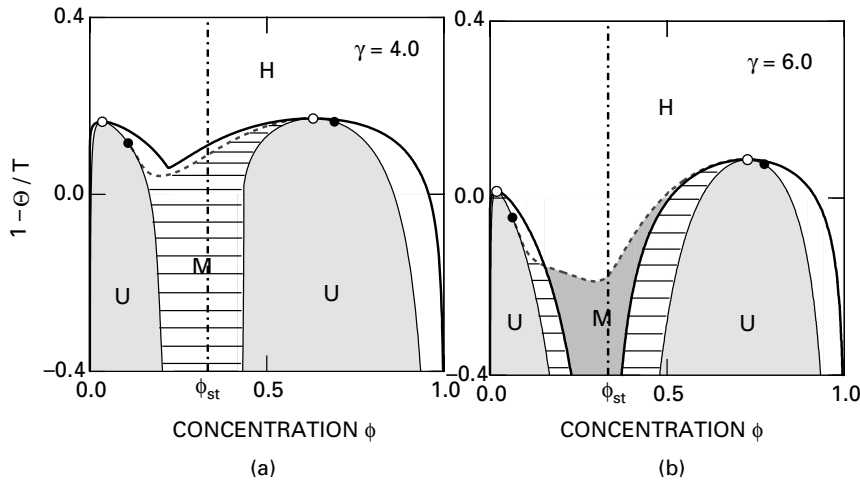
Fig. 6.5 Phase diagrams of side-chain association. The binodal (solid line), the spinodals (borderline of the gray areas), microphase separation transition line (broken line), critical solution points (white circles), and Lifshitz points (black circles) are shown. The homogeneous mixture region, microphase region, and the macroscopically unstable region are indicated by H, M, and U, respectively. Parameters are fixed at $n_A = 1000$, $f = 200$, $n_B = 10$, $\lambda_0 = 1.0$, and $\psi_1 = 1.0$. The concentration ϕ_{st} (vertical broken-dotted line) indicates the stoichiometric concentration. (a) $\gamma = 4.0$, (b) $\gamma = 6.0$. (Reprinted with permission from Ref. [26].)

Figures 6.5(a) and (b) compare the phase diagrams for two different binding energy parameters γ. The solid line shows the binodal, the broken line the MST, and the shaded areas the unstable regions with the spinodal lines at their boundaries. The area with horizontal lines indicates a phase with microstructure. In Figure 6.5(b), two segments of the binodal lines that lie inside the microphase region only indicate their existence near these positions.

The overall structure of the diagram is similar to that of the A/B blends with added A·B block copolymers, but it differs in detail near the concentration where the number of A groups coincides with that of B groups. We call this concentration the **stoichiometric concentration** ϕ_{st} (vertical broken-dotted line). It is explicitly given by

$$\phi_{st} \equiv n_A / (n_A + f n_B). \tag{6.77}$$

Around the stoichiometric concentration, miscibility of the mixture is sufficiently improved for the usual UCST miscibility dome to split into two gaps, each having a critical point (white circle). The intersections (black circles) between the MST and the SP lines are the **Lifshitz point**. As expected, the miscibility of the blend is improved with an increase in the association energy.

For a weak binding energy, the microphase region is mostly included inside the metastable region between the binodal and the spinodal (Figure 6.5(a)). For a stronger binding energy, however, the two miscibility gaps are completely separated from each other near the stoichiometric concentration, and a stable microphase appears in between
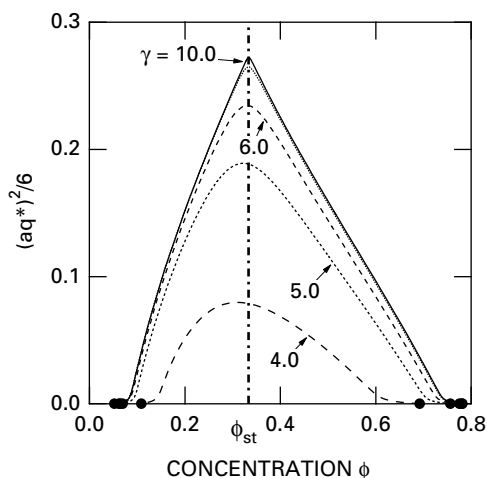
Fig. 6.6   Dimensionless wave number q^* along the MST curve as a function of the polymer concentration. The binding energy $\gamma \equiv \Delta\epsilon/k_B\Theta$ is changed from curve to curve. Black circles show the Lifshitz points where periodic structure starts to appear. (Reprinted with permission from Ref. [26].)

(the dark-shaded area in Figure 6.5(b)). This microphase differs from the conventional one found in chemical block-copolymers in that it is caused by molecular association between repulsively interacting polymers, and hence the entire phase is thermally controlled.

Figure 6.6 shows the inverse periodicity q^* as a function of the concentration along the MST line. The binding energy γ is varied from curve to curve. At the stoichiometric concentration the periodicity of the microphase is smallest (q^* largest). Also, as the binding energy is increased, the periodicity is reduced. In the limit of the infinite binding energy $\gamma \to \infty$, the periodicity approaches the limiting value. In the region away from the stoichiometric concentration, the excess unassociated chains swell the periodic structure formed by the saturated $(1, f)$-clusters, and modify its periodicity.

Ruokolainen and coworkers [30,31,32,33,34] observed MST in the mixture of poly(4-vinyl pyridine) (P4VP) and surfactant molecules 3-pentadecyl phenol (PDP). In this system the hydrogen bonds between the hydroxyl group of PDP and the basic amino nitrogen in the pyridine group lead to the formation of comb-shaped block copolymers with densely grafted short side chains (called a *molecular bottlebrush* [33]). They observed lamellar structures at low temperature. The lamellar period L was found to decrease in proportion to the reciprocal of x, the fraction of surfactant molecules per pyridine group in P4VP, and the MST temperature takes a minimum value (easiest MST) near the stoichiometric concentration $x = 1$. The structures of possible mesophases inside MS region were recently studied by Angerman and ten Brinke [35] by constructing RPA free energy of nonuniform systems. Structure and material properties of supramolecular hydrogen-bonded polymers and their applications are reviewed by ten Brinke *et al.* [36].

6.4 Hydration in aqueous polymer solutions and closed-loop miscibility gaps

For the study of aqueous polymer solutions in which water molecules are hydrogen-bonded onto polymer chains [29], we regard the water molecule as monofunctional molecules R{B$_1$} and fix $n_B = 1$ in the model system studied above. The number of repeat units of the polymers is $n_A = n$. PEO chains are known to take loose 11_2 helical conformation (with 1.8 nm period) on thermal average at room temperature. Water molecules are hydrogen-bonded into the pockets of the PEO helical turns, one by one with H-bonds through their two protons [37]. Each helical turn is assumed to serve a hydrogen bonding site, so that f is proportional to n. In this section, the solvent molecules are assumed to be randomly and independently hydrogen-bonded onto the polymer chains (see Figure 6.7). The more interesting case of cooperative hydration will be studied in the next section.

Since $bf/a = 1$, the spinodal condition becomes

$$\frac{1}{n\phi} + \frac{[1+\theta(y)]^2}{y+\phi\theta(y)\Delta\bar{m}} - 2\chi = 0. \tag{6.78}$$

Figure 6.8 (a)–(c) shows the possible phase diagrams. In Figure 6.8 (a), we fix the parameters as $\lambda_0 = 0.002$, and $\gamma = 3.5$ (from the measured strength of the hydrogen bond in a solution) as a typical example. The number n is varied from curve to curve. The functionality f (number of attaching sites on a polymer chain) is assumed to be equal to n because each monomer carries one hydrogen-bonding oxygen. For such a small value
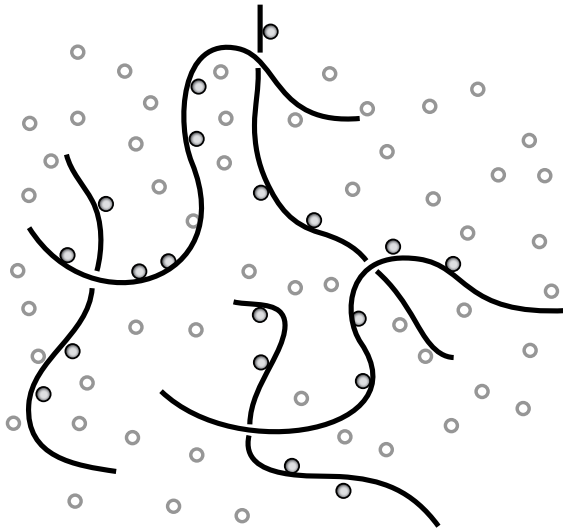
Fig. 6.7 Hydration of water-soluble polymers. Water molecules are hydrogen-bonded onto a polymer chain. Polymers partially wear clothes that are the same as the surrounding solvent environment.
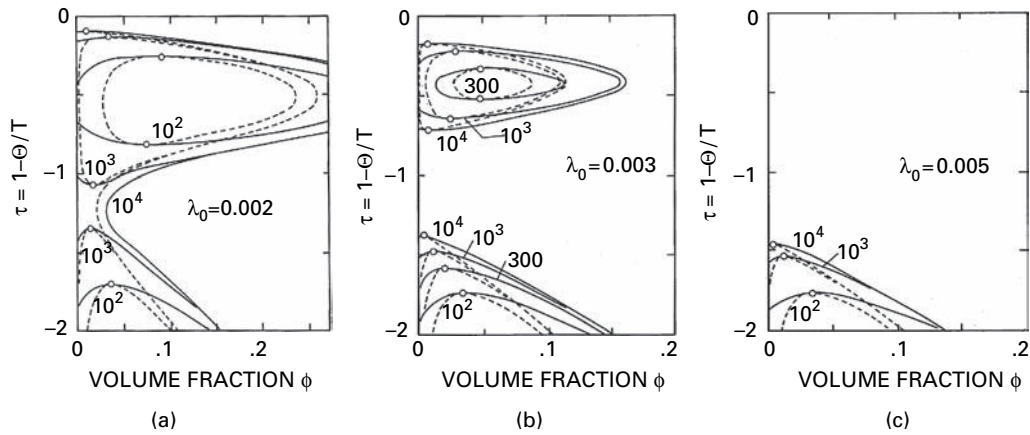
Fig. 6.8   Phase diagram of the hydrated polymer solutions. The number n of repeat units is varied from curve to curve. Binodals (solid lines) and spinodals (broken lines) are drawn. The critical solution points are indicated by the open circles. (a) $\lambda_0 = 0.002$, (b) $\lambda_0 = 0.003$, (c) $\lambda_0 = 0.005$. (Reprinted with permission from Ref. [29].)
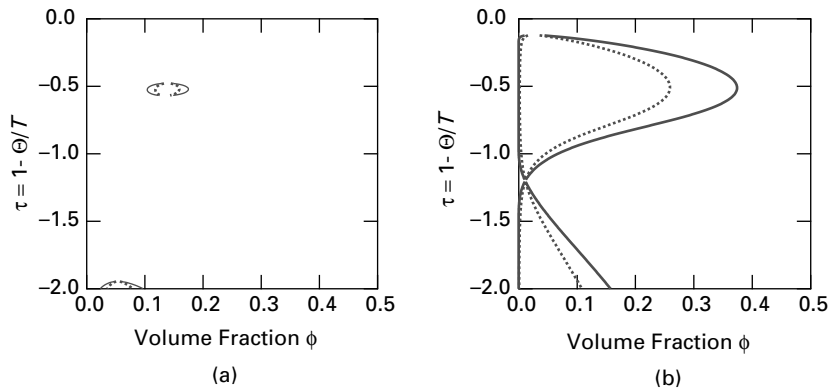

Fig. 6.9   (a) Hypercritical point where a miscibility loop shrinks to a point ($n = 37$). (b) Double critical point where the LCST of the miscibility loop merges with the UCST of the miscibility dome ($n = 1670$). $\lambda_0 = 0.002, \gamma = 3.5$.

of λ_0, there are two miscibility gaps for low molecular-weight polymers: one ordinary miscibility **dome** and one **closed miscibility loop** above the dome (see $n = 10^2$ curve).

The miscibility loop [38–42] has one **upper critical solution temperature** (UCST) at its top and one **lower critical solution temperature** (LCST) at its bottom. The **miscibility dome** has an ordinary UCST. As the molecular weight is increased, the LCST of the loop and the UCST of the dome come closer. Figure 6.9(b) shows how the miscibility loop and dome merge. At a certain value of n (1670 for the parameters given in this figure) the LCST and UCST merge into a higher-order critical point, which
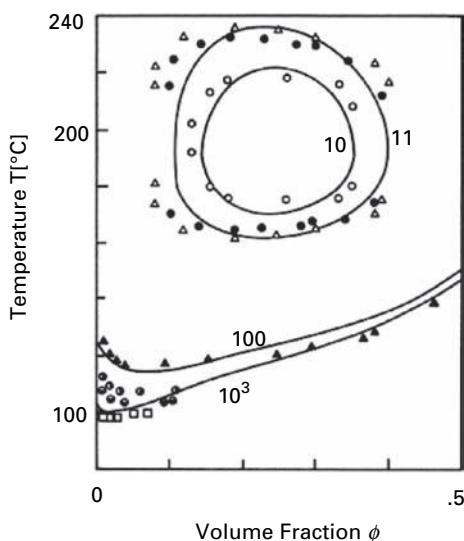
Fig. 6.10 Phase diagram of aqueous solutions of poly(ethylene oxide) showing the closed-loop miscibility gap. Theoretical curves (solid lines) are fitted to the experimental data of the cloud points (symbols) measured by Saeki *et al.* [45, 46]. The number-average molecular weight in the experiment covers the range 2.17×10^3–1.02×10^6. (Reprinted with permission from Ref. [29].)

is called the **double critical point** [43] (DCP). For a molecular weight higher than this critical value, the two gaps merge into a single **hourglass** shape.

However, the miscibility loop shrinks with a decrease in the molecular weight, and eventually vanishes at a certain critical molecular weight ($n = 37$ for the Figure 6.9(a)). This vanishing loop is called the **hypercritical point** (HCP).

For a slightly higher value of λ_0 as in Figure 6.8(b), however, it was found that the two miscibility gaps remain separated for any high molecular weight [29]. Under such conditions, there are three theta temperatures to which each critical point approaches in the limit of infinite molecular weight. In particular, the second is the critical point of the LCST phase separation. It approaches the **inverted theta temperature** in the limit of high molecular weight (about 100°C for PEO, see Figure 6.10 below.)

For a still larger value of λ_0 (Figure 6.9(c)), the closed loop does not appear; there is an ordinary miscibility dome only. Since the parameter λ_0 is small if the entropy loss during the bond formation is large, there must be a strong orientational or configurational constraint in the local geometry for the appearance of an hourglass.

Figure 6.10 compares the theoretical calculation with the observed phase diagram [44–46] of polyethylene oxide (PEO) in water. The miscibility loop expands with an increase in the molecular weight. The UCST phase separation expected at low temperatures cannot be observed due to crystallization of the PEO. The solid curves show the calculated binodals. The number n of the statistical units on a chain is varied from curve to curve. Parameters used for fitting are: $\psi = 1$, $\Theta = 730\,\text{K}$, $\gamma = 6$, and $\lambda_0 = 1.66 \times 10^{-5}$. Fitting is made mainly by adjusting the unkown parameter λ_0. The agreement is very good. The
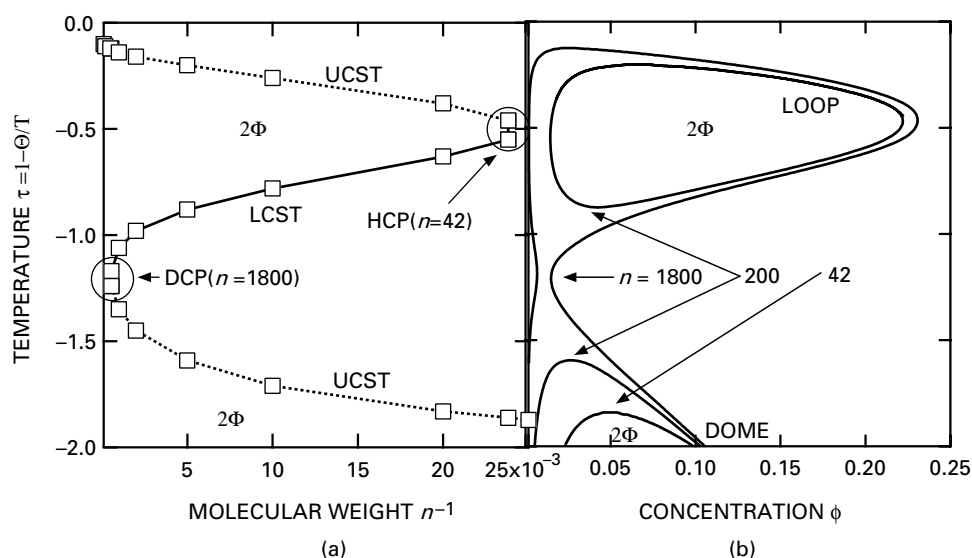
Fig. 6.11 (a) Shultz plot of PEO. UCST (dotted lines) and LCST (solid lines) of homopolymer PEO solutions as functions of n^{-1}. (b) Phase diagrams of PEO solutions on an ordinary temperature–concentration plane. The DP of the polymer is changed from curve to curve. (Reprinted with permission from Ref. [55].)

calculation of PEO/water phase diagrams was later examined by taking into account the hydrogen-bond networks in water [47]. The effect of pressure on the miscibility loop was studied to derive temperature–pressure phase diagrams [48].

Figure 6.11 (a) presents the theoretical plots of the LCST and UCST of homopolymer PEO solutions as functions of the reciprocal DP. This is an example of a Shultz plot applied to an associating polymer solution. Figure 6.11(b) displays the corresponding phase diagrams on the conventional temperature–concentration plane. DPC is the double critical point where the LCST and UCST merge into a single critical point. The HCP (hyper critical point) is where the phase separation region of the loop shape shrinks into one point. For PEO, the DCP occurs at $n = 1800$, while the HCP takes place at $n = 42$. The disappearance of the loop (HCP) was observed experimentally by Saeki *et al.* [45, 46] as in Figure 6.10.

6.5   Cooperative hydration in solutions of temperature-responsive polymers

In contrast to PEO, other water-soluble polymers, such as poly(*N*-isopropylacrylamide) (PNIPAM), show very flat LCST, whose cloud-point lines and spinodal lines are horizontal up to 20 wt% of polymer concentration and almost independent of the molecular weight [49–54]. The phase separation region takes a shape like the bottom part of a square, so that in what follows we refer to it as the **miscibility square**. Obviously, the miscibility square cannot be explained by *random* adsorption of water molecules. But,

if we introduce positive correlation between the neighboring hydrogen bonds along the polymer chain, i.e., if adsorption of a water molecule onto the sites adjacent to the already adsorbed ones is preferential, phase separation may take place in a narrow temperature region.

For PNIPAM, it is in fact the case because the hydrogen-bonding site (amide group) is blocked by a large hydrophobic group (isopropyl group). The random coil parts sharply turn into collapsed globules on approaching the phase separation temperature [50], so that hydrogen-bonding is easier at the boundary between an adsorbed water sequence and a collapsed coil part. Such steric hindrance by hydrophobic isopropyl side groups is the main origin of the strong cooperativity between neighboring water molecules. This section shows that the formation of sequential hydrogen bonds along the polymer chain, or **cooperative hydration**, in fact leads to miscibility square behavior of aqueous polymer solutions [55].

To describe adsorption of water, let $\mathbf{j} \equiv \{j_1, j_2, \ldots\}$ be the index specifying the polymer chain carrying the number j_ζ of sequences that consist of a run of H-bonded ζ consecutive water molecules, and let $N(\mathbf{j})$ be the number of such polymer–water complexes whose type is specified by $\mathbf{j}$ (Figures 6.7 and 6.12).

The total number of water molecules on a chain specified by $\mathbf{j}$ is given by $\sum \zeta j_\zeta$, and the DP of a complex is given by $n(\mathbf{j}) \equiv n[1 + \theta(\mathbf{j})]$, where

$$\theta(\mathbf{j}) \equiv \sum \zeta j_\zeta / n \qquad (6.79)$$

is the fraction of the bound water molecules counted relative to the DP of a polymer.

By the association equilibrium condition, we find

$$\nu(\mathbf{j}) = K(\mathbf{j}) x y^{n\theta(\mathbf{j})}, \qquad (6.80)$$
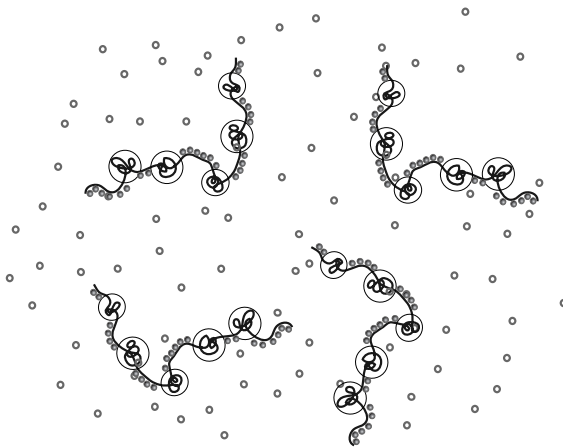
Fig. 6.12   Sequential hydrogen bonds formed along the polymer chain due to cooperative hydration. The type of polymer–water associated complex is specified by the index $\mathbf{j} \equiv (j_1, j_2, \ldots)$, where j_ζ is the number of sequences that consist of a run of hydrogen-bonded ζ consecutive water molecules (pearl-necklace conformation).

where $x \equiv \phi(\mathbf{j}_0)$, $y \equiv \phi_{\mathrm{fw}}$ for the number density of the hydrated chains specified by $\mathbf{j}$, and $K(\mathbf{j})$ is the equilibrium constant. The total polymer volume fraction ϕ is given by

$$\phi = x G_0(y). \tag{6.81}$$

The total volume fraction of water is given by

$$1 - \phi = y + x G_1(y). \tag{6.82}$$

Here the new functions $G_i(y)$ are defined by

$$G_0(y) \equiv \sum_{\mathbf{j}} K(\mathbf{j}) y^{n\theta(\mathbf{j})}, \quad G_1(y) \equiv \sum_{\mathbf{j}} \theta(\mathbf{j}) K(\mathbf{j}) y^{n\theta(\mathbf{j})}. \tag{6.83}$$

The coupled equations (6.81) and (6.82) should be solved for x and y to find the cluster distribution function in terms of the polymer volume fraction and the temperature.

Upon eliminating x, the second equation is transformed to

$$1 - \phi = y + \phi \theta(y), \tag{6.84}$$

to be solved for y, where the function θ is defined by

$$\theta(y) = G_1(y)/G_0(y) = \partial \ln G_0(y)/n\partial \ln y, \tag{6.85}$$

which is thermal average of the degree of hydration (6.79).

The total number ν^{S} of free water molecules and associated complex is given by

$$\nu^{\mathrm{S}} = y + \phi/n. \tag{6.86}$$

By the reaction equiliblium conditions, we find

$$\mathscr{F} = \mathscr{F}_{\mathrm{FH}} + \mathscr{F}_{\mathrm{AS}}, \tag{6.87}$$

where $\mathscr{F}_{\mathrm{FH}}$ is the usual Flory–Huggins mixing free energy (2.100), and

$$\mathscr{F}_{\mathrm{AS}}(\phi, T) = \frac{\phi}{n} \ln\left(\frac{x}{\phi}\right) + (1 - \phi) \ln\left(\frac{y}{1 - \phi}\right) + 1 - \phi - y \tag{6.88}$$

is the additional free energy due to hydrogen bonding association. This part can be written in the form

$$\mathscr{F}_{\mathrm{AS}}(\phi, T) = -\frac{\phi}{n} \ln G_0(y) + (1 - \phi) \ln[1 - \phi\theta(y)/(1 - \phi)] + \phi\theta(y), \tag{6.89}$$

by the substitution of the relations (6.81) and (6.82).

The osmotic pressure π can be found by the thermodynamic relation $\pi a^3 = -\Delta\mu_{\mathrm{fw}}$, and is given by

$$\beta\pi a^3 = -1 - \ln[1 - \phi - \phi\theta(y)] + [1 - \phi - \phi\theta(y) + \phi/n] - \chi\phi^2. \tag{6.90}$$

By expanding the function $\theta(y)$ in powers of the concentration as $\theta(y) = \theta_0 + \theta_1 \phi + \cdots$, we find the second virial coefficient in the form

$$A_2 = \frac{1}{2}(1+\theta_0)^2 - \chi, \tag{6.91}$$

where θ_0 is the value of $\theta(y)$ in the limit of infinite dilution.

The spinodal condition is found to be

$$\frac{1}{n\phi} + \frac{\kappa(\phi)}{1-\phi} - 2\chi = 0, \tag{6.92}$$

where

$$\kappa(\phi) \equiv \frac{[1+\theta(y)]^2(1-\phi)}{y+\phi\theta(y)\Delta\bar{m}} \tag{6.93}$$

gives the effect of hydration.

For random hydration, $K(\mathbf{j})$ should be replaced by $K_m = (1+m/n)_n C_m \lambda^m$. All results reduce to random hydration, as studied in the previous section.

For cooperative hydration, the equilibrium constant is most generally written as

$$K(\mathbf{j}) = \omega(\mathbf{j}) \prod_{\zeta=1}^{n} \eta_\zeta^{j_\zeta}, \tag{6.94}$$

as in Section 1.9, where

$$\omega(\mathbf{j}) \equiv (n - \sum \zeta j_\zeta)! / \Pi j_\zeta! [n - \sum(\zeta+1)j_\zeta]! \tag{6.95}$$

is the number of different ways to select sequences specified by $\mathbf{j}$ from a chain, and η_ζ is the statistical weight for a single water sequence of length ζ formed on the chain.

Because summing up all possible types $\mathbf{j}$ in the above functions is mathematically difficult, we replace the sum by the contribution from the most probable type $\mathbf{j}^*$ (**one-mode approximation**). The necessary functions are then given by

$$G_0(y) = \omega(\mathbf{j}^*) \prod_{\zeta=1}^{n} (\eta_\zeta y^\zeta)^{j_\zeta}, \tag{6.96}$$

and $G_1(y) = \theta(\mathbf{j}^*)G_0(y)$ and $\theta(y) = \theta(\mathbf{j}^*)$. The function θ reduces to the coverage θ of the bound water in the type $\mathbf{j}^*$.

The most probable type $\mathbf{j}$, or sequence distribution, can be found by minimizing the free energy $\mathscr{F}_{AS}$ by changing $\mathbf{j}$, i.e., by the condition $\partial\mathscr{F}_{AS}/\partial j_\zeta = 0$. We find that it is given by

$$j_\zeta/n = (1-\theta)t\eta_\zeta q^\zeta, \tag{6.97}$$

where q is defined by the equation

$$q \equiv (1-\phi-\theta\phi)z. \tag{6.98}$$

The parameter z is defined by $z \equiv 1 - \nu/(1 - \theta)$ as in Section 1.8.

Substituting this distribution function (6.97) into the definitions of θ and ν, we find

$$\theta(q) = [1 - \theta(q)]z(q)V_1(q), \tag{6.99}$$

and

$$\nu(q) = [1 - \theta(q)]z(q)V_0(q), \tag{6.100}$$

and hence

$$z(q) = 1/[1 + V_0(q)]. \tag{6.101}$$

Here the new functions V are defined by

$$V_0(q) \equiv \sum \eta_\zeta q^\zeta, \quad V_1(q) \equiv \sum \zeta \eta_\zeta q^\zeta. \tag{6.102a}$$

Now, θ and z must be regarded as functions of q, so that (6.98) is an equation for the unknown variable q to be solved in terms of the concentration ϕ.

The κ function in the spinodal condition (6.92) now takes the form

$$\kappa(q;\phi) = \frac{\lambda(1 - \phi)(1 + \theta)^2}{y - \lambda\phi(1 - \theta)Q}, \tag{6.103}$$

where

$$Q(q) \equiv \theta(q) - [1 - \theta(q)]\bar{\zeta}_w(q), \tag{6.104}$$

and

$$\bar{\zeta}_w(q) \equiv V_1(q)/V_0(q), \tag{6.105}$$

is the weight average sequence length of the bound water.

In order to carry out complete calculations, we employ the simplest form of Zimm and Bragg [56, 57]

$$\eta_\zeta = \sigma\lambda(T)^\zeta, \tag{6.106}$$

where σ is the **cooperativity parameter**.

Figure 6.13(a) draws the spinodal curves for different cooperative parameters σ with other parameters fixed. The bottom part of the miscibility square becomes flatter with decreasing σ. In the calculation, the usual miscibility domes with UCST appear at low temperatures, but these are not observable in the experiments because the water freezes. For polymer concentrations higher than $\phi = 0.5$, our theoretical description becomes poor because of the depletion of water molecules; the number of water molecules becomes insufficient to cover the polymers.

Figure 6.13(b) shows the dehydration curves. The coverage θ of a polymer chain by H-bonded water molecules is plotted against the temperature. The cooperative parameter
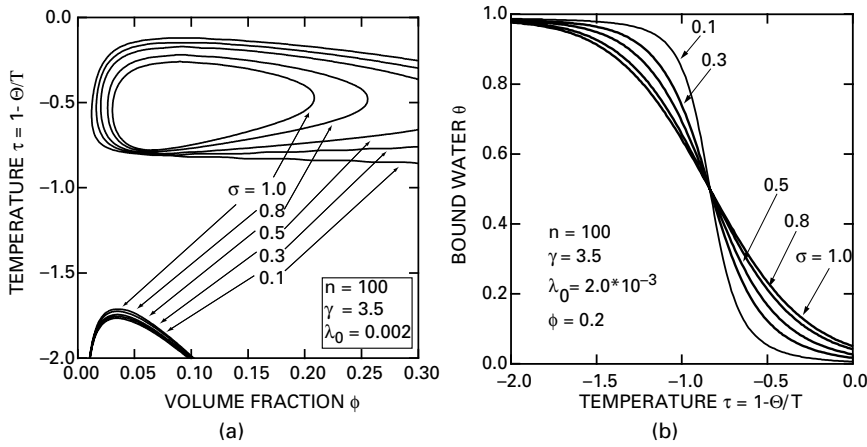
Fig. 6.13   (a) Spinodal lines drawn on the (reduced) temperature and concentration plane for different cooperative parameters σ. Other parameters are fixed at $n = 100$, $\psi = 1.0$, $\lambda_0 = 0.002$, and $\gamma = 3.5$. The bottom part of the miscibility square becomes flatter with an increase in the cooperativity (miscibilty square). (b) The coverage θ of a polymer chain by hydrogen-bonded water molecules plotted against the temperature. The cooperative parameter σ is changed from curve to curve. (Reprinted with permission from Ref. [55].)

σ is changed from curve to curve. Dehydration of bound water takes place near the phase separation temperature, and becomes sharper with an increase in the cooperativity.

From the curve θ of the bound water as a function of the temperature, we can find the enthalpy ΔH of dehydration. If a fraction $-\Delta\theta$ is dehydrated by a small temperature rise ΔT, the absorption of heat is given by

$$\Delta H = |\epsilon + \delta\epsilon|\phi\Delta\theta/M. \tag{6.107}$$

It shows a peak at the temperature where θ changes most sharply, i.e., at the phase separation temperature. The polymer chains collapse into compact globules as soon as the bound water is dissociated.

Figure 6.14 plots the critical points (UCST and LCST of the miscibility loop, and UCST of the miscibility dome) against the polymer molecular weight (**Shultz plot**). For random hydration ($\sigma = 1.0$), miscibility loop shrinks to a point at about $n = 40$ at the hyper critical point (HCP). Also, at a high molecular weight of about $n = 1800$, the loop merges with the miscibility dome at low temperatures, and turns into an hourglass. For cooperative hydration with $\sigma = 0.3$, however, the DCP does not appear. The HCP shifts to a smaller n, and has the shape of an angular square. From this plot, it is evident that cooperative hydration leads to a flat LCST with almost no molecular-weight dependence.

Figure 6.15(a) compares theoretical calculations with experimental data [52] on the spinodal points, and Figure 6.15(b) shows the fraction θ of the bound water molecules plotted as functions of the temperature for three different polymer concentrations. In the experiments, the upper part of the miscibility square cannot be observed because the
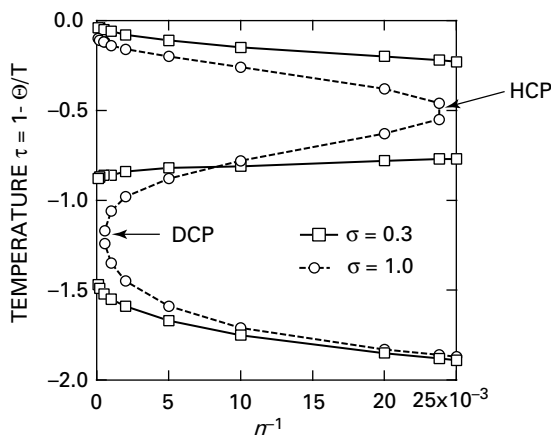
Fig. 6.14 Molecular-weight dependence of the LCST and UCST (Shultz plot). The critical temperatures are plotted against the reciprocal of DP. The hyper critical point (HCP) and double critical point (DCP) are indicated by arrows. (Reprinted with permission from Ref. [55].)
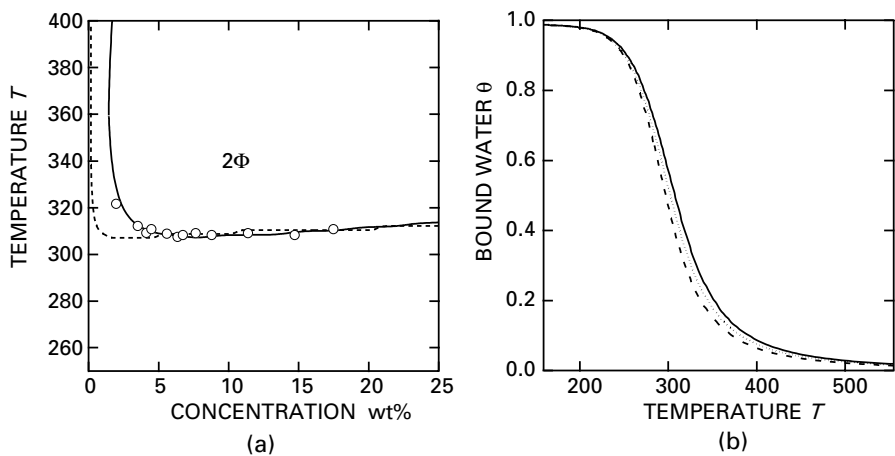
Fig. 6.15 (a) Experimental data (○) of the spinodal curve in an aqueous PNIPAM solution is compared with theoretical calculations. The DP of the polymer is $n = 100$ (solid line) and $n = 1000$ (broken line). The theoretical parameters used are $\Theta = 555$ and $\lambda_0 = 0.002$ for $n = 100$, and $\Theta = 565$ and $\lambda_0 = 0.003$ for $n = 1000$. Other parameters are fixed at $\gamma = 3.5, \sigma = 0.3$. (b) Content θ of the bound water plotted against temperature for three polymer volume fractions $\phi = 0.1$ (solid line), $\phi = 0.2$ (dotted line), and $\phi = 0.3$ (broken line) for $n = 100$. (Reprinted with permission from Ref. [55].)

temperature is too high. Also, UCST phase separation seen in the theoretical calculation is not observable because of the freezing of water. The molecular weight of the polymer used in the experiment is $M_w = 615\,500$, so that the nominal number of monomers is roughly given by $n = 5,400$. Since the statistical unit used in the lattice theory must be
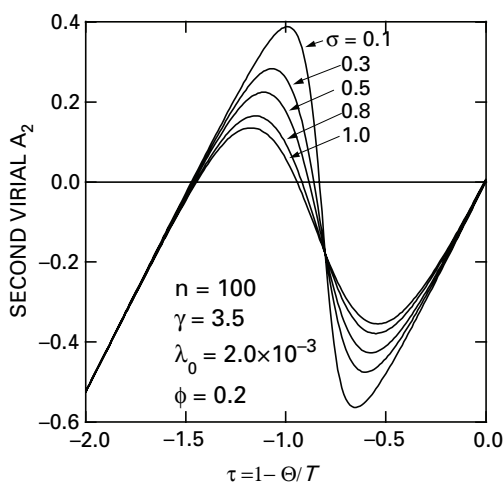
Fig. 6.16 Second virial coefficient A_2 plotted against temperature. The cooperative parameter σ is varied from curve to curve. (Reprinted with permission from Ref. [55].)

regarded as a group of monomers, fitting is tried for $n = 100$ and 1000. (Theoretical calculation does not depend so much upon the number n if it is larger than 500.)

Figure 6.16 plots the second virial coefficient A_2 as a function of the temperature. The cooperative parameter σ is varied from curve to curve. There are in principle three theta temperatures where A_2 (6.91) vanishes. The one lying in the middle temperature is the relevant theta temperature (inverted theta temperature) to which the observed LCST approaches for infinite molecular weight. With an increase in cooperativity, the dehydration becomes sharper, so that the (negative) slope of A_2 becomes larger.

An attempt to derive the phase diagram of the PNIPAM solution by using the effective interaction parameter $\chi_{\text{eff}}(T, \phi)$ was made by Baulin and Halperin [58, 59]. They used, however, the empirical power expansion formula of Afroze *et al.* [51] with many phenomenological numerical coefficients, whose molecular origin is unknown. Although the above renormalization formula (5.40) due to hydrogen-bonding depends implicitly upon the concentration, it can be expanded in power series in dilute regime, and directly compared with the experimental measurements on the second virial coefficient of the osmotic pressure.

6.6 Hydrogen-bonded liquid-crystalline supramolecules

Some rigid molecules are known to undergo liquid crystallization when H-bonded with each other. A typical example is a binary mixture of low-mass molecules $R\{A_f\}$ and $R\{B_g\}$, each carrying at least one rigid part A or B capable of pairwisely forming mesogenic core when associated. Dimer, trimer, main-chain type, side-chain type,
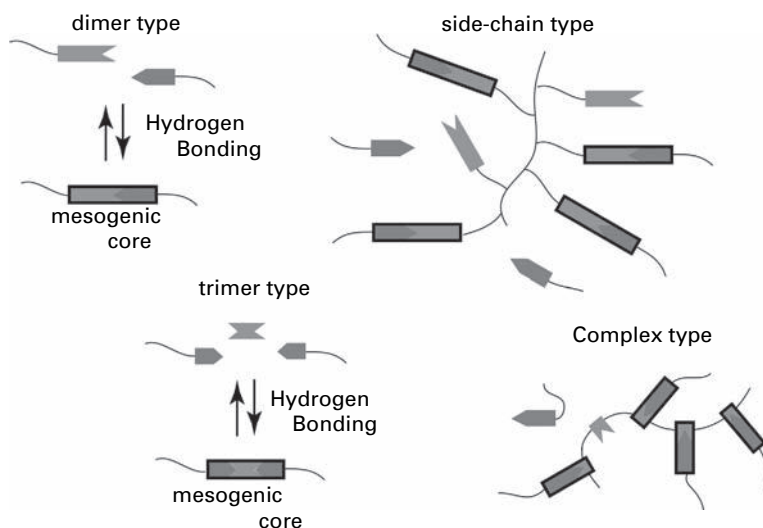
Fig. 6.17   Various types of hydrogen-bonded liquid crystals, such as dimer, trimer, side-chain, and main-chain complex.
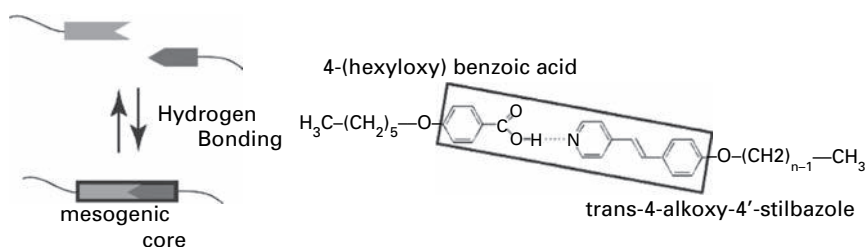
Fig. 6.18   Hydrogen-bonding liquid crystal by dimerization. The rigid heads become sufficiently long to be the mesogenic core when hydrogen-bonded.

combined type, and network type are known [13, 60] (Figure 6.17). These are called **hydrogen-bonded liquid crystals** (H-bonded LC).

For example, aromatic acid derivatives with alkoxy or alkyl terminal groups form dimers by H-bond between their carboxylic acid groups, and show mesomorphism [61–64]. The most remarkable case is that the non-mesogenic molecules form compounds with mesogenic cores when H-bonded (Figure 6.18). In such a combination of molecules, isotropic materials undergo liquid crystallization by mixing.

To describe liquid crystallization by association, we introduce the **orientational free energy** in addition to the free energy of reaction and mixing [65]. Let us assume that the $R\{A_f\}$ molecule (DP n'_A) carries f linear rigid associative groups A of length n^*_A, and $R\{B_g\}$ molecule (DP n'_B) carries g rigid groups B of length n^*_B. The total DPs are $n_A = n'_A + f n^*_A$ and $n_B = n'_B + g n^*_B$.

We start with the total free energy

$$\Delta F = \Delta_{\text{rea}} F + \Delta_{\text{mix}} F + \Delta_{\text{ori}} F, \qquad (6.108)$$

consisting of the reaction, mixing, and orientational parts [65].

For the orientational free energy, we employ the conventional molecular field theory of Maier and Saupe [66], or its extension by McMillan [67], which includes both orientational ordering of the mesogenic cores and translational ordering of their centers of mass. It is given by

$$\beta \Delta_{\text{ori}} F = \left\{ (-\ln Z) + \frac{1}{2} \zeta (\eta^2 + \alpha \sigma^2) \nu_{\text{M}} \right\} N_{\text{M}}, \qquad (6.109)$$

where N_{M} is the total number of mesogenic cores formed in the system, and $\nu_{\text{M}} \equiv N_{\text{M}}/\Omega$ is their number density.

In contrast to conventional liquid crystals, N_{M} changes depending on the temperature and composition, and should be decided by the equilibrium condition. The symbol η expresses the **nematic order parameter** defined by

$$\eta \equiv \langle P_2(\cos\theta) \rangle, \qquad (6.110)$$

and similarly

$$\sigma \equiv \langle P_2(\cos\theta) \cos(2\pi z/d) \rangle \qquad (6.111)$$

is the **smectic order parameter**.[1] The coupling constant ζ is the nematic interaction parameter (Maier–Saupe's nematic interaction parameter), and α is McMillan's smectic interaction parameter.

The averages $\langle \cdots \rangle$ refer to the statistical weight for orientation of each mesogenic core, whose partition function Z is defined by

$$Z(\eta, \sigma) \equiv \frac{1}{d} \int_0^d dz \int_0^1 d\cos\theta \exp\{\zeta[\eta + \alpha\sigma\cos(2\pi z/d)] P_2(\cos\theta)\nu_{\text{M}}\}, \qquad (6.112)$$

where d is the distance between the neighboring planes in the smectic A structure on which the centers of mass of mesogenic cores are located (layer thickness). The symbol θ shows the angle of the longitudinal axis of each mesogenic core measured from the preferential orientational axis.

By using this statistical weight, the definitions (6.110) and (6.111) become self-consistent coupled equations to find these order parameters. We solve the equations with equilibrium conditions for ν_{M}, and then by substitution find the chemical potential of each component as functions of the temperature and composition [65].

[1] The function $P_2(x) \equiv (3x^2 - 1)/2$ is the Legendre polynomial of degree 2, as in (1.39).
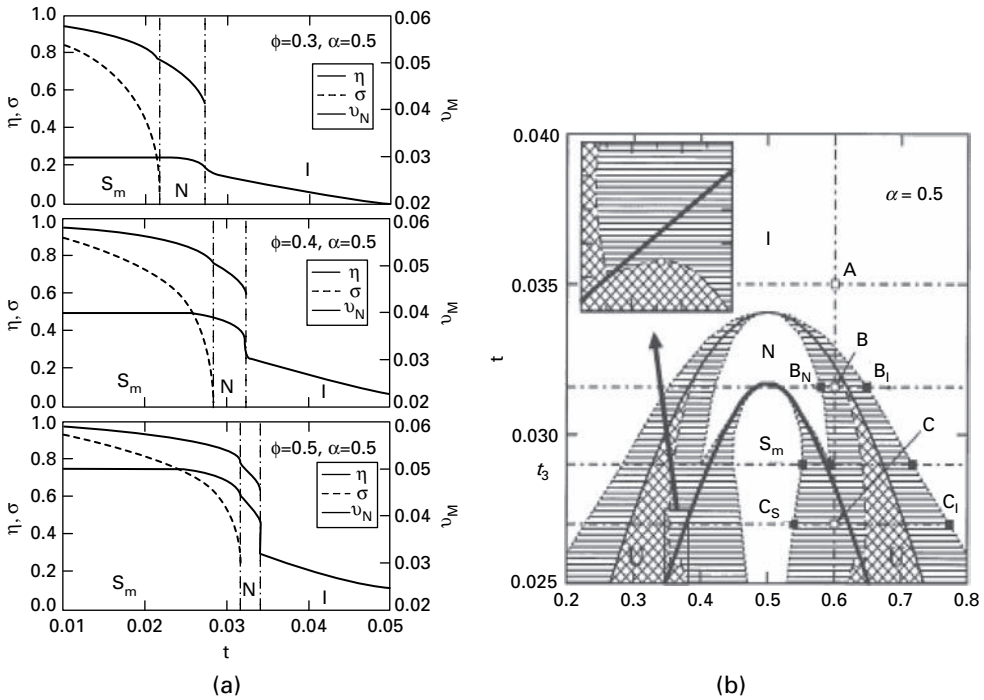
Fig. 6.19   (a) Number ν_M of mesogenic cores (dotted line, right axis), nematic order parameter η (solid line, left axis), and smectic order parameter σ (broken line, left axis) plotted against temperature at three compositions (top: $\phi = 0.3$, middle: $\phi = 0.4$, bottom: $\phi = 0.5$) in the dimer model $(n_A = n_B = 10, n_A^* = n_B^* = 1)$. The smectic interaction parameter is fixed at $\alpha = 0.5$. (b) Phase diagram of the athermal mixture corresponding to (a). The thin solid line is the I/N transition line, the thick solid line is the N/S transition line, and the dotted line is the binodal due to the I/N transition. The hatched area is the metastable region, and the gray area with U is the unstable region. The filled circle represents a critical end point.

Figure 6.19 shows an example phase diagram for the **athermal solvent** $\chi = 0$, together with the nematic and smectic order parameters, and the number of mesogenic cores ν_M as functions of the temperature for different composition.

Figure 6.20 shows the phase diagram for an athermal symmetric mixture with $n_A = n_B = 10$, and $n_A^* = n_B^* = 1$ (small rigid head groups carrying short aliphatic flexible tails). The temperature is measured by the ratio $t \equiv T/T_{NI}$ in the unit of the nematic/isotropic transition temperature T_{NI}.

We have assumed that Flory's χ-parameter takes the form (2.106) $\chi \equiv C_1 + C_2/t$ with constants C_1 and C_2 specified by the combination of molecular species. They are fixed at $C_1 = -0.5$ and $C_2 = 0.05$ in this figure. The association constant is assumed to take the form $\lambda(T) = \lambda_0 \exp(C/t)$, where $C \equiv |\Delta\epsilon|/k_B T_{NI}$ is the dimensionless energy of the hydrogen bond. We have fixed λ_0 at 30.0 and $C = 0.3$.

The inset magnifies the important part of the figure. The thin solid line is the I/N transition line, and the thick solid line the N/S$_m$ transition line. The letters I, N, and
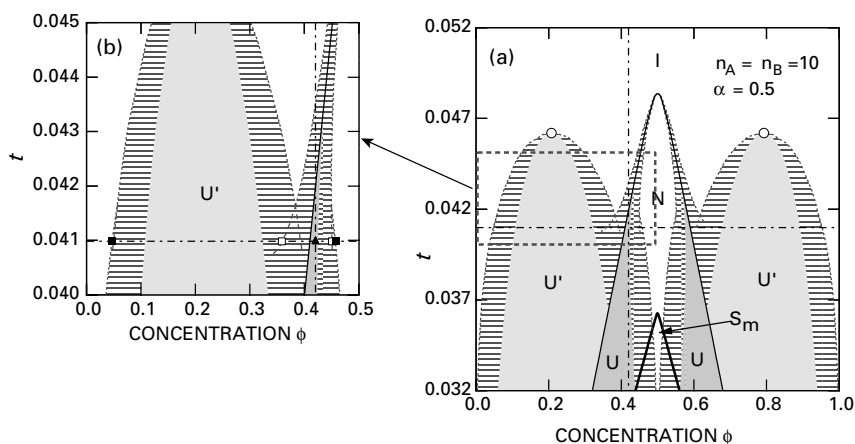
Fig. 6.20 Phase diagram of dimer-forming hydrogen-bonded liquid crystal. The thin solid line is the I/N transition line, the thick solid line is the N/S_m transition line, and the dotted line is the binodal. The hatched area is the metastable region. The dark gray area with U is the unstable region due to entropy difference between two different species of N structures. The light gray area with U$'$ is the unstable region due to mixing two different species of molecules. The open circle represents the critical solution point. Parameters are fixed at $n_A = n_B = 10$, $n_A^* = n_B^* = 1$, $\lambda_0 = 30.0$, $C = 0.3$, $C_1 = -0.5$, $C_2 = 0.05$, and $\alpha = 0.5$. (Reprinted with permission from Ref. [65].)

S_m represent the state whose free energy is lowest in the area. The dotted lines limiting the hatched metastable region are binodals. The dark gray area indicated by U is the unstable region hidden inside the coexistent region, whereas the light gray area with U$'$ is the conventional unstable region due to demixing. Open circles represent critical solution points.

An unstable region hidden in a two-phase coexistence region due to its first-order nature is well known in metallurgy as a metastable phase boundary [68]. Recently the existence of the spinodal curve hidden in a metastable region has been the focus of a study on the crystallization of polymers [69]. These hidden unstable regions usually accompany the first-order phase transitions, and lie in the region where the liquid state has the lowest free energy.

At high temperatures, the coexistence regions are caused by first-order I/N phase transition, and the two different species of molecules appear by demixing. Depending upon the composition, the mixture separates either into two I phases by the effect of mixing enthalpy, or into I phase and N phase by the I/N transition. At intermediate temperatures, the two coexistence regions merge, but the U and U$'$ regions remain separated.

At lower temperatures, the two unstable regions U and U$'$ also merge, so that the mixture separates directly into stable I and N phases, or into stable I and S_m phase by the cooperative driving force. If we divide the phase diagram into two at the middle and consider the left half, it is similar to the theoretical phase diagram of a lyotropic liquid crystal first derived by Flory [70], and later confirmed by an experiment by Miller *et al.* [71]. The narrow I/N coexisting region extending from the macroscopic phase

separation region is called the **miscibility chimney**. In lyotropic liquid crystals, the chimney goes straight up to high temperatures, but H-bonded LCs show that there is a limiting temperature (the top of the N phase) to which the chimney approaches, because the number of mesogenic cores decreases with increasing temperature.

6.7 Polymeric micellization

We next study the micellization of self-assembling solute molecules $R\{A_f\}$ in an inert solvent. Amphiphilic low-molecular weight molecules, polymers carrying hydrophobic groups, etc., are typical examples.

In the equilibrium state we have solvent $(0,1)$ and l-mers $(l,0)$, where $l = 1, 2, 3....$ To simplify the symbols, we contract the double suffices into single ones, and write l for an l-mer, 0 for a solvent. Our starting free energy is

$$\beta \Delta F = \sum_{l \geq 1} N_l \ln \phi_l + N_0 \ln \phi_0 + \chi \phi (1 - \phi)\Omega + \sum_{l \geq 1} \Delta_l N_l + \delta(\phi) N^G, \qquad (6.113)$$

where $\phi_0 \equiv 1 - \phi$ is the volume fraction of the solvent, and N^G the number of $R\{A_f\}$ molecules in the macroscopic cluster if it exists. In general, such a macroscopic cluster may have any structure; it can be a three-dimensional branched network, a worm-like micelle, an infinitely long string, etc. In what follows, we call the association that leads to such connected macroscopic aggregates **open association**. In contrast, we call it **closed association** if the association is limited to a finite size.

By differentiation, we find for the chemical potentials

$$\beta \Delta \mu_l / n = (1 + \Delta_l + \ln \phi_l)/n - l\nu^S + \chi l (1 - \phi)^2 + l \delta'(\phi)\nu^G (1 - \phi), \qquad (6.114a)$$

$$\beta \Delta \mu_0 = 1 + \ln(1 - \phi) - \nu^S + \chi \phi^2 - \delta'(\phi)\nu^G \phi, \qquad (6.114b)$$

where

$$\nu^S = 1 - \phi + \sum_{l \geq 1} \nu_l \qquad (6.115)$$

is the total degree of freedom for translational motion. The chemical equilibrium condition leads to the volume fraction of the clusters in the form

$$\phi_l = K_l x^l, \qquad (6.116)$$

where $x \equiv \phi_1$ is the volume fraction of the molecules that remain unassociated. It serves as an activity of the solute molecules. The equilibrium constant is given by

$$K_l = \exp(l - 1 - \Delta_l). \qquad (6.117)$$

We then have the total amount of materials in the sol

$$\phi^S(x, y) = 1 - \phi + \sum_{l=1}^{\infty} K_l x^l, \qquad (6.118)$$

and the total degree of translational freedom

$$v^S(x, y) = 1 - \phi + \sum_{l=1}^{\infty} b_l x^l, \tag{6.119}$$

where $b_l \equiv K_l/l$.

To study the convergence of the infinite sum

$$G_1(x) = \sum_{l=1}^{\infty} K_l x^l, \tag{6.120}$$

let us define the **binding free energy** $\delta_l \equiv \Delta_l/l$ required to connect a single molecule in a free state to a cluster of the size l. Application of the Cauchy–Hadamard theorem [72] gives the convergence radius x^* of the power series in the form

$$1/x^* = \overline{\lim_{l \to \infty}} (K_l)^{1/l} = e^{1-\delta_\infty}, \tag{6.121}$$

where the lower upper bound of the limit is indicated by the bar. The quatity $\delta_\infty \equiv \lim_{l \to \infty} \delta_l$ is defined by the limiting value of δ_l as $l \to \infty$. Within the radius of convergence, the normalization condition $G_1(x) = \phi$ gives a one-to-one relationship between ϕ and x.

The difference in spatial structures to be formed can be seen from the behavior of δ_l. Figure 6.21(a) schematically shows the exponent $\delta_l + 1/l - 1$ of the equilibrium constant $K_l^{-1/l}$ as a function of l. This function may either take a minimum at a certain finite

(a) (b)
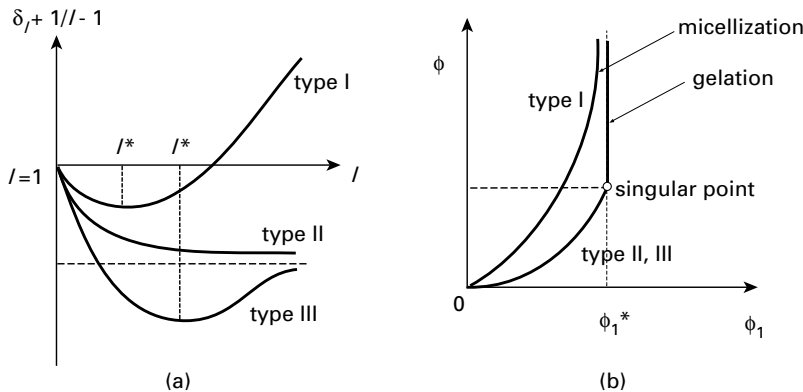
Fig. 6.21 (a) Binding free energy per molecule as a function of the aggregation number. (b) Total volume fraction as functions of the unimer concentration. Type I leads to micellization with finite aggregation number. Type II and III lead to macroscopic aggregates, such as infinitely long cylindrical micelles or three-dimensional networks. In the latter, the volume fraction ϕ_1 of unassociated molecules in the solution as a function of the total volume fraction ϕ of the molecules shows a singularity at the point where the weight-average molecular weight of aggregates becomes infinite.

l (curves I and III) or decrease monotonically to a finite value $\delta_\infty - 1$ (curve II). The former leads to closed association, while the latter open association. In either case, we find the l^* at which the curve shows a minimum using the condition

$$\frac{\partial \delta_l}{\partial l} - \frac{1}{l^2} = 0. \tag{6.122}$$

If we plot the total concentration ϕ as a function of the activity x, we can easily see the difference between open association and closed association (Figure 6.21(b)). For closed association, there is a convergence radius x^* to which the curve continuously approaches and asymptotically diverges. For open association the curve reaches a finite value at x^* and goes to infinity above x^*, and hence there is a singularity appearing x^*; the derivative of the curve shows discontinuity at x^*. Open association thus leads to a discontinuity of the thermodynamic quantities when the activity x is differentiated with respect to the concentration.

In contrast, closed association may lead to a sharp change in the number of micelles, but the transition is continuous as far as the size of micelles remains finite. There is no thermodynamic singularity because the number of molecules involved in the clusters remains finite.

Critical micelle concentration (CMC)

We can find the activity x as a function of the concentration ϕ by the inversion of the infinite series (6.120). The cluster size l for which the volume fraction ϕ_l reaches a maximum under a fixed value of the activity is given by

$$\partial \Delta_l / \partial l = 1 + \ln x. \tag{6.123}$$

Substituting the solution l^* of (6.122) into this condition, we find the activity.

In the case where l^* is finite, the total concentration corresponding to x is called the **critical micelle concentration** (CMC), since the volume fraction $x_{\mathrm{cmc}} = (K_{l^*})^{-1/l^*}$ of the clusters with aggregation number l^* takes a finite fraction at this value of the total volume fraction [73].

The sharpness in their appearance is controlled by the curvature of the function $\delta_l + 1/l - 1$ around l^*.

In the case where l^* is infinite, however, a macroscopic cluster appears as soon as x exceeds the critical value $x^* \equiv \exp(\delta^* - 1)$. The macroscopic clusters can be branched networks (gels) [74, 75], infinitely long polymers [17], or worm-like micelles [76–83], etc. We call the former case **gelation** and the latter case **polymerization** (including worm-like micellization). The total concentration ϕ^* obtained from x^* gives the concentration at which this transition takes place. It depends on the temperature through δ_∞. For ϕ above ϕ^*, the sum in (6.118) cannot reach ϕ. The remaining fraction $\phi - \sum \phi_l$ belongs to the macroscopic clusters.

(a)   (b)   (c)
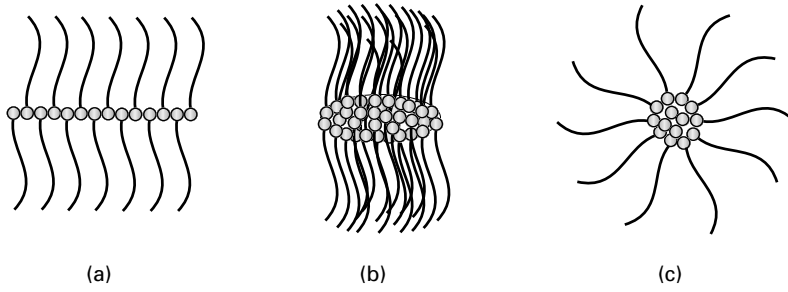
Fig. 6.22 Micellization of end-associative polymer chains: (a) linear association, (b) two-dimensional discotic association, (c) three-dimensional spherical association

Structure of aggregates and their distribution function

Let us see some simple examples. When molecules form a linear array as in Figure 6.22(a), the internal free energy of an aggregate is

$$\mu_l^\circ = -(l-1)\alpha k_B T, \tag{6.124}$$

where $\alpha k_B T$ is the free energy of a bond. We have

$$\delta_l + 1/l - 1 = -(1+\alpha) + \alpha/l^p + 1/l, \tag{6.125}$$

with $p = 1$.

For two-dimensional disk-like aggregates, as in Figure 6.22(b), we have the same equation with $p = 1/2$, because the aggregation number l is proportional to the area πR^2, and there are no bonds from outside along the edge. Similarly, we have $p = 1/3$ for the three-dimensional aggregates in Figure 6.22(c).

All these examples give monotonically decreasing curves of type II. Hence $(\phi_1)_{\text{cmc}} = \exp[-(1+\alpha)]$ for the critical micelle concentration. Above the CMC, the unimer concentration is nearly fixed at this value. The volume fraction of aggregates with specified number is given by $\phi_l \simeq \exp\left[-(1+\alpha l^{1-p})\right]$, or

$$\phi_l \simeq \left\{ \begin{array}{ll} e^{-\alpha} & (p=1) \\ e^{-\alpha l^{1/2}} \ll 1 & (p=1/2) \\ e^{-\alpha l^{2/3}} \ll 1 & (p=1/3) \end{array} \right\}. \tag{6.126}$$

We therefore expect a widely polydisperse distribution for linear aggregates because ϕ_l is almost constant. For two- and three-dimensional aggregates, the distribution function decays quickly with the aggregation number, and the sum (6.120) gives a finite number. Since the total concentration easily exceeds this finite number, aggregates of infinite size often appear.

Let us next consider types I and III where stable micelles of finite size are formed (see Figure 6.23). We expand the binding free energy around l^* as

$$1 - \delta_l - \frac{1}{l} \cong a - b(l - l^*)^2 + \cdots, \tag{6.127}$$
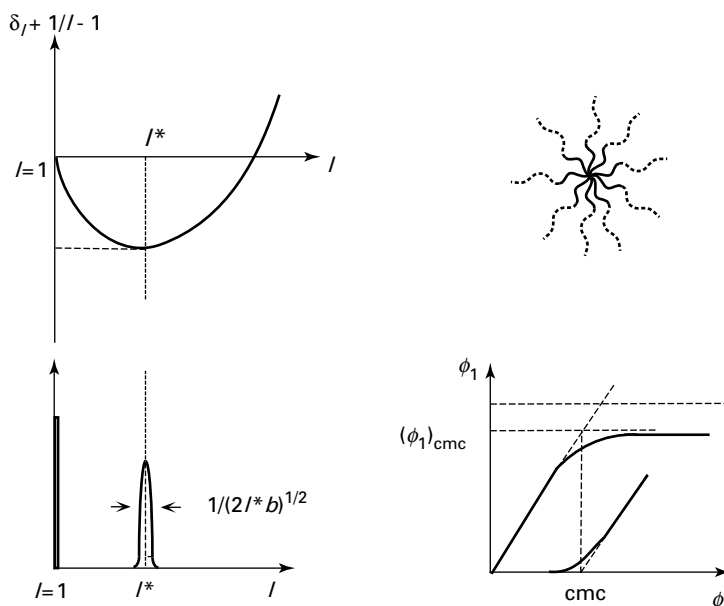
Fig. 6.23   Distribution function of the micellar aggregation number. Those corresponding to the minimum of the free energy give the largest population. The width of the distribution function is related to the curvature of the free energy at its minimum.

where a, b are positive constants. Since the volume fraction of l-mers is given by

$$\phi_l = e^{-bl(\Delta l)^2} (e^a \phi_1)^l, \tag{6.128}$$

CMC is decided from the condition

$$(\phi_1)_{\text{cmc}} = e^{-a}. \tag{6.129}$$

Hence we have

$$\phi_l \cong e^{-l^* b(\Delta l)^2}, \tag{6.130}$$

near $l = l^*$. The distribution function of the micelles becomes Gaussian with mean value l^* and variance $1/\sqrt{2l^* b}$.

It is well known that the geometrical form of the micelles varies with the type of surfactants and the concentration of the solutions (**micellar shape transition**) [84]. The spontaneous curvature is the fundamental factor to decide the micellar shape. For high spontaneous curvature the micelle takes a spherical shape. For intermediate spontaneous curvature, the micelle takes the shape of a cylinder terminated by two hemispheres. The cylinder can be very long, reaching several micrometers. In some situations, such worm-like giant cylindrical micelles are formed by tuning the value of the spontaneous curvature.

Typical examples of giant worm-like micelles are cationic surfactants cetylpyridinium bromide (CPyB) or cetylpyridinium cloride (CPyC) [76–79] with added NaBr, NaCl,

cetyltrimethylammonium bromide (CTAB) [85, 80, 81], or cetyltrimethylammonium cloride (CTAC) [86] mixed with ionic aromatic compounds such as sodium salicylate (NaSal), phthalimide potassium salt (PhIK). In the latter systems, one-to-one complexes of CTAB (or CTAC) and NaSal form long cylindrical micelles of uniform diameter of about 5–10 nm [85, 86]. Even at surfactant concentrations c as low as $10^{-2}\,\text{mol}\,\text{L}^{-1}$, the threadlike micelles grow long and are mutually entangled, so that the solutions show characteristic viscoelastic properties. The equilibrium distribution function of the cylinder length may be evaluated by the consideration of the formation free energy δ_l.

Polymeric micellization

Let us apply the above model to the micellization of amphiphilic diblock copolymers A-*block*-B. Let us assume that the A-block is hydrophilic and the B-block is hydrophobic. We split the free energy of association into two parts as usual

$$\Delta_l = \Delta_l^{\text{bond}} + \Delta_l^{\text{conf}}. \tag{6.131}$$

The binding free energy is given by $\Delta_l^{\text{bond}} = \beta(l-1)\Delta f_0 \ (\Delta f_0 < 0)$, while the conformational free energy is given by $\Delta_l^{\text{conf}} = \{S_{\text{dis}}(l) - lS_{\text{dis}}(1)\}/k_B$. The equilibrium constant then takes the form

$$K_l = l\gamma_l \left(\frac{\lambda(T)}{n}\right)^{l-1}, \tag{6.132}$$

where

$$\lambda(T) = \left[\sigma(\zeta-1)^2/\zeta\right]e^{-\beta\Delta f_0} \tag{6.133}$$

is the association constant, and Δf_0 is the free energy gain when a hydrophobic block is absorbed in the micellar core, which depends upon the length of the B-block and the interaction parameter χ_{BS} between the B-block and solvent.

Also, since the micelle is of finite size, there is interfacial free energy at the contact surface between the core of a micelle and solvent. Such an interfacial free energy in Δ_l^{bond} may take the form of $l^{2/3}$, which is included in the coefficient γ_l in the equilibrium constant. The volume fraction of the polymers is then given by

$$\frac{\lambda}{n}\phi = \sum_{l\geq 1} l\gamma_l x^l = G_1(x) \equiv x\tilde{u}(x), \tag{6.134}$$

while the number density of micelles is

$$\lambda v = \sum_{l\geq 1} \gamma_l x^l = G_0(x) \equiv x\tilde{U}(x), \tag{6.135}$$

where $x \equiv \lambda \phi_1 / n$ is the number density of unassociated polymers in the solution. The new functions are defined by

$$\tilde{u}(x) \equiv \sum_{l \geq 1} l \gamma_l x^{l-1}, \tag{6.136}$$

$$\tilde{U}(x) \equiv \sum_{l \geq 1} \gamma_l x^{l-1} = \frac{1}{x} \int_0^x \tilde{u}(x) dx. \tag{6.137}$$

Solving (6.134) for x, and substituting the result into (6.135), we can find ν as a function of the volume fraction.

The chemical potentials are

$$\beta \Delta \mu_1 / n = (1 + \ln x)/n - \nu^S + \chi (1 - \phi)^2, \tag{6.138a}$$

$$\beta \Delta \mu_0 = 1 + \ln(1 - \phi) - \nu^S + \chi \phi^2. \tag{6.138b}$$

The total number of clusters and molecules that possess a translational degree of freedom is

$$\nu^S = 1 - \phi + \nu. \tag{6.139}$$

We can find the osmotic pressure π from the chemical potential of the solvent $\Delta \mu_0$. The number average aggregation number of micelles is given by

$$\langle l \rangle_n = \tilde{u}(x)/\tilde{U}(x). \tag{6.140}$$

The weight average is

$$\langle l \rangle_w = 1 + x \tilde{u}'(x)/\tilde{u}(x). \tag{6.141}$$

In particular, we have $\gamma_l = 1$ for one-dimensional association because we can neglect the surface free energy. The function $\tilde{u}(x)$ becomes $\tilde{u}(x) = 1/(1-x)^2$, and hence we can express x explicitly in terms of the polymer number density $c \equiv \lambda \phi / n$ as

$$x = \frac{1}{2c} \left\{ 1 + 2c - \sqrt{1+4c} \right\}. \tag{6.142}$$

The CMC is estimated by the condition $c \simeq 1$, or equivalently

$$\lambda \phi_{\text{cmc}} / n \simeq 1. \tag{6.143}$$

At high concentrations where $c \gg 1$, we have approximately $x \simeq 1 - 1/\sqrt{c}$. The micellar distribution takes the form

$$\lambda \phi_l / n \simeq l(1 - 1/\sqrt{c})^l. \tag{6.144}$$

Hence, the aggregation number at which the volume fraction of micelles becomes largest is given by

$$l^* = \sqrt{c} = \sqrt{\phi / \phi_{\text{cmc}}}, \tag{6.145}$$

and the average aggregation number is

$$\langle l \rangle_\mathrm{n} = \sqrt{1+4c}. \tag{6.146}$$

We can see that it is 1 for $\phi << \phi_\mathrm{cmc}$, and $2\sqrt{\phi/\phi_\mathrm{cmc}}$ for $\phi >> \phi_\mathrm{cmc}$. The aggregation number increases with concentration in proportion to its square root.

References

[1] Tanaka, F.; Ishida, M.; Matsuyama, A., *Macromolecules* **24**, 5582 (1991).
[2] Tanaka, F., *Polym. J.* **34**, 479 (2002).
[3] Kielhorn, L.; Muthukumar, M., *J. Chem. Phys.* **107**, 5588 (1997).
[4] Tanaka, H.; Hashimoto, T., *Macromolecules* **24**, 5398; 5713 (1991).
[5] de Gennes, P. G., *Scaling Concepts in Polymer Physics*. Cornell University Press: Ithaca, NY, 1979.
[6] Leibler, L., *Macromolecules* **13**, 1602 (1980).
[7] Bates, F. S.; Fredrickson, G., *Ann. Rev. Phys. Chem.* **41**, 525 (1990).
[8] Hornreich, R. M.; Luban, M.; Shtrikman, S., *Phys. Rev. Lett.* **35**, 1678–1681 (1975).
[9] Haraguchi, M.; Nakagawa, T.; Nose, T., *Polymer* **36**, 2567 (1995).
[10] Haraguchi, M.; Nakagawa, T.; Nose, T., *Polymer* **37**, 3611; 4223 (1996).
[11] Lehn, J.-M., *Supramolecular Chemistry–Concepts and Perspectives*. VCH: Weinheim, 1995.
[12] Ciferri, C., *Supramolecular Polymers*. Marcel Dekker: New York, 2000.
[13] Kato, T., *Structure and Bonding* **96**, 95 (2000).
[14] Weiss, R. G.; Terech, P., *Molecular Gels: Materials with Self-Assembled Fibrillar Networks*. Springer: Dordrecht, 2006.
[15] Jacobson, H.; Stockmayer, W. H., *J. Chem. Phys.* **18**, 1600; 1607 (1950).
[16] Tobolsky, A. V.; Eisenberg, A., *JACS* **81**, 780 (1959).
[17] Scott, R. L., *J. Phys. Chem.* **1965**, *69*, 261; 352.
[18] Wheeler, J. C.; Pfeuty, P., *Phys. Rev. Lett.* **46**, 1409 (1981).
[19] Wheeler, J. C.; Pfeuty, P., *Phys. Rev. A* **24**, 1050 (1981).
[20] Wheeler, J. C.; Pfeuty, P., *J. Chem. Phys.* **74**, 6415 (1981).
[21] Mayer, J. E.; Mayer, M. G., *Statistical Mechanics*. Wiley: New York, 1940.
[22] Truesdell, C., *Annals of Mathematics* **46**, 144 (1945).
[23] Dudowicz, J.; Freed, K. F.; Douglas, J. F., *J. Chem. Phys.* **111**, 7116 (1999).
[24] Dudowicz, J.; Freed, K. F.; Douglas, J. F., *J. Chem. Phys.* **112**, 1002–1010 (2000).
[25] Terech, P.; Weiss, R. G., *Chem. Rev.* **97**, 3133 (1997).
[26] Tanaka, F.; Ishida, M., *Macromolecules* **30**, 1836 (1997).
[27] Tanaka, F., *Macromolecules* **37**, 605 (2004).
[28] Yashima, E.; Matsushima, T.; Okamoto, Y., *J. Am. Chem. Soc.* **119**, 6345 (1997).
[29] Matsuyama, A.; Tanaka, F., *Phys. Rev. Lett.* **65**, 341 (1990).
[30] Ruokolainen, J.; ten Brinke, G.; Ikkala, O.; Torkkeli, M.; Serimaa, R., *Macromolecules* **29**, 3409 (1996).
[31] Ruokolainen, J.; Torkkeli, M.; Serimaa, R. *et al.*, *Macromolecules* **29**, 6621 (1996).
[32] ten Brinke, G.; Ruokolainen, J.; Ikkala, O., *Europhys. Lett.* **35**, 91 (1996).
[33] ten Brinke, G.; Ikkala, O., *Trends Polym. Sci.* **5**, 213 (1997).
[34] Ruokolainen, J.; Torkkeli, M.; Serimaa, R.; Komanschek, B. E.; ten Brinke, G., *Phys. Rev. E* **54**, 6646 (1996).

[35] Angerman, H.; ten Brinke, G., *Macromolecules* **32**, 6813 (1999).

[36] ten Brinke, G.; Ruokolainen, J.; Ikkala, O., *Adv. Polym. Sci.* **207**, 113 (2007).

[37] Tasaki, K., *J. Am. Chem. Soc.* **118**, 8459 (1996).

[38] Koningsveld, R.; Stockmayer, W. H.; Nies, E., *Polymer Phase Diagrams–A Text Book*. Oxford University Press: Oxford, 2001, p. 341.

[39] Anderson, G. R.; Wheeler, J. C., *J. Chem. Phys.* **73**, 5778 (1980).

[40] Walker, J. S.; Vause, C. A., *Phys. Lett. A* **79**, 412 (1980).

[41] Goldstein, R. E.; Walker, J. S., *J. Chem. Phys.* **78**, 1942 (1983).

[42] Walker, J. S.; Vause, C. A., *Scientific American* **256**, 90 (1987).

[43] Narayanan, T.; Kumar, A., *Physics Reports* **249**, 135–218 (1994).

[44] Malcolm, G. N.; Rowlinson, J. S., *Trans. Faraday Soc.* **53**, 921 (1957).

[45] Saeki, S.; Kuwahara, N.; Konno, S.; Kaneko, M., *Macromolecules* **6**, 247 (1973).

[46] Saeki, S.; Kuwahara, N.; Nakata, M.; Kaneko, M., *Polymer* **17**, 685 (1976).

[47] Dormidontova, E. E., *Macromoles* **35**, 978 (2002).

[48] Bekiranov, S.; Bruinsma, R.; Pincus, P., *Phys. Rev. E* **55**, 577 (1997).

[49] Heskins, M.; Guillet, J. E., *J. Macromol. Sci.* **A2**, 1441 (1968).

[50] Fujishige, S.; Kubota, K.; Ando, I., *J. Phys. Chem.* **93**, 3311 (1989).

[51] Afroze, F.; Nies, E.; Berghmans, H., *J. Mol. Structure* **554**, 55 (2000).

[52] de Azevedo, R. G.; Rebelo, L. P. N.; Ramos, A. M.; Szydlowski, J.; de Sousa, H. C.; Klein, J., *Fluid Phase Eq.* **185**, 189 (2001).

[53] Rebelo, L. P. N.; Visak, Z. P.; de Sousa, H. C. *et al.*, *Macromolecules* **35**, 1887 (2002).

[54] Milewska, A.; Szydlowski, J.; Rebelo, L. P. N., *J. Polym. Sci., Polym. Phys. Ed.* **41**, 1219 (2003).

[55] Okada, Y.; Tanaka, F., *Macromolecules* **38**, 4465 (2005).

[56] Zimm, B. H.; Bragg, J. K., *J. Chem. Phys.* **31**, 526 (1959).

[57] Poland, P.; Scheraga, H. A., *Theory of Helix–Coil Transitions in Biopolymers*. Academic Press: San Diego, CA, 1970.

[58] Baulin, V. A.; Halperin, A., *Macromolecules* **35**, 6432 (2002).

[59] Baulin, V. A.; Halperin, A., *Macromol. Theory Simul.* **12**, 549 (2003).

[60] Bazuin, C. G., in *Mechanical and Thermophysical Properties of Polymer Liquid Crystals*, Brostow, W. (ed.) Chapman & Hall: London, 1998.

[61] Bradfield, A. E.; Jones, B., *J. Chem. Soc. Chem. Comm.* 2660 (1929).

[62] Jones, B., *J. Chem. Soc.* 1874 (1935).

[63] Weygand, C.; Gabler, G., *Z. Phys. Chem.* **1940**, *B46*, 270.

[64] Gray, J.; Jones, B., *J. Chem. Soc.,* 678–683 (1954).

[65] Shoji, M.; Tanaka, F., *Macromolecules* **35**, 7460 (2002).

[66] Maier, V. W.; Saupe, A., *Z. Naturforsch.* **13A**, 564 (1958); **14A**, 882 (1959); **15A**, 287 (1960).

[67] McMillan, W. L., *Phys. Rev. A* **4**, 1238 (1971).

[68] Cahn, J. W., *Tans. Metal. Soc. AIME* **242**, 166 (1968).

[69] Ormsted, P. D.; OPoon, W. C. K.; McLeish, T. C. B.; Terrill, N. J.; Ryan, A. J., *Phys. Rev. Lett.* **81**, 373 (1998).

[70] Flory, P. J., *Proc. Roy. Soc., London* **A234**, 73 (1956).

[71] Miller, W. G.; Kou, L.; Tohyama, K.; Voltaggio, V., *J. Polym. Sci.: Polymer Sym.* **65**, 91 (1978).

[72] Whittaker, E. T.; Watson, G. N., *A Course of Modern Analysis*, 6th edn. Cambridge University Press: Cambridge, 1969, p. 608.

[73] Tanford, C., *The Hydrophobic Effects*. Wiley: New York, 1980.

[74] Guenet, J. M., *Thermoreversible Gelation of Polymers and Biopolymers*. Academic Press: London, 1992.

[75] te Nijenhuis, K., *Adv. Polym. Sci.* **130**, 1 (1997).

[76] Porte, G; Appell, J.; Poggi, Y., *J. Phys. Chem.* **84**, 3105 (1980).

[77] Porte, G; Appell, J., *J. Phys. Chem.* **85**, 2511 (1981).

[78] Appell, J.; Porte, G., *J. Coll. Interface Sci.* **81**, 85 (1981).

[79] Appell, J.; Porte, G.; Poggi, Y., *J. Coll. Interface Sci. 87*, 492 (1981).

[80] Shikata, T.; Hirata, H.; Kotaka, T., *Langmuir* **3**, 1081 (1987); **4**, 354 (1988); **5**, 398 (1989).

[81] Shikata, T.; Hirata, H.; Kotaka, T., *J. Phys. Chem.* **94**, 3702 (1990).

[82] Candau, S. J.; Hirsch, E.; Zana, R.; Delsanti, M., *Langmuir* **2**, 1225 (1989).

[83] Hofmann, H.; Rehage, H., *Mol. Phys.* **5**, 1225 (1989).

[84] Degiorgio, V.; Corti, M., *Physics of Amphiphiles: Micelles, Vesicles and Microemulsions*. North-Holland: Amsterdan, 1985.

[85] Sakaguchi, Y.; Shikata, T.; Urakami, H.; Tamura, A.; Hirata, H., *J. Electron Microsc.* **36**, 168 (1987).

[86] Clausen, T. M.; Vinson, P. K.; Minter, J. R.; Davis, H. T.; Talmon, Y.; Miller, W. G., *J. Phys. Chem.* **96**, 474 (1992).

7   Thermoreversible gelation

This chapter presents several models of common gelling associating mixtures. They are constructed by combining the classical tree statistics of the branching reaction (Section 3.2) with the Flory–Huggins lattice theory of polymer solution (Section 2.3). They serve as the ideal models of thermoreversible gels and enable us to study the nature of gelation which interferes with phase separation. As application of the model, physical gels with multiple junctions are studied.

7.1   Models of thermoreversible gelation

Consider the self-assembling of polymer chain $R\{A_f\}$ $(n_A \equiv n)$ carrying a total of f associative groups A in an inert solvent B $(n_B = 1)$. We assume pairwise cross-linking of the associative groups leading to gels with one-component networks [1, 2, 3].

Let us start from the free energy (6.113)

$$\beta \Delta F = \sum_{l \geq 1} N_l \ln \phi_l + N_0 \ln \phi_0 + \chi(T)\phi(1-\phi)\Omega + \sum_{l \geq 1} \Delta_l N_l + \delta(\phi)N^G. \qquad (7.1)$$

In the last term, N^G is the number of polymer chains that belong to the network. It becomes a macroscopic variable after the gel point is passed. This additional term appears only in the postgel regime. The free energy $\delta(\phi)$ for a chain to be bound to the network depends on the concentration ϕ. It is negative, and its absolute value increases with the concentration because the network structure becomes tighter and denser with the concentration.

The chemical potentials of finite clusters composed of l chains, and that of the solvent molecules, are derived by the differentiation of the free energy as

$$\beta \Delta \mu_l / n = (\Delta_l + 1 + \ln \phi_l)/n - l\nu^S$$
$$+ \chi l(1-\phi)^2 + l\delta'(\phi)\nu^G(1-\phi), \qquad (7.2a)$$
$$\beta \Delta \mu_0 = 1 + \ln(1-\phi) - \nu^S + \chi \phi^2 - \delta'(\phi)\nu^G \phi, \qquad (7.2b)$$

where ν^S is the total density of the centers of mass in translational motion

$$\nu^S = 1 - \phi + \sum \nu_l. \qquad (7.3)$$

Similarly, the chemical potential of the polymer chain in the gel network is

$$\beta \Delta \mu_1^G / n = \delta/n - \nu^S + \chi(1-\phi)^2 + \delta'(\phi)\nu^G(1-\phi).$$

The condition for multiple equilibrium $\Delta \mu_l = l\Delta \mu_1$ leads to

$$\phi_l = K_l \phi_1{}^l \tag{7.4}$$

for the volume fraction of l-mers, where the equilibrium constant can be expressed as

$$K_l = e^{l-1-\Delta_l}, \tag{7.5}$$

by using the free energy Δ_l of l-mer formation.

In the postgel regime, the additional equilibrium condition $\Delta \mu_1 = \Delta \mu_1^G$ holds, and hence the relation

$$\delta(\phi) = 1 + \ln \phi_1 \tag{7.6}$$

is obtained. The binding free energy $\delta(\phi)$ per chain to the gel is uniquely related to the volume fraction ϕ_1 of unassociated chains. By relations (7.4) and (7.6), the volume fraction ϕ_1 serves as an activity of the polymer. Therefore, we use the symbol $\phi_1 = z$ to stress this property.

Substituting (7.4) and (7.6) into the free energy (7.1), and arranging the terms, we find the dimensionless free energy per lattice cell takes the form

$$\mathscr{F} \equiv \frac{\beta \Delta F}{\Omega} = -\frac{1}{n} G_0(z) + \frac{\phi}{n}(1 + \ln z) + (1-\phi)\ln(1-\phi) + \chi(T)\phi(1-\phi), \tag{7.7}$$

where functions

$$G_k(z) \equiv \sum_{l \geq 1} l^k b_l z^l \qquad (b_l \equiv K_l/l), \tag{7.8}$$

for $k = 0, 1, 2, \ldots$ have been introduced.

In terms of the gel fraction $w \equiv \phi^G/\phi$, the relation

$$\phi = \phi^S + \phi^G \tag{7.9}$$

is transformed to the equation for the volume fraction of the sol part

$$\phi(1-w) = G_1(z). \tag{7.10}$$

The total number of clusters is

$$\nu \equiv \sum_{l \geq 1} \nu_l = G_0(z)/n. \tag{7.11}$$

These results are analogous to the free energy of interacting gases

$$\mathscr{F} = \ln z - \nu G_0(z), \tag{7.12}$$

in Mayer's theory of condensation [4], where the volume v per particle and pressure p are given by

$$v^{-1} = G_1(z), \tag{7.13a}$$

$$p/kT = G_0(z). \tag{7.13b}$$

It is known [4] that the activity z can be eliminated from these equations, and the equation of state

$$p/k_B T = v^{-1} \left(1 - \sum_{k=1}^{\infty} \frac{k}{k+1} \beta_k v^{-k} \right) \tag{7.14}$$

is obtained, where β_k are the irreducible cluster integrals that are constructed from b_l. The coefficient b_l in the condensation theory is the l-th cluster integral, but in gelation problem it is replaced by the association equilibrium constant $b_l = K_l/l$. In the pregel regime, we therefore have

$$nv = \phi \left(1 - \sum_{k=1}^{\infty} \frac{k}{k+1} \beta_k \phi^k \right). \tag{7.15}$$

The coefficients β_k can be explicitly calculated in the present gel problem by using the Stockmayer factor.

As usual, we split the free energy into three parts

Assuming the structure of the gel for fixing the specific form of b_l and the gel fraction w, and solving (7.10) for the activity z in terms of the concentration ϕ and the temperature, we find the free energy (7.7) as a function of ϕ and T, and hence the entire problem is solved. We carry out this program for a simple model system for which the coefficients b_l can be explicitly found.

7.2   Application of the classical theory of gelation

To derive a specific form of the equilibrium constants b_l, let us introduce a simple model for the internal structure of clusters. Clusters are assumed to take a tree structure with no internal loops (**Cayley tree**). Cycle formation within a cluster is neglected. This is a crude approximation on the basis of the classical theory of gelation presented in Section 3.2 [5,6,7,8], but in fact it is known to work very well at least in the pregel regime.

As usual, we split the free energy into three parts

$$\Delta_l = \Delta_l^{\mathrm{comb}} + \Delta_l^{\mathrm{conf}} + \Delta_l^{\mathrm{bond}}. \tag{7.16}$$

To find the combinatorial part, we employ the entropy change on combining l identical f-functional molecules to form a single Cayley tree. The classical tree statistics in Section 3.2 give

$$\Delta S_l^{\mathrm{comb}} = k_B \ln[f^l \omega_l], \tag{7.17}$$

where

$$\omega_l \equiv \frac{(fl-l)!}{l!(fl-2l+2)!} \tag{7.18}$$

is Stockmayer's combinatorial factor (3.14) [6]. The free energy is given by $\Delta_l^{\text{comb}} = -\Delta S_l^{\text{comb}}/k_B$.

For the conformational free energy, we employ the lattice theoretical entropy of disorientation (2.90), and find

$$\Delta S_l^{\text{conf}} = S_{\text{dis}}(ln) - lS_{\text{dis}}(n) = k_B \ln\left[\left(\frac{\sigma(\zeta-1)^2}{\zeta en}\right)^{l-1} l\right]. \tag{7.19}$$

Finally, the free energy of bonding is given by

$$\Delta_l^{\text{bond}} = (l-1)\beta\Delta f_0, \tag{7.20}$$

because there are $l-1$ bonds in a tree of l molecules, where Δf_0 is the free energy change of a bond formation.

Combining all results together, we find

$$K_l = fl\omega_l\left(\frac{f\lambda}{n}\right)^{l-1}, \quad b_l = \left(\frac{n}{\lambda}\right)\omega_l\left(\frac{f\lambda}{n}\right)^l, \tag{7.21}$$

for the equilibrium constant, where $\lambda(T)$ is the association constant

$$\lambda(T) \equiv [\sigma(\zeta-1)^2/\zeta e]\exp(-\beta\Delta f_0). \tag{7.22}$$

The distribution of clusters (7.4) is simplified to

$$\lambda v_l = \omega_l x^l, \tag{7.23}$$

for the number density, where the independent variable x is defined by

$$x \equiv \lambda fz/n, \tag{7.24}$$

which gives the number of functional groups fz/n carried by the unassociated polymer chains in the solution.

The total number concentration of the finite clusters is then given by

$$\lambda \sum_{l\geq1} v_l = S_0(x). \tag{7.25}$$

Their volume fraction is

$$\frac{\lambda}{n}\sum_{l\geq1}\phi_l = S_1(x). \tag{7.26}$$

Therefore, the number-average of the cluster size is

$$\bar{l}_n \equiv \sum l v_l / \sum v_l = S_1(x)/S_0(x),$$ (7.27)

and the weight-average is

$$\bar{l}_w \equiv \sum l^2 v_l / \sum l v_l = S_2(x)/S_1(x).$$ (7.28)

These are written in terms of the moments of Stockmayer's distribution function, defined by

$$S_k(x) \equiv \sum_{l=1}^{\infty} l^k \omega_l x^l \quad (k=0,1,2,\ldots).$$ (7.29)

They are related to the functions (7.8) by $G_k(z) = n S_k(x)/\lambda$.

As in the Appendix to Chapter 3, these moments are explicitly written in terms of the extent α of reaction, which is defined by the equation

$$x \equiv \alpha(1-\alpha)^{f-2}.$$ (7.30)

To see the physical meaning of α, let us calculate the probability for a randomly chosen functional group to be associated. Since an l-mer includes the total of fl groups, among which $2(l-1)$ are associated, the probability of association (extent of reaction) is given by

$$2[S_1(x) - S_0(x)]/f S_1(x) = \alpha.$$ (7.31)

Thus, α in fact gives the extent of association.

By using α, the average cluster sizes are given by

$$\bar{l}_n = 1/(1 - f\alpha/2),$$ (7.32a)

$$\bar{l}_w = (1+\alpha)/[1 - (f-1)\alpha].$$ (7.32b)

7.2.1   Pregel regime

The weight-average cluster size diverges at $\alpha = 1/(f-1)$. This suggests that $\alpha = \alpha^* \equiv 1/(f-1)$ is the gel point. The number-average also diverges at $\alpha = \alpha_0 \equiv 2/f$, but since $2/f > 1/(f-1)$, we have to study the postgel regime to examine its behavior.

In the pregel regime ($\alpha < \alpha^*$), the volume fraction ϕ^S occupied by the polymer chains belonging to the sol must always be equal to the total polymer volume fraction ϕ. Thus, from (7.26), the total polymer volume fraction ϕ and the extent of association α satisfy the relation

$$\lambda \psi = \frac{\alpha}{(1-\alpha)^2},$$ (7.33)

where $\psi \equiv f\phi/n$ (the total number concentration of the functional groups) is used instead of the volume fraction ϕ.

We can solve this equation for α, and find

$$\alpha = \frac{1}{2\lambda\psi} \left\{ 1 + 2\lambda\psi - \sqrt{1 + 4\lambda\psi} \right\}, \tag{7.34}$$

through which we can express any physical quantity directly in terms of $\lambda\psi$. For instance, the total free energy per lattice cell is given by

$$\mathscr{F} = \frac{\phi}{n} \left\{ (f-2)\ln(1-\alpha) + \ln\alpha + \frac{1}{2}f\alpha \right\} + (1-\phi)\ln(1-\phi) + \chi\phi(1-\phi). \tag{7.35}$$

Hence the renormalization of the χ-parameter by association turns out to be

$$\Delta\chi(\phi) = \left[(f-2)\ln(1-\alpha) + \ln\alpha + \frac{1}{2}f\alpha - \ln\phi \right] / n(1-\phi). \tag{7.36}$$

It can be expanded in powers of the concentration as

$$\Delta\chi = -\frac{K_{2,0}}{2n_A}\phi + \cdots. \tag{7.37}$$

We thus describe the molecular origin of the concentration dependence of the χ-parameter in terms of the associative force.

In a similar way, the spinodal condition is

$$\frac{\kappa(\phi)}{n\phi} + \frac{1}{1-\phi} - 2\chi = 0, \tag{7.38}$$

where κ is given by

$$\kappa(\phi) = \frac{1-(f-1)\alpha}{1+\alpha} = \frac{1}{\bar{l}_{\mathrm{w}}(\alpha)} \tag{7.39}$$

in terms of α (7.34). It is the reciprocal of the weight-average cluster size.

7.2.2 The gel point

Let us next find the sol–gel transition point. The binding free energy per molecule

$$\delta_l = -(\ln K_l - l + 1)/l, \tag{7.40}$$

is a steadily decreasing function of l. It approaches the limiting value

$$\delta_\infty = 1 + \ln[f\lambda(T)/n] - (f-1)\ln(f-1) + (f-2)\ln(f-2), \tag{7.41}$$

as l goes to infinity. This model therefore falls into category II in Figure 6.21. The limit gives

$$z^* = \exp(\delta_\infty - 1),$$

for the convergence radius of the series (7.29), or equivalently,

$$x^* = (f-2)^{f-2}/(f-1)^{f-1}, \tag{7.42}$$

in terms of x, and

$$\alpha^* = 1/(f-1), \tag{7.43}$$

in terms of the extent of association, as was expected from the divergence of $\bar{l}_w$. The concentration of polymers at the gel point is then given by

$$\lambda(T)\psi^* = \frac{f-1}{(f-2)^2}. \tag{7.44}$$

This condition gives the sol–gel transition line on the temperature–concentration plane.

7.2.3   Postgel regime

In the postgel regime where $\phi > \phi^*$ ($\alpha > \alpha^*$), we have an additional condition (7.6). The activity z of the solute molecule is related to the binding free energy of the gel.

Since the reactivity in the sol can in general be different from that in the gel, let us write the former as α^S and the latter as α^G. The average reactivity α of the system as a whole is defined by

$$\alpha = \alpha^S(1-w) + \alpha^G w, \tag{7.45}$$

where w is the weight fraction of the gel.

The volume fraction ϕ^S of polymers belonging to the sol is consequently given by

$$\lambda\phi^S/n = S_1(\alpha^S), \tag{7.46}$$

in the postgel regime, so that it is different from the total ϕ given by $S_1(\alpha)$. The total number of finite clusters must also be replaced by

$$\lambda\nu = S_0(\alpha^S), \tag{7.47}$$

since it must give the number of molecules and clusters that have a translational degree of freedom. The gel network spans the entire solution and loses its translational degree of freedom.

By using $\nu^S = 1 - \phi + \nu$, the chemical potentials are given by

$$\frac{\beta\Delta\mu_1^*}{n} = \frac{1+\ln x}{n} - \nu^S + \chi(1-\phi)^2 + \delta'(\phi)(1-\phi)\nu^G, \tag{7.48a}$$

$$\beta\Delta\mu_0^* = 1 + \ln(1-\phi) - \nu^S + \chi\phi^2 - \delta'(\phi)\phi\nu^G. \tag{7.48b}$$

The function κ in the spinodal condition takes the form

$$\kappa(\phi) = \frac{d}{d\ln\phi}\left(1 + w\frac{d}{d\ln\phi}\right)\ln x(\alpha^S), \tag{7.49}$$

which is different from the one in the pregel regime.

Flory's treatment

By the definition (7.30) of α, x takes a maximum value $x^* = (f-2)^{f-2}/(f-1)^{f-1}$ at $\alpha = 1/(f-1)$. Therefore, two values of α can be found for a given value of x. Let us consider the postgel regime $\alpha > \alpha^*$. For a given α, the value of x is fixed by the relation $x \equiv \alpha(1-\alpha)^{f-2}$.

As described in Section 3.2, Flory postulated [5, 8] that another root α' (the shadow root) lying below α^* in this equation for a given value of x gives the extent of reaction in the sol. Hence we have

$$\alpha^S = \alpha'. \tag{7.50}$$

The volume fraction ϕ^S of polymers in the sol is given by

$$\frac{\lambda}{n}\phi^S = \frac{\alpha'}{f(1-\alpha')^2}, \tag{7.51}$$

and the gel fraction is given by

$$w = 1 - (1-\alpha)^2 \alpha'/(1-\alpha')^2 \alpha. \tag{7.52}$$

The larger one lying above α^* gives the reactivity for all functional groups in the system. It fulfills the relation

$$\lambda\psi = \alpha/(1-\alpha)^2. \tag{7.53}$$

The number of molecules that remain unassociated can be described either by $\lambda\psi^S$ $(1-\alpha^S)^f$ or by $\lambda\psi(1-\alpha)^f$. Hence we have

$$x = \alpha(1-\alpha)^{f-2} = \alpha^S(1-\alpha^S)^{f-2} \tag{7.54}$$

This gives a physical meaning to Flory's postulate of $\alpha^S = \alpha'$.

The gel fraction reaches unity only at the limit of complete reaction $\alpha = 1$. The extent of association α^G in the gel can be obtained by the definition of the total reactivity (7.45). Explicitly, it gives

$$\alpha^G = (\alpha + \alpha' - 2\alpha\alpha')/(1-\alpha\alpha'). \tag{7.55}$$

This value is obviously larger than that of the infinite limit in the tree approximation

$$\lim_{l\to\infty} [(f-2)l+2]/fl = 2/f \equiv \alpha_0, \tag{7.56}$$

so that, in Flory's picture, *cycle formation is allowed within the gel network*. Its cycle rank is given by

$$\xi = \frac{1}{2}\alpha^G - 1. \tag{7.57}$$

The main results obtained by Flory's picture are summarized in Figure 7.1.
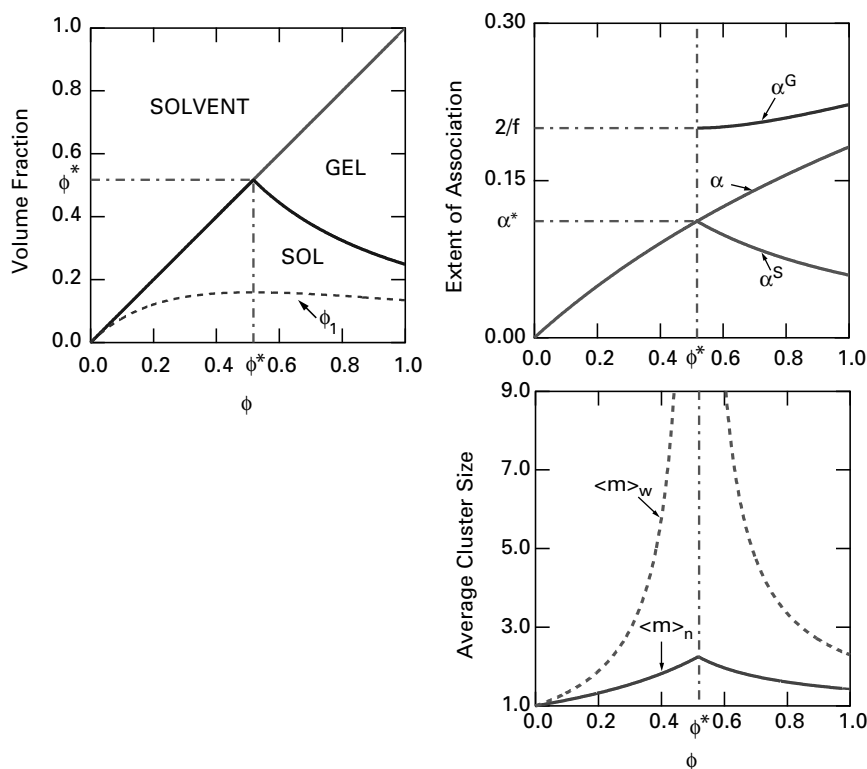
Fig. 7.1   Gel fraction, extent of association and average molecular weight $\langle m \rangle_n, \langle m \rangle_w$ calculated on the basis of Flory's postgel picture. The number-average has a discontinuous slope across the gel point, while the weight-average diverges. (Reprinted with permission from Ref. [9].)

The binding free energy $\delta(\phi)$ of a chain onto the gel network turns out to be

$$\delta(\lambda \psi) = 1 - (f-1)\ln(\lambda \psi) + f\ln[(\sqrt{1+4\lambda \psi}-1)/2], \qquad (7.58)$$

which is a monotonically decreasing function of the concentration. With an increase in the concentration, the network structure becomes tighter, so that the binding of a polymer chain becomes stronger. Since the average number of bonds per molecule is $(f/2)\alpha^G = \alpha^G/\alpha_0$, the binding free energy *per bond* is given by $\alpha_0 \delta(\phi)/\alpha^G$. This is not a constant, but changes as the reaction proceeds.

Stockmayer's treatment

Stockmayer [6] later remarked that Flory's result in the postgel regime is inconsistent with the tree assumption, however, since the treatment permits cycle formation in the gel network. To remove this inconsistency, he proposed another treatment of the postgel regime. He introduced a different assumption that the extent of reaction of functional groups in the finite clusters remains at the critical value $\alpha^* = 1/(f-1)$ throughout the postgel regime. He also proposed that in the postgel regime the extent of reaction in the

gel network should take the limiting value (7.56)

$$\alpha^G = \alpha_0, \tag{7.59}$$

which is appropriate to an infinite tree structure without cycles.

From the definition (7.45), the gel fraction w takes the form

$$w = \frac{(f-1)\alpha - 1}{1 - \alpha_0}, \tag{7.60}$$

where α $(> \alpha^*)$ is the extent of reaction of the entire system including all functional groups. It is a linear function of α, and reaches unity at $\alpha_0 = 2/f$ before the reaction is completed. The volume fraction of the sol remains constant at $\phi^S = \phi^*$. The number-average DP remains constant at $\bar{l}_n = (f-2)/2(f-1)$, while the weight-average is divergent $\bar{l}_w = \infty$ in the postgel regime. The binding free energy is fixed at δ_∞. The main results obtained by Stockmayer's picture are summarized in Figure 7.2.
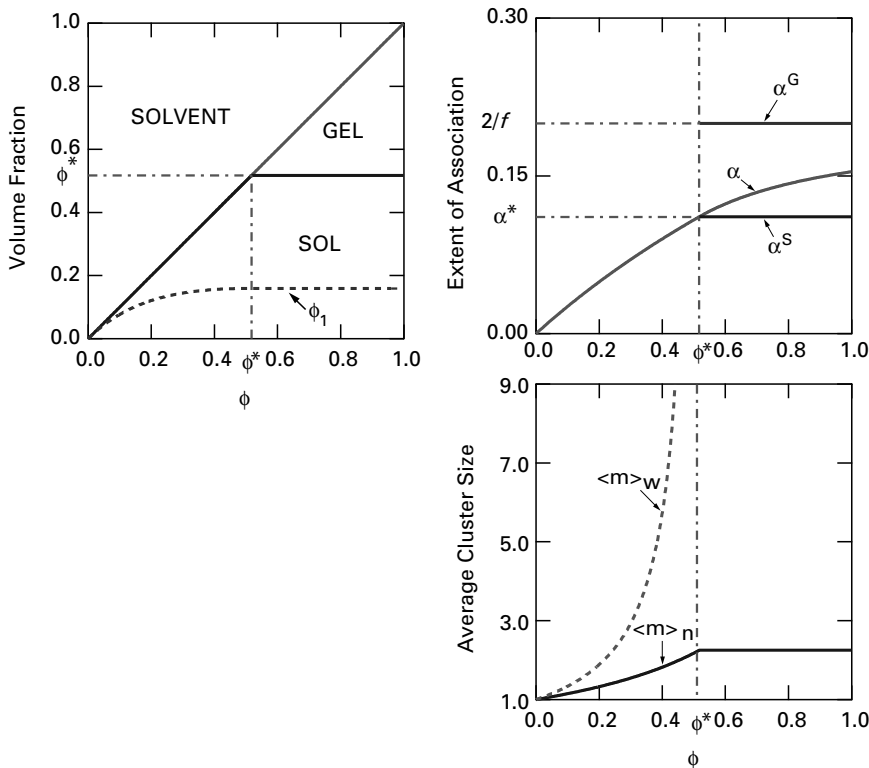
Fig. 7.2   Gel fraction, extent of association and average molecular weight calculated on the basis of Stockmayer's postgel picture. The number-average has a discontinuous slope across the gel point, while the weight-average remains divergent in the postgel regime. (Reprinted with permission from Ref. [9].)

From (7.10), which is now equivalent to

$$\lambda \psi (1 - w) = \lambda \psi^*, \tag{7.61}$$

we find

$$w = 1 - \phi^*/\phi. \tag{7.62}$$

7.2.4 Phase diagrams of thermoreversible gels

Figure 7.3(a) compares the phase diagrams calculated by the two treatments of the postgel regime [9, 10]. Binodals and spinodals appear at different positions. For the same association constant, Stockmayer's treatment gives a **tricritical point** (TCP) [11, 12] at the crossing of the sol–gel transition line and the binodal (spinodal), while Flory's treatment gives a **critical endpoint** (CEP) [12] at the shoulder of the binodal, and a critical point (CP) in the postgel regime. Existence of a CP in the postgel regime suggests that phase separation between dilute gel (with only a few cycles) and concentrated gel (with many cycles) in the postgel regime is possible.

Figure 7.3(b) compares the experimental phase diagram of atactic polystyrene (at-PS) solution in carbon disulfide (CS$_2$) [13–15]with theoretical calculations. This solution shows a TCP-type phase diagram, but CEP types were also reported for at-PS in
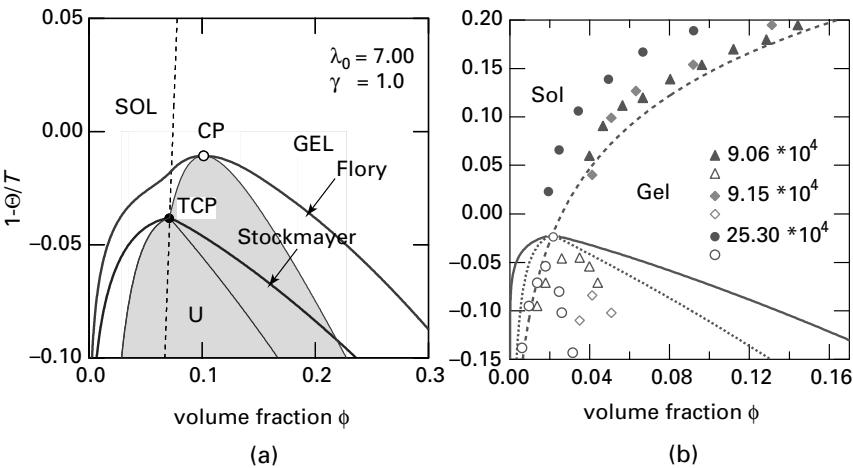
Fig. 7.3 (a) Comparison of the theoretical phase diagrams of low-molecular weight ($n = 1$) trifunctional ($f = 3$) molecules calculated by Flory's treatment (upper lines) and Stockmayer's treatment (lower lines) of the postgel regime for the same association constant. The sol–gel transition line (broken line), critical point (CP), tricritical point (TCP), and unstable region (gray area) are indicated. (b) Phase diagram of atactic polystyrene in carbon disulfide (at-PS/CS$_2$). The theoretical sol–gel transition line (broken line), binodal (solid line), and spinodal (dotted line) are drawn. The theta temperature is $\Theta = -70°C$. Experimental data of the gel points (black symbols) and cloud points (white symbols) are shown for three different molecular weights. The theoretical calculation is fitted to the data of $M = 9.06 \times 10^4$. (Reprinted with permission from Ref. [10].)

different solvents [14]. We attempted to fit the data by simple pairwise cross-linking in Stockmayer's picture.

The molecular origin of at-PS cross-linking has been the subject of a number of works [14,16–19], but there still remains a divergence in opinions. One series of studies [16] postulate the existence of short crystallizable stereoregular segment sequences on polymer chains, even if they are atactic, that are responsible for the formation of microcrystalline junctions.

Other studies [18, 17] propose that cross-linking takes place by specific interaction, such as the formation of stoichiometric compounds involving solvent molecules. If such complex formations were the mechanism of cross-linking, the gelation temperature should show a maximum at the stoichiometric concentration [17]. Existence of specific interaction was later suggested by a light scattering study of at-PS dilute solution mixture of CS_2 and toluene [20].

7.3 Thermodynamics of sol–gel transition as compared with Bose–Einstein condensation

At this stage, we recognize that our theory of thermoreversible gelation is mathematically analogous to those we encounter in the study of Bose–Einstein condensation (BEC) in ideal Bose gases [4, 21]. The number density N/V and the pressure p of an ideal Bose gas consisting of N molecules confined in a volume V is given by

$$\lambda_T^3 N/V = \sum_{l=1}^{\infty} x^l/l^{3/2}, \tag{7.63a}$$

$$p\lambda_T^3/k_{\mathrm{B}}T = \sum_{l=1}^{\infty} x^l/l^{5/2}, \tag{7.63b}$$

where x is the activity of the molecule, and $\lambda_T \equiv h/(2\pi m k_{\mathrm{B}}T)^{1/2}$ the thermal de Broglie wave length. The coefficient of the infinite series on the right-hand side is $1/l^{5/2}$ instead of Stockmayer's combinatorial factor ω_l, but other parts are completely analogous.

The infinite summations on the right-hand side of these equations are known as Truesdell functions [22] of order 3/2 and 5/2. Their singularity at the convergence radius $x = 1$ was studied in detail [22]. Since the internal energy of a Bose gas is related to its pressure by $U = 3pV/2$, the singularity in the compressibility and in the specific heat have the same nature; they reveal a discontinuity in their derivatives [21]. The transition (condensation of macroscopic number of molecules into a single quantum state) turns out to be a third-order phase transition [21].

We now show that a similar picture holds for our gelling solution; a finite fraction of the total number of primary molecules condenses into a single state (gel network), which has no center of mass translational degree of freedom (no momentum), although there is no quantum effect. Since the solution is spatially uniform, gelation can be seen as a *phase separation in the momentum space* into the zero momentum phase (gel) and the finite momentum phase (sol).

To find the nature of the singularity, we calculate the osmotic compressibility, defined by

$$K_T^{-1} \equiv \frac{k_B T}{a^3 \phi} \left(\frac{\partial \pi}{\partial \phi} \right)_T, \tag{7.64}$$

as a function of the temperature and the volume fraction. By taking the concentration derivative of the solvent chemical potential (7.2b), we find $K_T^{-1} = \phi^2 \sigma(\phi, T)$, where

$$\sigma(\phi, T) \equiv \frac{\kappa(\phi, T)}{n\phi} + \frac{1}{1 - \phi} - 2\chi. \tag{7.65}$$

Here, the function κ is defined by

$$\kappa \equiv n(\partial v / \partial \phi)_T. \tag{7.66}$$

The singularity in the osmotic pressure originates in this κ function: the translational entropy of clusters.

The analogy of BEC can be seen more clearly if we replace Stockmayer's combinatorial factor ω_l by its asymptotic form

$$\omega_l \simeq x^{*-1} / l^{5/2}, \tag{7.67}$$

for large l, where x^* is given by (7.42). This form is derived by applying Stirling's formula to (7.18). We find

$$\frac{\lambda \phi}{n} = \sum_{l=1}^{\infty} \frac{1}{l^{3/2}} \left(\frac{x}{x^*} \right)^l, \tag{7.68a}$$

$$\lambda v = \sum_{l=1}^{\infty} \frac{1}{l^{5/2}} \left(\frac{x}{x^*} \right)^l. \tag{7.68b}$$

Thus, we can see that the singularity at $x = x^*$ is identical to those in Truesdell's functions at $x = 1$.

Near the gel point, simple calculation gives

$$\bar{l}_w \simeq \frac{A}{\phi^* - \phi}, \tag{7.69}$$

with a constant amplitude

$$A \equiv \frac{fn}{(f-2)^3 \lambda(T)}, \tag{7.70}$$

for $\phi < \phi^*$. In Stockmayer's treatment $\bar{l}_w = \infty$ remains for all $\phi > \phi^*$. We thus find the discontinuity in the slope of the function κ is given by $\Delta(\partial \kappa / \partial \phi)_T = 1/A$. This leads to a discontinuity in the osmotic compressibility in the form

$$\Delta \left(\frac{\partial K_T}{\partial \phi} \right)_T = -K_T^2 \left(\frac{\phi^*}{n} \right) \Delta \left(\frac{\partial \kappa}{\partial \phi} \right)_T = -\frac{B}{\sigma(\phi^*, T)^2}, \tag{7.71}$$

where

$$B \equiv \frac{f^2(f-2)^9 \lambda(T)^4}{(f-1)^3 n^5} \tag{7.72}$$

is a constant depending only on the temperature, functionality, and the number of statistical units on a chain. For large molecular weight polymers, the amplitude B is small. This is the main reason why experimental detection of the singularity has so far been difficult. However, as we approach the spinodal point where the condition $\sigma(\phi^*, T) = 0$ is satisfied by changing the temperature under a fixed concentration, the discontinuity is enhanced by critical fluctuations, and there may be a chance to observe the singularity.

Similar calculation on the basis of Flory's treatment gives the factor $-4B$ instead of B. The sign changes, but the discontinuity remains.

We next consider the temperature derivatives of the free energy, such as entropy and specific heat. The temperature appears through the interaction parameter $\chi(T)$ and association constant $\lambda(T)$. Because it is evident that the former does not lead to any singularity, we consider the derivatives with respect to the latter.

Within Stockmayer's treatment of the postgel regime, after a complex calculation, it turns out that there is no singularity up to the second derivatives, but the third derivative contains a discontinuity

$$\Delta \left[\frac{\partial^3(\beta F)}{\partial(\ln \lambda)^3} \right]_\phi = C \frac{\phi}{n}, \tag{7.73}$$

where C is given by

$$C = \frac{f-2}{f^2(f-1)}. \tag{7.74}$$

Flory's treatment gives $[-4/(f-1)]C$ instead of C. Again, the sign changes, but the discontinuity remains. Collecting all results, we come to the conclusion that the ideal model of thermoreversible gelation treated here shows a third-order phase transition that is analogous to the Bose–Einstein condensation.

7.4 Thermoreversible gels with multiple cross-linking

7.4.1 Multiple association

Most thermoreversible gels of polymers and biopolymers have cross-link junctions that combine several distinct chains (**multiple junctions**) as shown in Figure 7.4. For instance, gelation by the micro-crystallization of chain segments (Figure 7.4(a)), by ionic (dipolar) aggregation (Figure 7.4(b)), and by the hydrophobic association of special groups attached to the polymer chains (Figure 7.4(c)), all fall on this important category [19, 23]. In some biopolymer gels, triple helices serve as extended cross-link junctions.

In this section, we attempt to extend our theory of thermoreversible gelation from pairwise association to the more general multiple association. As a model solution, we consider a mixture of associative molecules $R\{A_f\}$ in a solvent. Molecules are distinguished by the number f of associative groups they bear, each group being capable
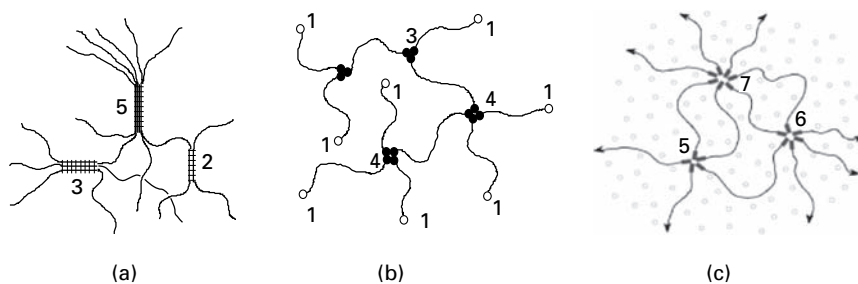
Fig. 7.4   Examples of multiple cross-links: (a) microcrystalline junctions, (b) ionic multiplets in a network of telechelic ionomers, (c) micellar junctions of hydrophobic aggregates in networks of telechelic associating polymers. Numbers near the junctions show their multiplicity.

of taking part in the junctions with variable multiplicity which may bind together any number k of such groups (Figure 7.5(a)) [3,24–27].We include $k = 1$ for unassociated groups, and allow junctions of all multiplicities to coexist, in proportions determined by the thermodynamic equilibrium conditions.

In order to incorporate polydispersity in the functionality, we allow the number f of associative groups to vary. Such polydispersity in the functionality of polymers is essential when associative groups are activated by the conformational transition of polymers, as in biopolymer gels. In such cases, the functionality f is not a fixed number but changes depending upon temperature, concentration, and other environmental parameters.

Let n_f be the number of statistical repeat units on an f-functional primary molecule, and let N_f be the total number of molecules in the solution. The number of repeat units per functional group $R \equiv n_f / f$ is assumed to be independent of f. The weight fraction ρ_f of the associative groups carried by the molecules with specified f relative to the total number of associative groups is given by

$$\rho_f = f N_f / \sum f N_f. \tag{7.75}$$

The number- and weight-average functionality of the primary molecules are then defined by

$$f_n \equiv \left(\sum \rho_f / f \right)^{-1}, \tag{7.76a}$$

$$f_w \equiv \sum f \rho_f. \tag{7.76b}$$

The volume fraction of f-functional molecules is given by $\phi_f = n_f \nu_f$, where $\nu_f \equiv N_f / \Omega$ is their number density, and the total volume fraction by $\phi = \sum_f \phi_f$.

In thermal equilibrium, the solution has a distribution of clusters with the population distribution fixed by the equilibrium conditions. As in Section 7.4, we define a cluster of type $(\mathbf{j};\mathbf{l})$ as consisting of j_k junctions of multiplicity k ($k = 1, 2, 3, ...$) and l_f molecules of functionality f ($f = 1, 2, 3, ...$). The bold letters $\mathbf{j} \equiv \{j_1, j_2, j_3, ...\}$ and $\mathbf{l} \equiv \{l_1, l_2, l_3, ...\}$ denote the sets of indices (Figure 7.5(b)). An isolated molecule of functionality f, for
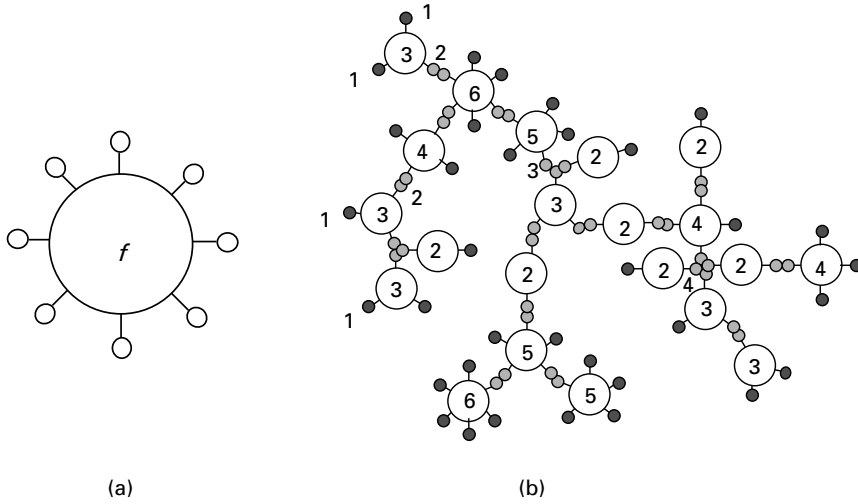
Fig. 7.5   (a) Symbolic picture of polyfunctional molecule R{A_f}. (b) A cluster formed by multiple association.

instance, is indicated by $\mathbf{j}_{0f} \equiv \{f, 0, 0, ...\}$, and $\mathbf{l}_{0f} \equiv \{0, ..., 1, 0, ...\}$. (The f-th number is unity, others are zero.)

In the multiple tree statistics described in Section 3.3, there are two fundamental relations (3.74) and (3.75) due to the geometrical constraints.

Let $N(\mathbf{j};\mathbf{l})$ be the number of $(\mathbf{j};\mathbf{l})$-clusters in the system. Their number density is given by $v(\mathbf{j};\mathbf{l}) = N(\mathbf{j};\mathbf{l})/\Omega$, and their volume fraction is given by

$$\phi(\mathbf{j};\mathbf{l}) = \left(\sum_{f \geq 1} n_f l_f\right) v(\mathbf{j};\mathbf{l}). \qquad (7.77)$$

The total volume fraction of the polymer component in the sol part is the sum over all possible cluster types

$$\phi(1-w) = \sum_{\mathbf{j},\mathbf{l}} \phi(\mathbf{j};\mathbf{l}), \qquad (7.78)$$

where w is the gel fraction.

7.4.2   Distribution function of multiple trees

The free energy change on passing from the reference state to the final solution, at equilibrium with respect to cluster formation, is

$$\mathscr{F} = \phi_0 \ln \phi_0 + \sum_{\mathbf{j},\mathbf{l}} v(\mathbf{j};\mathbf{l})[\Delta(\mathbf{j};\mathbf{l}) + \ln \phi(\mathbf{j};\mathbf{l})] + \chi(T)\phi_0\phi + \sum_f v_f^G \delta_f(\phi), \qquad (7.79)$$

which is a straightforward extension of (7.1).

Here, the free energy change $\Delta(\mathbf{j};\mathbf{l})$ accompanying the formation of a $(\mathbf{j};\mathbf{l})$-cluster in a hypothetical undiluted amorphous state from the separate primary molecules in their standard states is defined by

$$\Delta(\mathbf{j};\mathbf{l}) \equiv \beta \left[\mu^\circ(\mathbf{j};\mathbf{l}) - \sum_f l_f \mu^\circ(\mathbf{j}_{0f};\mathbf{l}_{0f}) \right]. \tag{7.80}$$

In the postgel regime, the last term for the gel part is necessary [9, 26].

By differentiating the free energy, we find the chemical potential

$$\beta \Delta \mu(\mathbf{j};\mathbf{l}) = 1 + \Delta(\mathbf{j};\mathbf{l}) + \ln \phi(\mathbf{j};\mathbf{l})$$
$$+ \left(\sum n_f l_f \right) \left[-\nu^S + \chi \phi_0^2 - \sum d_f^G \phi_f \right] + \sum n_f l_f d_f^G, \tag{7.81}$$

for the cluster of the type $(\mathbf{j};\mathbf{l})$,

$$\beta \Delta \mu_0 = 1 + \ln \phi_0 - \nu^S + \chi \phi^2 - \sum d_f^G \phi_f, \tag{7.82}$$

for the solvent molecule, and

$$\beta \Delta \mu_f^G = \delta_f + n_f \left[-\nu^S + \chi \phi_0^2 - \sum d_f^G \phi_f + d_f^G \right], \tag{7.83}$$

for a f-functional molecule in the gel, where ν^S, d_f^G are defined by

$$\nu^S \equiv 1 - \phi + \sum_{\mathbf{j};\mathbf{l}} \nu(\mathbf{j};\mathbf{l}), \qquad d_f^G \equiv \sum_g \frac{\partial \delta_g}{\partial \phi_f} \nu_g^G. \tag{7.84}$$

ν^S is the number of clusters and molecules that possess degree of freedom for translational motion.

We then impose chemical equilibrium conditions

$$\Delta \mu(\mathbf{j};\mathbf{l}) = \sum_f l_f \Delta \mu(\mathbf{j}_{0f};\mathbf{l}_{0f}), \tag{7.85}$$

to find the cluster size distribution function. The volume fraction of the clusters of a specified type is found to be

$$\phi(\mathbf{j};\mathbf{l}) = K(\mathbf{j};\mathbf{l}) \prod_f \phi(\mathbf{j}_{0f};\mathbf{l}_{0f})^{l_f}, \tag{7.86}$$

in terms of the volume fraction of the primary molecules that remain unassociated, where $K(\mathbf{j};\mathbf{l})$ is the equilibrium constant, and is related to the binding free energy as

$$K(\mathbf{j};\mathbf{l}) = \exp \left[\sum l_f - 1 - \Delta(\mathbf{j};\mathbf{l}) \right]. \tag{7.87}$$

In the postgel regime, we have the additional condition

$$\Delta\mu_f^G = \Delta\mu(\mathbf{j}_{0f}; \mathbf{l}_{0f}), \tag{7.88}$$

between the free molecule and the molecule bound to the gel network. Hence, we have the relation

$$\delta_f(\phi) = 1 + \ln\phi(\mathbf{j}_{0f}; \mathbf{l}_{0f}), \tag{7.89}$$

which is similar to (7.6).

Substituting the result (7.86) back into the starting free energy (7.79), we find it in the form of (5.37), where the association part is given by

$$\mathscr{F}_{AS}(\{\phi\}) = \sum_f \frac{\phi_f}{n_f} \ln\left(\frac{\phi_{0f}}{\phi_f}\right) + 1 - \phi + \sum_f \frac{\phi_f}{n_f} - \nu^S. \tag{7.90}$$

Here, $\phi_{0f} \equiv \phi(\mathbf{j}_{0f}; \mathbf{l}_{0f})$ is the volume fraction of f-molecules that remain unassociated in the solution. The number of different ways to form a cluster of the type $(\mathbf{j}; \mathbf{l})$ from separate primary molecules was found in the reaction theory of Section 3.3.

For the thermoreversible reaction under consideration, the probability p_k obeys the reaction equilibrium condition

$$\psi p_k / (\psi p_1)^k = K_k, \tag{7.91}$$

where

$$\psi \equiv \sum f N_f / \Omega \tag{7.92}$$

is the total number density of functional groups. Hence, p_k is given by

$$p_k = K_k \psi^{k-1} p_1{}^k. \tag{7.93}$$

Because there are $k-1$ bonds, we assume the form

$$K_k = \lambda(T)^{k-1} \gamma_k, \tag{7.94}$$

where $\lambda(T) = \exp(-\Delta f_0 / k_B T)$ is the association constant (Δf_0 being the binding free energy), and γ_k includes the free energy due to the existence of the surface on the micellar junction.

Substituting these relations into p_k and equilibrium constant $K(\mathbf{j}; \mathbf{l})$, and using the geometrical relations (3.74), the distribution function of the aggregates in terms of their number density is found to be

$$\lambda(T)\nu(\mathbf{j}; \mathbf{l}) = \left(\sum j_k - 1\right)! \left(\sum l_f - 1\right)! \prod_f \left(\frac{x_f^{l_f}}{l_f!}\right) \prod_k \left(\frac{\gamma_k^{j_k}}{j_k!}\right), \tag{7.95}$$

where

$$x_f \equiv f\lambda\nu(\mathbf{j}_{0f}; \mathbf{l}_{0f}) \equiv \lambda\psi\rho_f p_1{}^f \tag{7.96}$$

is the number density of unreacted primary molecules (multiplied by $f\lambda$).

Let us define

$$z \equiv \lambda \psi p_1, \qquad (7.97)$$

for the number density of *functional groups* that remain unassociated in the solution (scaled by the factor λ). The normalization condition $\sum p_k = 1$ then leads to the relation

$$\lambda \psi \equiv z\tilde{u}(z), \qquad (7.98)$$

by which we can find z as a function of the given concentration $\lambda \psi$. Here, the function $\tilde{u}(z)$ is defined by[1]

$$\tilde{u}(z) \equiv \sum_{k \geq 1} \gamma_k z^{k-1}. \qquad (7.99)$$

This relation can be transformed to

$$p_1 \tilde{u}(z) = 1. \qquad (7.100)$$

The reactivity (degree of association) α is related to the probability p_k by

$$p_1 = 1 - \alpha, \qquad (7.101)$$

or

$$\sum_{k \geq 2} p_k = \alpha, \qquad (7.102)$$

and hence we have the relation

$$\alpha = 1 - 1/\tilde{u}(z), \qquad (7.103)$$

which gives α as a function of the concentration and temperature. The number density x_f of unassociated primary molecules

$$x_f = (\lambda \psi) \rho_f p_1{}^f, \qquad (7.104)$$

can be written as

$$x_f = \rho_f \frac{z}{\tilde{u}(z)^{f-1}}, \qquad (7.105)$$

in terms of the parameter z, which is now a function of $\lambda \psi$.

7.4.3 The average molecular weight and the condition for the gel point

We first find the average molecular weight of the clusters for the distribution function $\nu(\mathbf{j};\mathbf{l})$. The number-average molecular weight defined by

$$\bar{l}_n \equiv \sum_{\mathbf{j};\mathbf{l}} \left(\Sigma n_f l_f\right) \nu(\mathbf{j};\mathbf{l}) / \sum_{\mathbf{j};\mathbf{l}} \nu(\mathbf{j};\mathbf{l}), \qquad (7.106)$$

---

[1] To distinguish from $u(x) \equiv \sum_{k \geq 1} p_k x^{k-1}$ in Section 8.2, we use the symbol $\tilde{u}$ for this function.

is found to be

$$\bar{l}_n = R \Big/ \left(\frac{1}{f_n} + \frac{1}{\bar{\mu}_n} - 1 \right), \tag{7.107}$$

where $\bar{\mu}_n$ is the number-average multiplicity of the junctions

$$\bar{\mu}_n \equiv \left(\sum \frac{p_k}{k} \right)^{-1}. \tag{7.108}$$

Substituting (7.93) for p_k, and using the relation between ψ and z, we find

$$\bar{\mu}_n = \tilde{u}(z)/\tilde{U}(z), \tag{7.109}$$

where the function $\tilde{U}(z)$ is the average of $\tilde{u}(z)$

$$\tilde{U}(z) \equiv \frac{1}{z} \int_0^z \tilde{u}(z) dz = \sum_{k \geq 1} \frac{\gamma_k}{k} z^{k-1}. \tag{7.110}$$

On the other hand, the weight-average molecular weight is defined by

$$\bar{l}_w \equiv \sum \left(\sum n_f l_f \right)^2 \nu(\mathbf{j};\mathbf{l}) \Big/ \sum \left(\sum n_f l_f \right) \nu(\mathbf{j};\mathbf{l}). \tag{7.111}$$

It is given by

$$\bar{l}_w = R \Big/ \left(\frac{1}{f_w} + \frac{1}{\bar{\mu}_w} - 1 \right). \tag{7.112}$$

Here, the weight-average multiplicity

$$\bar{\mu}_w \equiv \sum k p_k \tag{7.113}$$

has appeared. A calculation similar to $\bar{\mu}_n$ finds $\bar{\mu}_w$ as

$$\bar{\mu}_w = 1 + \frac{z\tilde{u}'(z)}{\tilde{u}(z)}. \tag{7.114}$$

The gel point where the weight-average molecular weight becomes infinite is found by the condition

$$(f_w - 1)(\bar{\mu}_w - 1) = 1, \tag{7.115}$$

or equivalently,

$$(f_w - 1)\frac{z\tilde{u}'(z)}{\tilde{u}(z)} = 1, \tag{7.116}$$

in terms of the parameter z. By combining with the relation (7.98) the sol–gel transition line is found on the phase plane.

7.4.4   Solution properties of thermoreversible gels with multiple junctions

Phase equilibria

Due to the association equilibrium condition, the chemical potential of solvent (7.82) and of f-functional molecules ($\mathbf{j}_{0f}, \mathbf{l}_{0f}$ in (7.81)) are transformed to

$$\beta \Delta \mu_0 = 1 + \ln(1-\phi) - \nu^{\mathrm{S}} + \chi \phi^2 - \left(\sum \delta'_f(\phi) \nu_f^{\mathrm{G}} \right) \phi, \tag{7.117}$$

and

$$\beta \Delta \mu_f / n_f = (1 + \ln x_f)/n_f - \nu^{\mathrm{S}} + \chi (1-\phi)^2 + \left(\sum \delta'_f(\phi) \nu_f^{\mathrm{G}} \right) (1-\phi), \tag{7.118}$$

where ν^{S} is

$$\lambda \nu^{\mathrm{S}} = \lambda(1-\phi) + z[(f_{\mathrm{n}}^{-1} - 1)\tilde{u}(z) + \tilde{U}(z)]. \tag{7.119}$$

The coexistence curve for a dilute phase with volume fraction ϕ^{α} to be in equilibrium with a concentrated phase with volume fraction ϕ^{β} is given by the coupled equations

$$\Delta \mu_0(\phi^{\alpha}, T) = \Delta \mu_0(\phi^{\beta}, T), \tag{7.120a}$$

$$\Delta \mu_f(\phi^{\alpha}, T) = \Delta \mu_f(\phi^{\beta}, T) \quad (f = 1, 2, \ldots). \tag{7.120b}$$

If the higher-concentration phase lies in the postgel regime, the postgel form of ν must be employed in the chemical potentials. These equilibrium conditions determine the total volume fractions ϕ^{α} and ϕ^{β} in each phase as well as the molecular distributions ρ_f^{α} and ρ_f^{β} in them.

Osmotic pressure

The osmotic pressure π is directly related to the solvent chemical potential through the relation (2.28) in Section 2.1. In the dilute region, this can be expanded in powers of the concentration

$$\pi \beta a^3 = \sum_{n=1}^{\infty} A_n \phi^n, \tag{7.121}$$

where the virial coefficients are formally written as

$$A_1 = 1/f_n R, \tag{7.122a}$$

$$A_2 = 1/2 - \chi - [\lambda(T)\gamma_2 / 2R^2], \tag{7.122b}$$

$$A_n = \frac{1}{n} \left\{ 1 - \frac{(n-1)\beta_{n-1}}{\lambda} \left(\frac{\lambda(T)}{R} \right)^n \right\} \quad \text{for} \quad n \geq 3. \tag{7.122c}$$

The coefficients β_n are the irreducible cluster coefficients [4] constructed from γ_k/k. The correction to the second virial coefficient is due to the existence of binary junctions ($k=2$), and should vanish if γ_2 in A_2 were made to vanish. Thus association does not affect the second virial coefficient if there is no binary cross-linking. The frequently

observed sudden gelation in physical gels without precursor suggests the dominance of high junction multiplicity.

The osmotic compressibility is found to be $K_T = \phi^2 \sigma(\phi, T)$ with

$$\sigma(\phi, T) \equiv \frac{1}{\bar{l}_{\mathrm{w}}(z)\phi} + \frac{1}{1-\phi} - 2\chi. \tag{7.123}$$

Stability analysis and Gibbs determinants

Let us consider the Gibbs determinant to study the stability of the homogeneous phase. Using Gibbs–Dühem relation described in Section 2.1, variation of one component among $0, f = 1, 2, \ldots$, can be expressed by the others. We take the solvent as the reference component, and consider the difference $\Delta\mu_f - \Delta\mu_0$. Its derivative by the composition of the g-component

$$G_{fg} \equiv \frac{\partial \beta(\Delta\mu_f - \Delta\mu_0)}{\partial \phi_g}, \tag{7.124}$$

for $g = 1, 2, \ldots$, serves as the (f, g) element of the Gibbs matrix. Specifically, it is

$$G_{fg} = \frac{1}{n_f} \frac{\partial}{\partial \phi_g} \sum_h \left(\delta_{fh} + \phi_h^G \frac{\partial}{\partial \phi_f} \right) \ln x_h + \frac{1}{1-\phi} - 2\chi. \tag{7.125}$$

The determinant $G \equiv |G_{fg}|$ of this matrix must be positive definite for the system to be thermodynamically stable.

For monodisperse primary chains, we have a strictly two-component system, and the thermodynamic stability limit (spinodal) is given by $\sigma(\phi, T) = 0$, where σ is the factor (7.123). Further, for such strictly binary systems, the critical solution point, if it exists in the pregel regime, can be found by the additional condition $\partial^2 \Delta\mu_0 / \partial \phi^2 = 0$. The condition is given explicitly by

$$\bar{l}_{\mathrm{z}}(\phi_c) / \bar{l}_{\mathrm{w}}(\phi_c)^2 = \phi_c^2 / (1 - \phi_c)^2. \tag{7.126}$$

For systems with polydisperse primary chains, the spinodal and critical conditions have to be determined from the appropriate Gibbs determinants.

7.4.5 Simple models of junction multiplicity

The multiplicity of the junctions is in principle determined automatically by the equilibrium requirement for a given associative interaction. In the case of hydrophobic interaction, the chain length of a hydrophobe, the strength of water–hydrophobe interaction, the geometric form of an aggregate, and other factors determine the association constant $\lambda(T)$ and the junction multiplicity k. For practical treatment, we avoid complexity in finding the precise form of the coefficients γ_k, but instead, we introduce model junctions [26].

In one of the practical models in commmon use, multiplicities lying in a certain range covering from $k = k_0$ to k_m are equally allowed (**mini-max junction**). In such cases we have

$$k = 1 \quad \text{(free)}, \qquad k = k_0, k_0 + 1, ..., k_m \quad \text{(associated)}. \tag{7.127}$$

The junction function takes the form

$$\tilde{u}(z) = 1 + \sum_{k=k_0}^{k_m} z^{k-1} = 1 + (z^{k_0-1} - z^{k_m})/(1 - z). \tag{7.128}$$

Such assumption of limited range can be, to some extent, justified in the case of micelles of hydrophobic chains [27].

When only a single value is allowed, i.e., $k_0 = k_m \equiv k$, we call the model the **fixed multiplicity model**. Thus, for $k = 2$, the fixed multiplicity model reduces to the pairwise association. The normalization relation (7.98) for the fixed multiplicity model of monodisperse polymers (f and n definite) is given by

$$\lambda(T)\psi = \alpha^{1/(k-1)}/(1 - \alpha)^{k/(k-1)}, \tag{7.129}$$

in terms of the extent α. This is the extension of (7.33) for pairwise junctions to multiple junctions. The gel point condition (3.77) gives $(f - 1)(k - 1)\alpha = 1$ and hence

$$\alpha^* \equiv 1/(f - 1)(k - 1), \tag{7.130}$$
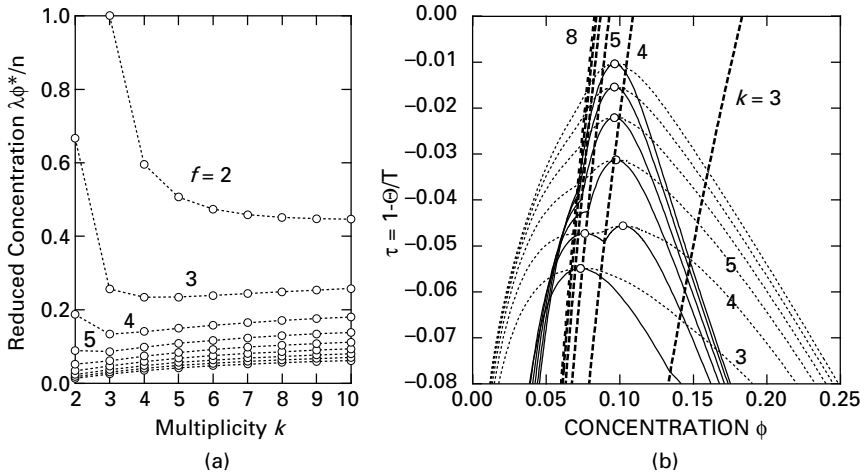
Fig. 7.6 (a) Reduced concentration $\lambda(T)\phi^*/n$ at the gel point plotted against junction multiplicity. The functionality is varied from curve to curve. (b) Sol–gel transition lines (thick broken lines), binodals (thin broken lines), and spinodal lines (solid lines) of bifunctional ($f = 2$) polymers with $n = 100$, $\lambda_0 = 10.0$ for association with fixed multiplicity ($k_0 = k_m \equiv k$). The multiplicity k is changed from 3 to 8.

which leads to the critical concentration

$$\lambda(T)\psi^* = \frac{(f-1)(k-1)}{[(f-1)(k-1)-1]^{k/(k-1)}}.\tag{7.131}$$

Figure 7.6(a) plots the reduced concentration $\lambda(T)\phi^*/n$ at the gel point as a function of the junction multiplicity. The functionality is changed from curve to curve. For bifunctional molecules $f = 2$, at least multiplicity 3 is necessary for gelling. The gelation concentration monotonically decreases with multiplicity. For functionalities higher than 2, however, there is an optimal multiplicity for which gelation is easiest. In such cases, network growth becomes difficult due to an increase in the number of branches at the junctions.

Figure 7.6(b) shows how the phase diagrams shift with increase in the multiplicity for bifunctional molecules. The sol–gel transition line (thick broken lines), binodals (thin broken line), and spinodals (solid lines) are drawn for a fixed multiplicity within Flory's postgel treatment. The transition line shifts to the high-temperature, low-concentration regions with the multiplicity. Above a certain critical multiplicity ($k = 5$ in the figure) the two critical solution points merge into one, and the phase diagram changes from the CEP type to the TCP type.

References

[1] Tanaka, F., *Macromolecules* **22**, 1988 (1989).

[2] Tanaka, F., *Macromolecules* **1990**, *23*, 3784; 3790.

[3] Tanaka, F., in *Molecular Gels–Materials with Self-Assembled Fibrillar Networks*, Terech, P.; Weiss, R. G. (eds.). Springer: Dordrecht, 2006; pp. 1–68.

[4] Mayer, J. E.; Mayer, M. G., *Statistical Mechanics*. Wiley: New York, 1940.

[5] Flory, P. J., *J. Am. Chem. Soc.* **63**, 3091 (1941).

[6] Stockmayer, W. H., *J. Chem. Phys.* **11**, 45 (1943).

[7] Stockmayer, W. H., *J. Chem. Phys.* **12**, 125 (1944).

[8] Flory, P. J., *Principles of Polymer Chemistry*. Cornell University Press: Ithaca, New York, 1953.

[9] Ishida, M.; Tanaka, F., *Macromolecules* **30**, 3900 (1997).

[10] Tanaka, F. *Polym. J.* **34**, 479 (2002).

[11] Knobler, C. M.; Scott, R. L., in *Phase Transitions and Critical Phenomeca*. Academic Press: New York, 1984.

[12] Pynn, R.; Skjeltorp, A., in *Multicritical Phenomena*. Plenum Press: New York and London, 1984.

[13] Wellinghoff, S.; Shaw, J.; Baer, E., *Macromolecules* **12**, 932 (1979).

[14] Tan, H. M.; Moet, A.; Hiltnet, A.; Baer, E., *Macromolecules* **16**, 28 (1983).

[15] Boyer, R. F.; Baer, E.; Hiltner, A., *Macromolecules* **18**, 427 (1985).

[16] Domszy, R. C.; Alamo, R.; Edwards, C. O.; Mandelkern, L., *Macromolecules* **19**, 310 (1986).

[17] Gan, J. Y. S.; Francois, J.; Guenet, J. M., *Macromolecules* **19**, 173 (1986).

[18] Guenet, J. M.; McKenna, G. B., *Macromolecules* **21**, 1752 (1988).

[19] Guenet, J. M., *Thermoreversible Gelation of Polymers and Biopolymers*. Academic Press: New York, 1992.

[20] Chen, S.-J.; Berry, G. C.; Plazek, D. J., *Macromolecules* **28**, 6539 (1995).

[21] London, F., *Superfluids*, Vol. II. Wiley: New York, 1954.

[22] Truesdell, C., *Annals of Mathematics* **46**, 144 (1945).

[23] te Nijenhuis, K., *Adv. Polym. Sci.* **130**, 1 (1997).

[24] Fukui, K.; Yamabe, T., *Bull. Chem. Soc. Jpn* **40**, 2052 (1967).

[25] Stockmayer, W. H., *Macromolecules* **24**, 6367 (1991).

[26] Tanaka, F.; Stockmayer, W. H., *Macromolecules* **27**, 3943 (1994).

[27] Tanaka, F.; Koga, T., *Bulletin Chem. Soc. Jpn* **74**, 201 (2001).

8 Structure of polymer networks

This chapter studies the local and global structures of polymer networks. For the local structure, we focus on the internal structure of cross-link junctions, and study how they affect the sol–gel transition. For the global structure, we focus on the topological connectivity of the network, such as cycle ranks, elastically effective chains, etc., and study how they affect the elastic properties of the networks. We then move to the self-similarity of the structures near the gel point, and derive some important scaling laws on the basis of percolation theory. Finally, we refer to the percolation in continuum media, focusing on the coexistence of gelation and phase separation in spherical colloid particles interacting with the adhesive square well potential.

8.1   Local structure of the networks–cross-linking regions

Most physical gels have complex multiple junctions. In Section 7.4, we studied thermoreversible gelation with junctions of variable multiplicity. In this section, we consider a new method to find the local structure of the networks, i.e., the structure of the network junctions.

Junction multiplicity k was defined by the number of chains connected to a single junction. Simple pairwise cross-links, for example, have multiplicity $k = 2$, whose sol–gel transition is detailed in Section 7.4 and in the classical literature [1]. For networks with junctions of multiplicity larger than two, the conventional Eldridge–Ferry procedure [2] to find the enthalpy of melting, which plots the logarithm of the gelation concentration $\ln c^*$ against the inverse temperature, does not work because it assumes pairwise cross-linking.

To find the number of statistical units taking part in a junction, let us consider a simple model junction that binds k chains with ζ sequential units per chain (Figure 8.1(a)). This model is suitable for the description of thermoreversible gels with junctions formed by **fringed-micellar crystallites**, but finds application to other important types of junctions.

The **Eldridge–Ferry method** [2] gives the total enthalpy melting ΔH_0 of a junction by finding the slope of $\ln c^*$ against $1/T$ through the relation

$$\ln c^* = \Delta H_0 / k_B T + \text{constant}, \tag{8.1}$$

where c^* is the gelation concentration, and T the absolute temperature. The enthalpy ΔH_0 is expected to be proportional to the number of segments participating in the junction. Since the total number of segments involved in a junction is given by ζk for
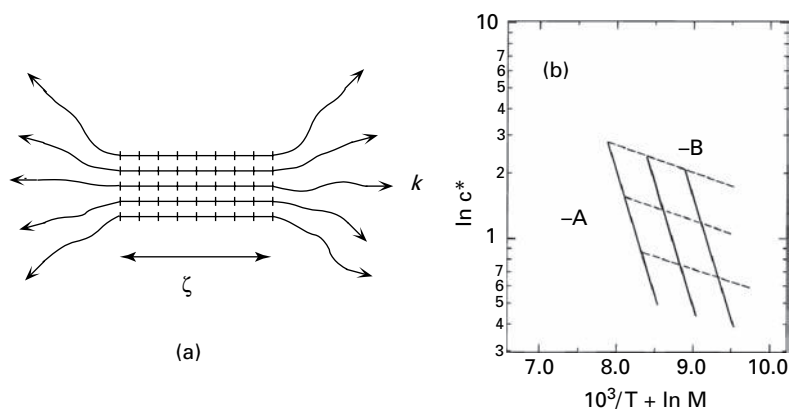
Fig. 8.1   (a) Model of a network junction. The multiplicity k and cross-link length ζ are two fundamental parameters for characterization of a junction. (b) Schematic drawing of the modified Eldridge–Ferry plot to find the junction multiplicity k and the number ζ of repeat units per chain in the junction. The constant temperature lines (broken lines) and constant molecular weight lines (solid lines) are shown.

the model junction described above, this equation holds under additional assumption that the sol–gel transition is independent of the junction multiplicity k, but depends only on the total number of segments ζk in a junction. This assumption, however, is incorrect in the case of multiple cross-links, because gelation is easier for higher multiplicity even if the total number of segments involved in a junction is the same [3]. We showed in Figure 7.6(b) [3] that the sol–gel transition line shifts toward the high-temperature, low-concentration region as the junction multiplicity is increased under a fixed association constant.

Another equation from which the Eldridge–Ferry method starts is the relation between the molecular weight M of a polymer and the gel melting temperature. It is given by

$$\ln M = \Delta H_0 / m k_{\mathrm{B}} T + \text{constant}, \tag{8.2}$$

where m is an integer to be adjusted to satisfy several thermodynamic requirements. (It was chosen as $m = 7$ in the original paper [2] under several assumptions.) This equation is more hypothetical than the first, and lacks molecular-theoretical justification.

In Section 7.4, we found the gelation concentration as a function of the number n of statistical units on a chain, its functionality f, and the junction multiplicity k. The result is given by (7.115)

$$\lambda(T)\phi^* / n = f'k' / f(f'k' - 1)^{k/k'}, \tag{8.3}$$

where ϕ^* is the volume fraction of the polymer at gelation, $f' \equiv f - 1$, and $k' \equiv k - 1$. The association constant $\lambda(T)$ is $\lambda(T) = \exp(-\beta \Delta f_0)$, where Δf_0 is the standard free energy change *per functional group*, i.e., the free energy change on binding a single functional group into a junction.

When a functional group involves ζ sequential repeat units as in the model junction, we can write the standard free energy change as

$$\Delta f_0 = \zeta(\Delta h - T\Delta s). \tag{8.4}$$

Here Δh is the enthalpy of bonding and Δs the entropy of bonding, both measured *per single repeat unit*. Taking the logarithm of (8.3), we find an important relation

$$\ln \phi^* = \zeta \frac{\Delta h}{k_B T} + \ln\left[\frac{f'k'n}{f(f'k'-1)^{k/k'}}\right] - \zeta \frac{\Delta s}{k_B}, \tag{8.5}$$

from which we find ζ and k.

For the model junction introduced above, each ζ sequence of repeat units along a chain may be regarded as a functional group. A polymer chain then carries $f = n/\zeta$ functional groups. Since we have large n, and hence large f, we can neglect 1 compared to n or f. We are thus led to an equation

$$\ln c^* = \zeta \frac{\Delta h}{k_B T} - \frac{1}{k-1} \ln M + \text{constant}, \tag{8.6}$$

where the weight concentration c^* has been preferred to the volume fraction. This equation enables us to find ζ and k independently from the data of c^*.

Let us plot $\ln c^*$ against $10^3/T + \ln M$. Then the slope $-B$ of the line at constant T gives $-1/(k-1)$, while the slope $-A$ of the line at constant M gives

$$\zeta = \frac{10^3 k_B}{|\Delta h|} A = \frac{10^3 R}{|(\Delta h)_{\text{mol}}|} A, \tag{8.7}$$

where $(\Delta h)_{\text{mol}}$ is the enthalpy of bonding per mol of the repeat units. This **modified Eldridge–Ferry procedure** is depicted schematically in Figure 8.1(b) [4–6].

As an example of the analysis, we consider the melting point of poly(vinyl alcohol) (PVA) gels in water. PVA is known to be a typical crystalline polymer, but it also gels in aqueous solution under large supercooling. There are several experimental evidences that the cross-links are formed by partial crystallization of the polymer segments in which syndiotactic sequence dominates, while subchains connecting the junctions consist of atactic non-crystalline sequences on the PVA chains [7]. The micro-crystals at the junctions are supposed to be stabilized by hydrogen bonds between the hydroxy groups.

Figure 8.2 shows the result of our modified Eldridge–Ferry plot for the gel melting concentration. The gel melting temperature T_m is estimated from the temperature at which the DSC heating curve shows an endotherm peak. The slope of the solid lines with
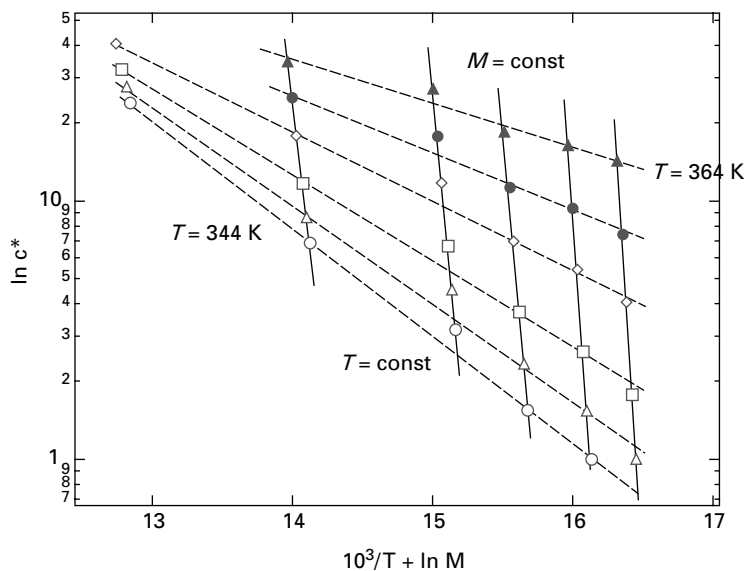
Fig. 8.2   Modified Eldridge–Ferry analysis for aqueous poly(vinyl alcohol) solutions. The gel melting concentration c^* measured at a constant temperature for different molecular weight polymers plotted against the molecular weight finds the junction multiplicity from the slope (broken lines), while those measured at constant molecular weight by changing the temperature find the number of the repeat units per chain in the junction (solid lines). (▲) 91°C; (●) 87°C; (◇) 83°C; (□) 78°C; (△) 74°C; (○) 71°C. (Reprinted with permission from Ref. [6].)

constant molecular weight gives $-A = 13.43$ almost independently of their molecular weights. Hence we find $\zeta = 26.7\,\text{kcal}\,\text{mol}^{-1}/|(\Delta h)_{\text{mol}}|$. If we use the heat of fusion $(\Delta h)_{\text{mol}} = 1.64\,\text{kcal}\,\text{mol}^{-1}$ in the bulk crystal [8], we find $\zeta = 16.3$. On the other hand, the slope of the dotted lines with constant temperature depends on their temperature. At the highest temperature $T = 91°C$ in the measurement, it is -0.38, while it gives a larger value of -0.9 at $T = 71°C$. The average multiplicity is estimated to decrease from 3.6 for high-temperature melting to 2.1 for low-temperature melting. From the thermodynamic stability of the junctions, a gel which has smaller junctions melts at lower temperature.

8.2   Global structure of the networks – elastically effective chains and elastic modulus

8.2.1   Fundamental parameters of the network topology

To characterize the global structure and connectivity of the networks, we start with the definition of the cross-links of the type (i, k); they are junctions of multiplicity k with a total of i paths connected to the network matrix (Figure 8.3). If chains carry no functional groups at their ends, the **path number** varies in the range $0 \leq i \leq 2k$. For end functional
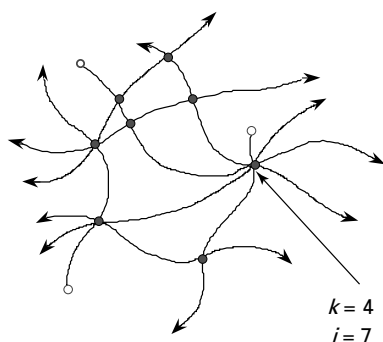
Fig. 8.3   Multiplicity k and path number i of a network junction.
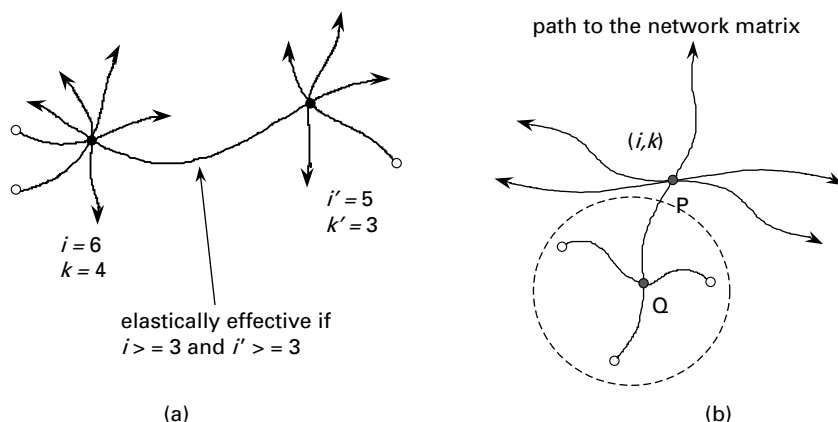
Fig. 8.4   (a) Scanlan–Case criterion to find the elastically effective chains. A chain with both ends connected to junctions with a path number larger or equal to 3 is elastically effective. (b) End group (dotted circle) and its branch point P.

groups, in particular telechelic polymers, there is only one path from a functional group in a junction, so that the path number varies in $0 \leq i \leq k$.

Let $\mu_{i,k}$ be the number of cross-link junctions of the type (i,k) in the network. The number of junctions of multiplicity k is

$$\mu_k = \sum_{i=1}^{2k} \mu_{i,k}. \tag{8.8}$$

The upper limit depends on whether there is an end group or not.

In Section 4.2, we introduced the Scanlan–Case (SC) criterion to find the elastically effective junctions and chains. SC proposes that a chain with both ends connected to **elastically effective junctions** (junctions whose path number is larger or equal to three) is elastically effective (Figure 8.4(a)) [9, 10].

The number of elastically effective junctions can be found by the sum

$$\mu_{\text{eff}} = \sum_{k=2}^{\infty} \sum_{i=3}^{2k} \mu_{i,k}. \tag{8.9}$$

Converting this to the number of chains, the number of elastically effective chains can be found by

$$\nu_{\text{eff}} = \frac{1}{2} \sum_{k=2}^{\infty} \sum_{i=3}^{2k} i \mu_{i,k}, \tag{8.10}$$

since an (i,k) junction has i paths. Double counting is corrected by dividing the sum by 2.

Next, let us count the number of branches that are dangling from a cross-link and free from external stress. Figure 8.4(b) shows an end group whose entire body is connected to the network by a single junction P of multiplicity k. This junction at the root is a **branch point**, and the group dangling from it is an **end group**. There may be some junctions in the end group, such as Q in the figure, from which **end branches** are extended. The number of end groups is the same as the number of the branch points, and hence we have

$$\nu_{\text{end}} = \sum_{k=2}^{\infty} \sum_{i=2}^{2k} (2k - i) \mu_{i,k}. \tag{8.11}$$

The number $2k - i$ is the number of paths that are not connected to the network matrix. The sum on i starts from 2 because $i = 1$ indicates that the branch point is the end branch point that has already been counted. The end groups do not contribute to elasticity of the network because they are free from external stress, but they contribute to the viscosity and the relaxation time of the network due to friction with the solvent molecules.

8.2.2   Structure parameters of multiply cross-linked gels

We generalize the treatments of the postgel regime by Pearson–Graessley [11–13] in classical gelation theory to multiple junctions [14]. Let q_k $(k = 2, 3, 4, \ldots)$ be the junction distribution defined by the number of functional groups in k-junctions divided by the total number of functional groups contained in the junctions (Figure 8.5(a)). The multiplicity $k = 1$ is excluded for true cross-links.

Let p_k $(k = 1, 2, 3, \ldots)$ be the probability for a randomly chosen functional group in the system to be in a k-junction, as in Section 7.4. The junction distribution is described by

$$q_k = p_k / \sum_{k \geq 2} p_k. \tag{8.12}$$

The probability p_1 for a functional group to remain unassociated can be expressed as $p_1 = 1 - \alpha$ in terms of the extent α of reaction

$$\alpha \equiv \sum_{k \geq 2} p_k. \tag{8.13}$$
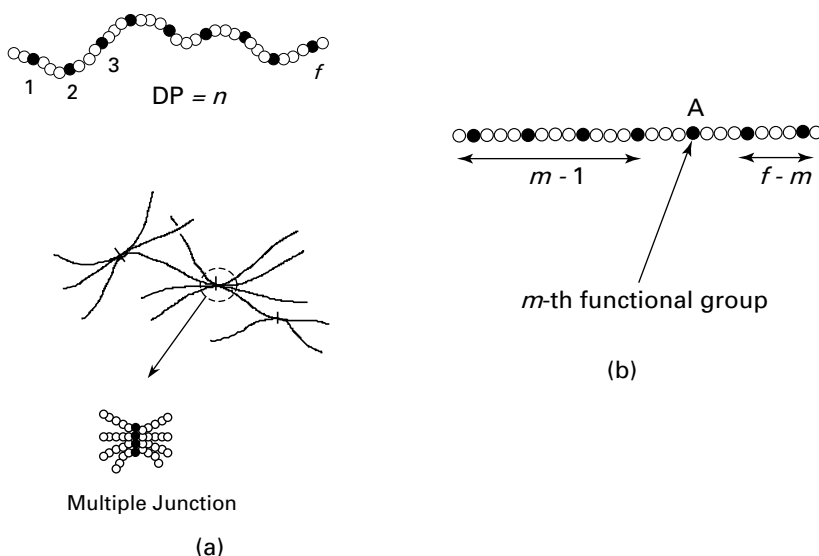
Fig. 8.5 (a) Model network consisting of f-functional primary polymer chains cross-linked by multiple junctions. (b) Connection probability. The probability ζ_j of connection through j paths are described using the parameter u.

We then have the relation

$$p_k = \alpha q_k, \tag{8.14}$$

for $k \geq 2$.

Connection probability

To study the connectivity of the network, we regard the cross-link junctions as **vertices**, and subchains as **paths** connecting the vertices in conventional graph theoretical terminology. Let ζ_j be the probability for an arbitrarily chosen *unreacted* functional group to be connected to the network matrix through j paths. For instance, $j = 0$ if the functional group belongs to a cluster of finite size that is separated from the network. Since we consider linear chains only as primary molecules, j takes only the values $0, 1, 2$.

Let u be the probability for an arbitrarily chosen functional group (A in Figure 8.5(b)) to be either unreacted or connected to the finite cluster in the sol. The probability ζ_0 is given by the condition that all functional groups on both sides of this chosen functional group on the chain are connected to the sol by probability u, and hence it is given by

$$\zeta_0 = \frac{1}{f} \sum_{m=1}^{f} u^{m-1} u^{f-m} = u^{f-1}. \tag{8.15}$$

Similarly, the paths on the both sides must be connected to the matrix for ζ_2, given by

$$\zeta_2 = \frac{1}{f} \sum_{m=1}^{f} (1 - u^{m-1})(1 - u^{f-m}) = 1 + u^{f-1} - \frac{2(1 - u^f)}{f(1-u)}. \tag{8.16}$$

From the normalization condition that the sum of the probability is unity, the remaining probability is given by

$$\zeta_1 = 1 - \zeta_0 - \zeta_2 = 2\left\{ \frac{1 - u^f}{f(1-u)} - u^{f-1} \right\}. \tag{8.17}$$

The probability u can be expressed in terms of ζ_0 by (8.15). The probability for an arbitrarily chosen functional group to be unreacted is $1 - \alpha$, to be connected only to the sol is $\alpha q_k \zeta_0^{k-1}$ if the connected functional group belongs to a k junction. Therefore, u turns out to be

$$u(\zeta_0) = 1 - \alpha + \alpha \sum_{k \geq 2} q_k \zeta_0^{k-1} \equiv 1 - \alpha + \alpha \theta(\zeta_0), \tag{8.18}$$

where a new function $\theta(x)$ is defined by

$$\theta(x) \equiv \sum_{k \geq 2} q_k x^{k-1}. \tag{8.19}$$

Also, from (8.14) and $p_1 = 1 - \alpha$, we have

$$u(\zeta_0) = \sum_{k \geq 1} p_k \zeta_0^{k-1}, \tag{8.20}$$

which is related to the function introduced in (7.99).[1]

From (8.15), the relation $u^{f-1} = \zeta_0$ holds, so that ζ_0 is a solution of the equation

$$x = \{1 - \alpha + \alpha \theta(x)\}^{f-1}, \tag{8.21}$$

lying in the region $0 < x < 1$ ($x = 1$ is always a solution. Hence ζ_0 is another solution smaller than 1).

If the primary molecules are an assembly of molecules carrying different numbers of functional groups, the equation for ζ_0 is given by

$$x = \sum_f \rho_f \{1 - \alpha + \alpha \theta(x)\}^{f-1}, \tag{8.22}$$

by using the distribution ρ_f of the functional groups.

The weight-average junction multiplicity is given by

$$\overline{\mu}_w \equiv \sum_{k \geq 1} k p_k = 1 - \alpha + \alpha \sum_{k \geq 2} k q_k, \tag{8.23}$$

---

[1] The function $\tilde{u}(z) \equiv \sum_{k \geq 1} \gamma_k z^{k-1}$ is derived from $u(x) \equiv \sum_{k \geq 1} p_k x^{k-1}$ by substituting the relation $p_k = \gamma_k (\lambda \psi)^{k-1}$.

ζ_0
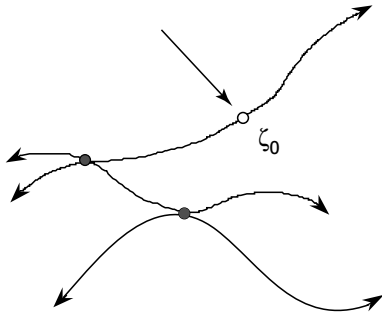
Fig. 8.6   Method to find the sol fraction.

using the probability q_k.

From the relation

$$\sum_{k\geq 2} kq_k = 1+\theta'(1), \tag{8.24}$$

by the help of the condition $\overline{\mu}_w - 1 = \alpha\theta'(1)$ of (8.23), the gel point is found by

$$\alpha\theta'(1)(f_w - 1) = 1, \tag{8.25}$$

in terms of the derivative of the function $\theta(x)$.

The sol fraction $1 - w$ is given by

$$1 - w = (1-\alpha)\zeta_0 + \alpha\theta(\zeta_0)\zeta_0 = \zeta_0 u(\zeta_0), \tag{8.26}$$

in terms of ζ_0, where the first term is the probability for an unreacted group to be not connected to the gel, and the second term is the probability that it is connected to the sol (Figure 8.6).

Effective junctions and effective chains

The total number of the junctions of multiplicity k is

$$\mu_k \equiv \sum_{i=0}^{2k} \mu_{i,k} = (f\nu\alpha)(q_k/k), \tag{8.27}$$

where ν is the total number of primary chains, and $f\nu\alpha$ is the number of reacted functional groups.

To find the number $\mu_{i,k}$ of the (i,k) junctions, let us first introduce the fraction $t_{i,k}$ of the junctions with path number i among the total μ_k of junctions of multiplicity k. Then the relation

$$\mu_{i,k} = \mu_k t_{i,k} \tag{8.28}$$

enables us to find the number of junctions of the type (i,k) from $t_{i,k}$. The fraction $t_{i,k}$ is found in the following way.
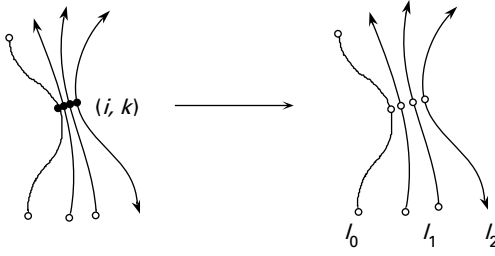
Fig. 8.7   The separation of an (i,k) junction.

First, we focus on an (i,k) junction. If all its bonds were cut, and the functional groups were separated from each other, a total of k independent paths would be generated (Figure 8.7).

Assume that, among these separated paths, the number l_0 is not connected to the network matrix, the number l_1 is singly connected, and the number l_2 is doubly connected. The probability $t_{i,k}$ is then

$$t_{i,k} = \sum_{\{l\}} \frac{k!}{l_0! l_1! l_2!} \zeta_0^{l_0} \zeta_1^{l_1} \zeta_2^{l_2}, \tag{8.29}$$

where the two relations $l_0 + l_1 + l_2 = k$, $l_1 + 2l_2 = i$ hold. If we write $l_2 = m$, we have $l_0 = k - i + m$, $l_1 = i - 2m$. The number m can vary $m = 0, 1, 2, \ldots, i/2$ for a given k.

From (8.27) and (8.29), we find the fundamental relation

$$\mu_{i,k} = (f \nu \alpha) q_k \sum_{m=0}^{i/2} \frac{(k-1)!}{(k-i+m)!(i-2m)!m!} \zeta_0^{k-i+m} \zeta_1^{i-2m} \zeta_2^m. \tag{8.30}$$

On substitution of this relation into the SC criterion (8.9), we find that the number of effective junctions is

$$\mu_{\text{eff}} = (f \nu \alpha) \left\{ \int_{\zeta_0}^1 \theta(x)dx - (\zeta_1 + \zeta_2)\theta(\zeta_0) - \frac{1}{2}\zeta_1^2 \theta'(\zeta_0) \right\}, \tag{8.31}$$

as a function of $\theta(\zeta_0)$ and its derivative $\theta'(\zeta_0)$, where ζ_0 is the solution of (8.21), which is smaller than 1. Similarly, the number of effective chains is

$$\nu_{\text{eff}} = \frac{1}{2}(f \nu \alpha) \left\{ (2\zeta_2 + \zeta_1)[1 - \theta(\zeta_0)] - \zeta_1^2 \theta'(\zeta_0) \right\}, \tag{8.32}$$

and the number of the end groups is

$$\nu_{\text{end}} = (f \nu \alpha) \left\{ (2\zeta_0 + \zeta_1)[1 - \theta(\zeta_0)] - 2\zeta_0 \zeta_1 \theta'(\zeta_0) \right\}. \tag{8.33}$$

The total number of the branch points in the end groups is

$$\mu_{\text{d}} = (f \nu \alpha)\theta(\zeta_0)\zeta_1. \tag{8.34}$$

These structural parameters enable us to find the global properties, such as the average length of the effective chains

$$n_{\text{eff}} = (nv)\zeta_2/v_{\text{eff}}, \tag{8.35}$$

and the average DP of the end groups

$$n_{\text{d}} = (nv)\zeta_1/v_{\text{end}}. \tag{8.36}$$

Telechelic chains

For the functional groups at the chain ends, the counting of paths is slightly different. In particular for the polymers carrying the functional groups at both ends, there remain no free ends in the completion of reaction $\alpha \to 1$, and hence $v_{\text{end}} \to 0$.

Let us study telechelic polymers ($f = 2$) in more detail. It is impossible for an unreacted group to have a double path $j = 2$ because it is at the chain end, and hence $\zeta_2 \equiv 0$ (Figure 8.8(a)). Also, because $\zeta_0 = u$ and $\zeta_1 = 1 - u$ for $f = 2$, we have

$$t_{i,k} = \frac{k!}{i!(k-i)!}\zeta_0^{k-i}\zeta_1^i, \tag{8.37}$$

for a junction of the type (i,k), where i varies as $0 \le i \le k$. The number of effective junctions is

$$\mu_{\text{eff}} = \sum_{k=3}^{\infty}\sum_{i=3}^{k}\mu_{i,k}, \tag{8.38}$$

since the maximum value of the path number i is k. This gives the same result as (8.31) with $\zeta_2 = 0$.

to matrix

dangling end

$k = 9, \quad i = 6$

(a)

(b)
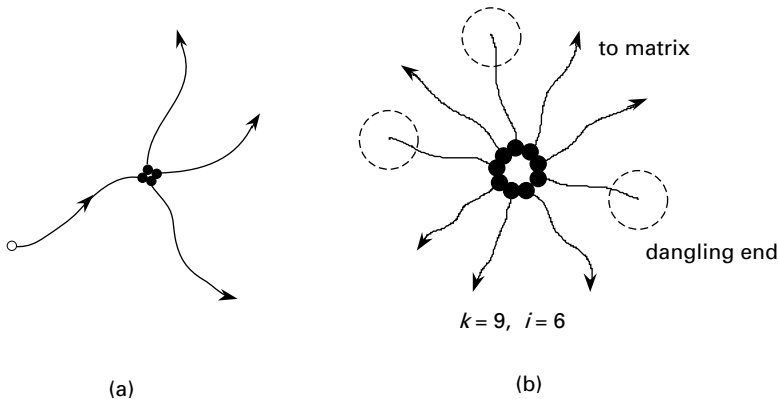
Fig. 8.8   (a) Connection paths of the telechelic polymers. (b) A cross-link junction formed by the functional groups of the telechelic polymers.

Similarly, the number of effective chains is

$$\nu_{\text{eff}} = \frac{1}{2} \sum_{k=3}^{\infty} \sum_{i=3}^{k} i \mu_{i,k}, \tag{8.39}$$

which is the same as (8.32) with $\zeta_2 = 0$. But the number of end groups

$$\nu_{\text{end}} = \sum_{k=2}^{\infty} \sum_{i=2}^{k} (k-i) \mu_{i,k}$$
$$= (f \nu \alpha)[1 - \theta(\zeta_0) - \zeta_1 \theta'(\zeta_0)]\zeta_0, \tag{8.40}$$

is different from the previous result. In the limit of $\alpha \to 1$, the relation $\nu_{\text{end}} \to 0$ is confirmed by $\zeta_0 \to 0$ (Figure 8.8(b)).

8.2.3   The number of elastically effective chains

We start from the definition of the function $u(x)$ (8.20) and $\tilde{u}(x)$ (7.99). They are related by

$$u(x) = (1-\alpha)\tilde{u}(zx), \tag{8.41}$$

where the parameter z is defined by $z \equiv \lambda(T)\psi p_1$. From the definition of the function $\theta(x)$, we find

$$\theta(x) = \frac{1-\alpha}{\alpha}[\tilde{u}(zx) - 1]. \tag{8.42}$$

The normalization condition $u(1) = 1$ then gives a relation (7.103)$(1-\alpha)\tilde{u}(z) = 1$. After eliminating α from (8.42), we find

$$\theta(x) = (\tilde{u}(zx) - 1)/(\tilde{u}(z) - 1), \tag{8.43}$$

which gives the function $\theta(x)$ in terms of the concentration.

Similarly, to find the zero path probability (8.22) is transformed to

$$x = [\tilde{u}(zx)/\tilde{u}(z)]^{f-1}. \tag{8.44}$$

The smaller solution x_1 of this equation can now be found as a function of $\lambda\psi$.

Finally we can readily check that $\theta(1) = 1$ holds, and its derivative is given by

$$\theta'(1) = \frac{d \ln[\tilde{u}(z) - 1]}{d \ln z}. \tag{8.45}$$

On substitution into the sol–gel transition criterion (8.25) and by the use of the relation (10.147), we find an equation

$$(f-1)\frac{d \ln \tilde{u}(z)}{d \ln z} = 1, \tag{8.46}$$

for finding the critical value of z as a function of the functionality and the multiplicity. This is the same as (7.116).

Before studying specific models of the junctions, we derive asymptotic forms of the network parameters in the extreme limit of complete reaction $\alpha \to 1$. In this limit, the smaller root of (8.44) goes to zero ($x_1 \to 0$), and hence

$$\zeta_0 \to 0, \tag{8.47a}$$

$$\zeta_1 \to 2/f, \tag{8.47b}$$

$$\zeta_2 \to 1 - 2/f. \tag{8.47c}$$

The effective chains and junctions therefore show a limiting behavior

$$\frac{\nu_{\text{eff}}}{\nu} \to f' - \frac{2}{f} q_2, \tag{8.48a}$$

$$\frac{\mu_{\text{eff}}}{\nu} \to \frac{f}{\bar{k}_n} - \frac{2}{f} q_2, \tag{8.48b}$$

where

$$\bar{k}_n \equiv \left(\sum_{k \geq 2} q_k/k \right)^{-1} \tag{8.49}$$

is the number-average junction multiplicity. For the dangling ends we find

$$\frac{\nu_{\text{end}}}{\nu} \to 2, \tag{8.50}$$

as expected, because only the two ends of the primary chains remain dangling at the completion of association.

In contrast, for telechelic polymers, we are led to the asymptotic behavior $\nu_{\text{end}}/\nu \to 0$ from (8.40), again as expected.

The first model we study allows only one fixed number k of the functional groups in a junction. We therefore have only $k = 1$ (unreacted) and k (reacted). Since $q_k = 1$, with the other q_k being zero, we find $\theta(x) = x^{k'}$, where $k' \equiv k - 1$, and

$$\tilde{u}(z) = 1 + z^{k'}. \tag{8.51}$$

Now the equation to find x_1 takes the form

$$x = (1 - \alpha + \alpha x^{k'})^{f'}, \tag{8.52}$$

whose solution is formally given by

$$x_1 = \left[\frac{\alpha'(1-\alpha)}{\alpha(1-\alpha')} \right]^{1/k'}. \tag{8.53}$$

Here α' is a solution of the equation

$$(\alpha')^{1/k'}(1-\alpha')^{f'-1/k'} = \alpha^{1/k'}(1-\alpha)^{f'-1/k'}, \tag{8.54}$$

which lies in the pregel regime ($\alpha' < \alpha^*$) for a given value of α ($> \alpha^*$). This smaller root refers to the average extent of reaction in the sol.

The simplest case is the pairwise association $k = 2$ for arbitrary functionality f. The number of elastically effective chains was calculated by Clark and Ross-Murphy [15]. Their result can be reproduced by choosing the function $\tilde{u}(x)$ as $\tilde{u}(x) = 1 + x$. Straightforward calculation leads to the result

$$\nu_{\text{eff}}/\nu = f\alpha(3\zeta_1 + 2\zeta_2)\zeta_2/2, \tag{8.55a}$$

$$\mu_{\text{eff}}/\nu = f\alpha(2\zeta_1 + \zeta_2)\zeta_2/2, \tag{8.55b}$$

where the values of ζ are found by (8.15)–(8.17) with x_1 being the root of (8.52). The above formulae for the effective chains and junctions were first derived by Langley [13]. For trifunctional ($f = 3$) primary chains, we find explicitly that

$$\nu_{\text{eff}}/\nu = (2\alpha - 1)^3(5 - \alpha)/3\alpha^3, \tag{8.56a}$$

$$\mu_{\text{eff}}/\nu = (2\alpha - 1)^3/\alpha^2. \tag{8.56b}$$

We now examine the opposite case where polymers carry only two functional groups $f = 2$, but form multiple junctions with $k \geq 3$. We find $\zeta_0 = x_1, \zeta_1 = 1 - x_1$, and $\zeta_2 = 0$. The last relation $\zeta_2 = 0$ is obvious because an unreacted functional group on a chain can only be connected to the gel through the chain carrying it (i.e., $i = 1$) in the special case of $f = 2$. The number of effective chains now becomes

$$\nu_{\text{eff}}/\nu = \alpha(1 - x_1)(1 - k'x_1^{k''} + k''x_1^{k'}). \tag{8.57}$$

Similarly, the number of effective junctions and dangling ends take the form

$$\mu_{\text{eff}}/\nu = (2\alpha/k)[1 - (x_1^{k''}/2)(k'k''x_1^2 - 2kk''x_1 + kk')], \tag{8.58}$$

and

$$\nu_{\text{end}}/\nu = (2\alpha)[1 + x_1 - (2k - 1)x_1^{k'} + (2k - 3)kx_1^k]. \tag{8.59}$$

The slightly modified form

$$\nu_{\text{end}}/\nu = (2\alpha)(1 - k'x_1^{k''} + k''x_1^{k'})x_1 \tag{8.60}$$

must be used for telechelic polymers.

Figure 8.9 shows the number of elastically effective chains for $f = 2$ with k varied from curve to curve as a function of (a) the extent of reaction, and (b) the reduced concentration [14]. The critical behavior obeys the mean-field scaling law

$$\nu_{\text{eff}}/\nu \simeq (\phi - \phi^*)^t, \tag{8.61}$$
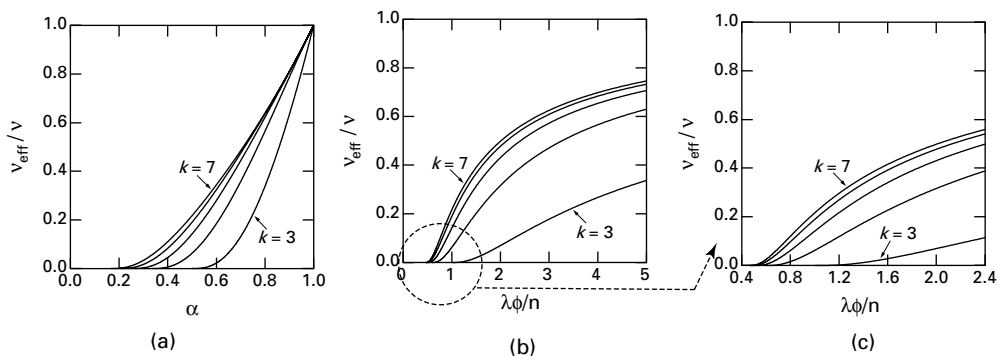
Fig. 8.9   The number of effective chains as a function of (a) reactivity and (b) the polymer concentration. (c) Magnification of (b) near the gel point. (Reprinted with permission from Ref. [14].)

with $t = 3$. The cubic power comes of course from the mean-field treatment (tree statistics). According to the percolation theory, we should expect a smaller power $t = 1.7$ [18]. At the completion of the reaction $\alpha = 1$ (and hence $\lambda\phi/c \to \infty$), and the curves asymptotically reach unity. The number of effective chains is proportional to the polymer concentration in this region.

The simplest model network is the one formed by bifunctional ($f = 2$) primary chains with triple junctions ($k = 3$). In this special case, we find $\alpha' = 1 - \alpha$, where α is the root of the third-order algebraic equation $(\lambda\psi)^2\alpha^3 + \alpha - 1 = 0$. The larger one lying in $0 \le \alpha \le 1$ must be chosen for α in order for α' to be the smaller root of (8.54). All network properties are analytically expressed. We have, for example, $\zeta_0 = (1 - \alpha)/\alpha$, $\zeta_1 = (2\alpha - 1)/\alpha$, $\zeta_2 = 0$, and

$$\nu_{\text{eff}}/\nu = (2\alpha - 1)^3/\alpha^2, \tag{8.62a}$$

$$\mu_{\text{eff}}/\nu = 2(2\alpha - 1)^3/3\alpha^3. \tag{8.62b}$$

Since the critical extent of reaction is given by $\alpha^* = 1/2$, the cubic power near above the sol–gel transition point is evident.

These curves can be compared with the experimental data on the high-frequency dynamic modulus for HEUR measured by Annable et al. [16]. Their experimental data for HEUR C16/35K (end-capped with $C_{16}H_{33}$, molecular weight of 35 000, Figure 19 in [16]) are replotted in Figure 8.10. If we choose $c^* = 1.0\%$ for the weight concentration at gelation, the scaling power at the critical region gives $t = 1.6$, close to the percolation value. But this power depends sensitively on how to choose c^*. In Figure 8.10 fitting the experimental curve to the theoretical calculation is attempted. At high concentrations, the multiplicity is estimated to be 6–7, and about 60% of chains are effective. In the direct measurement [17] of the junction multiplicity using fluorescence decay of pyrene excimer, the number of hydrophobic groups in a junction was estimated to be 20. The difference $20 - 7 = 14$ in the number of hydrophobes of these two measurements may

multiplicity
6 ~ 7

60%
effective

$k = 7$

$k = 3$

$\nu_{eff} \propto (c - c^*)^{1.7}$

$\ln(\nu_{eff}/\nu)$

$\ln(c - c^*) + \text{constant}$
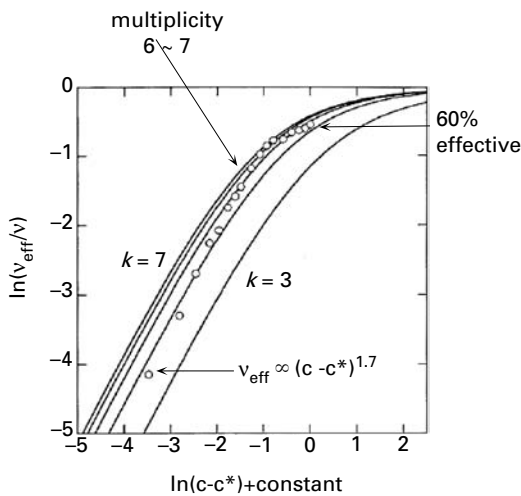
Fig. 8.10   Comparison of the high-frequency plateau modulus of aqueous HEUR C16/35K solutions (○) and theoretical calculation of the number of the elastically effective chains (solid lines). Both are plotted against the log of the concentration deviation. (Reprinted with permission from Ref. [14].)

be attributed to the hydrophobes attached to the loop chains dangling from the junction, which are elastically ineffective.

8.3   Percolation model

In a different way from the classical theory of gelation, the **percolation model of gelation** focuses on the geometrical structure and connectivity of the system. Percolation theory was originally developed to study how water pervades into sands, and has been applied to coffee percolation, irrigation of fields, spreading of diseases, propagation of fires in forests, etc. [19, 20]. We describe the theory with an attempt to apply it to the gelation problem [18, 20, 21].

Percolation models are roughly classified into percolation on regular lattices and percolation in continuum space. Both derive the scaling laws near the percolation threshold by focusing on the self-similarity of the connected objects. The percolation theory is suitable for the study of fluctuations in the critical region, but has a weak point in that the analytical description of the physical quantities in wider regions is difficult.

8.3.1   Percolation threshold

There are two types of percolation problems on regular lattices: **site percolation** and **bond percolation** (Figure 8.11).

In site percolation (Figure 8.11(a)), particles are randomly distributed on the lattice sites. The neighboring pairs are regarded as connected. Let Ω be the total number of

(a)   (b)
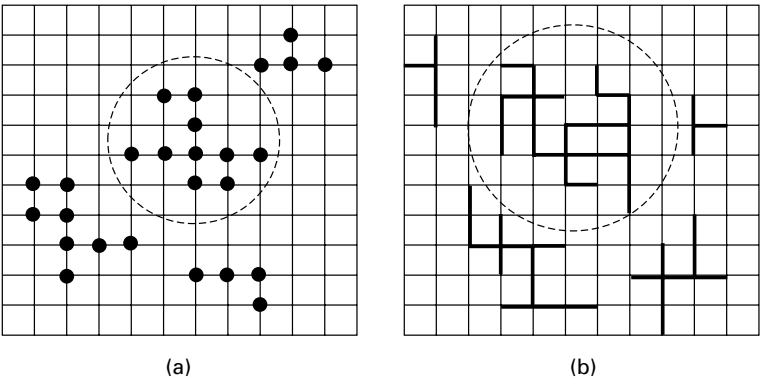
Fig. 8.11   Percolation problem on regular lattices: (a) site percolation, (b) bond percolation. Connected clusters are circled.

Table 8.1 Percolation threshold

d	Lattice A	z	f	Bond $p_c(b)$	Site $p_c(s)$	$zp_c(b)$	$fp_c(s)$
	H (honeycomb)	3	0.61	0.6527	0.70	1.96	0.427
$d=2$	S (square)	4	0.79	0.5000	0.59	2.00	0.466
	T (triangular)	6	0.91	0.3473	0.5000	2.08	0.455
	d (diamond)	4	0.34	0.39	0.43	1.56	0.143
	s.c.	6	0.52	0.25	0.31	1.50	0.161
$d=3$	b.c.c.	8	0.68	0.18	0.24	1.44	0.163
	f.c.c. ⎫ h.c.p. ⎭	12	0.74	0.12	0.20	1.44	0.148

the lattice sites, and N be the number of particles placed on them. The fraction p is defined by

$$p \equiv N/\Omega. \tag{8.63}$$

When p exceeds a certain threshold value p_c, a connected cluster of infinite size appears. This critical value p_c of the fraction depends on the space dimensions d and lattice structure (symbolically described as A), and hence it is indicated by $p_c(A, s)$. In two-dimensional space ($d = 2$), there are square lattices (A = S), triangular lattices (A = T), honeycomb lattices (A = H), etc. In three-dimensional space ($d = 3$), there are simple cubic lattices (A = sc), face-centered cubic lattices (A = fcc), body-centered cubic lattices (A = bcc), and hexagonal close packed lattices (A = hcp) (Table 8.1).

In contrast, in the bond percolation model (Figure 8.11(b)), the connection bonds are randomly placed on the lines between the nearest neighboring (n.n.) sites on the lattice. Bonds sharing the same lattice point are regarded as connected. The fraction p in this

(a)   (b)
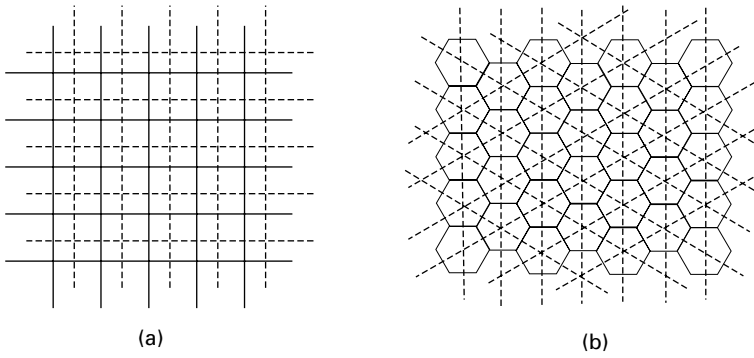
Fig. 8.12   Dual lattice and dual transformation. (a) Square lattice is self-dual S* = S. (b) The dual lattice of a honeycomb lattice is a triangular lattice H* = T and vice versa T* = H.

model is defined by

$$p = N_B/\Omega_B, \tag{8.64}$$

where Ω_B is the total number of n.n. pairs, and N_B is the total number of bonds. The percolation threshold of the bond percolation is designated as $p_c(A, b)$.

Some of the critical values of percolation can be derived using a simple method based on the **duality** of the lattices. In general, the new lattice A* constructed from A by connecting the centers of lattice cells is called the **dual lattice** of A. For instance, the dual lattice of the square lattice is a square lattice: (S* = S). It is self-dual. A honeycomb lattice and a triangular lattice are dual to each other: (T* = H, H* = T) (Figure 8.12).

Because bonds on the lattice A and bonds on its dual lattice A* cross each other, percolation problems on them are related by

$$p_c(A, b) + p_c(A^*, b) = 1. \tag{8.65}$$

The state on A where bonds are connected to infinity at p_c corresponds to the infinitely connected vacancies that appear on A* at $1 - p_c$. This relation is called the **matching relation**. We find immediately that the critical value of the percolation on a square lattice is $p_c(S, b) = 1/2$.

Also, triangular and honeycomb lattices have a matching relation $p_c(T, b) + p_c(H, b) = 1$. The critical values are not uniquely decided by this relation only, but there is another relation $1 - 3p_c(T, b) + p_c(T, b)^3 = 0$ that holds rigorously (the **Sykes–Essam relation**) [22]. Combination of these relations leads to the interesting results

$$p_c(T, b) = 1 - p_c(H, b) = 2\sin\left(\frac{\pi}{18}\right) = 0.347296. \tag{8.66}$$

A similar matching relation can be found between site and bond percolations. For instance, if the middle points of all bonds on a square lattice are tied, a triangular lattice is generated (Figure 8.13). Therefore, the bond percolation (S, b) on a square lattice is
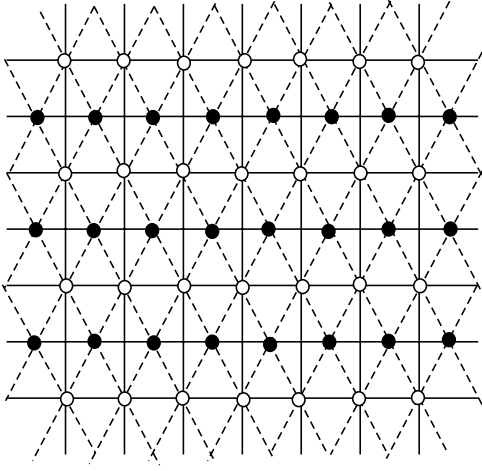
Fig. 8.13 Bond-site matching.

dual to the site percolation (T, s) on a triangular lattice: $(S, b)^* = (T, s)$, and hence

$$p_c(T, s) + p_c(S, b) = 1 \tag{8.67}$$

holds. Since $p_c(S, b) = 1/2$, we find $p_c(T, s) = 1/2$. Thus, the exact critical values of some percolation problems can be found by matching relations, but in general numerical estimation by computer simulation is necessary. Table 8.1 summarizes the values of p_c obtained so far.

8.3.2 Distribution function of clusters

The cluster distribution function f_m is defined by

$$f_m(p) \equiv N_m / N, \tag{8.68}$$

where N_m ($m = 1, 2, 3, \ldots$) is the number of clusters consisting of m particles (referred to as m-mer). The number density ν_m of m-mers is defined by

$$\nu_m(p) \equiv N_m / \Omega. \tag{8.69}$$

In the region $p > p_c$ after the percolation threshold is passed, the infinite cluster coexists with finite clusters (Figure 8.14). Let N_∞ be the number of particles in the infinite cluster. The total particles are decomposed into two parts

$$\sum_{m \geq 1} m N_m + N_\infty = N. \tag{8.70}$$
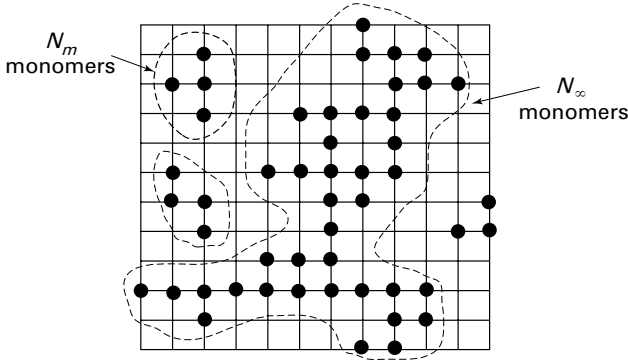
Fig. 8.14   Cluster distribution in the region where finite and infinite clusters coexist.

Dividing by Ω, we find the relation

$$\sum_{m=1}^{\infty} m v_m + P_\infty(p) = p, \tag{8.71}$$

where

$$P_\infty(p) \equiv N_\infty / \Omega \tag{8.72}$$

is the volume fraction of particles belonging to the infinite cluster. The gel fraction w is then given by

$$w = N_\infty / N = P_\infty(p)/p. \tag{8.73}$$

We study v_m and P_∞ as functions of the fraction p.

8.3.3   Percolation in one dimension

In one dimension, the probability for finding a continuous train of m particles is p^m, and the probability for both sides of this train to be empty is $(1-p)^2$ (Figure 8.15). Therefore we have

$$v_m = p^m (1-p)^2. \tag{8.74}$$

If $p < 1$, the identity $\sum_{m \geq 1} m v_m = p$ holds, so that the percolation threshold is $p_c = 1$. Because only one vacancy separates the train into two parts, all lattice sites must be occupied for the system to percolate. In other words, there is no postgel regime in one dimension.

By using this number density, we find $\langle m \rangle_n = 1/(1-p)$ for the number-average, and $\langle m \rangle_w = (1+p)/(1-p)$ for the weight-average, and $\langle m \rangle_z = (1+2p-p^2)/(1+p)(1-p)$ for the z-average. Let us introduce the deviation $\Delta p \equiv p_c - p$ from the critical value. The averages behave as $\langle m \rangle_n \simeq \langle m \rangle_w \simeq (\Delta p)^{-1}$, $\langle m \rangle_z \simeq (\Delta p)^{-1}$ near the threshold.

To specify the nature of the singularity near the threshold, we introduce the **critical indices** of percolation. The averages are

$$\langle m \rangle_w \simeq (\Delta p)^{-\gamma}, \tag{8.75}$$
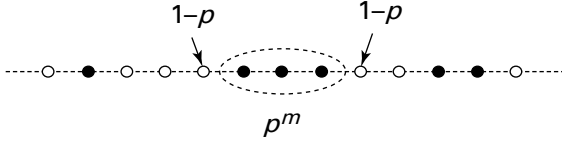
Fig. 8.15 Percolation in one dimension.

for the weight-average, and

$$\langle m \rangle_z \simeq (\Delta p)^{-1/\sigma}, \tag{8.76}$$

for the z-average. In one dimension, $\gamma = \sigma = 1$.

The cluster density can be transformed as

$$\nu_m = p^m (1-p)^2 = (1-p)^2 e^{m \ln p} \simeq (\Delta p)^2 e^{-m \Delta p}. \tag{8.77}$$

Hence, it is

$$\nu_m \simeq (m^*)^{-\tau} F(m/m^*), \tag{8.78}$$

by using a characteristic size m^*. Either $\langle m \rangle_w$ or $\langle m \rangle_z$ may be chosen as the characteristic size m^* in one dimension, but it turns out that m^* should be identified to be $\langle m \rangle_z$ in the space dimension larger than 1. The index τ is $\tau = 2$, whereas the function $F(x)$ is $F(x) = e^{-x}$. The index τ is called the **Fisher index**, the function $F(x)$ is the **scaling function**, and the relation (8.78) is the **scaling law**. The cluster distribution does not depend on the size m and the fraction p independently, but depends on the combination $m/m^*(p)$ due to the self-similarity of the structure.

We next introduce the **connectivity correlation function** $g^\dagger(r)$ of the particles defined by the average

$$g^\dagger(r) \equiv \frac{1}{N} \sum_{i,j} \langle \langle \delta(\mathbf{r} - \mathbf{r}_{i,j}) \rangle \rangle, \tag{8.79}$$

where the sum should be taken over all of the particles that belong to the *same cluster*. The symbol $\langle \langle \cdots \rangle \rangle$ indicates the average over all possible placements of the particles. Since this function includes only the *intra-cluster* particle correlation, it conveys information on the connectivity of the system [23–25].

In one dimension, we have

$$g^\dagger(r) = p^r, \tag{8.80}$$

by definition. Changing this equation into the form

$$g^\dagger(r) \simeq e^{-r/(-\ln p)} \simeq e^{-r/\xi}, \tag{8.81}$$

the correlation length ξ depends on the fraction p in the form

$$\xi = -1/\ln p \simeq (\Delta p)^{-1}. \tag{8.82}$$

As p approaches $p_c = 1$, the correlation length grows to infinity. If we introduce the critical index ν by the form

$$\xi \simeq (\Delta p)^{-\nu}, \tag{8.83}$$

the index turns out to be $\nu = 1$.

8.3.4   Site percolation on the Bethe lattice

In one dimension, the separation effect by the vacancies is so exaggerated that no post-percolation region appears. We improve this point by modelling the percolation on a **Bethe lattice** (**Cayley tree**) (Figure 8.16). The coodination number z of the Bethe lattice is $z = f$, where f is the number of the functional groups on a particle. Each particle is assumed to carry f functional groups which react at 100% when particles are placed on the n.n. sites. The reactivity α of the functional group is the same as the probability p for finding a particle on the n.n. site. The classical theory of gelation in Section 3.2 found for the number density of m-mers as

$$\nu_m \equiv \frac{N_m}{\Omega} = \left(\frac{fN}{\Omega} \right) \frac{(1-p)^2}{p} \omega_m \beta^m, \tag{8.84}$$

where $\beta \equiv p(1-p)^{f-2}$ and $\omega_m \equiv (fm-m)!/m!(fm-2m+2)!$ is the Stockmayer factor.

From the results in Section 3.2, the weight-average cluster size is

$$\langle m \rangle_w = (1+p)/[1-(f-1)p], \tag{8.85}$$

and hence the percolation threshold is $p_c = 1/(f-1)$. The special case of $f = 2$ reduces to the one-dimensiona problem. There is a post-percolation region when $f \geq 3$.

Let us next find the fraction P_∞ of the percolated cluster in the postgel regime ($p > p_c$). Let u be the probability for a functional group to be connected to the finite clusters only
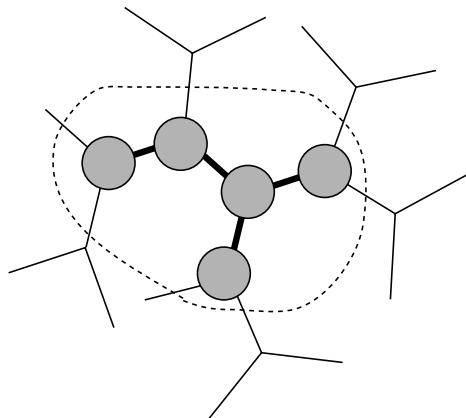
Fig. 8.16   Percolation on a Bethe lattice.

(Figure 8.16). Then, the relation

$$u = 1 - p + p\zeta_0 \tag{8.86}$$

holds, where ζ_0 is the probability for a particle to be connected only to the finite clusters, because the probability for a randomly chosen functional group to be unreacted is $1 - p$, and to be connected to a particle which is a member of a finite cluster is $p\zeta_0$.

Since all $f - 1$ paths starting from the particle must be connected to finite clusters, ζ_0 should be given by

$$\zeta_0 = u^{f-1}. \tag{8.87}$$

We then have from (8.86) the equation

$$u = 1 - p + pu^{f-1} \tag{8.88}$$

to find u. This is a special case of (8.21) for the pairwise association $k = 2$ only. Because the sol fraction is $w^S \equiv u^f = \zeta_0 u$, and the gel fraction is $w = P_\infty(p)/p$, the percolation probability is given by

$$P_\infty(p) = p(1 - u^f). \tag{8.89}$$

For the special case of $f = 3$, $u = (1 - p)/p$, $\zeta_0 = [(1 - p)/p]^2$, and hence the gel fraction reduces to

$$P_\infty(p) = p \left\{ 1 - \left(\frac{1 - p}{p} \right)^3 \right\}, \tag{8.90}$$

which is the same result as Flory's postgel treatment in the classical theory of gelation. Hence, Flory's assumption of the reactivity of the sol α' turned out to be the correct one. Comparing the gel fraction (3.29) by Flory with the relation $w = P_\infty(p)/p$, we find that the reactivity p^S of the sol part must be equal to $p^S = 1 - p$. This gives, however, $p^G = (1 - 2p + 2p^2)/(1 - p + p^2)$ if the reactivity of the gel part p^G is defined by the relation (3.37), which gives the correct total reactivity. The reactivity of the gel can therefore be larger than $\alpha_0 \equiv 2/3$ of the maximum reactivity of the tree with $f = 3$. Such an inconsistency in treatment originates in the assumption that the system is infinitely large, and that the recursion relation (8.88) holds.[2]

8.4   Self-similarity and scaling laws

8.4.1   Static scaling laws

In the critical region near the percolation threshold, the structure of the clusters are self-similar; the structure observed in a certain length scale looks similar to a part of it when the part is magnified λ times as large, and hence they are superimposable onto each other (Figure 8.17). Let us describe the **self-similarity** in a mathematical way by taking the

---

[2] The number of surface sites in a tree is of the same order as the total number of the sites (see Section 4.3), so that a simple thermodynamic limit without the surface correction may lead to an inconsistent result.
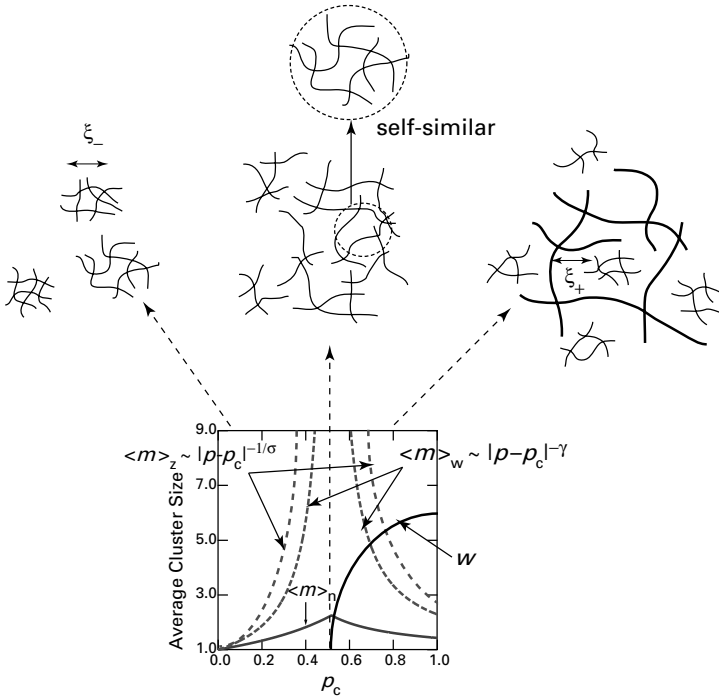
Fig. 8.17	Definition of self-similarity, correlation length, and average molecular weights.

mass M of the connected assembly of the identical particles as an example. Let $M(L)$ be the mass of the region of the assembly inside the radius L measured from the center of mass. The mass $M(\lambda L)$ inside the radius λL should satisfy

$$M(\lambda L) = \lambda^D M(L), \tag{8.91}$$

from the self-similarity. The index D is the **fractal dimension** of the object [26]. Taking a microscopic length as L, and the average radius of gyration $R(m)$ of the m-mers as λL, the mass $M(\lambda L)$ is the molecular weight M_m of the m-mer. Hence, self-similarity is described by the proportionality relation

$$M_m \simeq R(m)^D. \tag{8.92}$$

Power laws derived in this way from the self-similarity include the **scaling laws**.

In the critical region, the cluster distribution function obeys the scaling law

$$f_m(p) = m^{-\tau} F(m/m^*(p)), \tag{8.93}$$

where m is the number of particles in the connected cluster, τ is the **Fisher index**, and $m^*(p)$ is the reference size of the clusters [18, 19]. The size $m^*(p)$ is shown to be the z-average cluster size $\langle m \rangle_z$ in the following (8.98). Practically, it is the size of the largest

cluster. Since it diverges at p_c, the index σ is introduced in (8.76) by the scaling law

$$m^*(p) \simeq |p - p_c|^{-1/\sigma} = |\Delta p|^{-1/\sigma}. \tag{8.94}$$

The indexes σ and τ are two fundamental structural indices of percolation theory. The function $F(x)$ is a smooth **scaling function** which decays sufficiently fast.

Pregel regime

The number average cluster size takes a finite value at the percolation threshold, and hence

$$\langle m \rangle_n = \sum_{m \geq 1} m f_m = \text{constant}. \tag{8.95}$$

The weight-average is divergent as

$$\langle m \rangle_w = \sum m^2 f_m / \sum m f_m \simeq (m^*)^{3-\tau} \equiv (\Delta p)^{-\gamma}, \tag{8.96}$$

where the last equality is the definition of the index γ. We immediately have the relation

$$\gamma = \frac{3 - \tau}{\sigma}, \tag{8.97}$$

from the scaling form of f_m. The index γ can thus be described by the two fundamental indices τ and σ. The z-average is similarly

$$\langle m \rangle_z = \sum m^3 f_m / \sum m^2 f_m \simeq (m^*)^{4-\tau} / (m^*)^{3-\tau} \simeq m^*. \tag{8.98}$$

Thus, the reference cluster size m^* turned out to be the z-average.

In the derivation of these equations, the summation is replaced by the integral

$$\sum_{m \geq 1} m^k f_m \simeq \int_1^\infty m^k f_m dm = \int_1^\infty m^{k-\tau} F(m/m^*) dm$$

$$= (m^*)^{k+1-\tau} \int_{1/m^*}^\infty x^{k-\tau} F(x) dx. \tag{8.99}$$

Since the last integrals are convergent for $k = 2, 3, \ldots$ in the limit of $m^* \to \infty$, the moments are proportional to $\simeq (m^*)^{k+1-\tau}$ except for $k = 1$, for which the summation is a constant at $p = p_c$ (because of $\tau > 2$).

The correlation length of percolation is defined by the size of the largest cluster

$$\xi \simeq R(m^*) \simeq a(\Delta p)^{-\nu}. \tag{8.100}$$

The last equality is the definition of the critical index ν. Since $m^* \simeq R(m^*)^D \simeq (\Delta p)^{-\nu D}$ by using the fractal dimension D, the index ν is given by

$$\nu = 1/\sigma D. \tag{8.101}$$

In contrast, the weight average cluster size is

$$\langle R^2 \rangle_{\mathrm{w}} \equiv \frac{\sum R(m)^2 m f_m}{\sum m f_m} \simeq (m^*)^{2/D+2-\tau} \simeq \xi^2 (\Delta p)^{(\tau-2)/\sigma}, \tag{8.102}$$

so that the last factor makes the singularity weaker than the squared correlation length.

On the gel point

On the critical percolation threshold $p = p_c$, the cluster distribution becomes

$$f_m(p_c) \simeq F(0) m^{-\tau}, \tag{8.103}$$

where $F(0)$ is a finite constant, so that a power law holds due to the self-similarity. The average radius of gyration of m-mers obeys the scaling law $R(m) \simeq a m^{1/D}$, where a is the microscopic length scale.

Postgel regime

In the postgel regime ($\Delta p \equiv p - p_c > 0$), the volume fraction of the sol is given by the sum

$$S \equiv \sum_{m \geq 1} m v_m(p), \tag{8.104}$$

but since there is no contribution from the infinite cluster ($m = \infty$) in the sum, the gel part P_∞ can be calculated from the subtraction

$$P_\infty = p - \sum_{m \geq 1} m v_m(p). \tag{8.105}$$

The sol fraction is $1 - w = S/p$, while the gel fraction is $w = P_\infty/p$. The gel fraction obeys the power law

$$w \simeq (\Delta p)^\beta \tag{8.106}$$

near the threshold (Figure 8.17), where β is a new index. It is shown to be identical to

$$\beta = (\tau - 2)/\sigma \tag{8.107}$$

in terms of the two fundamental indices as follows.

Because $\sum_{m \geq 1} m v_m(p_c) = p_c$ holds, we find

$$P_\infty = p - \sum_{m \geq 1} m v_m(p) \simeq \sum_{m \geq 1} m \{ v_m(p_c) - v_m(p) \}.$$

Substituting the scaling law, we find

$$P_\infty = \sum_{m \geq 1} m^{1-\tau} \{ F(0) - F(m/m^*) \}.$$

Table 8.2 Critical indices of the percolation problem

| Index | Space dimensions | | | Cayley tree | Experiment |
	$d=1$	$d=2$	$d=3$		
σ	1	36/91	0.46	1/2	0.40±0.08
τ	2	187/91	2.20	5/2	2.28±0.03
β	–	5/36	0.45	1	0.7±0.2
γ	1	43/18	1.74	1	1.8±0.3
ν	1	4/3	0.88	1/2	1.1±0.2
δ	–	91/5	4.9	2	
D^{-1} $(p=p_c)$		48/91	0.40	1/4	
D^{-1} $(p<p_c)$		0.641	0.5	1/4	0.48±0.02
D^{-1} $(p>p_c)$		1/2	1/3	1/4	
s		–	0.7–0.9	0	1.4 ± 0.2
t		4/3	1.7–1.9	3	3.2 ± 0.5

If the sum is replaced by integration, the probability turns out to be

$$P_\infty \simeq \int_1^\infty m^{1-\tau}\{F(0)-F(m/m^*)\}dm$$

$$\simeq (m^*)^{2-\tau} \int_{1/m^*}^\infty x^{1-\tau}\{F(0)-F(x)\}dx$$

$$\simeq (m^*)^{2-\tau} \simeq (\Delta p)^{(\tau-2)/\sigma}. \tag{8.108}$$

The weight-average size of the finite clusters in the sol is usually written as $\langle m \rangle_{\mathrm{w}} \simeq (\Delta p)^{-\gamma'}$, but by symmetry, the relation $\gamma = \gamma'$ holds. The weight-average is related to the gel fraction as

$$\langle m \rangle_{\mathrm{w}} \simeq w^{1-\delta}, \tag{8.109}$$

in terms of the new index δ. Obviously, it is given by

$$\delta = 1 + \gamma'/\beta. \tag{8.110}$$

Table 8.2 summarizes the theoretical critical indices and their experimental values. The index s characterizes the divergence of the viscosity, and t characterizes the appearance of the elastic modulus. The index t is larger than β because not all the chains in the connected network are elastically effective. There are many free ends near the percolation threshold.

8.4.2 Viscoelastic scaling laws

Scaling laws hold not only for geometrical properties but also for viscoelastic properties. The steady-state (zero shear) viscosity (2.54) diverges as

$$\eta_0 \simeq (p_c - p)^{-s} \tag{8.111}$$
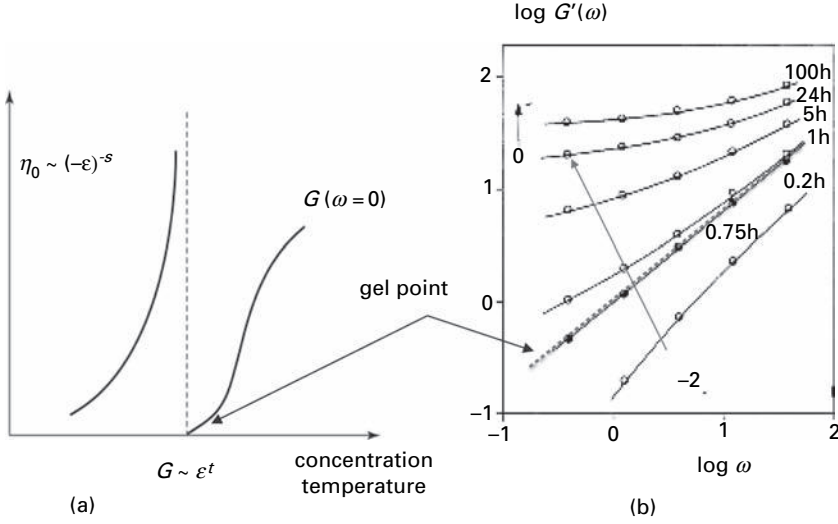
Fig. 8.18   (a) Steady-state viscosity η_0 and equilibrium modulus $G(\omega=0)$ near the percolation threshold. (b) Scaling law for the dynamic mechanical modulus $G(\omega)$ of poly(vinyle alcohol) solutions in di-(2-ethylhexyl)phthalate ($c=9.9$ wt %)

on approaching the percolation threshold, while the equilibrium modulus rises as

$$G_\infty \simeq (p-p_c)^t \qquad (8.112)$$

in the postgel region, where indices s, t are defined (see Figure 8.18). If the clusters obey Rouse motion under the condition of free draining, the viscosity index is $s=(D-d+2)\nu$. If there is strong hydrodynamic interaction, $s=0$ (logarithmic divergence). The evaluation of the effective chains in the gel fraction w may lead to the index t, but the judgement of the active chains is difficult, because even if the gel is geometrically percolated, it is not necessarily elastically percolated [21]. The concept of **rigidity percolation** was introduced to describe the difference [27].

By using these two indices, the **dynamic mechanical modulus** $G(\omega) = G'(\omega) + i G''(\omega) = i\omega[\eta'(\omega) - i\eta''(\omega)]$ is shown to obey the scaling law

$$G(\omega; \Delta p) \simeq (\Delta p)^t g_\pm\left(\frac{i\omega}{\omega^*}\right) \qquad (8.113)$$

near the gel point, where

$$\omega^* \equiv \omega_0 (\Delta p)^{s+t} \qquad (8.114)$$

(ω_0 is the frequency corresponding to a microscopic timescale), and the function $g_\pm(x)$ is a smooth scaling function which has no singularity [28–30].

In the limit of low frequency $\omega << \omega^*$, the scaling function must be expanded in the power series $g_-(x) = a_1 x + a_2 x^2 + \cdots$ in order for the scaling relation $\eta'(\omega) \simeq (\Delta p)^{-s}$ (8.111) to hold in the pregel regime. It must also be expanded in the form $g_+(x) = b_1 + b_2 x + \cdots$ in order for the scaling relation $G'(\omega) \simeq (\Delta p)^t$ (8.112) to hold in the postgel regime. For the intermediate frequencies in the range $\omega^* \ll \omega \ll \omega_0$, if the power form

$$g_\pm(x) \simeq x^\Delta \tag{8.115}$$

is assumed for scaling, the modulus is

$$G(\omega; \Delta p) = G_0 \left(\frac{\omega}{\omega_0}\right)^\Delta e^{i\pi\Delta/2}, \tag{8.116}$$

and the phase shift is $\delta(\omega) = \pi\Delta/2$, that is, the loss tangent is

$$\tan\delta(\omega) \equiv G''(\omega)/G'(\omega) = \tan\left(\frac{\pi}{2}\Delta\right), \tag{8.117}$$

which is independent of ω.

Furthermore, if $G(\omega; \Delta p)$ is independent of Δp in this frequency range, the scaling index of the complex modulus is expressed as

$$\Delta = t/(s+t) \tag{8.118}$$

in terms of the fundamental two indices of viscoelasticity. Usually $s = 0.7$–0.9, $t = 1.7$–1.9, the index takes the value around $\Delta \simeq 0.5$.

Such a scaling idea leads to the experimental identification of the gel point from the measurement of the dynamic mechanical moduli. Figures 8.18(b) and 8.19 show a typical example. In the course of the cross-linking reaction of poly(dimethyl siloxane) by tetra-functional silane, there is a time at which the storage and loss modulus exhibit

$t - t_c$	A
-6	2
-2	1
0	0
2	-1
6	-2

(a)

(b)
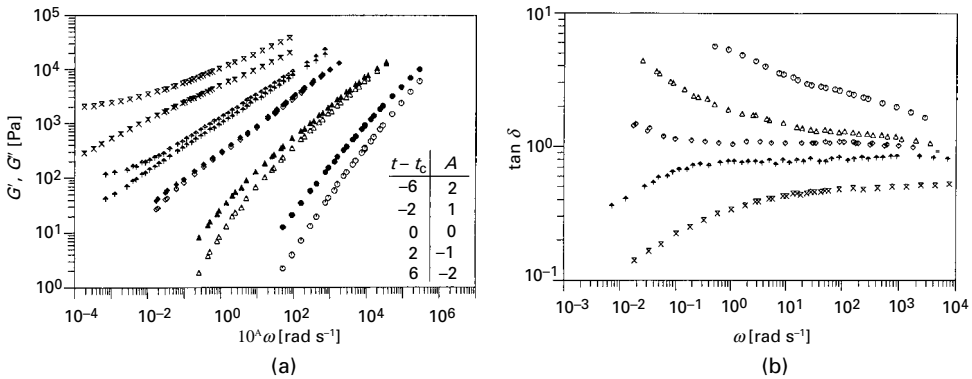
Fig. 8.19 Identification of the gel point on the basis of the dynamic mechanical scaling law. (a) $G'(\omega)$ (white symbols) and $G''(\omega)$ (black symbols) at different time. (b) Loss tangent plotted against the frequency. (Reprinted with permission from Ref. [30].)

the same slope in logarithmic scale (Figure 8.19(a)). The loss tangent is constant over a wide frequency range (Figure 8.19(b)). This is the gel point. This method of finding the gel point is referred to as the **Chambon–Winter method**.

8.5   Percolation in continuum media

8.5.1   Critical volume fraction of percolation

Let us move to the percolation problem in the continuum spaces [31]. This can be naturally done by first finding the **invariants** of the problem which do not depend on the details of the lattice structures but depend only on the space dimensions and symmetry, and then discard the lattices from which the problem started.

For instance, the threshold value $p_c(A, s)$ of the site percolation depends on the lattice structure A, but when it is multiplied by the **filling factor** $f(A)$, the product

$$\phi_c = f(A) p_c(A, s) \tag{8.119}$$

is known to depend only on the space dimensions d and is called the **critical volume fraction**. The filling factor $f(A)$ for the lattice A is defined by the ratio of the volume of the spherical balloons on the sites swollen until they come into contact with each other against the total volume of the lattice (Figure 8.20).

In the square lattice, the radius of the circle is $1/2$, and the filling factor is $f(S) = \pi(1/2)^2/1 = \pi/4$. Similarly, $f(sc) = (4\pi/3)(1/2)^3 = \pi/6$ for the simple cubic lattice.

The critical volume fraction is therefore $\phi_c = 1.00$ for the one-dimensional lattice, and $\phi_c = \pi(1/2)^2 \times 1/2 = 0.393$ for two dimensions as calculated in the square lattice. Scher and Zallen [32] found $\phi_c = 0.44 \pm 0.02$ in two dimensions $d = 2$, while $\phi_c = 0.154 \pm 0.005$ in three dimensions $d = 3$. It decreases with the space dimensions, because even if the cluster is percolated d dimensionally, it may not necessarily be percolated $d + 1$
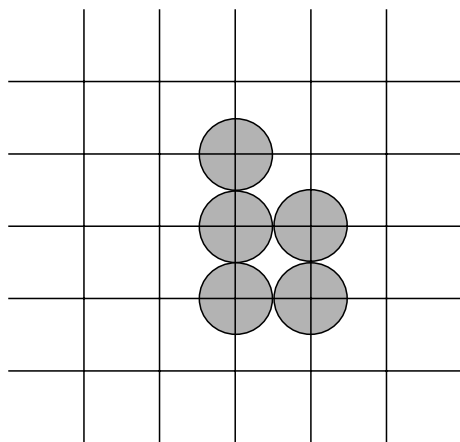
Fig. 8.20   Construction of the space filling factor f for the given lattice.

dimensionally (Table 8.1). The critical volume fraction is applicable to the percolation problem of randomly distributed hard spheres in three-dimensional space.

As another example of the invariant, let us take the critical bond number

$$\phi_c \equiv z p_c(A, b) \tag{8.120}$$

in the bond percolation problem, where z is the coordination number of the lattice A. It was found to be invariant by Ziman [33]. It is $\phi_c = 2.0 \pm 0.2$ in $d = 2$, while it is $\phi_c = 1.5 \pm 0.1$ in $d = 3$. The critical volume fraction is known to be approximately given by $\phi_c \simeq d/(d-1)$ (Table 8.1).

The percolation models discussed so far undergo purely geometrical transitions because the objects treated have no center of mass translational motion. They are only randomly placed either on the lattices or in the continuum space. Therefore, they don't reveal any thermodynamic singularities. If particles are moving in a space, however, the entropy associated with the translational motion may partly vanish at the percolation point since the mass center of the infinite cluster (gel) ceases to move. If its derivative with respect to the concentration across the percolation point has a discontinuity, the transition becomes a real thermodynamic one.

Studies along this line have been developed on the basis of the classical theory of condensation. For instance, Hill [34] introduced a formal method for calculating the number of **physical clusters** in imperfect gasses as contrasted with **Mayer's method** [35] of mathematical cluster expansion. The transition from low-temperature microcrystalline arrangement (droplet) to high-temperature spongelike structure (percolatiton) was studied by Stillinger [36] in the case of the pair potential with limited interaction range. The relation between condensation and gelation was discussed in more detail by Cohen *et al.* [37]. They derived Stockmayer distribution (3.19) of the polycondensation reaction using Hill's method of physical clusters, and pointed out that the singularity is associated with thermoreversible gelation. However, the thermodynamic scaling laws have not yet been established. In the next section, we will see some studies of the problem by focusing on the adhesive hard-sphere pair potential.

8.5.2 Gelation of sticky hard spheres (Baxter's problem)

To study gelation phenomena in globular proteins, colloid dispersions, etc., Baxter's **adhesive hard sphere** (AHS) system [38] is often used as a model system. Particles in the AHS system interact with each other through strongly attractive short-range square well potentials.

Consider N spherical particles of radius $\sigma/2$ in a container of volume V. The volume fraction $\phi = (4\pi/3)(\sigma/2)^3 N/V$ is used for the concentration. The attractive potential has a depth $-\varepsilon$ and width $\Delta \equiv d - \sigma$ (Figure 8.21(a)). In the Baxter limit [38] of short range $d \to \sigma$ and strong force $\epsilon \to \infty$, the spheres form branched spongelike clusters in which they are connected to each other. Above a certain volume fraction, the clusters percolate over the entire container (percolation line in Figure 8.21(b)) [23–25,39]. The condition for the existence of such percolation phenomena is roughly estimated as $\xi \equiv \Delta/\sigma < 0.1$.
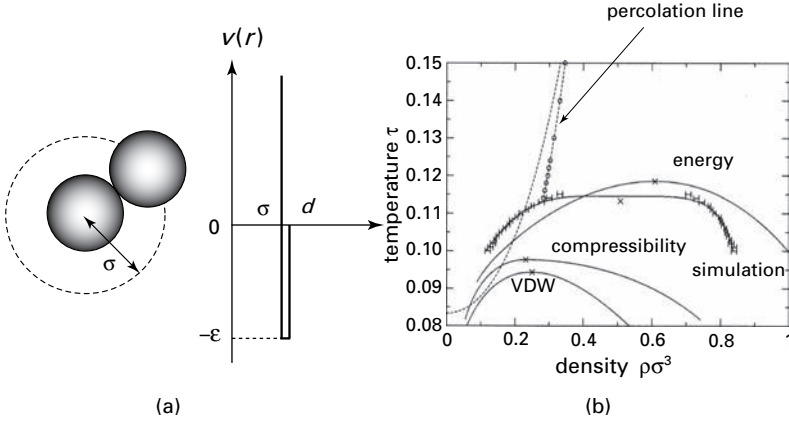
Fig. 8.21   (a) Baxter's adhesive hard sphere (AHS) system. (b) Its universal phase diagram. Coexisting percolation transition and phase separation in the system of hard spheres with short-range strongly attractive interaction are shown on the temperature–volume fraction phase plane. Data (○) of the percolation transition are produced by molecular simulation, while the theoretical result [24] is shown by the dotted line. Solid lines are gas–liquid transition lines. (Reprinted with permission from Ref. [40].)

The second virial coefficient

$$A_2(T) = \frac{1}{2}\int_0^\infty (1 - e^{-u(r)/k_BT})4\pi r^2 dr \qquad (8.121)$$

of the AHS system is normalized as $A_2^* \equiv A_2(T)/A_2^{HS}$ by using the hard sphere system $A_2^{HS} = (4\pi\sigma^3/3)$, and is used to measure the temperature in the form $\tau \equiv 1/4(A_2^* - 1)$. There have been attempts to construct phase diagrams on the τ–ϕ plane [24, 25].

AHS systems show interesting phase diagrams in which gas–liquid phase transition coexists with percolation transition (Figure 8.21(b)). The percolated cluster can be regarded as a porous gel comprising spherical particles. Within the Percus–Yevick approximation, Chiew and Glandt [24] found that the percolation line is given by

$$\tau = (19\phi^2 - 2\phi + 1)/12(1 - \phi)^2. \qquad (8.122)$$

If we apply Mayer's theory of condensation to AHS systems, we find that in the cluster expansions (7.13a) for the molar volume v and (7.13b) for the pressure p. The coefficients (cluster integrals) b_l are constructed by the special form

$$f(r) \equiv e^{-u(r)/k_BT} - 1 = \frac{\sigma}{12\tau}\delta(r - \sigma) + \theta(r - \sigma) - 1 \qquad (8.123)$$

of the Mayer function. They take a form similar to ω_l in tree statistics with the functionality $f \simeq z$ ($z \simeq 12$ is the coordination number of closely packed spheres.) There is a strong tendency to form tree-type clusters rather than spherical droplets.

As a result, the percolation transition splits from the gas–liquid transition line. Because the analytical solution of the problem is difficult to find, molecular simulations are used

to construct the phase diagram [40,41]. However, the nature of the singularity of the thermal properties such as compressibility, specific heat, etc., across the percolation line still remains an open question.

References

[1] Flory, P.J., *Principles of Polymer Chemistry*. Cornell University Press: Ithaca, NY, 1953.

[2] Eldridge, J.E.; Ferry, J.D., *J. Phys. Chem.* **58**, 992 (1954).

[3] Tanaka, F.; Stockmayer, W.H., *Macromolecules* **27**, 3943 (1994).

[4] Tanaka, F.; Nishinari, K., *Macromolecules* **29**, 3625 (1996).

[5] Nishinari, K.; Tanaka, F., *Journal de Chimie et Physique* **93**, 880 (1996).

[6] Tanaka, F., *Polym. J.* **34**, 479 (2002).

[7] Ohkura, M.; Kanaya, T.; KKaji, K., *Polymer* **33**, 3686 (1992).

[8] Brandrup, J.; Immergut, E.H., *Polymer Handbook*. Wiley: New York, 1975; p. III-13.

[9] Scanlan, J., *J. Polym. Sci.* **43**, 501 (1960).

[10] Case, L.C., *J. Polym. Sci.* **45**, 397 (1960).

[11] Pearson, D.S.; Graessley, W.W., *Macromolecules* **11**, 528 (1978).

[12] Graessley, W.W., *Polymeric Liquids & Networks: Structure and Properties*, Chapter 9. Garland Science: London, 2004.

[13] Langley, N.R., *Macromolecules* **1**, 348 (1968).

[14] Tanaka, F.; Ishida, M., *Macromolecules* **29**, 7571 (1996).

[15] Clark, A.H.; Ross-Murphy, S.B., *Adv. Polym. Sci.* **83**, 57 (1987).

[16] Annable, T.; Buscall, R.; Ettelaie, R.; Whittlestone, D., *J. Rheol.* **37**, 695 (1993).

[17] Yekta, A.; Xu, B.; Duhamel, J.; Adiwidjaja, H.; Winnik, M.A., *Macromolecules* **28**, 956 (1995).

[18] Stauffer, D.; Coniglio, A.; Adam, M., *Adv. Polym. Sci.* **44**, 103 (1982).

[19] Stauffer, D.; Aharony, A., *Introduction to Percolation Theory*, 2nd edn. Taylor & Francis: London, 1991.

[20] de Gennes, P.G., *Scaling Concepts in Polymer Physics*. Cornell University Press: Ithaca, NY, 1979.

[21] de Gennes, P.G., *J. Physique* **1976**, *37*, L1.

[22] Sykes, M.F.; Essam, J.W., *J. Math. Phys.* **5**, 1117 (1964).

[23] Coniglio, A.; Angelis, U.D.; Forlani, A., *J. Phys. A: Math. Gen.* **10**, 1123 (1977).

[24] Chiew, Y.C.; Glandt, E.D., *J. Phys. A: Math. Gen.* **16**, 2599 (1983).

[25] Stell, G., *J. Phys. A: Math. Gen.* **1984**, *17*, L855.

[26] Mandelbot, B.B.; Gouyet, J.-F., *Physics and Fractal Structures*. Springer: New york, 1996.

[27] Feng, S.; Sen, P.N., *Phys. Rev. Lett.* **52**, 216 (1984).

[28] Winter, H.H.; Chambon, F., *J. Rheol.* **30**, 367 (1986).

[29] Durand, D.; Delsanti, M.; Adam, M.; Luck, J.M., *Europhys. Lett.* **3**, 297 (1987).

[30] Winter, H.H.; Mours, M., *Adv. Polym. Sci.* **134**, 165 (1997).

[31] Ziman, J.M., *Models of Disorder*. Cambridge University Press: Cambridge, 1979.

[32] Scher, H.; Zallen, R., *J. Chem. Phys.* **53**, 3759 (1970).

[33] Ziman, J.M., *J. Phys. C* **1**, 1532 (1968).

[34] Hill, T.L., *J. Chem. Phys.* **23**, 617 (1955).

[35] Mayer, J.E.; Mayer, M.G., *Statistical Mechanics*. Wiley: New York, 1940.

[36] Stillinger, F.H., *J. Chem. Phys.* **38**, 1486 (1963).

[37] Cohen, C.; Gibbs, J. H.; Fleming III, P. D., *J. Chem. Phys.* **59**, 5511 (1973).

[38] Baxter, R. J., *J. Chem. Phys.* **49**, 2770 (1968).

[39] Xu, J.; Stell, G., *J. Chem. Phys.* **89**, 1101 (1988).

[40] Miller, M. A.; Frenkel, D., *Phys. Rev. Lett.* 2003, *90113*.

[41] Kranendonk, W. G.; Frenkel, D., *Mol. Phys.* **64**, 403 (1988).

9   Rheology of thermoreversible gels

This chapter is devoted to the molecular rheology of transient networks made up of associating polymers in which the network junctions break and recombine. After an introduction to theoretical description of the model networks, the linear response of the network to oscillatory deformations is studied in detail. The analysis is then developed to the nonlinear regime. Stationary nonlinear viscosity, and first and second normal stresses, are calculated and compared with the experiments. The criterion for thickening and thinning of the flows is presented in terms of the molecular parameters. Transient flows such as nonlinear relaxation, start-up flow, etc., are studied within the same theoretical framework. Macroscopic properties such as strain hardening and stress overshoot are related to the tension–elongation curve of the constituent network polymers.

9.1   Networks with temporal junctions

In most polymer blends and solutions of practical interest, the polymer chains carry functional groups that interact with each other by associative forces capable of forming reversible bonds. These forces include hydrogen bonding, ionic association, stereocomplex formation, cross-linking by the crystalline segments, or solvent complexation. Because the bond energy is often comparable to the thermal energy, bond formation is reversible by a change in temperature or concentration.

Typical examples are networks in aqueous solutions of polymers with short hydrophobic chains attached at both chain ends (**telechelic polymers**), such as hydrophobic poly(ethylene oxide), hydrophobic ethoxylated urethane (called HEUR) [1–5], hydrophobic poly(*N*-isopropylacrylamide) [6,7], poly(propylene oxide)-poly(ethylene oxide)-poly(propylene oxide) triblock copolymers [8–10], etc. These networks are analogous to the polymer networks whose elastic properties are studied in Chapter 4. They differ, however, in the important point that the network junctions can break and recombine. We extend the theoretical framework of rubber elasticity to suit for the study of polymer networks with temporal cross-link junctions.

There are two clearly distinct regimes: entangled networks and unentangled networks. In **unentangled networks**, the average molecular weight $M_\times$ of a chain connecting the temporal junctions is smaller than the entanglement molecular weight M_e, $M_\times \ll M_e$. The major part of the stress is supported by the elastically active chains connecting the junctions. In **entangled networks**, the opposite relation $M_\times \gg M_e$ holds. Localized entanglements play a role similar to the cross-linked junctions.

The first systematic study of the reversible networks was the **transient network theory** developed by Green and Tobolsky [11], in which stress relaxation in rubber-like polymer networks was treated by the kinetic theory of rubber elasticity suitably extended so as to allow the creation and annihilation of junctions during the network deformation.

In order to ensure a wider range of applicability, some arbitrary assumptions in their theory were later removed by Lodge [12] and Yamamoto [13] with an attempt to apply it to entangled polymer melts rather than reversible networks. In their studies, localized entanglements were regarded as temporal junctions that can be created and destroyed under macroscopic deformation. Because of a lack of detailed knowledge about the molecular mechanism of junction creation (the onset of entanglements), their theories, however, remained semiphenomenological.

Another stream of the study of temporal networks concerns a model network whose history involves cross-links added at a certain stage, a part of which is subsequently removed so as not to be present in the final stage of deformation (called an **addition–subtraction network**). On the basis of such model composite networks, Flory [14] calculated the stress relaxation, and found that it obeys slow dynamics including a logarithmic dependence of the stress, which is closer to power law rather than exponential.

Flory's intuitive argument was later confirmed by Fricker [15] with minor modification by a replica calculation. Owing to the rather arbitrary assumption about chain creation and annihilation, the addition–subtraction network model is difficult to apply to real physical gels.

In this chapter, we focus on the telechelic polymers, and construct a molecular rheology that contains only the molecular parameters whose origin can easily be identified [16–19].

9.1.1   Models of transient networks

Consider networks made up of telechelic polymers carrying short hydrophobic groups at their chain ends (Figure 9.1). Let ν be the number of chains in a unit volume, n be the number of statistical repeat units on a chain, and a be the size of the repeat unit. The total length of the chain is given by $l \equiv na$. We neglect finiteness in the length of the end chains by assuming that they are negligibly short compared with the middle chain.

Typical polymers used in the experiments are poly(ethylene oxide) (PEO) with a molecular weight ranging from 6×10^3 to 35×10^3 carrying alkyl chains $-C_mH_{2m+1}$ ranging from $m = 12$ to 22 [20–22], and poly(N-isopropylacrylamide) (PNIPAM) with a molecular weight ranging from 7×10^3 to 5.9×10^4 carrying alkyl chains of $m = 18$ [6, 7].

There are three kinds of chains in such networks: bridge chains (elastically effective chain), dangling chains and loop chains. A **bridge chain** connects two different junctions, while a **dangling chain** has one free end. There may be many **loops** attached to the junctions, but we neglect them because their effect is only to reduce the number of chains in the network from the total number given by the polymer concentration to the effective number decided by the thermodynamic equilibrium condition. We also neglect the free chains that are separated from the network and floating in the solution. The stress
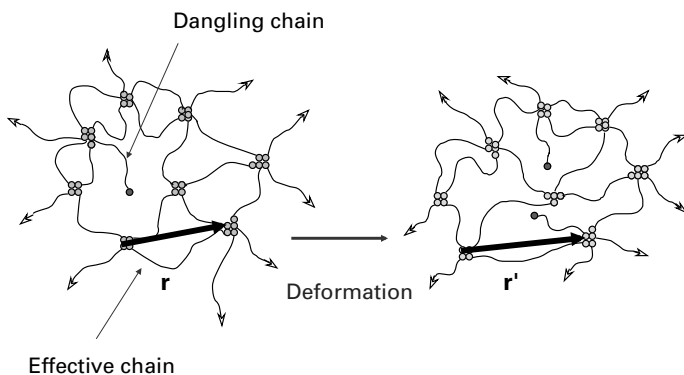
Fig. 9.1   Internal reorganization of the transient network induced by a macroscopic deformation. Bridge chains with high tension dissociate from the junctions and change to dangling chains, while some dangling ends catch the junctions in the course of Brownian movement.

transfer by a dangling chain is made only through friction with its surrounding chains and solvent molecules, which is negligibly small compared with that by the deformation of active chains.

If one end of an active chain dissociates from a junction due to thermal motion, or a tension caused by the external force, the chain becomes dangling and relaxes to an equilibrium state after the single-chain relaxation time τ, which is of the order of the Rouse relaxation time $\tau_R = (\zeta a^2/6\pi^2 k_B T)n^2$ in the unentangled regime. We are concerned with the change in macroscopic properties of a network that is slower than τ_R.

Suppose the network is subjected to a time-dependent deformation described by the tensor $\hat{\lambda}(t)$. It can be a shear flow, an elongational flow, etc., but needs not be specified at this stage. Let $\psi(\mathbf{r},t)$ be the number of bridge chains per unit volume at time t whose end-to-end vector is given by $\mathbf{r}$, and let $\phi(\mathbf{r},t)$ be that of the dangling chain (Figure 9.2) [23].

Let $\mathbf{f}(\mathbf{r})$ be the tension of a bridge chain with the end-to-end vector $\mathbf{r}$ working on the micelle at its end. The tension is a function of the vector $\mathbf{r}$. Similarly, let $\mathbf{f}_j (j = 1,2,3,\ldots)$ be the tensions given by the other chains connected to the same micelle. Then, the random motion of the micelle is described by the Langevin equation

$$m\frac{d\mathbf{v}}{dt} = -\zeta(\mathbf{v} - \bar{\mathbf{v}}(t)) + \mathbf{f} + \sum_j \mathbf{f}_j + \mathbf{R}(t), \tag{9.1}$$

where m is the mass of the micelle, ζ the friction coefficient of the micelle with the medium, $\mathbf{v}$ the instantaneous velocity vector of the micelle, $\bar{\mathbf{v}}(t)$ its average velocity vector, and $\mathbf{R}(t)$ the random force originating in the thermal motion of the medium.

For the average movement of the micellar junction, we follow the assumption JG1 in Section 4.3, and assume an affine deformation

$$\bar{\mathbf{r}}(t+\Delta t) = \hat{\lambda}(t+\Delta t) \cdot \hat{\lambda}(t)^{-1} \cdot \bar{\mathbf{r}}(t), \tag{9.2}$$
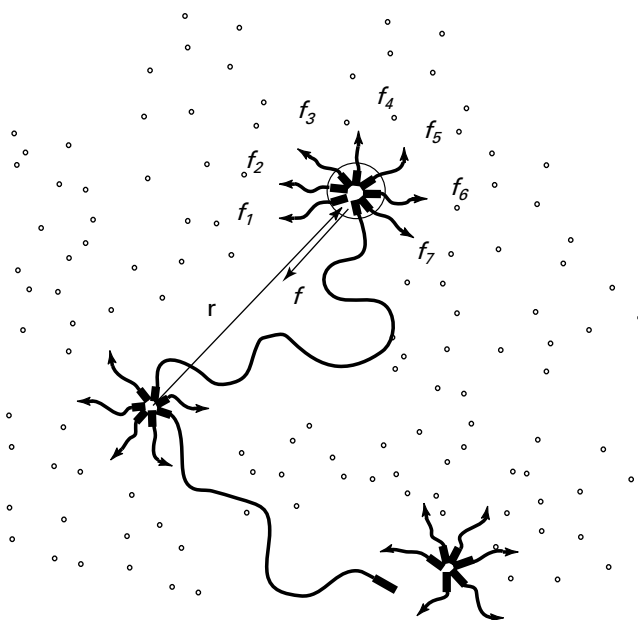
Fig. 9.2   Bridge chain with end-to-end vector **r**, and a dangling chain with one free end in a transient network made up of telechelic polymers. Micellar junctions make Brownian motion by the thermal force under tensions $\mathbf{f}_j$ given by the polymer chains whose ends are connected to them. The instantaneous vector **r** does not change affinely to the external deformation tensor. (Reprinted with permission from Ref. [23].)

for a small time interval Δt. By taking the limit of $\Delta t \to 0$, we have

$$\bar{\mathbf{v}}(t) = \hat{\kappa}(t)\bar{\mathbf{r}}(t), \tag{9.3}$$

for the average velocity [16], where

$$\hat{\kappa}(t) \equiv d\hat{\lambda}(t)/dt \cdot \hat{\lambda}(t)^{-1}. \tag{9.4}$$

We also assume as for JG2 in Section 4.3 that the random force has Gaussian white noise

$$< R_\alpha(t) R_\beta(t') >= 2\zeta k_{\mathrm{B}} T \delta_{\alpha,\beta} \delta(t - t'), \tag{9.5}$$

where the friction coefficient ζ is independent of the deformation.

Similarly, the equation of motion of the free end of a dangling chain is given by

$$m_1 \frac{d\mathbf{v}}{dt} = -\zeta_1 \mathbf{v} + \mathbf{f} + \mathbf{R}_1(t), \tag{9.6}$$

where m_1 is the mass of the end group, **v** its instantaneous velocity, and $\mathbf{R}_1(t)$ the random force acting on it. Since a dangling chain is free from macroscopic strain, the equation has no terms concerning the deformation. The mass m is related to m_1 through the

multiplicity k of the junction as $m = m_1 k$. The friction coefficient ζ of the micelle is also related to that of the end group ζ_1 through the multiplicity, but the relation depends on the structure of the micelle.

To study the time development of the two kinds of chains, let us next introduce their distribution functions. Let

$$\hat{\psi}(\mathbf{r},t) \equiv \delta(\mathbf{r} - \hat{\mathbf{r}}(t)) \tag{9.7}$$

be the density operator for the chain vector of the bridge chains, and let

$$\hat{\phi}(\mathbf{r},t) \equiv \delta(\mathbf{r} - \hat{\mathbf{r}}(t)) \tag{9.8}$$

be that for the dangling chains.[1] These are operators (dynamical variables) at this stage, but eventually give their distribution functions after the thermal average is taken.

These operators obey the chain conservation law

$$\frac{\partial}{\partial t}\hat{\psi}(\mathbf{r},t) + \nabla \cdot (\mathbf{v}(t)\hat{\psi}(\mathbf{r},t)) = -\beta(\mathbf{r})\hat{\psi}(\mathbf{r},t) + \alpha(\mathbf{r})\hat{\phi}(\mathbf{r},t), \tag{9.9a}$$

$$\frac{\partial}{\partial t}\hat{\phi}(\mathbf{r},t) + \nabla \cdot (\mathbf{v}(t)\hat{\phi}(\mathbf{r},t)) = \beta(\mathbf{r})\hat{\psi}(\mathbf{r},t) - \alpha(\mathbf{r})\hat{\phi}(\mathbf{r},t), \tag{9.9b}$$

where $\beta(\mathbf{r})$ is the **chain dissociation rate**, i.e., the probability per unit time for an end chain to dissociate from the junction it is attached to, and $\alpha(\mathbf{r})$ is the **chain recombination rate**, i.e., the probability per unit time for a free end to catch a junction in the neighborhood at the position specified by the chain vector $\mathbf{r}$.

We now neglect the inertia term (the acceleration term) in (9.1) as in the conventional treatment of the Brownian motion of polymer chains [24, 25], solve it in the form

$$\mathbf{v}(t) = \bar{\mathbf{v}}(t) - \zeta^{-1}\left[\mathbf{f} + \sum_j \mathbf{f}_j + \mathbf{R}(t)\right] \tag{9.10}$$

and substitute into (9.9a). After this procedure, we take the thermal average of the equation and find the equations for the distribution functions $\psi(\mathbf{r},t) = \langle\hat{\psi}(\mathbf{r},t)\rangle$ and $\phi(\mathbf{r},t) = \langle\hat{\phi}(\mathbf{r},t)\rangle$

The tensions $\mathbf{f}_j$ given by other members of the bridge chains connected to this junction are then averaged out, and give the **chemical affinity** of the association–dissociation process. If the change between a bridge chain and a dangling chain is regarded as a **reversible chemical reaction**, the equilibrium constant $K(\mathbf{r})$ is given by

$$K(\mathbf{r}) = \beta(\mathbf{r})/\alpha(\mathbf{r}). \tag{9.11}$$

Since the chemical affinity of the reaction is given by the Gibbs free energy $-k_\mathrm{B}T \ln K(\mathbf{r})$, the average tension should be given by

$$\left\langle\sum_j \mathbf{f}_j\right\rangle = \nabla[k_\mathrm{B}T \ln K(\mathbf{r})]. \tag{9.12}$$

---

[1] We indicate that the position vector is a dynamical variable by using a hat symbol on $\mathbf{r}$.

As for the random force due to thermal motion, we follow the conventional treatment of the Gaussian white noise [26] leading to a diffusion term in the time-development equation of the distribution function. We then finally have the coupled equations for the chain distribution functions in the forms

$$\frac{\partial}{\partial t}\psi(\mathbf{r},t)+\nabla\cdot(\bar{\mathbf{v}}(t)\psi(\mathbf{r},t))=D\nabla\cdot\left[\nabla+\mathbf{f}/k_{\mathrm{B}}T+\ln K(\mathbf{r})\right]\psi(\mathbf{r},t)$$

$$-\beta(\mathbf{r})\psi(\mathbf{r},t)+\alpha(\mathbf{r})\phi(\mathbf{r},t), \qquad (9.13\mathrm{a})$$

$$\frac{\partial}{\partial t}\phi(\mathbf{r},t)=D_1\nabla\cdot\left[\nabla+\mathbf{f}/k_{\mathrm{B}}T\right]\phi(\mathbf{r},t)$$

$$+\beta(\mathbf{r})\psi(\mathbf{r},t)-\alpha(\mathbf{r})\phi(\mathbf{r},t), \qquad (9.13\mathrm{b})$$

where the diffusion constants are given by $D = k_{\mathrm{B}}T/\zeta$ for the micellar junctions, and $D_1 = k_{\mathrm{B}}T/\zeta_1$ for the end chains. The characteristic time for diffusion is given by $\tau = l^2/D$ for the junctions, and $\tau_1 = l^2/D_1$ for the end chains. In the above equations, we have changed the sign of the tension so that it agrees with the conventional definition given by (1.12) in Section 1.2.

9.1.2   Equilibrium solutions

Since we have the situation of $D_1 \gg D$, the relaxation time of the free ends is much shorter than that of the micelles. We therefore assume that all the dangling chains instantaneously relax to their equilibrium conformation, and should fulfill the condition

$$(\nabla+\mathbf{f}/k_{\mathrm{B}}T)\phi(\mathbf{r},t)=\mathbf{0}. \qquad (9.14)$$

Hence, we find that their distribution function is given by

$$\phi(\mathbf{r},t)=\nu_{\mathrm{d}}(t)\Phi(\mathbf{r}), \qquad (9.15)$$

where $\nu_{\mathrm{d}}(t)$ is the number of dangling chains in a unit volume of the network at time t, and

$$\Phi(\mathbf{r})\equiv C_n\exp\left[-\int_0^{\mathbf{r}}(\mathbf{f}/k_{\mathrm{B}}T)\cdot d\mathbf{r}\right], \qquad (9.16)$$

where C_n is the normalization constant, is the distribution function of the end-to-end vector of a dangling chain.

Such an assumption of **complete relaxation** for the dangling chains has recently been examined theoretically [27, 28] and experimentally [29]. It was found that, under a certain condition, a high-frequency tail in the loss modulus appears due to the **incomplete relaxation** of the dangling chains within the time interval between their dissociation and recombination. In what follows, we assume the separability of the time scales τ_1 and τ due to the large size of the micellar junctions, and neglect the effect of incomplete relaxation.

The tension along the chain depends upon the nature of the polymer chain. For a Gaussian chain with

$$\mathbf{f}/k_BT = 3\mathbf{r}/na^2,\tag{9.17}$$

we have (1.34) the distribution

$$\Phi(\mathbf{r}) = C_n\exp(-3r^2/2na^2) \equiv \Phi_0(\mathbf{r}),\tag{9.18}$$

where the normalization constant is given by $C_n \equiv (3/2\pi na^2)^{3/2}$ under the assumption that the upper limit of the integral can be extended to infinity.

For a Langevin chain, we have

$$\Phi(\mathbf{r}) = C_n\exp\left[-\int_0^r L^{-1}(r/na)dr/a\right],\tag{9.19}$$

where $L(x)$ is Langevin function (1.27). If it is described by the phenomenological form (1.30) with amplitude A, we have

$$\Phi(\mathbf{r}) = C_n(1-\tilde{r}^2)^A e^{-(3/2-A)\tilde{r}^2},\tag{9.20}$$

which includes both Gaussian and Langevin chains.

Substituting the form (9.15) into (9.13b), and integrating the result over all possible values of $\mathbf{r}$, we find

$$dv_d(t)/dt = -\langle\alpha\rangle v_d(t) + \langle\beta\rangle_t,\tag{9.21}$$

where

$$\langle\alpha\rangle \equiv \int \alpha(\mathbf{r})\Phi(\mathbf{r})d\mathbf{r}\tag{9.22}$$

is the equilibrium average of the recombination rate of the free ends, and

$$\langle\beta\rangle_t \equiv \int d\mathbf{r}\beta(\mathbf{r})\psi(\mathbf{r},t)\tag{9.23}$$

is the instantaneous average of β at at time t.

The total number $v_e(t)$ of the effective chains in a unit volume at time t is then given by

$$v_e(t) \equiv \int \psi(\mathbf{r},t)d\mathbf{r} = v - v_d(t),\tag{9.24}$$

due to the chain conservation law.

Substituting (9.15) into (9.13a), we find the starting equation

$$\frac{\partial\psi}{\partial t} + \nabla\cdot(\bar{\mathbf{v}}(t)\psi) = D\nabla\cdot\left[\nabla + \mathbf{f}/k_BT + \ln K(\mathbf{r})\right]\psi(\mathbf{r},t)$$
$$- \beta(\mathbf{r})\psi + v_d(t)\alpha(\mathbf{r})\Phi(\mathbf{r}).\tag{9.25}$$

For the affine networks for which $D=0$, this equation reduces to [16–19]

$$\frac{\partial\psi}{\partial t} + \nabla\cdot(\bar{\mathbf{v}}(t)\psi) = -\beta(\mathbf{r})\psi + v_d(t)\alpha(\mathbf{r})\Phi(\mathbf{r}).\tag{9.26}$$

The mean square radius of the displacement that a junction to which the bridge chain is attached makes before its end is dissociated is estimated as $D\beta_0^{-1}$ (β_0 is the average dissociation rate). Let us compare this with the mean square end-to-end distance $\langle r^2 \rangle_0 = na^2$ of the bridge chain, and introduce an important dynamic parameter

$$\epsilon_D \equiv D\beta_0^{-1}/na^2 \tag{9.27}$$

If ϵ_D is small, the network is well described by the affine network [16]. But, if it is of order unity, the effect of the fluctuations is large. We will mostly start from affine networks in the following analyses, but show the effect of diffusion whenever it is significant.

For an aged system that has been kept quiescent for a long time under no deformation so that all chains have relaxed to the equilibrium state, we have

$$\phi(\mathbf{r}, \infty) = \phi_0(\mathbf{r}) = \nu_d(\infty)\Phi(\mathbf{r}). \tag{9.28}$$

We find the equilibrium distribution of the effective chains in the form

$$\psi_0(\mathbf{r}) = \nu_d(\infty)\alpha(\mathbf{r})\Phi(\mathbf{r})/\beta(\mathbf{r}). \tag{9.29}$$

The initial distribution is therefore *not Gaussian* if the chain dissociation rate β, or recombination rate α, depends on the end-to-end distance.

Since the ratio $\beta(\mathbf{r})/\alpha(\mathbf{r})$ is the equilibrium constant $K(\mathbf{r})$ of the chemical reaction, the above equation is transformed to

$$\psi_0(\mathbf{r}) = \nu_d(\infty)C_n \exp\left[-\int_0^{\mathbf{r}} (\mathbf{f}/k_B T + \nabla \ln K(\mathbf{r})) \cdot d\mathbf{r} \right]. \tag{9.30}$$

We see that an effective chain experiences, in addition to the direct tension $\mathbf{f}$, the chemical affinity $\nabla \ln K(\mathbf{r})$ originating in the tensions from other end chains connected to the same junction. The total force working on the end of an effective chain is given by

$$\mathbf{F}(\mathbf{r})/k_B T \equiv \mathbf{f}/k_B T + \nabla \ln K(\mathbf{r}). \tag{9.31}$$

Finally, by integrating (9.29) over all possible $\mathbf{r}$, we find

$$\nu_e(\infty)/\nu_d(\infty) = \int \alpha(\mathbf{r})\Phi(\mathbf{r})/\beta(\mathbf{r})d\mathbf{r} \equiv \langle \alpha\beta^{-1} \rangle, \tag{9.32}$$

and hence we have

$$\nu_d(\infty) = \nu/(1 + \langle \alpha\beta^{-1} \rangle), \tag{9.33a}$$

$$\nu_e(\infty) = \nu\langle \alpha\beta^{-1} \rangle/(1 + \langle \alpha\beta^{-1} \rangle). \tag{9.33b}$$

Among the total ν of the chains forming the network, the fraction $\langle \alpha\beta^{-1} \rangle/(1 + \langle \alpha\beta^{-1} \rangle)$ turns out to be active.

9.1.3 Stress–strain relation

The free energy of the entire network is given by the sum of the free energy stored in each individual chain and the internal energy caused by the molecular interactions between the chain segments.

The former is analogous to (1.12), and given by

$$F(t) = \int d\mathbf{r}\epsilon(\mathbf{r})\psi(\mathbf{r},t), \tag{9.34}$$

where the elastic free energy stored in a single chain is

$$\epsilon(\mathbf{r}) = \int \mathbf{f} \cdot d\mathbf{r}. \tag{9.35}$$

For the Gaussian chain (1.34), it takes the form (1.36)[2]

$$\epsilon(\mathbf{r}) = \frac{3k_B T}{2na^2} r^2. \tag{9.36}$$

The latter is assumed to depend only on the density ρ of the segments. It is proportional to $vnV_0/V(t)$, where $V(t)$ is the instantaneous volume of the system at time t. The volume change under deformation is given by $V(t) = V_0|\hat{\lambda}(t)|$ in terms of the initial volume V_0, and the determinant of the strain tensor.

This assumption leads to the total free energy

$$F_{\text{tot}}(t) = F(t) + E(|\hat{\lambda}(t)|), \tag{9.37}$$

where E represents the internal free energy due to the chain interaction.

The stress tensor corresponding to a given deformation $\hat{\lambda}(t)$ is derived by the limit

$$\hat{\Sigma}(t)a^3 = \lim_{\hat{\Delta} \to 0} [F_{\text{tot}}((\hat{1} + \hat{\Delta}) \cdot \hat{\lambda}) - F_{\text{tot}}(\hat{\lambda})] \cdot \hat{\Delta}^{-1}, \tag{9.38}$$

which explicitly gives

$$\hat{\Sigma}(t)a^3 = \int d\mathbf{r}(\mathbf{r}\,{}^t\mathbf{f})\psi(\mathbf{r},t) - P\hat{1}, \tag{9.39}$$

where $\mathbf{r}^t\mathbf{f}$ is a dyadic, and P is the isotropic pressure due to the internal energy.[3] Specifically for the Gaussian chain (1.34), the stress tensor is

$$\hat{\Sigma}(t)a^3 = \frac{3k_B T}{na^2}\langle\mathbf{r}\,{}^t\mathbf{r}\rangle_t - P\hat{1}. \tag{9.40}$$

---

[2] The single-chain free energy F_0 in Section 1.2 is designated here as ϵ.
[3] The superscript t on the left shoulder of $\mathbf{f}$ indicates the transpose of the vector $\mathbf{f}$.

9.1.4   Integral form of the equation

The solution of the initial value problem for the differential equation (9.26) is formally expressed by [16]

$$\psi(\mathbf{r},t)d\mathbf{r} = \Theta(\mathbf{r},t;\mathbf{r}_0,0)\psi(\mathbf{r}_0,0)d\mathbf{r}_0$$
$$+ \int_0^t dt'\Theta(\mathbf{r},t;\mathbf{r}',t')m(\mathbf{r}',t')\Phi(\mathbf{r}')d\mathbf{r}', \tag{9.41}$$

where the two-point function Θ is defined by

$$\Theta(\mathbf{r},t;\mathbf{r}',t') \equiv \exp\left[-\int_{t'}^t \beta(\mathbf{r}_{t'',t'})dt''\right]. \tag{9.42}$$

This function provides the **chain survival probability**, which is the probability for a given active chain with end-to-end vector $\mathbf{r}'$ at time t' to remain active until time t with end vector $\mathbf{r}$.

Thanks to the affineness assumption, $\mathbf{r}$ is uniquely related to $\mathbf{r}'$ through the equation

$$\mathbf{r} = \mathbf{r}_{t,t'} = \hat{\lambda}(t) \cdot \hat{\lambda}(t')^{-1} \cdot \mathbf{r}'. \tag{9.43}$$

The first term in (9.41) gives the number of chains that, being active in the initial state, remain active until time t. The function $m(\mathbf{r},t)$ in the second term is the number of active chains created at t in a unit time

$$m(\mathbf{r},t) = \alpha(\mathbf{r})v_{\mathrm{d}}(t) = \alpha(\mathbf{r})[v - v_{\mathrm{e}}(t)]. \tag{9.44}$$

The second term in (9.41) therefore gives the number of active chains that are created at time t' with end-to-end vector $\mathbf{r}'$ and remain active until t. Since this term depends on the space integral of $\psi(\mathbf{r}',t')$ through $v_{\mathrm{e}}(t')$, (9.41) is not an explicit solution of the initial value problem, but gives an *integral equation* for $\psi(\mathbf{r},t)$.

Let us first consider the time development of the number of active chains. Spatial integration of (9.41) gives

$$v_{\mathrm{e}}(t) = v_{\mathrm{e}}^{\circ}(t) + \int_0^t \theta(t;t')[v - v_{\mathrm{e}}(t')]dt', \tag{9.45}$$

where

$$v_{\mathrm{e}}^{\circ}(t) \equiv \int \Theta(\mathbf{r},t;\mathbf{r}_0,0)\psi_0(\mathbf{r}_0)d\mathbf{r}_0, \tag{9.46}$$

and

$$\theta(t;t') \equiv \int \Theta(\mathbf{r},t;\mathbf{r}',t')\alpha(\mathbf{r}')\Phi(\mathbf{r}')d\mathbf{r}'. \tag{9.47}$$

The first term $v_{\mathrm{e}}^{\circ}(t)$ gives the number of chains that were initially active and remain active until time t. It is therefore a steadily decreasing function of the time; it goes down to 0 at $t = \infty$ in most cases. It can reach a finite value at $t = \infty$ when the chain dissociation rate $\beta(\mathbf{r})$ vanishes in a certain finite region of $\mathbf{r}$.

The function $\theta(t;t')$ gives the survival probability averaged over the distribution at the creation time t'

Substituting the integral form for $\psi(\mathbf{r},t)$ into the stress tensor, we find

$$\hat{\Sigma}(t) = \hat{\Sigma}^{\circ}(t) + \int_0^t \hat{\sigma}(t;t')[v - v_e(t')]dt' - P\hat{1}, \tag{9.48}$$

for the time development of the stress tensor, where

$$\hat{\Sigma}^{\circ}(t)a^3 \equiv \int (\mathbf{r}^t\mathbf{f})\Theta(\mathbf{r},t;\mathbf{r}_0,0)\psi_0(\mathbf{r}_0)d\mathbf{r}_0 \tag{9.49}$$

is the stress supported by the initially active chains, and

$$\hat{\sigma}(t;t')a^3 \equiv \int (\mathbf{r}^t\mathbf{f})\Theta(\mathbf{r},t;\mathbf{r}',t')\alpha(\mathbf{r}')\Phi(\mathbf{r}')d\mathbf{r}' \tag{9.50}$$

is the time propagator for the stress survival.

The isotropic pressure stays constant under a volume conserving deformation $\hat{\lambda}(t)$ for which $|\hat{\lambda}(t)| = 1$ holds, but there should be a coupling between the chain elasticity and the segment interaction if the volume is not conserved during the deformation.

The solution of the integral equation (9.45) can formally be found by Laplace transformation. Let

$$\tilde{v}_e(s) \equiv \int_0^{\infty} e^{-st} v_e(t)dt \tag{9.51}$$

be the Laplace transform of $v_e(t)$. Equation (9.45) then gives

$$\tilde{v}_e(s) = \frac{v\tilde{\theta}(s) + s\tilde{v}_e^{\circ}(s)}{s[1 + \tilde{\theta}(s)]} \tag{9.52}$$

For the stationary viscoelastic properties, it is sufficient to find a solution at $t = \infty$. The simple pole at $s = 0$ gives

$$v_e(t = \infty) = \frac{v\tilde{\theta}(0)}{1 + \tilde{\theta}(0)} \tag{9.53}$$

for the number of active chains.[4]

Similarly we find that the number of active chains generated in a unit time is given by

$$\tilde{m}(\mathbf{r},s) = \alpha(\mathbf{r})\frac{v - s\tilde{v}_e(s)}{s[1 + \tilde{\theta}(s)]}, \tag{9.54}$$

and hence we have for the steady state

$$m(\mathbf{r},t = \infty) = \alpha(\mathbf{r})\frac{v}{1 + \tilde{\theta}(0)}. \tag{9.55}$$

---

[4] The number $\tilde{v}_e^{\circ}(0)$ has been assumed to be finite, because $v_e^{\circ}(t)$ is a rapidly decaying function.

9.1.5   Generalization of the model

At this stage, we can see easily that our present model is a special case of the two-state transient network model in which chains take either A-state or B-state. The conversion between them

$$A(\mathbf{r}) \rightleftharpoons B(\mathbf{r}) \qquad (9.56)$$

is allowed. If we neglect the diffusion terms, and confine in the affine networks, the time development of the number of chains obeys

$$\frac{\partial \psi_A(\mathbf{r},t)}{\partial t} + \nabla \cdot (\bar{\mathbf{v}}_A(t)\psi_A(\mathbf{r},t)) = -\beta(\mathbf{r})\psi_A(\mathbf{r},t) + \alpha(\mathbf{r})\psi_B(\mathbf{r},t) \qquad (9.57a)$$

$$\frac{\partial \psi_B(\mathbf{r},t)}{\partial t} + \nabla \cdot (\bar{\mathbf{v}}_B(t)\psi_B(\mathbf{r},t)) = \beta(\mathbf{r})\psi_A(\mathbf{r},t) - \alpha(\mathbf{r})\psi_B(\mathbf{r},t) \qquad (9.57b)$$

In the present poblem of telechelic polymers, the A-state corresponds to the bridge chain connecting the micellar junctions, while the B-state is the dangling chain. In affine network theory, $\bar{\mathbf{v}}_A = (\frac{d\hat{\lambda}}{dt} \cdot \hat{\lambda}^{-1}) \cdot \mathbf{r}$ as in (9.3), and $\bar{\mathbf{v}}_B = 0$. But $\bar{\mathbf{v}}_B$ may also be affine if the B-state is another type of the elastically effective state, such as helical conformation or globular conformation of the same chain. We can study the stress relaxation in rubber networks in which chains change their conformation by deformation [30].

9.2   Linear response of transient networks

Consider the linear response of the affine network (9.26) to a small oscillatory shear flow defined by the deformation tensor

$$\hat{\lambda}(t) = \begin{bmatrix} 1 & \epsilon e^{i\omega t} & 0 \\ 0 & 1 & 0 \\ 0 & 0 & 1 \end{bmatrix}, \qquad (9.58)$$

with a small amplitude ϵ. The velocity tensor is given by

$$\hat{\kappa}(t) = \begin{bmatrix} 0 & i\epsilon\omega e^{i\omega t} & 0 \\ 0 & 0 & 0 \\ 0 & 0 & 0 \end{bmatrix}, \qquad (9.59)$$

so that the average velocity of the junction is

$$\bar{\mathbf{v}}(t) = \begin{bmatrix} i\epsilon\omega y e^{i\omega t} \\ 0 \\ 0 \end{bmatrix}. \qquad (9.60)$$

The amplitude ϵ is assumed to be sufficiently small, and hence we can expand the chain distribution functions in powers of ϵ.

Let us find the solution within the linear term

$$\psi(\mathbf{r},t) = \psi_0(\mathbf{r})[1 + \epsilon \xi(\mathbf{r},t)], \tag{9.61}$$

where $\xi(\mathbf{r},t)$ is the deviation from the equilibrium, and

$$\phi(\mathbf{r},t) = \phi_0(\mathbf{r}). \tag{9.62}$$

(The linear term in ϕ is zero.) Substituting into (9.26), we find

$$\frac{\partial \xi}{\partial t} + i\omega y e^{i\omega t} \frac{\partial \ln \psi_0}{\partial x} = -\beta(\mathbf{r})\xi \tag{9.63}$$

for the linear term in ϵ. The solution of this equation is

$$\xi(\mathbf{r}) = \frac{i\omega y F_x / k_B T}{i\omega + \beta} e^{i\omega t}. \tag{9.64}$$

The complex modulus is defined by the proportionality constant between the stress and deformation as

$$\Sigma_{x,y} a^3 \equiv G(\omega)\epsilon e^{i\omega t}. \tag{9.65}$$

Hence we have

$$\frac{G(\omega)}{k_B T} = \int d\mathbf{r}\,\psi_0(\mathbf{r}) \left(x \frac{f_y(r)}{k_B T} \right) \frac{i\omega}{i\omega + \beta(\mathbf{r})} \left(y \frac{F_x(r)}{k_B T} \right), \tag{9.66}$$

for the complex modulus. Taking the real and imaginary parts, we find [23]

$$\frac{G'(\omega)}{k_B T} = \int d\mathbf{r}\,\psi_0(\mathbf{r}) \left(\frac{x f_y(r)}{k_B T} \right) \frac{\omega^2}{\omega^2 + \beta(\mathbf{r})^2} \left(\frac{y F_x(r)}{k_B T} \right), \tag{9.67a}$$

$$\frac{G''(\omega)}{k_B T} = \int d\mathbf{r}\,\psi_0(\mathbf{r}) \left(\frac{x f_y(r)}{k_B T} \right) \frac{\beta(\mathbf{r})\omega}{\omega^2 + \beta(\mathbf{r})^2} \left(\frac{y F_x(r)}{k_B T} \right). \tag{9.67b}$$

By spherical symmetry, these are transformed to

$$\frac{G(\omega)}{k_B T} = \int d\mathbf{r}\,\psi_0(\mathbf{r}) \left(\frac{xy}{r} \frac{f(r)}{k_B T} \right) \frac{i\omega}{i\omega + \beta(\mathbf{r})} \left(\frac{xy}{r} \frac{F(r)}{k_B T} \right), \tag{9.68}$$

where $f(r)/k_B T = -d \ln \Phi/dr$, $F(r)/k_B T = -d \ln \psi_0/dr$. By partial integration, we find

$$\begin{aligned}
\frac{G(\omega)}{k_B T} &= \int d\mathbf{r}\,\psi_0(\mathbf{r}) \frac{d}{dr} \left[\left(\frac{xy}{r} \right)^2 \frac{f(r)}{k_B T} \frac{i\omega}{i\omega + \beta(r)} \right] \\
&= \frac{\nu_e}{\langle \alpha\beta^{-1} \rangle} \left\langle \frac{\alpha}{\beta} \frac{i\omega}{i\omega + \beta} \left[\frac{d}{dr} \left(\frac{r^2 f}{k_B T} \right) - \left(\frac{r^2 f}{k_B T} \right) \frac{\beta'}{i\omega + \beta} \right] \right\rangle,
\end{aligned} \tag{9.69}$$

for an isotropic $\beta(r)$.

In particular, for a Gaussian chain with a constant recombination rate α, we find [17]

$$\frac{G'(\omega)}{\nu_e k_B T} = \frac{1}{\langle \beta^{-1} \rangle_0 n a^2} \left\langle \frac{\omega^2 r^2}{\beta(r)[\omega^2 + \beta(r)^2]} \left[1 - \frac{2r\beta(r)\beta'(r)}{5[\omega^2 + \beta(r)^2]} \right] \right\rangle_0, \tag{9.70a}$$

$$\frac{G''(\omega)}{\nu_e k_B T} = \frac{1}{\langle \beta^{-1} \rangle_0 n a^2} \left\langle \frac{\omega r^2}{\omega^2 + \beta(r)^2} \left[1 + \frac{[\omega^2 - \beta(r)^2]r\beta'(r)}{5\beta(r)^2[\omega^2 + \beta(r)^2]} \right] \right\rangle_0. \tag{9.70b}$$

The frequency-dependent linear viscosity is defined by

$$\eta(\omega) \equiv G''(\omega)/\omega. \tag{9.71}$$

The **complex viscosity**, defined by

$$\eta^*(\omega) \equiv \frac{\{G'(\omega)^2 + G''(\omega)^2\}^{1/2}}{\omega}, \tag{9.72}$$

is sometimes referred to instead of $\eta(\omega)$.

By taking the $\omega \to 0$ limit, we find

$$\eta_0 \equiv \eta(\omega = 0) = k_B T \int d\mathbf{r} \psi_0(\mathbf{r}) \left(\frac{xy}{r} \frac{f(r)}{k_B T} \right) \frac{1}{\beta(\mathbf{r})} \left(\frac{xy}{r} \frac{F(r)}{k_B T} \right), \tag{9.73}$$

for the zero-frequency viscosity. We will show in Section 9.3 that this agrees with the zero shear-rate limit ($\dot{\gamma} \to 0$) of the nonlinear stationary viscosity $\eta_{st}(\dot{\gamma})$.

Also, we find that the slope for the high-frequency region

$$-\lim_{\omega \to \infty} \omega G''(\omega) = k_B T \int d\mathbf{r} \psi_0(\mathbf{r}) \left(\frac{xy}{r} \frac{f(r)}{k_B T} \right) \frac{1}{\beta(\mathbf{r})} \left(\frac{xy}{r} \frac{F(r)}{k_B T} \right), \tag{9.74}$$

must be equal to η_0. The **high-frequency plateau modulus** is

$$G_\infty \equiv \lim_{\omega \to \infty} G'(\omega) = k_B T \int d\mathbf{r} \psi_0(\mathbf{r}) \left(\frac{xy}{r} \frac{f(r)}{k_B T} \right) \left(\frac{xy}{r} \frac{F(r)}{k_B T} \right). \tag{9.75}$$

As for the storage modulus, the limit

$$\lim_{\omega \to 0} \frac{G'(\omega, T)}{\omega^2} = k_B T \int d\mathbf{r} \psi_0(\mathbf{r}) \left(\frac{xy}{r} \frac{f(r)}{k_B T} \right) \frac{1}{\beta(\mathbf{r})^2} \left(\frac{xy}{r} \frac{F(r)}{k_B T} \right) \tag{9.76}$$

gives exactly half the value of the zero-shear limit of the stationary first normal stress difference coefficient $\Psi_1(\dot{\gamma} = 0)$ (see Section 9.3).

The static recovery compliance J_e^0 is therefore given by

$$J_e^0 = \lim_{\omega \to 0} G'(\omega)/\omega^2 \eta_0^2, \tag{9.77}$$

and hence the terminal relaxation time τ_m defined by $\tau_m \equiv \eta_0 J_e^0$ is identical to the ratio

$$\tau_m = \eta_0/G_\infty, \tag{9.78}$$

irrespective of the chain dissociation rate $\beta(\mathbf{r})$.

9.2.1 The Green–Tobolsky limit

Let us next consider the special case where the chain dissociation rate $\beta(r)$ is a constant. This limit is called the **Green–Tobolsky limit** (GT limit). Since $\beta(r) = \beta_0$ ($\beta'(r) = 0$), we find from (9.70a,b)

$$G'(\omega, T) = \nu_e k_B T \frac{\omega^2}{\omega^2 + \beta_0^2}, \tag{9.79}$$

$$G''(\omega, T) = \nu_e k_B T \frac{\beta_0 \omega}{\omega^2 + \beta_0^2}, \tag{9.80}$$

for any tension profile $f(r)$. Thus our network reduces to a **Maxwell fluid** with a single relaxation time $\tau_m = \beta_0^{-1}$. The complex viscosity in the GT limit is

$$\eta^*(\omega, T) = \frac{\nu_e k_B T}{(\omega^2 + \beta_0^2)^{1/2}}. \tag{9.81}$$

The dissociation rate per unit time takes the activation form

$$\beta_0(T) = \omega_0 e^{-\Delta E / k_B T}, \tag{9.82}$$

where ω_0 is the natural frequency of thermal vibration of the reactive group. It is a microscopic measure of the time, and should take a typical value in the order of 10^8–10^9 s^{-1} in ordinary circumstances.

Temperature dependence of the rheological time scale in temporal networks is different from that of uncross-linked polymer melts. In the latter systems, both Rouse relaxation time and the reptation time are virtually proportional to T^{-1} apart from the indirect dependence through the friction coefficient.

Upon substitution of (9.82) into the moduli (9.68), we find the **frequency–temperature superposition principle** such that a modulus–frequency curve at any temperature T can be superimposed onto a single curve at the reference temperature T_0, if it is vertically and horizontally shifted properly. Such construction of the **master curve** is described by the equation

$$\frac{G(\omega, T)}{\nu_e(T_0) k_B T_0} b_T = \mathcal{G}\left(\frac{\omega}{\beta_0(T_0)} a_T\right), \tag{9.83}$$

for both G' and G'', where $\mathcal{G}$ is a scaling function,

$$a_T \equiv \beta_0(T_0) / \beta_0(T) = \exp\left[-\frac{\Delta E}{k_B}\left(\frac{1}{T_0} - \frac{1}{T}\right)\right] \tag{9.84}$$

is the frequency (horizontal) shift factor, and

$$b_T \equiv \nu_e(T_0) k_B T_0 / \nu_e(T) k_B T \tag{9.85}$$

is the modulus (vertical) shift factor. The frequency shift factor a_T depends exponentially on the reciprocal of the temperature due to the activation process (9.82) of the dissociation.

HEUR C16/ 35K
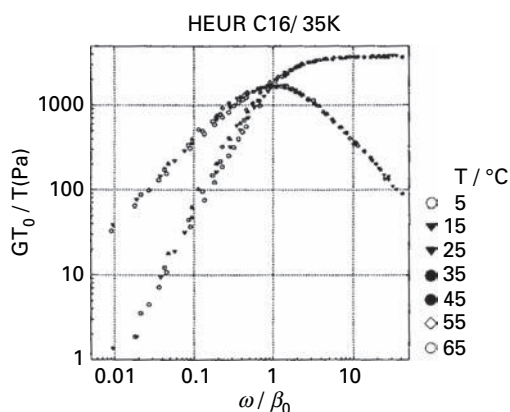
Viscoelastic master curve of HEUR with $M_{\mathrm{w}} = 35\mathrm{K}$ and 16 carbons in the end chain [2]. The reference temperature is 5°C. The activation energy and the number of elastically effective chains can be found from the shift factors. (Reprinted with permission from Ref. [2].)

A typical example of the master curve [2] is shown in Figure 9.3 for HEUR (polyethylene oxide) end-capped with $-C_{16}H_{33}$. The reference temperature is chosen at 5°C. From the horizontal shift factor, the activation energy is found to be $67\,\mathrm{kJ\,mol^{-1}}$. From the high-frequency plateau of the storage modulus, the number of elastically effective chains is found as a function of the polymer concentration, which was already studied in Section 8.2 (Figure 8.10).

9.2.2   Exponential dissociation rate

Because the reactive group is attached on the chain end, it is pulled by the tension f from the chain. Hence, the potential barrier for the associative group to dissociate is effectively reduced to $\Delta E - fa$. The chain dissociation rate is therefore enhanced to

$$\beta(r) = \omega_0 \exp[-(\Delta E - fa)/k_{\mathrm{B}}T] \equiv \beta_0 e^{\kappa r}, \tag{9.86}$$

for a Gaussian chain, where $\kappa \equiv 3/na$ is a small parameter that depends on the molecular weight of the polymer chain [17].

The length r^* of the end-to-end separation above which the reactive group spontaneously dissociates can be roughly estimated by the condition $\Delta E - fa \simeq 0$, and hence

$$r^* \simeq \frac{na}{3k_{\mathrm{B}}T} \Delta E. \tag{9.87}$$

For the physical association, whose binding energy is comparable to the thermal energy, the cutoff lies in the high extension region, i.e., $r^* \simeq l = na$.

Figure 9.4(a) shows the numerical calculation of the master curves for the exponential $\beta(r)$ on a logarithmic scale. The solid lines show the storage modulus, and the broken lines the loss modulus. The degree of polymerization n is varied from curve to curve. Both moduli shift to a lower-frequency region with the molecular weight, but because of
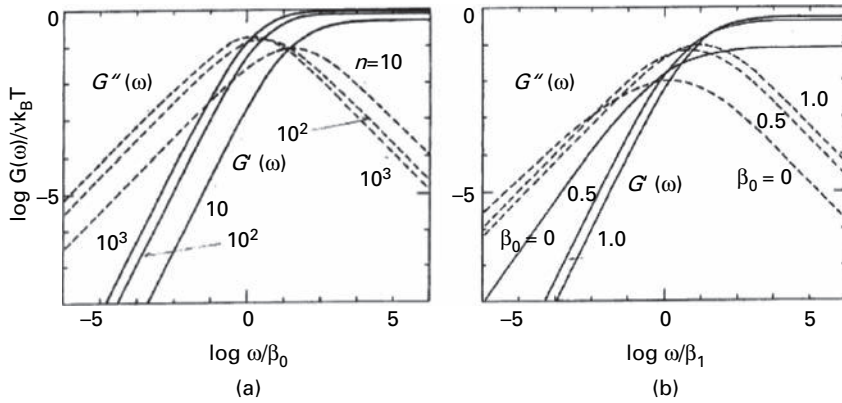
Fig. 9.4 (a) Modulus–frequency master curve for the chain dissociation rate $\beta(r) = \beta_0 \exp(\kappa r)$. The number n of statistical units on a chain is varied from curve to curve. (b) Master curve for $\beta(r) = \beta_0 + (3/2)\beta_1 r^2/\langle r^2 \rangle_0$ for $n = 100$. The parameter β_0 is changed from curve to curve. (Reprinted with permission from Ref. [18].)

the weak dependence of the chain dissociation rate on the molecular weight, any change in n alters the master curves only a little.

Insensitivity to the molecular weight indicates that the viscoelasticity is caused by conformational entropy change of the stretched active chains rather than monomeric friction.

9.2.3 Power-law dissociation rate

In order to illustrate the insensitivity of the master curve to the detailed form of $\beta(r)$, we show in Figure 9.4(b) the result for the power-law model [17]

$$\beta(r) = \beta_0 + \frac{3}{2}\beta_1 \left(\frac{r^2}{\langle r^2 \rangle_0}\right)^m, \tag{9.88}$$

where $m = 1, 2, \ldots$, $\langle r^2 \rangle_0 = na^2$. (The factor 3/2 is for calculational simplicity.) The frequency is scaled by the unit β_1, while the modulus is measured in the unit of $\nu_e(T)k_B T$. The chain dissociation rate β_0 is changed from curve to curve. As β_0 is increased, both moduli decrease in the low-frequency region, while they increase in the high-frequency region. The entire form of the master, however, remains the same.

Figure 9.5 shows the numerical result with m varied for a fixed β_0. The figures beside the curves show the values of the power $2m$. As $2m$ is increased from 0.5 to 2.5, the slope of G' at low frequencies decreases from 2.0 to 1.0, while that of G'' remains 1.0. In fact, the lower bound of the integrals shown in (9.70b) controls the low-frequency slopes of the moduli.

By making a scaling $r \equiv \omega^{1/m} x$ for the integral variables, one can easily find that $G'(\omega) \approx \omega^{(5-2m)/2m}$ for $2m > 5/3$, while $G'(\omega) \approx \omega^2$ for $2m < 5/3$. Similarly $G''(\omega) \approx \omega^{(5-2m)/2m}$ for $2m > 5/2$, while $G''(\omega) \approx \omega$ for $2m < 5/2$.
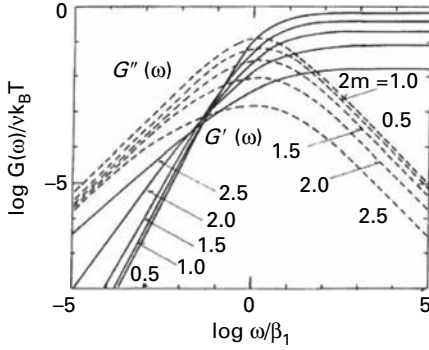
Fig. 9.5   Master curve for the dissociation rate $\beta(r) = (3/2)\beta_1(r^2/\langle r^2\rangle_0)^m$. The figures beside the curves show the value of $2m$. The slope of the low-frequency tail of the storage modulus changes with m. (Reprinted with permission from Ref. [18].)

Thus for sufficiently high powers m of $\beta(r)$, the storage and loss modulus both turn out to have low-frequency asymptotic tails behaving $\approx \omega^{(5-2m)/2m}$. This asymptotic evaluation breaks down for $2m > 5/2$, because the integrals diverge.

9.2.4   Coupling to the tension

To incorporate stretching of the chain beyond the linear regime, we consider the nonlinear profile (1.30)

$$\tilde{f}(\tilde{r}) = 3\tilde{r}\left(1 + \frac{2}{3}A\frac{\tilde{r}^2}{1-\tilde{r}^2}\right) \tag{9.89}$$

of the tension–elongation curve discussed in Section 1.2. The nonlinearity of the chain depends on the amplitude A; $A = 0$ gives a Gaussian, while $A = 1$ gives a Langevin chain within a very high accuracy. The chain nonlinearity increases with the amplitude A. The measurement by atomic force spectroscopy [31], and molecular dynamic simulation [32] suggest that $A \approx 5.0$ for a PEO chain, and $A \approx 1.0$ for a PNIPAM chain in water at room temperature.

We introduce the effect of chain tension on the dissociation rate in the form

$$\beta(r) = \beta_0(T)[1 + g\tilde{f}(\tilde{r})^2], \tag{9.90}$$

where $\beta_0(T)$ is the thermal dissociation rate (9.82), and g the **coupling constant** between the dissociation rate and the chain tension [33,23]. This form may be derived by applying the conventional Kramers method [34] to calculate the first passage time required for a trapped Brownian particle to overcome the barrier of the force potential. The coupling constant g provides a measure for how easily the end chains are extruded from the micelles. If there is no coupling ($g = 0$), the model reduces to the GT limit. If the chain is Gaussian, the model reduces to the power-law ($m = 1$) in the previous section.

Figure 9.6 shows the calculated modulus of the nonlinear chain with $A = 10$ with a fixed coupling constant $g = 0.2$. Although we are studying linear viscoelasticity, the
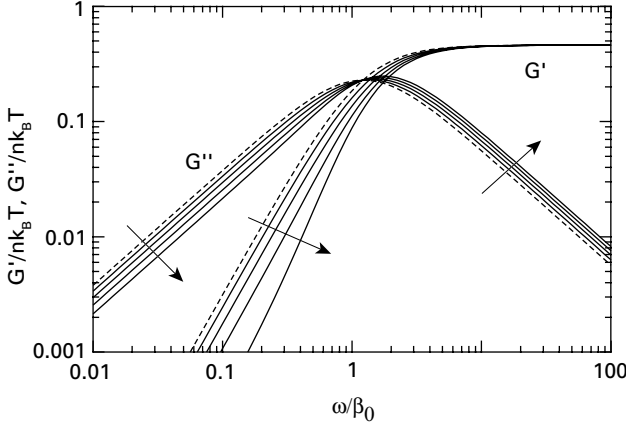
Fig. 9.6   Dynamic mechanical moduli of the nonlinear chain $A = 10$ with tension-dissociation coupling $g = 0.2$. The dimensionless diffusion parameter ϵ_D is changed from 0 (affine network, broken line) to 0.20 (solid lines). (Reprinted with permission from Ref. [23].)

effect of nonlinear stretching of the main chain turns out to be significant [23]. We have included the effect of the diffusion (nonaffine effect) in this figure by changing the diffusion constant D from curve to curve. There is a shift of the maximum point in $G''(\omega)$ to the high-frequency region, leading to softening of the modulus in the low ω region and appearance of a tail in the high ω region. This is because there are more chances for the bridge chains to be highly stretched if the fluctuations of the junction positions are large.

9.3   Stationary flows

We next consider the stationary solution under a shear flow along the x-axis with a constant shear rate $\dot{\gamma}$. The average velocity is given by

$$\bar{\mathbf{v}}(t) = \begin{bmatrix} \dot{\gamma} y \\ 0 \\ 0 \end{bmatrix}. \tag{9.91}$$

The equation for the distribution of the bridge chains in a steady state takes the form

$$\dot{\gamma} y \frac{\partial \psi}{\partial x} = -\beta(\mathbf{r})\psi + \nu_d \alpha(\mathbf{r})\Phi(\mathbf{r}), \tag{9.92}$$

where $\nu_d \equiv \nu_d(\dot{\gamma})$ is the number of the dangling chains in a stationary state under the steady shear flow. For the deviation $\xi(\mathbf{r})$ from the equilibrium distribution defined by $\psi(\mathbf{r}) \equiv \psi_0(\mathbf{r})\xi(\mathbf{r})$, we find

$$\dot{\gamma} y \left[\frac{\partial}{\partial x} - \frac{x}{r} F(r) \right] \xi = -\beta(\mathbf{r})\xi + \beta(\mathbf{r})\zeta(\dot{\gamma}), \tag{9.93}$$

where

$$\zeta(\dot{\gamma}) \equiv \nu_{\mathrm{d}}(\dot{\gamma})/\nu_{\mathrm{d}}(0) \tag{9.94}$$

is the ratio of ν_{d} to its equilibrium value without shear.

Our starting equation is then written in a compact form as

$$(\dot{\gamma}\hat{P} + \beta)\xi = \beta\zeta, \tag{9.95}$$

by using the differential operator

$$\hat{P} \equiv y\left[\frac{\partial}{\partial x} - \frac{x}{r}F(r)\right]. \tag{9.96}$$

The ij component of the stress tensor can be calculated by

$$\Sigma_{ij}(\dot{\gamma})a^3 = \int d\mathbf{r}(x_i f_j)\psi_0(\mathbf{r})\xi(\mathbf{r})$$
$$= \zeta(\dot{\gamma})\int d\mathbf{r}(x_i f_j)(\beta + \dot{\gamma}\hat{P})^{-1}\beta, \tag{9.97}$$

from (9.39). The stationary shear viscosity is obtained from the shear stress by

$$\eta(\dot{\gamma}) = \Sigma_{xy}(\dot{\gamma})/\dot{\gamma}. \tag{9.98}$$

Hence, in the limit of high shear rate, we find

$$\eta(\dot{\gamma}) \simeq \zeta(\dot{\gamma})/\dot{\gamma}^2, \tag{9.99}$$

by neglecting β in the inverse operator $(\beta + \dot{\gamma}\hat{P})^{-1}$.

The normal stress differences are defined by

$$N_1 = \Sigma_{xx} - \Sigma_{yy}, \tag{9.100a}$$
$$N_2 = \Sigma_{yy} - \Sigma_{zz}, \tag{9.100b}$$

and the normal stress coefficients Ψ_i are defined by

$$\Psi_i = N_i/\dot{\gamma}^2. \tag{9.101}$$

9.3.1   GT limit and quadratic β

In the GT limit, the steady-state number of active chains is independent of the shear rate. It remains the same as the equilibrium value under no external forces

$$\nu_{\mathrm{e}}(\infty) = \nu_{\mathrm{e}}. \tag{9.102}$$

The shear viscosity is given by

$$\eta_{st}(\dot{\gamma}) = \frac{\nu_e k_B T}{\beta_0} = G_\infty \tau_m, \tag{9.103}$$

which is independent of the shear rate, where $G_\infty \equiv \nu_e k_B T$ is the linear elastic modulus. Therefore an inequality

$$\eta(\omega) < \eta^*(\omega) < \eta_{st}(\dot{\gamma}) \tag{9.104}$$

between linear viscosity and the stationary nonlinear viscosity holds, when compared at $\omega = \dot{\gamma}$.

In ordinary polymer solutions in which polymers interact by nonspecific van der Waals type potentials, it is known that the phenomenological relation $\eta(\omega) = \eta_{st}(\dot{\gamma})$ (the **Cox–Merz rule**) often holds [35]. Disagreement between the complex viscosity and the stationary viscosity at finite frequencies is one of the common features of the hydrogen-bonded networks.

The first normal stress difference coefficient can be similarly obtained from (9.101) as

$$\Psi_1 = \frac{2\nu_e k_B T}{\beta_0^2} = 2\eta_0 \tau_m, \tag{9.105}$$

which is a positive constant independent of the shear rate. The second normal stress difference coefficient vanishes

$$\Psi_2 = 0. \tag{9.106}$$

To study the dependence on the shear rate, let us consider quadratic dissociation rate. For the particular form (9.88) with $m = 1$, we can find analytic solution of the integral equation. Mathematical detail is given in Appendix 9.B. We show in Figure 9.7 the complex viscosity and the stationary viscosity plotted against the frequency ω, or the same value of the shear rate $\dot{\gamma}$. Comparison is specifically made for the quadratic model
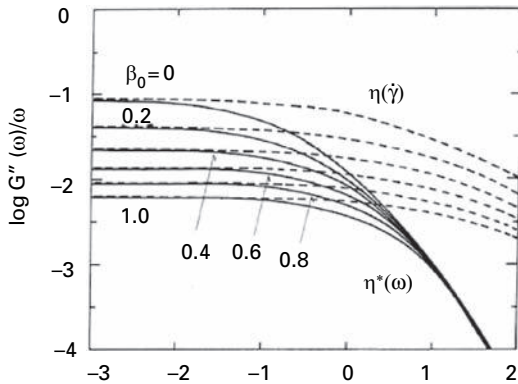
Fig. 9.7 Deviation from the Cox–Merz rule. The frequency-dependent linear viscosity $\eta(\omega)$ (solid lines) is compared to the nonlinear stationary viscosity $\eta_{st}(\dot{\gamma})$ (broken lines). The quadratic $\beta(r)$ is assumed. The parameter β_0 is varied from curve to curve. (Reprinted with permission from Ref. [17].)

$(m = 1)$ with β_0 varied from 0 to 1.0. The stationary viscosity decreases with the shear rate (**shear thinning**) due to the enhancement of the dissociation rate by chain stretching. However, it is still larger than the linear viscosity $\eta(\omega)$ at all frequencies, thus suggesting a breakdown of the Cox–Merz rule.

9.3.2   Coupling to the tension

We next examine the stationary stresses of the tension–dissociation coupling model. Typical numerical results for the affine transient networks are presented in Figure 9.8 for the thinning case (a) $g = 1$, and the thickening case (b) $g = 0.01$ under shear flow [36]. The stresses and the shear rate are presented in the units of $\nu k_B T$ and β_0. The shear viscosity shows thinning in (a) and thickening in (b).

Roughly, the chain must be highly nonlinear (large A) and the coupling constant must be sufficiently small (small g) for thickening (see Figure 9.8) [33, 36]. In the thinning case of the shear viscosity, the first normal stress coefficient Ψ_1 also shows thinning. The
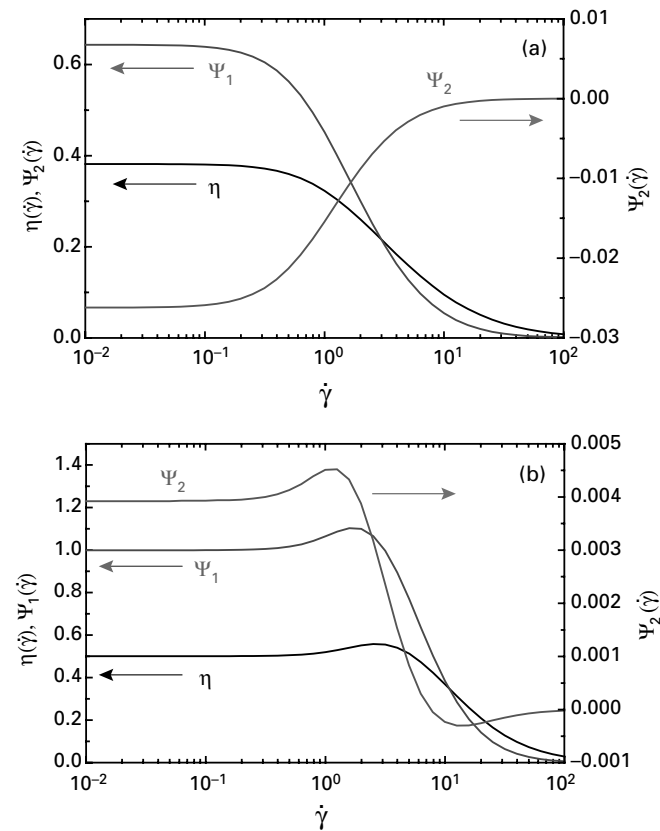
Fig. 9.8   Stationary shear viscosity and normal stress coefficients for a polymer chain of $n = 100$ as a function of shear rate (a) in the shear-thinning regime ($A = 1, g = 1$), and (b) in the shear-thickening regime ($A = 1, g = 0.01$). (Reprinted with permission from Ref. [36].)

sign of the second normal stress coefficient Ψ_2 remains always negative, and its absolute value decreases with the shear rate.

In the thickening case as in Figure 9.8(b) for the viscosity, the first normal stress coefficient Ψ_1 also shows thickening although the peak appears at a lower $\dot{\gamma}$. The second normal stress coefficient Ψ_2 is positive in the small shear-rate region, and shows thickening at $\dot{\gamma} \simeq 1$. For higher shear rates, Ψ_2 rapidly decreases and *changes its sign* at $\dot{\gamma}$ where the viscosity shows a maximum. Therefore, the peak appears first in Ψ_2, then in Ψ_1, and finally in η.

Let $\dot{\gamma}_{\max}(\eta)$ and $\dot{\gamma}_{\max}(\Psi_i)$ be their peak positions, and let $\dot{\gamma}_0(\Psi_2)$ be the shear rate where **sign inversion** occurs in the second normal stress coefficient. Then, an inequality $\dot{\gamma}_0(\Psi_2) < \dot{\gamma}_{\max}(\Psi_1) < \dot{\gamma}_{\max}(\eta)$ holds except for the small-A region ($A < 0.15$). The sign inversion occurs at a larger shear rate than that of the viscosity peak.

9.3.3 Expansion in powers of the shear rate

To study the shear-rate dependence of the stresses at small $\dot{\gamma}$ analytically, we first expand ξ and ζ in power series of $\dot{\gamma}$ as

$$\zeta(\dot{\gamma}) = \zeta^{(0)} + \zeta^{(1)}\dot{\gamma} + \zeta^{(2)}\dot{\gamma}^2 + \cdots, \tag{9.107a}$$

$$\xi(\dot{\gamma}) = \xi^{(0)} + \xi^{(1)}\dot{\gamma} + \xi^{(2)}\dot{\gamma}^2 + \cdots. \tag{9.107b}$$

The odd terms $\zeta^{(1)} = \zeta^{(3)} = \cdots = 0$ vanish by symmetry. A simple calculation from Appendix 9.A finds $\zeta^{(0)} = \xi^{(0)} = 1$, and

$$\zeta^{(2)} = \frac{c_{20}}{\nu} \int dr \psi_0 \frac{r^4 F \beta'}{\beta^3}. \tag{9.108}$$

The numerical coefficient c_{20} appears from the angular integral, and is calculated in Appendix 9.A. The explicit forms of $\xi^{(i)} (i = 1 \sim 4)$ are also presented in Appendix 9.A.

Nonlinear viscosity

Since the even-order terms are zero due to symmetry, the shear viscosity is written as

$$\eta(\dot{\gamma}) = \eta^{(0)} + \eta^{(2)}\dot{\gamma}^2 + \cdots, \tag{9.109}$$

where the coefficients are explicitly given by the integrals as

$$\eta^{(0)} = c_{20} \int dr \psi_0 \frac{r^4 f F}{\beta}, \tag{9.110a}$$

$$\eta^{(2)} = c_{40} \int dr \psi_0 \frac{r^6 f F}{\beta^3} \left(\frac{f'}{f} - \frac{1}{r} \right) \left(F - \frac{F'}{F} + \frac{1}{r} + \frac{\beta'}{\beta} \right) \left(\frac{f'}{f} - \frac{1}{r} \right)$$

$$- c_{40} \int dr \psi_0 \frac{r^6 f F}{\beta^3} \frac{\beta'}{\beta} \left(F - \frac{F'}{F} + \frac{4}{r} + \frac{\beta'}{\beta} \right) + \zeta^{(2)} \eta^{(0)}. \tag{9.110b}$$
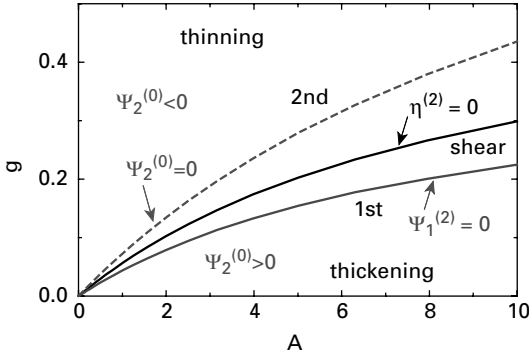
Fig. 9.9 Thickening–thinning diagram of the shear viscosity (solid line) and the first normal stress coefficient (thin solid line). The line of the sign inversion for the second normal stress coefficient (broken line) for the polymer chain of $n = 100$ also shown in linear scale. (Reprinted with permission from Ref. [36].)

The first term $\eta^{(0)}$ agrees with the zero shear viscosity η_0 (9.73). The numerical coefficient c_{40} is given in Appendix 9.A.

The shear-rate dependence of the shear viscosity is determined by the sign of $\eta^{(2)}$. In order to show how the condition for shear thickening depends on the parameters g and A, we draw in Figure 9.9 the thickening and thinning regions on the A–g plane (called the **thickening diagram**) [33, 36] by the criterion $\eta^{(2)} = 0$.

To understand the molecular mechanism of shear thickening, we focus on the two factors, $(f'/f - 1/r)$ and β' in $\eta^{(2)}$. The first one can be written as

$$\frac{f'}{f} - \frac{1}{r} = \frac{4A\tilde{r}/3l}{(1 - \tilde{r}^2 + 2A\tilde{r}^2/3)(1 - \tilde{r}^2)}. \tag{9.111}$$

This is 0 for Gaussian chains ($A = 0$), and positive for nonlinear chains ($A > 0$). On the other hand, $\beta' = 0$ in the GT limit.

In the GT limit ($g = 0$) of Gaussian chains ($A = 0$), $\eta^{(2)}$ is always 0, hence the network lies on the boundary between the thickening and thinning boundaries (Figure 9.9). If the coupling g increases for Gaussian chains ($A = 0$), $\eta^{(2)}$ becomes negative, leading to thinning. If the nonlinearity A increases in the GT limit ($g = 0$), $\eta^{(2)}$ becomes positive showing thickening. This indicates that shear thickening is caused by the stretching of bridge chains into the nonlinear regime.

Normal stress differences

For the normal stress coefficients, we find

$$\Psi_i = \Psi_i^{(0)} + \Psi_i^{(2)}\dot{\gamma}^2 + \cdots. \tag{9.112}$$

(The odd terms vanish due to symmetry.)

By the use of $\xi^{(2)}$ in Appendix 9.A, we find explicitly

$$
\begin{aligned}
\Psi_i^{(0)} = &-c_{02}^{(i)} \int dr \psi_0 \frac{r^4 f F}{\beta^2} \\
&-c_{20}^{(i)} \int dr \psi_0 \frac{r^5 f F}{\beta^2} \left(\frac{F'}{F} - F - \frac{1}{r} - \frac{\beta'}{\beta} \right),
\end{aligned}
\tag{9.113}
$$

for $i = 1, 2$. The coefficients $c_{20}^{(2)}, c_{02}^{(2)}$ are given in Appendix 9.A.

For the first normal stress coefficient ($i = 1$), we have

$$
\Psi_1^{(0)} = \frac{8\pi}{15} \int dr \psi_0 \frac{r^4 f F}{\beta^2},
\tag{9.114}
$$

which is in agreement with the low-frequency slope (9.76) of the storage modulus.

For the second normal stress coefficient ($i = 2$), we have

$$
\Psi_2^{(0)} = c_{20}^{(2)} \int dr \psi_0 \frac{r^5 f F}{\beta^2} \left(\frac{f'}{f} - \frac{1}{r} \right) - c_{20}^{(2)} \int dr \psi_0 \frac{r^5 f F}{\beta^2} \frac{\beta'}{\beta}.
\tag{9.115}
$$

The first term is zero for a Gaussian chain ($A = 0$), while the second term is zero in the GT limit ($g = 0$). Therefore, $\Psi_2^{(0)} = 0$ in the GT limit of Gaussian chains.

If $g > 0, A = 0$, then $\Psi_2^{(0)} < 0$ by the second term. In the GT limit of nonlinear chains ($g = 0, A > 0$), $\Psi_2^{(0)}$ becomes positive by the first term.

In general, the sign of the second normal stress coefficient is determined by the competition between these two terms. If the contribution from the nonlinear stretching is dominant, $\Psi_2^{(0)}$ is positive. Hence, the sign inversion of the second normal coefficient is related to the thickening of the viscosity. In Figure 9.9, the line for the sign inversion of $\Psi_2^{(0)}$ lies close to the line of thickening for $\eta^{(2)}$.

Figure 9.10 compares the theoretical calculation and the experimental data measured on C16 HEUR ($M_w = 20\,000$) [37]. The nonlinear amplitude A in the tension curve is fixed at $A = 5$ by fitting the direct measurement of the tension–elongation profile by AFM [38]. Other model parameters used are $\beta_0 = 9.5\,\mathrm{s}^{-1}$, $g = 0.16$, and $\alpha = 1.48\,\mathrm{s}^{-1}$.

9.3.4 Elongational flows

In other types of flow, polymer chains may behave in a different way and exhibit different flow characteristics. In order to study sensitivity to the type of deformation and flow, let us consider the **elongational flow** described in Section 4.2. The time-dependent
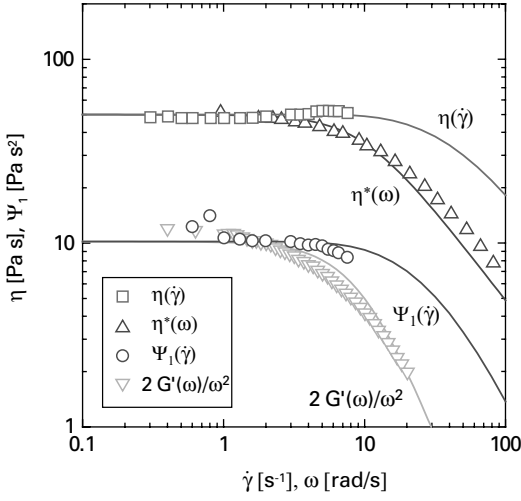
Fig. 9.10   Theoretical curves for the steady shear viscosity and the first normal stress coefficient fitted to the experimental data (symbols) on HEUR in literature [37]. (Reprinted with permission from Ref. [36].)

deformation tensor for a simple elongational deformation along the x-axis with constant elongational rate $\dot{\epsilon}$ is given by

$$\hat{\lambda}(t) = \begin{bmatrix} \lambda(t) & 0 & 0 \\ 0 & 1/\sqrt{\lambda(t)} & 0 \\ 0 & 0 & 1/\sqrt{\lambda(t)} \end{bmatrix}, \tag{9.116}$$

where

$$\lambda(t) = \exp(\dot{\epsilon}t) \tag{9.117}$$

is the deformation ratio. Apart from the geometry of the deformation, steady elongational flow differs from steady shear flow in that the flow lines grow exponentially in time while in shear they grow linearly in time.

We focus on a Gaussian chain with a constant recombination rate [17]. The number of active chains in the stationary state is again given by (9.53), with $\tilde{\theta}(0)$ being replaced by the one corresponding to the elongational flow

$$\tilde{\theta}(0) = \alpha \int_0^\infty dt \left\langle \exp[-\int_0^t \beta(r(t'))dt'] \right\rangle_0, \tag{9.118}$$

where the end-to-end distance at time t' is given by

$$r(t') \equiv [\lambda(t')^2 x^2 + (x^2 + y^2)/\lambda(t')]^{1/2}. \tag{9.119}$$

For small values of $\dot{\epsilon}$, $\tilde{\theta}(0)$ can be expanded as

$$\tilde{\theta}(0) = \theta_0 + \theta_1 \dot{\epsilon} + \theta_2 \dot{\epsilon}^2 + \cdots. \tag{9.120}$$

In contrast to the shear flow, there is no symmetry between $\dot{\epsilon}$ and $-\dot{\epsilon}$; an elongational flow changes to a compressional flow if the sign of $\dot{\epsilon}$ is changed. The 0-th order value $\theta_0 = \alpha \langle \beta^{-1} \rangle$ is the same as for the shear. The first-order coefficient θ_1 vanishes because the chain dissociation rate is spherically symmetric. The coefficient of the second-order term is explicitly given by

$$\theta_2 = -\frac{\alpha}{15} \left\langle \frac{r}{\beta^4} \left(4\beta' + r\beta'' - \frac{3r\beta'^2}{\beta} \right) \right\rangle_0, \tag{9.121}$$

which turns out to be negative for most physical forms of $\beta(r)$.

The equilibrium number of active chains then takes the form

$$\nu_e(\dot{\epsilon}) = \nu_e \left\{ 1 + \frac{\theta_2}{\alpha \langle \beta^{-1} \rangle_0 (1 + \theta_0)} \dot{\epsilon}^2 + \cdots \right\}, \tag{9.122}$$

for small $\dot{\epsilon}$, so that it is reduced by the increase of the elongational rate.

In the following we use the boundary condition such that the side of the sample is free from external forces, i.e., $\Sigma_{yy} = \Sigma_{zz} = 0$. Solving these conditions with respect to the presssure P, and substituting the result into Σ_{xx}, we obtain the normal stress in the flow direction:

$$\Sigma_{||} = \nu_e \tilde{\sigma}_{||}(\dot{\epsilon}), \tag{9.123}$$

where

$$\tilde{\sigma}_{||}(\dot{\epsilon}) = \frac{3k_B T}{\langle \beta^{-1} \rangle_0 n a^2} \int_0^\infty dt \left\langle \left[\lambda(t)^2 x^2 - \frac{y^2 + z^2}{2\lambda(t)} \right] \exp \left[-\int_0^t \beta(r(t')) dt' \right] \right\rangle_0 \tag{9.124}$$

is the elongational stress supported by a single chain.

Elongational viscosity $\mu(\dot{\epsilon})$, being defined by

$$\mu(\dot{\epsilon}) \equiv \Sigma_{||}(t = \infty)/\dot{\epsilon}, \tag{9.125}$$

is therefore calculated by the formula

$$\mu(\dot{\epsilon}) = \nu_e \tilde{\sigma}_{||}(\dot{\epsilon})/\dot{\epsilon}. \tag{9.126}$$

In the GT limit, it is

$$\mu(\dot{\epsilon}) = 3\nu_e k_B T \frac{\beta_0}{(\beta_0 + \dot{\epsilon})(\beta_0 - 2\dot{\epsilon})}. \tag{9.127}$$

The elongational viscosity increases with the increasing $\dot{\epsilon}$, and eventually exhibits a singularity at $\beta_0 = 2\dot{\epsilon}$. This divergence in $\mu(\dot{\epsilon})$ suggests that infinitely large stress is

required to stretch the system at the rate faster than $\beta_0/2$. This artifact is caused by the unphysical assumption of constant dissociation rate.

In general, the viscosity has a power expansion

$$\mu(\dot{\epsilon}) = \mu_0 + \mu_1\dot{\epsilon} + \mu_2\dot{\epsilon}^2 + \cdots, \tag{9.128}$$

for small $\dot{\epsilon}$, where the first two coefficients are given by

$$\mu_0 = \frac{3\nu_e k_B T}{\langle \beta^{-1}\rangle_0 na^2}\left\langle \frac{r^2}{\beta^2}\left(1 - \frac{r\beta'}{5\beta}\right)\right\rangle_0, \tag{9.129}$$

$$\mu_1 = \frac{3\nu_e k_B T}{\langle \beta^{-1}\rangle_0 na^2}\left\langle \frac{r^2}{\beta^3}\left[1 - \frac{26}{35}\frac{r\beta'}{\beta} - \frac{2r^2}{35}\left(\frac{\beta''}{\beta} - 3\left(\frac{\beta'}{\beta}\right)^2\right)\right]\right\rangle_0. \tag{9.130}$$

The limiting value μ_0 for vanishing $\dot{\epsilon}$ is exactly three times as large as the shear viscosity (9.73) η_0 in the limit of small shear rate: $\mu_0 = 3\eta_0$. Hence, **Trouton's rule**, $\mu = 3\eta$, which is known to hold at any elongational rate for Newtonian fluids, holds for our transient network with arbitrary $\beta(r)$ in the limit of small strain rate.

Unlike the shear viscosity, the first coefficient μ_1 for the elongational viscosity starts from a term that is independent of any derivatives of β, hence giving a large positive contribution. It is therefore clear that our network has a tendency to **elongational thickening** irrespective of the detailed form of $\beta(r)$.

For a quadratic dissociation rate, we can find the exact solution [17]. Figure 9.11 shows the calculated (a) number of elastically effective chains and (b) elongational viscosity as a function of the elongation rate. It always shows a peak (thickening). The peak position shifts to a lower rate and becomes sharper as the constant term β_0 in the dissociation rate is reduced. Detailed calculation is given in Appendix 9.B.
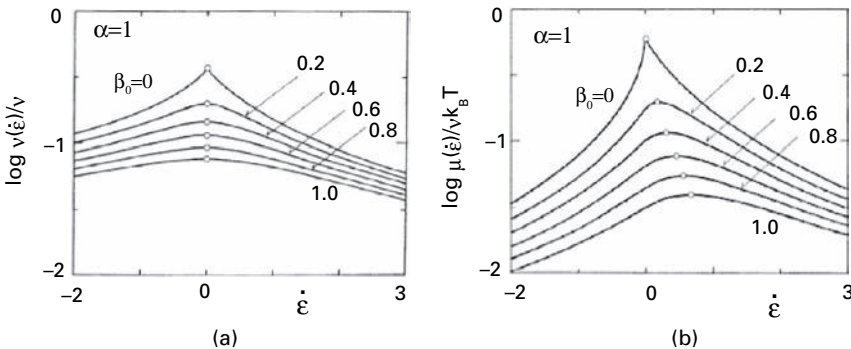
Fig. 9.11   (a) Number of active chains, and (b) elongational viscosity, both plotted against the elongational rate on a semilogarithmic scale. The viscosity exhibits a maximum at finite positive $\dot{\epsilon}$. The elongational rate giving the maximum decreases with decreasing β_0 and eventually becomes singular at $\dot{\epsilon} = 0$ when β_0 vanishes. (Reprinted with permission from Ref. [17].)

9.4 Time-dependent flows

In the experiments, two main types of time-dependent flows have been studied: start-up flows and stress relaxation. In the **start-up flow** experiments, shear flows with constant shear rates and elongational flows with constant elongational rates are started in the system in equilibrium under no external force, and the time-dependent stress build-up in the system is measured. In the **stress relaxation** experiments, constant deformations are applied to or removed from the system, and the time-dependent relaxation of the stress is measured. In this section, we study these two types within the framework of transient network theory.

9.4.1 Transient flows of Gaussian networks in the GT limit

We first study a shear flow with a constant shear rate $\dot{\gamma}$ along the x-axis, which is started at time $t = 0$ in a transient network in equilibrium [19]. In the GT limit, we find $\nu_e^\circ(t) = \nu_e e^{-\beta_0 t}$, where ν_e is the unperturbed equilibrium number of the active chains, which stays constant after a steady flow is started.

Similarly we find

$$\hat{\sigma}(t;t') = k_B T \hat{\lambda}(t) \cdot^t \hat{\lambda}(t-t')e^{-\beta_0 t}, \tag{9.131}$$

for the stress propagator, and hence we have

$$\hat{\Sigma}(t)/k_B T = \nu_e \hat{g}(t) + \alpha \nu_d \int_0^t \hat{g}(t')dt' - P(t)\hat{1}, \tag{9.132}$$

for the stress tensor, where a new tensor $\hat{g}$ is introduced by

$$\hat{g}(t) \equiv \hat{\lambda}(t) \cdot^t \hat{\lambda}(t)e^{-\beta_0 t}. \tag{9.133}$$

It is proportional to the squared deformation tensor.

For a steady shear flow, we have specifically

$$g_{xy}(t) = (\dot{\gamma}t)e^{-\beta_0 t}, \tag{9.134a}$$

$$g_{xx}(t) - g_{yy}(t) = (\dot{\gamma}t)^2 e^{-\beta_0 t}, \tag{9.134b}$$

$$g_{yy}(t) - g_{zz}(t) = 0. \tag{9.134c}$$

The shear component of the stress then takes the form

$$\Sigma_{xy}(t)/k_B T = \nu_e(\dot{\gamma}t)e^{-\beta_0 t} + \alpha \nu_d \frac{\dot{\gamma}}{\beta_0^2}\left[1 - (1 + \beta_0 t)e^{-\beta_0 t}\right]. \tag{9.135}$$

Similarly the first and second normal stress differences obey

$$N_1(t)/k_B T = \nu_e(\dot{\gamma}t)^2 e^{-\beta_0 t} + \alpha \nu_d \frac{2\dot{\gamma}^2}{\beta_0^3}\left[1 - \left(1 - \beta_0 t + \frac{1}{2}(\beta_0 t)^2\right)e^{-\beta_0 t}\right], \tag{9.136}$$
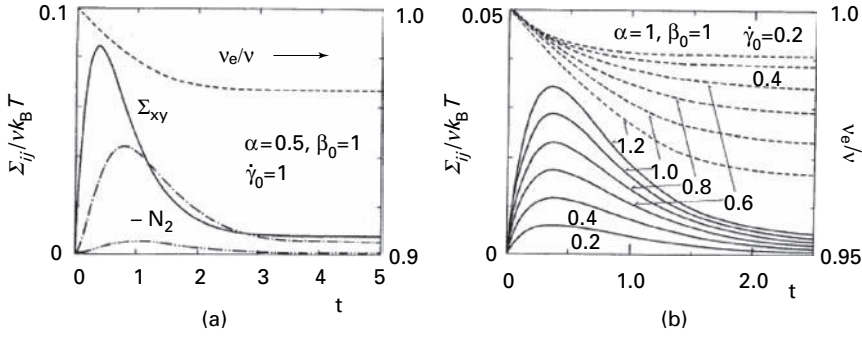
Fig. 9.12   (a) Stress overshoot of the transient network model under shear flow. The total number of active chains, the shear stress, and the first and second normal stress difference are shown as functions of time after a shear flow with the shear rate $\dot{\gamma} = 1$ is started. The decay rate is fixed as $\beta_0 = 1$. Each component of the stress shows an overshoot at a different time. (b) Number of active chains and shear stress plotted against the time. The shear rate $\dot{\gamma}$ is changed from curve to curve. The overshoot time is almost independent of the shear rate. (Reprinted with permission from Ref. [19].)

and

$$N_2(t)/k_B T = 0. \tag{9.137}$$

It is easy to see that these stresses are steadily increasing functions; they exhibit no overshoot for any large shear rate $\dot{\gamma}$. The coupling between the dissociation rate and the chain tension brings about the stress overshoot.

To see the relation between chain stretching and stress overshoot, the quadratic coupling ($m = 1$ in (9.88)) is detailed. Figure 9.12 shows a model calculation (a) of the total number of active chains, the shear and normal stresses as functions of time for a fixed shear rate $\dot{\gamma} = 1$, and (b) the shear stress for varied shear rate $\dot{\gamma}$. It turns out that the overshoot time is almost independent of the shear rate. A detailed calculation is presented in Appendix 9.A.

The stress tensor of the elongational flow (9.116) takes the form (9.133) in the GT limit. The component of the tensor $\hat{g}$ parallel to the flow direction is given by

$$g_{||}(t) = \left[\lambda(t)^2 - \frac{1}{\lambda(t)}\right] e^{-\beta_0 t}, \tag{9.138}$$

and hence we have

$$\Sigma_{||}(t)/k_B T = \nu_e (e^{-(\beta_0 - 2\dot{\epsilon})t} - e^{-(\beta_0 + \dot{\epsilon})t})$$

$$+ \alpha \nu_d \left(\frac{1 - e^{-(\beta_0 - 2\dot{\epsilon})t}}{\beta_0 - 2\dot{\epsilon}} - \frac{1 - e^{-(\beta_0 + \dot{\epsilon})t}}{\beta_0 + \dot{\epsilon}}\right), \tag{9.139}$$

due to the free boundary condition on the side surface. This stress is again a steadily increasing function without overshoot. However, any chain dissociation rate can lead to the overshoot in the elongational stress, if it depends on r.
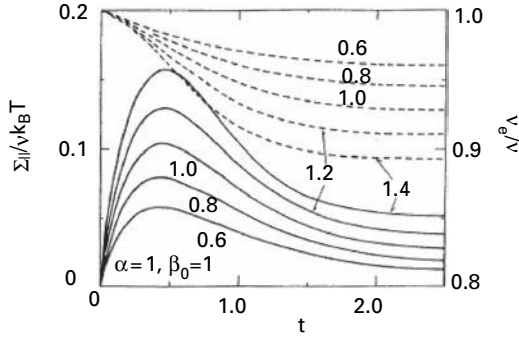
Number of effective chains and longitudinal stress in the case of an elongational flow. The elongational rate $\dot{\epsilon}$ is changed from curve to curve. (Reprinted with permission from Ref. [19].)

Figure 9.13 shows the numerical result for the quadratic model as discussed above. We have fixed $\beta_0 = 1$ and $\alpha = 1$. The fraction of the active chains in a quiescent state is given by $\nu_e/\nu = 0.326\,261$ in this case. The elongational rate $\dot{\epsilon}$ is changed from curve to curve. Large-scale variation of the curves is essentially the same as in the shear flow, although it is different in minor quantitative details.

9.4.2 Start-up shear flows with tension–dissociation coupling

For a shear flow, the equation for the time development of the active chains takes the form

$$\frac{\partial \psi}{\partial t} + \dot{\gamma} y \frac{\partial \psi}{\partial x} = -\beta(\mathbf{r})\psi + \nu_d(t)\alpha(\mathbf{r})\Phi(\mathbf{r}), \qquad (9.140)$$

with the initial condition (9.30). The deviation $\xi(\mathbf{r},t)$ from the equilibrium distribution defined by $\psi(\mathbf{r},t) \equiv \psi_0(\mathbf{r})\xi(\mathbf{r},t)$ obeys [39]

$$\frac{\partial \xi}{\partial t} + [\dot{\gamma}\hat{P} + \beta(\mathbf{r})]\xi = \beta(\mathbf{r})\zeta(t), \qquad (9.141)$$

where the operator $\hat{P}$ is defined by (9.96), and

$$\zeta(t) \equiv \nu_d(t)/\nu_d(t=0) \qquad (9.142)$$

is the number of the dangling chains at time t counted relative to its initial equilibrium value $\nu_d(t=0)$ without shear. The initial value $\nu_d(t=0)$ is $\nu_d(\infty)$ in (9.29).

The formal solution of this equation with the initial condition $\xi(\mathbf{r},0) = 1$ can be written as

$$\xi(\mathbf{r},t) = e^{-\hat{\Gamma}t}\left[1 + \int_0^t e^{\hat{\Gamma}t'}\beta(\mathbf{r})\zeta(t')dt'\right], \qquad (9.143)$$

by using the time-development operator

$$\hat{\Gamma} \equiv \dot{\gamma}\hat{P} + \beta(\mathbf{r}). \qquad (9.144)$$

The i, j component of the stress as a function of time can then be calculated from the relation (9.39) [16]

$$\Sigma_{i,j}(t)a^3 = \int d\mathbf{r}\psi_0(\mathbf{r})(x_i f_j)\xi(\mathbf{r},t). \tag{9.145}$$

To study the short-term behavior, we find the solution in power series of time. The formal expansion of the exponential in (9.143) in powers of t leads to

$$\xi(\mathbf{r},t) = 1 + t\xi^{(1)} + \frac{t^2}{2}\xi^{(2)} + \frac{t^3}{3!}\xi^{(3)} + \frac{t^4}{4!}\xi^{(4)} + \cdots, \tag{9.146}$$

where the explicit forms of $\xi^{(n)}$ are given in Appendix 9.A.

Shear stress

We first study the shear stress $\Sigma_{x,y}(t)$ as a function of time. Since it is of the order of $\dot{\gamma}$, the shear viscosity buildup function

$$\eta^+(t) \equiv \Sigma_{x,y}(t)/\dot{\gamma} \tag{9.147}$$

is commonly used. Substituting the expansion (9.146) into the stress (9.145), and integrating over all possible end-to-end vectors, we find

$$\eta^+(t) = t\eta^{(1)} + \frac{t^2}{2}\eta^{(2)} + \frac{t^3}{3!}\eta^{(3)} + \frac{t^4}{4!}\eta^{(4)} + \cdots. \tag{9.148}$$

After integration, the first term takes the form

$$\eta^{(1)} = c_{2,0}\int_0^l dr\psi_0(r)(r^4 fF), \tag{9.149}$$

where the numerical coefficient $c_{2,0} = 4\pi/15$ appears from the angular integral. The high-frequency limit of the storage modulus is given by the same integral (9.75). Hence, we confirm that the initial slope of the viscosity growth function is the same as the high-frequency modulus

$$\eta^{(1)} = \lim_{\omega\to\infty} G'(\omega) \equiv g_1, \tag{9.150}$$

as it should.

The second term takes the form

$$\eta^{(2)} = -c_{2,0}\int_0^l dr\psi_0(r)(r^4\beta fF). \tag{9.151}$$

The slope of the loss modulus (9.74) is the same integral in the limit of high frequency. We thus find a new result

$$\eta^{(2)} = -\lim_{\omega\to\infty} \omega G''(\omega) \equiv -g_2. \tag{9.152}$$

The coefficient $\eta^{(2)}$ is negative definite and independent of the shear rate. The specific values of g_1 and g_2 depend upon the chain property (in particular the amplitude A), and the coupling constant g through $\beta(\mathbf{r})$.

The third term can be written in the form

$$\eta^{(3)} = Q_0 + Q_2 \dot{\gamma}^2, \tag{9.153}$$

where

$$Q_0 = c_{2,0} \int_0^l dr \psi_0(r)(r^4 \beta^2 f F), \tag{9.154a}$$

$$Q_2 = \frac{1}{3} c_{2,2} \int_0^l dr \psi_0(r)(r^6 f F) \left(F + \frac{1}{r} - \frac{F'}{F} \right) \left(\frac{f'}{f} - \frac{1}{r} \right), \tag{9.154b}$$

with $c_{2,2} = 4\pi/35$.

Strain hardening

We have derived the power expansion in the form

$$\eta^+(t) = g_1 t - \frac{g_2}{2} t^2 + \frac{1}{6}(Q_0 + Q_2 \dot{\gamma}^2) t^3 + \cdots, \tag{9.155}$$

up to the third order. It is an alternating power series, so that the long-term behavior is basically difficult to predict.

Let us first examine the sign of this third coefficient. If it is negative, the viscosity decreases as time goes on. If it is positive, the viscosity may deviate upwards from the baseline $\eta^+(t) = g_1 t$ fixed by the linear modulus. In other words, it shows an upturn at a certain time from the linear baseline. Such a stress growth beyond the linear baseline caused by a large deformation is called **strain hardening**.

Figure 9.14(a) schematically shows the relation between strain hardening, **stress overshoot**, and the steady nonlinear viscosity in a shear-thinning regime. For a sufficiently high shear rate, the viscosity first shows an upward deviation due to strain hardening, followed by an **overshoot peak**, and then asymptotically decreases to the stationary value. The stationary viscosity is plotted in Figure 9.14(b).

More precisely, the critical shear rate $\dot{\gamma}$ at which strain hardening appears can be found by the condition

$$-g_2 + \frac{1}{3}(Q_0 + Q_2 \dot{\gamma}^2) t = 0, \tag{9.156}$$

for the cancelation of the second and third terms.

In Figure 9.15(a), we show the exact numerical integration. (The numerical values of the stresses are presented in the unit of $\nu k_B T$.) The shear rate $\dot{\gamma}$ is varied from curve to curve. The DP of the chain is assumed to be $n = 20$, and the coupling constant in the dissociation rate is fixed at $g = 0.2$.

In Figure 9.15(b), the linear baseline $g_1 t$ is subtracted from each curve, and shown by broken lines. In order to examine the accuracy of the power series (9.155) up to the
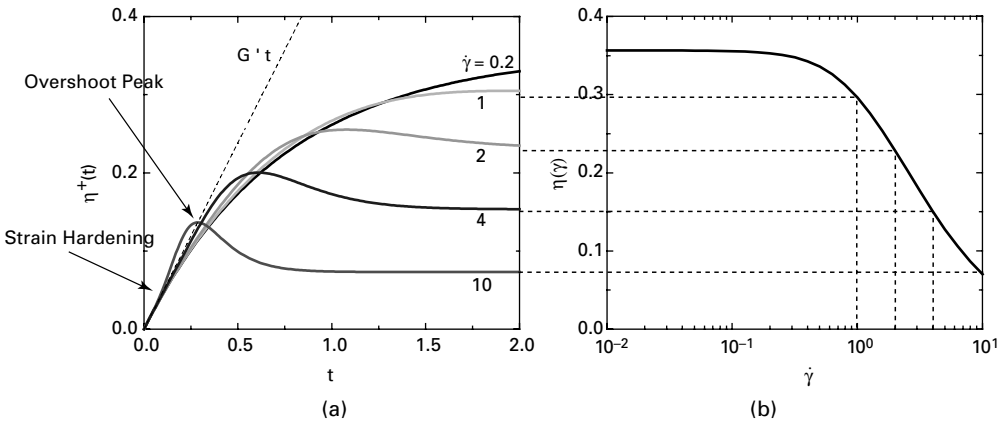
Fig. 9.14   Concepts of strain hardening, stress overshoot, and nonlinear stationary viscosity shown by taking the typical theoretical result of the stress buildup function. (a) Time development of the viscosity for different shear rates. The initial slope is given by the linear storage modulus. The linear baseline is defined by $\eta^+(t) = g_1 t$ (dotted line). For large $\dot{\gamma}$, the viscosity shows hardening and overshoot. (b) Nonlinear stationary viscosity plotted as a function of the shear rate. (Reprinted with permission from Ref. [39].)
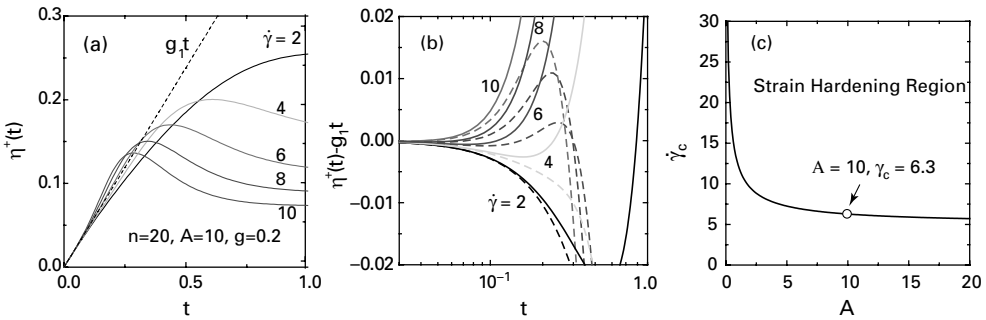
Fig. 9.15   (a) Growth curves $\eta^+(t)$ of the viscosity numerically calculated for the affine transient network equation (9.143). The shear rate $\dot{\gamma}$ is changed from curve to curve for a nonlinear chain with $A = 10$. (b) Deviation $\eta^+(t) - g_1 t$ of the viscosity from the reference baseline defined by the linear modulus plotted against time (broken lines), and the same for the third-order approximation (9.155). (c) Critical shear rate $\dot{\gamma}_c$ for the appearance of strain hardening found by (9.156) plotted against the nonlinear amplitude A of the tension–elongation curve of a polymer chain. The higher the nonlinearity of the chain, the easier the strain hardening. (Reprinted with permission from Ref. [39].)

third order, we carry out the same procedure for (9.155), and show $-g_2 t^2/2 + (Q_0 + Q_2 \dot{\gamma}^2) t^3/6$ by solid lines in the same figure. We can see that the change of the sign in the slope at around $t \simeq 0.1$ decides the occurrence of hardening. Therefore, we put $t = 0.1$ in the hardening condition (9.156), and solve it for $\dot{\gamma}$ to find the critical shear rate $\dot{\gamma}_c$ for hardening. The result is plotted against the nonlinear amplitude A in Figure 9.15(c).

Gaussian chains ($A = 0$) show no hardening. For a nonlinear chain with $A = 10$, for instance, the critical value obtained in this way is $\dot{\gamma}_c = 6.3$.

Stress overshoot

For polymer solutions and melts, it is often claimed that the deformation $\gamma_{max} \equiv \dot{\gamma} t_{max}$ accumulated before the stress reaches the maximum is independent of the shear rate and takes a value of order unity (1.0 in the literature [40]). In other studies [41,42], it depends on the shear rate, and is approximately described by the formula $\gamma_{max} = a[b + (\dot{\gamma}\tau)^{2/3}]^{3/2}$, where a and b are numerical constants of order unity, and τ is the relaxation time. In gelling solutions, γ_{max} seems to depend on the system. For aqueous solutions of Guar galactomannan [43] at 3 wt% has $\gamma_{max} \simeq 2$, while in aqueous solutions of xanthan polysaccharides [44] at 2 wt% it increases with the shear rate from 0.5 to 1.0.

For the transient networks under present study, it is highly probable that the stress shows a maximum at a certain time t_{max} in the regime where it shows a strain hardening. But it may also show a maximum even in the regime where there is no strain hardening (for instance, the curves for small $\dot{\gamma}$ in Figure 9.15(a)). We therefore first carry out numerical integration by using different values A of chain nonlinearity for a fixed coupling constant $g = 0.2$, and found t_{max} as a function of $\dot{\gamma}$. The results are shown in Figure 9.16. We can see that the accumulated deformation γ_{max} is almost independent of the shear rate for both Gaussian ($A = 0$) and nonlinear ($A = 10$) chains (Figure 9.16(b)). The viscosity $\eta_{max} \equiv \eta(t_{max})$ at the maximum time decreases with the shear rate (Figure 9.16(c)).

The result can be interpreted physically by using the power series expansion

$$\eta^+(t) = g_1 t - \frac{g_2}{2} t^2 + \frac{g_3(\dot{\gamma})}{6} t^3 - \cdots + \frac{g_{2n-1}(\dot{\gamma})}{(2n-1)!} t^{2n-1} - \frac{g_{2n}(\dot{\gamma})}{(2n)!} t^{2n} + \cdots, \quad (9.157)$$
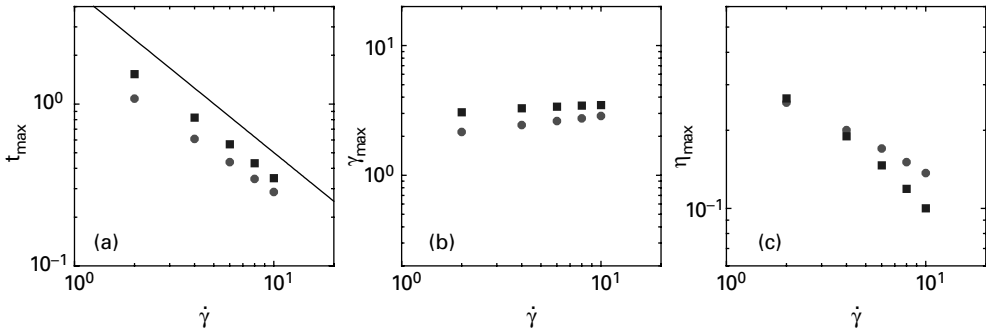
Fig. 9.16 Numerical calculation of the affine network with coupling constant $g = 0.2$ for the chains $A = 0$ (squares), and 10 (circles) with $n = 20$. (a) Overshoot time t_{max}, (b) accumulated deformation γ_{max}, and (c) viscosity at the maximum time, all plotted against the shear rate. (Reprinted with permission from Ref. [39].)

which has alternating signs. For a high shear rate $\dot{\gamma}$, all intermediate terms cancel alternately, and a peak appears when the first term is balanced by the last term, i.e., when the condition

$$\frac{g_{2n}}{2n!}t^{2n-1} \simeq g_1 \tag{9.158}$$

is fulfilled. Because $g_{2n} \sim \dot{\gamma}^{2(n-1)}$ for large $\dot{\gamma}$, the peak time is roughly estimated to be

$$t_{\max} \simeq \dot{\gamma}^{-(2n-2)/(2n-1)} \simeq \dot{\gamma}^{-1}, \tag{9.159}$$

for large n. Hence we expect that the accumulated deformation is asymptotically independent of the shear rate, and is given as a function of the coupling constant g and the nonlinearity A.

Normal stress differences

Normal stress coefficients have the power expansions

$$\Psi_i^+(t) = \frac{t^2}{2}\psi_i^{(2)} + \frac{t^3}{3!}\psi_i^{(3)} + \frac{t^4}{4!}\psi_i^{(4)} + \cdots, \tag{9.160}$$

by (9.146). They start from $O(t^2)$.

Upon substitution of $\xi^{(2)}$, we find for the first coefficient

$$\psi_1^{(2)} = 2G'(\omega = \infty) = 2g_1, \tag{9.161}$$

i.e., twice as large as the plateau modulus. After straightforward but tedious calculation, we find $\psi_1^{(3)} = -4g_2$ for higher terms.

Similarly, we find for the second normal stress coefficient

$$\psi_2^{(2)} = -c_{2,0}^{(2)} \int_0^l dr\, \psi_0(r)(r^5 f F)\left(\frac{F'}{F} - F + \frac{6}{r}\right). \tag{9.162}$$

It incidentally vanishes by cancelation between the positive and negative regions if the chain is Gaussian and the upper limit of the integral is extended to infinity. Even with an upper cutoff, it is as small as 10^{-9}. For a nonlinear chain, however, it changes sign with A, so that the sign of the initial slope in the second normal stress changes its sign depending upon the nature of the chain.

9.4.3   Nonlinear stress relaxation

This section treats the time evolution of the stress after a sudden deformation is given to an equilibrium state of the network. The deformation, being followed by a constant strain, creates a stress which gradually relaxes with time. The long-term behavior of stress relaxation following a large stepwise deformation is frequently measured in rheological experiments. It is known as the **nonlinear stress relaxation**.

Let us consider a **stepwise deformation** [19]

$$\hat{\lambda}(t) = \hat{\lambda}\theta(t), \tag{9.163}$$

which starts at $t = 0$ with a constant strain tensor $\hat{\lambda}$. Within the affiness assumption of the active chains, the end-to-end vector $\mathbf{r}$ of an active chain in equilibrium configuration before the deformation ($t < 0$) is deformed to $\mathbf{r}_{t,0} = \hat{\lambda} \cdot \mathbf{r}$ at later time t after the deformation is given ($t > 0$). Similarly, if the end-to-end vector of an active chain is $\mathbf{r}$ at time $t'(> 0)$, it will remain active in later time, because the strain stays constant for $t > 0$. Hence we have $\mathbf{r}_{t'',t'} = \mathbf{r}$ for $0 < t' < t''$. Under such assumption, the chain survival function takes a simple form

$$\theta(t;t') = \langle \alpha(r)e^{-\beta(r)(t-t')} \rangle \quad \text{for} \quad 0 < t' \le t, \tag{9.164}$$

while the number of chains that were active in the initial equilibrium state decays according to

$$v_e^\circ(t) = \frac{v_e}{\langle \alpha\beta^{-1} \rangle} \left\langle \frac{\alpha(r)}{\beta(r)} \frac{e^{-\beta(|\hat{\lambda}\cdot\mathbf{r}|)t}}{\beta(r)} \right\rangle \quad \text{for} \quad 0 < t. \tag{9.165}$$

The integral equation (9.41), together with the specific forms of $\theta(t;t')$ and $v_e^\circ(t)$, determine the time developement of $v_e(t)$.

Due to the affineness assumption, the stress propagator reduces to an isotropic form

$$\hat{\sigma}(t;t') = \sigma_0(t - t')\hat{1}, \tag{9.166}$$

whose diagonal element takes the form

$$\sigma_0(t) \equiv \left\langle \alpha(r) \left[\frac{r}{3} f(r)e^{-\beta(r)t} \right] \right\rangle. \tag{9.167}$$

The stress supported by the chains that are initially active decays according to the law

$$\hat{\Sigma}^\circ(t) = \frac{v_e}{\langle \alpha\beta^{-1} \rangle} \hat{\lambda} \cdot \left\langle \frac{\alpha(r)}{\beta(r)} (\mathbf{r}^t\mathbf{f}) \frac{e^{-\beta(|\hat{\lambda}\cdot\mathbf{r}|)t}}{\beta(r)} \right\rangle \cdot {}^t\hat{\lambda}. \tag{9.168}$$

Shear deformation

We focus on Gaussian chains with a constant recombination rate α in this subsection. Consider a shear deformation

$$\hat{\lambda} = \begin{bmatrix} 1 & \gamma & 0 \\ 0 & 1 & 0 \\ 0 & 0 & 1 \end{bmatrix}, \tag{9.169}$$

with constant shear γ. The number of active chains in the network, which are initially active and stay active until time t, is written explicitly by

$$v_e^\circ(t) = \frac{v_e}{\langle \beta^{-1} \rangle_0} \left\langle \frac{1}{\beta(r)} e^{-\beta(\sqrt{(x+\gamma y)^2+y^2+z^2})t} \right\rangle_0, \tag{9.170}$$

$$\Sigma_{xy}^\circ(t) = \frac{3\nu_e k_B T}{\langle \beta^{-1}\rangle_0 n a^2} \left\langle \frac{(x+\gamma y)y}{\beta(r)} e^{-\beta(\sqrt{(x+\gamma y)^2+y^2+z^2})t} \right\rangle_0, \tag{9.171}$$

$$N_1(t) \equiv \Sigma_{xx}(t) - \Sigma_{yy}(t)$$
$$= \frac{3\nu_e k_B T}{\langle \beta^{-1}\rangle_0 n a^2} \times \left\langle \frac{[(x+\gamma y)^2 - y^2]}{\beta(r)} e^{-\beta(\sqrt{(x+\gamma y)^2+y^2+z^2})t} \right\rangle_0, \tag{9.172}$$

$$N_2(t) \equiv \Sigma_{yy}(t) - \Sigma_{zz}(t)$$
$$= \frac{3\nu_e k_B T}{\langle \beta^{-1}\rangle_0 n a^2} \times \left\langle \frac{(y^2 - z^2)}{\beta(r)} e^{-\beta(\sqrt{(x+\gamma y)^2+y^2+z^2})t} \right\rangle_0. \tag{9.173}$$

In the GT limit of a constant β_0, the number of initially active chains decays exponentially as

$$\nu_e^\circ(t) = \nu_e e^{-\beta_0 t}. \tag{9.174}$$

The total number $\nu(t)$ of the active chains, however, remains constant at the equilibrium value ν_e. Stresses are given by

$$\Sigma_{xy}(t) = \nu_e^\circ(t) k_B T \gamma, \tag{9.175}$$

$$N_1(t) = \nu_e^\circ(t) k_B T \gamma^2, \tag{9.176}$$

$$N_2(t) = 0. \tag{9.177}$$

In all these stresses, time dependence can be separated from the strain. For instance, we have

$$\Sigma_{xy}(\gamma, t) = h(\gamma) G(t), \tag{9.178}$$

for the shear stress. Thus, **time–strain separability** holds in the limit where there is no coupling between the chain conformation and the dissociation rate. The measurement of the stress ratio $\Sigma_{xy}(t)/\Sigma_{xy}(0)$ therefore gives the fraction $\nu_e^\circ(t)/\nu_e$ of the network chains that remain active after deformation until time t, as in conventional theories [11, 12].

The first normal stress difference after a step shear deformation is related to the shear stress by the equation

$$N_1(\gamma, t) = \gamma \Sigma_{xy}(\gamma, t). \tag{9.179}$$

This proportionality relation is called the **Lodge–Meissner relation** [45, 46].

Figure 9.17 shows the results of numerical calculation for the power-law dissociation rate (9.88), plotted on a logarithmic scale. Reduced values of the number of chains relative to the stationary value ν_e are plotted against the time, and stresses are measured in the unit of $\nu_e k_B T$. The unit of time is β_1^{-1}. The amplitude of the strain is fixed as $\gamma = 0.5$ in both figures, while β_0 (the chain dissociation rate at $r = 0$) is given by (a) $\beta_0 = 0$ and (b) $\beta_0 = 1$.

As shown in the figures, the number $\nu_e^\circ(t)$ of initially active chains steadily decreases. The total number $\nu_e(t)$, however, restores the stationary value ν_e, although it initially
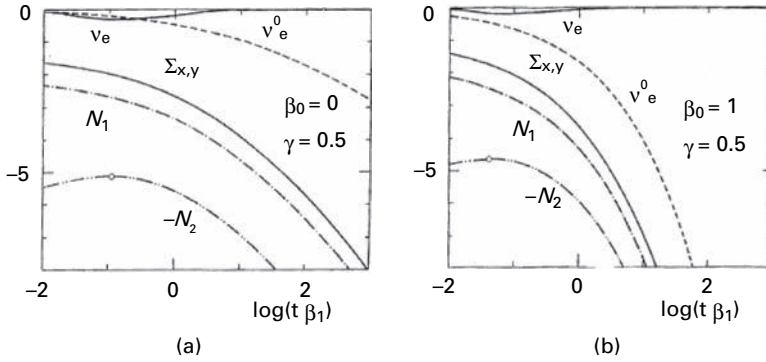
Fig. 9.17 Nonlinear stress relaxation of the transient network model with a quadratic chain dissociation rate under a constant shear deformation for $\gamma = 0.5$. The decay rate is fixed as (a) $\beta_0 = 0$ and (b) $\beta_0 = 1$. The total number ν_e of active chains and the number ν_e^0 of chains that remain active from the initial state are shown on a logarithmic scale. These are normalized by the stationary value of ν_e. The shear stress Σ_{xy}, the first normal stress difference N_1, and the second normal stress difference N_2 are shown in the unit of $\nu_e k_B T$. (Reprinted with permission from Ref. [19].)

decreases. The first normal stress difference is proportional to the shear stress at arbitrary time (**Lodge–Meissner relation**) [45, 46], although their relative magnitudes change with increase in the shear strain γ. One of the remarkable results of the numerical demonstration is that the absolute value of the second normal stress difference shows a maximum at the time at which the number $\nu_e(t)$ shows a minimum. In the particular case where $\beta_0 = 0$, stress relaxation obeys a power law rather than an exponential one. More specifically, Σ_{xy}, N_1, and N_2 all decay as $\sim t^{-5/2}$ for sufficiently large t.

In order to study the asymptotic decay of the stresses more generally, let us assume that the chain dissociation rate behaves $\beta(r) \sim r^{2m}$ in the high stretching limit, where m is an arbitrary number. For large γ, $\beta(|\hat{\lambda} \cdot \mathbf{r}|)$ can be approximately replaced by $\beta(|\hat{\lambda} \cdot \mathbf{r}|) \sim (\gamma y)^{2m}$, so that the space coordinate must be scaled as $y \sim t^{-1/2m}/\gamma$. This scaling gives an asymptotic form

$$\Sigma_{xy}(t) \sim \frac{t^{-5/2m}}{\gamma}, \tag{9.180}$$

for the shear stress.

Elongational deformation
In order to study how the nonlinear stress relaxation depends on the type of deformation, we next consider an elongational strain for which the strain tensor is given by

$$\hat{\lambda} = \begin{bmatrix} \lambda & 0 & 0 \\ 0 & 1/\sqrt{\lambda} & 0 \\ 0 & 0 & 1/\sqrt{\lambda} \end{bmatrix}, \tag{9.181}$$

where λ is a constant elongational ratio. Since $(\hat{\lambda} \cdot \mathbf{r})^2 = \lambda^2 x^2 + (y^2 + z^2)/\lambda$, the general formulae (9.165) and (9.168) lead to

$$\nu_e^{\circ}(t) = \frac{\nu_e}{\langle \beta^{-1} \rangle_0} \left\langle \frac{1}{\beta(r)} e^{-\beta(\sqrt{\lambda^2 x^2 + (y^2+z^2)/\lambda})t} \right\rangle_0 , \tag{9.182}$$

and

$$\Sigma_{||}(t) = \frac{3\nu_e k_B T}{\langle \beta^{-1} \rangle_0 n a^2} \left\langle \frac{[\lambda^2 x^2 - (y^2+z^2)/2\lambda]}{\beta(r)} e^{-\beta(\sqrt{\lambda^2 x^2 + (y^2+z^2)/\lambda})t} \right\rangle_0 , \tag{9.183}$$

where the free boundary condition on the sample side parallel to the elongational axis has been used to derive the elongational stress $\Sigma_{||}$.

In the GT limit, where $\beta(r) = \beta_0$, we find $\nu_e^{\circ}(t) = \nu_0 e^{-\beta_0 t}$ again, and

$$\Sigma_{||}(t) = \nu_e^{\circ}(t) k_B T \left(\lambda^2 - \frac{1}{\lambda} \right), \tag{9.184}$$

which is in agreement with the force–deformation relation (4.23) for rubbers. Stress is supported by the initially active chains only, the number of which decays exponentially.

From the analytic solution for the quadratic $\beta(r)$ detailed in Appendix 9.B, we can find the numerical results. In Figure 9.18, the number ν_e° of the initially active chains, and elongational stress are plotted against time on a logarithmic scale for $\beta_0 = 0$ and $\beta_0 = 1$. The elongational ratio is fixed as $\lambda = 2$ as a typical example. Since this model has a finite probability of dissociation for any active chains irrespective of their configurations, they must eventually dissociate. Hence, there is no residual stress at $t = \infty$.

If the dissociation rate $\beta(r)$ has a region of r in which $\beta(r) = 0$, the chains with an end-to-end distance lying in this region survive to $t = \infty$.

For example, the cutoff model, for which $\beta(r) = 0$ $(0 < r < r^*)$ and $\beta(r) = \infty$ $(r^* < r)$ hold, allows the residual stress to remain finite in a deformed equilibrium state.
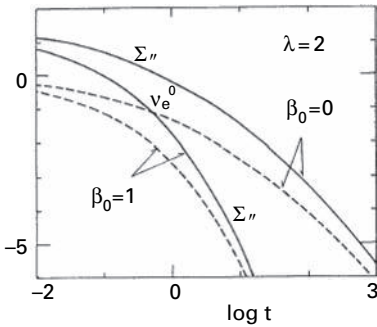
Fig. 9.18   Nonlinear relaxation under an elongational deformation with the elongational strain $\lambda = 2$ for quadratic $\beta(r)$ model. (Reprinted with permission from Ref. [19].)

Appendices to Chapter 9

9.A Expansion in powers of the shear rate and time

For the stationary flows (9.107), we find the following relations for each order of $\dot{\gamma}$:

$$\beta \xi^{(0)} = \beta \zeta^{(0)},$$
$$\hat{P} \xi^{(0)} + \beta \xi^{(1)} = \beta \zeta^{(1)},$$
$$\hat{P} \xi^{(1)} + \beta \xi^{(2)} = \beta \zeta^{(2)},$$
$$\hat{P} \xi^{(2)} + \beta \xi^{(3)} = \beta \zeta^{(3)},$$
$$\hat{P} \xi^{(3)} + \beta \xi^{(4)} = \beta \zeta^{(4)},$$

and so on.

By solving these equations order by order, we obtain

$$\xi^{(0)}(\mathbf{r}) = \zeta^{(0)} = 1,$$

$$\xi^{(1)}(\mathbf{r}) = \Theta \frac{rF}{\beta},$$

$$\xi^{(2)}(\mathbf{r}) = -\frac{1}{\beta} \left[\Phi^2 + \Theta^2(\hat{p} - 2) \right] \frac{rF}{\beta} + \zeta^{(2)},$$

$$\xi^{(3)}(\mathbf{r}) = -\frac{1}{\nu} \Theta \frac{r\beta'}{\beta^2} \left[\Phi^2 + \Theta^2(\hat{p} - 2) \right] \frac{rF}{\beta}$$
$$- \Theta \frac{1}{\beta} \left[3\Phi^2 + \Theta^2(\hat{p} - 4) \right] (\hat{p} - 2) \frac{rF}{\beta} - \Theta r F \zeta^{(2)}.$$

The angular factors $\Theta(\theta, \phi) \equiv \sin^2\theta \sin\phi \cos\phi$ and $\Phi(\theta, \phi) \equiv \sin\theta \sin\phi$ are separated as the prefactors of the radial differential operator

$$\hat{p} \equiv r \left[\frac{d}{dr} - F(r) \right],$$

in the spherical coordinates.

Similarly, for the start-up flows (9.146), each order in the time expansion is given by

$$\xi^{(1)}(\mathbf{r}) = \dot{\gamma} \Theta (rF),$$

$$\xi^{(2)}(\mathbf{r}) = -\dot{\gamma} \left\{ \Theta\beta + \dot{\gamma}[\Phi^2 + \Theta^2(\hat{p} - 2)] \right\} (rF),$$

$$\xi^{(3)}(\mathbf{r}) = \ddot{\zeta}_0 \beta(\mathbf{r}) + \dot{\gamma} \left\{ \Theta\beta^2 + \dot{\gamma} \hat{\Xi}_1 + \dot{\gamma}^2 \Theta[3\Phi^2 + \Theta^2(\hat{p} - 4)](\hat{p} - 2) \right\} (rF),$$

$$\xi^{(4)}(\mathbf{r}) = \dddot{\zeta}_0 \beta(\mathbf{r}) - \dot{\gamma} \{ \Theta\beta^3 + \dot{\gamma} \hat{\Xi}_2 + \dot{\gamma}^2 \hat{\Xi}_3$$
$$- \dot{\gamma}^3 [3\Phi^4 + 6\Phi^2\Theta^2(\hat{p} - 4) + \Theta^4(\hat{p} - 6)(\hat{p} - 4)](\hat{p} - 2) \} (rF).$$

Definitions of the operators $\hat{\Xi}_1 \sim \hat{\Xi}_3$ are

$$\hat{\Xi}_1 \equiv 2\Phi^2\beta + \Theta^2\left[(\hat{p}-2)\beta + \beta(\hat{p}-2)\right],$$

$$\hat{\Xi}_2 \equiv \Phi^2\beta^2 + \Theta^2\left[(\hat{p}-2)\beta^2 + \beta(\hat{p}-2)\beta - \beta^2(\hat{p}-2)\right],$$

$$\hat{\Xi}_3 \equiv \Theta\Phi^2\left[3(\hat{p}-2)\beta + (\hat{p}-2)\beta - \beta(\hat{p}-2)\right]$$
$$+ \Theta^3\left\{(\hat{p}-4)(\hat{p}-2)\beta[(\hat{p}-4)\beta - \beta(\hat{p}-4)](\hat{p}-2)\right\}.$$

Upon such decomposition, we are led to the three types of angular integrals. They are defined by

$$c_{l,m} \equiv \int \sin\theta\, d\theta\, d\phi\ \Theta^l\Phi^m,$$

$$c_{m,n}^{(1)} \equiv \int \sin\theta\, d\theta\, d\phi\, \Theta_1\Theta^m\Phi^n,$$

$$c_{m,n}^{(2)} \equiv \int \sin\theta\, d\theta\, d\phi\, \Theta_2\Theta^m\Phi^n,$$

where $\Theta_1 \equiv \sin^2\theta(1 - 2\sin^2\phi)$ and $\Theta_2 \equiv \sin^2\theta(1 + \sin^2\phi) - 1$.

The numerical constants arising from the angular integrals are

$$c_{2,0} = \frac{4\pi}{15}, \quad c_{2,2} = \frac{4\pi}{35}, \quad c_{4,0} = \frac{4\pi}{105},$$

$$c_{2,0}^{(1)} = 0, \quad c_{0,2}^{(1)} = -\frac{8\pi}{15}, \quad c_{2,0}^{(2)} = \frac{8\pi}{105}, \quad c_{0,2}^{(2)} = \frac{8\pi}{15},$$

$$c_{4,0}^{(1)} = 0, \quad c_{2,2}^{(1)} = -\frac{8\pi}{315}, \quad c_{0,4}^{(1)} = -\frac{16\pi}{35},$$

$$c_{4,0}^{(2)} = \frac{16\pi}{1155}, \quad c_{2,2}^{(2)} = \frac{16\pi}{315}, \quad c_{0,4}^{(2)} = \frac{16\pi}{35}.$$

After carrying out all angular integrals, we are left with the radial integrals.

9.B   Solvable model of the quadratic dissociation rate

In this appendix, we study in detail a specific form of the chain dissociation rate

$$\beta(r) = \beta_0 + \frac{3}{2}\beta_1 r^2.$$

For a Gaussian chain, the tension–dissociation coupling model (9.90) reduces to this quadratic rate. The quadratic r-dependence allows rigorous calculation of the viscoelastic properties of the network by using Gaussian integrals, and thus presents a result from which a great deal can be inferred.

For a constant recombination rate α, a similar calculation was done by Fuller *et al.* [47] to study the effect of entanglements in the polymer melts. They found that the number density of entanglement junctions is a decreasing function of the flow rate, and that shear thinning and elongational thickening are two major characteristics shared by all transient networks that fall into this category.

9.B.1 Start-up and stationary flows

We first consider a shear flow. By carrying out the Gaussian integral, we find that the chain survival function of this model network is explicitly given by

$$\theta(t) = \frac{e^{-\beta_0 t}}{(1+t)[(1+t)^2 + \frac{1}{3}(1+\frac{1}{4}t)t^3\dot{\gamma}^2]^{1/2}}.$$

Similarly, the stress propagators turn out to be

$$\frac{\sigma_{xy}(t)}{k_B T} = \frac{(\dot{\gamma}t)(1+\frac{1}{2}t)e^{-\beta_0 t}}{(1+t)^{1/2}[(1+t)^2 + \frac{1}{3}(1+\frac{1}{4}t)t^3\dot{\gamma}^2]^{3/2}},$$

for the shear component,

$$\frac{n_1(t)}{k_B T} = \frac{(\dot{\gamma}t)^2(1+\frac{4}{3}t+\frac{1}{3}t^2)e^{-\beta_0 t}}{(1+t)^{3/2}[(1+t)^2 + \frac{1}{3}(1+\frac{1}{4}t)t^3\dot{\gamma}^2]^{3/2}},$$

for the first normal stress difference, and

$$\frac{n_2(t)}{k_B T} = -\frac{\frac{1}{3}(\dot{\gamma}t)^2 t(1+\frac{1}{4}t)e^{-\beta_0 t}}{(1+t)^{3/2}[(1+t)^2 + \frac{1}{3}(1+\frac{1}{4}t)t^3\dot{\gamma}^2]^{3/2}},$$

for the second normal stress difference.

Similarly, for the initial terms we carry out the coordinate Gaussian integrals, and find

$$v_e^\circ(t) = \frac{v_e}{\langle\beta^{-1}\rangle_0}\int_0^\infty dt' A(t,t'),$$

for the number of active chains, where the function $A(t,t')$ is defined by

$$A(t,t') = \frac{e^{-\beta_0(t+t')}}{[a(t,t')b(t,t')]^{1/2}},$$

in terms of the two functions $a(t,t') \equiv 1+t+t'$, and $b(t,t') \equiv (1+t+t')^2 + \frac{1}{3}(1+\frac{1}{4}t + t')t(\dot{\gamma}t)^2$. By the use of this function, we can write the chain survival function in the simple form $\theta(t) = A(t,0)$.

In a similar way, we find

$$\Sigma_{x,y}^\circ(t) = \frac{v_e k_B T}{\langle\beta^{-1}\rangle_0}\int_0^\infty dt' S_{xy}(t,t'),$$

for the shear component of the stress, where

$$S_{xy}(t,t') \equiv \frac{(\dot{\gamma}t)(1+\frac{1}{2}t+t')e^{-\beta_0(t+t')}}{a(t,t')^{1/2}b(t,t')^{3/2}}$$

is another new function. Similar integration leads to

$$N_i^\circ(t) \equiv \frac{\nu_e k_B T}{\langle \beta^{-1}\rangle_0} \int_0^\infty dt'\, S_i(t,t') \quad \text{for} \quad i=1,2,$$

for the first and second normal stress difference, where

$$S_1(t,t') \equiv \frac{(\dot{\gamma}t)^2(1+\frac{4}{3}t+\frac{1}{3}t^2+\frac{4}{3}tt'+2t'+t'^2)e^{-\beta_0(t+t')}}{[a(t,t')b(t,t')]^{3/2}},$$

and

$$S_2(t,t') \equiv \frac{(\dot{\gamma}t)^2(\frac{1}{3}t)(1+\frac{1}{4}t+t')e^{-\beta_0(t+t')}}{[a(t,t')b(t,t')]^{3/2}}$$

are the corresponding integrals.

The stress propagators can be expressed as $\sigma_{xy}(t)=k_B T S_{xy}(t,0), n_1(t)=k_B T S_1(t,0)$, and $n_1(t)=k_B T S_2(t,0)$ in terms of these functions in a similar way as above.

In the case of an elongational flow with a constant flow rate $\dot{\epsilon}$, a similar procedure leads to the same form for the time evolution of the number of active chains $\nu_e^\circ(t)$ that have been active from the initial stage, but the function $A(t,t')$ must now be replaced by

$$A(t,t') \equiv \frac{e^{-\beta_0(t+t')}}{c(t,t')[d(t,t')]^{1/2}},$$

where two newly introduced functions are defined by $c(t,t') \equiv 1+(1-e^{-\dot{\epsilon}t})/\dot{\epsilon}+t'$, and $d(t,t') \equiv 1+(e^{2\dot{\epsilon}t}-1)/2\dot{\epsilon}+t'$. The chain survival function is again given by $\theta(t)=A(t,0)$.

Quite analogously, the elongational stress supported by the initially active chains can be found by

$$\Sigma_{||}^\circ(t) = \frac{\nu_e k_B T}{\langle \beta^{-1}\rangle_0} \int_0^\infty dt'\, S_{||}(t,t'),$$

where

$$S_{||}(t,t') = A(t,t')\left[\frac{e^{2\dot{\epsilon}t}}{b(t,t')} - \frac{1}{e^{\dot{\epsilon}t}a(t,t')}\right].$$

The $t'=0$ component of this function gives the stress propagator for the elongational flow $\sigma_{||}(t)=k_B T S_{||}(t,0)$.

We have now reached the explicit form of the coupled equations for $\nu_e(t)$ and $\hat{\Sigma}(t)$, the solution of which can be found numerically. Some typical results are shown in the text.

To study the stationary state, we find the Laplace transform of the chain survival function. It takes the form

$$\tilde{\theta}(s) = \frac{1}{\beta_1} \phi\left(\frac{\dot{\gamma}}{\beta_1}, \frac{s+\beta_0}{\beta_1}\right),$$

where the function $\phi(x,y)$ of the two variables is defined by the integral

$$\phi(x,y) \equiv \int_0^\infty dt \frac{e^{-yt}}{\sqrt{(1+t)[(1+t)^2 + \frac{1}{3}(1+\frac{1}{4}t)t^3 x^2]}}.$$

The number of chains that remain active in the stationary state is then given by

$$\frac{v_e(\dot{\gamma})}{v} = \frac{\alpha\phi(\dot{\gamma}/\beta_1, \beta_0/\beta_1)}{\beta_1 + \alpha\phi(\dot{\gamma}/\beta_1, \beta_0/\beta_1)}.$$

Upon integration we get the expression

$$\frac{\eta(\dot{\gamma})}{vk_B T/\beta_1} = \frac{\alpha\psi(\dot{\gamma}/\beta_1, \beta_0/\beta_1)}{\beta_1 + \alpha\phi(\dot{\gamma}/\beta_1, \beta_0/\beta_1)},$$

for the reduced viscosity, and

$$\frac{\Psi_1(\dot{\gamma})}{vk_B T/\beta_1^2} = \frac{\alpha\psi_1(\dot{\gamma}/\beta_1, \beta_0/\beta_1)}{\beta_1 + \alpha\phi(\dot{\gamma}/\beta_1, \beta_0/\beta_1)},$$

$$\frac{\Psi_2(\dot{\gamma})}{vk_B T/\beta_1^2} = -\frac{\alpha\psi_2(\dot{\gamma}/\beta_1, \beta_0/\beta_1)}{\beta_1 + p\phi(\dot{\gamma}/\beta_1, \beta_0/\beta_1)},$$

for the reduced first and second normal stress difference coefficients. The new functions ψ, ψ_1, and ψ_2 are defined by the integrals

$$\psi(x,y) \equiv \int_0^\infty \frac{t(1+\frac{1}{2}t)e^{-yt}}{(1+t)^{1/2}[(1+t)^2 + \frac{1}{3}(1+\frac{1}{4}t)t^3 x^2]^{3/2}},$$

$$\psi_1(x,y) \equiv \int_0^\infty \frac{t^2(1+\frac{4}{3}t+\frac{1}{3}t^2)e^{-yt}}{(1+t)^{3/2}[(1+t)^2 + \frac{1}{3}(1+\frac{1}{4}t)t^3 x^2]^{3/2}},$$

$$\psi_2(x,y) \equiv \int_0^\infty \frac{\frac{1}{3}t^3(1+\frac{1}{4}t)e^{-yt}}{(1+t)^{3/2}[(1+t)^2 + \frac{1}{3}(1+\frac{1}{4}t)t^3 x^2]^{3/2}}.$$

The number of active chains for the shear flow is plotted in Figure 9.19(a) as a function of the shear rate on a logarithmic scale. The recombination rate α is chosen to be unity as a typical example and the chain breakage rate β_0 at the vanishing end-to-end distance is varied from curve to curve. Both the shear rate $\dot{\gamma}$ and the chain breakage rate β_0 are measured in the unit of the coefficient β_1, or equivalently, β_1 is set to be unity. For all β_0 the number of active chains decreases steadily as a function of $\dot{\gamma}$.
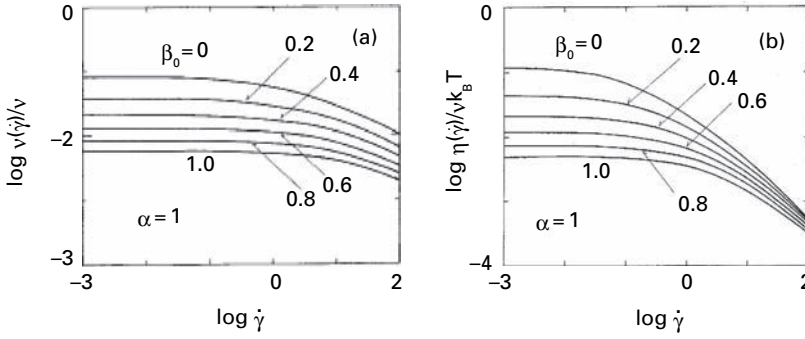
Fig. 9.19   (a) Number of active chains, and (b) nonlinear shear viscosity, plotted against the shear rate on a logarithmic scale. $\alpha = 1$. β_0 is varied from curve to curve. The curves have a common asymptotic slope in the high shear region. (Reprinted with permission from Ref. [17].)
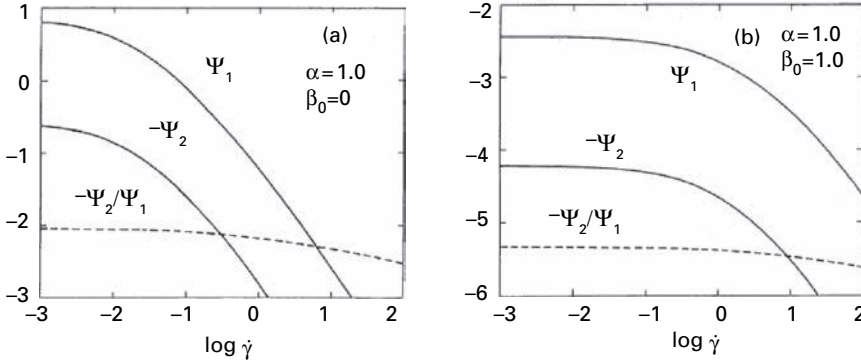
Fig. 9.20   First and second normal stress differences plotted against the shear rate on a logarithmic scale, using $\alpha = 1$ as a typical example. The second coefficient is negative and its ratio is virtually constant over a wide range of shear rates. (a) $\beta_0 = 0$, (b) $\beta_0 = 1$. (Reprinted with permission from Ref. [17].)

Figure 9.19(b) shows the shear viscosity plotted against the shear rate. The network exhibits shear thinning for all β_0. The increase in β_0 physically corresponds to the increase in temperature. Calculation for other values of α shows that the viscosity curve is insensitive to a change in α.

The asymptotic slope of the tail of the viscosity curve is approximately -0.98 for all β_0 in the highest $\dot{\gamma}$ region shown in the figure.

Figure 9.20(a) and (b) show the two normal stress coefficients Ψ_1 and $-\Psi_2$ (solid lines) and their ratio $-\Psi_2/\Psi_1$ (broken line) as a function of $\log \dot{\gamma}$. The ratio turned out to be virtually constant over a wide range of $\dot{\gamma}$, though we have no specific analytical reason for this. Both coefficients are monotonic functions of $\dot{\gamma}$ and show only a minor quantitative difference.

Since the time variable in the integral is scaled as $t \approx \dot{\gamma}^{1/2}$ as $\dot{\gamma} \to \infty$, we expect that the viscosity behaves as $\eta \approx \dot{\gamma}^{-4/3}$ in the limit of high shear rate. Similarly $\Psi_1 \approx \dot{\gamma}^{-2}$ and

$\Psi_2 \approx \dot{\gamma}^{-8/3}$ are expected for the normal stresses. Because the index $4/3$ is larger than unity, it can lead to mechanical instability (as noted by Doi and Edwards [48]); the shear stress $\eta\dot{\gamma}$ passes a maximum as the shear rate is increased. The flow may take either value of the two shear rates giving the same value of the shear stress (**shear banding**) [48]. The same remark holds also for the normal stresses.

The calculation given above allows us to find the asymptotic behavior of a network with the more general form of $\beta(r)$, which increases as $\beta(r) \approx r^m$ at high stretching. For large $\dot{\gamma}$ the integral in the exponent of the decay factor can be replaced by the dominant term

$$\int_0^t \beta(|\hat{\lambda}(t) \cdot \mathbf{r}|) dt \approx \int_0^t dt (\dot{\gamma} yt)^m = y^m \dot{\gamma}^m t^{m+1},$$

so that the time variable must be scaled as

$$t \approx \tau \dot{\gamma}^{m/(m+1)}$$

where τ is a dimensionless time. From the definition of the functions we find $\phi(x, y) \approx x^{-m/(m+1)}$ and $\psi(x, y) \approx x^{-2m/(m+1)}$ as $x \to \infty$ for any fixed y. The shear viscosity turns out to take an asymptotic form

$$\eta(\dot{\gamma}) \approx \dot{\gamma}^{-2m/(m+1)}$$

at high shear rate. Smaller values of m, and hence slower variation of $\beta(r)$, give smaller values of the exponent of η under high shear. For instance $\eta(\dot{\gamma}) \approx \dot{\gamma}^{-2/3}$ for $m = 1/2$ causes no mechanical instability. Similar dimensional analysis leads to $\Psi_1 \approx \dot{\gamma}^{-3m/(m+1)}$ and $\Psi_2 \approx -\dot{\gamma}^{-4m/(m+1)}$.

Studies can be carried out for elongational flow. The quadratic form of $\beta(r)$ leads to the same form for the survival function, but $\dot{\gamma}$ is replaced by $\dot{\epsilon}$, and the function $\phi(x, y)$ is now defined by a different integral

$$\phi(x, y) \equiv \sqrt{2} x^{3/2} \int_0^\infty dt \, \frac{e^{(x-y)t}}{[(1+x)e^{xt} - 1](e^{2xt} + 2x - 1)^{1/2}}.$$

The elongational viscosity also takes the same form as before:

$$\frac{\mu(\dot{\epsilon})}{vk_B T/\beta_1} = \frac{\alpha\psi(\dot{\epsilon}/\beta_1, \beta_0/\beta_1)}{\beta_1 + \alpha\phi(\dot{\epsilon}/\beta_1, \beta_0\beta_1)},$$

but the function $\psi(x, y)$ here is defined by

$$\psi(x, y) \equiv \sqrt{2} x^{3/2} \int_0^\infty dt \, \frac{2(1+x)e^{3xt} - 3e^{2xt} - (2x - 1)}{[(1+x)e^{xt} - 1]^2 (e^{2xt} + 2x - 1)^{3/2}} e^{(x-y)t}.$$

Because an elongational flow is changed to a compressional flow when the flow rate $\dot{\epsilon}$ goes negative, both the number of active chains $v(\dot{\epsilon})$ and the viscosity $\mu(\dot{\epsilon})$ have no symmetry between $\dot{\epsilon}$ and $-\dot{\epsilon}$. The functions $\phi(x, y)$ for shear and elongational flow take

the same value at $x = 0$, while the function $\psi(x, y)$ for the elongation is three times as large as that for the shear at $x = 0$.

Figure 9.11(b) shows the elongational viscosity plotted against the flow rate. The most remarkable feature of the nonlinear viscosity for elongational flow is that it exhibits a maximum at finite positive flow rate. The network therefore undergoes elongational thickening for smaller values of $\dot{\epsilon}$, followed by thinning. The case $\beta_0 = 0$ is rather exceptional: the viscosity shows a singularity at $\dot{\epsilon} = 0$, as in a number of active chains, and steadily decreases for either compression or elongation. The elongational rate at which the viscosity shows a maximum increases with increasing β_0 (or increasing the temperature), although the viscosity itself is lowered.

9.B.2   Stress relaxation

In order to express the bilinear form $(\hat{\lambda} \cdot \mathbf{r})^2$ as a sum of three independent coordinate variables, let us first find the eigenvalues of the matrix ${}^t\hat{\lambda} \cdot \hat{\lambda}$. For a shear deformation (9.169), they are given by

$$\lambda_1^2 = 1 + \frac{\gamma^2}{2} - \frac{\gamma}{2}\sqrt{\gamma^2 + 4},$$

$$\lambda_2^2 = 1 + \frac{\gamma^2}{2} + \frac{\gamma}{2}\sqrt{\gamma^2 + 4},$$

$$\lambda_3^2 = 1.$$

Hence we can decompose as $(\hat{\lambda} \cdot \mathbf{r})^2 = \sum_{i=1}^{3} \lambda_i^2 \xi_i^2$, where ξ_i are the principal coordinates. Upon moving onto these coordinates, the average over a Gaussian chain distribution can be explicitly carried out by performing Gaussian integrals.

In order to do this, we first use an identity using the identity

$$1/\beta(r) = \int_0^{\infty} e^{-\beta(r)t'} dt',$$

and then carry out the Gaussian integrals. We find

$$\nu_e(t) = \frac{\nu_e}{\langle \beta^{-1} \rangle_0} \int_0^{\infty} dt' \frac{e^{-\beta_0(t+t')}}{(\prod_{i=1}^{3} \Lambda_i)^{1/2}},$$

for the number of active chains, where the three functions $\Lambda_i(t, t')(i = 1, 2, 3)$ are defined by

$$\Lambda_i(t, t') = 1 + \beta_1(\lambda_i^2 t + t').$$

Similarly, for the stress components we find

$$\Sigma_{xy}(t) = \frac{\nu_e k_B T}{\langle \beta^{-1} \rangle_0 \sqrt{\gamma^2 + 4}} \int_0^{\infty} dt' \frac{e^{-\beta_0(t+t')}}{(\prod_{i=1}^{3} \Lambda_i)^{1/2}} \left(-\frac{\lambda_1^2}{\Lambda_1} + \frac{\lambda_2^2}{\Lambda_2} \right),$$

$$N_1(t) = \gamma \Sigma_{xy}(t),$$

$$N_2(t) = \frac{\nu_e k_B T}{\zeta_0 \sqrt{\gamma^2+4}} \int_0^\infty dt' \frac{e^{-\beta_0(t+t')}}{(\prod_{i=1}^3 \Lambda_i)^{1/2}}$$
$$\times \left(\frac{\sqrt{\gamma^2+4}-\gamma}{2\Lambda_1} + \frac{\sqrt{\gamma^2+4}+\gamma}{2\Lambda_2} - \frac{\sqrt{\gamma^2+4}}{\Lambda_3} \right).$$

The Lodge–Meissner relation is automatically fulfilled.

In a similar way, the three eigenvalues of the strain tensor (9.116) in the case of elongational deformation are given by $\lambda_1^2 = \lambda^2$ and $\lambda_2^2 = \lambda_3^2 = 1/\lambda$. Hence we have

$$\Lambda_1 = 1 + \beta_1(\lambda^2 t + t'),$$

$$\Lambda_2 = \Lambda_3 = 1 + \beta_1(\frac{t}{\lambda} + t').$$

The number of active chains is given by the same formula as above, but the Λ_is must be replaced. The elongational stress takes the form

$$\Sigma_{||}(t) = \frac{\nu_e k_B T}{\langle \beta^{-1} \rangle_0} \int_0^\infty dt' \frac{e^{-\beta_0(t+t')}}{(\prod_{i=1}^3 \Lambda_i)^{1/2}} \left(\frac{\lambda^2}{\Lambda_1} - \frac{1}{\lambda\Lambda_2} \right).$$

References

[1] Jenkins, R. D.; Silebi, C. A.; El-Asser, M. S., *ACS Symp. Ser.* **462**, 222 (1991).

[2] Annable, T.; Buscall, R.; Ettelaie, R.; Whittlestone, D., *J. Rheol.* **37**, 695 (1993).

[3] Annable, T.; Ettelaie, R., *Macromolecules* **27**, 5616 (1994).

[4] Annable, T.; Buscall, R.; Ettelaie, R.; Shepherd, P.; Whittlestone, D., *Langmuir* **10**, 1060 (1994).

[5] Yekta, A.; Xu, B.; Duhamel, J.; Adiwidjaja, H.; Winnik, M. A., *Macromolecules* **28**, 956 (1995).

[6] Kujawa, P.; Watanabe, H.; Tanaka, F.; Winnik, F. M., *Eur. Phys. J. E* **17**, 129 (2005).

[7] Kujawa, P.; Segui, F.; Shaban, S. *et al. Macromolecules* **39**, 341 (2006).

[8] Quellet, C.; Eicke, H.-F.; Xu, G.; Hauger, Y., *Macromolecules* **23**, 3347 (1990).

[9] Mortensen, K.; Brown, W.; Jorgensen, E., *Macromolecules* **27**, 5654 (1994).

[10] Odenwald, M.; Eicke, H.-F.; Meier, W., *Macromolecules* **28**, 5069 (1995).

[11] Green, M. S.; Tobolsky, A. V., *J. Chem. Phys.* **14**, 80 (1946).

[12] Lodge, A. S., *Trans. Faraday Soc.* **52**, 120 (1956).

[13] Yamamoto, M., *J. Phys. Soc. Jpn.* **11**, 413 (1956); **12**, 1148 (1957); **13**, 1200 (1958).

[14] Flory, P. J., *Trans. Faraday Soc.* **56**, 722 (1960).

[15] Fricker, H. S., *Proc. Roy. Soc. London A* **335**, 267; **335**, 289 (1973).

[16] Tanaka, F.; Edwards, S. F., *Macromolecules* **25**, 1516 (1992).

[17] Tanaka, F.; Edwards, S. F., *J. Non-Newtonian Fluid Mech.* **43**, 247 (1992).

[18] Tanaka, F.; Edwards, S. F., *J. Non-Newtonian Fluid Mech.* **43**, 272 (1992).

[19] Tanaka, F.; Edwards, S. F., *J. Non-Newtonian Fluid Mech.* **43**, 289 (1992).

[20] Alami, E.; Rawiso, M.; Isel, F.; Beinert, G.; Binana-Limbele, W.; Francois, J., *Model Hydrophobically End-Capped Poly(ethylene oxide) in Water*. Advances in Chemistry Series, Vol. 248. American Chemical Society: Washington, DC, 1996.

[21] Alami, E.; Almgren, M.; Brown, W.; Francois, J., *Macromolecules* **29**, 2229 (1996).

[22] Alami, E.; Almgren, M.; Brown, W., *Macromolecules* **29**, 5026 (1996).

[23] Tanaka, F.; Koga, T., *Macromolecules* **39**, 5913 (2006).

[24] Rouse Jr., P. E., *J. Chem. Phys.* **21**, 1272 (1953).

[25] Bird, B. B.; Curtiss, C. F.; Armstrong, R. C.; Hassager, O., *Dynamics of Polymeric Liquids*, Vol. 1, *Fluid Mechanics*; Vol. 2, *Kinetic Theory*. Wiley: Chichester, 1987.

[26] Chandrasekhar, S., *Rev. Mod. Phys.* **15**, 1 (1943).

[27] Marrucci, G.; Bhargava, S.; Cooper, S. L., *Macromolecules* **26**, 6483 (1993).

[28] Vaccaro, A.; Marrucci, G., *J. Non-Newtonian Fluid Mech.* **121**, 261 (2000).

[29] Pellens, L.; Ahn, K. H.; Lee, S. J.; Mewis, J., *J. Non-Newtonian Fluid Mech.* **121**, 87 (2004).

[30] Tanaka, F., *Langmuir* **26**, 5374 (2010).

[31] Zhang, W.; Zou, S.; Wang, C.; Zhang, X., *J. Phys. Chem. B* **104**, 10258 (2000).

[32] Bedrov, D.; Smith, D., *J. Chem. Phys.* **118**, 6656 (2003).

[33] Indei, T.; Tanaka, F., *Macromol. Rapid Commun.* **26**, 701 (2005).

[34] Kramers, H. A., *Phys. Rev.* **1940**, *VII*, 284.

[35] Cox, W. P.; Merz, E. H., *J. Polym. Sci.* **118**, 619 (1958).

[36] Koga, T.; Tanaka, F., *Macromolecules* **43**, 3052 (2010).

[37] Pellens, L.; Corrales, R. G.; Mewis, J., *J. Rheol.* **48**, 379 (2004).

[38] Oesterhelt, F.; Rief, M.; Gaub, H. E., *New J. Physics* **1**, 6 (1999).1.

[39] Koga, T.; Tanaka, F.; Kaneda, I.; Winnik, F. M., *Langmuir* **25**, 8626 (2009).

[40] Menezes, E. V.; Graessley, W. W., *Rheol. Acta* **19**, 38 (1980).

[41] Pearson, D.; Herbolzheimer, E.; Grizzuti, N.; Marrucci, G., *J. Polym. Sci., Part B: Polym. Phys.* **29**, 1589 (1991).

[42] Osaki, K.; Inoue, T.; Isomura, T., *J. Polym. Sci., Part B: Polym. Phys.* **38**, 1917 (2000).

[43] Richardson, R. K.; Ross-Murphy, S. B., *Int. J. Bio. Macromolecules* **9**, 250 (1987).

[44] Richardson, R. K.; Ross-Murphy, S. B., *Int. J. Bio. Macromolecules* **9**, 257 (1987).

[45] Lodge, A. S.; Meissner, J. M., *Rheol. Acta* **11**, 351 (1972).

[46] Lodge, A. S., *Rheol. Acta* **14**, 664 (1975).

[47] Fuller, G. G.; Leal, L. G., *J. Polym. Sci.: Polym. Phys. Ed.* **59**, 531 (1981).

[48] Doi, M.; Edwards, S. F., *The Theory of Polymer Dynamics*. Oxford University Press: Oxford, 1986.

10 Some important thermoreversible gels

This chapter applies the thermodynamic and rheological theories developed so far to the specific important network-forming associating polymer solutions. The topics include modification of the phase separation and gelation of associating polymers by added surfactants, transition from intramolecular association to intermolecular association, competitive and coexisting hydration and hydrophobic association, and thermoreversible gelation strongly coupled to the polymer conformational change. With an increase in the number of components, or the degree of freedom in the system, phase transitions and flow properties become complex. However, the basic ideas to treat them stay within the fundamental theoretical framework presented in the preceding chapters. All systems are modeled from a unified point of view.

10.1 Polymer–surfactant interaction

The problem of the interaction between polymers and surfactants was laid initially in the study of proteins associated with natural lipids, and later extended to their association with synthetic surfactants [1, 2]. More recently, the interaction of water-soluble synthetic polymers such as poly(ethylene oxide) with ionic and non-ionic surfactants [3–7] has attracted the interest of researchers because of its scientific and technological implications.

Adding surfactants to polymer solutions, or vice versa, followed by the formation of a polymer/surfactant complex, can substantially alter the original physical properties substances involved. The effects can be summarized in the following four categories:

- Conformational transition of polymers such as **coil–globule transition** [8, 9] and **coil–rod transition** [10, 11] induced by surfactant binding.
- Expansion and shift of the phase separation region on the polymer/solvent phase plane [12].
- Formation of microphases [13], and gels [14].
- Shift of the sol–gel transition line [15–17] accompanied by modification of the rheological properties [18–20].
- Viscoelastic synergy of wormlike surfactant micelles with hydrophobically modified associating polymers [21–26]

When polymers carry a small fraction of hydrophobic groups, the effects are dramatically enhanced. Such hydrophobically modified polymers (associating polymers)
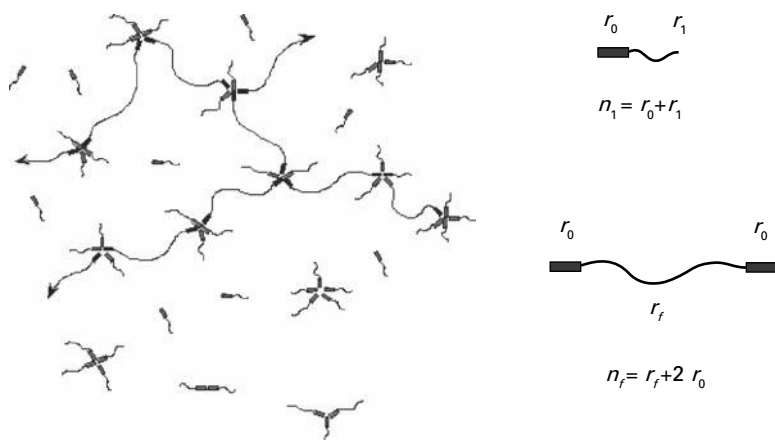
Fig. 10.1   Network junctions mixed with surfactant molecules, and pure micelles consisting of surfactant molecules only.

show a tendency towards self-assembly, eventually leading to gelation caused by the aggregation of hydrophobes, as studied in Section 7.4.

The ability of surfactant binding is enhanced through the hydrophobic interaction between polymer hydrophobes and surfactant hydrophobes. Typical model polymers such as hydrophobically ethoxylated urethane (HEUR), ethyl hydroxyethyl cellulose (EHEC), and hydroxypropyl methyl cellulose (HPMC) have been the focus of study.

To model the polymer–surfactant system, we consider a mixture of polymers and low-molecular weight surfactant molecules in a solvent. Each polymer is assumed to carry the number f (≥ 2) of associative groups of the volume r_0 along its chain, which is composed of r_f statistical units. Each surfactant molecule is modeled as a molecule of a volume r_1 carrying a single hydrophobe connected to the hydrophilic head (see Figure 10.1) [1].

The hydrophobe on a surfactant molecule may be different from that on a polymer chain, but we assume that they are the same to maximize the mixing properties within the micelles. The difference of the hydrophobes could be included easily by considering the phase separation within the formed micelles (**intramicellar phase separation**) [27] at the network junctions.

The total number of statistical units on a polymer is then given by $n_f = r_f + f r_0$, and that of a surfactant molecule is $n_1 = r_1 + r_0$. Such a mixture of f-molecules and $f = 1$ molecules in a solvent is a special case of the general model solution studied in Section 7.4.

The volume fraction of each species is given by $\phi_i = n_i N_i / \Omega$ ($i = 1, f$), and the number of hydrophobes carried by each species is $\psi_i = i \phi_i / n_i = i \nu_i$ ($i = 1, f$), where $\nu_i \equiv \phi_i / n_i$ is the number density of molecules of type i.

Since the total number of hydrophobes in the solution is given by $\psi = \psi_1 + \psi_f$, the weight distribution ρ_i of associative groups on the species i is given by $\rho_i = \psi_i / \psi$,

whose number- and weight-average functionalities are given by

$$1/f_{\mathrm{n}} \equiv \sum \rho_i/i = (\nu_1 + \nu_f)/\psi, \tag{10.1}$$

$$f_{\mathrm{w}} \equiv \sum i\rho_i = (\nu_1 + f^2\nu_f)/\psi. \tag{10.2}$$

In equilibrium, hydrophobes on the polymers and on the surfactants aggregate into mixed micelles that serve as cross-link junctions of various multiplicity k. Let p_k be the probability for a randomly chosen hydrophobe to belong to a junction of multiplicity k at a certain given temperature and polymer and surfactant concentration. Then $p_1 \equiv 1 - \alpha$ is the probability for a hydrophobe to remain unassociated, where α is the extent of reaction in the conventional meaning.

If we use the **reduced concentration** $c_f \equiv \lambda(T) f\phi_f/n_f$ instead of ψ_f for polymers, and $c_1 \equiv \lambda(T)\phi_1/n_1$ for surfactants, the relation (7.98) can be transformed into

$$c_f(1+\eta) = z\tilde{u}(z), \tag{10.3}$$

where

$$\eta \equiv c_1/c_f \tag{10.4}$$

is the ratio of the surfactant concentration to the polymer concentration. Solving this relation with respect to z, we find z, and hence the reactivity α, as a function of a given temperature and concentration.

By using the ratio η, we can write the weight distribution ρ_i as

$$\rho_1 = \eta/(1+\eta) \quad \text{(for surfactant),}$$
$$\rho_f = 1/(1+\eta) \quad \text{(for polymer).} \tag{10.5}$$

10.1.1 Modification of the gel point by surfactants

For the polymer/surfactant system, the sol–gel transition condition (7.116) is explicitly given by

$$(f-1)z\tilde{u}'(z)/(1+\eta)\tilde{u}(z) = 1. \tag{10.6}$$

Combining this condition with the relation (10.3), we find the sol–gel transition curve on the temperature–concentration plane.

To describe the observed nonmonotonic behavior of the mechanical modulus and viscosity of the polymer–surfactant mixtures, we introduce a mini-max model of the junctions (7.127), for which

$$\tilde{u}(z) = 1 + \sum_{k=k_0}^{k_{\mathrm{m}}} z^{k-1} = 1 + (z^{k_0-1} - z^{k_{\mathrm{m}}})/(1-z), \tag{10.7}$$

where k_0 is the **minimum multiplicity** and k_{m} the **maximum multiplicity** allowed. We have neglected any possible contribution to the free energy from the micellar surface, and set all $\gamma_k = 1$ for $k_0 \leq k \leq k_{\mathrm{m}}$.

Small micelles whose aggregation numbers are less than k_0 and large micelles with aggregation numbers larger than k_m are assumed to be unstable and dissociate. In fact, sufactant molecules are known to form micelles of a very narrow size distribution. The upper and lower bounds here are determined by the geometrical suitability of the hydrophobes for spatial packing, the flexibility of the polymer chains, and other factors.

When the polymer concentration is so low that the number of hydrophobes is not enough to form junctions, the addition of surfactants combines the unassociated hydrophobes until their aggregation number exceeds k_0 and stabilizes them. The surfactant works as a cross-linker.

However, when the polymer concentration is sufficiently large and many junctions are already formed, some of the polymer hydrophobes in the junctions are replaced by surfactant hydrophobes. The path number (connectivity) of the network junctions is reduced.

Figure 10.2(a) shows how junctions are formed and destroyed by added surfactants in the special case where the multiplicity is fixed at $k_0 = k_m = 5$. The average branching number is $(5+5)/2 = 5$ (top figure), $(5+5+2)/3 = 4$ (middle figure), $(2+2+1+1)/4 = 1.5$ (bottom figure). It decreases monotonically with surfactant concentration.

From these considerations, we expect that there is no surfactant-mediated process if the minimum multiplicity is $k_0 = 2$, i.e., if there is no gap in the size distribution. Under

(a)   (b)
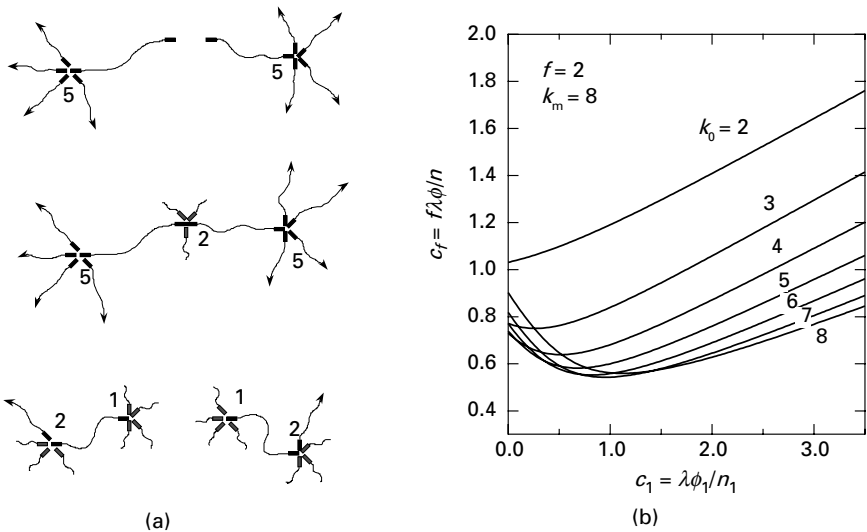
Fig. 10.2   (a) Formation of a junction with the help of surfactant molecules (surfactant-mediated association) and destruction of a junction by excess surfactant molecules. The allowed multiplicity is fixed at $k = 5$. Numbers near the junctions indicate their branching numbers. (b) Polymer concentration at sol–gel transition as a function of the concentration of added surfactant. The minimum multiplicity k_0 is varied from curve to curve under a fixed maximum multiplicity k_m. A minimum appears at a certain surfactant concentration for $k_0 \geq 3$. (Reprinted with permission from Ref. [1].)

such conditions, hydrophobes form stable junctions with any aggregation number less than k_m. The addition of surfactants therefore merely destroys the existing junctions.

To demonstrate these ideas, we calculate from (10.6) the sol–gel transition concentration as a function of the concentration of the added surfactant. Figure 10.2(b) shows the result for telechelic ($f = 2$) polymers. To clarify the effect of the **minimum multiplicity**, k_0 is varied from curve to curve, while the **maximum multiplicity** is fixed at $k_m = 8$. It is clear that the sol–gel concentration c_f^* monotonically increases with the surfactant concentration for $k_0 = 2$ (no lower bound). Gelation is blocked by the surfactant. But if there is a gap between $k = 1$ (unassociated) and $k = k_0$, a minimum in c_f^* appears where gelation is easiest, as can be seen for $k_0 \geq 3$ in Figure 10.2(b). The surfactant concentration at which c_f^* becomes minimum, referred to as the **surfactant-mediated gel point** (SMG), increases as the gap becomes larger.

10.1.2 Surfactant binding isotherms

The clusters consisting of surfactant molecules only are indicated by $l_f = 0$, so that we have $\mathbf{l} = \{l_1, 0\}$ in the distribution function (7.95). There are junctions of multiplicity $k = l_1$ only in such **pure surfactant micelles**. We then have $j_k = 1$ for $k = l_1$, otherwise $j_k = 0$. The distribution function becomes

$$\lambda \nu(\mathbf{j}; \mathbf{l}) = \gamma_{l_1}(x_1)^{l_1}/l_1, \tag{10.8}$$

where $x_1 \equiv \lambda(T)\nu(\mathbf{j}_{0,1}; \mathbf{l}_{0,1})$ is the concentration of unassociated surfactant molecules. The total number density of pure surfactant micelles (including unassociated molecules) is then given by

$$\lambda \nu_1^\circ \equiv \lambda \sum_{l_1 \geq 1} \nu(\mathbf{j}; \mathbf{l}) = \int_0^{x_1} \tilde{u}(x)dx, \tag{10.9}$$

while the total volume fraction of pure surfactant micelles is given by

$$\lambda \phi_1^\circ/n_1 \equiv \lambda \sum_{l_1 \geq 1} l_1 \nu(\mathbf{j}; \mathbf{l}) = x_1 \tilde{u}(x_1) \tag{10.10}$$

(The symbol $^\circ$ indicates clusters that are made up of surfactant molecules only, including unassociated ones.)

Since

$$x_1 = c_1(1 - \alpha) = c_1/\tilde{u}(z), \tag{10.11}$$

by definition, we find

$$\lambda \phi_1^\circ/n_1 = x_1 \tilde{u}(x_1) = c_1 \tilde{u}(x_1)/\tilde{u}(z), \tag{10.12}$$

and hence

$$\phi_1^\circ = [\tilde{u}(x_1)/\tilde{u}(z)]\phi_1. \tag{10.13}$$
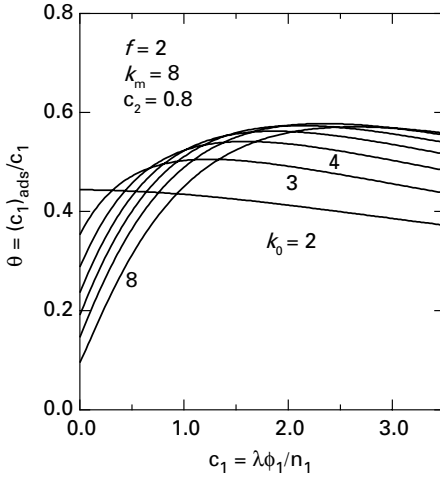
Fig. 10.3   Isotherm of surfactant molecules bound by bifunctional ($f = 2$) polymers. The fraction θ of the adsorbed surfactant molecules is plotted against their total concentration. The minimum multiplicity k_0 of the junctions is changed from curve to curve with fixed $k_m = 8$. The curve starts from a finite value and shows a peak at the SMG concentration. (Reprinted with permission from Ref. [1].)

The fraction $\tilde{u}(x_1)/\tilde{u}(z)$ out of the total volume fraction ϕ_1 of surfactants remains unassociated to the polymers. The rest

$$\theta \equiv \phi_1^{\text{ads}}/\phi_1 = 1 - \tilde{u}(x_1)/\tilde{u}(z) \tag{10.14}$$

is the fraction of surfactant molecules that are adsorbed into the network junctions. The fraction θ as a function of ϕ_1 is the **binding isotherm** of surfactant adsorption.

Figure 10.3 shows the binding isotherm θ of the adsorbed surfactant molecules as a function of the total surfactant concentration. The maximum multiplicity is fixed at 8, while the minimum multiplicity is varied from curve to curve. The polymer concentration is fixed at $c_f = 0.8$ at which polymers are in the postgel regime for $k_0 = 3, 4, 5, 6$, but in the pregel regime for $k_0 = 2, 7, 8$, as can be seen from Figure 10.4(a). The fraction θ changes continuously across the sol–gel transition point, and takes a maximum value at the surfactant concentration where gelation is easiest (the micellization–gelation point, MGP, defined below), except in the case for $k_0 = 2$, for which there is no gap in k.

10.1.3   CMC of the surfactant molecules

It is known that surfactant molecules form micelles above a certain concentration (see Section 6.7). The concentration at which micelles appear is referred to as the **critical micelle concentration** (CMC). For mixed solutions of associating polymers and surfactants, the concentration at which mixed micelles starts to form is referred to as the **critical aggregation concentration** (CAC). To see how the CMC of the surfactant is affected by the presence of polymers, let us consider the surfactant molecules that are
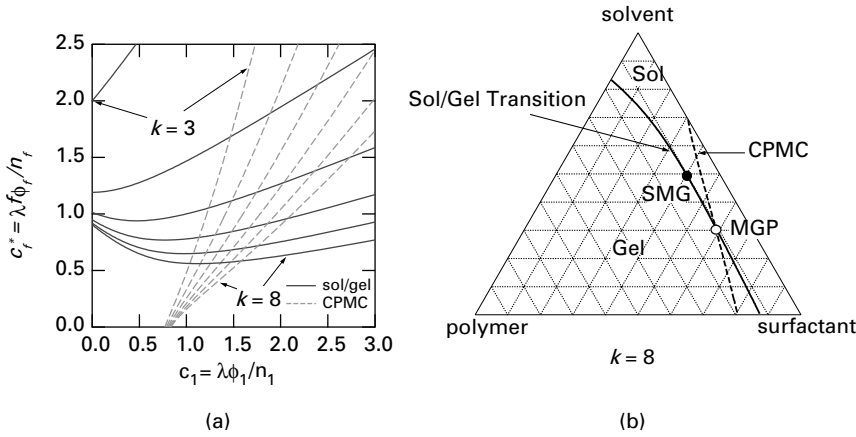
Fig. 10.4   (a) Polymer concentration (solid lines) at the sol–gel transition, and the critical pure micelle concentration (broken lines) plotted as a function of the concentration of added surfactant for a fixed multiplicity $k_0 = k_m = 8$. (b) Sol–gel transition and CPMC lines drawn on the ternary phase plane of the polymer/surfactant/solvent system. The minimum gelation point (SMG point) is indicated by a black circle. The white circle shows a special point at which gelation and micellization take place simultaneously (MGP). (Reprinted with permission from Ref. [1].)

not associated to any polymers, and define the CMC by the surfactant concentration at which micelles consisting only of surfactant molecules appear. This concentration is referred to as the **critical pure micelle concentration** (CPMC). By definition CPMC lies above CAC.

One conventional criterion for CMC is to find the concentration at which the osmotic pressure changes its slope most rapidly [28]. The contribution to the osmotic pressure from the surfactant molecules that are not connected to the polymers is proportional to (10.9) at low concentrations. Their volume fraction is given by (10.10). If we try to solve (10.10) for x_1 as a function of ϕ_1°, we will fail to find the solution whenever the condition

$$d(x\tilde{u}(x))/dx = \tilde{u}(x) + x\tilde{u}'(x) = 0 \tag{10.15}$$

holds. This equation is an algebraic equation for x, and has its roots on the complex x-plane. These roots are the branch points of the inverse function. When the concentration x_1 of the unassociated surfactant passes near the root that lies closest to the real x-axis, the osmotic pressure (10.9) due to surfactant molecules changes its slope most rapidly.

To study the relative positions of CPMC and SMG concentration, we consider a fixed multiplicity model in which the multiplicity is fixed at a single value $k_0 = k_m \equiv k$. The function $\tilde{u}(x)$ in this fixed multiplicity model takes the form $\tilde{u}(x) = 1 + x^{k-1}$, and leads to a set of equations

$$\lambda v_1^\circ = x_1 + x_1^k/k, \tag{10.16}$$

$$\lambda \phi_1^\circ / n_1 = x_1 + x_1^k. \tag{10.17}$$

The equation (10.15) now gives the roots

$$x_j = k^{-1/(k-1)} \exp[2\pi i (j+1/2)/(k-1)] \quad (j=0,1,2,\ldots,k-2), \tag{10.18}$$

which lie on a circle of radius $r \equiv k^{-1/(k-1)}$ on the complex x-plane.

Now setting $x_1 = r$ in (10.11), we find the CPMC by

$$c_1/(1+z^{k-1}) = r, \tag{10.19}$$

where the parameter z is expressed in terms of c_f and c_1 by solving (10.3), which now takes the form

$$c_f + c_1 = z(1+z^{k-1}). \tag{10.20}$$

Figure 10.4(a) shows the sol–gel transition concentration (vertical axis) as a function of the surfactant concentration (horizontal axis) (solid lines), and the CPMC (horizontal axis) as a function of polymer concentration (vertical axis) (broken lines). The multiplicity is changed from $k=3$ to $k=8$.

There is an intersection between the solid broken lines for each multiplicity k. This is a special point where the sol–gel transition and the CPMC take place simultaneously. We call this special point the **micellization gelation point** (MGP). For instance, for $k=8$ this point is located at a surfactant concentration that is nearly twice as large as the SMG concentration.

To see the situation more clearly, we draw these two lines on the ternary phase plane. Figure 10.4(b) shows the sol–gel transition (solid line) and CPMC lines (broken line) on the triangular plane of the polymer/surfactant/water system. SMG and MGP are indicated by the black and white circles. Their relative positions may change if we allow the binding free energy of polymer hydrophobe and surfactant hydrophobe to change.

10.1.4   High-frequency elastic modulus

In the experiment on the HEUR/SDS system [18], the addition of surfactant resulted in several effects. (1) The moduli are no longer described by the simple **Maxwell element** with a single relaxation time, but a shoulder appears on the loss modulus at higher frequencies. (2) The high-frequency plateau in the storage modulus reveals nonmonotonic dependence on the SDS concentration. At low polymer concentration, it initially rises, and reaches a peak and then decreases monotonically, falling eventually to zero at a higher SDS concentration (Figure 10.5(a)). With an increase in the polymer concentration, the height of the peak decreases and its position shifts to a lower SDS concentration. Above a certain polymer concentration, the peak disappears. (3) The average rheological relaxation time also shows a peak for all polymer concentrations measured.

To see how these new rheological features appear, we calculate the number μ_{eff} of elastically effective junctions in a unit volume from (8.31), and the number of elastically effective chains ν_{eff} from (8.32).

Figure 10.5(b) shows the number $\nu_{\text{eff}}(c_1)$ of elastically effective chains plotted against the surfactant concentration c_1. The number is normalized by the value $\nu_{\text{eff}}(0)$ under the
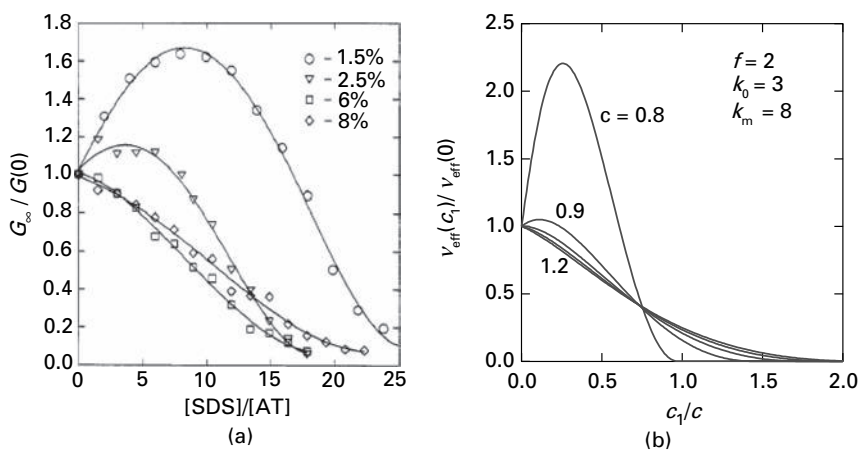
Fig. 10.5 (a) Experimental data on the high-frequency storage modulus as a function of the surfactant concentration. The polymer concentration is changed from curve to curve. (Reprinted with permission from Ref. [18].) (b) Theoretical calculation of the number of elastically effective chains plotted against the ratio of the surfactant concentration and the polymer concentration. The polymer concentration is varied from curve to curve. (Reprinted with permission from Ref. [1].)

absence of the surfactant. This ratio therefore gives the relative strength $G_\infty(c_1)/G_\infty(0)$ of the **high-frequency plateau value** in the storage modulus. Polymers are assumed to carry two functional groups ($f = 2$). The allowed multiplicity of a junction ranges from 3 to 8. The polymer concentration is changed from curve to curve.

As expected, the curves for low polymer concentrations first increase to a peak and then monotonically decrease to zero where the gel network is broken into sol pieces by the surfactant. For higher polymer concentrations, however, the curves do not show any peak because the junctions are well developed without surfactant molecules. The added surfactant only destroys the junctions.

These calculations reproduce, at least qualitatively, the experimental observations HEUR/SDS reported by Annable *et al.* [18] (Figure 10.5(a)), apart from that in the theory all curves cross each other at a certain surfactant concentration, whereas the experimental data reveal the same tendency only for relatively higher polymer concentrations. The maximum in the modulus appears as a result of the existence of a forbidden gap (from $k = 2$ to $k_0 - 1$) in the multiplicity of the network junctions.

10.2 Loop-bridge transition

Polymers carrying many hydrophobes undergo the simultaneous formation of intramolecular micelles with a dense core of hydrophobic groups surrounded by a corona of small loops (**flowers**) and interchain micellar cross-links (Figure 10.6). A subchain connecting two junctions on different micelles is called a **bridge chain**. This
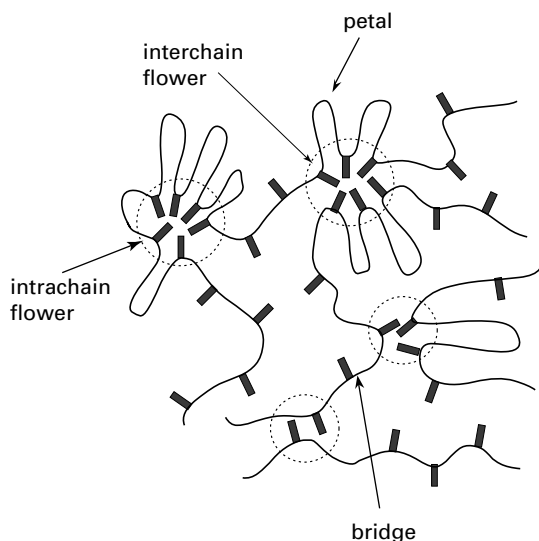
Fig. 10.6　Intra- and intermolecular flowers formed by hydrophobically modified associating polymers. (Reprinted with permission from Ref. [29].)

section studies the transition from **intramolecular association** (**closed association**) to **intermolecular association** (**open association**) by changing the polymer concentration.

In general, the CMC of the flower micelles is very low; it can be as low as 10^{-3} polymer wt%. At low concentrations, intramolecular flowers dominate. With an increase in the polymer concentration, loops dissociate and have more chance to form an open association with many bridges, thus eventually leading to gelation. The sharpness of the transition depends on the association constant and the aggregation number of the micelles.

If we can assume association to be an entire equilibrium and reversible, it can be decomposed into intra- and intermolecular association. In intramolecular association, each chain has a conformation carrying several intramolecular flowers along the chain [29]. The hydrophobic cores are regarded as composite associative groups. In intermolecular association, such composite chains are connected with each other by intermolecular association. Thus, the system is modeled as a polymer solution in which polymers carry many associative groups of different sizes that may form junctions of variable multiplicity. The functionality of each chain is not fixed, but is controlled by the thermodynamic requirement.

Let us specifically consider **telechelic polymers**. The intramolecular association of telechelic polymers is unique, namely, they form a **single loop** (petal). The probability to form such a loop is decided by the thermodynamic equilibrium condition. It is given by the **cyclization parameter** introduced in Section 6.2 [30]

$$\zeta_n(T) = B\lambda(T)/n^{3/2}, \tag{10.21}$$

where $\lambda(T)$ is the association constant, n the total number of statistical units on a chain, and B is some numerical constant that may depend upon chain flexibility, the chemical species of the polymers, and solvent quality.

Strictly, the power 3/2 in (10.21) should be replaced by $d\nu + \gamma - 1$ for swollen polymers in a good solvent, where $d = 3$ is the space dimension, $\nu = 3/5$ Flory's exponent (Section 1.6), and $\gamma = 7/6$ the critical exponent for the total number of self-avoiding random walks [31]. However, we neglect the excluded-volume effect since both our solution theory and gelation theory are based on the mean-field treatment.

The loop parameter (10.21) is a new parameter that depends on the association constant. It may also be written as

$$\zeta_n(T) = \exp(-\beta \Delta A), \qquad (10.22)$$

where $\Delta A \equiv A_1 - A_2$ is the difference in the conformational free energy between the reference conformation (an open chain with two unassociated groups indicated by the subscript 2) and the excited conformation (a loop with a single composite associative group indicated by the subscript 1). Thermoreversible gelation driven by such an intramolecular conformation change can be treated more generally for the functional groups that are activated by the conformational change (see Section 10.5).

A petal is regarded as a monofunctional molecule carrying a single composite associative group formed by the doublet of the original associative groups (see Figure 10.7). We have the model solution in which bifunctional telechelic polymers are mixed with monofunctional loops, which is mathematically equivalent to the mixture of the associating
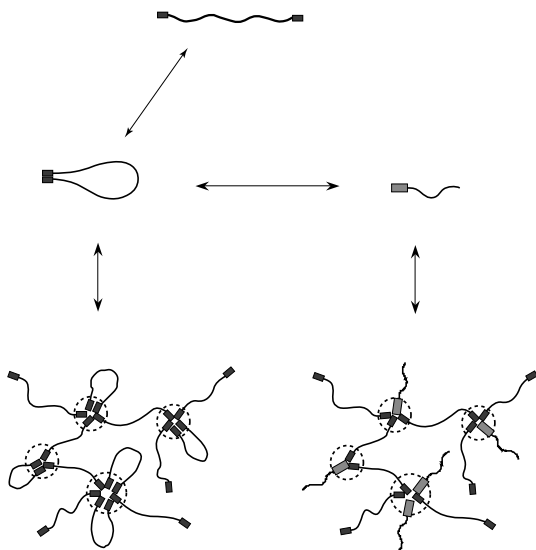
Fig. 10.7 Mixture of petals and telechelic chains. A petal can be regarded as a monofunctional composite chain. (Reprinted with permission from Ref. [29].)

polymers and surfactant molecules studied in the preceding section. The only difference lies in that the population of loops (corresponding to surfactants) is automatically controlled by the thermodynamic equilibrium condition.

Let ϕ_1 be the volume fraction of the loops ($f = 1$), and ϕ_2 be that of the open chains ($f = 2$). The total volume fraction ϕ of the polymers in the solution is $\phi = \phi_1 + \phi_2$. The total number density of the associative groups is $\psi = (\phi_1 + 2\phi_2)/n$. Their ratio is decided by the equilibrium loop parameter as

$$v_1^\circ/v_2^\circ = \zeta_n(T), \tag{10.23}$$

where the superscript ∘ indicates that the chains remain isolated in the solution.

By definition, we have $v_f^\circ = v_f(1-\alpha)^f = v_f/\tilde{u}(z)^f$ for $f = 1, 2$, where α and $\tilde{u}(z)$ are defined in the usual way. Hence, the relation

$$\phi_1/\phi_2 = \zeta_n(T)/\tilde{u}(z) \tag{10.24}$$

holds. On substitution into (7.99), we find

$$\left(\frac{\lambda}{n}\phi\right)\frac{\zeta_n(T) + 2\tilde{u}(z)}{\zeta_n(T) + \tilde{u}(z)} = z\tilde{u}(z), \tag{10.25}$$

so that the number-average functionality f_n of the loop/chain mixture turns out to be

$$f_n = [\zeta_n + 2\tilde{u}(z)]/[\zeta_n + \tilde{u}(z)]. \tag{10.26}$$

By definition, the weight-average f_w is

$$f_w = (1^2 v_1 + 2^2 v_2)/(v_1 + 2v_2) = [\zeta_n + 4\tilde{u}(z)]/[\zeta_n + 2\tilde{u}(z)]. \tag{10.27}$$

The gel point can be found by (7.115). Putting (7.115) and (10.27) together, the parameter z^* at the gel point is found to be the solution of the equation

$$2zu'(z)/[\zeta_n + 2\tilde{u}(z)] = 1. \tag{10.28}$$

To calculate the gel point concentration, we introduce the reduced polymer concentration $c \equiv 2\lambda(T)\phi/n$, the total number density of the associative groups. From (10.25) for $z = z^*$, the concentration c^* at the gel point for the fixed multiplicity model takes the form

$$c^* = k'(1 + \zeta_n/2k')[1 + (1 + 2k'')\zeta_n/2k']/(k'')^{k/k'}(1 + \zeta_n/2)^{k''/k'}, \tag{10.29}$$

where the abbreviated notations $k' \equiv k - 1$ and $k'' \equiv k - 2$ have been used.

Figure 10.8(a) shows c^* as a function of the loop parameter for the min-max model ($k_0 = 5, k_m = 8$) of the junction multiplicity. Two of λ, ζ_n, and n are independent variables. In other words, λ and ζ_n can be independently changed only through a change of n (for a given prefactor B). The two axes in this figure (and also in Figure 10.8(b)) must therefore
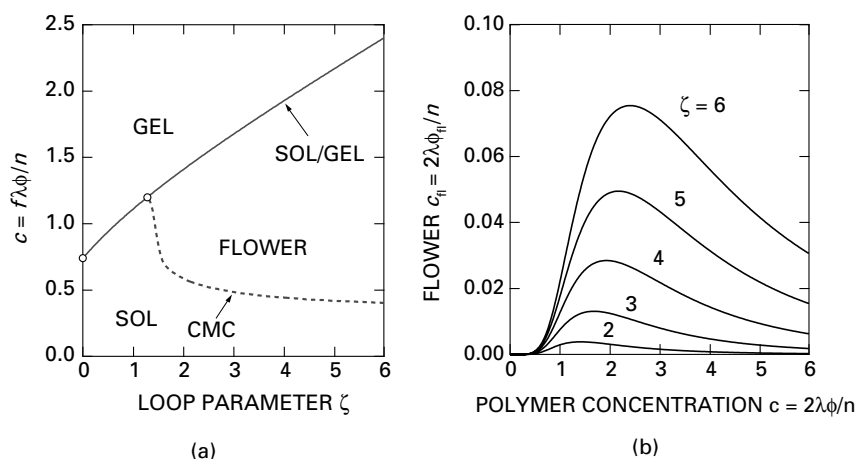
Fig. 10.8 (a) Relative position of CFMC and sol–gel transition of telechelic polymers with min-max junction ($k_0 = 5, k_m = 8$). (b) Population of flower micelles as a function of the polymer concentration. (Reprinted with permission from Ref. [29].)
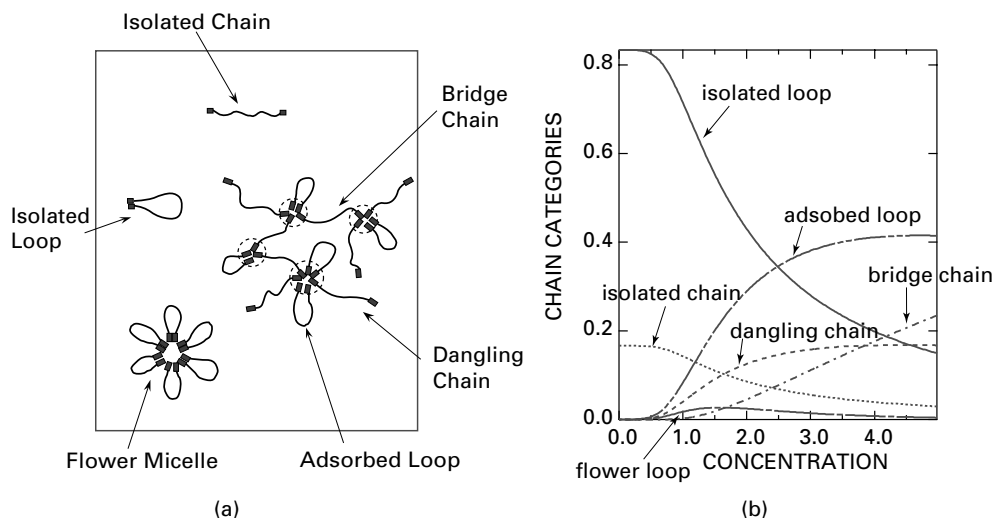
Fig. 10.9 (a) Six association categories of the chains in the solution of telechelic polymers. (b) Their relative population plotted against the polymer concentration for $\zeta_n = 5$. (Reprinted with permission from Ref. [29].)

be understood as the variables changed in this context. The gel point concentration is monotonically increasing function of ζ_n because loop formation prevents gelation.

To see how closed association changes into open association, we first summarize all possible types of chain association. There are six categories altogether (Figure 10.9(a)): isolated open chain, isolated loop, cluster consisting only of loops (called **flower micelle**), bridge chain, dangling chain, dangling loop in a cluster. In particular, the concentration

at which the flowers appear is referred to as the **critical flower micelle concentration** (CFMC).

Figure 10.9(b) shows the relative population of each chain category as a function of the total polymer concentration. These results are calculated within the theoretical framework for the model mixture of $f = 1$ and $f = 2$ associative molecules. The multiplicity of the junctions is allowed in the range between k_0 and $k_m = 8$ for a fixed loop parameter $\zeta_n(T) = 5$. These curves are normalized to give unity when summed up. Isolated loops and isolated chains start with a ratio of 5 to 1, but both decrease with the polymer concentration, because they are adsorbed into the mixed clusters.

Dangling chains, adsorbed loops, and bridge chains increase with the concentration, but bridge chains eventually dominate at high concentrations. Flower loops appear in a certain range of the concentration. Their curve exhibits a single maximum near $c = 1.5$. Since the gel point concentration for this solution is given by $c^* = 2.2$, flowers appear before the gel point. The fraction of the free ends as functions of the polymer concentration and temperature was experimentally measured for fluorinated telechelic PEO solutions by using ^{19}F NMR relaxation method [32].

The reactivity α used so far is the superficial degree of association calculated under the assumption that the composite group on a loop is regarded as one associative group. The real reactivity α_0 is defined by the number of associated functional groups divided by the total number of groups. Therefore the relation

$$\alpha_0 = \frac{2(\phi_1 + \phi_2\alpha)}{2(\phi_1 + \phi_2)} = \frac{\alpha + \zeta_n(1 - \alpha)}{1 + \zeta_n(1 - \alpha)} \tag{10.30}$$

holds. As a function of the loop parameter ζ_n, it starts from α and monotonically increases to unity.

The volume fraction ϕ_{fl} of the flower micelles is written as

$$\phi_{fl} = L_{fl}\phi = \frac{\zeta_n[\tilde{u}(x_1) - 1]\phi}{[\zeta_n + \tilde{u}(z)]\tilde{u}(z)}, \tag{10.31}$$

from the probability L_{fl} for the loops to attach to the junctions. Since the parameters z and x_1 are functions of the total polymer concentration, ϕ_{fl} is regarded as a function of the concentration. By differentiation, the concentration at which the volume fraction of flowers becomes maximum satisfies the condition $dx_1/dc = 0$, but since this is equivalent to the condition for the gel point, we find the *concentration of flower micelles reaches a maximum value at the gel point*.

Figure 10.8(b) shows the volume fraction ϕ_{fl} of flower micelles plotted against the total polymer concentration. The loop parameter is varied from curve to curve for the multiplicity in the allowed range $5 \leq k \leq 8$. The concentration at which ϕ_{fl} rises from zero is CFMC. Since it slowly increases in the figure, the conventional method to identify CMC (the population curve of the micelles bends most sharply) is not directly applicable. As a rough estimate, we here employ a simple criterion that the concentration where the absolute value of ϕ_{fl} reaches a certain threshold value is CFMC. The actual value of the

CFMC obtained in this simple method depends sensitively upon the chosen threshold value. We have fixed this value at $\phi_{fl} = 0.001$, although it is somewhat arbitrary.

10.3   Competing hydration and gelation

Solutions of natural polymers often gel on heating. A typical example that has long been studied is methylcellulose with a nearly full degree of substitution by methoxyl groups [33, 34]. Substitution by large side-chain groups prevents polymers from undergoing hydrogen-bonding crystallization.

In an aqueous solution at low temperatures, polymer chains are hydrated with water molecules attached by hydrogen bond (p-w H-bond), so that direct association between polymer segments is prohibited by the bound water molecules. As the temperature is raised, chains gradually lose bound waters, and polymer–polymer association (p-p H-bond), which is initiated by hydrophobic force, being stabilized by direct hydrogen bonds, begins to take place. As dehydration proceeds, the number of direct interchain associations increases, and eventually reaches a critical value for gelation. This sol–gel transition is signaled by a sharp rise in viscosity. It is reversible in the sense that the gel liquefies to the original constituents on cooling [33].

Because the hydrophobic segments on polymer chains are partly exposed to water in the postgel regime, the solution tends to separate into two macroscopic phases by hydrophobic association. Thus gelation and phase separation compete as the temperature goes up. The solution reveals an interesting multi-critical phase behavior [33].

10.3.1   Models of competitive hydration and gelation

The model we study is the polymer solution in which each primary polymer chain carries f reactive groups attached along the chain backbone. Each reactive group is assumed to be capable of forming pairwise hydrogen bond with either solvent molecule (water molecule in an aqueous solution) or other reactive group on a different chain.

To specify the type of the clusters, we use a set of numbers (l, m) for a cluster consisting of l cross-linked polymer chains which are hydrated by a total m of solvent molecules (Figure 10.10). Specifically a free solvent molecule is described by $(0, 1)$.

The total free energy of the solution is given by the sum of the general form (5.13). The chemical potential of an (l, m)-cluster is

$$\beta \Delta \mu_{l,m} = 1 + \Delta_{l,m} + \ln \phi_{l,m} - (nl + m)\nu^{S} + \chi[nl(1 - \phi) + m\phi - (nl + m)\phi(1 - \phi)],$$
(10.32)

where

$$\nu^{S} \equiv \sum_{l,m} \nu_{l,m}$$
(10.33)

is the total number of clusters per unit cell.
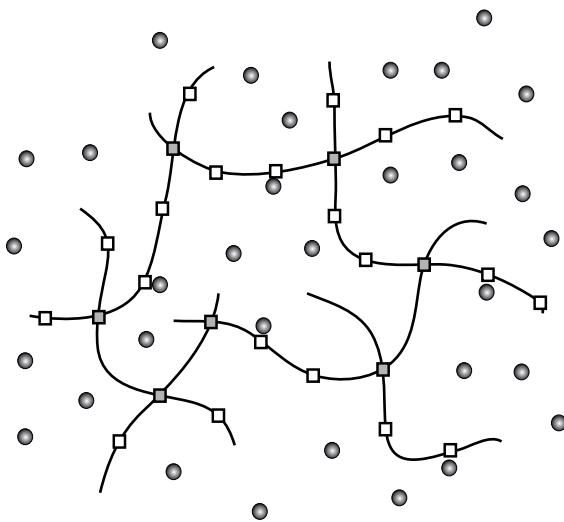
Fig. 10.10 Competing hydration and association. If polymers carry associative groups at or near the hydration sites, polymer–polymer association is prevented by hydration. The solution gels after dehydration upon heating.

By the multiple-equilibrium condition

$$\Delta\mu_{l,m} = l\Delta\mu_{1,0} + m\Delta\mu_{0,1}, \tag{10.34}$$

for arbitrary l and m, we find the volume fraction of the (l,m) clusters as

$$\phi_{l,m} = K_{l,m}(\phi_{1,0})^l(\phi_{0,1})^m, \tag{10.35}$$

where

$$K_{l,m} \equiv \exp(l + m - 1 - \Delta_{l,m}) \tag{10.36}$$

is the equilibrium constant.

Now, as usual, we split the free energy of cluster formation into three parts:

$$\Delta_{l,m} = \Delta_{l,m}^{\text{comb}} + \Delta_{l,m}^{\text{conf}} + \Delta_{l,m}^{\text{bond}}. \tag{10.37}$$

An (l,m)-cluster has $l-1$ cross-links connecting l constituent polymer chains, and $fl - 2l + 2$ unreacted functional groups, m of which are hydrated by solvent molecules. The combinatorial factor is given by $f^l\omega_l$ for the connection of the f-functional polymers into a tree, where $\omega_l \equiv (fl-l)!/l!(fl-2l+2)!$ is the Stockmayer factor (3.19). For each type of the polymer tree, m attaching sites must be chosen from $fl - 2l + 2$ open sites for hydration. This selection gives a binomial factor $_{fl-2l+2}C_m$. The total combinatorial free energy change then takes the form

$$\Delta_{l,m}^{\text{comb}} = -\ln(_{fl-2l+2}C_m \, f^l\omega_l). \tag{10.38}$$

To find the configurational entropy, we employ the conventional lattice-theoretical formula for the entropy of disorientation (2.90)

$$S_{\text{dis}}(l,m) \equiv k_B \ln\left[\frac{(nl+m)\zeta(\zeta-1)^{nl+m-2}}{\sigma\exp(nl+m-1)}\right], \tag{10.39}$$

where ζ is the lattice coordination number, and σ the symmetry number of the polymer chain. The configurational free energy is then given by

$$\Delta_{l,m}^{\text{conf}} = -\beta T[S_{\text{dis}}(l,m) - l\,S_{\text{dis}}(1,0) - m\,S_{\text{dis}}(0,1)]$$
$$= -\ln\left\{(nl+m)\left[\frac{\sigma(\zeta-1)^2}{\zeta e}\right]^{l+m-1}/n^l\right\}. \tag{10.40}$$

Finally the free energy of bond formation is given by

$$\Delta_{l,m}^{\text{bond}} = \beta[(l-1)\Delta f_0 + m\Delta g_0], \tag{10.41}$$

where Δf_0 is the standard free energy change of p-p bond formation, and Δg_0 is that of a p-w bond.

Combining all these results, we are led to

$$K_{l,m} = (nl+m)_{\,fl-2l+2}C_m\,\omega_l\frac{f}{n}\left[\frac{f\lambda(T)}{n}\right]^{l-1}\mu(T)^m, \tag{10.42}$$

for the equilibrium constant, where a temperature-dependent association constant

$$\lambda(T) \equiv [\sigma(\zeta-1)^2/\zeta e]\exp(-\beta\Delta f_0) \tag{10.43}$$

depends on the strength of a single p-p pairwise bond. The p-w association constant is similarly defined by

$$\mu(T) = [\sigma(\zeta-1)^2/\zeta e]\exp(-\beta\Delta g_0). \tag{10.44}$$

A variety of phase diagrams appear depending on their relative strengths, some of which correspond to the actually observed phase diagrams of the solutions of cellulose derivatives.

Upon substitution of (10.42) into (10.35) and rearranging the result, we find that the number distribution of clusters is given by

$$\nu_{l,m} = \frac{1}{\lambda(T)}\,_{fl-2l+2}C_m\,\omega_l x^l y^m + \frac{1}{\mu(T)}y\delta_{l,0}\delta_{m,1}, \tag{10.45}$$

where δ is the Kronecker's delta. We have introduced two variables

$$x \equiv f\lambda(T)\phi_{1,0}/n \quad\text{and}\quad y \equiv \mu(T)\phi_{0,1}, \tag{10.46}$$

each corresponding to the number density of the isolated molecules, acompanied by the temperature shift factor λ or μ.

When there is no p-w coupling ($\mu = 0$), the model reduces to the simple gelation by pairwise cross-linking studied in Section 7.1. On the contrary, when there is no p-p coupling ($\lambda = 0$), it reduces to the random hydration in aqueous polymer solutions studied in Section 6.4.

Our next step is to express x and y in terms of the total concentration ϕ of the polymer. This is most conveniently carried out by calculating the moments of the cluster distribution. For instance, the volume fraction ϕ_P^S of the polymers belonging to the finite clusters is found to be

$$\phi_P^S = n \sum_{l \geq 1, m} l \nu_{l,m} = n(1+y)^2 S_1(z)/\lambda, \qquad (10.47)$$

by the use of a combined variable

$$z \equiv x(1+y)^{f-2}. \qquad (10.48)$$

The reactivity α is defined by the equation $z = \alpha(1-\alpha)^{f-2}$. It gives the degree of p-p reaction, i.e., the number of associating groups cross-linked to the groups on different chains divided by the total number of groups.

In the pregel regime ϕ_P^S agrees with the total volume fraction ϕ of polymers, but it can be smaller than ϕ in the postgel regime.

Quite similarly, the volume fraction of the solvent is given by

$$1 - \phi = \phi_H^S + y/\mu, \qquad (10.49)$$

where the first term ϕ_H^S is the volume fraction of the solvent molecules bound to the polymer chains, and the second term gives that of the free solvent. The hydration part is given by

$$\phi_H^S = \sum_{l,m \geq 1} m \nu_{l,m} = y(1+y) S(z)/\lambda, \qquad (10.50)$$

with $S(z)$ defined by $S(z) \equiv (f-2) S_1(z) + 2 S_0(z) = \alpha/(1-\alpha)$.

Solving the coupled equations (10.47) and (10.49) with respect to y and z, we can express them in terms of the total volume fraction ϕ. The explicit forms of the coupled equations in the pregel regime are

$$(1+y)^2 \alpha/(1-\alpha)^2 = c_f, \qquad (10.51a)$$

$$\zeta y(1+y)\alpha/(1-\alpha) + y = c_1, \qquad (10.51b)$$

with the variables $c_f \equiv f\lambda(T)\phi/n$ and $c_1 \equiv \mu(1-\phi)$. The ratio $\zeta \equiv \mu/\lambda$ is the relative strength of the p-w and p-p H-bonds.

The second equation gives

$$\alpha = (c_1 - y)/[\zeta y(1+y) + c_1 - y], \qquad (10.52)$$

for the reactivity. Substituting this relation into the first equation, we find

$$\zeta y^3 - (1 - \zeta - \zeta^2 c_f + \zeta c_1) y^2 + (2 - \zeta) c_1 y - c_1^2 = 0. \qquad (10.53)$$

The volume fraction y of the free solvent is the one solution of this algebraic equation that tends to $\mu(1 - \phi)$ in the limit of small ϕ.

10.3.2 Degree of hydration and the gel point

The chemical potential of each species is

$$\beta \Delta \mu_P = (1 + \ln x)/n - \nu^S(x, y) + \chi (1 - \phi)^2, \qquad (10.54)$$

for the polymer segment, and

$$\beta \Delta \mu_0 = 1 + \ln y - \nu^S(x, y) + \chi \phi^2, \qquad (10.55)$$

for the solvent molecule, where the total number of clusters is

$$\nu^S(x, y) \equiv \sum_{l,m} \nu_{l,m} = (1 + y)^2 \alpha (1 - f\alpha/2)/\lambda f (1 - \alpha)^2 + y/\mu. \qquad (10.56)$$

Since these chemical potentials are now given as functions of the temperature and concentration through the parameters x and y, we can find the solution properties.

For instance, the second virial coefficient is found to be

$$A_2 = \frac{1}{2} \left(1 + \frac{\mu f/n}{1 + \mu} \right)^2 - \frac{\lambda}{2} \left(\frac{f/n}{1 + \mu} \right)^2 - \chi. \qquad (10.57)$$

The gel point can be found by the divergence of the weight-average $\bar{l}_w$ of the cluster size, which leads to the usual condition $\alpha = 1/(f - 1) \equiv \alpha^*$. We find the gelation concentration as a function of the temperature as

$$\lambda(T)\phi^* = A(T)\{1 + B(T) - [1 + 2B(T)]^{1/2}\}, \qquad (10.58)$$

where
$$A(T) \equiv ff'(f''\lambda - \mu)^2/2\mu^2(f' + ff''/n)^2 \qquad (10.59)$$

and
$$B(T) \equiv 2n\lambda\mu(1 + \mu)(f' + ff''/n)/f(\lambda f'' - \mu)^2 \qquad (10.60)$$

are functions of the temperature only. To simplify the notation, we have used condensed notations $f' \equiv f - 1$ and $f'' \equiv f - 2$.

Since A and B are complex functions of the temperature, (10.58) suggests that it is experimentally impossible to find the standard enthalpy ΔH_0 of cross-linking–which is contained in the factor $\lambda(T)$–by the conventional Eldridge–Ferry method, which plots $\ln \phi^*$ against $1/k_B T$.

In the postgel regime we follow Stockmayer's treatment, and assume that the degree of reaction α in the sol part remains at constant α^*. The corresponding value of z is given by $z^* = (f-2)^{f-2}/(f-1)^{f-1}$. The polymer volume fraction of the sol part

$$\phi_P^S = n(1+y)^2 S_1(z^*)/\lambda \tag{10.61}$$

then becomes smaller than the total volume fraction ϕ. The excess fraction

$$\phi_P^G \equiv \phi - \phi_P^S \tag{10.62}$$

gives the polymer volume fraction of the part that is forming the gel network.

The volume fraction of the solvent molecules that are bound to the gel network is similarly given by

$$\phi_H^G = 1 - \phi - \phi_H^S - y/\mu, \tag{10.63}$$

where

$$\phi_H^S = y(1+y)S(z^*)/\lambda \tag{10.64}$$

is the volume fraction of the solvent molecules that are attached to the *finite* clusters in the sol. The total volume fraction of the bound solvent molecules is given by

$$\phi_H = \phi_H^S + \phi_H^G = 1 - \phi - y/\mu. \tag{10.65}$$

The osmotic compressibility takes the form (7.64), where the function σ is given by

$$\sigma(\phi, T) = \frac{\kappa_P(\phi)}{n\phi} + \frac{\kappa_0(\phi)}{1-\phi} - 2\chi. \tag{10.66}$$

The general relations (5.47a) lead to

$$\kappa_P(\phi) = \frac{1}{1+\alpha}\left[1 - f'\alpha\frac{f\lambda y(1-\alpha)(1+\alpha\phi - y/\mu)}{(1+y)[\lambda(1-\phi)(1+\alpha) - \alpha y^2]}\right], \tag{10.67a}$$

$$\kappa_0(\phi) = \frac{\lambda y(1-\phi)(1+\alpha\phi - y/\mu)}{\phi[\lambda(1-\phi)(1+\alpha) - \alpha y^2]}. \tag{10.67b}$$

In the limit of no hydration ($\mu = 0$), they reduce to $\kappa_P = (1 - f'\alpha)/(1+\alpha)$ and $\kappa_0 = 1$ as given in Section 7.1. The function κ_P therefore gives the reciprocal of the weight-average cluster size $\bar{l}_w = (1+\alpha)/(1 - f'\alpha)$ in this limit. In the limit of no gelation [35] ($\lambda = 0$), $\kappa_P = (1 - \phi + y)/(1 - \phi + y^2/\mu)$ and $\kappa_0 = (1-\phi)(1+y)(1 - y/\mu)/\phi(1 - \phi + y^2/\mu)$, which agrees with the result in Section 6.4.

The association constants are assumed to take the forms

$$\lambda(T) = \lambda_0 \exp(-\gamma_1\tau), \quad \mu(T) = \mu_0 \exp(-\gamma_2\tau), \tag{10.68}$$

by splitting the standard free energy changes into the entropy part and the energy part, where $\gamma_1 \equiv |\Delta\epsilon_1|/k_B\Theta$ ($\Delta\epsilon_1 < 0$) is the p-p bond strength relative to the thermal energy.

The p-w bond γ_2 is similarly defined. Effect of the entropy change on bonding is included in the prefactors.

We confine our argument in the special case $\gamma_1 = \gamma_2 = 3.5$ for simplicity to restore the the phase diagram of polyethylene oxide in Section 6.4. We regard it as a prototype and see how the phase diagrams change as the relative strength of λ_0 and μ_0 is changed.

Figure 10.11(a)–(c) shows how the sol–gel transition line passes through the miscibility gap and interferes with phase separation as the p-p association constant λ_0 is increased. Broken lines show the sol–gel transition, solid lines the spinodals, and dotted lines the binodals. The parameter λ_0 is changed from figure to figure ((a) $\lambda_0 = 0.001$,
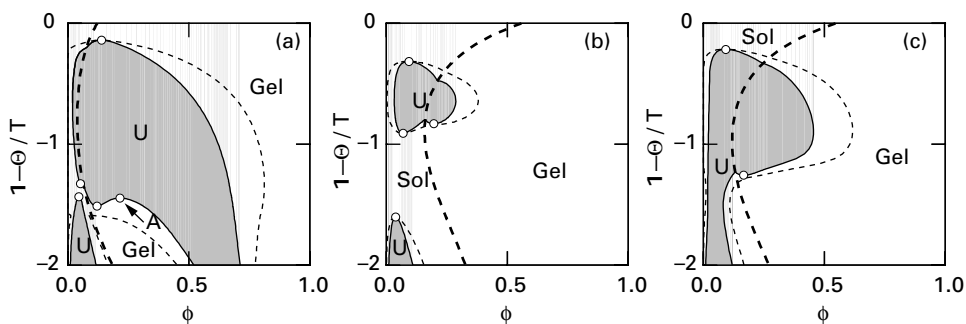
Fig. 10.11 Sol–gel transition line (thick broken line), binodal (thin dotted line), and spinodal (solid line) shown on the reduced temperature–concentration plane. The amplitude λ_0 of the association constant is changed: (a) $\lambda_0 = 0.001$, (b) 0.01, (c) 0.05.
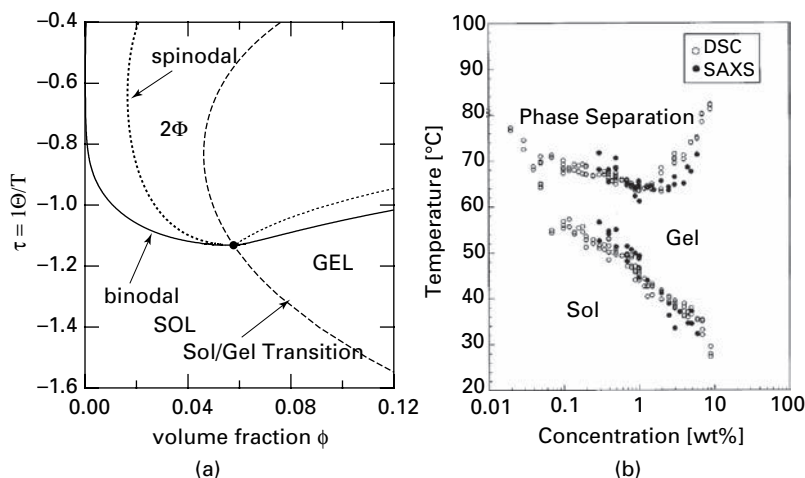
Fig. 10.12 (a) Theoretical phase diagram for methyl cellulose in water. Sol–gel transition line (broken line), binodal (solid line), and spinodal (dotted line) are shown on the reduced temperature–concentration plane. Gelation and phase separation compete on heating the solution. (b) Experimental phase diagram of methyl cellulose ($M_w = 9.36 \times 10^5$, $DS = 1.78$) constructed from DSC and SAXS data [36]. (Reprinted with permission from Ref. [36].)

(b) 0.01, and (c) 0.1), while other parameters are fixed at $n = f = 100$, $\mu_0 = 0.05$, and $\psi_1 = 1$.

As λ_0 becomes larger, two miscibility gaps come closer to each other, and the sol–gel line shifts to the low-concentration region. As the temperature becomes higher, some of the bound solvent molecules are dissociated from the chains, and the chance to form direct bonds becomes higher, thus resulting in gelation on heating.

Figure 10.12 shows our theoretical description of what we see in the experiments of methyl cellulose in water. The upper half of the miscibility loop is beyond the range of the experimental observation, so that we see the binodal of the LCST only. The sol–gel line intersects the binodal from below. However, there is no lower critical solution point. Instead a new inverted tricritical point (TCP) exists.

10.4   Coexisting hydration and gelation

In some aqueous polymer solutions, hydration is noncompetitive with association. For instance, in solutions of telechelic polymers, main chain hydration only indirectly affects the end-chain association. There is interference only in the region very close to the chain end. Dehydration and chain collapse start near the core of the flower micelles in the form of heterogeneous nucleation. The solutions with such coexisting hydration and association turn into gels on cooling (**low-temperature gelation**), while they phase separate at high temperatures.

Experimentally, the effect of end-chain association is evidenced by the lower shift of the LCST line and its inverted molecular-weight dependence. Experimental values of the LCST and maximum temperature (collapse transition) recorded in the endotherm by differential scanning calorimetry (DSC) for solutions of telechelic C18-PNIPAMs of various concentrations [37] are presented in Figure 10.13(b) for various molecular weight of polymers. The data of the homopolymer are also presented as reference data.

In the solutions of homopolymers, the onset temperature of phase separation coincides with the coil–globule transition temperature. In contrast, telechelic PNIPAM solutions have a cloud-point temperature that is several degrees lower than the collapse temperature. The solution becomes turbid by the scattering of the light due to the formation of aggregates (of flower micelles) whose size is comparable to the wavelength of the light. Thus, the LCST splits from the collapse transition temperature.

Existence of the aggregates can be seen from the molecular weight dependence of the LCST lines. In the usual polymer solutions, the phase separation region expands with the polymer molecular weight, but for hydrated associating polymers, it shrinks; shorter chains have a lower LCST. The shift ΔT_{cl} from the homopolymer LCST is as large as 10 K for the shortest chain ($M_n = 12000 \, \text{g} \, \text{mol}^{-1}$) measured. There are more end chains for the shorter polymers when compared at the same weight concentration, and hence the average molecular weight of the aggregates may become higher, and solubility is reduced.

Experimental cloud points of telechelic PNIPAM with $M_w = 37000 \, \text{g} \, \text{mol}^{-1}$ recorded for solutions of various concentrations are presented in Figure 10.13(a) together with
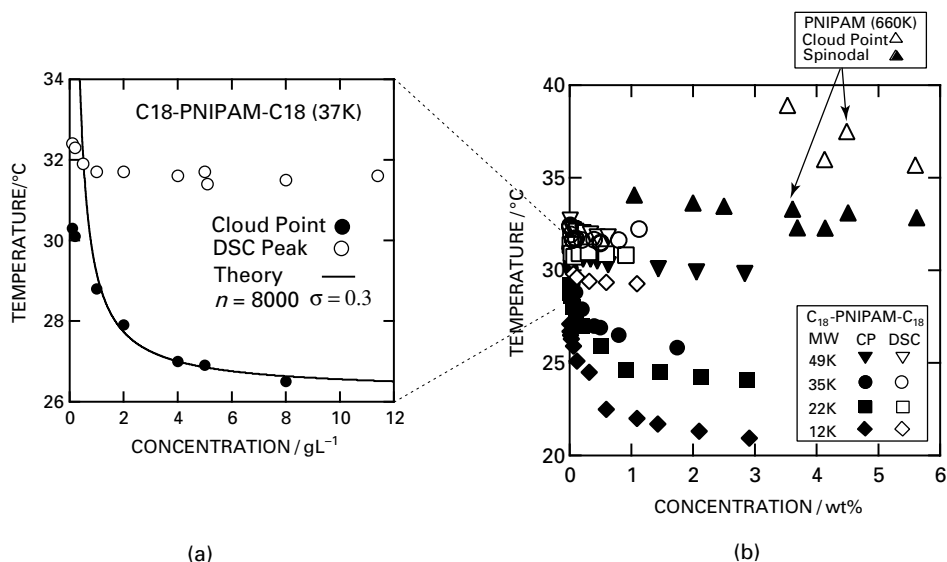
Fig. 10.13 (b) Experimental cloud points (black symbols) of aqueous telechelic PNIPAM solutions determined from temperature-induced changes in the light scattering intensity of polymer solutions, and temperatures of maximum intensity (open symbols) of the endotherms recorded by DSC for aqueous solutions of telechelic PNIPAMs of four different molecular weights. (a) Magnification of (b) for $M_w = 37\,000\,\mathrm{g\,mol^{-1}}$. The coil–globule transition temperatures detected by DSC are also plotted (open circles). The cloud points (onset of phase separation) lie below the coil–globule transition temperature due to hydrophobic end-association. (Reprinted with permission from Refs. [37, 38].)

the theoretical spinodal line. Because their spinodal lines are expected to lie above the binodal lines (cloud points), the comparison is only qualitative. The discrepancy between the binodal and spinodal becomes larger at lower concentrations.

Let us consider a model solution consisting of N telechelic polymer chains (main chain of DP$=n$) carrying two end groups of DP n^*. The total DP of the polymer chains is $n_t \equiv n + 2n^*$. The chains are mixed with a number N_0 of water molecules. To describe the hydration of the main chains by water, let $\mathbf{i} \equiv \{i_1, i_2, \ldots\}$ be the index specifying the hydration type carrying the number i_ζ of sequences that consist of a run of ζ consecutive hydrogen-bonded water molecules, and let $N(\mathbf{i})$ be the number of such p-w complexes of type $\mathbf{i}$ (Figure 10.14) [38]. In particular, we have $\mathbf{i}_0 \equiv (0, 0, \ldots)$ for a bare polymer chain with no bound water. The total number of water molecules on a chain specified by $\mathbf{i}$ is given by $\sum_\zeta \zeta i_\zeta$, and the DP of a complex is given by $n(\mathbf{i}) \equiv n[1 + \theta(\mathbf{i})] + 2n^*$, where

$$\theta(\mathbf{i}) \equiv \sum_{\zeta=1}^{n} \zeta i_\zeta / n \tag{10.69}$$

is the fraction of the bound water molecules relative to the total number of H-bonding sites (DP of a polymer).
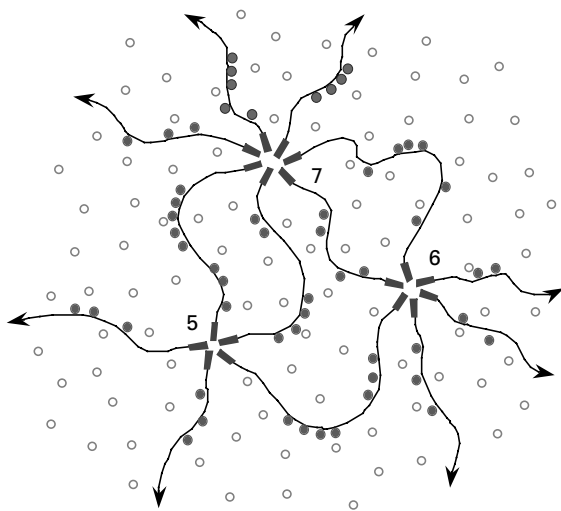
Fig. 10.14   Pictorial representation of a telechelic polymer network made up of hydrated polymer chains. The polymer chains are cross-linked by the micellar junctions formed by hydrophobic association of the end chains. Chain association and hydration are expected to be independent except in the region near the junctions.

We define a cluster type $(\mathbf{j};\mathbf{m})$ if it consists of j_k junctions of multiplicity k ($k = 1, 2, 3, ...$) and $\mathbf{m(i)}$ molecules of the hydration type $\mathbf{i}$. The bold letters $\mathbf{j} \equiv \{j_1, j_2, j_3, ...\}$ and $\mathbf{m} \equiv \{m(\mathbf{i})\}$ denote the sets of indices. The multiplicity is equivalent to the number of hydrophobes in a micelle. A $(\mathbf{j};\mathbf{m})$ cluster is a connected cluster consisting of the number $m(\mathbf{i})$ of hydrated chains of type $\mathbf{i}$. An isolated molecule of the type $\mathbf{i}$, for instance, is indicated by the labels $\mathbf{j}_0 \equiv \{f, 0, 0, ...\}$ (the first element is $j_1 = f$, in particular for a $f = 2$ telechelic chain), and $\mathbf{m}_0(\mathbf{i}) \equiv 1$ (for the type specified by $\mathbf{i}$), $\equiv 0$ (for others).

Let $N(\mathbf{j};\mathbf{m})$ be the number of $(\mathbf{j};\mathbf{m})$-clusters in the system. Their number density is given by $\nu(\mathbf{j};\mathbf{m}) = N(\mathbf{j};\mathbf{m})/\Omega$, and their volume fraction is

$$\phi(\mathbf{j};\mathbf{m}) = \tilde{n}(\mathbf{m})\nu(\mathbf{j};\mathbf{m}), \tag{10.70}$$

where $\tilde{n}(\mathbf{m}) \equiv \sum_{\mathbf{i}} n(\mathbf{i})m(\mathbf{i})$ and $n(\mathbf{i}) \equiv n(1 + \theta(\mathbf{i}) + 2n^*/n)$ is the total DP of a p-w complex of type $\mathbf{i}$. It is approximately given by $n(\mathbf{i}) \simeq n(1 + \theta(\mathbf{i}))$ for a polymer in which the main chain is much longer than the end groups. This gives the volume of a cluster including the bound water. The total volume fraction of the p-w complexes is then given by $\sum_{\mathbf{j},\mathbf{m}} \phi(\mathbf{j};\mathbf{m})$.

In the postgel regime where hydrated gel networks exist, one needs consider the number $N(\mathbf{i})$ of polymer chains of type $\mathbf{i}$ involved in the network. Their number density is given by $\nu^{\mathrm{G}}(\mathbf{i}) = N^{\mathrm{G}}(\mathbf{i})/\Omega$, and their volume fraction by $\phi^{\mathrm{G}}(\mathbf{i}) = n(\mathbf{i})\nu^{\mathrm{G}}(\mathbf{i})$.

The total number of polymer chains in the solution is

$$N = \sum_{\mathbf{j},\mathbf{m}} \left[\sum_{\mathbf{i}} m(\mathbf{i})\right] N(\mathbf{j};\mathbf{m}) + \sum_{\mathbf{i}} N^{\mathrm{G}}(\mathbf{i}). \tag{10.71}$$

In particular, the number of polymer chains of hydration type $\mathbf{i}$ that remain unassociated in solution is given by $N(\mathbf{j}_0; \mathbf{m}_0(\mathbf{i}))$. Similarly, the number of bound water molecules is

$$N_{\text{bw}} = \sum_{\mathbf{j},\mathbf{m}} \left[\sum_{\mathbf{i}} n\theta(\mathbf{i})m(\mathbf{i}) \right] N(\mathbf{j};\mathbf{m}) + \sum_{\mathbf{i}} n\theta(\mathbf{i}) N^G(\mathbf{i}), \qquad (10.72)$$

and the number of free water molecules is

$$N_{\text{fw}} = (1-\phi)\Omega - N_{\text{bw}}. \qquad (10.73)$$

The total volume $\Omega \equiv N_0 + nN$ of the solution is now given by

$$\Omega = \sum_{\mathbf{j},\mathbf{m}} \tilde{n}(\mathbf{m}) N(\mathbf{j};\mathbf{m}) + \sum_{\mathbf{i}} n(\mathbf{i}) N^G(\mathbf{i}) + N_{\text{fw}}. \qquad (10.74)$$

To study the interaction, let us consider the number of contacts between polymers and water. Since the volume fraction of the main chain is $\phi_c = (n/n_t)\phi$, and that of the end chain is $\phi_e = (2n^*/n_t)\phi$, the number of main chain–water contacts (m-w) is $\phi_c(1-\phi)$, and the end chain–water contacts (e-w) is $\phi_e(1-\phi)$. We introduce the conventional χ parameter for each contact type, and find that the enthalpy of p-w interaction per lattice cell is given by $\bar{\chi}(T)\phi(1-\phi)$, where

$$\bar{\chi}(T) \equiv \chi_{\text{mw}}(T)(n/n_t) + \chi_{\text{ew}}(T)(2n^*/n_t). \qquad (10.75)$$

For linear alkyl chains in water near room temperature, a detailed study [39] of **hydrophobic interaction** finds

$$n^*\chi_{\text{ew}}(T) = 2.102\, n_{\text{CH}_3} + 0.884\, n_{\text{CH}_2}/k_\text{B}T \ \left[\text{kcal}\,\text{mol}^{-1}\right]. \qquad (10.76)$$

In particular, for the octadecyl group, for which $n_{\text{CH}_3} = 1, n_{\text{CH}_2} = 17$, we find

$$n^*\chi_{\text{ew}}(T) = 2.102 + 0.884 \times 17/k_\text{B}T. \qquad (10.77)$$

It is approximately $28.5\,\text{kcal}\,\text{mol}^{-1}$ at room temperature.

When we can neglect the length n^* of the end chain compared to n, the effective contact interaction parameter is approximately

$$\bar{\chi}(T) \equiv \chi_{\text{mw}}(T) + \chi_1(T)/n, \qquad (10.78)$$

where $\chi_1 \simeq 2n^*\chi_{\text{ew}}$ is the effective interaction parameter between the end chain and water. The direct interaction between the hydrophobic groups and water gives an $O(1/n)$ correction, and is stronger for shorter chains.

At this stage, we realize that we can study monofunctional polymers ($f = 1$) and telechelic polymers ($f = 2$) (and also their mixtures) from the unified point of view described above. Important examples of the monofunctional case are amphiphilic diblock

copolymers made up of a hydrophilic block and a hydrophobic block, such as PEO-PPO diblock copolymers, PEO-PNIPAM diblock copolymers [40], etc. Another common example is that of the nonionic surfactants C_iE_j, made up of a short alkyl chain and an ethyleneoxide chain [41]. The LCST phase separation depends sensitively on the number of ethyleneoxide units [41]. The phase separation and mixing law of the end-chains in the mixtures of telechelic PEO and semi-telechelic hydrophobic PEO have been studied in detail in the literature [42]

The free energy of the model solution has three contributions:

$$\Delta F = \Delta_{\mathrm{mix}} F + \Delta_{\mathrm{hyd}} F + \Delta_{\mathrm{as}} F. \tag{10.79}$$

The free energy of mixing is given by

$$\beta \Delta_{\mathrm{mix}} F = N_{\mathrm{fw}} \ln \phi_{\mathrm{fw}} + \sum_{\mathbf{j},\mathbf{m}} N(\mathbf{j};\mathbf{m}) \ln \phi(\mathbf{j};\mathbf{m}) + \bar{\chi} \Omega \phi (1-\phi), \tag{10.80}$$

as in Section 5.2, by applying the Flory–Huggins mixing entropy for polydisperse polymer solutions [43].

The free energy of hydration is

$$\beta \Delta_{\mathrm{hyd}} F = \sum_{\mathbf{j},\mathbf{m}} \left[\sum_{\mathbf{i}} \beta \Delta A(\mathbf{i}) m(\mathbf{i}) \right] N(\mathbf{j};\mathbf{m}) + \sum_{\mathbf{i}} \beta \Delta A(\mathbf{i}) N^{\mathrm{G}}(\mathbf{i}), \tag{10.81}$$

where $\Delta A(\mathbf{i}) \equiv A(\mathbf{i}) - A(\mathbf{i}_0)$ is the free energy of hydration to form a complex of type $\mathbf{i}$ starting from a bare polymer of reference conformation $\mathbf{i}_0 \equiv \{0,0,\ldots\}$.

The free energy of hydrophobic association is

$$\beta \Delta_{\mathrm{as}} F = \sum_{\mathbf{j},\mathbf{m}} \Delta(\mathbf{j};\mathbf{m}) N(\mathbf{j};\mathbf{m}) + \sum_{\mathbf{i}} \delta_{\mathbf{i}}(\phi) N^{\mathrm{G}}(\mathbf{i}), \tag{10.82}$$

where $\Delta(\mathbf{j};\mathbf{m}) \equiv \beta[\mu^{\circ}(\mathbf{j};\mathbf{m}) - \sum_{\mathbf{i}} \mu^{\circ}(\mathbf{j}_0;\mathbf{m}_0(\mathbf{i})) m(\mathbf{i})]$ is the free energy change upon formation of a cluster of type $(\mathbf{j};\mathbf{m})$ from separated chains of type $\mathbf{i}$, and where $\delta_{\mathbf{i}}(\phi)$ is the dimensionless free energy gain when a polymer chain of type $\mathbf{i}$ is connected to the network (see Section 5.2). The terms that include the number $N^{\mathrm{G}}(\mathbf{i})$ of polymer chains of type $\mathbf{i}$ in the gel network need to be introduced only in the postgel regime.

The free energy per lattice cell of the solution becomes

$$\mathscr{F}(\phi, T) \equiv \mathscr{F}_{\mathrm{FH}} + \mathscr{F}_{\mathrm{AS}}, \tag{10.83}$$

where

$$\mathscr{F}_{\mathrm{FH}} \equiv \frac{\phi}{n} \ln \phi + (1-\phi) \ln(1-\phi) + \bar{\chi}(T) \phi (1-\phi), \tag{10.84}$$

and

$$\mathscr{F}_{\mathrm{AS}} \equiv \frac{\phi}{n} \ln \left(\frac{\phi_{\lambda}}{\phi} \right) + (1-\phi) \ln \left(\frac{\phi_{\mathrm{fw}}}{1-\phi} \right) + \Delta \nu, \tag{10.85}$$

with

$$\Delta v \equiv 1 - \phi + \phi/n - v^{S} \qquad (10.86)$$

being the loss in the degree of center of mass translational motion as a result of intermolecular association; ϕ_{λ} is the volume fraction of unhydrated and unassociated chains.

We follow the general theoretical procedure described in Section 5.2 and find the following set of equations to relate z and ϕ_{fw} to the polymer concentration:

$$\lambda(T)\psi = z\tilde{u}(z), \qquad (10.87a)$$

$$\phi = \tilde{u}(z)^{f}\phi_{\lambda}G_{0}(\phi_{fw}), \qquad (10.87b)$$

$$1 - \phi = \phi_{fw} + \phi\theta(\phi_{fw}). \qquad (10.87c)$$

The spinodal condition is

$$\frac{\kappa_{\lambda}(\phi)}{n\phi} + \frac{\kappa_{fw}(\phi)}{1-\phi} - 2\bar{\chi} = 0, \qquad (10.88)$$

where the κ-functions take the form

$$\kappa_{\lambda}(\phi) = [1 - (f-1)(\bar{\mu}_{w} - 1)]/\bar{\mu}_{w}, \qquad (10.89a)$$

$$\kappa_{fw}(\phi) = [1 + \theta(\phi_{fw})]^{2}(1-\phi)/\phi_{fw}[1 + \phi\theta'(\phi_{fw})], \qquad (10.89b)$$

in the pregel regime. Here, μ_{w} is the weight-average multiplicity of the network junctions. Because the gel point in multiple tree statistics is given by the divergence condition (7.116), we find that κ_{λ} vanishes at the gel point.

For cooperative hydration, the equilibrium constant for the hydration part is most generally written as

$$K_{H}(\mathbf{i}) = \omega(\mathbf{i}) \prod_{\zeta=1}^{n} \eta_{\zeta}^{i_{\zeta}}, \qquad (10.90)$$

as was shown in Section 6.5, where $\omega(\mathbf{i})$ is the number of different ways to select the sequence specified by $\mathbf{i}$ from a chain, and is given by (1.90). In the *one-mode approximation*, the most probable type is found by minimizing the free energy $\mathscr{F}_{AS}$ by changing $\mathbf{i}$.

For numerical calculation of the phase diagrams, we fix the necessary parameters in the following way. For the interaction between the end-chains and water, we have $\chi_{1} \simeq 2 \times 28.5 \,\mathrm{kcal\,mol^{-1}}/k_{B}T$. To have the sol–gel transition lines in the observed concentration range near 2%, we tried two fixed values of $\chi_{1}(T) = 3.0$ and 10.0. The association constant of the hydrophobic aggregation of the end chains is then given by $\lambda(T) \equiv \lambda_{0}\exp(|\Delta\epsilon|/k_{B}T) = \lambda_{0}\exp[\gamma(1-\tau)]$ in terms of the reduced temperature, where $\gamma \equiv |\Delta\epsilon|/k_{B}\Theta$ is the association energy in a unit of thermal energy at the reference temperature.
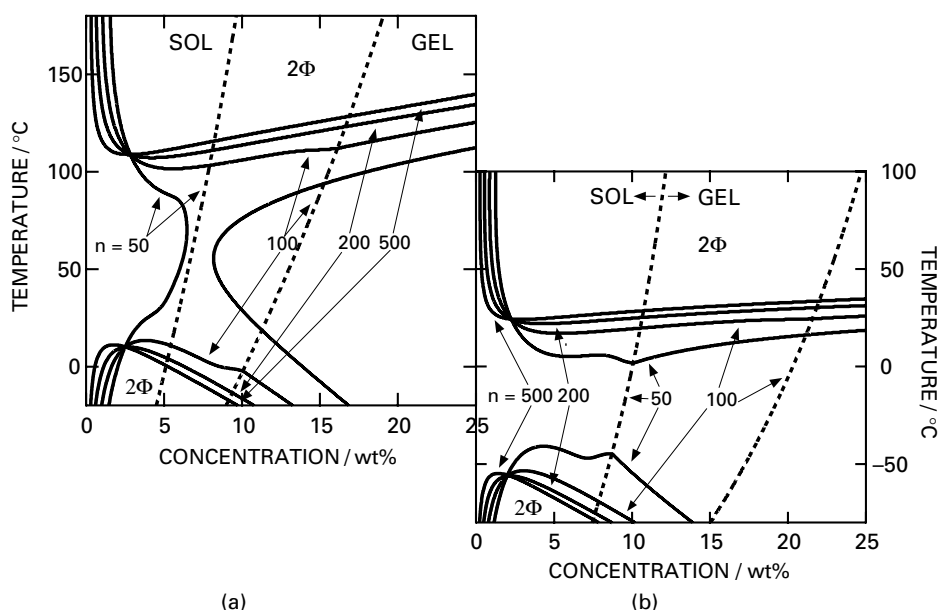
Fig. 10.15   Comparison of the phase diagrams of telechelic associating polymers: (a) random hydration ($\sigma = 1.0$) for telechelic PEO, (b) cooperative hydration ($\sigma = 0.3$) for telechelic PNIPAM. Spinodal lines (solid lines) and sol–gel transition lines (broken lines) are shown. The various curves correspond to polymers of different molecular weights. Other parameters are fixed at the values obtained from the single-chain study. (Reprinted with permission from Ref. [38].)

Similarly, the association constant for hydration is expressed as $\mu(T) = \mu_0 \exp(|\epsilon_H + \Delta\epsilon_H|/k_B T) = \mu_0 \exp[\gamma_H(1-\tau)]$ in terms of the reduced temperature, where μ_0 gives the entropy part of the binding free energy, and $\gamma_H \equiv |\epsilon_H + \Delta\epsilon_H|/k_B \Theta$ is the dimensionless binding energy.

The reference temperature Θ is not the true theta temperature at which the second virial coefficient of the osmotic pressure vanishes. The latter lies far below Θ due to H-bonding and hydrophobic interaction in addition to the van der Waals interaction in the background. The parameters related to the strength of hydration, such as μ_0, γ_H, were taken from Section 6.4 for PEO, and Section 6.5 for PNIPAM.

In Figure 10.15 we compare the calculated phase diagrams of aqueous solutions of telechelic associating polymers undergoing random hydration ((a) $\sigma = 1.0$) or cooperative hydration ((b) $\sigma = 0.3$). The spinodal lines (solid lines) and the sol–gel transition lines (broken lines) are shown over a wide concentration range up to 25 wt%. The molecular weights of the polymers vary from $n = 50$ to 1000. For the polymer concentrations higher than 2 wt%, the LCST moves upwards and the UCST moves downwards with increasing molecular weight.

For the solutions of concentration lower than 2 wt%, however, the opposite trend is observed; the shorter the polymer chains, the higher the spinodal temperature. In such a low-concentration region, intermolecular end chain association is so limited that the

average molecular weight of the aggregates of shorter chains remains smaller than that of longer chains. Hence, the tendency for phase separation is stronger for longer chains, as in homopolymer solutions. For a higher concentration, however, open association develops to such an extent that the average molecular weight of the associated shorter chains exceeds that of the longer chains. As a result, shorter chains show a more profound tendency for phase separation. Such an **inversion in the molecular weight effect** takes place at the point where the LCST curves for different molecular weights meet each other.

For random hydration, the LCST and UCST merge at a molecular a weight between $n = 50$ and 100, and the phase separation region turns into an hourglass. For cooperative hydration, the LCST curves are very flat up to high polymer concentration. Molecular weight effect is weak.

Since the critical micelle concentration is reported to be extremely small ($c < 10^{-3}$wt%), the spinodal curves for solutions of telechelic polymers with concentration lower than 1 wt% are expected to be substantially modified due to the formation of flower micelles. Within the present tree approximation, however, it is not sufficient to study the formation of flower micelles; the critical point is identical to the crossing point of the spinodal curve and the sol–gel transition curve.

10.5   Thermoreversible gelation driven by polymer conformational change

Most natural polymers undergo conformational transition preceding to gelation. Activation of the particular functional groups on a polymer chain accompanied by a proper three-dimensional conformation change is a necessary prerequisite for interchain cross-linking.

For instance, water-soluble natural polymers, such as agarose and κ-carrageenan, first change their conformation from a random coil to a partially helical one. The helical parts then aggregate into network junctions (Figure 10.16(a)) [34,44,46–48].

A similar two-step mechanism of gelation through coil–helix transition was confirmed for synthetic polymers with stereo-regularity. For instance, in solutions of syndiotactic poly(methyl methacrylate) (PMMA) in toluene, a fast intramolecular conformational change is followed by the intermolecular association leading eventually to gelation [49, 50].

Gelation accompanied by polymer conformation change can also be found in polymer solutions where the coil–globule transition of polymer chains plays a dominant role (Figure 10.16(b)). Upon cooling, globular nuclei are randomly formed on a random coil polymer chain due to van der Waals attraction. Some of them associate to similar globular nuclei on different chains in the spatial neighborhood, and form cross-links of densely packed submolecular aggregates. Networks thus take structure in which random coil subchain sequences are connected to each other by the junctions of compact globular aggregates [51, 52].

Other important examples are globular proteins. Proteins, such as ovalbumin and human serum albumin, are believed to form gels after some of the intramolecular bonds
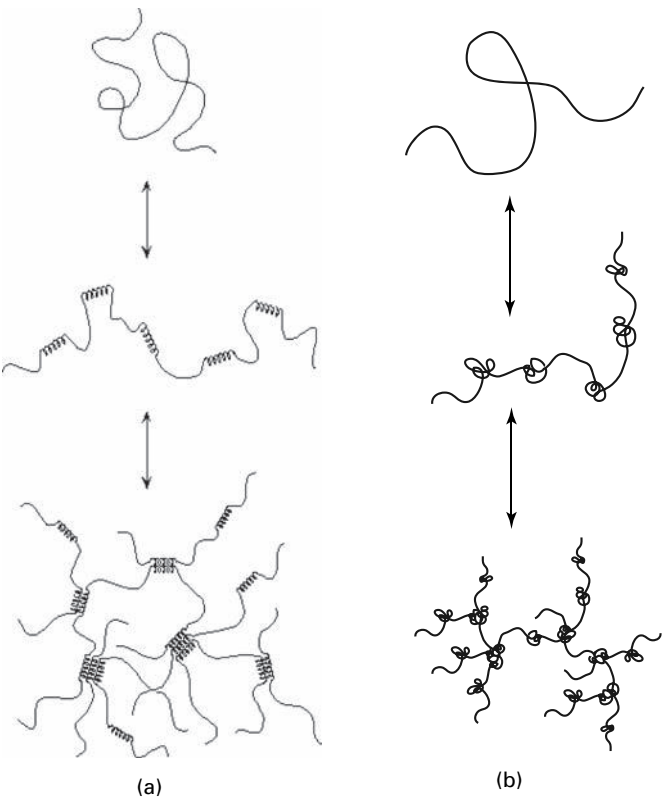
Fig. 10.16   (a) Coil–helix transition of polymer chains followed by the aggregation of helices leading to gelation. (b) Cross-linking by association of globular segments.
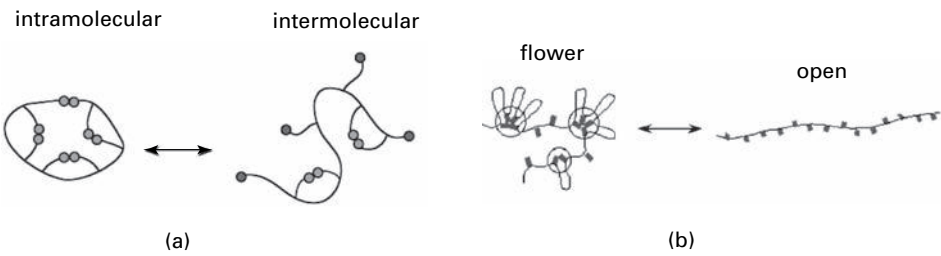
Fig. 10.17   (a) Dissociation of intramolecular bonds, and (b) dissociation of intramolecular flower micelles, by changing the temperature, concentration, pH, etc. (Reprinted with permission from Ref. [57].)

in the native state are broken during denaturation, with their functional groups being exposed to the water in the bulk (Figure 10.17(a)), followed by intermolecular recombination of the groups (**intra–inter transition** studied in Section 10.2) [53–55]. A certain degree of unfolding to expose functional groups is a neccessary condition for gelation in these examples.

Important synthetic polymers whose gelation is strongly coupled to the polymer conformational change are the associating polymers studied in Section 10.2. At low polymer concentrations, intramolecular association (flower micelles) is dominant, but with increase in the concentration, or by raising temperature, some hydrophobic groups are exposed to water (Figure 10.17(b)), and open association (inter-micellar bridging) increases. Bridge chains eventually form networks with multiple cross-link junctions.

10.5.1 Models of conformational transition

The diverse types of gelation may be summarized as follows.

(1) Intra–inter transition
The functional groups hidden inside a polymer molecule are activated by a change in environmental conditions, such as temperature, polymer concentration, pH, concentration of another component, etc., and this leads to gelation by the formation of intermolecular bonds. This transition is often referred to as **loop–bridge transition** or **flower–bridge transition** [56]. In the case where functional groups are thermally activated, this type of conformational transition leads to high-temperature gels.

(2) Coil–helix, coil–rod, or coil–globule transition
Polymers in random coil conformation first partially form helices (or rods or globules) as the temperature is lowered (or raised), and then helices (rods, globules) aggregate into network junctions. This mechanism results in low-temperature gelation as complex cross-linking regions are formed by the attractive interactions. At extremely low temperatures, however, the helix sequences become so long that the total *number* of helices on a chain decreases. Hence, helices tend to form dimers, trimers, etc., and prevent gelation.

(3) Two-state transition
Each monomeric unit A along a polymer chain can take either an active state A* or an inert state A (**two-state model**) [57, 58]. The active monomeric units form cross-links of type $(A^*)_k$ with multiplicity k ($k = 2, 3, 4, ...$) (Figure 10.18). This type may also lead to high-temperature gelation.

At this stage, it should be remarked that the equilibrium polymerization of sulfur [59, 60] is a special case of the above intra–inter transition. A ring polymer S_8 (called λ-sulfur), which is inert at room temperature, first opens its ring to form a linear chain carrying reactive groups on both its ends (called μ-sulfur) as the temperature is raised, and then polymerized through interchain bonding at 160°C. Since the reaction takes place pairwisely, and the functionality f (number of active sites on a molecule) of μ-sulfur is two, the molecules form linear chains instead of three-dimensional networks.

In analogy to sulfur polymerization, we may therefore generally call a molecule staying in the inert state "λ-*molecule*," and one in the active state "μ-*molecule*" for our gel-forming polymer solutions. The **λ/μ-transition** described above in an extended meaning is schematically summarized in Figure 10.19.
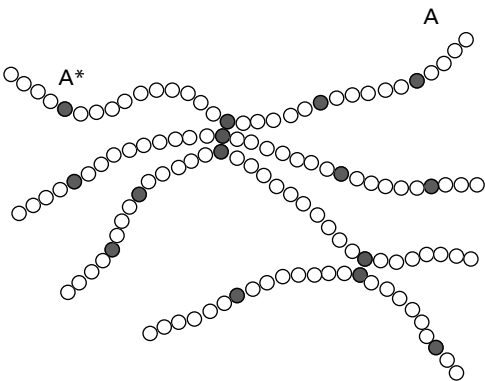
Fig. 10.18 Model two-state polymer chain whose repeat units can take either an inert state (A) or an active state (A*). Repeat units in the active state can form junctions of variable multiplicity. (Reprinted with permission from Ref. [57].)

λ-molecule

$f = 1$ $f = 2$ $f = 3$ $f = 4$ ...... $f = f_{max}$
A_1 A_2 A_3 A_4 A_{fmax}

μ-molecule (active)
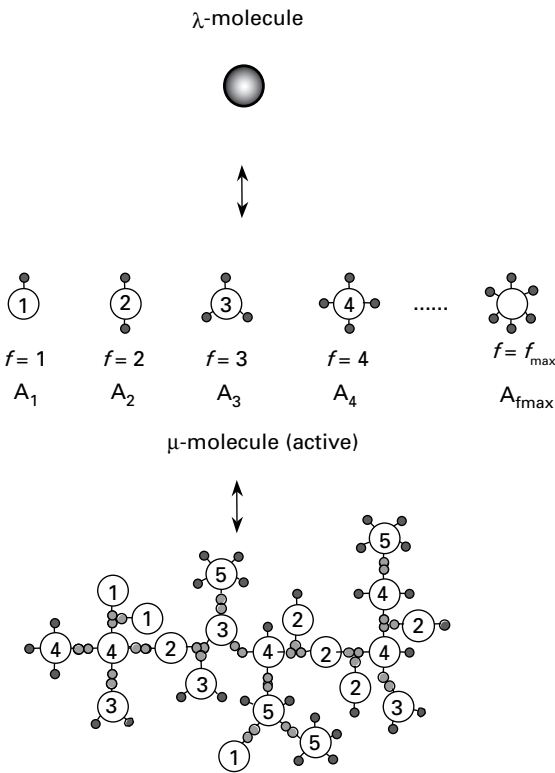
Fig. 10.19 λ/μ transition followed by gelation. Inactive primary molecules called λ-molecules are activated to molecules carrying variable numbers of functional groups, and then form a network with junctions of variable multiplicity. Figures in circles show their functionalities.

10.5.2 Theory of gelation with conformation change

To study the equilibrium gelation strongly coupled to the polymer conformational change, we consider a polydisperse mixture of primary polymer chains carrying variable numbers of functional groups in a solvent. A molecule is distinguished by the number f of active functional groups it carries, which is a variable that depends on the temperature and polymer concentration, as well as other environmental parameters [57].

Let N_λ be the number of λ-molecules, and $\phi_\lambda \equiv nN_\lambda/\Omega$ be their volume fraction. The subscript λ indicates $f = 0$. The volume fraction of μ-molecules is then given by

$$\phi_\mu = \phi - \phi_\lambda = \sum_{f \geq 1} \phi_f, \qquad (10.91)$$

where

$$\phi_f = nN_f/\Omega = n\nu_f \qquad (10.92)$$

is the volume fraction of the f-functional molecules. The total number density of the functional groups is

$$\psi = \sum_{f \geq 1} f\nu_f. \qquad (10.93)$$

The weight distribution ρ_f of the functional groups is

$$\rho_f = f\nu_f/\psi. \qquad (10.94)$$

The number-average functionality f_n of the μ-molecules is then given by

$$f_n \equiv \psi/\sum_{f \geq 1} \nu_f, \qquad (10.95)$$

and the weight-average functionality f_w by

$$f_w \equiv \sum_{f \geq 1} f^2 \nu_f/\psi. \qquad (10.96)$$

These depend on the temperature and the concentration, and play a central role in the following analysis of the sol–gel transition.

The free energy change on passing from the reference states to the final solution, at equilibrium with respect to cluster formation, consists of three parts:

$$\Delta F = \Delta_{\text{conf}} F + \Delta_{\text{rea}} F + \Delta_{\text{mix}} F, \qquad (10.97)$$

where $\Delta_{\text{conf}} F$ is the free energy for the change in molecular conformation, $\Delta_{\text{rea}} F$ the free energy of reaction required to connect μ-molecules into clusters, and $\Delta_{\text{mix}} F$ the free energy produced on mixing all clusters with the solvent.

The first term is introduced to study conformational change of polymer chains. It is written as

$$\Delta_{\text{conf}} F = A_\lambda N_\lambda + \sum_{\mathbf{j},\mathbf{l}} \left(\sum_{f \geq 1} A_f l_f \right) N(\mathbf{j};\mathbf{l}) + \sum_{f \geq 1} A_f N_f^G, \qquad (10.98)$$

where $N(\mathbf{j};\mathbf{l})$ is the number of clusters of the type $(\mathbf{j};\mathbf{l})$, N_f^G is the number of primary molecules in the gel network in the state with f active functional groups, A_λ the conformational free energy in the reference λ-state, and A_f the same for a μ-molecule with f active groups.

The free energy required for activation of a molecule is therefore given by

$$\Delta A_f \equiv A_f - A_\lambda. \tag{10.99}$$

The second term $\Delta_{\mathrm{rea}} F$ in (10.97) is the free energy required to form $N(\mathbf{j};\mathbf{l})$ clusters of the type $(\mathbf{j};\mathbf{l})$ from the primary chains, and also to form a gel network containing N_f^G polymer chains of functionality f. It is written as

$$\beta \Delta_{\mathrm{rea}} F = \sum \Delta(\mathbf{j};\mathbf{l}) N(\mathbf{j};\mathbf{l}) + \sum_{f \geq 1} \delta_f(\phi) N_f^G, \tag{10.100}$$

where $\Delta(\mathbf{j};\mathbf{l})$, as in (7.80), is the free energy change accompanying the formation of a $(\mathbf{j};\mathbf{l})$ cluster in a hypothetical undiluted amorphous state from the separate primary molecules with partially activated states.

The second term on the r.h.s. of (10.100) is necessary only after the gel point is passed; it contains the number N_f^G of f-functional primary molecules connected to the network. The free-energy change $\delta_f(\phi)$ is the free energy required to attach an isolated primary f-molecule to the network.

Finally, the last term $\Delta_{\mathrm{mix}} F$ in (10.97) gives the free energy for mixing the above clusters and the networks with the solvent

$$\beta \Delta_{\mathrm{mix}} F = N_0 \ln \phi_0 + N_\lambda \ln \phi_\lambda + \sum_{\mathbf{j},\mathbf{l}} N(\mathbf{j};\mathbf{l}) \ln \phi(\mathbf{j};\mathbf{l}) + \Omega \chi(T) \phi_0 \phi, \tag{10.101}$$

as in (7.79), where χ is Flory's interaction parameter for the van der Waals interaction.

First let us consider the activation equilibrium, i.e., the equilibrium between λ-molecules and f-molecules in the μ-state ($\boldsymbol{\lambda/\mu}$ **equilibrium**)

$$\Delta \mu_\lambda = \Delta \mu(\mathbf{j}_{0f};\mathbf{l}_{0f}), \tag{10.102}$$

from which we find that the volume fraction of f-molecules in the solution is uniquely related to the volume fraction of λ-molecules by

$$\phi(\mathbf{j}_{0f};\mathbf{l}_{0f}) = \phi_\lambda \exp(-\beta \Delta A_f). \tag{10.103}$$

Let us next consider the equilibrium cluster formation

$$\Delta \mu(\mathbf{j};\mathbf{l}) = \sum_{f \geq 1} l_f \Delta \mu(\mathbf{j}_{0f};\mathbf{l}_{0f}). \tag{10.104}$$

These conditions lead to the most probable distribution of clusters for which the volume fraction of the type $(\mathbf{j};\mathbf{l})$ is connected to the power products of the isolated μ-molecules as

$$\phi(\mathbf{j};\mathbf{l}) = K(\mathbf{j};\mathbf{l}) \prod_{f \geq 1} \phi(\mathbf{j}_{0f};\mathbf{l}_{0f})^{l_f}, \tag{10.105}$$

by the reaction constant

$$K(\mathbf{j};\mathbf{l}) \equiv \exp[l - 1 - \Delta(\mathbf{j};\mathbf{l})]. \tag{10.106}$$

Finally, an isolated f-molecule should also be in equilibrium with an f-molecule attached to the gel network in the postgel regime. Hence we have

$$\Delta\mu_f^{\mathrm{G}} = \Delta\mu(\mathbf{j}_{0f};\mathbf{l}_{0f}), \tag{10.107}$$

which leads to the relation

$$\phi(\mathbf{j}_{0f},\mathbf{l}_{0f}) = \exp(\delta_f - 1). \tag{10.108}$$

With the help of all these relations, the volume fraction of molecules or clusters of any type can be expressed in terms of a single unknown, for which we choose the volume fraction ϕ_λ of the λ-molecules.

The total number density of chains can be split into sol and gel:

$$\nu_f = \nu_f^{\mathrm{S}} + \nu_f^{\mathrm{G}}. \tag{10.109}$$

The total concentration ψ of associative groups is related to that of unassociated groups $z \equiv \lambda(T)\psi p_1$ by

$$\lambda\psi = z\tilde{u}(z), \tag{10.110}$$

as in (7.98).

The number density of functional groups carried by the unassociated μ-molecules is

$$x_f = \frac{f\lambda}{n}\phi(\mathbf{j}_{0f},\mathbf{l}_{0f}). \tag{10.111}$$

By definition, x_f is given by

$$x_f \equiv \lambda\psi\rho_f p_1{}^f = \rho_f z/\tilde{u}(z)^{f'}, \tag{10.112}$$

where $f' \equiv f - 1$. The equilibrium condition (10.103) leads to

$$x_f = f x_\lambda \exp(-\beta\Delta A_f), \tag{10.113}$$

where x_λ is the scaled number density of λ-molecules

$$x_\lambda \equiv \frac{\lambda(T)}{n}\phi_\lambda. \tag{10.114}$$

Thus, we have

$$\rho_f = \frac{\tilde{u}(z)^{f'}}{z} f x_\lambda e^{-\beta \Delta A_f} = \frac{f x_\lambda}{\lambda \psi} \tilde{u}(z)^f e^{-\beta \Delta A_f}, \tag{10.115}$$

for the distribution function of the functional group. By the normalization condition $\sum \rho_f = 1$, the parameter x_λ is expressed by

$$x_\lambda = \lambda \psi / F_1(z) = z \tilde{u}(z) / F_1(z), \tag{10.116}$$

as a function of z, where the new functions $F_m(z) (m = 0, 1, 2, ...)$ are introduced by the definition

$$F_m(z) \equiv \sum_{f \geq 1} f^m \tilde{u}(z)^f e^{-\beta \Delta A_f}. \tag{10.117}$$

Substituting this result into (10.115), we find

$$\rho_f = f \tilde{u}(z)^f e^{-\beta \Delta A_f} / F_1(z). \tag{10.118}$$

Thus the weight distribution ρ_f of associative groups is expressed in terms of the conformational excitation free energy ΔA_f and the number density z of associative groups that remain unreacted in the solution.

On substitution into (10.95), we find

$$f_n = F_1(z) / F_0(z). \tag{10.119}$$

Similarly, the weight-average functionality is

$$f_w = F_2(z) / F_1(z). \tag{10.120}$$

The volume fraction of μ-molecules is

$$\phi_\mu \equiv n \sum_{f \geq 1} \nu_f = n \psi / f_n. \tag{10.121}$$

Hence we find for the total volume fraction of polymers

$$\frac{\lambda}{n} \phi = x_\lambda + \frac{\lambda \psi}{f_n} = [1 + F_0(z)] x_\lambda = \frac{1 + F_0(z)}{F_1(z)} z \tilde{u}(z), \tag{10.122}$$

or equivalently,

$$\frac{\lambda f_{av}(z)}{n} \phi = z \tilde{u}(z), \tag{10.123}$$

where

$$f_{av}(z) \equiv F_1(z) / [1 + F_0(z)]. \tag{10.124}$$

This is a relation that enables us to find the number density z of unassociated functional groups as functions of the total polymer concentration. By solving this relation, we find z, and hence x_λ, as a function of ϕ.

The sol–gel transition point is given by the condition

$$(f_w - 1)(\mu_w - 1) = 1, \tag{10.125}$$

or equivalently,

$$[f_w(z) - 1]z\tilde{u}'(z)/\tilde{u}(z) = 1. \tag{10.126}$$

Here, the average functionality f_w is given by (10.120) as a function of z, which is related to the total polymer concentration through (10.123).

10.5.3 Simple models of excitation

Independent excitation model

In this model a polymer chain is assumed to carry a fixed number f of associative groups, each of which may independently take either an active or inert state. The energy difference between the two states is assumed to be given by ΔA_1.

Then the functions $F_m(z)$ in (10.117) take the form

$$F_m(z) = \sum_{g=0}^{f} g^m u(z)^g \frac{f!}{g!(f-g)!} \left(e^{-\beta \Delta A_1}\right)^g = \left(x \frac{d}{dx}\right)^m (1+x)^f, \tag{10.127}$$

where $x \equiv \eta \tilde{u}(z)$ with $\eta \equiv \exp(-\beta \Delta A_1)$. The average functionalities are given by $f_{av} = fx/(1+x)$, $f_w = (1+fx)/(1+x)$, and $f_n = fx(1+x)^{f-1}/[(1+x)^f - 1]$. The fundamental relation (7.98) now takes the form

$$\frac{f\lambda}{n}\phi = z\tilde{u}(z)\left[1 + \frac{1}{\eta \tilde{u}(z)}\right], \tag{10.128}$$

and the sol–gel transition point is found by the condition

$$f'\eta z\tilde{u}'(z)/[1 + \eta \tilde{u}(z)] = 1. \tag{10.129}$$

The reduced concentration of λ-molecules is given by

$$x_\lambda = z/f\eta[1 + \eta \tilde{u}(z)]^{f'}. \tag{10.130}$$

In the postgel regime, the variable z in these equations must be replaced by the smaller root z' of Flory's condition $x_\lambda(z) = x_\lambda(z')$. The parameter z refers to the conversion of the entire system, while z' refers to that of the sol part only.

The weight fraction of the sol is obtained by the ratio

$$w^S = z'\left[1 + \eta \tilde{u}(z')\right]/\{z[1 + \eta \tilde{u}(z)]\}, \tag{10.131}$$

and that of the gel is given by $w^G = 1 - w^S$.

The association and excitation constants are assumed to take the following form:

$$\lambda(T) = \lambda_0 \exp[\lambda_1(1 - \tau)], \qquad \eta(T) = \eta_0 \exp[\eta_1(\tau - 1)]. \tag{10.132}$$
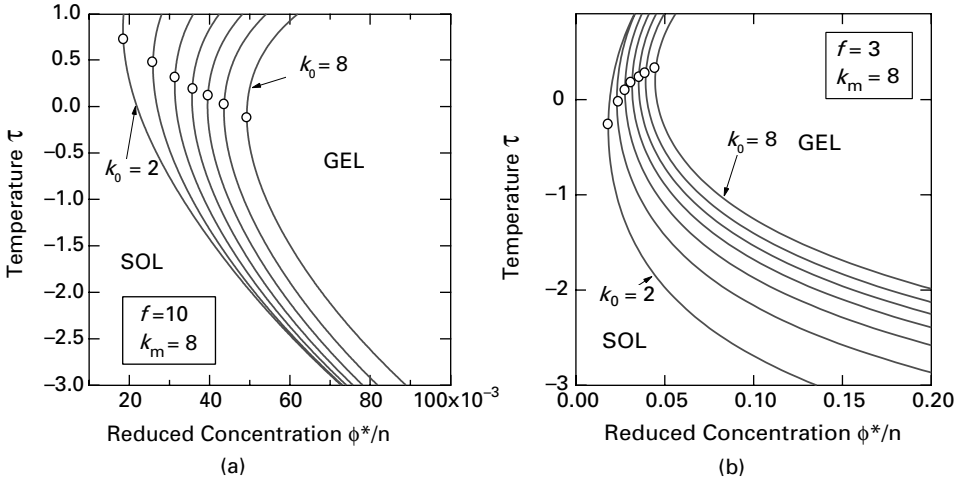
Fig. 10.20   Sol–gel transition line on the temperature–concentration plane. Functionality $f = 10$, with maximum allowed multiplicity $k_m = 8$, and minimum multiplicity varied from $k_0 = 2$ to 8. The minimum concentration for gelation is indicated by circles. (a) Independent excitation model with multiple junctions: $\lambda_0 = 2.0, \lambda_1 = 1.2, \eta_0 = 1.0, \eta_1 = 1.3$. (b) All-or-none excitation model: $f = 3, k_m = 8, k_0$ varied from 2 to 8, $\lambda_0 = 5.0, \lambda_1 = 1.0, \eta_0 = 4.0, \eta_1 = 2.0$. (Reprinted with permission from Ref. [57].)

Figure 10.20(a) shows the effect of junction multiplicity on the sol–gel transition. The functionality is fixed at $f = 10$. The association constants are fixed at $\lambda_0 = 2.0, \lambda_1 = 1.2$. The excitation constants are fixed at $\eta_0 = 1.0, \eta_1 = 1.3$. The junction multiplicity between k_0 and $k_m = 8$ is allowed. The minimum multiplicity k_0 is varied from curve to curve. The gel region shrinks as k_0 approaches k_m because the allowed multiplicity range becomes smaller. Most of the curves have temperature T^*_{min} at which the gelation concentration becomes minimum. This is the optimal temperature of gelation. Under a fixed concentration, the solution gels on heating, but goes back to sol on further heating (**reentrant sol**). Such nonmonotonic behavior was theoretically pointed out by Higgs and Ball [47], and experimentally reported in [46].

All-or-none model

This model assumes that all associative groups are either active or inactive simultaneously. We have functionality f for the excited state and 0 for the ground state, so that $f_{av} = f \eta \tilde{u}^f / (1 + \eta u^f), f_n = f_w = f$, where $\eta \equiv \exp(-\beta \Delta A_f)$. When $f = 2$ and association is restricted to pairwise connection, this model reduces to Scott's theory of sulfur polymerization [60]. The fundamental relation in this model takes the form

$$\frac{f\lambda}{n}\phi = z\tilde{u}(z)\left[1 + 1/\eta\tilde{u}(z)^f\right],$$ (10.133)

and the sol–gel transition point is found by the condition

$$f'z\tilde{u}'(z)/\tilde{u}(z) = 1.$$ (10.134)
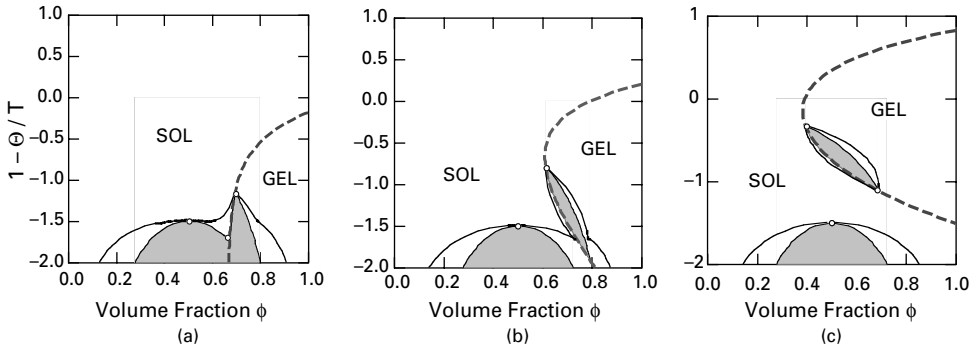
Fig. 10.21 Phase diagrams of low-molecular weight primary molecules ($n = 1$) with triple associative groups ($f = 3$). Independent excitation followed by triple association ($k = 3$) is assumed. Association constant and excitation constant are fixed at (a) $\lambda_0 = 0.49, \lambda_1 = 2.50, \eta_0 = 1.00$, $\eta_1 = 2.50$; (b) $\lambda_0 = 0.73, \lambda_1 = 2.50, \eta_0 = 1.00, \eta_1 = 2.80$; (c) $\lambda_0 = 1.48, \lambda_1 = 2.00$, $\eta_0 = 1.00, \eta_1 = 3.00$. (Reprinted with permission from Ref. [57].)

In the postgel regime, z' must be found by the condition

$$z/\tilde{u}(z)^{f'} = z'/\tilde{u}(z')^{f'}. \tag{10.135}$$

The sol fraction is then given by

$$w^S = \left[1 + \eta\tilde{u}(z')^f\right] / \left[1 + \eta\tilde{u}(z)^f\right]. \tag{10.136}$$

Figure 10.20(b) shows the transition lines for the all-or-none excitation model with varied multiplicity for a functionality of $f = 3$. Though the detailed shape of the curves is different, the overall behavior is the same as that of the independent excitation model.

Figures 10.21(a)–(c) shows how the phase behavior changes depending upon the relative strength of the association constant λ and the excitation constant η. All phase diagrams are calculated for trifunctional ($f = 3$) low-molecular weight molecules ($n = 1$) with triple junctions ($k = 3$). All-or-none excitation of the functional groups is assumed. In all three diagrams, solid lines show the binodal, broken lines the sol–gel transition, and the shaded areas are unstable regions.

When the association constant is large as in Figure 10.21(a), the solution exhibits UCST-type phase separation intersecting with the low-temperature sol–gel transition line at the top of the phase separation region. With a decrease in the strength of the association constant (Figure 10.21(b)), or an increase in the excitation constant (Figure 10.21(c)), association in the low-temperature region becomes less favorable, and the lower part of the sol–gel line tends to shift to a higher-concentration region. The unstable region around the sol–gel transition line moves upwards following the shift of the sol–gel transition line. In Figure 10.21(c), the two-phase region splits into two parts. This diagram resembles that of the equilibrium polymerization of sulfur in a solution [60], but the polymerization line is replaced by the gelation line.

Tobitani and Ross-Murphy [55] confirmed the existence of a similar gelation line in their study of heat-induced gelation in an aqueous solution of a globular protein (bovine serum albumin).

10.6   Thermoreversible gelation driven by the coil–helix transition of polymers

We focus on the polymer solutions in which polymers in random-coil conformation (reference conformation λ) form partial helices on cooling, and then aggregate into multiple network junctions (Figure 10.22). Helical sequences are regarded as functional groups.

If a chain carries many short helices, its functionality is high, but the association energy is small because the energy is proportional to the helix length. If a chain carries a small number of long helices, its functionality is low, but the association energy is large. Therefore, there is a competition between helix growth and helix association.

This competition is described by the relative magnitude of the probability for the formation of a helix of length ζ

$$\eta_\zeta(T) \equiv \exp(-\Delta A_\zeta / k_B T), \tag{10.137}$$

where ΔA_ζ is the free energy of a helix measured relative to the random coil, and the association constant

$$\lambda_\zeta(T) \equiv \exp(-\Delta f_\zeta / k_B T) \tag{10.138}$$

where Δf_ζ is the free energy change for binding a helix of length ζ into a junction. In the following study, we assume that the time scale of helix growth is sufficiently fast compared to that of helix association, so that the helix distribution on a chain reaches an

(a)   (b)
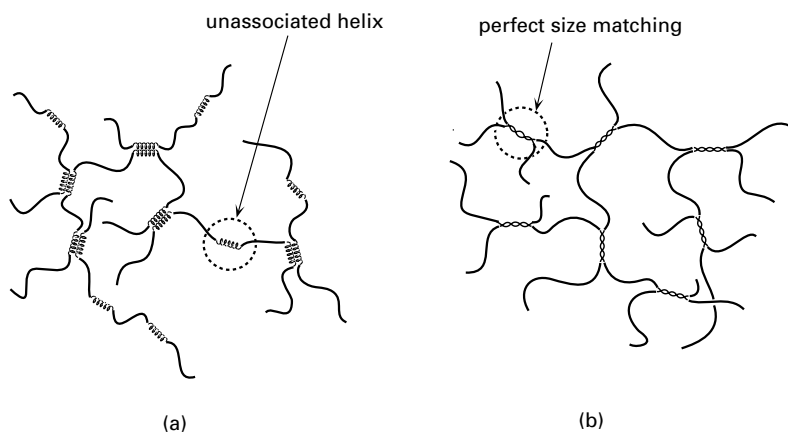
Fig. 10.22   Two fundamentally different types of networks cross-linked by helices: (a) multiple association of single helices, (b) association by multiple helices. (Reprinted with permission from Ref. [67].)

equilibrium before association. Both **strong association** ($\lambda_\zeta > \eta_\zeta$) and **weak association** ($\lambda_\zeta < \eta_\zeta$) are possible.

Let us distinguish between two fundamentally different cases: the multiple association of **single helices** and association by **multiple helices** (Figure 10.22). These are fundamentally different in the following ways:

(1) Unassociated helices remain in the networks in the single-helix case; while there are no isolated helices in the multiple-helix case. In the former the helix content is not necessarily proportional to the elastic modulus of the network.
(2) In the multiple-helix case, there is by definition perfect size matching among the sequence lengths joining in a junction; while in the single-helix case, small helices may associate with longer ones, so that the helix length in a junction is not necessarily uniform.
(3) In the single-helix case, two neighboring helices on the same chain may merge into one when they grow; while in the multiple-helix case they collide and never merge.

In most biopolymer gels, experimental distinction between pairwise association of single helices and interwined double helices is very difficult, so that the more general term **helical dimer** is used in the literature [61, 62]. We treat them in a different way, but, for simplicity, assume perfect **size matching** when single helices associate. Helices of different length are regarded as different functional groups.

In addition to the double helices formed in biopolymers such as κ-carrageenen, gellan, etc., we can treat other types of junction zones, such as hydrogen-bonded ladder type junctions as seen in polyacid–polybase complexes [63, 64], or association by forming stereocomplex eggbox junction zones [65, 66] in which metalic ions are captured (Figure 10.23). For such pairwise association of polymer chains, Higgs and Ball [47] suggested
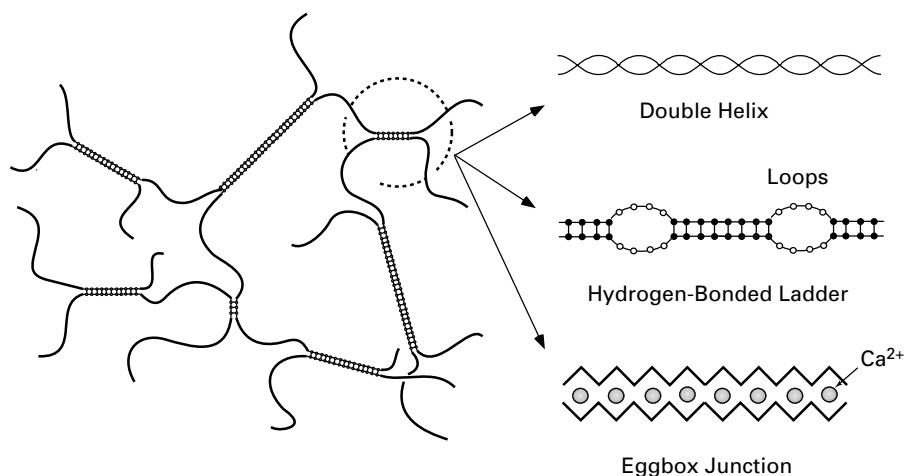
Fig. 10.23 Three examples of zipper type junction zones: double helix, hydrogen-bonded ladder (with small loops), and eggbox junction. (Reprinted with permission from Ref. [67].)

the occurrence of **pairing transition**, where the mean length of bound sequences reaches the total polymer chain length. We will study this transition in detail using the theory of associating polymer solutions.

10.6.1   Models of helix association

We extend the single chain coil–helix transition studied in Section 1.8 to many-chain problems [67]. In a solution, polymer chains carry helices whose length distribution along the chain is specified by j_ζ. A polymer chain is regarded as a functional molecule carrying j_ζ of functional groups specified by the length ζ of helices (Figure 10.24). Helices of different length are regarded as different functional groups.

We can apply the model of thermoreversible gelation of functional molecules whose functionality is not a fixed number but varies depending on the temperature.

We are then led to

$$\mathscr{F} = \mathscr{F}_{\mathrm{FH}}(\phi) + \mathscr{F}_{\mathrm{AS}}(\phi), \tag{10.139}$$

for the free energy per lattice cell, where $\mathscr{F}_{\mathrm{FH}}(\phi)$ (5.38) is the Flory–Huggins free energy in the absense of association, and

$$\mathscr{F}_{\mathrm{AS}}(\phi) \equiv \frac{\phi}{n} \ln\left(\frac{\phi_\lambda}{\phi}\right) + \sum_\zeta \frac{1}{\lambda_\zeta} \int_0^{z_\zeta} z\tilde{u}'(z)dz \tag{10.140}$$

is the free energy due to the conformational change and association [57]. Here, ϕ_λ is the volume fraction of λ-molecules (polymers that remain in the random coil with no helix).

We need the parameters z and λ for each ζ, so we have introduced the suffix. The temperature-dependent parameter $\lambda_\zeta(T)$ is the association constant (10.138) for helices of length ζ. The parameter z_ζ is related to the polymer volume fraction through (10.123), which takes the form

$$\lambda_\zeta \langle j_\zeta \rangle \phi/n = z_\zeta \tilde{u}(z_\zeta), \tag{10.141}$$

for each ζ.
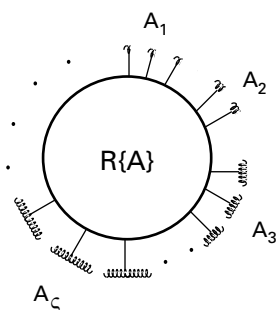
Fig. 10.24   Schematic picture of a functional molecule carrying different species of functional groups A_1, A_2, …. (Reprinted with permission from Ref. [67].)

The function $\tilde{u}(z)$ refers to the multiplicity of the junction. It is defined by (7.99). For k-ple association of single helices, it is

$$\tilde{u}(z) = 1 + z^{k-1}. \tag{10.142}$$

For association by k-ple helices, it is

$$\tilde{u}(z) = z^{k-1}. \tag{10.143}$$

The first term for $k=1$ doesn't exist in the latter because there is no isolated helix.

Minimizing the free energy(10.140) by changing the helix distribution function $\{j\}$ leads to the most probable distribution function

$$j_\zeta/n = (1 - \theta - \nu)\eta_\zeta \tilde{u}(z_\zeta)t^\zeta, \tag{10.144}$$

where the parameter t is defined by the relation $t = 1 - \nu/(1-\theta)$ (1.98) as before,[1] but now depends upon the polymer concentration. The distribution function $\{j\}$ can also be written as

$$j_\zeta/n = (1 - \theta)\eta_\zeta \tilde{u}(z_\zeta)t^{\zeta+1}. \tag{10.145}$$

Comparing this result with the single-chain helix distribution (1.95), we find that interchain association is included in the front factor junction function $\tilde{u}(z)$.

The parameter t is related to the volume fraction ϕ_λ by

$$\phi_\lambda/\phi = t^n. \tag{10.146}$$

Therefore, it gives the probability for a randomly chosen monomer on a chain to belong to a random-coil sequence.

The parameter z_ζ is related to the polymer concentration by (10.122), which now produces the relation

$$z_\zeta = (1-\theta)\phi\lambda_\zeta\eta_\zeta t^{\zeta+1}, \tag{10.147}$$

for the most probable distribution found above.

Upon substitution of the junction function (10.142) for $\tilde{u}(z)$ into the distribution function, we find that the helix content θ per chain is given by $\theta = \sum_{k\geq 1}\theta_k$, and the number of helices ν per chain by $\nu = \sum_{k\geq 1}\nu_k$, where

$$\theta_k \equiv \gamma_k(1-\theta)t\sum_{\zeta=1}^{n}\zeta\eta_\zeta z_\zeta^{k-1}t^\zeta \tag{10.148}$$

is the total helical monomers in the junctions of multiplicity k, and

$$\nu_k \equiv \gamma_k(1-\theta)t\sum_{\zeta=1}^{n}\eta_\zeta z_\zeta^{k-1}t^\zeta \tag{10.149}$$

---

[1] The solution z of the ZB equation (1.146) is denoted as t to avoid confusion with z_ζ.

is their number.

Since the average multiplicity for the helices of length ζ is given by (see Section 7.4)

$$\bar{\mu}_\zeta = 1 + z_\zeta \tilde{u}'(z_\zeta)/\tilde{u}(z_\zeta), \tag{10.150}$$

the gel point condition is found by the condition

$$\sum_{\zeta=1}^{n} \frac{\tilde{u}(z_\zeta)}{\tilde{u}(z_\zeta) + z_\zeta \tilde{u}'(z_\zeta)} j_\zeta = n\nu - 1. \tag{10.151}$$

10.6.2   Multiple helices

We first study the formation of multiple helices with a fixed multiplicity k. For such k-ple helices, the junction function takes the form

$$\tilde{u}(z) = z^{k-1}. \tag{10.152}$$

Let us focus on the double helices $k = 2$, for which θ and ν turn out to be [67]

$$\theta = (1-\theta)^2 \phi t^2 W_1^{(2)}(t^2), \tag{10.153}$$

and

$$\nu = (1-\theta)^2 \phi t^2 W_0^{(2)}(t^2), \tag{10.154}$$

where

$$W_0^{(k)}(x) \equiv \sum_{\zeta=1}^{n} \lambda_\zeta^{k-1} \eta_\zeta^k x^\zeta, \qquad W_1^{(k)}(x) \equiv \sum_{\zeta=1}^{n} \zeta \lambda_\zeta^{k-1} \eta_\zeta^k x^\zeta \tag{10.155}$$

are defined as before.

For the statistical weight of a double helix with sequence length ζ, we assume ZB form

$$\eta_\zeta = 1, \qquad \lambda_\zeta = \sigma_2 \lambda(T)^\zeta. \tag{10.156}$$

The first equation of (10.156) ensures that a chain doesn't form helices by itself. The second equation is described by the weight σ_2 for the initiation (nucleation) of a double helix, i.e., the probability for an arbitrarily chosen pair of monomers on different chains to start winding. This is the counterpart of σ_1 of a single-chain helix nucleation. The cooperativity parameter σ_1 is expected to be small, but σ_2 can be of order unity if there is no strict restriction on monomer conformation in starting chain winding.

The weight $\lambda(T)$, associated with a monomer belonging to a helix, originates in the hydrogen bond between the monomer pair in a helix, and can be regarded as the association constant. It is written as

$$\ln \lambda(T) = \Delta s/k_B - \epsilon_A/k_B T, \tag{10.157}$$

in terms of the entropy and energy of association.

We then have

$$W_0^{(2)}(t^2) = \sigma_2 \lambda t^2 w_0(\lambda t^2), \qquad (10.158a)$$

$$W_1^{(2)}(t^2) = \sigma_2 \lambda t^2 w_1(\lambda t^2), \qquad (10.158b)$$

where functions w_0 and w_1 are defined by (1.107). The equation to find t becomes

$$(1-t)\left\{1 + \frac{w_1(\lambda t^2)(1-t)}{w_0(\lambda t^2)}\right\} = \sigma_2 \lambda \phi t^4 w_0(\lambda t^2). \qquad (10.159)$$

In the limit of infinite dilution, the solution is $t_0 = 1$. At finite concentration, t monotonically decreases as temperature is lowered.

Figure 10.25(a) shows the helix content, number of helices, and average helix length as functions of the temperature for polymers with $n = 100$ repeat units. The temperature is measured in terms of $\ln \lambda \simeq |\epsilon_A|/k_B T$. The polymer volume fraction is changed from curve to curve. The coil–helix transition takes place at around $\ln \lambda = 0$, and shifts slightly to a higher temperature with the polymer concentration. The helix initiation parameter is fixed at $\sigma_2 = 1.0$ by assuming the simplest case where there is no restriction for a pair of chains to start winding.

The total helix content in the solution is proportional to $\theta \times \phi$, and is an increasing function of the polymer concentration for all temperature regions (Figure 10.25(b)). It is expected to be proportional to the rotation angle of the polarization plane in optical measurements.

Near the transition temperature, many short helices are nucleated. At low temperatures, helices grow longer and longer, so that there are only a few long helices on a chain. For
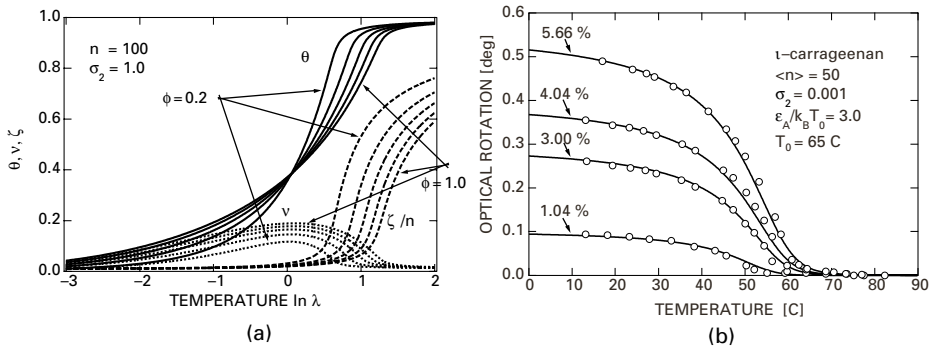
Fig. 10.25 (a) Theoretical helix content θ (solid lines), number of helices ν (dotted lines), mean helix length $\bar{\zeta}$ per chain (broken lines) plotted against the temperature. Temperature is measured in terms of $\ln \lambda = const + |\epsilon_A|/k_B T$. Polymer volume fraction is changed from curve to curve. The total DP of a polymer is fixed at $n = 100$. The helix initiation factor is fixed at $\sigma_2 = 1.0$. (b) Comparison of the experimentally measured optical rotation angles (circles) and theoretically calculated total content of helices in a solution (solid lines). Experimental data were obtained from degraded ι-carrageenan solution with 0.1 mol salt. Polymer concentration is varied from curve to curve. (Reprinted with permission from Ref. [67].)

instance, their length reaches about 80% at $\ln \lambda = 2$. The double helices with 80% long are practically rod-like rigid pairs of polymers. Hence they form various anisotropic liquid-crystalline mesophases [68–70].

Figure 10.25(b) compares the experimentally measured optical rotation angle for the degraded ι-carrageenan aqueous solution with 0.1 mol of added salt [71] with theoretically calculated total helix content in the solution. The molecular distribution of degraded carrageenan was measured in the experiment and the average chain length was estimated to be 47 residues. The optical rotation was measured at four concentrations by changing the temperature. The ι-carrageenan with such a small molecular weight (47 residues) does not form gels in this temperature–concentration region. DSC measurement on cooling and heating process in the same temperature range was also carried out together with optical measurement. The result on cooling and on heating did not show any significant difference, and gave a unique value for the enthalpy of coil–helix transition. Therefore, the solution was treated as in thermal equilibrium.

The proportionality constant between theoretical helix content and optical rotation is found by fitting the data at the highest concentration of 5.66% measured. Then, theoretical results at other concentrations automatically fit the experimental data with high accuracy. It turned out that, for $\langle n \rangle = 50$, the helix initiation parameter σ_2 should be as small as 0.001 to obtain good fit. One of the main reasons why ι-carrageenan does not form gels is the smallness of this helix initiation probability. The coil–helix transition temperature at dilute limit is fixed at $T_0 = 65°C$.

Figure 10.26(a) summarizes the theoretical results in the form of a phase diagram. The solid line shows the sol–gel transition line as decided by the condition (10.151) for $k = 2$. Broken lines show the contours with a constant helix length. Along the right most line with $\zeta/n = 0.8$, for example, double helices have average length of 80 % of the total length. The sol–gel transition concentration is not a monotonic function of the temperature.
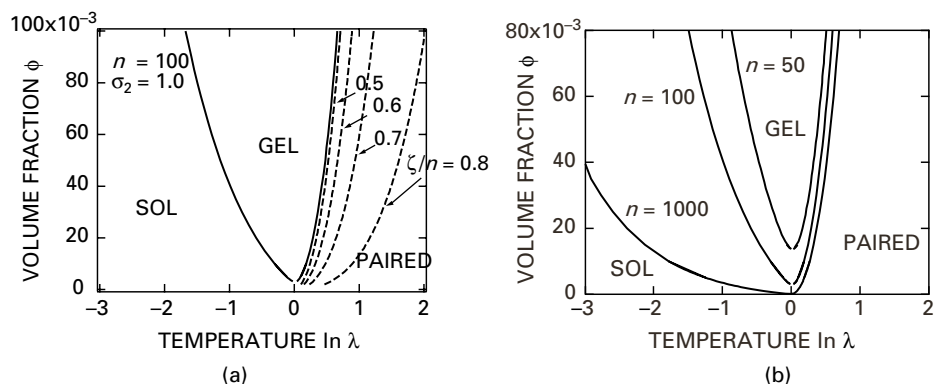
Fig. 10.26 (a) Temperature–concentration phase diagram of a polymer solution forming networks by double helices. The solid line shows the sol–gel transition line. The broken lines show the contour along which the average helix length takes a fixed value. (b) Molecular weight dependence of the sol–gel transition line. (Reprinted with permission from Ref. [67].)

Helices grow so long at low concentrations that the number of network junctions becomes insufficient for gelation. The phase plane is roughly divided into four regions: a sol region with separate chains in the high-temperature dilute regime; a gel region with **type I networks** (long random coils cross-linked by short helices) in the high-temperature side of the postgel regime; a gel region with type II networks (long double helices cross-linked by short free joints of random coils) in the low-temperature side of the postgel regime; and a pairing region in the low-temperature dilute regime (**pairing transition**) [47].

Figure 10.26(b) shows the molecular weight dependence of the sol–gel transition line. The upper branch of the transition line significantly shifts to the high-temperature and low-concentration region with the molecular weight, while the lower branch remains at almost the same position. Such a general tendency was predicted by Higgs and Ball [47] by a simple kinetic analysis in which the helix initiation parameter (σ_2 in the present notation) was assumed to be proportional to the polymer concentration. Their result is justified by the present more precise calculation on the basis of equilibrium statistical mechanics.

Figure 10.27 shows the structure of a **type II network** (the almost pairing phase) found in the Monte Carlo simulation using bead–spring model chains [72]. In addition to the H-bonding energy ϵ, the simulation incorporates the interaction $\Delta\epsilon = 0.3\epsilon$ between neighboring H-bonds.

Figure 10.28 shows more snapshots of the Monte Carlo simulation at three different temperatures along the fixed polymer volume fraction $\phi = 0.05$ [72]. At the highest temperature $\epsilon/k_\mathrm{B}T = 0.2$ (ϵ is the H-bonding energy), it is a uniform molecularly dispersed
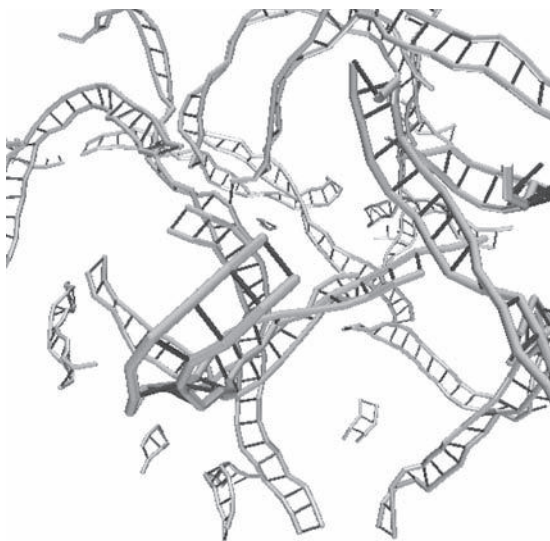
Fig. 10.27   Snapshot of the Monte Carlo simulation on H-bonding polymers using bead–spring model chains. The interaction between neighboring H-bonds is incorporated for the cooperativity in the bond formation.
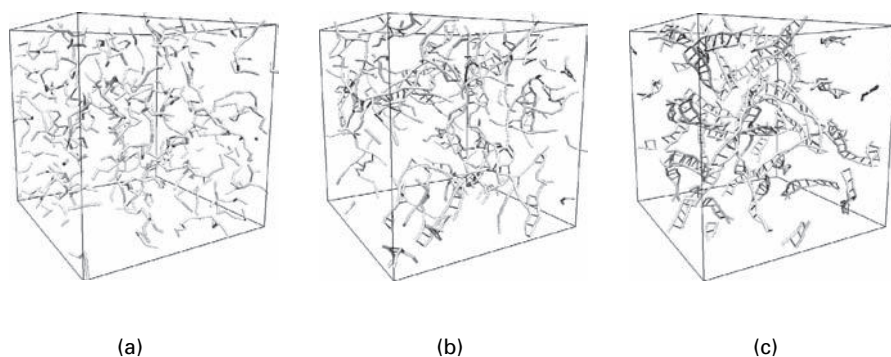
solution (Figure 10.28(a)). The chains are separated from each other. As the temperature goes down, short zippers start to form. A type I network is formed at this temperature $\epsilon/k_B T = 2.2$ (Figure 10.28(b)). As the solution is cooled further, zippers grow, and the network turns into a type II where long zippers are cross-linked by short random coils. At the lowest temperature $\epsilon/k_B T = 4.0$ outside the gel region, most chains are paired. Long ladders are formed, most of which are separated from each other (**pairing phase**) (Figure 10.28(c)).

10.6.3   Multiple association of single helices

For the multiple association of single helices [67], the junction function is

$$\tilde{u}(z) = 1 + z^{k-1}. \tag{10.160}$$

By the assumption of the perfect size matching, the helix content and number of helices are then decomposed into two terms

$$\nu = (1-\theta)t V_0(t) + (1-\theta)^k \phi^{k-1} t^k W_0^{(k)}(t^k), \tag{10.161}$$

$$\theta = (1-\theta)t V_1(t) + (1-\theta)^k \phi^{k-1} t^k W_1^{(k)}(t^k). \tag{10.162}$$

The existence of the first terms in ν and θ discriminates single helices from multiple helices. The equation for t takes the form

$$[1-t-t V_0(t)] \left\{ 1 + t V_1(t) + \bar{\zeta}_k(t)[1-t-t V_0(t)] \right\}^{k-1} = \phi^{k-1} t^k W_0^{(k)}(t^k). \tag{10.163}$$

Two cooperativity parameters are necessary: σ_1 for helix formation, and σ_2 for helix association. We can study the weak association case ($\epsilon_A/\epsilon_H \ll 1$), and the strong association case ($\epsilon_A/\epsilon_H \gg 1$).

In weak association for pairwise association ($k = 2$), most helices are short and unassociated at high temperatures. Helices grow and association starts to take place near the coil–helix transition temperature. The elastic modulus of the network in this region is not related to the total helix content. Pair formation is sharply enhanced around the transition temperature, and paired helices dominate below this temperature. Networks formed around this temperature are basically type II in which short unassociated helices (20% of the total length) are connected by long paired helices (70% of the total length) at junctions via short random coils. At lower temperatures, the helices condense into long paired ones; the system becomes a concentrated solution of rod-like molecules of helix pairs.

In strong association, there is a sharp rise in θ_2, where the total helix content $\theta = \theta_1 + \theta_2$ shows a sudden increase (except for infinite dilution, where $\phi \to 0$). Type I networks exist just above this temperature, but they disappear at a certain temperature. In the special case of infinite dilution, where $\phi \to 0$, all curves reduce to those predicted by ZB theory for a single chain.

References

[1] Tanaka, F., *Macromolecules* **31**, 384 (1998).
[2] Goddard, E. D.; Ananthapadmanabhan, K. P., *Interactions of Surfactants with Polymers and Proteins*. CRC Press: Boca Raton, CA, 1993.
[3] Cabane, B., *J. Phys. Chem.* **81**, 1639 (1977).
[4] Brown, G.; Chakrabarti, A., *J. Chem. Phys.* **96**, 3251 (1992).
[5] Feitosa, E.; Brown, W.; Hansson, P., *Macromolecules* **29**, 2169 (1996).
[6] Feitosa, E.; Brown, W.; Vasilescu, M.; Swason-Vethamuthu, M., *Macromolecules* **29**, 6837 (1996).
[7] Feitosa, E.; Brown, W.; Wang, K.; Barreleiro, P. C. A., *Macromolecules* **35**, 201 (2002).
[8] Ricka, J.; Meewes, M.; Nyffenegger, R.; Binkert, T., *Phys. Rev. Lett.* **65**, 657 (1990).
[9] Meewes, M.; Ricka, J.; de Silva, M.; Nyffenegger, R.; Binkert, T., *Macromolecules* **24**, 5811 (1991).
[10] Fredrickson, G. H., *Macromolecules* **26**, 2825 (1993).
[11] Seki, T.; Tohnai, A.; Tamaki, T.; Kaito, A., *Macromolecules* **29**, 4813 (1996).
[12] Alami, E.; Almgren, M.; Brown, W., *Macromolecules* **29**, 5026 (1996).
[13] Cabane, B.; Lindell, K.; Engström, S.; Lindman, B., *Macromolecules* **29**, 3188 (1996).
[14] Nyström, B.; Lindman, B., *Macromolecules* **28**, 967 (1995).
[15] Nyström, B.; Walderhaug, H.; Hansen, F. K.; Lindman, B., *Langmuir* **11**, 750 (1995).
[16] Nyström, B.; Kjonisken, A. L.; Lindman, B., *Langmuir* **12**, 3233 (1996).
[17] Wang, G.; Lindell, K.; Olofsson, G., *Macromolecules* **30**, 105 (1997).
[18] Annable, T.; Buscall, R.; Ettelaie, R.; Shepherd, P.; Whittlestone, D., *Langmuir* **10**, 1060 (1994).
[19] Nilsson, S., *Macromolecules* **28**, 7837 (1995).
[20] Xie, X.; Hogen-Esch, T. E., *Macromolecules* **29**, 1734 (1996).
[21] Sgashkina, J. A.; Philippova, O. E.; Zaroslov, Y. D.; Khokhlov, A. R.; Pryakhina, T. A., *Langmuir* **21**, 1524 (2005).
[22] Couillet, I.; Hughes, T.; Maitland, G.; Candau, F., *Macromolecules* **38**, 5271 (2005).

[23] Yoshida, T.; Taribagil, R.; Hillmyer, M.A.; Lodge, T.P., *Macromolecules* **40**, 1615 (2007).

[24] Lodge, T.P.; Taribagil, R.; Yoshida, T.; Hillmyer, M.C., *Macromolecules* **40**, 4728 (2007).

[25] Nakaya, K.; Ramos, L.; Tabuteau, H.; Ligoure, C., *J. Rheology* **52**, 359 (2008).

[26] Tabuteau, H.; Ramos, L.; Nakaya-Yaegashi, K.; Imai, M.; Ligoure, C., *Langmuir* **25**, 2467 (2009).

[27] D'Errico, G.; Ciccarelli, D.; Ortona, O.; Vitagliano, V., *J. Mol. Liquids* **100**, 241 (2002).

[28] Stillinger, F.H.; Ben-Naim, A., *J. Chem. Phys.* **74**, 2510 (1981).

[29] Tanaka, F.; Koga, T., *Comp. Theor. Polym. Sci.* **10**, 259 (2000).

[30] Jacobson, H.; Stochmayer, W.H., *J. Chem. Phys.* **18**, 1600 (1950).

[31] de Gennes, P.G., *Scaling Concepts in Polymer Physics*. Cornell University Press: Ithaca, NY, 1979.

[32] Preuschen, J.; Menchen, S.; Winnik, M.A.; Heuer, A.; Spiess, H.W., *Macromolecules* **32**, 2690 (1999).

[33] Sarkar, N., *J. Appl. Polym. Sci.* **24**, 1073 (1979).

[34] Guenet, J.M., *Thermoreversible Gelation of Polymers and Biopolymers*. Academic Press: London, 1992.

[35] Matsuyama, A.; Tanaka, F., *Phys. Rev. Lett.* **65**, 341 (1990).

[36] Takahashi, M.; Shimazaki, M.; Yamamoto, J., *J. Polym. Sci., Part B: Polym. Phys.* **39**, 91 (2001).

[37] Kujawa, P.; Segui, F.; Shaban, S. *et al.*, *Macromolecules* **39**, 341 (2006).

[38] Okada, Y.; Tanaka, F.; Kujawa, P.; Winnik, F.M., *J. Chem. Phys.* **2006**, *125*, 244902[1].

[39] Tanford, C., *The Hydrophobic Effect*, 2nd edn. Wiley: New York, 1980.

[40] Motokawa, R.; Morishita, K.; Koizumi, S.; Nakahira, T.; Annaka, M., *Macromolecules* **38**, 5748 (2005).

[41] Degiorgio, V.; Corti, M., *Physics of Amphiphiles: Micelles, Vesicles and Microemulsions*, Chap. V. North-Holland: Amsterdam, 1985.

[42] Lafleche, F.; Durand, D.; Nicolai, T., *Macromolecules* **2003**, *36*, 1331; 1341.

[43] Flory, P.J., *Principles of Polymer Chemistry*. Cornell University Press: Ithaca, NY, 1953.

[44] Burchard, W., *British Polym. J.* **17**, 154 (1985).

[45] Clark, A.H.; Ross-Murphy, S.B., *British Polym. J.* **17**, 164 (1985).

[46] te Nijenhuis, K., *Adv. Polym. Sci.* **130**, 1 (1997).

[47] Higgs, P.G.; Ball, R.C., *J. Phys. Paris* **50**, 3285 (1989).

[48] Viebke, C.; Piculell, L.; Nilsson, S., *Macromolecules* **27**, 4160 (1994).

[49] Berghmans, M.; Thijs, S.; Cornette, M. *et al.*, *Macromolecules* **27**, 7669 (1994).

[50] Buyse, K.; Berghmans, H.; Bosco, M.; Paoletti, S., *Macromolecules* **31**, 9224 (1998).

[51] Hikmet, R.M.; Callister, S.; Keller, A., *Polymer* **29**, 1378 (1988).

[52] Callister, S.; Keller, A.; Hikmet, R.M., *Makromol. Chem., Macromol. Symp.* **39**, 19 (1990).

[53] Clark, A.H.; Ross-Murphy, S.B., *Adv. Polym. Sci.* **83**, 57 (1987).

[54] Biagio, P.L.; Palma, M.U., *Biophys. J.* **60**, 508 (1991).

[55] Tobitani, A.; Ross-Murphy, S.B., *Macromolecules* **1997**, *30*, 4845; 4855.

[56] Xu, B.; Yekta, A.; Winnik, M.A., *Langmuir* **13**, 6903 (1997).

[57] Tanaka, F., *Macromolecules* **33**, 4249 (2000).

[58] Baulin, V.A.; Halperin, A., *Macromolecules* **35**, 6432 (2002).

[59] Tobolsky, A.V.; Eisenberg, A., *J. Am. Chem. Soc.* **81**, 780 (1959).

[60] Scott, R.L., *J. Phys. Chem.* **1965**, *69*, 261; **71**, 352 (1967).

[61] Rochas, C.; Rinaudo, M., *Biopolymers* **19**, 1675 (1980).

[62] Rochas, C.; Rinaudo, M., *Biopolymers* **23**, 735 (1984).

[63] Iliopoulos, I.; Audebert, R., *Eur. Polym. J.* **24**, 171 (1988).

[64] Iliopoulos, I.; Halary, J. L.; Audebert, R., *J. Polym. Sci., Part A, Polym. Chem.* **26**, 275 (1988).

[65] Morris, E. R.; Rees, D. A.; Thom, D.; Boyd, J., *J. Carbohydro. Res.* **66**, 145 (1978).

[66] Cuppo, F.; Reynaers, H.; Paoletti, S., *Macromolecules* **35**, 539 (2002).

[67] Tanaka, F., *Macromolecules* **36**, 5392 (2003).

[68] Borgström, J.; Quist, P.-O.; Piculell, L., *Macromolecules* **29**, 5926 (1996).

[69] Borgström, J.; Egermayer, M.; Sparrman, T.; Qest, P.-O.; Piculell, L., *Langmuir* **14**, 4935 (1998).

[70] Ramzi, M.; Borgström, J.; Piculell, L., *Macromolecules* **32**, 2250 (1999).

[71] Reid, D. S.; Bryce, T. A.; Clark, A. H.; Rees, D. A., *Faraday Disc. Chem. Soc.* **57**, 230 (1974).

[72] Tamura, Y.; Tanaka, F., *J. Polym. Sci. Part B: Polym. Phys.* **43**, 3331 (2005).

Index